# Novel Amphiphilic Branched Copolymer Nanoparticles as Candidates for Drug Delivery

Thesis submitted in accordance with the requirements of the
University of Liverpool
for the degree of Doctor in Philosophy

by

Rebecca Slater

[B. Sc. (Hons)., University of Liverpool]

August 2013

For Mum and Dad,

Only your unconditional love and support made this possible.

I’m forever grateful.

# Acknowledgements

Thank you Steve for your patience and guidance over these years, I can't explain how much your support has meant to me. This project has been full of ups and downs both experimentally and personally and now that it's finished I will truly miss working for you. Thank you for taking a chance and offering me this PhD. I wish you every success in your future research, you really deserve it. You picked me up and pushed me to do this when I doubted that I could and were the best supervisor I could have hoped for. Huge thanks also goes to my other supervisor Dr. Jonathan Weaver who sadly passed away in 2012. Jon passed on his enthusiasm and love for this work and I will always be grateful for the time he spent with me.

A huge thank you to everyone in the department, and thanks to those who helped with my experiments.

Andy, you've been my everything for the last 8 years and always will be; thanks for putting up with me through all of this! I love you more than I could ever put into words.

Mum and Dad, I can never thank you enough for everything you've done. You're unwavering love and support has helped me through this, you both mean the world to me.

# Table of Contents

# Abstract

The methanolic atom transfer radical polymerisation (ATRP) of 2-hydroxypropyl methacrylate (HPMA) to controllably form the hydrophobic polymer *p*(HPMA) using a one-pot methodology at ambient temperature has been demonstrated, where polymerisations were shown to reach >99 % conversion. By simple variation of initiator:monomer feed ratio, polymers of varying chain length were synthesised. Using identical polymerisation conditions, addition of a small amount of ethylene glycol dimethacrylate (EGDMA) divinyl brancher resulted in the generation of high molecular weight branched copolymers without any modification of reaction kinetics. This approach was extended to include the first synthesis of linear and branched amphiphilic A-B block copolymers using polyethylene oxide (PEG) macroinitiators without loss of the ATRP controlled polymerisation. A series of systematically varying copolymers, containing variation in PEG length and/or variation in *p*(HPMA) primary chain length, have been synthesised to allow direct comparison of the impact of architectural variation on polymer properties.

Nanopreciptation approaches were investigated for the linear and branched copolymers and extremely stable hydrophobic nanoparticles were produced using copolymers with branched architecture. Moreover, it has been shown that nanoparticle z-average diameter can be controlled using extremely facile methods. The loading capacity of amphiphilic branched A-B block copolymer nanoparticles with various guest-molecules has been systematically investigated. The world leading HIV/AIDS antiretroviral drug Lopinavir (LPV) was used in a preliminary loading screen and shown to produce candidate LPV/drug nanocarrier options for future studies and optimisation.

# List of Abbreviations

| | |
|---|---|
| AIBN | 2,2'-Azobisisobutyronitrile |
| AIDS | Acquired immunodeficiency syndrome |
| ATRP | Atom transfer radical polymerisation |
| BDA | but-2-ene-1,4-diacrylate |
| BPY | 2,2'-Bipyridine |
| BuMA | *n*-butyl methacrylate |
| CDMSS | 4-(chlorodimethylsilyl) styrene |
| CMC | Critical micelle concentration |
| CNS | Central nervous system |
| CTA | Chain transfer agent |
| DDT | 1-dodecanethiol |
| DEA | 2-(diethylamino)ethyl methacrylate |
| DLS | Dynamic light scattering |
| DMAP | 4-Dimethylaminopyridine |
| DMEAMA | 2-(dimethylamino)ethyl methacrylate |
| DMF | *N*,*N*-Dimethylformamide |
| DMSO | Dimethyl sulfoxide |
| DNA | Deoxy ribonucleic acid |
| $DP_n$ | Number-average degree of polymerisation |
| DVB | Divinylbenzene |
| EA | Ethyl acrylate |
| EBiB | α-bromoisobutyrate |
| EGDA | Ethylene glycol diacrylate |
| EGDMA | Ethylene glycol dimethacrylate |
| FDA | Food and drug association |
| FI | Fusion Inhibitor |
| GMA | Glycerol monomethacrylate |
| GPC | Gel permeation chromatography |
| HAART | Highly active antiretroviral therapy |
| HEMA | 2-Hydroxyethyl methacrylate |

| | |
|---|---|
| HIV | Human immunodeficiency virus |
| HPMA | 2-Hydroxypropyl methacrylate |
| IPA | Propan-2-ol |
| IV | Intrinsic viscosity |
| LALS | Low angle light scattering |
| LCST | Lower critical solution temperature |
| LPV | Lopinavir |
| MA | Methyl acrylate |
| MMA | Methyl methacrylate |
| $M_n$ | Number-average molecular weight |
| MPC | 2-Methacryloyloxyethyl phosphorylcholine |
| mRNA | messenger ribonucleic acid |
| $M_w$ | Weight-average molecular weight |
| $M_w/M_n$ | Polydispersity |
| *n*BuMA | *n*-Butyl methacrylate |
| NIPAAm | *N*-isopropylacrylamide |
| NMP | Nitroxide-mediated radical polymerisation |
| NMR | Nuclear magnetic resonance spectroscopy |
| NNRTI | Non nucleoside reverse transcriptase inhibitor |
| NRTI | Nucleoside reverse transcriptase inhibitor |
| OEGA | Monomethoxy-capped oligo(ethylene glycol) acrylate |
| OEGMA | Monomethoxy-capped oligo(ethylene glycol) methacrylate |
| PEG | Poly(ethylene glycol) |
| PEGMA | Poly(ethylene glycol) methyl ether methacrylate |
| PEG-OH | Poly(ethylene glycol) methyl ether methacrylate |
| PGA | Poly(glycolic acid) |
| PI | Protease inhibitor |
| PLA | Poly(lactic acid) |
| PLGA | Poly(lactic acid-*co*-glycolic acid |
| RAFT | Reversible addition-fragmentation chain transfer |
| RALS | Right angle light scattering |
| RI | Refractive index |
| RIF | Rifampicin |

| | |
|---|---|
| SCL | Shell cross-linked |
| SCVP | Self-condensing vinyl polymerisation |
| tBuMA | *tert*-Butyl methacrylate |
| TEA | Triethylamine |
| THF | Tetrahydrofuran |
| tRNA | transfer ribonucleic acid |
| UV | Ultra violet |
| VAc | Vinyl acetate |
| VBC | Vinyl benzyl chloride |
| WHO | World health organisation |

# List of Figures

# List of Schemes

# List of Tables

# 1. Introduction

"The ultimate success of a biomaterial is determined by the ability to tailor its properties". This short quote encapsulates the essence of this thesis.[1]

Due to their versatility, polymers (and structures comprised thereof) are a class of material extensively used in a wide range of biomedical applications such as contact lenses,[2] tissue engineering,[3] artificial organs,[4] and orthopaedic devices[5] to name a few.

This introduction aims to highlight some routes to the production of successful biomaterials and therefore lead to the rationale of the research carried out in subsequent chapters. The field of materials science for biomedical applications is extremely vast and here it is limited to those comprised of polymers with the aim of drug delivery. Creating carriers is of extremely high importance as a large fraction of new drugs have poor water solubility and if dosed orally, achieving an adequate therapeutic dose is extremely difficult. Alongside this, drugs can have adverse side effects and are often toxic (leading to poor patient compliance); by effectively "hiding" the drug within a polymeric vector these unwanted effects can be reduced.[6]

## 1.1 Human Immunodeficiency Virus (HIV)

### 1.1.1 Statistics

The huge surge in research in this area is because HIV/AIDS constitutes one of the most serious infectious diseases we face today. Shockingly, over 60 million people have been infected globally[7] and it was estimated that approximately 34 million people are presently living with the disease.[8] The infection has claimed over 25

million lives worldwide[9] since its discovery in the 1980's. The first published research about Acquired Immunodeficiency Syndrome (AIDS) was in 1981 written by Gottlieb *et al.*[10] However, the discovery of the HIV virus is attributed to Montagnier.[11] The effects of HIV/AIDS are most prevalent in sub-Saharan Africa, where around two thirds of HIV sufferers reside and is responsible for the death of 2 million Africans in 2005 alone.[12]

Anti-retroviral drugs and their subsequent delivery systems have been shown to convert the once fatal infection to a more manageable chronic infection. Although this is a huge achievement; according to the World Health Organisation (WHO) guidelines in 2011 only 56 % of HIV sufferers were able to receive treatment in sub-Saharan Africa and globally only 54 % of people with HIV received treatment; [13] clearly much more research still needs to be done to help combat this epidemic.

### 1.1.2 Infection

A brief overview of the replication cycle of the HIV virus is given here and can be seen in Figure 1.1. Human HIV infection is mainly achieved through fusion with CD4+ cells and through self–replication *via* integration of the viral genome into a host cell in the human body (mainly immune system cells) after which the virus can quickly spread through the body. Once entered, mucosal surface CD4+ antigens and either the CCR5 or CXCR4 chemokine receptors on the virus are recognised by T lymphocytes and are subsequently bound by interactions mediated by the transmembrane gp120 glycoprotein, leading to opening of the host cell membrane (Figure 1.1 (1)). Once successfully fused and transported across the cell membrane reverse transcriptase and transfer ribonucleic acid (tRNA) can produce proviral deoxyribonucleic acid (DNA) (Figure 1.1 (2)), which is then integrated into the

genome using integrase (Figure 1.1 (3)). The cell will now convert the HIV genes into messenger ribonucleic acid (mRNA) and leave the nucleus ready to be used for producing more HIV proteins and enzymes. New viral particles are also formed and these contain the entire HIV genome which, together with HIV proteins and enzymes will migrate to the cell surface and leave in a process known as "budding". These are now free to infect other immune system cells and start the replication cycle again. The virus replication cycle requires energy and resources (e.g. enzymes) from the host cell in order for each process to take place and produce new mature particles. Eventually the T lymphocytes' energy sources will be depleted and the cell will die in a form of apoptosis. As the virus can rapidly spread throughout the body, plasma viral load increases and the number of T lymphocytes and other cells drops significantly, this leaves the patient unable to fight off infection effectively. Weight loss and acquiring opportunistic infections (namely pneumonia and tuberculosis) along with other illnesses such as cancer (e.g. lymphoma and Kaposi's sarcoma) and dementia are the main contributors to death in HIV/AIDS sufferers. Once infected by either a mucosal or parenteral route, a person may suffer symptoms such as fever, diarrhoea and lymphadenopathy due to the initial high level of virus, however, generally these symptoms are not synonymous to HIV and therefore the disease can remains undetected for many years and those infected may pass on the virus through bodily fluids.[14,15,16,17]

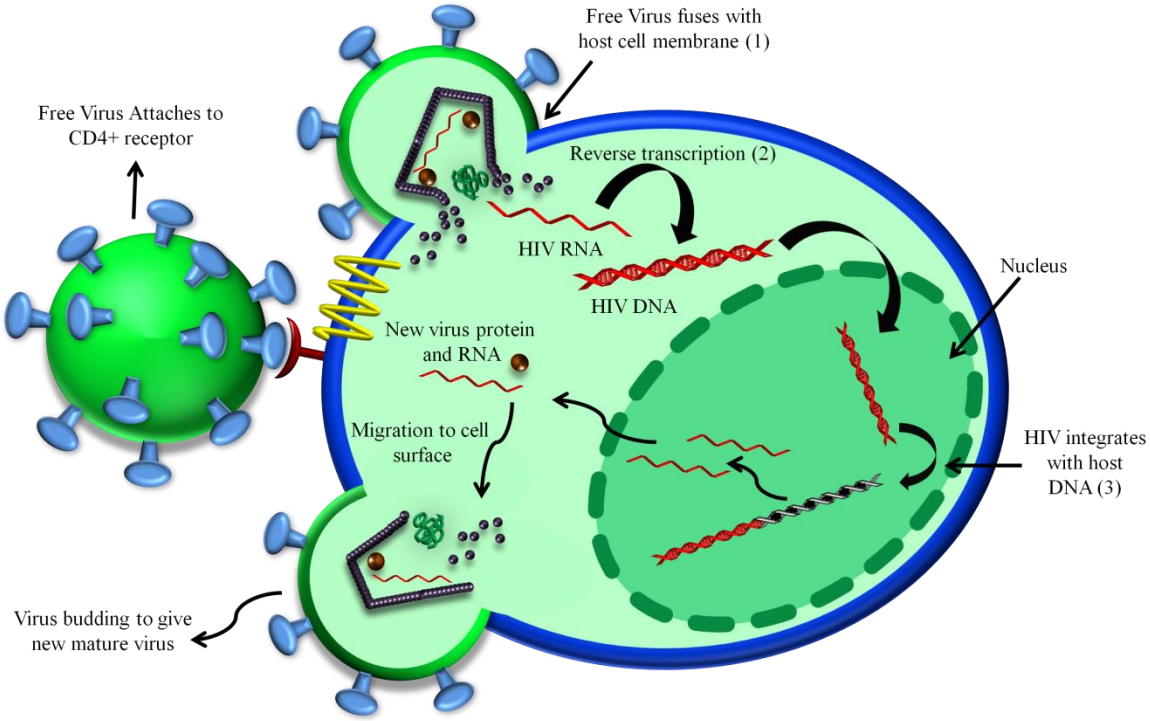


Figure 1.1: HIV replication cycle.

### 1.1.3 Treatment

Treatment for HIV/AIDS comes in the form of a class of drugs known as anti-retrovirals, which target specific stages in the replication cycle and inhibit viral replication. Currently there are 24 drugs approved by the Food and Drug Association (FDA) on the market for the treatment of the HIV-1 virus[18] (a complete list can be found in Appendix 1. There are 5 subgroups of antiretroviral drugs: nucleoside reverse transcriptase inhibitors (NRTIs), non- nucleoside- reverse transcriptase inhibitors (NNRTIs), protease inhibitors (PIs), integrase inhibitors and fusion inhibitors (FIs).

The first antiretroviral drug for the treatment of HIV-1 was an NRTI (Zidovudine) and there are currently eight within this drug class currently available. These inhibit viral reverse transcriptase by DNA chain termination, shown in Figure 1.1 (2). The

drugs have similar structures to natural deoxynucleoside without the 3'- hydroxyl group which elongates DNA and these drugs compete for binding sites.[19] Three different NNRTIs exist, which act non-competitively and bind to pockets within reverse transcriptase which changes conformations of subunits close to the active site of the polymerase enzyme and the active site becomes inactive[20] (see Figure 1.1 (2)). A PI selectively inhibits enzyme activity impeding the production of new virus by inhibition of precursor polyprotein cleavage (which produce immature infectious virus).[21, 22] There are now seven different PIs available for administration to patients. There is only one integrase inhibitor on the market currently (Raltegravir) and this catalyses integration of viral DNA into host DNA (see Figure 1.1 (3)); the diketo acids (integrase inhibitor) selectively bind to the enzyme and inhibits the transfer of viral and host DNA.[23, 24]

As the virus can readily mutate and become resistant to single drugs[25, 26] it became common to administer two or more drugs simultaneously, known as Highly Active Anti-Retroviral Therapy (HAART). Developed in 1996, it is thought that this approach has altered HIV/AIDS from being a certain death sentence, to a chronic condition and shown a huge decrease in mortality among AIDS patients.

Prior to 1996 people aged 15-24 were expected to survive for 12.5 years after infection and those aged 45-54 had an average life expectancy of 7.9 years.[27] Post 1996 a decrease in the risk and death due to AIDS has been reported and is more than likely attributed to HAART.[28, 29, 30] The correct time for initiating antiretroviral drugs is debated,[31] however, US guidelines recommend treatment when CD4+ cell count reaches below 500 per $mm^3$ or a viral load greater than 10 000 – 20 000 copies per mL.[32] Although this has been debated, and it is argued that it is more beneficial to start patients on HAART at a much earlier stage, irrespective of the CD4+ cell

count.[33] The drugs themselves exert toxicities which will be unfavourable to what are considered "healthy" patients.

### 1.1.4 Treatment Failures

There are many advantages of HAART with research suggesting suppression of viral replication for decades therefore increasing life expectancies of sufferers, provided patients comply with recommended regimens.[18] The increased viral suppression makes the attainment of resistance much more difficult as the virus must mutate in such a way to overcome the effects of a cocktail of drugs rather than just one.[34]

Despite these positives, there exist many downfalls to the current administration of antiretroviral drugs including extensive first pass metabolism where little drug reaches the blood stream. This occurs when certain drugs are dosed orally and are metabolised by the liver after absorption from the gastrointestinal tract *via* the hepatic portal vain, leading to poor bioavailability.[35] The drugs tend to have short half-lives which increased the frequency of administration and this in turn decreases patient compliance (also known as 'pill burden').[36]

Poor bioavailability is primarily linked to 'reservoir' or 'sanctuary' sites in the body; this is where the virus can reside and replicate where dissolved drugs struggle to enter.[37] Cellular sites include CD+ T lymphocytes and monocytes/macrophages where as anatomical sites include the Central Nervous System (CNS), liver, lungs, lymphatic system and genitals.[38] It is thought that alongside poor bioavailability/targeting, limited access to sanctuary sites is linked to the development of multi-drug resistance.[39]

The administration of these toxic antiretroviral drugs (in some patients) can induce undesirable side effects. PI's can cause nephrotoxicity,[40] lypodystrophy, hyperlipidaemia and insulin resistance.[41] Administration of NRT's can result in liver steatosis, myopathy, lactic acidosis,[42] and lipoatrophy[43] where as NNRTIs can cause hypersensitivity[44] and hepatotoxicity.[45]

Literature suggests that there are no significant side effects associated with Raltegravir[46] (Integrase inhibitor) and the same is true for FIs, although 96 % of patients receiving enfuvirtide experienced hypersensitivity at injection site.[47,48,49] In order to increase life expectancies, HIV sufferers must take combinations of these drugs (based on individual requirements) and unfortunately encounter some of the aforementioned side effects.

Perhaps most shocking of all is the cost of production and distribution of antiretroviral drugs; particularly to Africa which is resource limited.[50] The global budget required just to treat (research not included) HIV patients from 2009 to 2031 is predicted to be approximately US$ 397-727 billion.[51] Clearly, much more research is desperately needed in this field in developing new drug delivery vehicles for HIV/AIDS drugs.

## 1.2 Polymers for Drug Delivery

The field of polymer synthesis is ever expanding, where synthetic techniques are becoming highly sophisticated generating new and structurally complex materials which have the ability to encapsulate and deliver drugs. The necessity for this is due to the often hydrophobic nature of drugs which limits their interaction within the body and therefore limits therapeutic effect. The scope of materials from which

scientists can choose in this area is enormous and reviewing all polymers (considered and currently approved) is almost impossible. However, it is the intent here to give an overview of perhaps the most commonly reported and used polymers, strategies and drug delivery systems.

### 1.2.1 Naturally occurring polymers

As naturally occurring polymers are high in abundance and usually biodegradable they are a good choice of material for the development of drug delivery systems or other biomedical devices. These polymers fall mainly into the categories of proteins and polysaccharides which can offer good biocompatibility.[52]

To reduce the risk of infection in wounds,[53] collagen (see Figure 1.2 (A)) "sponges" have been generated for the delivery of antibiotics. Immobilisation of drugs into collagen matrices is achieved by simply soaking in antibiotic solutions,[54] however, significant research into the optimisation of drug release kinetics has been described where the density of collagen can be increased[55] or cross-linked[56] therefore decreasing the rate of drug release. Collagen can also be combined with other naturally occurring polymers such as α-hydroxy acids[57] to achieve the same effect. Also described in the literature are collagen gels[58] and collagen microparticulates[59] which can be used as drug delivery vehicles.

The polysaccharide chitosan is perhaps the most widely researched naturally occurring polymer used in therapies, with approximately 6500 references found when entering "chitosan drug delivery" into the Scifinder database. This material shows good biocompatibility and its positive charge under acidic conditions through protonation of amino groups[60] (see Figure 1.2 (B)) means it can be exploited in drug delivery vehicles by interactions with oppositely charged cells/membranes and also

DNA. Material can be encapsulated by chitosan forming colloidally stable particles by a variety of mechanisms which include chemical crosslinking and ionic crosslinking; [61] promising research is briefly outlined here in relation to chitosan based drug delivery systems. Through a spray-drying process[62] insulin loaded (65-85 %) chitosan microparticles have been synthesised for nasal delivery and were found to be superior to chitosan solutions[63]. Chitosan based systems have also been effective in the delivery of growth factors *via* immobilisation into hydrogels enhancing lesion[64] and cartilage repair[65]. Magnetic nanoparticles of chitosan have been developed for the targeted delivery of antibiotics. Both bleomcyin and neomycin were successfully encapsulated by chitosan and transported (through diffusion) across inner ear membranes with no detrimental effects to surrounding tissue.[66] Anti-inflammatory drugs can also be delivered through chitosan based systems,[67, 68] as well as antigens for parental and mucosal delivery achieved by chitosan based powders and nanoparticles.[69]

Undoubtedly huge advances have been made by utilising natural polymers for drug delivery and steps are being taken to modify the materials to suit new applications. However, due to their structural complexities synthetic modification is often difficult. For example, extremely strong and stable hydrogen bonding exists within chitosan (inter and intra molecular) from the amino and two hydroxyl groups in the hexosaminide repeating unit (see Figure 1.2 (B)) leading to difficulties in solubilising the material in organic solvents. As it is insoluble in water, reactions can be carried out in aqueous organic acids (acetic and formic acid) and some inorganic acids generating highly viscous solutions. The high viscosity coupled with the corrosiveness (requiring alkaline solutions for purification) are undesirable for the development of drug delivery systems; consequently new processing strategies

are needed in the development of new chitosan based materials.[70,71] Other naturally occurring polymers which have been used specifically as drug delivery vectors are albumin[72, 73, 74] and gelatin.[75, 76]

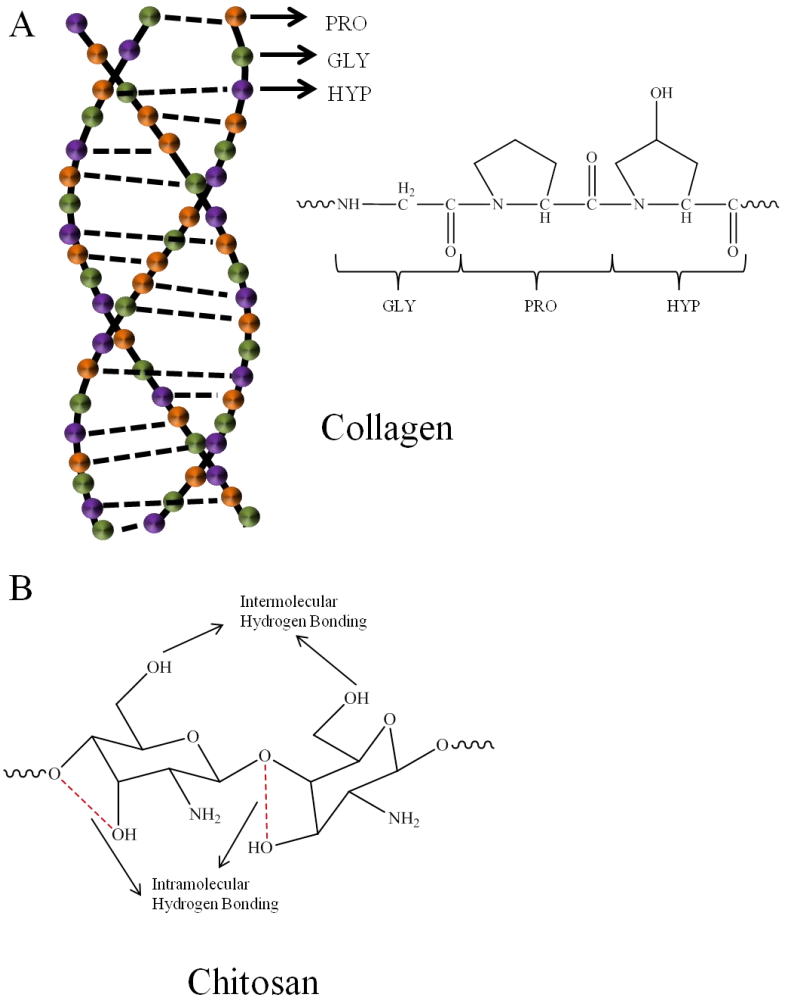


Figure 1.2: Structural examples of naturally occurring polymers. Collagen (A) and Chitosan (B).

## 1.2.2 Synthetic Polymers

The ability to control the chemical and architectural properties of synthetic polymeric materials perhaps offers considerably more options than those available through the use of naturally occurring polymers for the purpose of drug delivery. Described here are some polymers which have been synthesised for use in the field of medicine. The key to all systems which are intended for use in the human body is

biocompatibility; this may be defined as "the ability of a material to perform with an appropriate host response in a specific application".[77] This definition is vague as the number of interactions and processes between materials and biological systems is extremely vast and therefore a precise definition of biocompatibility does not exist i.e. a material may biocompatible in one application yet bioincompatible in another. However, for the purposes of this thesis the criteria of a material to offer good biocompatibility will be the acceptance to living tissue and/or blood. The role polymers play in terms of haemocompatibility, immunocompatibility and also carcinogenicity has been researched.[78, 79]

### 1.2.3 Biodegradable and non-biodegradable polymers

Polymers used in bio-applications are not limited to those which are biodegradable; as non-biodegradable materials may be biocompatible and excreted by renal processes.[80] Materials which are approximately 4 nm to 14 nm in diameter can permeate epithelial cell walls within the glomerulus and are excreted in urine.[81] This size roughly equates to a molecular weight range of between 30000 to 150000 g $mol^{-1}$ (however, this is highly dependable on the structure and chemistry of the material).[82] Those which exceed this threshold may circulate in the body for extended periods of time.[80] The liver and spleen can also eliminate non degradable polymer whose size exceeds 200 nm *via* opsonisation; material is engulfed by phagocytes in the blood stream, yet only hydrophobic and neutral polymers tend to bind to the opsonin proteins.[83]

Polymers which do not contain C-C backbones e.g. polyesters are degraded through hydrolysis of the chains' backbone. For materials which are semi-crystalline this hydrolysis occurs *via* a two step process; first the long peripheral polymer chains (which are amorphous) are converted to shorter (and water soluble) segments. This

molecular weight reduction does not immediately impact the mechanical strength of the crystalline core; however, as water begins to permeate, fragmentation occurs. Enzymes then metabolise these fragments leading to a dramatic decrease in molecular weight.[84] This process is much faster at the periphery of the material due to the large surface area and low molecular weight products can be completely removed into the surrounding fluid. Bulk erosion of the material ensues when the rate of water penetration exceeds the rate of conversion to water soluble material.[85] This polymer erosion is inevitable (provided that the structure contains hydrolysable bonds), however, fast rates are often undesirable as this leads to a decrease in the drug delivery devices' mechanical stability alongside risks of toxicity associated with large quantities of small fragments produced within short timescales.[86]

Polymers containing ester groups within the backbone (poly(lactic acid) (PLA), poly(glycolic acid) (PGA) and poly(lactic acid-*co*-glycolic acid (PLGA)) (see Figure 1.3) will degrade *via* hydrolysis, however, their metabolism may result in increased acidity leading to tissue irritation.[87]

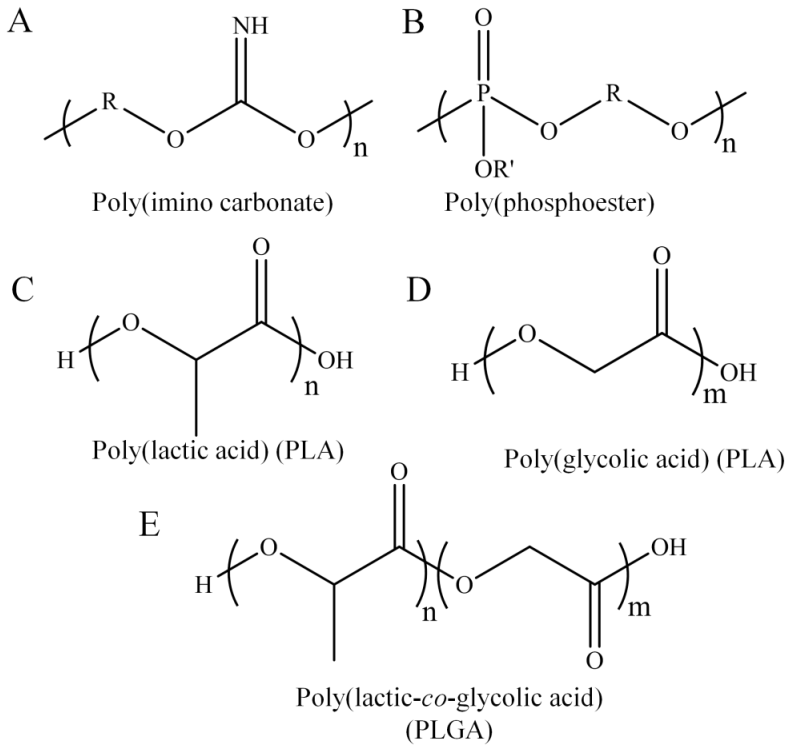


Figure 1.3: Examples of polymers used in drug delivery systems. Poly(imino carbonate) (A), poly(phosphoester) (B), poly(lactic acid) (C), poly(glycolic acid) (C) and poly(lactic-*co*-glycolic acid) (D).

For materials which encapsulate proteins, this increased acidity can be detrimental to the stability of the protein.[88] Degradation of polyanhydrides and polyesters is achieved by the hydrolytic cleavage of chain backbones yet the rate of degradation and drug release can be affected by molecular weight, polydispersity, monomer choice and their relative ratios (for copolymers).[89, 90] Polypeptides can successfully encapsulate drugs yet their capabilities of release are limited as certain enzymes in the body are necessary for their bio-degradation. To overcome this 'pseudo' poly(amino acids) can be synthesised (i.e. poly(imino carbonates) (see Figure 1.3 (A)), which do not depend on these enzymes.[87] Atoms of phosphorous (bonded to either carbon or oxygen) in poly(phosphoesters) (see Figure 1.3 (B)) means that

chemical modification of side chains is relatively straightforward, significantly affecting the rate of bio-degradation; important in terms of drug release.[91]

In conclusion, mechanisms of bio-degradation vary with polymer composition (i.e. functional groups) alongside architecture, administration route, molecular weight distribution, morphology, pH, structure of overall delivery vehicle and its concentration. This means that determination of toxicity/degradation/clearance/accumulation of polymeric systems is extremely complicated yet of high importance in order to successfully manufacture a polymeric drug delivery system.

### 1.2.4 Monomethyl PEG

This relatively simple molecule is usually synthesised *via* living anionic polymerisation where nucleophilic attack of the methoxide ion on an epoxide ring initiates the reaction,[92,93] (see Scheme 1.1) giving molecular weight distributions ranging from 1.01 ($M_w$ = 3000-5000 g mol$^{-1}$) to 1.2 ($M_w$ = > 20000 g mol$^{-1}$).[94] However, due to the nature of living anionic polymerisation dihydroxy poly(ethylene oxide) is also formed (typically between 1 – 10 % of overall product depending on the molecular weight) due to water/oxygen and other impurities present in the reaction which act as initiators and/ or chain transfer agents in the polymerisation.[95]

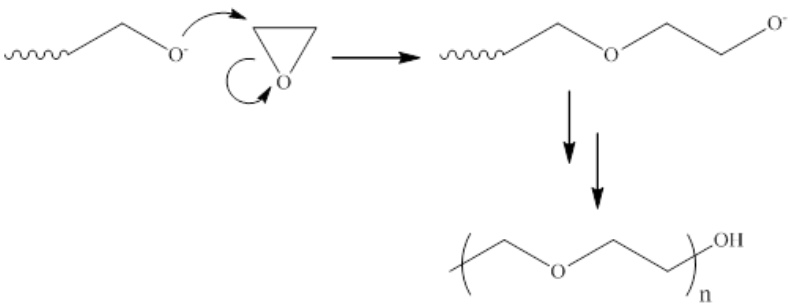


Scheme 1.1: Synthesis of monomethyl PEG by nucleophilic attack of an epoxide ring.

Below 1000 g $mol^{-1}$ PEG is a viscous colourless liquid, however, at higher molecular weights it exists as a white waxy solid.[96, 97] PEG is soluble in water, toluene, methylene chloride and many organic solvents yet is insoluble in ethyl ether, hexane and ethylene glycol (despite its similar structure and composition).[98]

PEG is non-toxic and has the ability to extend the half life of active materials when chemically conjugated to a drug (mainly due to the increased overall molecular weight reducing renal clearance).[99, 100] PEG has been shown to interact with cell membranes by associating with phospholipid head groups of and once fused its uptake is mainly through endocytosis.[101]

Drugs can be bonded to PEG (known as prodrugs) through the activation of the hydroxy (or dihydroxy) groups. When bonded, PEG increases the hydrophilicity of drugs which in turn reduces the toxicity of the drug; an example of this is the prodrug PEG-palitaxel (anti cancer drug) which when administered (5.25 μ mol dose) showed no acute toxicity compared to taxol® (comprising cremophor® and palitaxel) which is highly toxic.[99, 102] The huge volume of research dedicated to PEG and its derivatives make it the polymer of choice for drug delivery systems; however, for the purpose of this thesis the main focus is the co-polymerisation of PEG and the (non-bonded) encapsulation of drugs within varied structures.

## 1.3 Polymeric Drug Delivery Systems

The majority of new drug delivery systems have sizes within the nanometre (nm) scale. The advantages of these extremely small dimensions are an increased surface to volume ratio which is thought to improve pharmacokinetics and biodistribution of active substances leading to increased accumulation at preferential sites in the body.[103] As research has suggested that approximately 40 % of active substances (i.e. drugs) are poorly water soluble,[104, 105] nanometre sized vehicles are extremely

desirable. Estimates suggest that by 2015 approximately US$1 trillion will be made through sales of nanotechnologies[106] of which approximately US$53 billion is specifically related to medical products.[107]

Specific polymers have been discussed in their relation to drug delivery systems, however, the majority of the systems have one common characteristic which is amphiphilicity. In an aqueous solution a hydrophobic drug will reside/solubilise in hydrophobic domains and is thus encapsulated by the hydrophilic corona which is hydrated. This is a very simplistic rationale; the mechanisms of vector generation can vary widely as well as overall vector structure/shape. Here, examples of polymeric drug delivery vehicles are given.

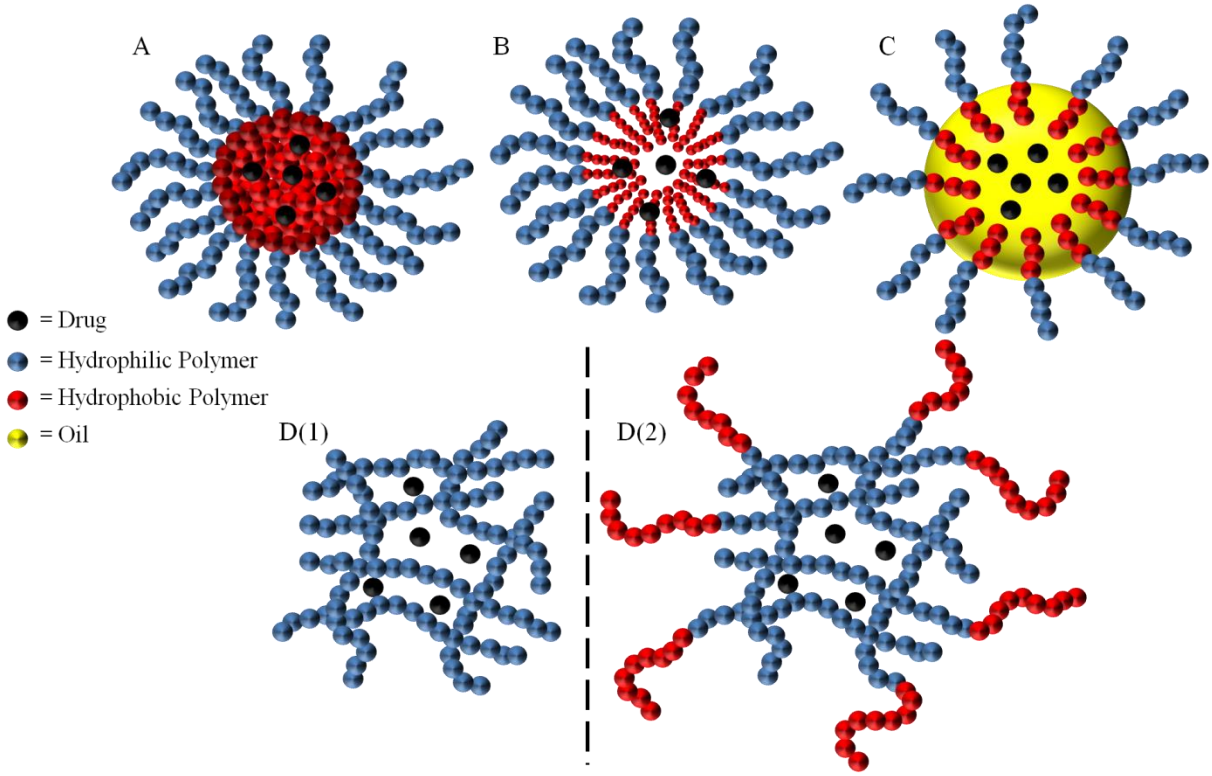


Figure 1.4: Representation of common polymeric drug nanocarriers in aqueous medium (not to scale). A) Nanoparticle B) Micelle C) Nanoemulsion D(1) Hydrogel D(2) Sol-gel.

### 1.3.1 Micelles

Formed from amphiphilic block copolymers which self-assemble (see Figure 1.5), micelles have core shell architectures in water where hydrophobic drug may resides in the hydrophobic domain, shown in Figure 1.4 (B).

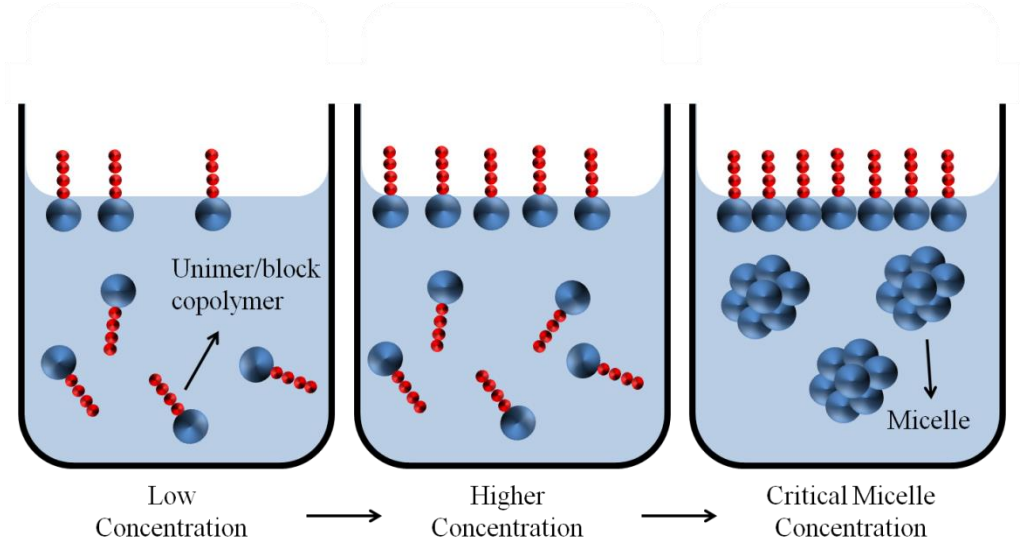


Figure 1.5: Micelle formation.

The driving force of micellisation is interfacial tension; at the Critical Micelle Concentration (CMC) the interfacial tension is minimised by the formation of micelles, below which polymers exist as single entities` known as unimers. Once de-solvated (e.g. through dialysis) van der waals forces exist between hydrophobic segments and form domains which are stabilised by a hydrated corona comprised of the hydrophilic block segments.[108, 109]

In addition to linear block copolymers other polymer architectures can form micelles such as the novel scorpion like amphiphilic macromolecules (shown in Figure 1.6) have been synthesised which aggregate in water and form micelles and star-like macromolecules which form unimolecular micelles, both of which can be used for drug encapsulation.[110]

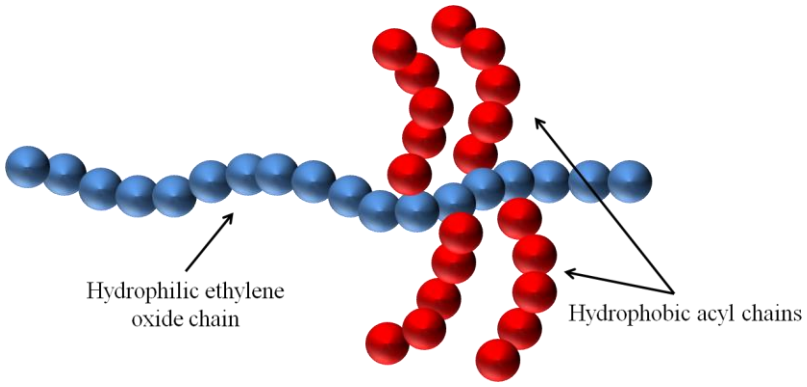


Figure 1.6: Representation of a novel scorpion like macromolecule.

As micelles are formed *via* self-assembly, physiological, thermal and chemical changes dramatically affect their stability; to overcome this it is common to crosslink a selected domain of the micelle. Wooley and co-workers were the first to report shell crosslinked (SCL) micelles in 1996[111] involving UV radiation although more recently 'click' chemistry has been employed by the same group to achieve crosslinked micelle coronas, however, the final concentrations of micelles is often low (approximately 0.2 mg $mL^{-1}$) and their preparation involves multiple purification steps such as dialysis.[112] The core domain of polymeric micelles can also be crosslinked[113, 114, 115] and is usually achieved through the addition of a free radical initiator and have been shown to release drug *via* a pH trigger.[116]

### 1.3.2 Nanoemulsions (oil in water)

Emulsions and nanoemulsions are described as dispersions of one liquid phase in another immiscible liquid phase and are usually formed under mechanical shearing.[117, 118] Amphiphilic copolymers can decrease the interfacial tension of oil droplets by partitioning themselves between the two liquids; however, the solubility of both polymer segments can vary considerably.[119] Similar to micelles, hydrophobic drugs will reside within the oil phase (see Figure 1.4 (C)) due to

hydrophobic interactions and are usually dissolved within the oil prior to nanoemulsion formation.[120]

### 1.3.3 Hydrogels

Hydrogels are crosslinked polymers which are soluble in water and maintain a 3D structure.[121] A true hydrogel is dissimilar to other drug delivery devices as they are comprised of water soluble polymers only, shown in Figure 1.4 (D(1)). Crosslinking in hydrogels can be achieved by hydrogen bonding,[122] covalent crosslinking,[123] and physical cross-linking,[124] between either a polymer or a small molecule[125] or two oppositely charged polymers[126] where crosslinking can be triggered by pH changes. Their porosity allows the loading of drugs into matrices and release is diffusion controlled. Due to their low tensile strength, it has been shown that drug loading is limited.[127]

Sol-gels are partially crosslinked amphiphilic materials whose hydrophobic cores become crosslinked at elevated temperatures. Usually drugs are loaded into hydrogels and sol-gels post formation; their solutions are freeze dried and the material is re-dispersed in a drug containing solution followed by filtration.[128] A representation of a sol-gel is shown in Figure 1.4 (D(1)).

### 1.3.4 Nanoparticles

It may be possible to consider any polymer containing system whose size is within the nanometre size range as a nanoparticle, including those mentioned above; these systems also have the potential to load material (see Figure 1.4 (A)). For the purposes of this thesis polymeric nanoparticles will be defined as systems prepared by the methods described below; it should be noted that other methods of preparation exist that are not described here.

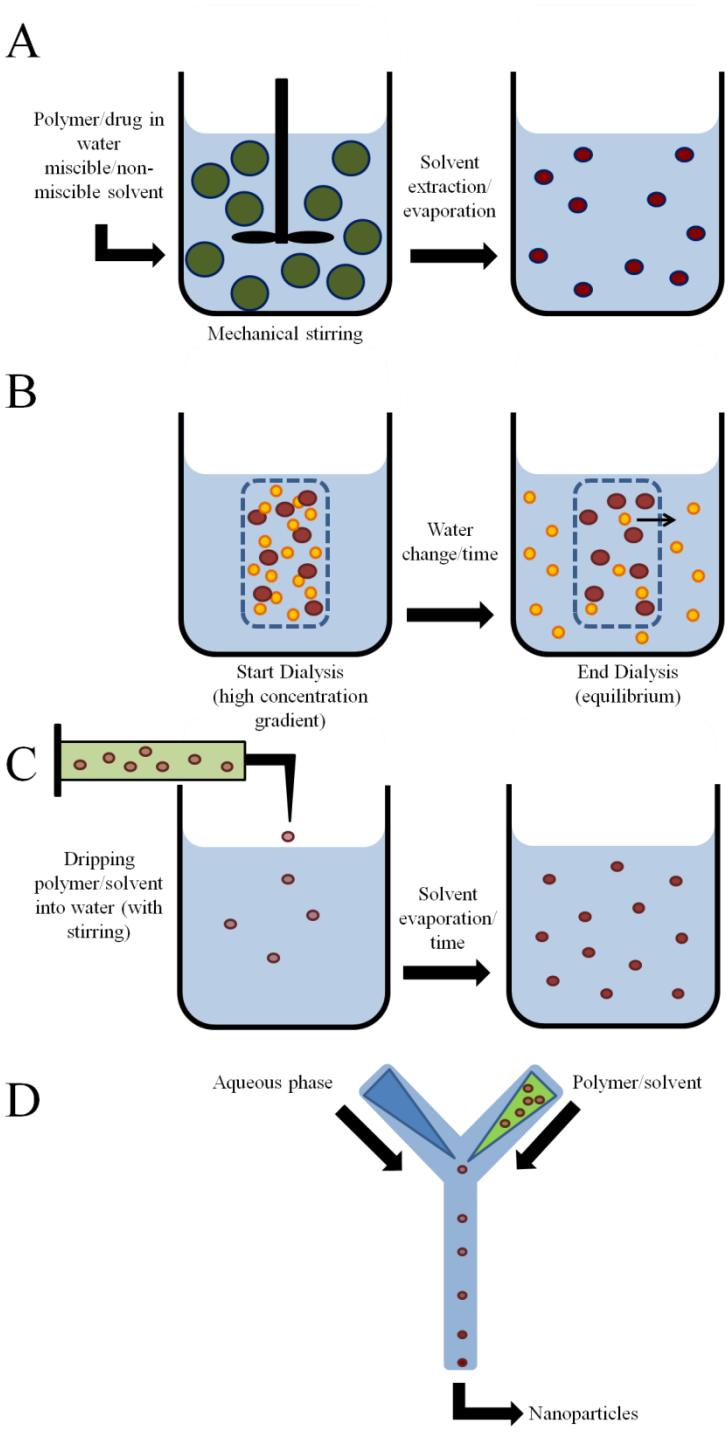


Figure 1.7: Nanoparticle preparation methods. A) Emulsification-solvent evaporation. B) Dialysis. C) Nanoprecipitation. D) Microfluidics.

#### 1.3.4.1 Synthesis by Emulsification-Solvent Evaporation

This was the first method employed to prepare nanoparticles comprised of pre-formed polymers.[129] In short, emulsions from polymer solutions and volatile solvents such as chloroform are prepared through mechanical stirring after which solvent is allowed to diffuse through the continuous phase,[130] however, coalescence is often observed and surfactants are utilized in the process; a representation of this process is shown in Figure 1.7 (A). Amphiphilic copolymers such as PEG-PLA[131] have been used to generate nanoparticles using this method. This is a two step route (emulsion preparation and solvent extraction) to nanoparticle production and may involve the use of toxic solvents and therefore it is not optimum for many applications.

#### 1.3.4.2 Synthesis by Emulsification Reverse Salting out

This method is similar to that described above, however, the solvent chosen to dissolve the polymer must be miscible with water. Acetone is often favoured for this purpose.[132] Concentrated aqueous salt solutions are employed to form the emulsion after which large excesses of water are added. This induces precipitation of the polymer within emulsion droplets. It is possible to encapsulate lipophilic material within nanoparticles by addition to the polymer solution prior to emulsification.[130] However, this method involves extensive purification to completely eliminate both the volatile solvent and the salting-out agent.

#### 1.3.4.3 Synthesis by Nanoprecipitation

This method essentially consists of three components (polymer, solvent, non-solvent) precipitation and offers an experimentally facile method of preparing polymeric nanoparticles. Developed by Fessi and co-workers,[133] nanoparticles form

due to an almost instantaneous solvent switch (both solvent and non-solvent must be miscible) where the polymer rapidly de-solvates and aggregates to form colloidally stable entities usually within the nanometre size range with low polydispersities. This phenomenon can be exploited experimentally where different experimental protocols can be developed to suit certain applications; some of which are outlined here.

Through the simple addition of a solution of polymer in a water miscible solvent to water and subsequent evaporation of the organic solvent, it is possible to obtain colloidally stable nanoparticles; a representation of this process is shown in Figure 1.7 (C). This method was first described by Fessi[133] and has been used by Schubert and co-workers[134] who employed a slow dripping technique to prepare stable nanoparticles and it is noted that parameters such as polymer concentration has a direct effect on nanoparticle size.[135]

Essentially any organic solvent which is volatile and will solubilise a chosen copolymer and/ or drug could potentially be used in this technique as long as it is miscible with water, however, the time consuming dripping approach often employed and the extensive purification (dialysis and filtration) are drawbacks to this method.

The nanoprecipitation approach has been exploited by BIND Therapeutics; predominantly manufacturing drug loaded nanoparticles using PEG-PLGA block copolymers; synthesised by the simple conjugation of COOH-PEG-$NH_2$ and PLGA-COOH. By combining these block copolymers with drug in a suitable organic solvent, stable drug loaded nanoparticles can be prepared. It should be noted that

these nanoprecipitates are in clinical trials for cancer therapies, demonstrating the feasibility of industrial scale production of drug loaded nanoparticles.[136, 137]

#### 1.3.4.4 Synthesis by Dialysis

This simple technique involves solubilising a copolymer and/ or drug in a selected solvent which is transferred into a dialysis membrane and into a large volume of water which is changed regularly; a representation of this process is shown in Figure 1.7 (B). It is thought that this method allows for slow solvent exchange as it often takes > 24 hours for complete solvent removal, however, this may be debated. Nevertheless many research groups have reported stable nanoparticle suspensions prepared by this method[138] and is useful for micelle formation if a good solvent can be found for both blocks of an amphiphilic copolymer.

#### 1.3.4.5 Synthesis using Microfluidics

It is possible to control the mixing of solutions of polymers in organic solvents with water by using microfluidic devices to achieve controlled polymer precipitation; a representation of this process is shown in Figure 1.7 (D). The hydrodynamic flow is tunable allowing a degree of control within the system which may be advantageous as scale up can be easily achieved. Drugs may be dissolved in the initial polymer/solvent mixture and may therefore become encapsulated in the final nanoparticle solution.[139]

## 1.4 Polymer Architecture-Towards Drug Delivery

Various polymerisation methods are reviewed here in order to highlight their advantages and limitations with respect to the generation of subsequent polymeric drug delivery systems. Literature shows that polymers with complicated

architectures can be synthesised such as star-branched (Figure 1.8 (A)), star block[140] (Figure 1.8 (B) and pentablock copolymers[141] (Figure 1.8 (C). As a general rule, the more complicated the architecture becomes the more synthetic/purification steps are necessary; therefore the likelihood of these polymers being used on an industrial scale will be diminished.

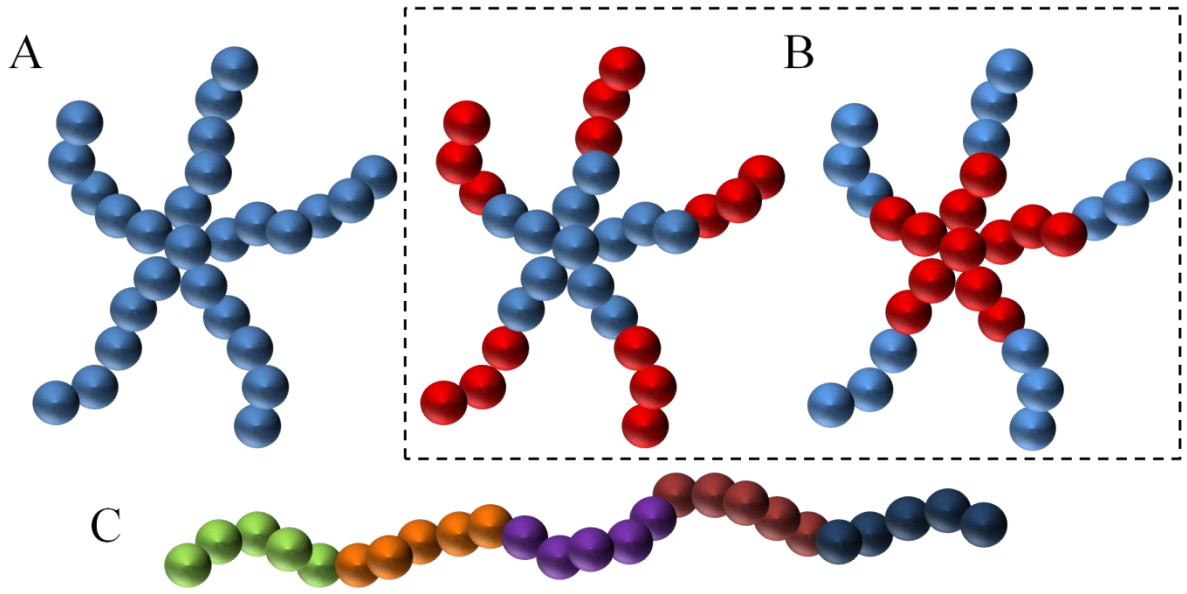


Figure 1.8: Examples of various polymer architectures. A) Star branched polymer. B) Star block copolymer. C) Pentablock copolymer.

### 1.4.1 Hyperbranched polymers and Dendrimers

Dendrimers are highly branched materials synthesised using either a convergent[142] (Scheme 1.2 (B) (1)) or divergent[143] approach (Scheme 1.2 (B) (1)) where complexity increases with each 'generation' or 'layer' of functional groups. These ordered structures can produce near monodisperse materials with a large number of functional end groups (dependant on generation).[144] Unfortunately dendrimer synthesis involves a multitude of reaction and purification steps[145] and yields are often low and reactions are often incomplete.[146] An excellent review on dendrimers

and dendronised materials explores new strategies to limit time consuming reaction steps.[147]

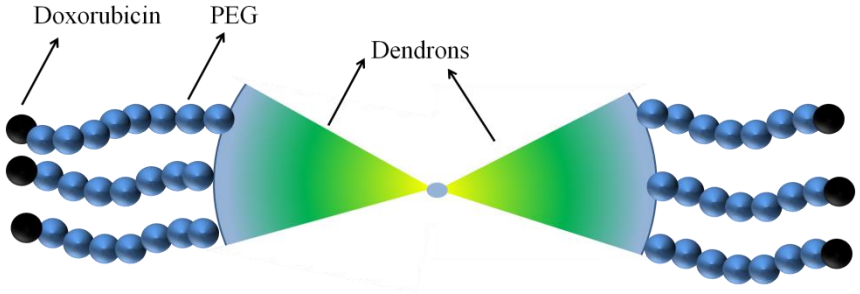


Figure 1.9: Representation of doxorubicin-functionalised dendrimers.

Fréchet and co-workers have reported the synthesis of novel polyester dendritic 'bow-tie' molecules for drug delivery purposes. The dendritic molecules (of various generations) can have various peripheral functional groups and can be coupled to PEG (of various chain lengths) to generate a catalogue of novel architectures. Coupling doxorubicin to these macromolecules has shown an increase in circulation time (compared to parent drug) and also significant antitumor activity; a representation of the structure of doxorubicin-functionalised dendrimers[148, 149] is shown in Figure 1.9.

Hyperbranched polymers can be synthesised by the Flory $AB_x$ approach (shown in Scheme 1.2 (A)) where $AB_2$ monomers are very common[150] but monomers such as $AB_3$ and even $AB_6$ have been reported using a one-pot step-growth polymerisation. The criteria for a successful step growth polymerisation are that A must react only with B without side reactions and $B_x$ must have equal reactivity.[152] Besides polyesters[153] a wide variety of polymers can be synthesised using this polycondensation approach.[152]

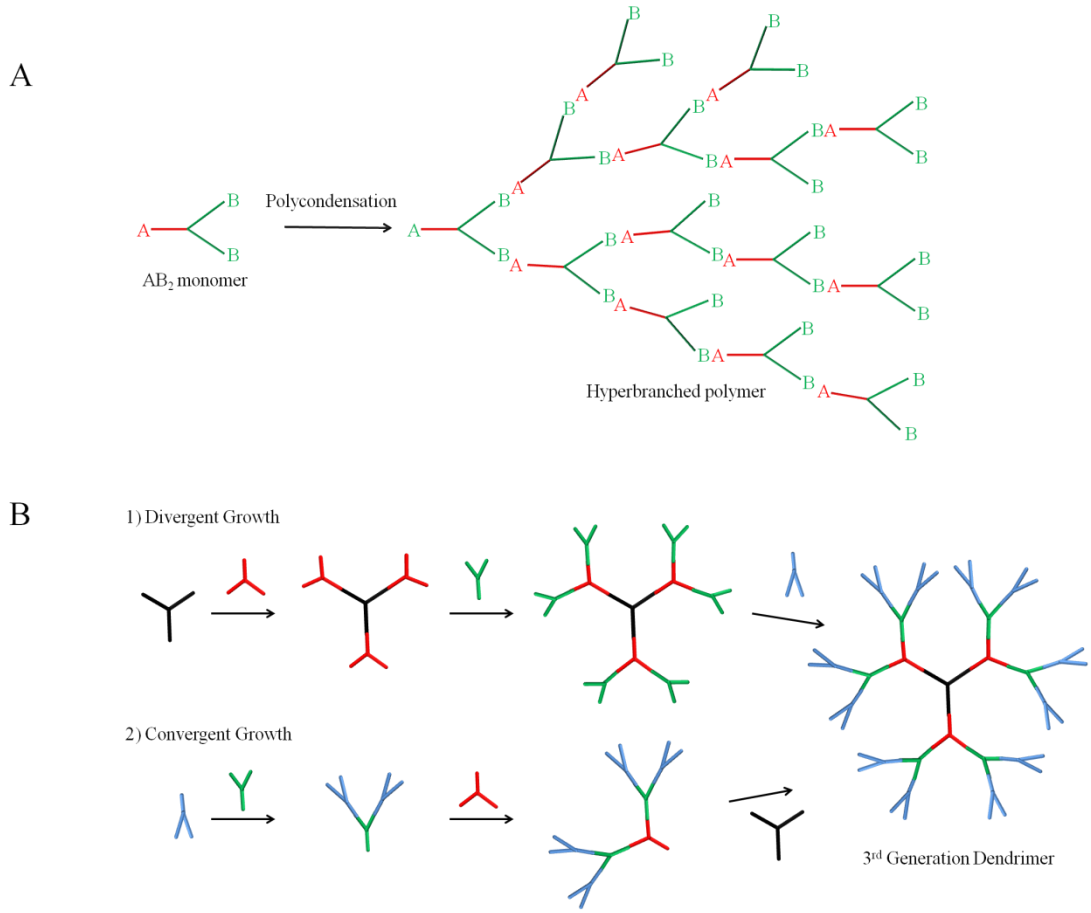


Scheme 1.2: Representation of hyperbranched polymer and dendrimers synthesis. A) Polycondensation of an $AB_2$ monomer to give a hyperbranched polymer B) 1) Divergent growth and 2) convergent growth giving a third generation dendrimer.

Recently more complicated monomer combinations (such as $A_2 + B_y$) can be used to generate complicated and multifunctional polymers.[154] Using this approach, gelation can occur and is highly dependent on functionality ratio, temperature, reaction time etc.[155] For these reasons it can be experimentally difficult to isolate hyperbranched polymers without fractionation, which can lead to sample loss and affecting polymer distribution.[152] Hyperbranched polymers synthesised through polycondensation have also been investigated as drug delivery devices.[156, 157]

## 1.5 Polymerisation Techniques

### 1.5.1 Free Radical Polymerisation

It has been reported that conventional free radical polymerisation is the most widely used polymerisation technique using unsaturated vinyl monomers.[158] Briefly the reaction consists of three distinct steps:

1) Initiation involves the homolytic scission of a single bond achieved either thermally or photolytically. The reactive (and short-lived) radicals are capable of attacking monomer π bonds generating new radical centres. The most common initiators include peroxides,[159] azo[160] and photolabile compounds,[161] yet monomers such as styrene and some acrylates can be thermally induced.[162] Propagation is the addition of monomer units to active radical centres until termination occurs and is thought to be chain length independent. Termination is an irreversible process terminating polymer chain growth. This can occur either by combination of active chains or disproportionation by hydrogen abstraction and is also chain length dependant where diffusion coefficients are considered.[163] These steps are shown in Scheme 1.3.

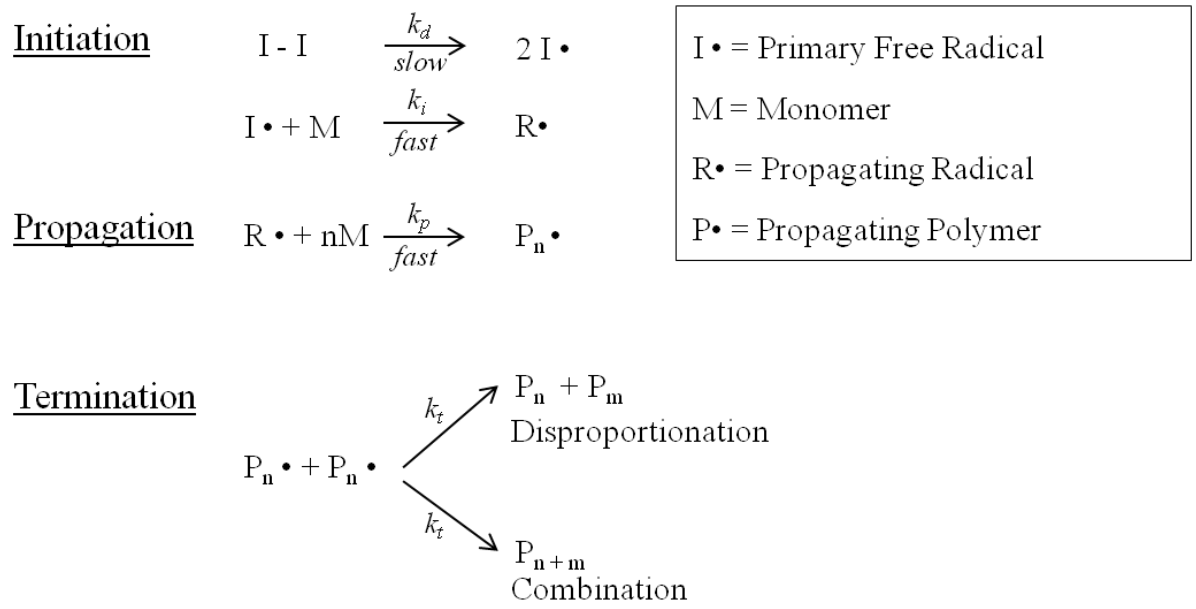


Scheme 1.3: Representation of individual steps of conventional free radical polymerisation.

1.5.1.1 General aspects of Free Radical Polymerisation

Free radical polymerisation is tolerable to a wide range of monomers, i.e. almost any monomer containing a vinyl group has the potential to polymerise. It can also be carried out in bulk and many organic solvents, only limited by potential transfer reactions. As shown in Scheme 1.3, propagation is extremely fast and therefore high molecular weight polymer chains are achieved relatively quickly and therefore at longer reaction times conversion will undoubtedly increase yet $M_n$ is little affected (see Figure 1.10).

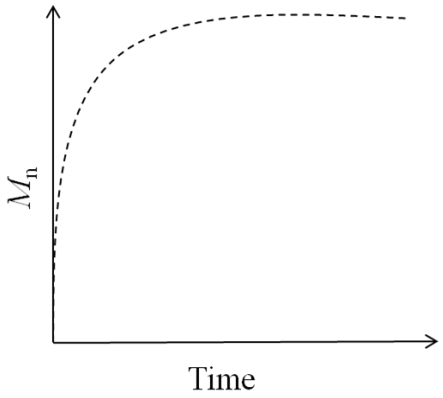


Figure 1.10: Evolution of $M_n$ with time for conventional free radical polymerisation.

Despite being experimentally facile, conventional free radical polymerisation has major limitations. Perhaps under-reported in the literature, the initiators used in these reactions can often be explosive and are therefore hazardous;[164] a scheme of the decomposition of the initiator azobisisobutyronitrile (AIBN) is shown in Scheme 1.4. Synonymous with conventional free radical polymerisation is its lack of direct control of specific chain lengths and the formation of monodisperse materials. This is due to initiation and termination occurrence throughout the reaction. Polydispersities are generally > 2 if polymerisations are left to reach high conversion, however, this may be reduced if reactions are terminated at low conversion.[161]

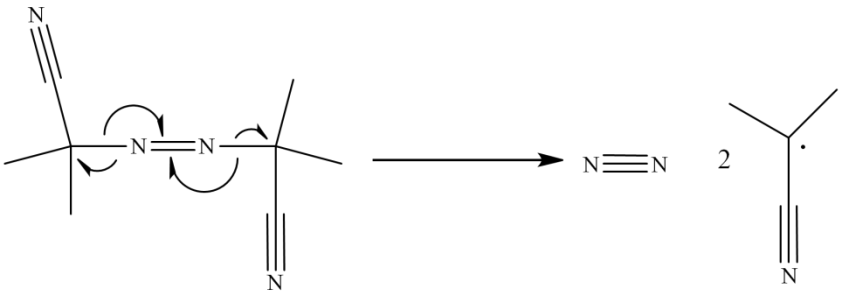


Scheme 1.4: Decomposition of AIBN producing radicals.

### 1.5.1.2 Achieving Control in Free Radical Polymerisation

The addition of Chain Transfer Agents (CTAs) (e.g. carbon tetrabromide and thiols with labile hydrogen atoms) is one way to achieve some control in these reactions. Hydrogen abstraction of a CTA results in a terminated polymer chain, leaving a CTA radical capable of propagation with unreacted monomer, resulting in lower molecular weight polymers; reported as early as 1943.[165] Carefully chosen, a CTA can also be used to gain chain-end functionality yet it is almost impossible to ensure every polymer chain contains a CTA as many chains will be initiated by other species. It has been reported that mostly CTA capped polymer chains could be prepared if the initiator and the CTA contain identical functional groups, however, this only highlights the limited choice of materials which can be used.[166]

It is possible to obtain copolymers using conventional free radical polymerisation, however, the mode of incorporation is highly dependent on steric hindrance and reactivity ratios of each monomer. Theoretically if monomers are carefully chosen gradient copolymers could be synthesised yet block copolymers could never form by this method. The use of macroazoinitiators consisting of polymeric or oligomeric units with one or more azo group is one way of forming block copolymers using conventional free radical polymerisation,[167] yet this relies on the macroazoinitiators initiating all chains when it is known that monomers can often polymerise thermally.

### 1.5.1.3 Branching in Free Radical Polymerisation

Sherrington and co-workers introduced a new simple route to manipulate free radical polymerisation to achieve complex branched architectures using the "Strathclyde" approach.[168, 169] In short they proposed that soluble branched polymers of any vinyl monomer (such as methyl methacrylate (MMA)) could be prepared by inclusion of a

bi-functional vinyl monomer (such as but-2-ene-1,4-diacrylate (BDA)) and a CTA (1-dodecanethiol (DDT)) depicted in Scheme 1.5.

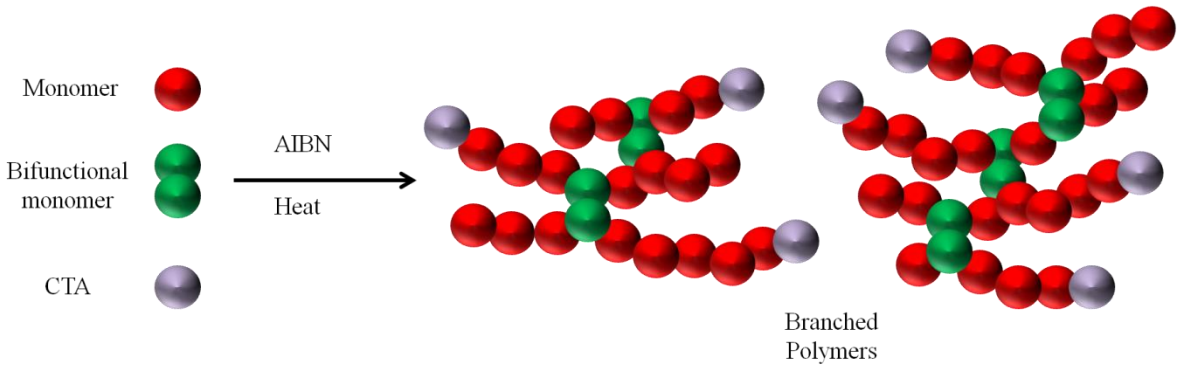


Scheme 1.5: Strathclyde route to branched polymers using a bifunctional initiator and CTA.

These reactions were generally carried out in toluene and had relatively short reaction times (approximately 5 hours) after which polymers were precipitated into *n*-hexane. It was reported that the molecular weight of these polymers could be controlled by variation of monomer: CTA: bifunctional monomer feed ratio and molecular weights (characterised by dual detection Gel Permeation Chromatography (GPC)) obtained were approximately 150000 g $mol^{-1}$. However, using ethylene glycol diacrylate (EGDA) as the bifunctional monomer with a molar feed ratio of MMA:EGDA:DDT 100:15:6 a soluble branched polymer was obtained with a molecular weight of 3774000 g $mol^{-1}$.[170] This process could in principal be applied to all vinyl monomers and branchers and has scope for developing different branched architectures such as core cross-linked star clusters.

Little research has been reported with regard to nanometre structures comprised of polymers synthesised by this method. Weaver *et al*. described pH-responsive nanoparticles (16 nm to 46 nm) of 2-(diethylamino)ethyl methacrylate (DEA) and

poly(ethyleneglycol) methacrylate (PEGMA) ($M_n$ = 1 100 g mol$^{-1}$) with an ethylene glycol dimethacrylate (EGDMA) brancher which are capable of encapsulating fluorescent material.[171]

In short summary, despite this facile one-pot approach to generating branched polymers, absolute control of primary chain length cannot be achieved using this free radical polymerisation approach.

### 1.5.2 Anionic Polymerisation

Anionic polymerisation is a method which was first reported by Szwarc[172] and the first example of a 'living' polymerisation. Under the correct conditions there exist a constant number of propagating chains with anion active functionalities present throughout the reaction demonstrated by linear plots of i) $M_n$ *vs.* conversion; and ii) ln([$M_0$/[M]) *vs.* time. The molecular weight distribution also remains extremely narrow throughout the polymerisation. These polymerisations can also self-block (i.e. introducing a second monomer feed) and have tuneable chain lengths controlled by the monomer to initiator ratio and polymerisation will continue until all monomer is consumed. In order to be an ideal 'living' system, termination does not occur, however, in practice this is extremely difficult to realise as the active chain ends can abstract protons from solvent and therefore it is necessary to use aprotic solvents which are extensively deoxygenated and are anhydrous. Furthermore vessels must be dry and the reaction atmosphere must also be completely inert; these stringent conditions make anionic polymerisation an unfavourable synthetic method. The reactions are usually initiated by organometallics reagents which have a carbanion capable of propagating chain ends; a simple reaction is shown in Scheme 1.6.

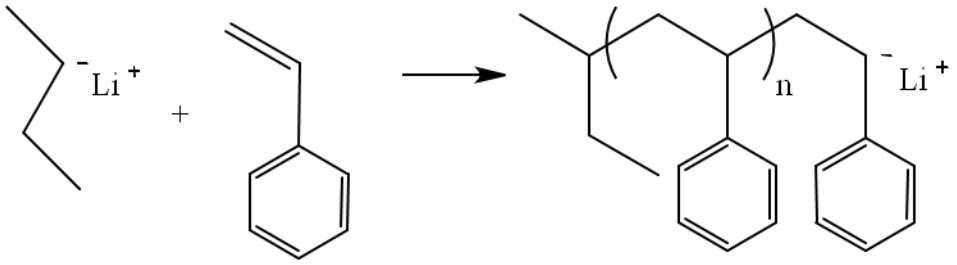


Scheme 1.6: Anionic polymerisation of styrene using *sec*-Butyl Lithium as the initiator.

As well as benzene rings other functional groups can be incorporated into polymer chains such as carboxyls, hydroxyls and halogens. These groups can be placed at the beginning, middle or the end of (typically polystyrene) chains. Carboxylic acid groups can be introduced through carboxylation of the carbanionic living group and hydroxyl chain ends can be prepared by a simple quenching reaction in methanol. Halogens can be introduced by the reaction of dihaloalkanes to the polystyryl ions yielding haloalkyl terminated polymers, however, this reaction is not quantitative and coupling of polystyrene chains also occurs.[173]

### 1.5.2.1 Branching in Anionic Polymerisation

A dendritic style of branching can be achieved using anionic polymerisation and a convergent process through the addition of 4-(chlorodimethylsilyl) styrene (CDMSS), which contains a polymerisable vinyl group in addition to a dimethyl silyl group, capeable of an $S_N2$ reaction generating star shaped polymers[174] (Figure 1.11 (A)) or through a coupling reaction which also yields star branched polymers[175] (Figure 1.11 (B)). Star polymers of polystyrene can also be prepared by a divinyl benzene (DVB) coupling reaction (shown in Figure 1.11 (C)), where nanometre sized polymers with up to 41 arms has been synthesised. The area of branched polymers synthesised *via* anionic methods is relatively small despite the near ideal

nature of this polymerisation method, mostly due to the above mentioned experimental criteria and the limited number of suitable monomers.

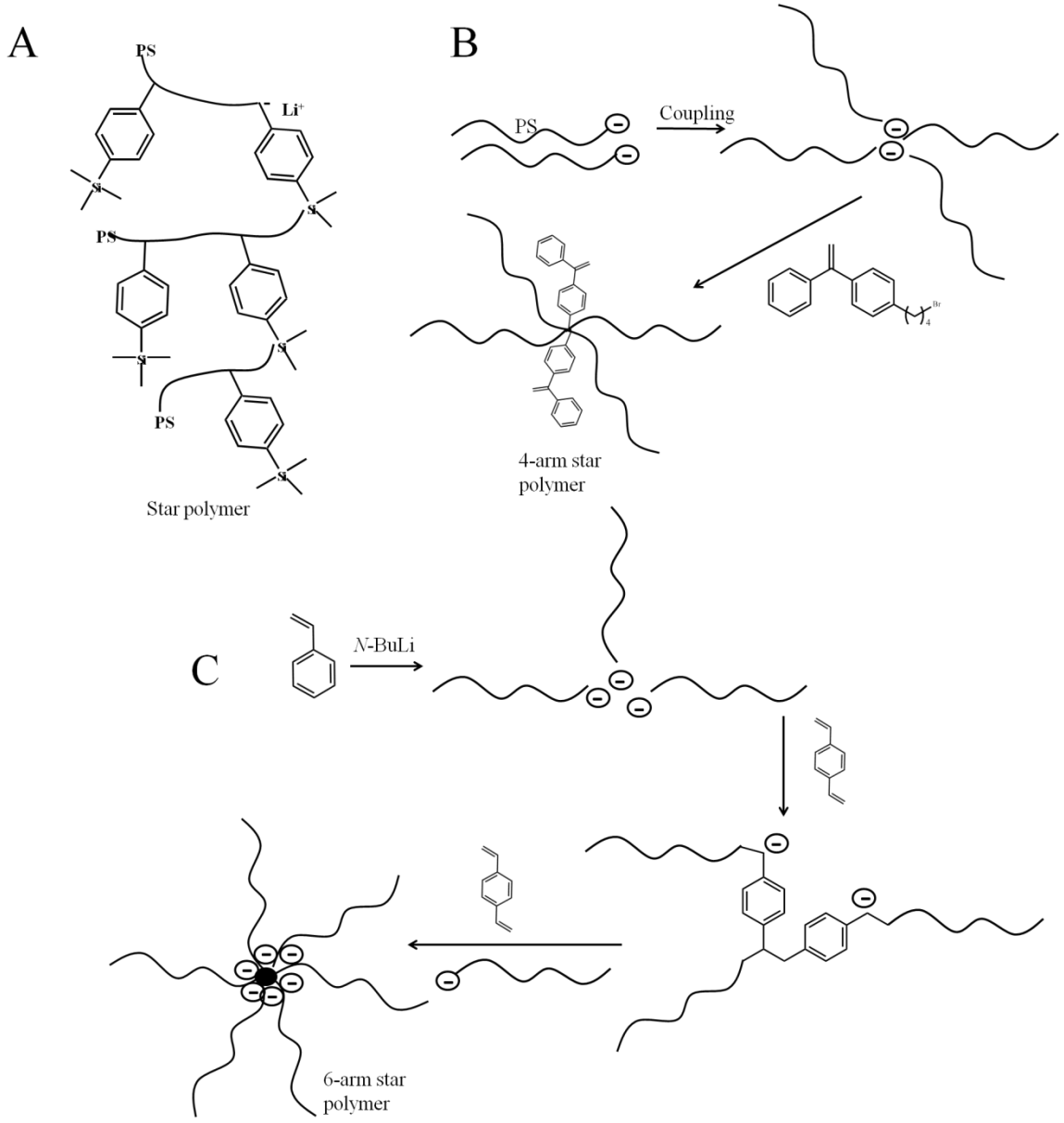


Figure 1.11: Methods of branching using anionic polymerisation. A) Using anionic and convergent synthesis. B) Coupling reaction. C) Coupling with divinyl benzene (DVB).

It has been shown that anionic polymerisation can be used to generate nano systems which can load drugs. These ABC miktoarm star terpolymers form multicomponent micelles in solution. [176, 177] (shown in Figure 1.12).

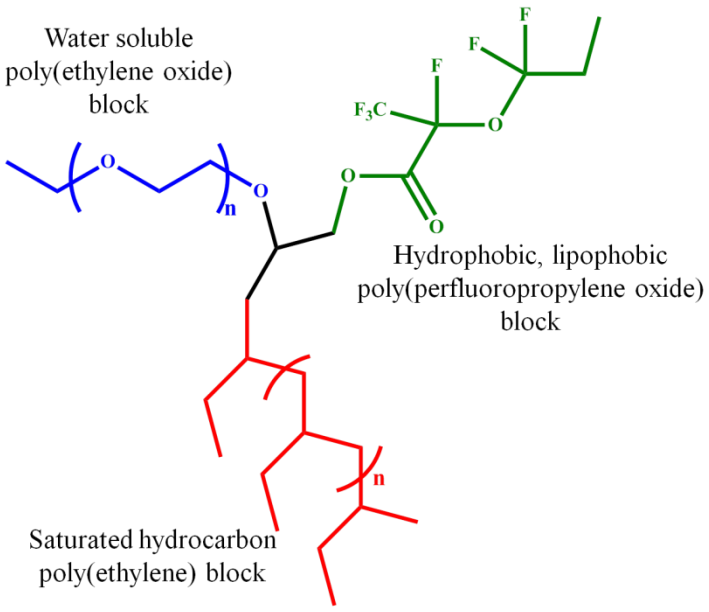


Figure 1.12: Example of an ABC miktoarm star terpolymer.

### 1.5.3 Nitroxide Mediated Polymerisation (NMP)

NMP is a controlled polymerisation first reported by Georges *et al*.[178] who described the polymerisation of styrene using a benzoyl peroxide initiator and mediated by 2,2,6,6-tetramethyl-1-piperidinyloxy, (TEMPO). Other researchers successfully used this method utilising the reversible end-capping of chains with a controls the rate of monomer addition.[179]

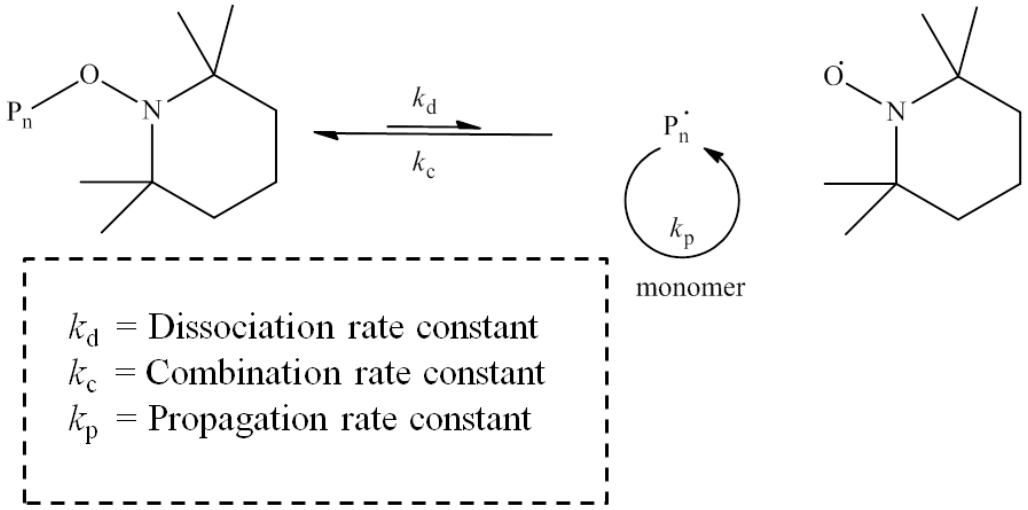


Scheme 1.7: NMP polymerisation mechanism.

Styrene and substituted styrenic monomers are the most common monomers used in NMP,[180, 181] however, acrylate, acrylamide and acrylonitriles monomers can also be polymerised using this method where polydispersities of < 1.20 can be achieved.[182] Unfortunately methacrylates are not suitable monomers as irreversible termination can occur due to the proton transfer from methacrylates to the nitroxide radical species.[183]

### 1.5.3.1 Branching in NMP

Branched polystyrene polymers using bifunctional divinyl benzene (DVB) can be synthesised using a straightforward NMP approach, where adjustment of the mole feed ratio of brancher can result in either soluble branched polymers or cross-linked gels. Analysis of these polymers showed that molecular weights were in the range of 150000 g $mol^{-1}$, however, this report did not include details of linear analogues or

even initial initiator: monomer ratios and therefore primary chain length of these polymers was not be determined.[184]

To date, polymers synthesised *via* NMP, have not been directly used in the development of drug delivery devices. Nicolas *et al.*[185] have synthesised amphiphilic polymers using styrene, methyl methacrylate and polyethylene glycol methyl ether methacrylate (PEGMA) (ethylene oxide repeat unit = 4-5) where a modified nitroxide and small amount of styrene were added to the reaction mixture to overcome methacrylate induced termination. These polymers may have the ability to self-assemble in water and host hydrophobic material but such properties were not discussed in this report.[184]

### 1.5.4 Reversible Addition-Fragmentation chain Transfer Polymerisation (RAFT)

RAFT is a controlled polymerisation technique introduced by Moad and co-workers;[186] reactions are based on the transfer of an end-group (from a RAFT agent) where the chain end is in equilibrium as an active and dormant species. A general mechanism of this reaction is shown in Scheme 1.8 (A). Essentially RAFT is a conventional free radical polymerisation with the addition of a chain transfer agent which is usually a dithioester but can be trithiocarbonates or xanthates (general RAFT agent features are seen in Scheme 1.8 (C)) which controls monomer addition. Following initation, radical species add across the C=S bond of the RAFT agent generating an intermediate which fragments yielding a new radical and a dormant capped polymer chain. This radical will re-initiate the polymerisation with the capped polymer behaving as the RAFT agent.

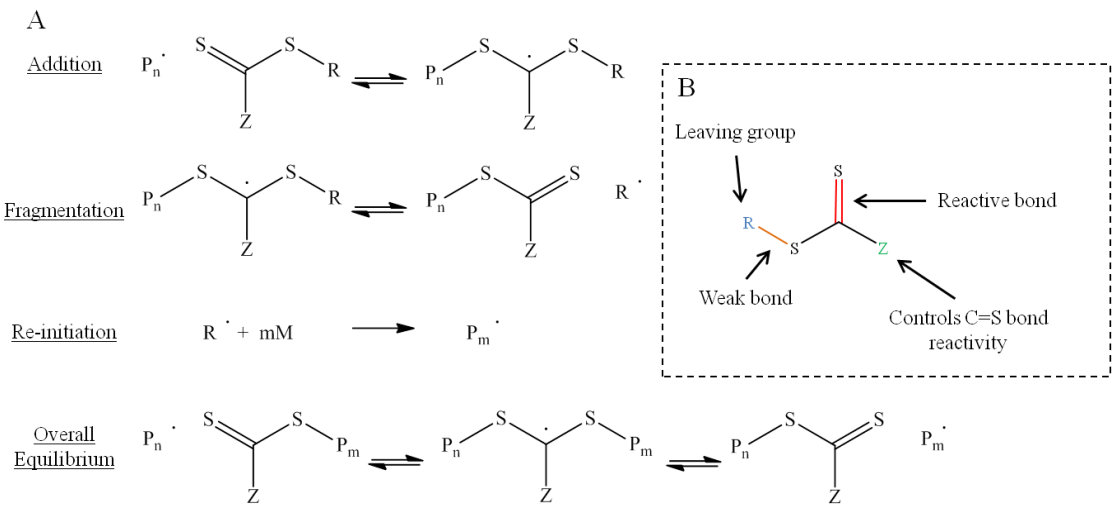


Scheme 1.8: RAFT process. A) General reaction mechanism. B) RAFT agent features.

As well as styrene (and its derivatives), a wide variety of (meth)acrylate monomers can be utilised in RAFT polymerisation.[187] Reactions can proceed in a controlled manner at temperatures ranging from ambient to 140°C and, for certain systems, increased reaction temperatures can yield polymers with narrow polydispersities,[161] however, an increased temperature in the polymerisation of MMA (using a trithiocarbonate RAFT agent) had no effect on polydispersity.[188] In most polymerisations an increased temperature leads to an increased rate of polymerisation and shorter reaction times. Higher molecular weights can also be achieved by increasing reaction pressure (this slows the rate of radical-radical termination).[189]

Reactions can be carried out in protic solvents such as alcohols and water, however, suitability of the RAFT agent in these solvents must be considered.[186 190] For the polymerisation of vinyl acetate (VAc) and MMA (both using AIBN initiator) conversions of 96 % and 90 % can be achieved respectively, however, different RAFT agents were used for these reactions.[188]

The ability to synthesise RAFT agents with different chemistries (which must be compatible with the chosen monomer and solvent) gives polymer chain end functionality which can be highly desirable. As a consequence, the dithioester group of the RAFT agent will remain at the terminus of each polymer chain which colours the final material. This colour, coupled with the dithioester functionality may be undesirable for further reactions and/ or applications of the polymers, for example toxicity issues when used in drug delivery systems.[191] These groups can be cleaved through aminolysis, thermal emimination and UV irradiation[192, 193] depending on the individual RAFT agent.

Statistical copolymers copolymers can be prepared by RAFT polymerisation but it should be noted that these are generally gradient copolymers dependant on the chemistry of both/multiple monomers and their reactivity ratios.[188] It should be noted that the monomers used in copolymerisations must compliment the chosen RAFT agent. Diblock copolymers copolymers can also be readily synthesised through addition of a second monomer batch after high conversion of the original monomer batch, and as this is experimentally facile, polymers with ABA and ABC compositions can be produced.[194, 195]

#### 1.5.4.1 Branching in RAFT Polymerisation

A RAFT monomer with a dithioester group and a double bond has been shown to copolymerise with styrene (in bulk) to give highly branched structures with a molecular weight of 600000 g $mol^{-1}$ at 83 % conversion (24 hours)[196] but Perrier was the first to report the synthesis of PMMA hyperbranched polymers using EGDMA as a brancher in 2005 where near 100 % conversion could be reached. An example of a dithioester RAFT agent used in this branched polymerisation[197] is shown in Figure

1.13. This one-pot system produced a branched polymer with a molecular weight of approximately 686 000 g $mol^{-1}$ (polydispersity = 38.63) using a molar ratio of CTA: MMA: EGDMA 1: 34: 1.82 and it was also shown that this material could be successfully chain extended using styrene monomer. These examples of branched polymerisations were found to be controlled reactions where linear plots of $M_n$ *vs.* conversion and ln([$M_0$/[M]) *vs.* time were recorded.

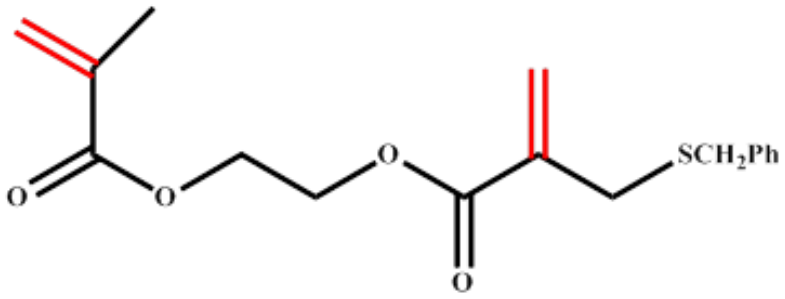


Figure 1.13: Example of a dithioester RAFT agent bearing double bonds.

1.5.4.2 RAFT Polymers in Drug Delivery

There have been very few reports on the *in vitro* toxicity[198, 199] and blood compatibility[200] associated with polymers synthesised by RAFT, and it is thought the thiocarbonyl groups will have different toxicities to different tissues in the body. Nevertheless numerous micelles using amphiphilic copolymers synthesised *via* RAFT have been shown to self-assemble where relative ratios and block length has been shown to affect size, stability and CMC of the resulting micelles.[201, 202] Reversible shell-crosslinked micelles (with a poly(ethylene oxide) corona) have shown controlled release of a model drug[203] and there have also been reports of pH[204] and temperature sensitive[205] micelles often using *p*(*N*-isopropylacrylamide) (NIPAAm). It has been shown that acid-degradable crosslinked core-shell particles with average diameters of approximately 150 - 500 nm can be generated by RAFT-

mediated dispersion polymerisation.[206] These consist of *n*-butyl acrylate cores and *p*(oligoethylene glycol acrylate) (OEGA) shells which are acid cleavable, resulting in release of a hydrophobic payload. Thermoresponsive hydrogels for use in tissue engineering scaffolds can be assembled using BAB triblock copolymers containing *p*(NIPAAm) and *p*( *N, N*-dimethacrylamide) synthesised using RAFT.[207]

#### 1.5.4.3 RAFT Limitations

Despite the versatility of RAFT polymerisation in terms of monomer choice and architecture, there are a number of negative aspects which will be briefly outlined here. Invariably overlooked is the widespread use of AIBN initiator, which has been reported to be a potentially explosive material and extra care must be taken during its use.[208] Perhaps the most significant limitation is the time consuming synthesis and characterisation of individual RAFT agents which must compliment the chosen monomer making it extremely difficult during the synthesis of multicomponent and branched polymers. To use these polymers in applications such as drug delivery or any other biomedical purpose further modification/ purification may be necessary to cleave the dithioester moieties present on each chain, to prevent any toxic side effects associated with this functional group.

### 1.5.5 Atom Transfer Radical Polymerisation (ATRP)

ATRP is a popular method of controlled free radical polymerisation. It was developed independently by Sawamoto[209] and Matyjaszewski[210] in 1995. 13 papers (SciFinder Scholar) based on the technique were published in the same year; since then interest has increased dramatically with 929 papers published in 2012 alone (SciFinder Scholar). The process is a development of Atom Transfer Radical Addition; a free radical addition of alkyl halides and alkenes produced in a 1:1 ratio.

### 1.5.5.1 ATRP Mechanism

Radicals are generated by a reversible redox process which is catalysed by a transition metal complex ($M_t^n$ – Y / Ligand) which can abstract a halogen atom (X) from an alkyl halide initiator (R – X) to give an alkyl radical and an oxidised metal complex (X - $M_t^{n+1}$ – Y / Ligand); this is the activation step. As the metal complex is in a higher oxidation state it acts as a deactivator and will rapidly re-generate a halogen capped polymer chain. A fast equilibrium between these active and dormant species is quickly set up where monomer addition occurs in a controlled manner (basic mechanism is shown in Scheme 1.9).

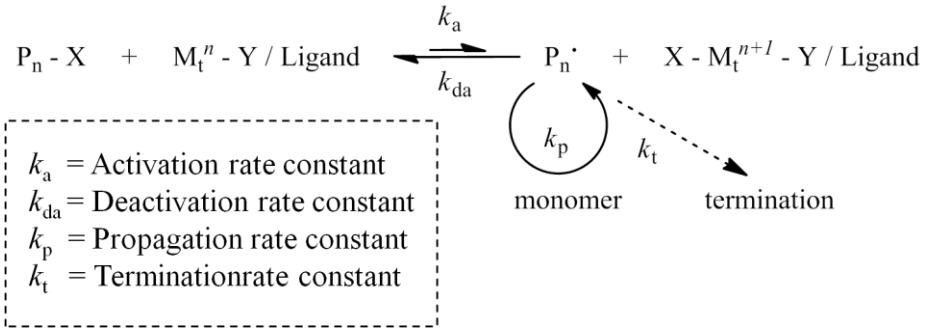


Scheme 1.9: General ATRP mechanism.

This outlined reversible capping of polymer chain ends is a feature similar to the nitroxide capping in NMP and the RAFT process (section 1.5.3 and section 1.5.4), the addition of monomer is similar to that found in free radical polymerisation (section 1.5.1).

### 1.5.5.2 ATRP Rate Law

This rate law predicts a linear relationship between $\ln([M]_0/[M])$ and conversion with time should be observed during an ATRP process. The linearity indicates a constant concentration of radical species in the reaction and first order kinetics with

respect to monomer consumption. Deviation from linearity may occur due to termination reactions where the concentration of $Cu^{II}$ increases; this can happen when the initial concentration of $Cu^{II}$ is not large enough to ensure fast rates of deactivation resulting in coupling of radicals and therefore increasing the concentration of $Cu^{II}$.

$$R_p = k_p[M][P^\bullet] = k_p K_{eq}[M][I]_0 \cdot \frac{[Cu^I]}{[X\text{-}Cu^{II}]}$$

Equation 1.1: Rate law of ATRP.

1.5.5.3 Molecular weight Determination

In the case of living polymerisations, molecular weights can be pre-determined and predicted by tailoring of initiator: monomer ratio. The number of monomers in a primary chain is referred to as the Degree of Polymerisation ($DP_n$) and is equal to $[M]/[I]_0$ and polymers with molecular weights above 100000 g $mol^{-1}$ can be prepared, however, by targeting these high molecular weights termination is thought to occur more readily.

As these reactions proceed in a controlled manner, i.e. only transient periods of monomer addition, polymer chains synthesised by ATRP have relatively narrow polydispersities typically 1.01 – 1.5. The polydispersity relates to initiator (RX) deactivator (D), propagation rate constant ($k_p$) and deactivation rate constant ($k_p$) and monomer conversion (P) seen in Equation 1.2.

$$\frac{M_w}{M_n} = 1 + \left( \frac{([RX]_0 - [RX]_t) \cdot k_p}{k_{da} \cdot [D]} \right) \left( \frac{2}{P} - 1 \right)$$

Equation 1.2: Polydispersity determination in ATRP.

This equation assumes no chain termination or transfer reactions take place in the polymerisation, which in practice is unlikely to be the case. Higher polydispersities are often found for acrylates compared to methacrylates as the former generally have higher rates of propagation, consistent with Equation 1.2. Shorter polymer chains also tend to have larger polydispersities in comparison to long chains due to the higher initial initiator concentration.

1.5.5.4 Experimental Procedure for ATRP

ATRP polymerisations are mostly carried out in solvent but bulk ATRP has been shown in the literature. Solvents aid the diffusion of polymer chains at high conversion when the solution becomes more viscous. ATRP can also be carried out in emulsion,[211] miniemulsion,[212] dispersion[213] and suspension polymerisation.[214] For the purposes of this study these systems will not be discussed further. Preparation for an ATRP reaction begins by the addition of either the initiator or $Cu^I$ / Ligand complex to a deoxygenated vessel containing monomer and solvent. ATRP is oxygen sensitive (as are all free radical polymerisations) but can proceed with small amounts of oxygen which is scavenged by the catalyst but large amounts leads to oxidation of catalyst reducing its concentration which decreases the polymerisation rate. De-gassing the initial monomer/solvent solution and providing an inert atmosphere is necessary to remove oxygen as it reacts with active polymer chains leading to unwanted termination. Once initiated, chain ends should remain active

until manual termination which is usually carried out by the addition of solvent and exposure to the atmosphere with stirring.

#### 1.5.5.5 Components of ATRP

##### 1.5.5.5.1 Choice of monomer

A wide variety of monomers can be used in ATRP including (meth)acrylates,[215, 216] (meth)acrylamides,[217, 218] styrenics,[219, 220] and acrylonitriles,[221] where polymerisations proceed in a controlled manner yielding polymers with narrow polydispersities. All of these monomers contain a stabilising group (often carbonyl) which ensures limited interference with propagating radicals and catalytic systems. It should be noted that optimisation of concentration and catalyst may be necessary to ensure controlled monomer chain addition with respect to radical concentration.

Methacrylates are favoured in ATRP as they generate highly stable radicals (due to their methyl group) affording more controlled reactions (when compared to acrylates), and *n*-butyl methacrylate (BuMA),[222, 223] 2-(dimethylamino) ethyl methacrylate (DMAEMA),[220] 2-hydroxy ethyl methacrylate (HEMA)[224, 225] and oligo (ethylene glycol) methyl ether methacrylate[226] have all been successfully polymerised (amongst many others) using ATRP.

2-Hydroxypropyl methacrylate (HPMA) is a relatively unused monomer in ATRP; however, it has been used in free radical polymerisation[227] and NMP.[228] HPMA has interesting solution properties as the monomer is highly water soluble yet *p*(HPMA) is extremely hydrophobic. The first report of direct *p*(HPMA) polymerisation using ATRP was in 2002[229] where reaction kinetics were investigated in various protic solvent systems achieving a polydispersity of 1.09 in methanol (97 % conversion,

target $DP_n$ = 50). Since then it has been used as a model monomer for investigating initiator efficiencies through $^{13}C$-radiolabelling[230] and for performing polymerisations in microfluidic systems.[231] The polymerisation of *p*(HPMA) has been shown to be facile, and when coupled with its tolerance to different solvents/initiators makes it an ideal candidate for further studies and its hydrophobicity may be exploited for the use in an amphiphilic polymer system.

1.5.5.5.2 Choice of Catalyst

The addition of a halogenated transition metal catalyst is necessary in ATRP to ensure control of the equilibrium between active and dormant moieties. The metal ion must undergo a one electron transfer i.e. oxidation/reduction and must successfully form a complex with a suitable ligand where the metal increases its coordination number by one. It must also have a strong affinity for halogen atoms but not hydrogen and alkyl radicals. The first ATRP reactions used ruthenium[209] (Sawamoto) and copper[210] (Matyjaszewski); since then a wide variety of metals including nickel,[232] rhodium,[233] molybdenum,[234] palladium[235] and iron[236] have been used; however, due to its relatively low toxicity, versatility and availability copper is generally preferred.

The halogenated metal and the initiator can contain the same halogen atom, however, it is common to used a mixed system as this can afford increased control in polymerisations, for example, bromine containing initiators compliment chlorinated catalysts. As the Cu-Cl bond is stronger than Cu-Br, halogen exchange occurs following initiation where most chains are terminated by Cl atoms.[237] Therefore the rate of initiation increases with respect to propagation and as such, using CuCl with a brominated initiator leads to better controlled polymerisations.[238]

1.5.5.5.3 Choice of ligand

Ligands in ATRP aid the solubilisation of the transition metal catalyst and also control the equilibrium position between active and dormant moieties through adjustment of the redox potential.[239] The most widely used are nitrogen-based, particularly for Cu containing systems where as phosphorous ligands are generally less effective. Other ligands used in Cu mediated ATRP have been reviewed.[239] The chosen ligand should form a strong complex with the transition metal and allow an increase in coordination number with no side reactions. Bidentate ligands such as 2, 2'-Bipyridine (BPY) are used in Cu mediated ATRP as its steric hindrance does not result in reduced catalytic activity and the nitrogen substituent is not excessively electron withdrawing.[237]

1.5.5.5.4 Choice of Initiator

The reaction of a chosen initiator influences the amount of control in a polymerisation and the ratio of initiator: monomer determines the primary chain length. To ensure radical generation the initiator must be equally (or more) reactive than the propagating species. If it is highly reactive control would be lost as the concentration of radicals would be too high. In short, any halide containing molecule with a stabilising group at the α-carbon can be used as an ATRP initiator[240] and faster initiation can occur as a result of a highly stable initiator radical. Weak initiator- halogen bonds i.e. C-I do not effectively initiate reactions, conversely C-F bonds are too strong and the same result is found and as such C-Br bonds are found to be most effective.[237]

To achieve chain end functionality, straightforward esterification reactions between acids (with various functional groups) and acyl halides can give a variety of ATRP

initiators.[226, 241] As ATRP is highly tolerant to functional groups it is possible to synthesise macroinitiators in the same way. These can be (relatively low molecular weight) polymers which have been previously synthesised and can be used as an alternative to conventional block copolymerisations. The solubility of both segments may be different but both must have sufficient solubility in the solvent used in polymerisation.[242]

1.5.5.5.5 Choice of Solvent

ATRP can be carried out in bulk,[243] however, as many polymers aren't soluble in their monomer, solvents are invariably used as a reaction medium. MMA,[244] PEGMA,[245] and DMAEMA[246] have all been polymerised in toluene. Polar solvents such as dimethyl sulfoxide (DMSO),[246] dimethyl formamide (DMF),[247] tetrahydrofuran (THF)[248] and acetone[249] have also been used in ATRP.

In 1998 polymerisation of *p*(HEMA) was successfully carried out in water (40 °C)[250] and can now be carried out at ambient temperature shown by Armes and co-workers who polymerised OEGMA to 95 % conversion (1.12 polydispersity)[251, 226] and Perrier *et al.* were able to polymerise PEGMA (higher molecular weight OEGMA) in the same manner.[252]

Alcoholic solvents are also utilised in ATRP, such as isopropyl alcohol (IPA) for the polymerisation of 4-vinyl pyridine (40 °C, 1.1 polydispersity); Rannard and co-workers were also able to polymerise BuMA in IPA: water mixtures.[222, 223] Monomers with hydroxy functionality such as HPMA and glycerol methacrylate (GMA) have been shown to polymerise in methanol (and methanol/water mixtures) in a controlled manner characterised by linear plots of $M_n$ *vs.* conversion and $\ln([M_0]/[M])$ *vs.* time. Using the same experimental protocol, Armes and co-workers

were able to use a PEG based macroinitiator (EO repeat unit = 45) to polymerise HPMA (target $DP_n$ = 25) to 100 % conversion at 50°C, yielding a polymer with a polydispersity of 1.17.[229] The addition of water to an ATRP reaction has been shown to increase the rates of polymerisation;[253, 254] thought to be due to the reduced concentration of the deactivator which leads to a reduction in the rate of deactivation and therefore monomer addition becomes faster (and less controlled). It is reported that water can act as a ligand in the Cu complex thereby eliminating the halogen atom. This complex becomes unable to act as a deactivator as it is no longer in a +2 oxidation state and as such reactions proceed at a faster rate, limiting control of monomer addition.[237]

#### 1.5.5.5.6 Temperature

As well as increasing polymerisation rate and catalyst solubility, elevated reaction temperatures also increase the chance of chain transfer and other undesirable side reactions and in some cases catalyst decomposition.[255] Optimal reaction temperatures are highly dependent on monomer, catalyst and target $DP_n$ and as such can vary considerably.[237]

## 1.6 Different Polymer Architectures using ATRP

Outlined here are various polymer architectures prepared by ATRP which may be manipulated to form drug delivery vehicles. Several graphical representations of these architectures are shown in Figure 1.14.

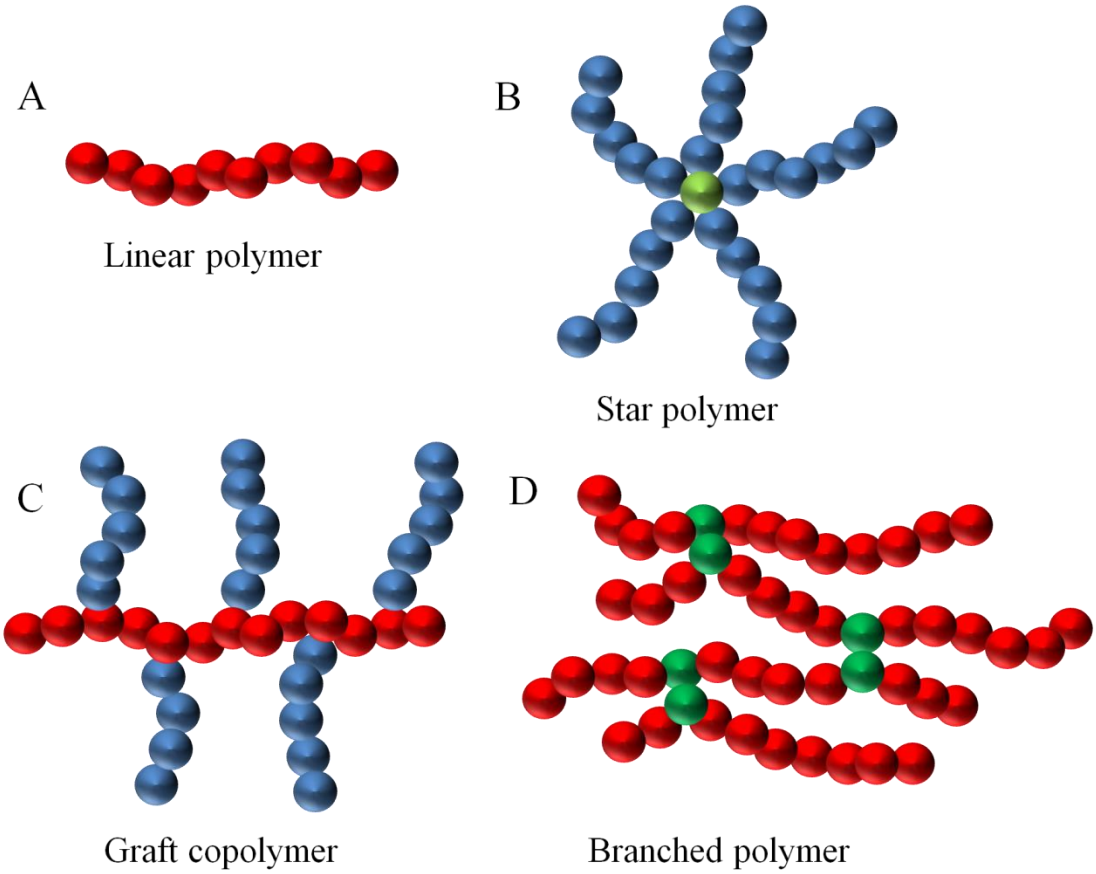


Figure 1.14: Representation of various polymer architectures obtained by ATRP. Linear polymer (A), star polymer (B), graft copolymer (C) and branched polymer (D).

### 1.6.1 Linear Polymers

Apart from homopolymers, various polymer compositions may be obtained through ATRP. Block copolymers can be generated by either a macroinitiator approach[256, 229] or by the sequential addition of monomers.[257] A decablock copolymer comprised of methyl acrylate (MA), ethyl acrylate (EA), *n*-butyl acrylate (*n*-BA) and *t*-butyl acrylate (*t*-BA) has been reported. Each block had a target molecular weight of 2000 g mol$^{-1}$ achieving a final molecular weight of 21 000 g mol$^{-1}$ (polydispersity =

1.72).[258] During each successive monomer addition some chain end functionality was lost, verified by low molecular weight shoulders in GPC analysis.

### 1.6.2 Star Polymers

These structures can be generated by the use of multifunctional initiators[259, 260] generating 'arms' as monomer growth proceeds away from the core initiating site (Figure 1.14 (B)) and may be called a 'core-first approach'. Star polymers may also be generated using an 'arms-first' approach where linear polymers are synthesised followed by addition of a crosslinking agent (such as DVB or EGDMA) leading to dense core formation.[261]

### 1.6.3 Graft Copolymers

Seen in Figure 1.14 (C), these structures can be obtained using three methods:

1) Grafting onto: Polymer chains are attached to a pre-synthesised polymer chain.[262]

2) Grafting from: The functional groups present within a polymer backbone can be converted to initiators followed by monomer addition.[263]

3) Grafting through: This technique utilises macromonomers which are polymer chains containing a polymerisable group.[264, 265]

Parameters such as grafting density and side chain length can be altered using this approach to produce polymers with desired properties.

### 1.6.4 Branched Copolymers

ATRP can be used to prepare hyperbranched polymers using self-condensing vinyl polymerisation (SCVP).[266] This utilised AB* monomers *via* a controlled free-radical process where A = vinyl group and B* = an ATRP initiator (see Figure 1.14 (D). Monomers such as vinyl benzyl chloride (VBC) can be polymerised using this method. When B* is active a "T" shaped linkage forms and without significant termination the number of branch points is equal to the $DP_n$. Gelation can never occur in conventional SCVP as the chains are all tethered at one end and there is no inter-chain reactivity that occurs when the reaction is proceeding.

The synthesis of soluble branched polymers using ATRP can be achieved through addition of a small amount of divinyl monomer (brancher) i.e. the Strathclyde approach. This molecule is statistically incorporated into a propagating polymer chain leaving a pendant unreacted vinyl group which will react with another propagating polymer chain leading to irreversible linkage. If this branching applied to every chain in a reaction pot an infinite network gel will be produced. The amount of divinyl monomer needed to produce highly branched polymers varies and is dependent on several factors including the reactivity ratios monomer and brancher (becoming more complex when using > 1 monomer), however, it is common practice for the initiator/brancher mole ratio to be less than unity.[267, 268]

If the branching process is random and provided all monomers have equal reactivities, it is inevitable that some chains will contain > 1 brancher molecule and conversely some will contain no brancher. Intramolecular cyclisation of brancher may occur during polymerisation where the pendant vinyl group of a brancher reacts with the chain end forming a loop. It has been shown that more dilute conditions increases the amount of intramolecular cyclisation.[269] Armes and co-workers have

used Monte Carlo modelling to predict molecular weights, polydispersities and architecture as a function of time; the results from which were compared to a branched copolymerisation of *p*(HPMA) using EGDMA as a brancher. Here it is shown that a multitude of architectures are formed after almost complete conversion.[270] A schematic representation of the various architectures that may form when using a divinyl monomer in an ATRP synthesis is shown in Figure 1.15.

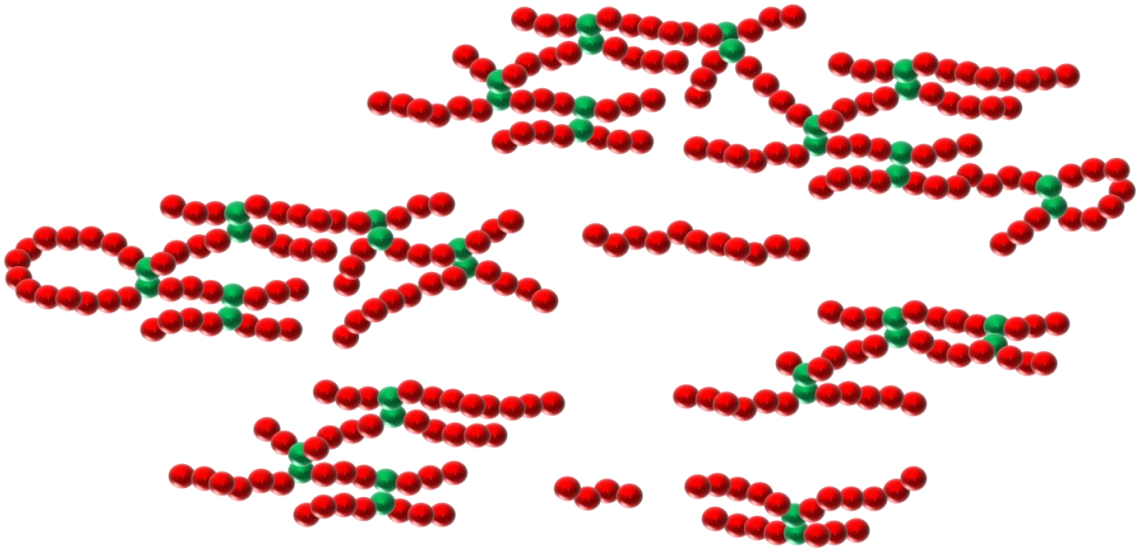

Figure 1.15: Representation of various architectures which may be present in a branched ATRP reaction.

### 1.6.5 ATRP Polymers for Drug Delivery

There are few reports of the encapsulation of drugs (or indeed any hydrophobic material) into polymeric systems synthesised *via* ATRP. However, pH responsive polymer micelles have been shown to successfully load and release rifampicin (RIF);[271] it should be noted that these polymers also contained cellulose segments which were not synthesised by ATRP. Micelles consisting of novel folic acid-functionalised diblock copolymers synthesised by ATRP have been shown to

successfully load a hydrophobic drug,[272] however, their preparation involved processes such as centrifugation, sonication and filtration. These procedures are time consuming and scale up experiments may prove difficult. To date, branched copolymers synthesised by ATRP have not been used for drug delivery purposes.

## 1.7 Project Outline

The aim of this project is to develop a strategy that will allow the controlled synthesis of high molecular weight amphiphilic copolymers with complex architectures. ATRP was chosen as the polymerisation method due to limitations of other systems, which are briefly highlighted here. The synthesis and purification of dendrimers/dendronised polymers is highly complex and time consuming, where as one-pot hyperbranched polymers offer no scope of chain length control; as is the case for free radical polymerisation. Monomer choice is limited in anionic polymerisation where reactions require extremely stringent conditions, which are unfavourable for this project. NMP was not utilised in this body of work as the scope of materials which may be synthesised using this route is limited, despite relatively facile polymer synthesis. Despite the complex architectures and wide range of monomer choice, RAFT was not used as a polymerisation technique; this is due to the synthesis of RAFT agents and subsequent dithioester cleavage post-polymerisation.

Hydrophobic *p*(HPMA) was chosen as the ATRP synthesis has been shown to proceed in a controlled manner, with and without a hydrophilic macroinitiator using Cu(Cl)/BPY as the catalyst/ligand at ambient temperature. The addition of water has been shown to increase the rate of polymerisation of *p*(HPMA), however, it was anticipated that complete removal of water may be experimentally difficult,

particularly if using a hygroscopic macroinitiator. To ensure polymerisations proceed in a controlled manner, detailed kinetic analysis of linear and branched *p*(HPMA) (using EGDMA brancher) will be performed with and without a PEG block. A catalogue of linear and branched polymers with varying amphiphilicity (through tailoring the chain lengths) will be synthesised which may be used to generate polymeric nanoparticles in water. Branched polymers will form micelle-like structures with dense hydrophobic cores without self-assembly or crosslinking in water and by using various nanoprecipitation approaches, aqueous nanoparticle dispersions comprising of these copolymers will be generated and their behaviour explored. A methodical approach will be taken, aiming to control nanoparticle z-average diameter utilising a rapid solvent exchange method, achieved simply through variation of concentration parameters. This work will show that these nanoparticles are capable of loading various hydrophobic materials including the human immunodeficiency virus/acquired immunodeficiency syndrome (HIV/AIDS) drug Lopinavir. The ultimate goal would be to generate a universal drug carrier alongside tailoring its z-average diameter to suit its biological application and it is believed progress towards this has been achieved.

## 1.8 References


1 V. Malinova and W. Meier, *Polymer Based Nanostructures: Medical Applications*, ed. P. Broz, Royal Society of Chemistry, 1st edn, 2010, ch. 1 pp. 3-15.

2 Nicolson. P. C, Vogt. J,. *Biomaterials*, **2001**, *22,* (*24*), 3273.

3 Hutmacher. D. W,. *Biomaterials*, **2000**, *21,* (*24*), 2529.

4 Ishihara. K., *Sci Technol Adv Mat*, **2000**, *1,* (*3*), 131.

5 Middleton. J.C., Tipton. J. A., *Biomaterials*, **2000**, *21*, (*23*), 2335.

6 Kumar. M. N. V. R., *J Pharm Pharmaceut Sci*, **2000**, *3*, (*2*), 234.

7 Stover. J., Walker. N., Garnett. G. P., Salomon. J. A., Stanecki. K. A., Ghys. P. D., Grassly. N. C., Anderson. R. M., Schwartländer. B., *Lancet*, **2002**, *360*, (*9326*), 73.

8 Esparza. J., Bhamarapravati. N., *Lancet*, **2000**, *355*, (*9220*), 2061.

9 Merson. M. H., *N Engl J Med*, **2006**, *354*, 2414.

10 Gottlieb. M. S., Schanker. H. M., Fan. P. T., Saxon. A., Weisman. J. D., *MMWR Morb Mortal Wkly Rep*, **1981**, *30*, (*21*), 250.

11 Barre-Sinoussi. F., Chermann. J. C., Rey. F., Nugeyre. M. T., Chamaret. S., Gruest. J., Dauguet. C., Axler-Blin. C., Vezinet-Brun. F., Rouzioux. C., Rozenbaum. W., Montagnier. L., *Science*, **1983**, *220*, (*4599*), 868.

12 Fortson. J. G., *Rev Econ Statistics*, **2011**, *93*, (*1*), 1.

13 https://www.unaids.org/en/media/unaids/contentassets/documents/epidemiology/2012/gr2012/2012_FS_regional_ssa_en.pdf. Accessed on 15th November 2013.

14 Weiss. R. A., ***Clin. Exp Immunol*, 2008**, *152*, 201.

15 Freed. E. O., *Somatic Cell and Molecular Genetics*, **2001**, *26*, 13.

16 Engelman. A., Cherepanov. P., *Nat Rev Microbiol*, **2012**, *10*, 279.

17 Vyas. T. K., Shah. L., Amiji. M. M., *Expert Opin Drug Deliv*, **2006**, *3*, (*5*), 613.

18 Arts. E. J., Hazuda. D. J., *Cold Spring Harb Perspect Med*, **2012**, *2*, 1.

19 Menendez-Arias. L., *Virus Res*, **2008**, *134*, 124.

20 Balzarini. J., *Curr Top Med Chem*, **2004**, *4*, 921.

21 Martinez-Cajas. J. L., Wainberg. M. A., *Antiviral Res*, **2007**, *76*, 203.

22 Velazquez-Campoy. A., Muzammil. S., Ohtaka. H., Schön. A., Vega. S., Freire. E., *Curr Drug Targets Infect Disord*, **2003**, *3*, (*4*), 311.

23 Espeseth. A. S., Felock. P., Wolfe. A., Witmer. M., Grobler. J.,Anthony. N., Egbertson. M., Melamed. J. Y., Young. S., Hamill. T., Cole. J. L., Hazuda. D. J., *Proc Natl Acad Sci USA*, **2000**, *97*, 11244.

24 Grobler. J. A., Stillmock. K., Hu. B., Witmer. M., Felock. P., Espeseth. A. S., Wolfe. A., Egbertson. M., Bourgeois. M., Melamed. J., Wai. J. S. Young. S., Vacca. J., D. J. Hazuda., *Proc Natl Acad Sci USA*, **2002**, *99*, 6661.

25 Molla. A., Korneyeva. M., Gao. Q., Vasavanonda. S., Schipper. P. J., Mo. H. M., Markowitz. M., Chernyavskiy. T., Niu. P., Lyons. N., Hsu. A., Granneman. G. R. , Ho. D. D., Boucher. C. A., Leonard. J. M., Norbeck. D. W., Kempf. D. J., *Nat Med*, **1996**, *2*, 760.

26 Samson. M., Libert. F., Doranz. B. J., Rucker. J., Liesnard. C., Farber. C. M., Saragosti. S., Lapoumeroulie. C., Cognaux. J., Forceille. C., Muyldermans. G., Verhofstede. C., Burtonboy. G., Georges. M., Imai. T., Rana. S., Yi. Y., Smyth. R. J., Collman. R. G., Doms. R. W., Vassart. G., Parmentier. M., *Nature*, **1996**, *382*, 722.

27 Collaborative Group on AIDS Incubation and HIV Survival., *Lancet*, **2000**, *355*, 1131.

28 Mocroft. A., Vella. S., Benfield. T. L, Chiesi. A., Miller. V., Gargalianos. P., d'Arminio Monforte. A., Yust. I., Bruun. J. N., Phillips. A. N., Lundgren. J. D., *Lancet*, **1998**, *352*, 1725.

29 Palella. F. J. Jr., Delaney. K. M., Moorman. A. C., Loveless. M. O., Fuhrer. J., Satten. G. A., Aschman. D. J., Holmberg. S. D., *N Engl J Med*, **1998**, *338*, 853.

30 Detels. R., Munoz. A., McFarlane. G., Kingsley. L. A., Margolick. J. B., Giorgi. J., Schrager. L. K., Phair. J. P., *JAMA*, **1998**, *280*, 1497.

31 Henry. K., *Ann Intern Med*, **2000**, *132*, 306.

32 Carpenter. C. C., Cooper. D. A., Fischi. M. A., Gatell. J. M., Gazzard. B. G., Hammer. S. M., Hirsch. M. S., Jacobsen. D. M., Katzenstein. D. A., Montaner. J. S. G., Richman. D. D., Saag. M. S., Schechter. M., Schooley. R. T., Thompson. M. A., Vella. S., Yeni. P. G., Volberding. P. A., *JAMA*, **2000**, *283*, 381.

33 Chaisson. R. E., Keruly. J., Moore. R. D., *JAMA*, **2000**, *284*, 3129.

34 Stengel. R. F., *Math Biosci*, **2008**, *213*, 93.

35 Ojewole. E., Mackraj. I., Naidoo. P., Govender. T., *Eur J Pharm Biopharm*, **2008**, *70*, 697.

36 Li. X. L., Chan. W. K., *Adv Drug Del Rev*, **1999**, *39*, 81.

37 Obaru. K., Mitsuya. H., *Nippon Rinsho*, **1998**, *56*, 769.

38 Aquaro. S., Calio. R., Balzarini. J., Bellocchi. M. C., *Antiviral Res*, **2002**, *55*, 209.

39 Amji. M. M., Vyas. T . K., Shah. L. K., *Discov Med*, **2006**, *6*, 157.

40 Harris. M., *Expert Opin Drug Saf*, **2008**, *7*, 4.

41 Carr. A., Samaras. K., Burton. S., Law. M., Freund. J., Chisholm. D. J., Cooper. D. A., *AIDS*, **1998**, *12*, F51.

42 Chariot. P., Drogou. I., de Lacroix-Szmania. I., Eliezer-Vanerot. M. C., Chazaud. B., Lombès. A., Schaeffer. A., Zafrani. E. S., *J Hepatol*, **1999**, *30*, 156.

43 Jacobson. D. L., Knox. T., Speigelman. D., Skinner. S., Gorbach. S., Wanke. C., *Clin Infect Dis*, **2005**, *40*, 1837.

44 Pirmohamed. M., Park. K. B., *Curr Opin Allergy Cl*, **2001**, *1*, (*4*), 311.

45 Rodríguez-Rosado. R., Garcia-Samaniego. J., Soriano. V., *AIDS*, **1998**, *12*, 1256.

46 Grinsztejn. B., Nguyen. B., Katlama. C., *Lancet*, **2007**, *369*, 1261.

47 LaBonte. J., Lebbos. J., Kirkpatrick., P., *Nat Rev Drug Discov*, **2003**, *2*, 345.

48 Esser. S., Helbig. D., Hillen. U., Dissemond. J., Grabbe. S., *J Dt Sch Dermatol Ges*, **2007**, *9*, 745.

49 Vandekerckhove. L., Verhofstede. C., D. Vogelaers., *J Antimicrob Chemoth*, **2009**, *63*, 1087.

50 Le Douce1. V., Janossy. A., Hallay. H., *J Antimicrob Chemother*, **2012**, *67*, 1074.

51 Hecht. R., Stover. J., Bollinger. L., Muhib. F., Case. K., de Ferranti. D., *Lancet*, **2010**, *376*, 1254.

52 Georges. M., Abraham. T. E., *J Control Release*, **2006**, *114*, 1.

53 Taylor, E.W., *Eur. J. Surg*, **1997**, *163*,(S558), 5.

54 Wachol-Drewek, Z., Pfeiffer, M., Scholl, E., *Biomaterials*, **1996**, *17*, 1733.

55 Fujioka. K., Takada. Y., Sato. S., Miyata. T., *J Control Release*, **1995**, *33*, 307.

56 Minabe. M., Uematsu. A., Nishijima. K., Tomomatsu. E., Tamura. T., Hori. T., Umemoto. T., Hino. T., *J Periodontol*, **1989**, *60*, (*2*), 113.

57 Stemberger. A., Unkauf. M., Arnold. D. E., Blümel. G., *Cosm Pharm Appl Polym*, **1990**, 263.

58 Singh. M. P., Stefko. J., Lumpkin. J. A., Rosenblatt. J., *Pharm. Res*, **1995**, *12* (*8*) 1205.

59 El-Samaligy. M. S., Rohdewald. P., *J Pharm Pharmacol*, **1983**, *35*, 537.

60 Satturwar. P. M., Fulzele. S. V., Dorle. A. K., *AAPS Pharm Sci Tech*, **2003**, *4*, 434.

61 Prabaharan. M., Mano. J. F., *Drug Deliv*, **2005**, *12*, 41.

62 Grenha. A., Grainger. C. I., Dailey. L. A., Seijo. B., Martin. G. P., Remunan-Lopez. C., Forbes. B., *Eur J Pharm Sci*, **2007**, *31*, 73.

63 Zhang. X., Zhang. H., Wu. Z., Wang. Z., Niu. H., Li. C., *Eur J Pharm Biopharm*, **2008**, *68*, 526.

64 Mattioli-Belmonte. M., Gigante. A., Muzzarelli. R. A., Politano. R., De Benedittis. A., Specchia. N., Buffa. A., Biagini. G., Greco, F,. *Med Biol Eng Comput*, **1999**, *37*, 130.

65 Suh. J. K., Matthew. H. W., *Biomaterials*, **2000**, *21*, 2589.

66 Sabera. A., Strand. S. P., Ulfendahla. M., *Eur J Pharm Sci*, **2010**, *39*, 110.

67 Ahn. J. S., Choi. H. K., Cho. C. S., *Biomaterials*,**2001**, *22*, 923.

68 Aggarwal. A., Kaur. S., Tiwary. A. K., Gupta. S., *J Microencapsul*, **2001**, *18*, 819.

69 Vila. A., Sanchez. A., Janes. K., Behrens. I., Kissel. T., Jato. J. L. V., Alonso, M.J., *Eur J Pharm Biopharm*, **2004**, *57*, 123.

70 Majeti. N.V., Ravi. K., *React Funct Polm*, **2000**, *46*, (*1*), 1.

71 Mathur. M. K., Narang. C. H., *J Chem Educ*, **1990**, *67*, 938.

72 Damascelli. B., Patelli. G .L., Lanocita. R., Di Tolla. G., Frigerio. L. F., Marchianò. A., Garbagnati. F., Spreafico. C., Tichà. V., Gladin. C. R., Palazzi. M., Crippa. F., Oldini. C., Calò. S., Bonaccorsi. A., Mattavelli. F., Costa.L., Mariani. L., Cantù. G., *Am J Roentgenol*, **2003**, *181*, 253.

73 Kramer. P. A., *J Pharm Sci*, **1974**, *63*, 1646.

74 Willmott. N., Harrison. P. J., *Int J Pharm*, **1988**, *43*, 161.

75 Cascone. M. G., Lazzeri. L., Carmignani. C., Zhu. Z., *J Mat Sci Mat in Med*, **2002**, *13*, 523.

76 Yoshioka. T., Hashida. M., Muranishi. S., Sezaki. H., *Int J Pharm*, **1981**, *81*, 131.

77 *Biomaterials Science: an introduction to materials in medicine*, ed. B. D. Ratner, A. S. Hoffman, F. J. Schoen and J. E Lemons, Elsevier Inc, Oxford, 2004, pp. xxv-vxxxix.

78 Rihova. B., Riha. I., *Ther Drug Carrier Syst*, **1985**, *1*, 311.

79 Rihova. B., *Adv Drug Deliv Rev*, **1996**, *21*, 157.

80 Duncan. R., *Adv Polym Sci*, **1984**, *57*, 51.

81 Venkatachalam. M. A., Rennke. H. G., *Circ Res*, **1978**, *43*, 337.

82 Duncan. R., *Nat Rev Drug Discovery*, **2003**, *2*, 347.

83 Owens. D. E., III., Peppas. N. A., *Int J Pharm*. **2006**, *307*, 93.

84 Pietrzak. W. S., Sarver. D. R., Verstynen. B.S., *J Craniofaxial Surg*, **1997**, *2*, 87.

85 *J. Kohn and R. Langer. Biomaterials science: An introduction to Materials in Medicine*, ed. B. D. Ratner, A. S. Hoffman, F. J. Schoen and J. E. Lemons, Academic Press, San Diego, CA, 1996, pp. 64-73.

86 Engelberg. I., Kohn. J., *Biomaterials*, **1991**, *12*, 292.

87 Uhrich. K. E., Cannizzaro. S. M., Langer. R. S., Shakesheff. K. M., *Chem Rev*, **1999**, *99*, 3181.

88 Fu. K., Pack. D. W., Kilbanov. A. M., Langer. R., *Pharm Res*, **2000**, *17*, 100.

89 Anderson. J. M., Shive. M. S., *Adv Drug Deliv Rev*, **1997**, *28*, 5.

90 *Encyclopaedia of Controlled Drug Delivery*, Vol 1, ed. E. Mathowitz, John Wiley and Sons, New York, 1999, pp.71-93.

91 *Encyclopaedia of Controlled Drug Delivery*, Vol 1, ed. E. Mathowitz, John Wiley and Sons, New York, 1999, pp.45-60.

92 Mangold. C., Wurm. F., Frey. H., *Polym Chem*, **2012**, *3*, 1714.

93 Itoh. A., Honda. S., Matsui. T., Hayashi. Y., U.S. Pat, 6780928, **2004**.

94 Veronese, F. M., *Biomaterials*, **2001**, *22*, 405.

95 Grodzinski. J. J., *React Funct Polym*, **2001**, *49*, 1.

96 F. E. Bailey Jr and K. V. Koleske, *Poly(Ethylene Oxide)*, Academic Press, New York, **1976**, ch. 3, pp. 13-29.

97 Serajuddin. A. T. M., Sheen. P., Mufson. D., Bernstein. D. F., Augustine. M. A., *J Pharm Sci*, **1988**, *77*, (*5*), 414.

98 *Poly(Ethylene Glycol) Chemistry: Biotechnical and Biomedical Applications*, ed. M. J. Harris, Plenum Press, New York, **1992**, ch. 1, pp. 1-12.

99 Greenwald. R. B., *J Control Release*, **2001**, *74*, 159.

100 Yamaoka. T., Tabata. Y., Ikada. Y., *J Pharm Sci*, **1994**, *83*, 601.

101 Knutton. S., *J Cell Sci*, **1979**, *36*, 61.

102 Greenwald. R. B., Gilbert. C. W., Pendri. A.,Conover. C. D., Xia. J.,Martinez. A., *J Med Chem*, **1996**, *39*, 424.

103 Alexis. F., Rhee. J. W., Richie. J. P., Radovic-Moreno. A. F., Langer. R., Farokhzad. O. C., *Urol Oncol*, **2008**, *26*, 74.

104 Lipinksi. C. A., *Curr Drug Dis*, **2001**, *1*, 17.

105 Lipinski. C. A., *Am Pharm Rev*, **2002**, *5*, 82.

106 Xia. T., Li. N., Nel. A. E., *Annu Rev Public Health*, **2009**, *30*, 137.

107 Jones. C. F., Grainger. D. W., *Adv Drug Delivery Rev*, **2009**, *61*, 438.

108 Oerlemans. C., Bult. W., Bos. M., Storm. G., *Pharm Res*, **2010**, *27*, 2569.

109 Rosler. A., Vandermeulen. G. W. M., Klock. H., *Adv Drug Deliver Rev*, **2012**, *64*, 270.

110 Tao. L., Uhrich. K. E., *J Colloid Interf Sci*, **2004**, *298*, 102.

111 Thurmond. K. B., Kowalewski. T., Wooley. K. L., *J Am Chem Soc,* **1996**, *118*, 7239.

112 O'Reilly. R. K., Joralemon. M. J., Wooley. K. L., Hawker. C. J., *Chem Mater*, **2005**, *17*, 5976.

113 Bontha. S., Kabanov. A. V., Bronich. T. K., *J Control Release*, **2006**, *114*, 163.

114 Yang,.Z., Zheng. S., Harrison. W. J., Harder. J., Wen. X., Gelovan., J. G., Qiao. A., Li. C., *Biomacromolecules*, **2007**, *8*, 3422.

115 Huang. H., Hoogenboom. R., Leenen. M. A. M., Guillet. P., Jonas. A. M., Schubert. U. S., Gohy. J. F., *J Am Chem Soc*, **2006**, *128*, 3784.

116 Chan. Y., Wong. T., Byrne. F., Kavallaris. M., Bulmus. V., *Biomacromolecules*, **2008**, *9*, 1826.

117 Mason. T. G., Graves. S. M., Wilking. J. N., Lin. M. Y., *Condens Matter Phys*, **2006**, *9*, (*45*), 193.

118 Bibette. J., Leal-Calderon.F., Poulin. P., *Rep Prog Phys*, **1999**, *62*, 969.

119 D. Myers, *Surfaces, Interfaces and Colloids*, Wiley, New York, 2nd ed, **1999**, ch. 3, pp. 21-40.

120 Chhabra. G., Chuttanik. K., Mishra. A .K., Pathak. K., *Drug Dev Ind Pharm*, **2011**, *37*, 907.

121 Kim. S. W., Bae. Y. H., Okano. T., *Pharm Res*, **1992**, *9*, (*3*), 283.

122 Ricciardi. R., Gaillet. C., Ducouret. G., Lafuma. F., Laupretre. F., *Polymer*, **2003**, *44*, (*11*), 3375.

123 Kurisawa. M., Chung. J. E., Yang. Y. Y., Gao. S. J., Uyama. H., *Chem Commun*, **2005**, *34*, 4312.

124 Ying. L., Sun. J. A., Jiang. G. Q., Jia. Z., Ding. F. X. *Chinese J Chem Eng*, **2007**, *15*, (*4*), 566.

125 Lim. D. W., Nettles. D. L., Setton. L. A., Chilkoti. A., *Biomacromolecules*, **2007**, *8*, (*5*), 1463.

126 Chen. P., *Colloid Surface A*, **2005**, *261*, 3.

127 Hoare. T. R., Kohane. D. S., *Polymer*, **2008**, *49*, 1997.

128 Gupta. P., Vermani. K., Garg. S., *Drug Discov Today*, **2002**, *7*, 569.

129 J. W. Vanderhoff, M. S. El Aasser, and J. Ugelstad., US Pat, 4177177, **1979**.

130 Allémann. E., Gurny. R., Doelker. E., *Eur J Pharm Biopharm*, **1993**, *39*, 1732.

131 Avgoustakis. K., *Curr Drug Deliv*, **2004**, *1*, (*4*), 321.

132 Ibrahim. H., Bindschaedler. C., Doelker. E., Buri. P, Gurny. R., *Int J Pharm*, **1992**, *87*, 239.

133 Fessi. H., Puisieux. F., Devissaguet. J. P., Ammoury. N., Benita. S., *Int J Pharm*, **1989**, *55*, RI-R4.

134 Schubert. S., Delaney. J. T., Schubert. U. S., *Soft Matter*, **2011**, *7*, 1581.

135 Bilati. U., Allemann. E., Doelker. E., *Eur J Pharm Sci*, **2005**, *24*, 67.

136 Cheng. J., Teply. B. A., Sherifi. I., Sung. J., Luther. G., Gu. F. X., Levy-Nissenbaum. E., Radovic-Moreno. A. F., Langer. R., Farokhzad. O. C., *Biomaterials*, **2007**, *28*, (*5*), 869.

137 Valencia. P. M., Hanewich-Hollatz. M. H., Gao. W., Karim. F., Langer. R., Karnik. R., Farokhzad. O. C., *Biomaterials*, **2011**, *32*, (*26*), 6226.

138 Zhang. Z., Feng. S., *Biomacromolecules*, **2006**, *7*, 1139.

139 Karnik. R., Gu. F., Basto. P., Cannizzaro. C., Dean. L., Kyei-Manu. W., Langer. R., Farokhzad. O. C., *Nano Lett*, **2008**, *8*, 2906.

140 Hirao. A., Inushima. R., T. Nakayama., Watanabe. T., Yoo. H., Ishizone. T, Sugiyama. K., Kakuchi. T., Carlotti. S., Deffieux. A., *Eur Polym J*, **2011**, *47*, 713.

141 Determana. M. D., Coxa. J. P., Seifert. S., Thiyagarajanc. P., Mallapragadaa. S. K., *Polymer*, **2005**, *46*, 6933.

142 Hawker. C. J., Fréchet. J. M. J., *J Am Chem Soc*, **1990**, *112*, 7638.

143 Tomalia. D. A., Baker. H., Dewald. J., Hall. M., Kallos. G., Martin. S., Roeck. J., Ryder. J., Smith. P., *Polym J*, **1985**, *17*, 117.

144 Svenson. S., Tomalia. D. A., *Adv Drug Deliver Rev*, **2012**, *64*, 102.

145 Dykes. G. M., *J Chem Technol Biotechnol*, **2001**, *76*, 903.

146 Frauenrath. H., *Prog Polym Sci*, **2005**, *30*, 325.

147 Carlmark. A., Hawker. C., Hult. A., Malkoch. M., *Chem Soc Rev*, **2009**, *38*, 352.

148 Gillies. E. R., Fréchet. J. M. J., *J Org Chem*, **2004**, *69*, 46.

149 Lee. C. C., Gillies. E. R., Fox. M. E., Guillaudeu. S. J., Fréchet. J. M. J., Dy. E. E., Szoka. F. C., *Proc Natl Acad Sci USA*, **2006**, *103*, (*45*), 16649.

150 Hunter. W. H., Woolet. G. H., *J Am Chem Soc*, **1974**, *39*, 65.

151 Miravet. J. F., Fréchet. J. M. J., *Macromolecules*, **1998**, *31*, 3461.

152 Voit. B. I., Lederer. A., *Chem Rev*, **2009**, *109*, 5924.

153 McKee. M. G., Unal. S., Wilkes. G. l., Long. T. E., *Prog Polym Sci*, **2005**, *30*, 507.

154 Gao. C., Yan. D., *Prog Polym Sci*, **2004**, *29*, 183.

155 Monticelli. O., Mariani. A., Voit. B., Komber. H., Mendichi. R., Pitto. V., Tabuani. D., Russo. S., *High Perform Polym*, **2001**, *13*, 45.

156 Chen. S., Zhang. X. Z., Cheng. S. X., Zhuo. R. X., Gu. Z. W., *Biomacromolecules*, **2008**, *9*, 2578.

157 Prabaharan. M., Grailer. J. J., Pilla. S., Steeber. D. A., Gong. S., *Biomaterials*, **2009**, *30*, 3009.

158 Hawker. C. J., Fréchet. J. M. J., Grubbs. R. B., Dao. J., *J Am Chem Soc*, **1995**, *117*, 10763.

159 Sheppard. C. S., Kamath. V. R., *Polym Eng Sci*, **1979**, *19*, (*9*), 597.

160 Engel. P. S., *Chem. Rev*, **1980**, *80*, 99.

161 J. Chiefari and E. Rizzardo, *Handbook of Radical Polymerization*, ed. K. Matyjaszewski and T. P. Davis, John Wiley and Sons Inc, Hoboken, 2002, ch. 12, pp 629-691.

162 Pryor. W. A., Lasswell. L. D., *Adv Free Radical Chem*, **1975**, *5*, 27.

163 Scheren. P. A. G. M., Russell. G. T., Sangster., D. F.,Gilbert. R. G., German. A. L., *Macromolecules*, **1995**, *28*, 3637.

164 S. Guo., W. Wan., C. Chen., W. H. Chen., *J Therm Anal Calorim*, **2013**, 1.

165 Mayo. F. R., *J Am Chem Soc*, **1943**, *65*, 2324.

166 Ici. (1967). *Synthetic Polymers*, UK Patent, GB1096912.

167 A. Ueda., S. Nagai., *J Polym Sci Part A Polym Chem*, **1986**, *24*, 405.

168 O'Brien. N., McKee. A., Sherrington. D. C., Slark. A.T., Titterton. A., *Polymer*, **2000**, *41*, 6027.

169 Slark. A. T., Sherrington. D. C., Titterton. A., Martin. I. K., *J Mater Chem*, **2003**, *13*, 2711.

170 Isaure. F., Cormack. P. A. G., Sherrington. D. C., *Macromolecules*, **2004**, *37*, 2096.

171 Weaver. J. V. M., Williams. R. T., Royles. B. J. L., Findlay. P. H., Cooper. A. I., Rannard. S. P., *Soft Matter*, **2008**, *4*, 985.

172 Szwarc. M., *Nature*, **1956**, *178*, 1168.

173 Jagur-Grodzinski. J., *J Polym Sci A1*, **2002**, *40*, 2116.

174 Knauss. D. M., Al-Muallem. H. A., Huang. T., Wu. D. T., *Macromolecules*, **2000,** *33*, 3557.

175 Higashihara. T., Nagura. M., Inoue. K., Haraguchi. N., Hirao. A., *Macromolecules*, **2005,** *38*, 4577.

176 Li. Z., Kesselman. E., Talmon. Y., Hillmyer. M. A., Lodge. T. P., *Science*, **2004**, *306*, 98.

177 Li. Z., Hillmyer. M. A., Lodge. T. P., *Langmuir*, **2006**, *22*, 9409.

178 Georges. M. K., Veregin. R. P. N., Kazmaier. P. M., Hamer. G. K., *Macromolecules*, **1993**, *26*, 2987.

179 Griffiths. P. G., Rizzardo. E., Solomon. D. H., *Tetrahedron Lett*, **1982**, *23*, 1309.

180 Georges. M. K., Veregin. R. P. N., Hamer. G. K., Kazmaier. P. M., *Macromol Symp*, **1994**, *88*, 89,

181 Jousset. S., Hammouch. S. O., Catala. J. M., *Macromolecules*, **1997**, *30*, 6685.

182 Benoit. D., Chaplinski. V., Braslau. R., Hawker. C. J., *J Am Chem Soc*, **1999**, *121*, 3904.

183 Steenbock. M., Klapper. M., Mullen. K., Pinhal. N., Hubrich. M., *Acta Polym*, **1996**, *47*, 276.

184 Ide. N., Fukuda. T., *Macromolecules*, **1999**, *32*, 95.

185 Nicolas. J., Couvreur. P., Charleux. B., *Macromolecules*, **2008**, *41*, 3758.

186 Chiefari. J., Chong. Y. K., Ercole. F., Krstina. J. Jeffery. J., Le. T. P. T., Mayadunne. R. T. A., Meijs. G. F., Moad. C. L., Moad. G., Rizzardo. E., Thang. S. H., *Macromolecules*, **1998,** *31*, 5559.

187 Moad. G., Mayadunne. R. T. A., Rizzardo. E., Skidmore. M., Thang. S. H., *Macromol Symp*, **2003**, *192*, 1.

188 Moad. G., Rizzardo. E., Thang. S. H., *Aust J Chem*, **2005**, *58*, 379.

189 Ladaviere. C., Dorr. N., Claverie. J. P., *Macromolecules*, **2001**, *34*, 5370.

190 Charmot. D., Corpart. P., Adam. H., Zard. S. Z., Biadatti. T., Bouhadir. G., *Macromol Symp*, **2000** *150*, 23.

191 Moad. G., Rizzardo. E., Thang. S. H., *Aust J Chem*, **2009**, *62*, 1402.

192 Moad. G., Chong. Y. K., Postma.A., Rizzardo. E., Thang. S. H., *Polymer*, **2005**, *46*, 8458.

193 de Brouwer. H., Schellekends. M. A. J., Klumperman. B., German. A. C., *J Polym Sci Part A: Polym Chem*, **2000**, *35*, 3596.

194 Du Pont, Commw Scient Ind Res Org, (1999). *Polymerisation process with living characteristics and polymers made therfrom*, Int. Patent, WO9931144.

195 Chong. B. Y. K., Le. T. P. T., Moad. G., Rizzardo. T., Thang. S. H., *Macromolecules*, **1999**, *32*, 207.

196 Wang. Z.,He. J., Tao. Y., Yang. L., Jiang. H., Yang. Y., *Macromolecules*, **2003**, *36*, 7446.

197 Liu. B., Kazlauciunas. A., Guthrie. J. T., Perrier. S., *Macromolecules*, **2005**, *38*, 2131.

198 Zhu. J. L., Cheng. H., Jin. Y., Cheng. S. X., Zhang. X. Z., Zhuo. R. X., *J Mater Chem*, **2008**, *18*, 4433.

199 Zhang. L., Nguyen. T. L. U., Bernard. J., Davis, T. P., Barner-Kowollik. C., Stenzel. M. H., *Biomacromolecules*, **2007**, *8*, 2890.

200 Rossi. N. A. A., Mustafa. I., Jackson. J. K., Burt. H. M., Horte. S. A., Scott. M. D., Kizhakkedathu. J. N., Biomaterials, **2009**, *30*, 638.

201 York. A. W., Kirkland. S. E., McCormick. C. L., *Adv Drug Deliver Rev*, **2008**, *60*, 1018.

202 Stenzel. M. H., *Chem Commun*, **2008**, *30*, 3486.

203 Li. Y. T., Lokitz. B. S., Armes. S. P., McCormick. C. L., *Macromolecules*, **2006**, *39*, 2726.

204 Jia. Z. F., Wong L. J., Davis. T. P., Bulmus. V., *Biomacromolecules*, **2008**, *9*, 3106.

205 Akimoto. J., Nakayama. M., Sakai. K., Okano. T., *J Polym Sci Part A: Polym Chem*, **2008**, *46*, 7127.

206 Chan. Y., Bulmus. V., Zareie. M. H., Byrne. F. L., Barner. L., Kavallaris. M., *J Control Release*, **2006**, *115*, 197.

207 Kirkland. S. E., Hensarling. R. M., McConaughy. S. D., Guo. Y., Jarrett. W. L., McCormick. C. L., *Biomacromolecules* **2008**, *9*, 481.

208 Li. X., Wang. X., Koseki. H., *J Hazard Mater*, **2008**, *159*, (*1*), 13.

209 Sawamoto. M., Kamigaito. M., *Trends Polym Sci*, **1996,** *4*, 371.

210 Wang. J. S., Matyjaszewski. K., *J Am Chem Soc*, **1995,** *117*, 5614.

211 Qiu. J., Gaynor. S., Matyjaszewski. K., *Macromolecules*, **1999**, *32*, 2872.

212 Matyjaszewski. K., Qiu. J., Tsarevsky. N. V., Charleux. B., *J Polym Sci Part A: Polym Chem*, **2000**, *38*, 4724.

213 Xia. J., Johnson. T., Gaynor. S., Matyjaszewski. K., DeSimone. J., *Macromolecules*, **1999**, *32*, 4802.

214 Wan. X., Ying. S., *J Appl Polym Sci*, **2000**, *75*, 802.

215 Davis. K. A., Matyjaszewski. K., *Polym Prepr*, **1999**, *40*, 430.

216 Paik. H. J., Matyjaszewski. K.., *Polym Prepr*, **1996**, *37*, 274.

217 Jewrajka. S. K., Mandal. B. M., *J Polym Sci Part A: Polym Chem*, **2004**, *42*, 2483.

218 Masci. G., Giacomelli. L., Crescenzi. V., *Macromol Rapid Comm*, **2004**, *25*, 559.

219 Shen. Y. Q., Zhu. S. P., Zeng. F. Q., Pelton. R., *Macromolecules*, **2000,** *33*, 5399.

220 Zhang. X., Xia. J. H., Matyjaszewski. K., *Macromolecules*, **1998**, *31*, 5167.

221 Matyjaszewski. K., Jo. S. M., Paik. H. J., Gaynor. S. G., *Macromolecules*, **1997,** *30*, 6398.

222 McDonald. S., Rannard. S. P., *Macromolecules*, **2001**, *34*, 8600.

223 Gaynor. S., Qiu. J., Matyjaszewski. K., *Macromolecules*, **1998**, *31*, 5951.

224 Demonceau. S. A., Noels. A. F., *Angew Chem Int Ed Engl*, **1999**, *38*, 538.

225 Beers. K. L.,Boo. S., Gaynor. S. G., Matyjaszewski. K., *Macromolecules*, **1999**, *32*, 5772.

226 Wang. S. X., Armes. S. P., *Macromolecules*, **2000**, *33*, 6640.

227 Hutchinson. R. A., Beuermann. S., Jackson. C., *Macromolecules*, **1998**, *31*, 1542.

228 Chen. J. M., Yang. Y. L., *Spectrosc Spectral Anal*, **2001**, *21*, 47.

229 Save. M., Weaver. J. V. M., Armes. S. P., *Macromolecules*, **2002**, *35*, 1152.

230 Long. M., Thornwaite. D. W., Rogers. S. H., Bonzi. G., Livens. F. R., Rannard. S. P., *Chem Commun*, **2009**, *42*, 6406.

231 Wu. T., Mei. Y., Cabral. J. T., Xu. C., Beers. K. L., *J Am Chem Soc*, **2004**, *126*, 9880.

232 Uegaki. H., Kotani. Y., Kamigaito. M., Sawamoto. M., *Macromolecules*, **1997**, *30*, 2249.

233 Kotani. Y., Kamigaito. M., Sawamoto. M., *Macromolecules*, **2000**, *33*, 6746.

234 Brandts. J. A. M., van de Geijn. P., van Faassen. E. E., Boersma. J., Van Koten. G., *J Organomet Chem*, **1999**, *584*, 246.

235 Lecomte. P., Drapier. I., Dubois. P., Teyssie. P., Jerome. R., *Macromolecules*, **1997**, *30*, 7631.

236 Matyjaszewski. K., Wei. M. L., Xia. J. H., McDermott. N. E., *Macromolecules*, **1997**, *30*, 8161.

237 K. Matyjaszewski and J. Xia, *Handbook of Radical Polymerization*, ed. K. Matyjaszewski and T. P. Davis, John Wiley and Sons Inc, Hoboken, 2002, ch. 11, pp 523-629.

238 Matyjaszewski.K., Shipp. D. A., Wang. J. L., Grimaud. T., Patten. T. E., *Macromolecules*, **1998**, *1*, 6836.

239 Xia. J., Zhang. X., Matyjaszewski. K., *ACS Symp Ser*, **2000**, *760*, 207.

240 Ando. T., Kamigaito. M., Sawamoto. M., *Tetrahedron*, **1997**, *53*, 15445.

241 Jankova. K., Chen. X. Y., Kops. J., Batsberg. W. *Macromolecules*, **1998**, *31*, 538.

242 Hansen. N. M. L., Haddleton. D. M., Hvilsted. S., *J Polym Sci Part A: Polym Chem*, **2007**, *45*, 5770.

243 Vargün. E., Usanmaz. A., *J Polym Sci Part A: Polym Chem*, **2005**, *43*, 3957.

244 Haddleton. D. M., Waterson. C., Derrick. P. J., Jasieczek. C. B., Shooter. A. J., *Chem Commun*, **1997**, 683.

245 Haddleton. D. M., Perrier. S., Bon. S. A. F., *Macromolecules*, **2000**, *33*, 8246.

246 Monge. S., Darcos., V., Haddleton. D. M., *J Polym Sci Part A: Polym Chem*, **2004**, *42*, 6299.

247 Iovu. M., Maithufi. N., Mapolie. S., *Macromol Symp*, **2003**, *193*, 209.

248 Moineau. G., Granel. C., Dubois. P., Jerome. R., Teyssie. P., *Macromolecules*, **1998**, *31*, 542.

249 Davis. K. A., Matyjaszewski. K., *Chinese J Polym Sci*, **2004**, *22*, 195.

250 Coca. S., Jasieczek. C. B., Beers. K. L., Matyjaszewski. K., *J Polym Sci Part A: Polym Chem*, **1998**, *36*, 1417.

251 Wang. X. S., Lascelles. S. F., Jackson. R. A., Armes. S. P., *Chem Commun*, **1999**, 817.

252 Perrier. S., Armes. S. P., Wang. X. S., Malet. F., Haddleton. D. M., *J Polym Sci Part A: Polym Chem*, **2001**, *39*, 1696.

253 Mao. B., Gan. L. H., Gan. Y. Y., Li. X., Ravi. P., Tam. K. C., *J Polym Sci Part A: Polym Chem*, **2004**, *42*, 5161.

254 Malet. F. L. G., Billingham. N. C., Armes. S. P., *Polym Prepr*, **2000**, *41*, 1811.

255 Percec. V., Barboiu. B., Neumann. A., *Macromolecules*, **1996**, *29*, 3665.

256 Darcos. V., Haddleton. D. M., *Eur Polym J*, **2003**, *39*, 855.

257 Ma. Y. H., Tang. Y. Q., Billingham. N. C., Armes. S. P., Lewis. A. L., Lloyd. A. W., Salvage. J. P., *Macromolecules*, **2003**, *36*, 3475.

258 Boyer, C., Soeriyadi. A. H., Zetterlund. P. B., Whittaker. M. R., *Macromolecules*, **2011**, *44*, 8028.

259 Li. J., Xiao, H., Kim. Y. S., Lowe. T. L., *J Polym Sci Part A: Polym Chem*, **2005**, *43*, 6345.

260 Matyjaszewski. K., Miller. P. J., Pyun. J., Kickelbick. G., Diamanti, S., *Macromolecules*, **1999**, *32*, 6526.

261 Zhang. X., Xia. J., Matyjaszewski. K., *Macromolecules*, **2000**, *33*, 2340.

262 Brandts. J. A. M., van de Geijn. P., van Faassen. E. E., Boersma. J., Van Koten. G., *J Organomet Chem*, **1999**, *584*, 246.

263 Borner. H. G., Beers. K., Matyjaszewski. K., Sheiko. S. S., Moller. M., *Macromolecules*, **2001**, *34*, 4375.

264 Neugebauer. D., Zhang. Y., Pakula. T., Sheiko. S. S., Matyjaszewski. K., *Macromolecules*, **2003**, *36*, 6746.

265 Yamada. K., Miyazaki. M., Ohno. K., Fukuda. T., Minoda. M., *Macromolecules*, **1999**, *32*, 290.

266 Fréchet. J. M. J., Henmi. M., Gitsov. I., Aoshima. S., Leduc. M. R., Grubbs. R.B., *Science*, **1995**, *269*, 1080.

267 Wang. A. R., Zhu. S., *Polym Eng Sci*, **2005**, *45*, (*5*), 720.

268 Wang. A. R., Zhu. S., *J Polym Sci A1*, **2005**, *43*, 5710.

269 Li. W., Yoon. J. A, Zhong. M.,Matyjaszewski. K., *Macromolecules*, **2011**, *44*, 3270.

270 Bannister. I., Billingham. N. C., Armes. S. P., *Soft Matter*, **2009**, *5*, 3495.

271 Wanga. D., Tana. J., Kanga. H., Maa. L., Jin. X., Liua. R., Huanga. Y.,*Carbohyd Polym*, **2001**, *84*, 195.

272 Licciardi. M., Giammona. G., Du. J., Armes. S. P., Tang. Y., Lewis. A. L., *Polymer*, **2006**, *47*, 2955.

# 2. Experimental Section

## 2.1 Materials used during this study.

Hydroxypropyl methacrylate (HPMA) 97 %, ethylene glycol dimethacrylate 98 % (EGDMA), ethyl α-bromoisobutyrate (EBiB) 98 %, α-bromoisobutyryl bromide 98 %, methoxypolyethylene glycol average mol wt 750, 2000, 5000 g $mol^{-1}$, Cu(I)Cl >99 %, 2,2,'-bipyridyl >99 %, aluminium oxide (activated, basic), Dowex Marathon exchange resin, Celite, Oil Red O, ibuprofen >98 %, pyrene > 99 %, 4-(dimethylamino) pyridine >98 %, triethylamine (TEA) >99 %, Amberlyst resin, anisole (anhydrous) 99.7 %, methanol (HPLC grade), tetrahydrofuran (HPLC grade), *n*-hexane, acetone (HPLC grade), toluene (anhydrous), dialysis tubing (benzoylated) molecular weight cut off = 2000 g $mol^{-1}$, Whatman 200 nm PTFE syringe filters were all purchased from Sigma-Aldrich and used without any further purification.

$CDCl_3$ and $d_6$-DMSO solvents were purchased from GOSS Scientific. Lopinavir was purchased from LGM Pharmaecuticals (Chicago).

## 2.2 Equipment utilised during the characterisation of linear and branched polymers and nanoparticles formed from the polymers

### 2.2.1 $^1$H NMR Spectroscopy

$^1$H NMR spectra were recorded in either DMSO-$d_6$, $CDCl_3$ or $D_2O$ using a 400 MHz Brüker Avance spectrometer. Chemical shifts (δ) are reported in parts per million (ppm) with respect to an internal reference of tetramethylsilane.

NMR spectroscopy can be used to calculate $M_n$ values using end-group analysis where a clear resonance from the polymer chain end-group is necessary. By

comparing the strength of end-group signals to signals originating from the polymer backbone, the ratio of end group: repeat unit can be calculated, ($DP_n$). Samples were prepared by dissolving approximately 0.05 g of product in 1-2 mL of solvent.

This method is subject to inaccuracy, especially as chain length increases and the end-group signal becomes weaker. For copolymers, the solvent also has a great influence, where solubility of copolymer components may be different. However, with appropriate solvent choice, end-group analysis can be a useful technique allowing determination of composition and $M_n$ of complex structures such.

### 2.2.2 Gel Permeation Chromatography

Triple detection gel permeation chromatography (GPC) (either HPLC grade tetrahydrofuran (THF) stabilized with 2,6-di-*tert*-butyl-4-methylphenol, or HPLC grade acetone eluent) with a flow rate of 1 mL $min^{-1}$ was performed using a Malvern Viscotek 270 Max instrument using T6000M x's 2 + guard column set. All samples were dissolved at 5 mg $mL^{-1}$ and passed through a 200 nm syringe filter prior to injection (100µL) with a run time of 60 minutes.

GPC (also known as size exclusion chromatography) analysis relies on different hydrodynamic sizes of polymer molecules in solution which are separated. Columns are packed with porous beads, and dilute samples of polymer are injected into these columns. Depending on polymer sizes in solution, chains are able to penetrate the beads and are eventually eluted. Larger polymer chains are less able to diffuse through pores than small chains, therefore they pass through columns faster. The smallest polymer molecules will penetrate the most pores, and are therefore eluted at longer retention times. Detector signals are plotted against elution volume or time. Elution volume for a given molecule is given by: $V_e = V_0 + K_e V_i$, where $V_e$ is elution

volume, $V_0$ is void volume; i.e. the volume between the beads. $V_i$ is the internal volume (i.e. the volume inside porous beads) and $K_e$ is a coefficient defined by the partition of the polymer molecules between voids and the beads. If all chains are large chains are excluded from all bead pores, $K_e = 0$ and $V_e = V_0$. If all chains are very small and penetrate all bead pores, $K_e = 1$ and $V_e = V_0 + V_i$. For a polymer sample to be separated, elution volume must lie between the limits i.e. $V_i < V_e < V_0 + V_i$.

Triple detection GPC uses a concentration detector (refractive index detector (RI)) which is based on deflection of light passing through a dual component flow cell (one containing a reference solvent and the other containing solvent and sample). The difference in refractive index can be used to determine sample concentration with respect to time during polymer separation; plotted as a detector response *vs.* elution volume (or time). For light scattering detectors to determine molecular weight, they use the Rayleigh Equation:

$$R\theta\Big|_{\theta \to 0} \simeq KCM$$

Where the intensity of scattered light is equal to an optical constant (K) multiplied by concentration (C) and molecular weight (M). To record the intensity of scattered light the measuring angle must be 0°; since this is not possible, angles close to 0° are used. Low angle light scattering is performed at angles typically >10 °. Right angle light scattering data (at 90°) is used in conjunction to viscosity measurements to correct the angle back to 0°. The viscometer measures intrinsic viscosity of samples, which may allow determination of molecular size.

### 2.2.3 Dynamic light scattering (DLS)

DLS studies of nanoparticle dispersions were performed using a Malvern Zetasizer Nano ZS equipped with a 4 mW He–Ne, 633 nm at a temperature of 25 °C and using plastic disposable cuvettes for aqueous dispersions. Glass cuvettes were used for solutions containing organic solvents. Malvern Zetasizer software version 6.20 was used for data analysis using the instruments automatic optimisation settings. It should be noted that measurements were taken directly from the nanoparticle dispersions without any additional filtration or centrifugation.

#### 2.2.3.1 Zeta potential measurements

Carried out at 1 mg $mL^{-1}$, at 25 °C, pH of 6.5, using disposable capillary zeta cells; measurements were obtained using the instruments automatic optimisation settings.

### 2.2.4 Scanning Electron Microscopy (SEM)

SEM images were recorded using a Hitachi S-4800 FE-SEM at 3 kV. Aqueous nanoparticle solutions (50 mL, containing approximately 0.1 mg $mL^{-1}$ polymer) were pipetted onto aluminium stubs. Clinical tissue was used to lightly dab the solution and the stubs were left to dry for approximately 3 hours. The dry samples were gold coated for 2 minutes at 15 mA using a sputter-coater (EMITECH K550X) prior to imaging.

## 2.3 Synthesis and Characterisation of linear and branched *p*(HPMA) by Ambient Temperature Methanolic ATRP

### 2.3.1 ATRP polymerisation of linear and branched *p*(HPMA$_x$) initiated by EBiB ATRP polymerisation of linear and branched *p*(HPMA$_x$) initiated by EBiB

For a typical ATRP homopolymerisation of linear *p*(HPMA) (target DP$_n$ = 50 monomer units), HPMA (7.39 g, 51.26 mmol), EBiB (0.2 g, 1.03 mmol) plus anisole as an internal standard (20 w/v % based on HPMA feed) were added to a 100 mL round-bottomed flask fitted with a magnetic stirrer bar. Methanol (HPLC grade) (50 v/v % based on HPMA feed) were then added and the solution was degassed with a nitrogen purge for approximately 10 minutes whilst stirring. Following this, Cu(I)Cl (0.10 g, 1.03 mmol) and BPY (0.33 g, 2.10 mmol) were weighed together and quickly added to the stirring solution whilst maintaining a positive nitrogen flow. After initiation, the nitrogen flow was removed and the flask was made air-tight using parafilm. The solution was allowed to polymerise at ambient temperature. After approximately > 99 % conversion which was judged by $^1$H NMR spectroscopy, when detectable vinyl signals could not be distinguished from the baseline. The reactions were exposed to the atmosphere and manually terminated *via* THF addition (approximately 200 mL). Once fully terminated, Dowex Marathon exchange beads (~ 10 g) were added to the solution (with stirring) for approximately 20 minutes, in order to remove the catalyst. The beads were filtered off using a Buchner funnel and the remaining solution was passed over a basic alumina column to remove residual catalyst/ligand. The mixture was concentrated under vacuum which removed the majority of THF and the viscous solution was precipitated into cold hexane and filtered to yield white powders. For *p*((HPMA$_{50}$)-*co*-EGDMA$_{0.95}$), EGDMA (0.193 g, 0.98 mmol) was added to reaction mixtures alongside monomer, where

copolymerisations were carried out using identical protocol as described in this section.

### 2.3.2 Kinetic Studies for ATRP linear and branched polymerisation of *p*(HPMA)

For kinetic studies, identical protocol was followed in addition to regular sampling *via* removal of ~0.5 mL of the solution where a nitrogen purge was applied. A small amount of this was added to ~ 1 mL of $d_6$-DMSO for $^1$H NMR spectroscopic analysis. The remaining sample was diluted into THF (~ 5 mL) and shaken to ensure efficient termination followed by passing over a small basic alumina column and into a pre-weighed sample vial. THF was allowed to completely evaporate and the vial was then re-weighed and THF was added to achieve 5 mg $mL^{-1}$ solution for triple detection GPC analysis.

The copolymerisation of branched *p*(HPMA) and kinetic studies of branched *p*(HPMA) were performed using the same protocol that is described above. For a typical polymerisation (target $DP_n$ = 50 monomer units), HPMA (7.39 g, 51.26 mmol), EBiB (0.2 g, 1.03 mmol) and EGDMA (0.19 g, 0.97 mmol) plus anisole as an internal standard (20 w/v % based on HPMA feed) were utilised. This 1: 0.95 monomer : brancher ratio was used for all of the branching polymerisations.

### 2.3.3 ATRP Synthesis of *p*($HPMA_{30}$)-*b*-*p*($HPMA_{50}$)

For a typical ATRP chain extension polymerisation of *p*($HPMA_{30}$)-*b*-*p*($HPMA_{50}$), first block synthesis was performed as described for the homopolymerisation of *p*(HPMA). Briefly, for a target $DP_n$ = 30 monomer units (for first block), HPMA, (5.62 g, 39 mmol), EBiB (0.2 g, 1.03 mmol) plus anisole as an internal standard (20

w/v % based on HPMA feed) were added to a 100 mL round-bottomed flask fitted with a magnetic stirrer bar. Methanol (HPLC grade) (50 w/v % based on HPMA feed) were then added and the solution was degassed with a nitrogen purge for approximately 10 minutes whilst stirring. Following this, Cu(I)Cl (0.10 g, 1.03 mmol) and BPY (0.33 g, 2.10 mmol) were weighed together and quickly added to the stirring solution whilst maintaining a positive nitrogen flow. After initiation, the nitrogen flow was removed and the flask was made air-tight using parafilm. The solution was allowed to polymerise at ambient temperature. HPMA (7.39 g, 51.26 mmol) and methanol (HPLC grade) (50 w/v % based on monomer) were added to a glass vial (40 mL) and de-gassed separately. After approximately 85-95 % conversion, a positive nitrogen flow was re-introduced to the polymerisation pot, the HPMA/methanol solution was added rapidly to the polymerisation with vigorous stirring using a large (20 mL) glass syringe. Positive nitrogen flow was maintained for approximately 5 minutes before removal, and reaction was sealed with parafilm. The polymerisation was allowed to reach > 99 % conversion before manual termination.

### 2.3.4 ATRP self-block branched polymerisation of *p*($HPMA_{30}$)-*b*-*p*($HPMA_{50}$-$EGDMA_{0.95}$)

EBiB initiator (0.2 g, 1.03 mmol), HPMA (4.45 g, 30.9 mmol; target $DP_n$ = 30) and the internal standard anisole (20 % w/v based on monomer) were placed into a 100 mL round-bottomed flask fitted with a magnetic stirrer bar. Methanol (HPLC grade) was added (50 % w/v based on HPMA monomer) and the solution was stirred and degassed using a nitrogen purge for approximately 10 minutes. Cu(I)Cl (0.10 g, 1.03 mmol) and BPY (0.33 g, 2.10 mmol) were weighed together and promptly added to

the flask whilst still maintaining a positive nitrogen flow. The nitrogen flow was removed and reaction flask sealed leaving the mixture to polymerise at ambient temperature. After ~ 80 % conversion of the initial monomer feed (previous kinetic studies determined this approximate timing and sampling of the reaction at this time gave the exact conversion), HPMA (7.39 g, 51.26 mmol; target $DP_n$ = 50 monomer units), EGDMA (0.19 g, 0.97 mmol) and methanol (50 % v/v based on HPMA monomer) was degassed in a separate flask and quickly added to the reaction *via* a double-ended needle whilst maintaining a positive nitrogen flow to the reaction flask. The nitrogen purge was removed and the reaction was sealed and left to polymerise under ambient conditions only subjected to termination and purification after high conversion was reached. Samples were analysed as described above.

## 2.3.5 $^1$H NMR Spectroscopic analysis of EBiB initiated *p*(HPMA) synthesised using Ambient Temperature Methanolic ATRP

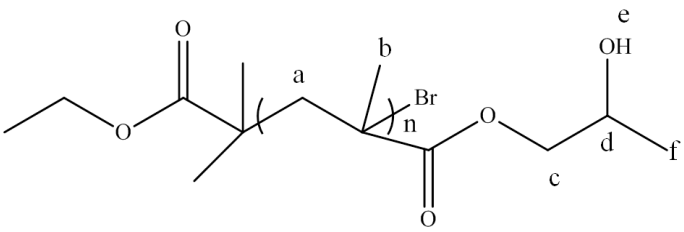


Figure 2.1: $^1$H NMR ($d_6$-DMSO - ppm) peak assignment for *p*(HPMA). 0.59-1.02 (b), 1.02-1.26 (f), 1.6-2.11 (a), 3.39-3.92 (c, d), 4.51-4.91 (e).

End group analysis could not be accurately performed due to overlap within polymer backbone signal (a) in Figure 2.1. In branched copolymer samples, proton signals in EGDMA were undetectable as the ratio of HPMA:EGDMA was extremely small and overlapped with (a) in spectra.

Monomer conversion was calculated by comparing peak integrals of an internal aromatic standard (see Figure 2.2) (anisole protons at 6.87–7.33 ppm; $d_6$-DMSO (a)) to those of the monomer vinyl signals (5.62–6.1 ppm; $d_6$-DMSO (b)).

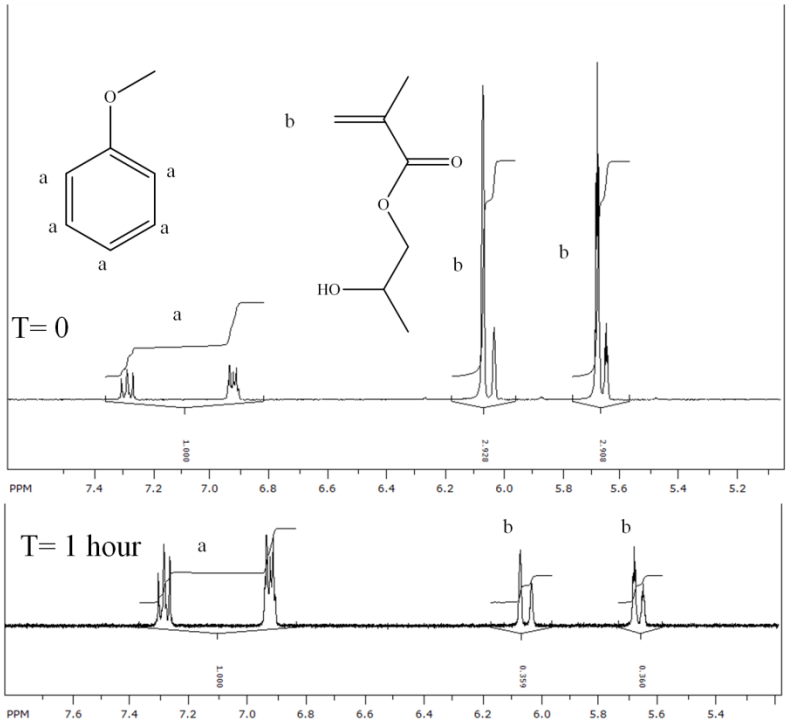


Figure 2.2: Calculation of monomer conversion using $^1$H NMR ($d_6$-DMSO).

Generating a ratio between (a) and (b) signals at T= 0 allows for calculation of monomer conversion by simply calculating percentage difference between vinyl signals as anisole signals remain unchanged throughout reactions.

## 2.3.6 Solubility testing of *p*(HPMA) oligomers

Saturated aqueous solutions of p(HPMA) (target $DP_n$ = 5, 7, 10, 13, 15, 17, 20, 50, 80 and 120 monomer units) were prepared by adding approximately 500 mg of each polymer to water (14 mL). Each sample was left to dissolve on a roller for three days at ambient temperature. After which each sample was left to stand for 2 hours, the supernatant (10 mL) was carefully pipetted into three pre-weighed aluminium dishes and left (covered) to evaporate for 1 week. After re-weighing, the subsequent

polymer mass was calculated and the saturated concentration was recorded as the average of the three samples. Saturated aqueous solutions of *p*(HPMA) with target $DP_n$ = 5, 7, 10, 13, 15, 17, 20, 50, 80 and 120 monomer units were generated by dissolving approximately 500 mg of each polymer in distilled water (14 mL) in glass vials (40 mL). Each sample was thoroughly sealed using parafilm and left to dissolve on a rolling machine at ambient temperature for three days. Sample vials were left to stand upright for 2 hours, the supernatant (10 mL) was carefully removed and pipetted into three pre-weighed aluminium dishes, which were covered with foil and small holes were added for evaporation. These were left at ambient temperature and water was allowed to evaporate for one week. The aluminium dishes were re-weighed and the polymer mass was calculated. The saturated concentration was recorded as the average of the three samples.

## 2.4 Synthesis and Characterisation of linear and branched PEG-*p*(HPMA) A-B block copolymers by Ambient Temperature Methanolic ATRP

### 2.4.1 PEG-Br Macroinitiator Synthesis

#### 2.4.1.1 Methods

A typical procedure for the preparation of methoxy-capped poly(ethylene glycol) initiator (PEG-Br) from a poly(ethylene glycol) mono-methyl ether (PEG-OH) with $M_n$ = 750 is outlined below.

PEG-OH $M_n$ = 750 (20 g, 26.6 mmol, 1 eq.), toluene (anhydrous) (150 mL), 4-Dimethylaminopyridine (DMAP) (0.32 g, 2.66 mmol, 0.1 eq.), and triethylamine (TEA) (4.08 mL, 2.96 g, 29.26 mmol, 1.1 eq.) were placed in a round-bottomed flask

fitted with a magnetic stirrer bar. 2-Bromoisobutyryl bromide (3.62 ml, 2.96 g, 29.26 mmol, 1.1 eq.) was added dropwise to the solution via a syringe over around one hour. The solution was stirred overnight, after which Amberlyst resin A21 (20 g) was added to remove residual acid bromide and the mixture stirred for about one hour. The solution was then filtered over celite to remove any insoluble materials. Solvent was removed under vacuum from the resulting clear pale yellow filtrate. The white oily product was dried at 60 °C in a vacuum oven overnight and stored at ~-2°C. The method was slightly altered for the preparation of the higher molecular weight initiators. Toluene was warmed to around 50 °C in order to dissolve the PEG-OH with molecular weights of 2000 g $mol^{-1}$ and 5000 g $mol^{-1}$. These products were purified by evaporation of the toluene to around a third of the original volume before precipitation into cold petroleum ether. The macroinitiator was collected on filter paper and dried under vacuum yielding white powdery products.

2.4.1.2 $^{1}$H NMR Spectroscopic analysis of $PEG_x$-Br macroinitiators.

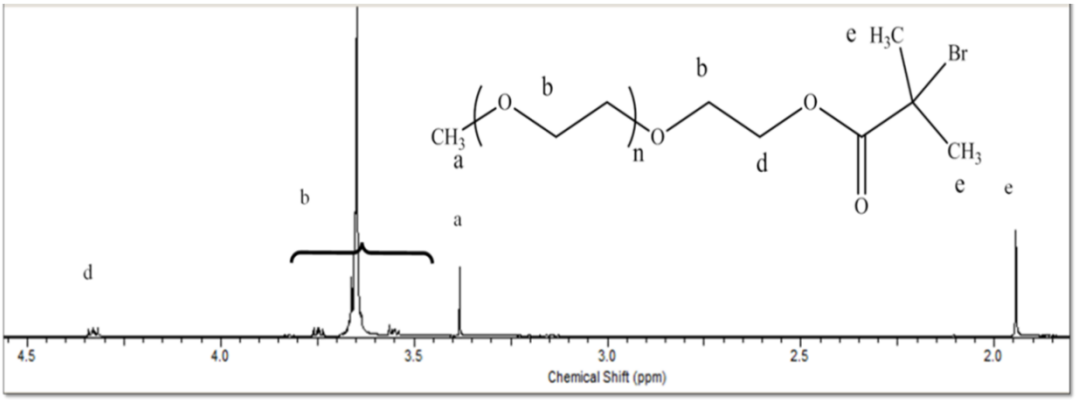


Figure 2.3: $^{1}$H NMR ($CDCl_3$ - ppm) analysis of a $PEG_x$-Br macroinitiator.

Peaks were assigned as follows: 1.94 (ester $CH_3$) (e), 3.38 (methoxy $CH_3$) (a), 3.50-3.80 (PEG $CH_2$) (b), 4.32 ($CH_2$-O-CO) (d).

Extent of esterification: The signal at 1.94 ppm can be attributed to the two

equivalent methyl groups of the tertiary bromide group. The signal at 4.33 ppm corresponds to the methylene adjacent to the ester group a ratio of the integrals of signals to the mono-methyl end-group indicated the extent of the esterification. $^{13}C$ NMR (100 MHz, $D_2O$) δ ppm 174.0, 71.5, 70.4, 70.1, 70.0, 68.8, 58.6, 30.5.

GPC (THF eluent): Initiators were diluted in THF or acetone (5 $mL^{-1}$) and passed through a 200 nm syringe filter prior to injection. $PEG_{17}$-Br could not be analysed by GPC, the elution time of this initiator was not within the detection limits of the separation columns.

## 2.4.2 ATRP polymerisation of linear and branched linear and branched $PEG_x$-*b*-*p*(HPMA) block copolymers

In a typical synthesis, $PEG_{117}$-Br initiator (0.94 g, 1.03 mmol) and HPMA (7.39 g, 51.26 mmol; target $DP_n$ = 50 monomer units, and anisole (20 % w/v based on monomer) were placed into a 100 mL round-bottomed flask. HPLC grade methanol was added (50 % w/v (initiator, monomer/solvent)) and the solution was stirred/deoxygenated using a nitrogen purge for 10 minutes. Cu(I)Cl (0.10 g,1.03 mmol) and BPY (0.19 g, 0.97 mmol) were added to the flask whilst maintaining a positive nitrogen flow. Samples of the reaction (~0.5 mL) were taken and diluted into THF for GPC analysis and $d_6$-DMSO for $^1H$ NMR spectroscopic analysis. End group analysis could be performed when utilising $PEG_{17}$, where integration of the methoxy chain end (3.2 ppm) and terminal methyl group of *p*(HPMA) (1 – 1.22 ppm), however, this was very inaccurate and unreliable, where the peak for water (~3.19 ppm) could shift, resulting in peak overlap. For copolymers with higher molecular weight PEG (2000 and 5000 g $mol^{-1}$) the methoxy chain end (3.2 ppm) could not be distinguished from the baseline, therefore end group analysis could not

be performed, For GPC analysis, HPLC grade THF as the eluent, stabilized with 2,6-ditert-butyl-4-methylphenol, with a flow rate of 1 mL $min^{-1}$. Samples for analysis of polymerisation kinetics were purified by passing over basic alumina column before removal of solvent. Dried samples were re-dissolved in THF to a concentration of 5 mg $mL^{-1}$ and passed through a syringe filter (0.2 mm) prior to injection.

2.4.2.1 $^{1}$H NMR Spectroscopic analysis of $PEG_x$-Br initiated *p*(HPMA)

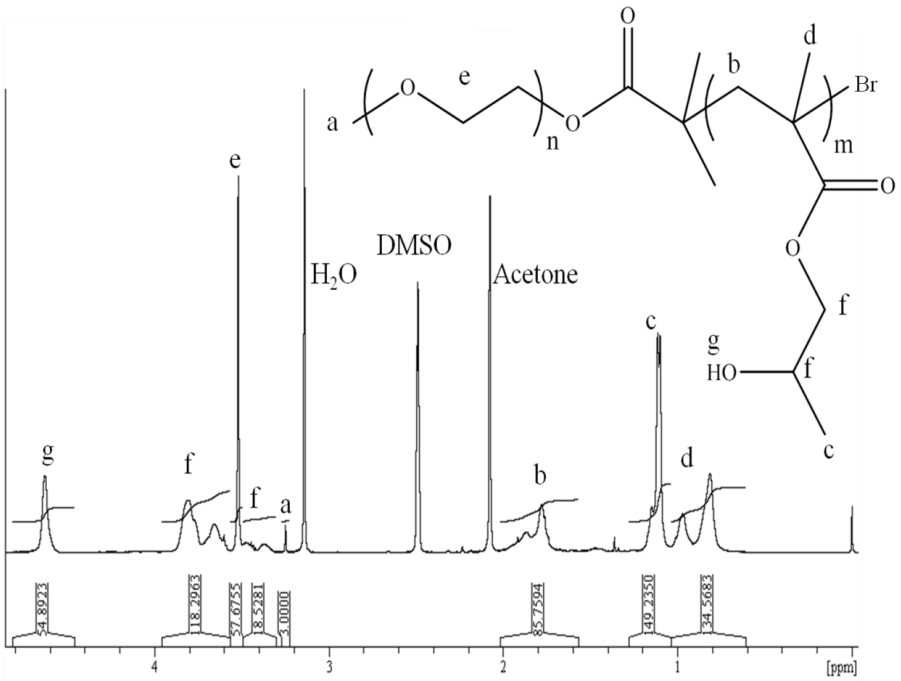


Figure 2.4: $^{1}$H NMR ($CDCl_3$ - ppm) analysis of $PEG_x$-Br initiated *p*(HPMA).

$PEG_{17}$-*b*-*p*($HPMA_{50}$): $^{1}$H NMR ($d_6$-DMSO - ppm): 0.65-1.02 (d), 1.02-1.26 (c), 1.64-2.01 (b), 3.22-3.26 (a), 3.3-3.5 (f), 3.49-3.54 (e), 3.56-3.87 (f), 4.53-4.71 (g).

End group analysis of $PEG_x$ copolymers to determine $DP_n$ could not be accurately performed due to overlap with water signals and (f) the small signal also deviated from the baseline when spectrum scaling was increased leading to inaccurate integration and therefore calculated $DP_n$. In branched copolymer samples, proton

signals in EGDMA were undetectable as the ratio of HPMA:EGDMA was extremely small and overlapped with (f) in spectra.

2.4.2.2 Kinetic Studies for ATRP linear and branched polymerisation of $PEG_x$-*b*-*p*(HPMA)

For kinetic studies, identical copolymerisation protocol was followed, in addition to regular sampling *via* removal of ~0.5 mL of the solution where a nitrogen purge was applied. A small amount of this was added to ~ 1 mL of $d_6$-DMSO for $^1$H NMR spectroscopic analysis. The remaining sample was diluted into THF (~ 5 mL) and shaken to ensure efficient termination followed by passing over a small basic alumina column and into a pre-weighed sample vial. THF was allowed to completely evaporate and the vial was then re-weighed and THF was added to achieve 5 mg $mL^{-1}$ solution for triple detection GPC analysis.

The copolymerisation of branched $PEG_x$-*b*-*p*(HPMA) and kinetic studies of branched *p*(HPMA) were performed using the same protocol that is described above. For a typical polymerisation (target $DP_n$ = 50 monomer units), HPMA (9.61 g, 66.5 mmol), $PEG_{17}Br$ (1 g, 1.33 mmol) and EGDMA (0.25 g, 1.26 mmol) plus anisole as an internal standard (20 w/v % based on HPMA feed) and methanol, 50 w/v % (initiator+monomer/methanol) were utilised. This 1: 0.95 monomer : brancher ratio was used for all of the branching polymerisations.

2.4.2.3 Chain Extension of $PEG_{17}$-*b*-*p*($HPMA_x$) Block Copolymer

A typical procedure for the chain extension of $PEG_{17}$-*b*-*p*($HPMA_{30}$) to $PEG_{17}$-*b*-*p*($HPMA_{30}$)-*b*-*p*($HPMA_{50}$) is outlined here. $PEG_{17}Br$ initiator (1 g, 1.33 mmol), HPMA (5.75 g, 39.9 mmol; target $DP_n$ = 30) and the internal standard anisole (20 %

w/v based on monomer) were placed into a 100 mL round-bottomed flask fitted with a magnetic stirrer bar. Methanol (HPLC grade) was added (50 % w/v based on initiator and monomer) and the solution was stirred and degassed using a nitrogen purge for approximately 10 minutes. Cu(I)Cl (0.13 g, 1.33 mmol) and BPY (0.52 g, 3.32 mmol) were weighed together and promptly added to the flask whilst still maintaining a positive nitrogen flow. The nitrogen flow was removed and reaction flask sealed leaving the mixture to polymerise at ambient temperature. After ~ 80 % conversion of the initial monomer feed (previous kinetic studies determined this approximate timing and sampling of the reaction at this time gave the exact conversion), HPMA (9.57 g, 66.5 mmol; target $DP_n$ = 50 monomer units) and methanol (50 % v/v based on HPMA monomer) was degassed in a separate flask and quickly added to the reaction *via* a double-ended needle whilst maintaining a positive nitrogen flow to the reaction flask. The nitrogen purge was removed and the reaction was sealed and left to polymerise under ambient conditions only subjected to termination and purification after high conversion was reached. Samples were analysed as described above.

## 2.5 Nanoparticle synthesis and Characterisation

### 2.5.1 Particle preparation by nanoprecipitation

#### 2.5.1.1 Rapid precipitation.

Polymer was dissolved in acetone overnight on a rolling machine in a sealed glass vial (made air-tight by parafilm) to give concentrations of 10, 5 or 1 mg $mL^{-1}$ (and others where indicated). To achieve a five-fold dilution, polymer+acetone (1 mL ) was added to distilled water (5 mL, 40 °C) using an adjustable pipette and left to stir overnight in a glass vial (12 mL) on a hotplate. Polymer+acetone volume was

adjusted, for example (0.8 mL) was added to water (5 mL) to give a dilution ratio of 0.8 mg $mL^{-1}$; the volume of water remained constant (5 mL) unless indicated.)

2.5.1.2 Slow/dropwise precipitation.

Polymer/acetone solutions were prepared to the concentrations and volumes as described above. A syringe pump operating at 0.1 mL $min^{-1}$ was employed to drip the polymer/acetone solution slowly into the stirring water vials (12 mL), these were left to stir overnight on a hotplate set to 40 °C.

2.5.1.3 Precipitation/dialysis.

Following the protocol of slowly dripping the polymer/acetone solution into the stirring water (as described above) the entire mixture of polymer/acetone/polymer was carefully poured into sections of dialysis tubing (2000 g $mol^{-1}$ molecular weight cut-off) and placed into large water filled beakers for 2 days where water was changed approximately every 8 hours. Nanosuspensions were carefully poured into glass vials for storage at room temperature (sealed).

2.5.1.4 Loaded nanoparticle Preparation

An example of a loaded nanoparticle preparation protocol is described here for the preparation of $PEG_{17}$-*b*-*p*((HPMA$_{50}$)-EGDMA$_{0.95}$)/Oil red nanoparticles using a copolymer starting concentration of 5 mg $mL^{-1}$ and a final concentration of 1 mg $mL^{-1}$ and an oil red starting concentration of 1 mg $mL^{-1}$ and a final concentration of 0.2 mg $mL^{-1}$. Polymer was dissolved in acetone overnight (total volume was variable, but was typically between 10 mL stock solutions were prepared) on a rolling machine in a sealed glass vial (made air-tight by parafilm) to achieve a

concentration of 5 mg $mL^{-1}$, oil red was carefully weighed out (2 mg) in a clean glass vial (12 mL) and the polymer+acetone solution was carefully added (2 mL). The vial was sealed and shaken until oil red has visually dissolved. 1 mL of this mixture was pipetted into warmed stirring water and left to evaporate. Although only 1 mL of the polymer/acetone/oil red solution was used for nanoprecipitation, a 2 mL solution was prepared to overcome error in pipetting accuracy.

## 2.5.2 Evaluation of nanoparticle stability

### 2.5.2.1 Sonication

A Covaris S2x acoustic homogenisation system was used to subject nanoparticle dispersions to high intensity focussed sonic waves (water-bath temperature controlled to 10 °C). Nanoparticle dispersions (1 mg $mL^{-1}$) were initially sized using DLS then transferred to a glass vial and submerged into the water bath (5 °C) of the sonicator. After 5 seconds using 100 % intensity and a duty cycle of 100, the solution was promptly re-analysed by DLS. The same sample was further sonicated and sized as reported above. As the nanoparticles appeared to be highly stable to the intense sound waves (indicated by relatively narrow polydispersity and lack of precipitate), no further measurements were recorded.

### 2.5.2.2 Aqueous stability.

A nanoparticle dispersion (1 mg $mL^{-1}$, 1 mL) was serially diluted (two-fold) with distilled water using an adjustable pipette followed by DLS sizing measurements using the technique described above to give a final concentration of $1.22 \times 10^{-2}$ mg $mL^{-1}$. After this concentration was reached, extremely low scattering was observed

in the DLS measurements and therefore accurate measurement was no longer possible.

2.5.2.3 Methanol addition.

A nanoparticle dispersion (1 mg mL $^{-1}$, 1 mL) was pipetted into a glass sizing cuvette fitted with a lid to prevent any significant evaporation where DLS measurements followed. Fixed volumes of methanol were carefully pipetted into the glass cuvette and promptly swirled gently by hand prior to each sizing measurement. DLS measurements became unreliable (due to very low scattering) at a volume ratio of almost 1 : 1 water : methanol.

2.5.2.4 Electrolyte addition.

A nanoparticle suspension (1 mg mL $^{-1}$, 0.5 mL) was pipetted into a low volume plastic cuvette and DLS measurements were performed (an average of six measurements). Aliquots of an aqueous NaCl solution (0.5 M, 0.2 μL) were added and the cuvette was gently shaken by hand to ensure a homogeneous mixture. The cuvette was rapidly returned to the DLS instrument and sized as described above. A total of eight aliquots were added and subsequently measured.

2.5.2.5 Loaded Nanoparticle stability evaluation

Unstable nanoparticles were characterised by the visual appearance of precipitated material at the bottom of sample vials. Samples were also determined to be unstable if DLS measurements could not be performed. This occurred when the instrument measurement criteria could not be met e.g. due to the presence of aggregating material.

The research described in Chapter 3 has been partially published as

"Architecture-driven aqueous stability of hydrophobic, branched polymer nanoparticles prepared by rapid nanoprecipitation."

R. A. Slater, T. O. McDonald, D. J. Adams, E. R. Draper, J. V. M. Weaver and S. P. Rannard.

*Soft Matter*, **2012**, 8(38), 9816 – 9827.

# 3. Linear and Branched ATRP of 2-Hydroxypropyl Methacrylate

## 3.1 Introduction

The ATRP of HPMA using different initiator:monomer ratios was studied here in order to optimise the reaction conditions for linear polymerisation, which could then be applied to further branched copolymerisations. Although many monomers have been shown to be successful using ATRP including methacrylates, methacrylamides, acrylonitriles and styrenes,[1, 2] The HPMA monomer was chosen as it has been shown to polymerise well using ATRP[3] but as yet has not been widely reported in the literature using this method of polymerisation.

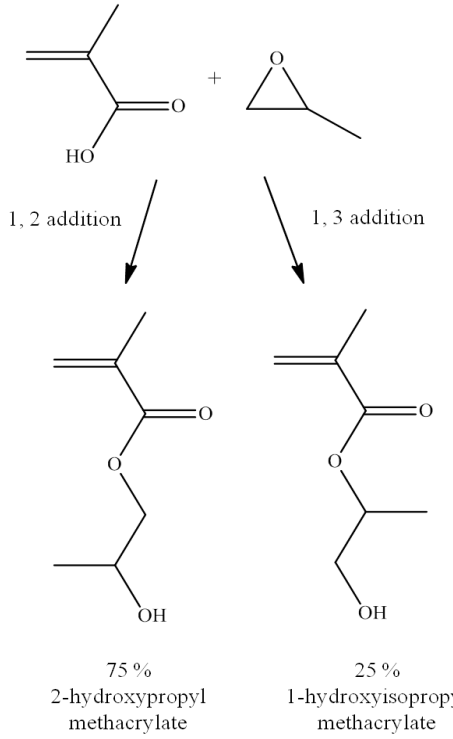


Scheme 3.1: Preparation route to HPMA monomer. Due to the poor regioselectivity of this reaction, both 2-hydroxypropyl methacrylate and 1-hydroxyisopropyl methacrylate isomers are formed.

HPMA has, however, been reported in polymerisations using nitroxide-mediated radical polymerisation (NMP),[4] free radical chemistry,[5] dispersion[6] and suspension techniques.[7]

Scheme 3.1 depicts the nucleophilic attack of propylene oxide by methacrylic acid. This can occur at two positions on the epoxide; reaction at the secondary carbon gives the major product 2-hydroxypropyl methacrylate whilst attack of the tertiary carbon yields the minor 1-hydroxyisopropyl methacrylate. As these two isomers co-exist in the commercial monomer feed, homopolymerisations should be properly described as statistical copolymerisations[3] when using this monomer.

Figure 3.1(A) shows a $^1$1 H NMR spectrum of HPMA in $D_2O$ where integration of the vinyl proton resonances (5.6-6.1 ppm) and terminal $CH_3$ protons (1.2 ppm) give a ratio of 2:3; other proton environments are also highlighted. As HPMA is a mixture of two isomers, the separate protons of the two different C=C double bond environments can be distinguished; shown in Figure 3.1(B). Integration indicates a ratio of the proton environments to be approximately 73/27.

## 3.2 Homopolymerisation of Linear *p*(HPMA$_x$) ($x$ = 50, 80, 120)

Methanol was chosen as a solvent for the ATRP synthesis of *p*(HPMA$_x$) as it has previously been reported,[3] although the same research group also conducted polymerisations of HPMA in methanol/water mixtures, achieving good control. It has been shown in the literature that this solvent system has been successful in other studies also.[8,9] The concentration of solvent was kept at 50/50 w/v % (monomer/solvent) throughout the polymerisation studies, as this has also been previously reported[10] and further dilutions were deemed unnecessary. Varying

dilution would also impact the reaction kinetics, leading to possibly slower reaction rates and more polydisperse materials.

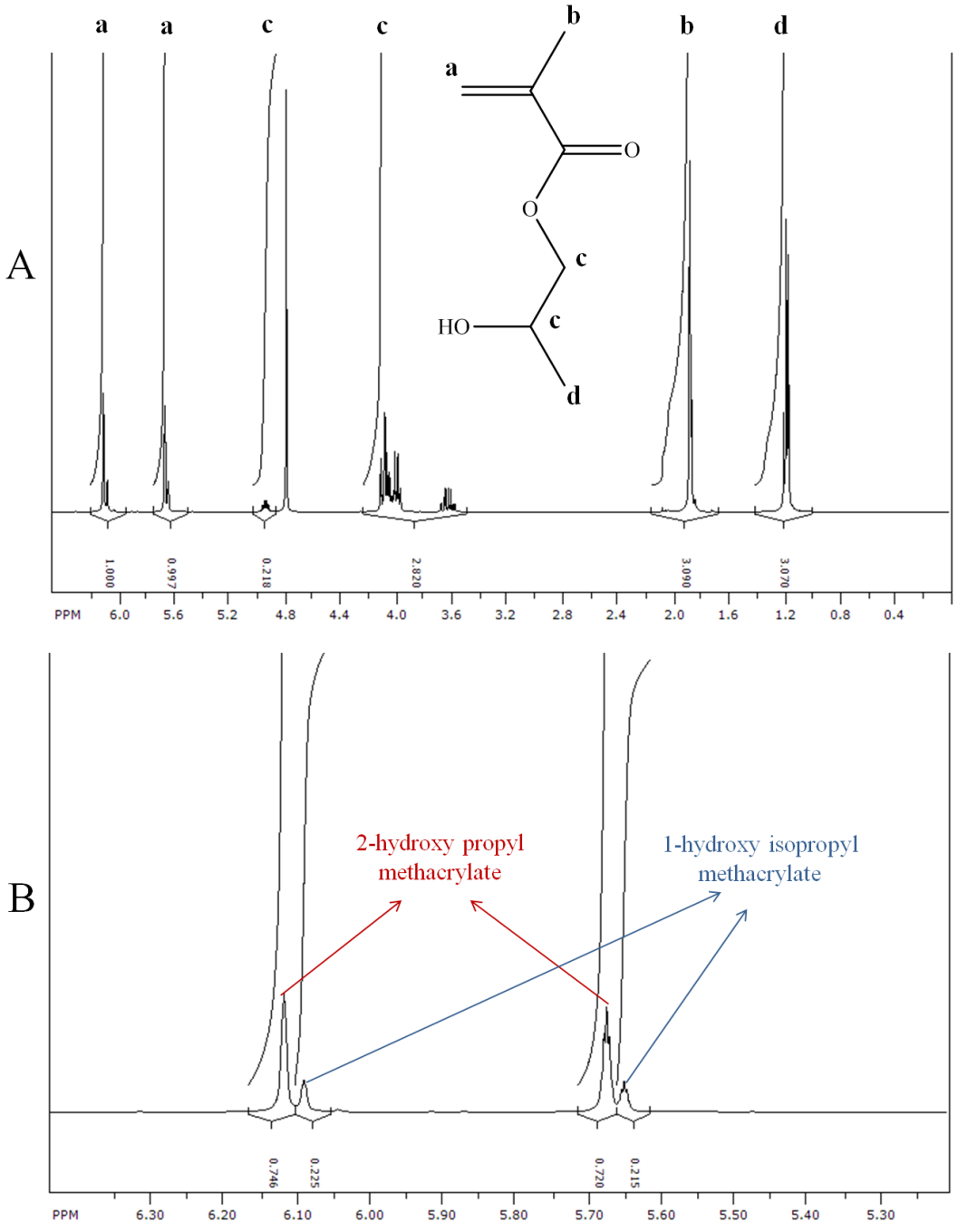


Figure 3.1: $^{1}$H HMR spectra of HPMA monomer in $D_2O$. (A) Entire spectrum. (B) HPMA vinyl signals.

The commonly used ethyl 2-bromoisobutyrate (EBiB) was chosen as the initiator for these polymerisations as it has been widely utilised for many methacrylate ATRP reactions.[11,12] It has been used effectively as an initiator to polymerise HPMA.[10] EBiB has several advantages; it is commercially available and due to its relatively small size and inert chemistry, it allows the investigation of polymer properties without any significant role being played by the presence of the initiator residue at the chain end.

Cu(I)Cl/BPY was chosen as the catalyst/ligand system due to reports of its compatibility in ATRP systems,[13] the commercial availability of both materials and the widespread success within a range of polymerisations. Armes and co-workers generally utilise this catalyst/ligand system in their ATRP reactions for methacrylates[14] as well as Sherrington and co-workers[15] and many other groups worldwide.

Initial polymerisations in methanol at ambient temperature (see Chapter 2 section 2.3.1), were investigated utilising EBiB as the initiator. The reaction protocol was chosen to allow > 99 % monomer conversion, to be judged by $^{1}$H NMR spectroscopy followed by manual termination, purification and subsequent analysis by triple detection GPC using tetrahydrofuran (THF) as eluent. The aim of these experiments was to identify reaction conditions that would allow the facile synthesis of polymers with identical chemistry but with varying chain lengths. All of the polymerisations were left to reach > 99 % conversion, rather than terminating at lower conversions whilst chains are still propagating and significant monomer remains in solution, as this allows all chains the potential to incorporate the entire monomer feed and therefore fully achieve the original target $DP_n$. Reaction kinetics can be followed to determine if reactions proceed in a controlled manner; final number average

molecular weights should be close to the predicted number average molecular weight (targeted by initiator:monomer feed ratios) and a relatively low molecular weight distribution should be found throughout the reaction. Assuming the reactions are controlled and reach > 99 % conversion, it is believed this experimental protocol is extremely facile and would be able to achieve polymer chains with varying chain length. The process is represented in Scheme 3.2.

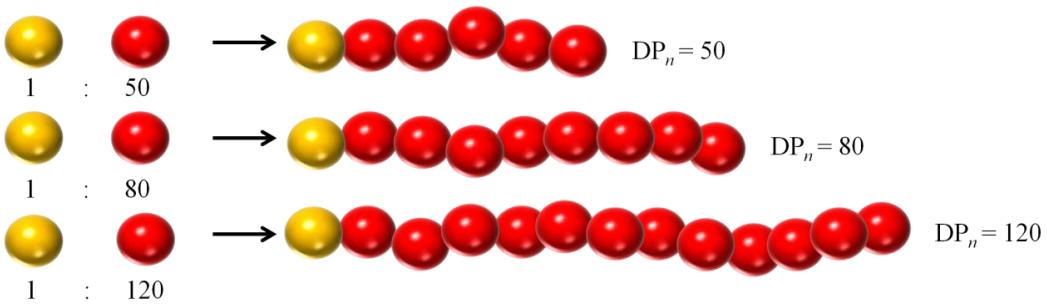


Scheme 3.2: A simple schematic representation of three linear polymers consisting of EBiB initiator (yellow spheres) and HPMA monomer (red spheres) of varying chain length (or $DP_n$).

Prior to any kinetic analysis of *p*(HPMA) reactions, three polymerisations were conducted with target $DP_n$ = 50, 80 and 120 monomer units; achieved simply by simply adjusting the initiator:monomer ratio. These reactions were left for approximately 15 hours after which $^1$H NMR spectroscopic analysis revealed that monomers had reached full conversion as judged by no detectable vinyl signals at 5.6-6.1 ppm (DMSO-$d_6$). These reactions were manually terminated and purified as explained in the Chapter 2 section 2.3.1. $DP_n$ could not be estimated directly using $^1$H NMR as the $CH_2$-$CH_3$ protons in the initiator overlapped with $^1$H signals from *p*(HPMA).

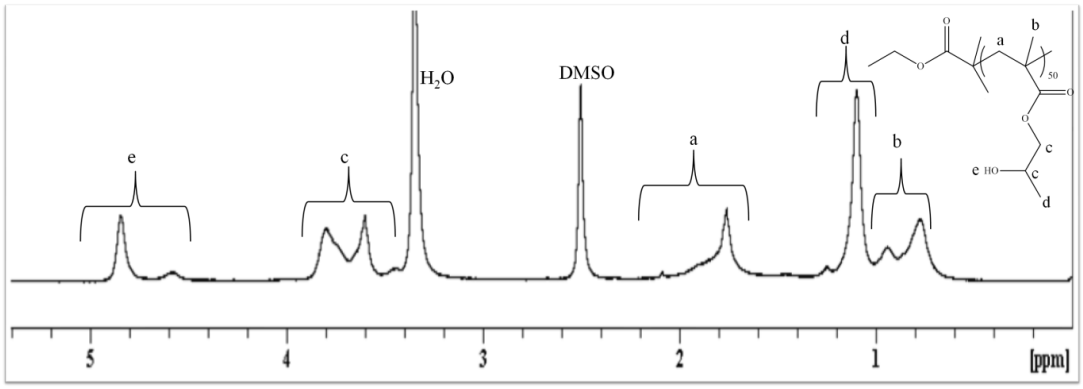


Figure 3.2: $^{1}$H HMR spectrum of *p*(HPMA$_{50}$) in DMSO-d$_6$.

The $^{1}$H NMR spectrum (DMSO-d$_6$) of a purified sample of *p*(HPMA$_{50}$) is shown in Figure 3.2 highlighting the various proton environments. The three *p*(HPMA) polymers with increasing targeted DP$_n$ values were diluted to reach a concentration of 5 mg mL$^{-1}$ in THF and subjected to triple detection GPC analysis, shown in Figure 3.3.

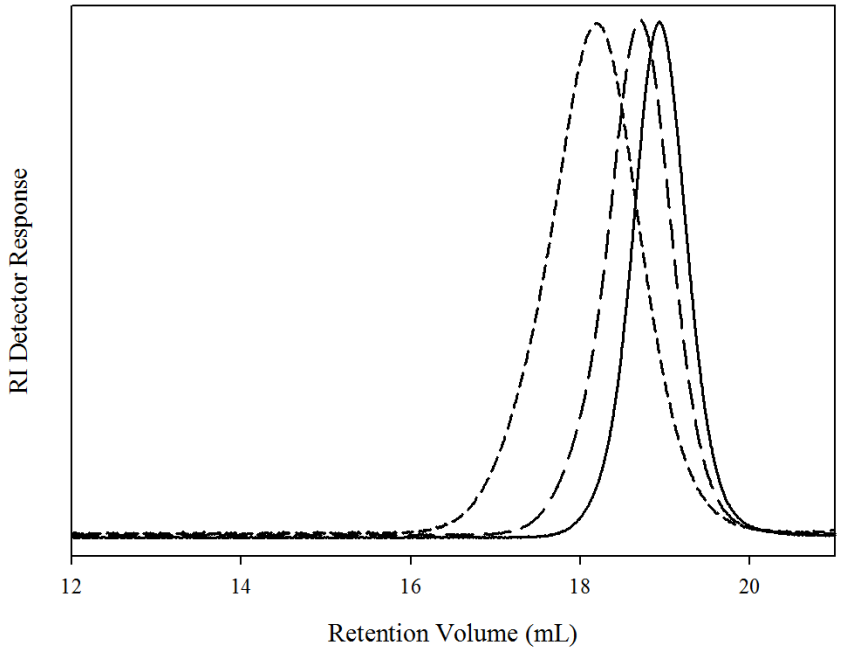


Figure 3.3: GPC (THF) chromatograms for linear homopolymers. *p*(HPMA$_{50}$) (solid line), *p*(HPMA$_{80}$) (medium dashed line), *p*(HPMA$_{120}$) (small dashed line).

As expected for a controlled polymerisation, the chromatograms are symmetrical and move to a lower retention volume with increasing target $DP_n$; indicative of formation of higher molecular weight material. A small summary of the data obtained from these polymers is shown below in Table 3.1.

| Sample | $M_n$ (g mol$^{-1}$) (theory) | $M_n$ (g mol$^{-1}$) (GPC) | $M_w$ (g mol$^{-1}$) (GPC) | $M_w/M_n$ | Conversion (%) |
|---|---|---|---|---|---|
| *p*(HPMA$_{50}$) | 7400 | 7900 | 11900 | 1.18 | > 99 |
| *p*(HPMA$_{80}$) | 11700 | 15200 | 19100 | 1.16 | > 99 |
| *p*(HPMA$_{120}$) | 17300 | 18100 | 29000 | 1.60 | > 99 |

Table 3.1: Data obtained *via* triple detection GPC (THF eluent) for the homopolymerisation of *p*(HPMA$_x$).

Observed $M_n$ values for *p*(HPMA$_{50}$) and *p*(HPMA$_{80}$) are extremely close to those predicted, with low molecular weight distributions obtained, which was expected using ATRP. The longest targeted chain length ($DP_n$ = 120 monomer units) produced a polymer with a significantly higher $M_n$ value of 18100 g mol$^{-1}$ in comparison to the targeted value of 17300 g mol$^{-1}$. The observed variation in $M_n$ may be due to some initiator inefficiency, where the polymerisation had a lack of initiating sites at the beginning of the reaction and therefore more monomer was added to fewer than expected chains. It is also possible that termination by combination of active polymer chains occurred at extremely high conversion; chain mobility will be reduced at high conversions due to the high viscosity of the solution, leading to end-group radical reaction and causing an increase in the observed $M_w$ and, thereby, affecting the overall molecular weight distribution. The dispersity value

of 1.60 for this sample which was notably higher than those found for the shorter targeted chains ($DP_n$ = 50, 80 monomer units). By overlaying the outputs of the Refractive Index (RI), Right Angle Light Scattering (RALS), Low Angle Light Scattering (LALS) and the Intrinsic Viscosity (IV) detectors of the linear polymer analysis, it is found that all traces are monomodal and symmetrical indicating no high, or indeed extremely low, molecular weight material is present in any of the samples prepared across the different chain lengths, demonstrated in Figure 3.4.

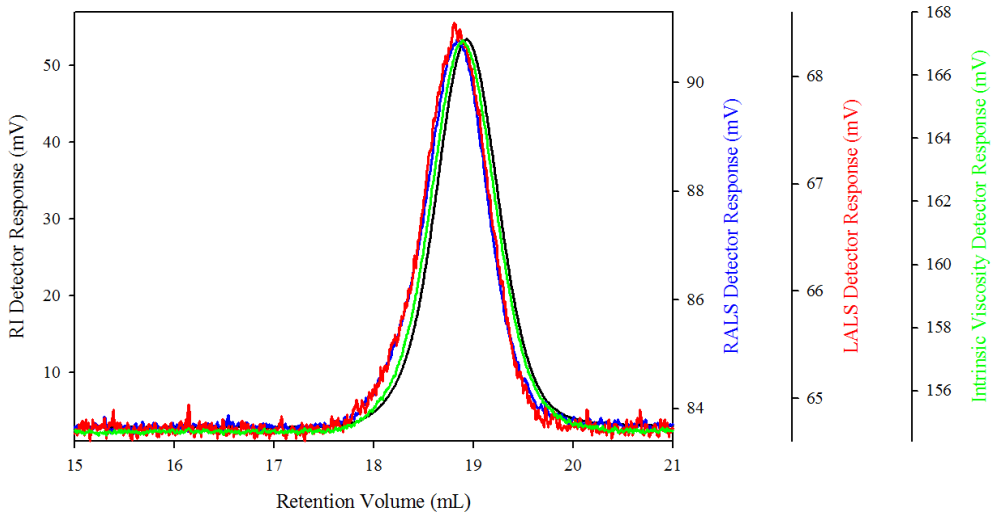


Figure 3.4: GPC chromatogram of *p*($HPMA_{50}$) showing RI (black line), RALS (blue line), LALS (red line) and Intrinsic Viscosity (green line) responses.

Excellent agreement of targeted and observed number average molecular weight was found for *p*($HPMA_{50}$), *p*($HPMA_{80}$) and *p*($HPMA_{120}$), with relatively low molecular weight distributions obtained, and therefore these reaction conditions were accepted for future polymerisations. No further experiments to target higher chain lengths were explored in this work.

### 3.2.1 Reproducibility of ATRP to form linear *p*(HPMA$_x$) homopolymers (*x* = 50, 80, 120)

To investigate the reproducibility of ATRP polymerisation of HPMA under ambient methanolic conditions, The formation of *p*(HPMA$_{50}$), *p*(HPMA$_{80}$) and *p*(HPMA$_{120}$) was repeated on two separate occasions using the same experimental protocol as previously described. Polymer concentration in (THF) for analysis *via* triple detection GPC was also kept constant at 5 mg/ml. In principle, signals observed by each of the detectors attached to the GPC instrument should be identical, but due to experimental error complete overlap was not observed. The overlap was, however, in very close agreement and examples of the RI chromatograms or the six polymers (2 repeats of each polymerisation) are shown in Figure 3.5.

Good agreement is found for each targeted DP$_n$, although the polymerisations were conducted at ambient temperature which was therefore not controlled between polymerisations. Differences in temperature, when conducting the repeat experiments, would affect the reaction kinetics and lead to deviation of molecular weights and molecular weight distributions.

It should also be noted that there are no literature reports on the reproducibility of *p*(HPMA) synthesis using methanolic ATRP under identical feed ratios and, as such, to the best of our knowledge, this is the first report of its type.

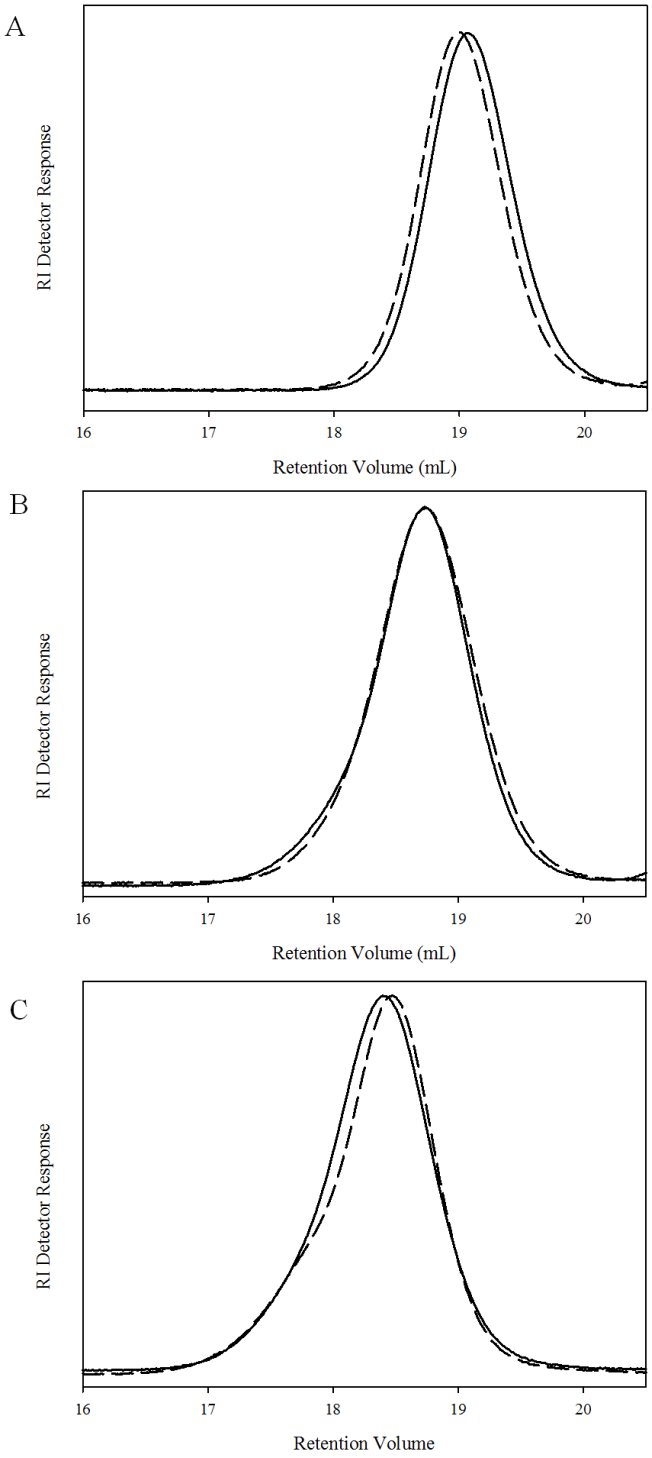


Figure 3.5: GPC (THF eluent) chromatograms of *p*(HPMA) homopolymers synthesised on separate occasions. A) *p*($HPMA_{50}$). B) *p*($HPMA_{80}$). C) *p*($HPMA_{120}$).

## 3.2.2 Kinetic Studies for the Linear Homopolymerisation of HPMA ($DP_n$ = 50, 80, 120)

To confirm the previously synthesised polymers proceeded under controlled radical polymerisation conditions, homopolymerisation kinetics studies were conducted for the linear polymerisations with number average degree of polymerisation values of 50, 80 and 120 monomer units, utilising EBiB as the initiator.

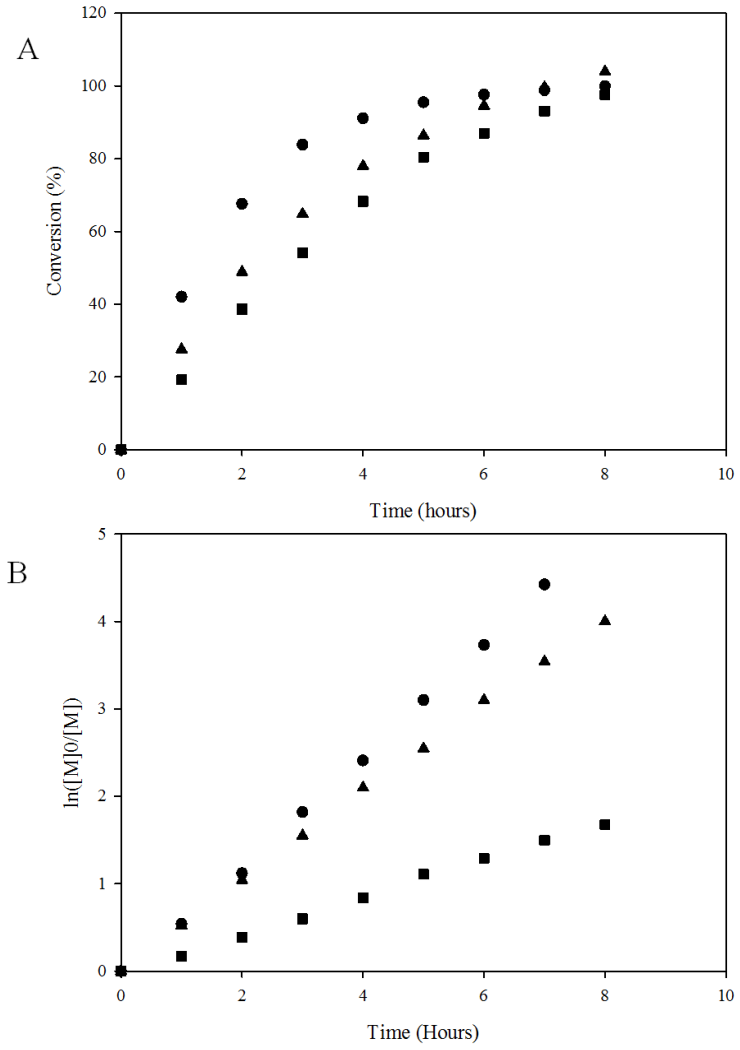


Figure 3.6: Kinetics studies of HPMA ATRP polymerisation. (A) Conversion *vs.* Time plot for *p*($HPMA_{50}$) (circle), *p*($HPMA_{80}$) (triangle) and *p*($HPMA_{120}$) (square). (B) Semi-logarithmic plot for ($HPMA_{50}$) (circle), *p*($HPMA_{80}$) (triangle) and *p*($HPMA_{120}$) (square).

Kinetic experiments were carried out in parallel, ensuring the molar ratio of EBiB was constant and the molar ratio of HPMA monomer was varied in order to achieve the desired target $DP_n$. The reactions were monitored for eight hours with regular hourly sampling of the polymerisation mixture and analysed by $^1H$ NMR spectroscopy and triple detection GPC (THF eluent).

Figure 3.6(A) shows percentage conversion as a function of time for the three polymers *p*($HPMA_{50}$), *p*($HPMA_{80}$) and *p*($HPMA_{120}$). For *p*($HPMA_{50}$), 42 % of the monomer has been polymerised within the first hour, compared to 23 % for *p*($HPMA_{80}$), and just 16 % for *p*($HPMA_{120}$). Despite these seemingly different conversions (for the same given time), the three polymerisations produced chains containing approximately 21 monomer units. It may have been expected that these figures would be more similar, given that the components are identical in the three reactions. The semi-logarithmic plots shown in Figure 3.6(B) all increase linearly with time, indicating the absence of termination and a constant concentration of propagating radicals within the polymerisation. If any termination was present, it was not seen within this experiment.

It is clear that under these polymerisation conditions, the rate of polymerisation is related to targeted chain length, where higher conversions are reached within shorter reaction times, when the targeted primary chain length is shorter. Alongside this, reaction rates decrease as target $DP_n$ increases (Figure 3.6(B)). These results are in near complete contrast to Armes and co-workers who report reduced reaction times and increased reaction rates with increasing primary chain length (when polymerising 2-methacryloyloxyethyl phosphorylcholine utilising an oligo(ethylene glycol)-based water-soluble initiator).[16]

This clearly demonstrates how dramatically different kinetic data can be obtained when using different monomers and initiators (both reactions were carried out in methanol). Varying temperature leads to altered rates within ATRP systems[17] and from the outset, this could be believed to be the reason for the different observed reaction rates, as they were carried out at ambient temperature, which could have changed slightly when performing each experiment. However, the reactions were performed within one week of each other, and the possibility of dramatic temperature change was discarded. In order to rationalise the differences observed during reactions, it is proposed that reaction kinetics are affected by the concentration of initiator in the monomer solution. As stated previously, a ratio of 50 w/v % (monomer/solvent) was utilised and as such, despite varying the target $DP_n$ of the polymer chain, there remains the same monomer/solvent ratio, discounting the possibility of this ratio affecting the kinetic differences between reactions. However, by keeping the monomer/ solvent ratio constant, the concentration of initiator within the reaction becomes unavoidably changed when altering the target $DP_n$. As the target $DP_n$ increases, the concentration of initiator becomes reduced with respect to monomer and solvent.

As a result, the concentration of Cu(I)Cl and BPY also becomes inevitably reduced in the solution. Both of these lead to changes in propagating radical concentration which would have a dramatic impact on the observed reaction rates between the three polymerisations with different targeted primary chain length.

Figure 3.7 shows that the molecular weight distribution decreases during the formation of *p*($HPMA_{80}$) ranging from 1.55 (23 % conversion) to 1.17 (99 % conversion). At low conversion higher molecular weight distributions are observed,

due the statistical nature of the catalyst activation/deactivation during propagation and the need to establish a significant Cu(II) concentration before a stable equilibrium can be achieved. Different numbers of monomer units are therefore added to the chain ends during each activation step within the early stages and the initiators are not activated simultaneously but rather a time period is required for a steady state of propagating radicals to be formed. The chains eventually become more uniform throughout the reaction due to the statistical nature of the continuous activation/deactivation reactions; eventually, all chains will have propagated for approximately the same time periods.

$M_n$ increases nearly linearly over time, suggesting monomer is being consumed at a relatively steady rate throughout the reaction. The behaviour seen here is characteristic of a fast initiation step with an insignificant amount of chain transfer or termination and good exchange of active species.

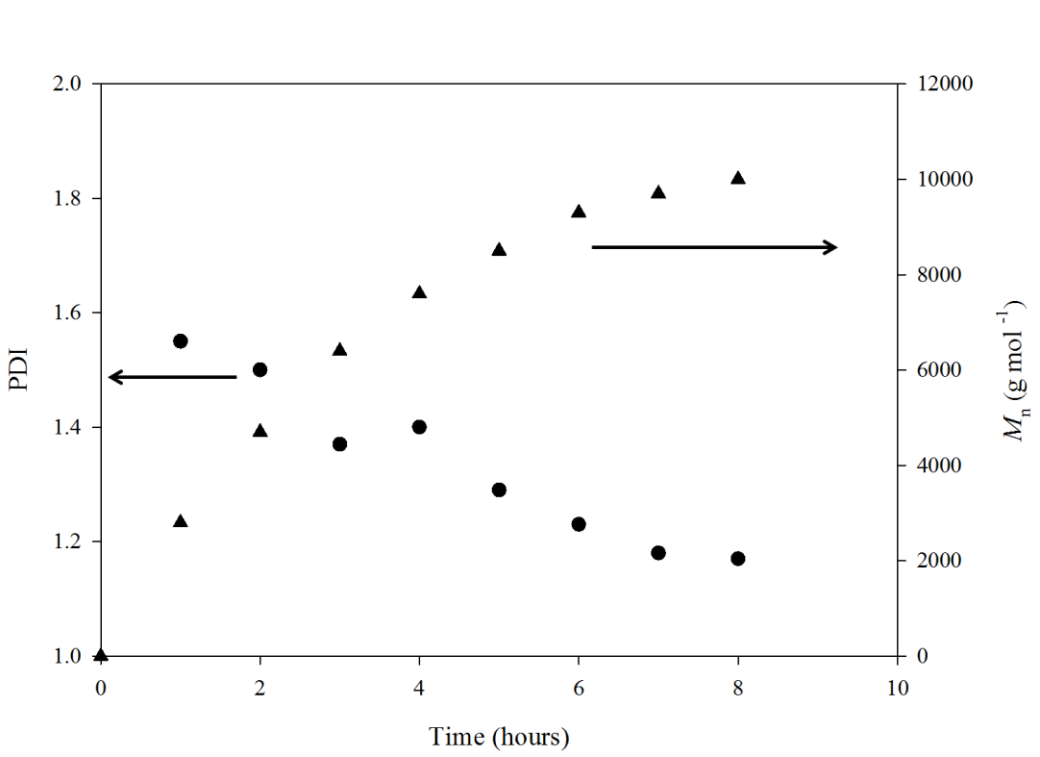


Figure 3.7: Evolution of molecular weight with conversion over time for the homopolymerisation of *p*(HPMA$_{80}$).

Figure 3.8 shows the development of molecular weight with time for *p*(HPMA$_{50}$), *p*(HPMA$_{80}$) and *p*(HPMA$_{120}$). Molecular weight distributions are narrow, monomodal and shift to a lower retention volume with time (and conversion) corresponding to higher molecular weights as expected for a controlled polymerisation. There is no obvious broadening of peaks, which would have indicated an increase of the molecular weight distribution of the polymers.

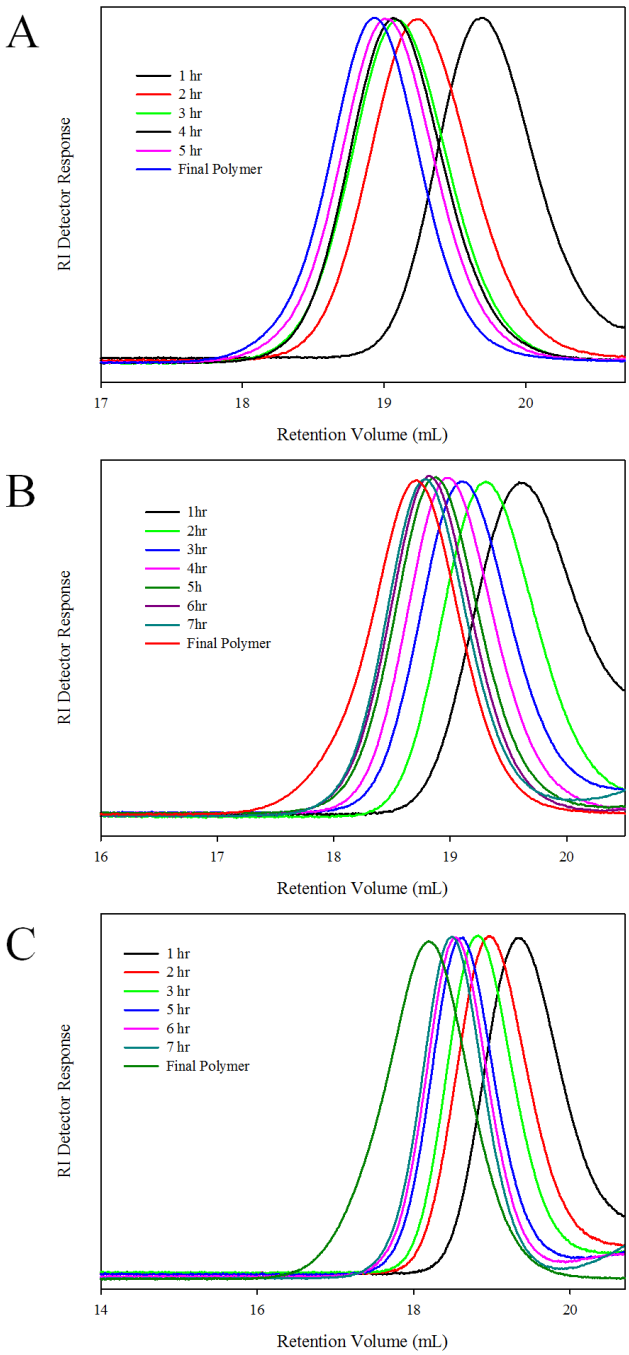


Figure 3.8: Evolution of molecular weight during the ATRP of HPMA (GPC (THF) chromatograms) (A) *p*(HPMA$_{50}$), (B) *p*(HPMA$_{80}$), (C) *p*(HPMA$_{120}$).

Conversion of monomer to polymer in the kinetic studies of *p*(HPMA) was calculated using a ratio of the aromatic signals from the internal standard anisole and an average of the two vinyl signals from HPMA monomer. Anisole was chosen as an internal standard due to its non-reactivity in the polymerisation and its clear

aromatic signals at 6.9 and 7.3 ppm. The terminal protons of the EBiB initiator on polymer chains would also prove difficult to quantify; the single proton signal at 2.5 ppm would not be sufficiently well resolved to allow any accuracy in determination of chain length using conventional chain-end analysis. The other proton shifts unfortunately overlap with those in the main chain. Figure 3.9 indicates the consumption of vinyl bonds during polymerisation.

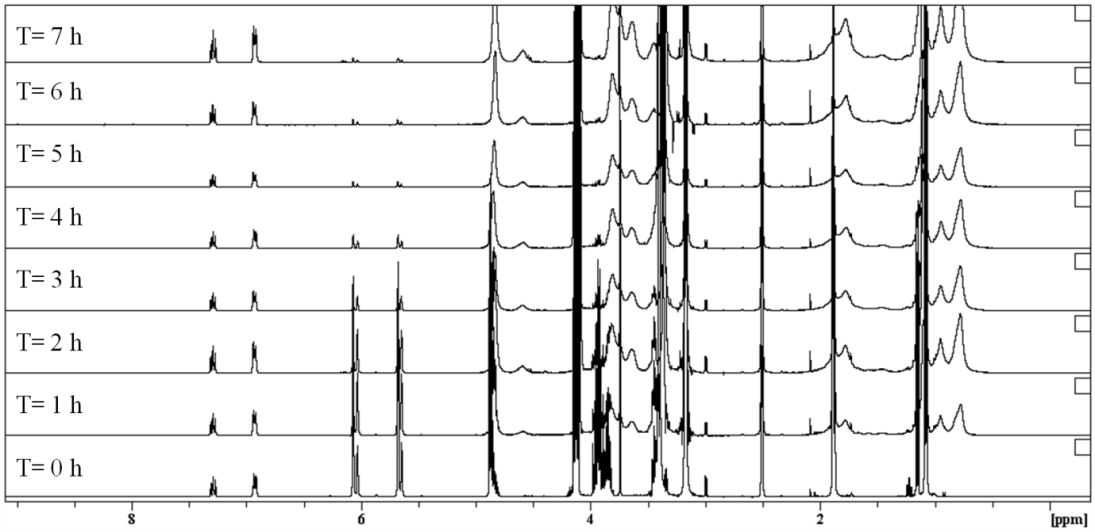


Figure 3.9: $^{1}$H NMR spectra (DMSO-$d_6$) of samples taken for the kinetic study of the ATRP of HPMA - target *p*(HPMA$_{50}$).

Having found that polymerisation in methanol produced well-defined polymers with low molecular weight distributions, over a range of target DP$_n$ (50, 80 and 120 monomer units) it seemed unnecessary to alter any reaction conditions. It has been reported that the addition of water to the polymerisation of *p*(HPMA) increased the rate[3], although it also incurred a loss of control, resulting in higher molecular weight distributions of the polymers. Using methanol as the sole solvent also made the

work-up of polymers more experimentally facile, as higher temperatures/extraction/ freeze drying would be necessary for complete removal of any added water.

The data generated suggests that increasing the targeted $DP_n$ leads to increases molecular weight distribution at high conversion (Figure 3.8). ATRP polymerisations are often terminated at approximately 80 % conversion when chain end functionality is still very high, and molecular weight distribution is narrow. The data in this chapter shows molecular weight distribution increases at high conversion, which is attributed to bimolecular termination of active chains which are starved of monomer (when conversion reaches > 99 %), however, the aims of the project are to utilise branched vinyl polymerisation to form complex architectures and therefore very high conversions are required.

Abstraction of protons from solution, leading to terminated chains, would not result in this broadening of GPC traces and it is therefore believed that it is due to radical-radical combination. Although this has not been widely reported in the literature, Matyjaszewski and others have demonstrated this occurrence in their ATRP reactions.[18,19]

In summary, three linear *p*(HPMA) polymers have been synthesised with their individual kinetics explored. Conventional ATRP mechanisms and controlled polymerisation appears to operate under the chosen conditions, even though no direct control of temperature was employed.

### 3.2.3 Linear Chain Extension of *p*(HPMA$_{30}$) to *p*(HPMA$_{30}$)-*b*-*p*(HPMA$_{50}$).

In order to investigate the control present within the ATRP polymerisations further, chain extension experiments were conducted. In this study a chain extension or "self-blocking" experiment in methanol was performed using EBiB as the initiator. A linear block of *p*(HPMA) (target DP$_n$ = 30 monomer units) was synthesised to relatively high conversion (~ 80-95 %) after which, a second HPMA monomer feed (equivalent to a target DP$_n$ = 50 monomer units) was added to the polymerising solution (see Chapter 2 section 2.3.4). Complete chain extension should occur provided that polymer chain ends are either active or capped with halogen atoms and significant termination had not occurred. Monomer will therefore add to all propagating chains in a controlled fashion (as was the case with the original polymer chain) to give a final polymer with an overall DP$_n$ of 80 monomer units. Analysis by GPC (THF eluent) was performed on a sample taken of the polymerising solution prior to second aliquot addition; samples were also taken post addition until polymerisation reached high conversion. In this case, the polymer is denoted *p*(HPMA$_{30}$)-*b*-*p*(HPMA$_{50}$).

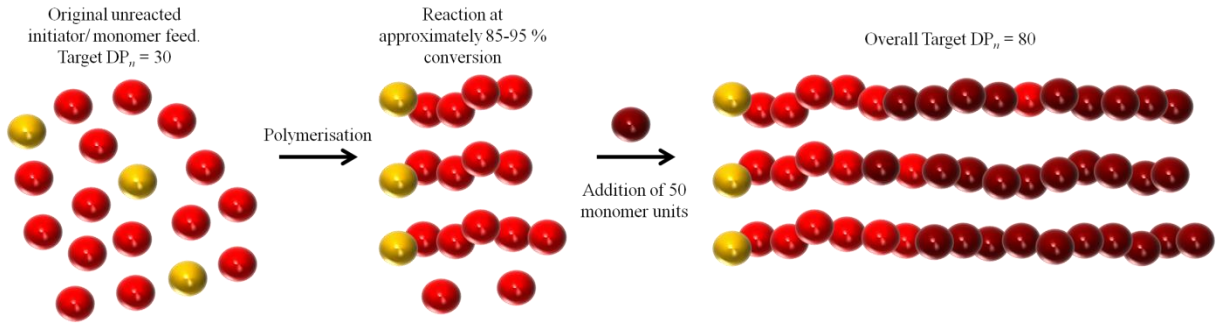


Scheme3.3: Representation of the chain extension process in methanol for linear *p*(HPMA) employing EBiB as the initiator. (Initiator: monomer feed is not to scale).

Scheme 3.3 aims to show the chain extension process of *p*(HPMA) where red spheres represent the first HPMA monomer feed (target $DP_n$ = 30 monomer units), which is polymerised until approximately 80-95 % conversion has been reached, after which the second batch of HPMA monomer (represented by the maroon spheres) is added to the reaction and left to polymerised until > 99 % conversion has been reached overall.

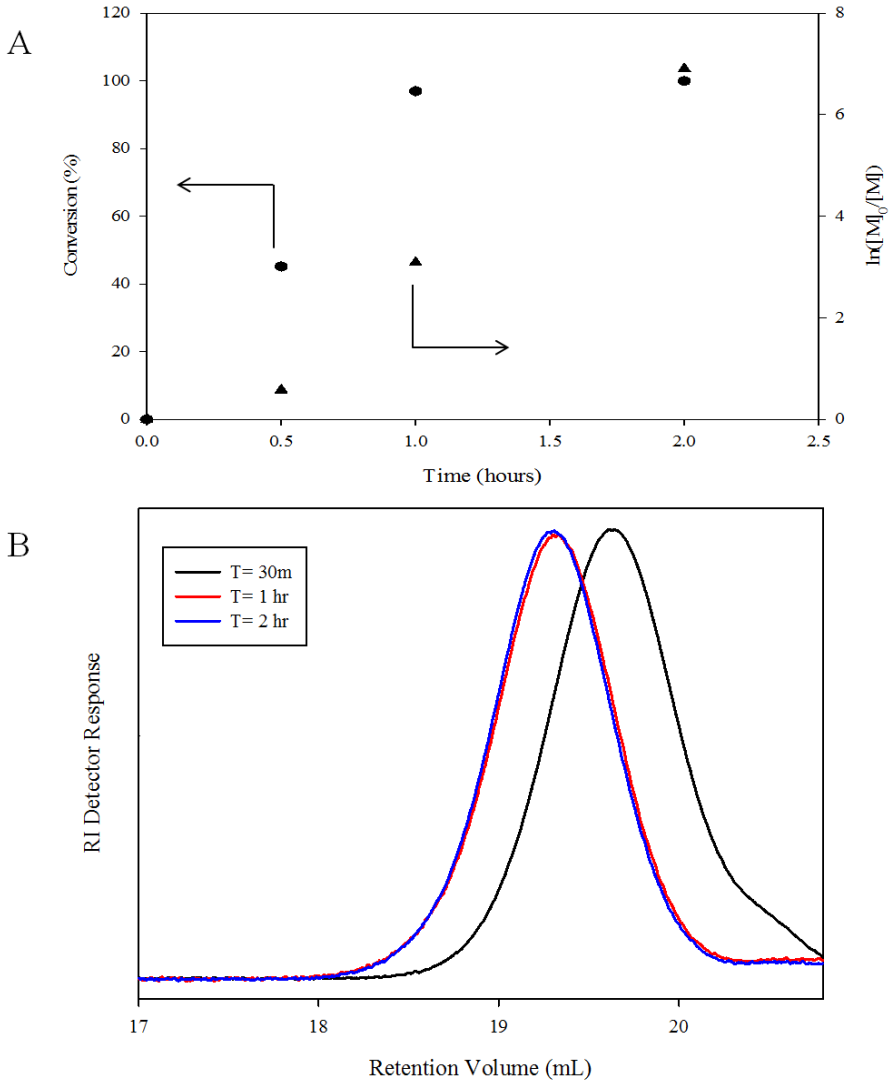


Figure 3.10: Kinetic data results for the polymerisation of *p*(HPMA) (target $DP_n$ = 30 monomer units). A) Conversion *vs*. time plot. B) GPC (THF eluent) analysis.

In order to determine when approximately 80-95 % had been reached for the polymerisation of *p(*$HPMA_{30}$) (the first block); a simple kinetics experiment was conducted. This was performed using the same protocol as the previous kinetics experiments. It was assumed the reaction would reach full conversion in a relatively short space of time in comparison to *p*($HPMA_{50}$) as there are fewer monomer units per chain, and therefore an extra sample was taken after 30 minutes reaction time (as well as after 1 hour and 2 hours). The kinetic analysis for the reaction of *p*($HPMA_{30}$) showed > 99 % conversion after only 2 hours with a linear semi-logarithm plot indicating a constant concentration of radicals and therefore the reaction was assumed to have proceeded in a controlled manner (Figure 3.10(A)). In addition, GPC analysis of the polymer reveals a final $M_n$ of 4400 g $mol^{-1}$ and a relatively low molecular weight distribution of 1.18 (Figure 3.10 (b)).

As a comparison, the polymerisation of *p*($HPMA_{50}$) should reach an approximate $M_n$ = 4400 g $mol^{-1}$ after 2 hours, given the kinetic analysis presented earlier although the conversions for each polymerisation are considerably different at this number average molecular weight, i.e. > 99 % conversion for the *p*($HPMA_{30}$) polymerisation and only 68 % conversion for *p*$HPMA_{50}$. As can be seen from Figure 3.11, after chromatograms taken at these timepoints for the different ATRP polymerisations overlap well; the polymerisation targeting *p*($HPMA_{50}$) had reached an $M_n$ value of 5100 g $mol^{-1}$ with a dispersity of 1.27. These values are similar to the *p*($HPMA_{30}$) polymerisation at > 99 % conversion, which achieved an $M_n$ of 4400 g $mol^{-1}$ and a molecular weight distribution of 1.18.

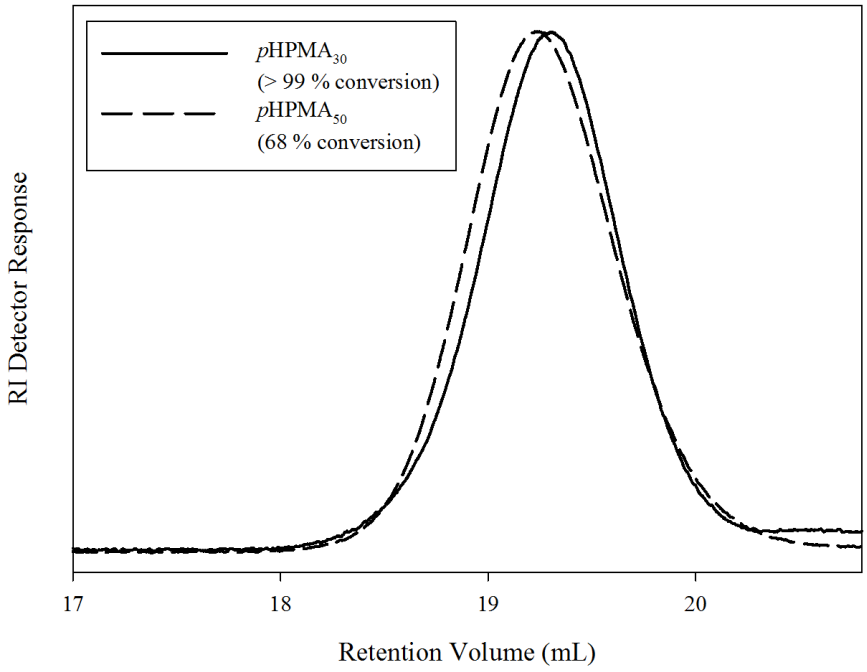


Figure 3.11: GPC (THF eluent) chromatograms of *p*(HPMA$_{30}$) at 99 % conversion (solid line) and *p*(HPMA$_{50}$) at 68 % conversion (dashed line).

The polymerisation was monitored further after the addition of the second monomer feed. Figure 3.12 shows the evolution of molecular weight for this reaction, where the black trace is the sample taken prior to addition of the second monomer batch and, as expected, this trace is monomodal and symmetrical with a measured monomer conversion = 88 %. Similarly, the subsequent polymer samples are also monomodal and their retention volumes decrease as polymerisation reaches high conversion. $^{1}$H NMR spectroscopy was used alongside GPC analysis to monitor this reaction and in similar fashion to the analysis of the kinetics for homopolymerisation, anisole was used as an internal standard and allowed conversion to be calculated throughout the polymerisation.

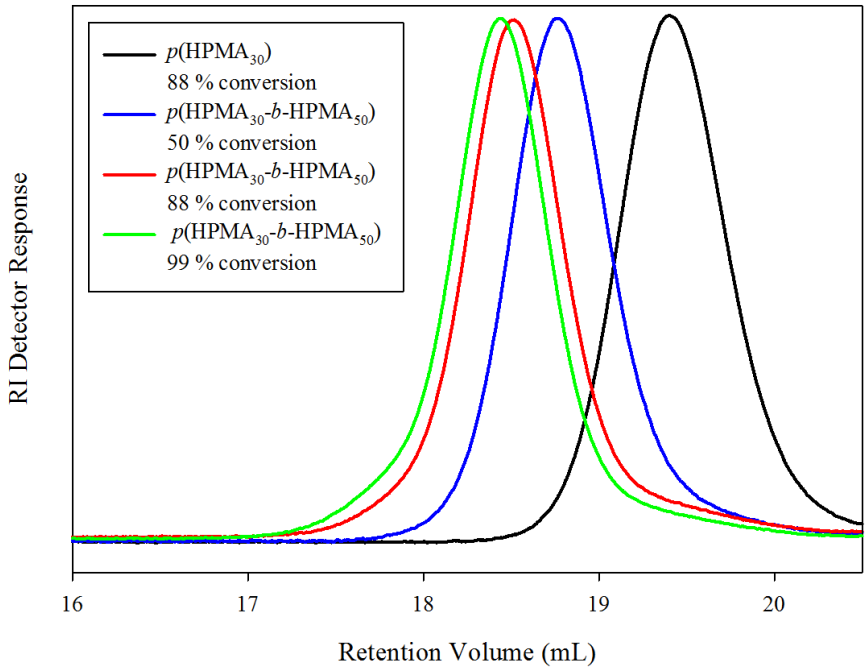


Figure 3.12: GPC (THF eluent) chromatograms for the chain extension of *p*(HPMA$_{30}$) to a final (*p*(HPMA$_{30}$)-*b*-*p*(HPMA$_{50}$)).

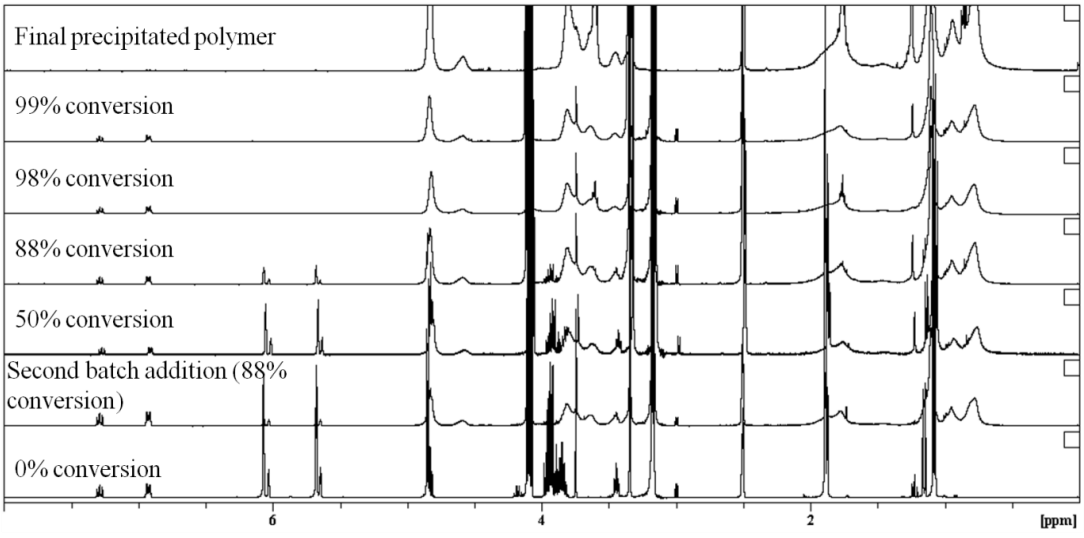


Figure 3.13: $^{1}$H NMR spectra in DMSO-d$_6$ for the kinetic study of *p*(HPMA$_{30}$-*b*-HPMA$_{50}$) over time.

As can be seen from Table 3.2, low molecular weight distributions are seen throughout the experiment, suggesting monomer is added to the growing chains in a controlled manner, yielding a polymer with a final molecular weight of 16000 g $mol^{-1}$ and a molecular weight distribution of 1.09. The observed $M_n$ is significantly higher than the expected molecular weight of 11500 g $mol^{-1}$, this increase can be attributed to insufficient initiation during the first polymerisation (where a lower than expected molecular weight was found) and therefore more monomer was added to fewer active chains during the second stage of polymerisation.

| Sample | $M_n$ (g $mol^{-1}$ ) (theoretical) | $M_n$ (g $mol^{-1}$) (GPC) | $M_w$ (g $mol^{-1}$) (GPC) | $M_w/M_n$ | Conversion (%) |
|---|---|---|---|---|---|
| *p*($HPMA_{30}$) | 3500 | 3 800 | 4200 | 1.11 | 88 |
| *p*($HPMA_{30}$)-*b*-($HPMA_{50}$) | 5800 | 8000 | 9600 | 1.20 | 50 |
| *p*($HPMA_{30}$)-*b*-($HPMA_{50}$) | 10200 | 15300 | 18400 | 1.20 | 88 |
| *p*($HPMA_{30}$)-*b*-($HPMA_{50}$) | 11500 | 16000 | 17600 | 1.08 | 99 |

Table 3.2: Data for the chain extension of *p*(HPMA). *Theoretical $M_n$ (g $mol^{-1}$) is based on the conversion values that were measured.

This is also supported by the fact that molecular weight distribution remains monomodal and the dispersity values are relatively low during all stages of the

polymerisation, therefore suggesting the majority of chain ends remained active and continued to polymerise effectively after the second batch of monomer was added. To show how apparent the difference is to the homopolymerisation of a single batch of HPMA monomer to a target $DP_n$ of 80 monomer units, Figure 3.14 shows chromatograms of both *p*($HPMA_{30}$)-*b*-($HPMA_{50}$) and *p*($HPMA_{80}$).

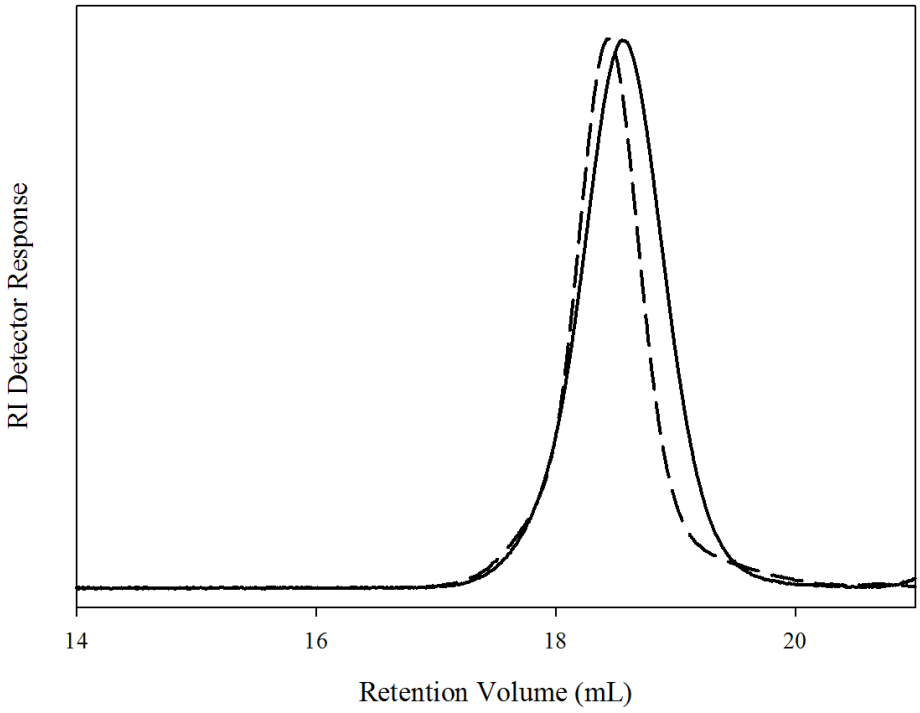


Figure 3.14: GPC (THF eluent) chromatograms for *p*($HPMA_{80}$) (solid line) and *p*($HPMA_{30}$)-*b*-($HPMA_{50}$) (dashed line).

Figure 3.14 shows that the homopolymer produced through a single monomer addition elutes at higher retention volumes, and therefore lower molecular weight than that of the self-blocked polymer at a nominal identical chain length. The self-blocked polymer also shows an absence of peaks at high retention volumes which would indicate blocking inefficiency. Although both GPC chromatograms peak at very similar retention volumes (approximately 18.5 mL), it is interesting that the

self-blocked copolymer (despite reaching > 99 % conversion), actually has a lower molecular weight distribution (1.09) than the homopolymer (1.18).

## 3.3 Copolymerisation of HPMA and EGDMA to form Branched (*p*((HPMA$_x$)-*co*-EGDMA$_{0.95}$)) (*x* = 50, 80, 120)

Herein the synthesis and characterisation of branched statistical copolymers comprising EGDMA and HPMA (*p*((HPMA$_x$)-*co*-EGDMA$_{0.95}$)) utilising EBiB as the initiator in methanol at ambient temperature is introduced. A simplistic approach to generating high molecular weight materials is used, in which the synthetic protocol is identical to approach employed to generate linear *p*(HPMA) homopolymers, apart from the addition of the EGDMA brancher within the HPMA monomer feed.

The controlled radical copolymerisation of a monovinylic monomer and a small amount of divinyl brancher inevitably generates a polymer with a branched architecture. This occurs *via* incorporation of one of the vinyl groups of the brancher into the growing copolymer chain followed by the reaction of the pendant vinyl group intermolecularly to form a covalent branch to another polymer chain. That is, unless the pendant group reacts with the radical chain end of the copolymer chain in which case may react intramolecularly and form a cycle.[20] The consumption of brancher in this way diminishes the copolymers' ability to reach high molecular weights. Analysis *via* GPC does not conventionally indicate the presence of intramolecular cycles, although Armes and co-workers have utilised $^1$H NMR spectroscopy to investigate and quantify how much brancher is incorporated in the

reaction of MMA and a disulfide-based cleavable bifunctional monomer.[21] The number average and weight average molecular weight of copolymers increases dramatically as lightly branched polymers become covalently bonded at high conversion.[22] A complex copolymer architecture will ensue if enough brancher has been added and it is predominantly incorporated intermolecularly.[23] If too much brancher is added, an insoluble polymer network will form, often described as a crosslinked gel.

The conditions for the copolymerisations are identical to those described above for linear polymerisation of HPMA with the exception of using a molar ratio of 1:0.95 for the initiator and brancher, respectively (see Chapter 2 section 2.3.1). The aim was to avoid gelation of the copolymer and form a highly branched soluble hydrophobic material. Although controlling the brancher molar ratio is unfortunately not sufficient to completely ensure that gelation does not occur, the key ratio is actually the molar ratio of reacted brancher to primary polymer chains; if the copolymer system has a low initiator efficiency it is highly likely to form a gelled network, despite an apparent feed ratio of brancher to initiator which is equal to < 1. This is due to the amount of reacted brancher being larger than the amount of primary chains produced. Additionally, if the copolymerisation is too concentrated (with respect to solvent), gelation can also ensue despite monomer to brancher ratios being below 1: 1.[24] Within the reactions described below, no gelation occurred and it is thought that a relatively high initiator efficiency was evident and therefore an inititator to brancher ratio of 1:0.95 was used throughout the range of reported polymerisations. The consistency of concentrations and initiator:brancher ratios allows a series of distinct comparisons to be made whereas any alterations would

undoubtedly lead to different architectures and reaction kinetics, leading to inaccurate comparisons between branched copolymers.

This method of forming soluble branched polymers is dissimilar to the work described by Sherrington and co-workers using conventional free radical polymerisation,[25] where very high molecular weight copolymer chains are obtained at low conversion. In this case branched copolymers are generated in early polymerisation stages in complete contrast to controlled radical polymerisation. In ATRP, it is suggested that the degree of branching is negligible at low conversions; in the early stages of copolymerisation, propagating chains are more likely to incorporate mono-vinylic monomer than successfully link two chains through intermolecular reaction. The fundamental question of at what conversion branching becomes significant will be investigated in this study. This is achieved by periodic sampling of three copolymerisations and their analysis by triple detection GPC (THF eluent) and $^{1}$H NMR spectroscopy (DMSO-$d_6$).

Primary chain lengths of $DP_n$ = 50 (*p*((HPMA$_{50}$)-*co*-EGDMA$_{0.95}$)), 80 (*p*((HPMA$_{80}$)-*co*-EGDMA$_{0.95}$)) and 120 (*p*((HPMA$_{120}$)-*co*-EGDMA$_{0.95}$)) monomer units were targeted. Reactions were left to copolymerise until vinyl monomer resonances ere not detectable within the $^{1}$H NMR spectroscopic analysis (> 99 % conversion) and subsequently terminated *via* exposure to the atmosphere and addition of oxygenated methanol. Under these conditions (1:0.95 monomer:brancher, 50 w/v % (monomer/solvent) all three copolymers remained soluble in THF and methanol with no visual gelation detectable, although the viscosity increased dramatically in the latter stages of copolymerisation. Copolymers were analysed by triple detection GPC in THF and their GPC chromatograms are shown in Figure 3.15. It should be noted that although it was possible to obtain soluble branched polymers at > 99 %

conversion, copolymerisations formed gel-networks when left for a significant period of time after reaching this conversion. This suggests after complete monomer consumption, the active chain ends (of the soluble branched copolymers) react with each other in a termination by combination type reaction, resulting in insoluble gel-networks. This type of reaction has also been postulated in Section 3.2.3 for linear polymers (due to the increase in molecular weight distribution at high conversion). The broad traces seen in Figure 3.15 are indicative of very high molecular weight materials within the copolymer samples; eluting as low at 10 mL for *p*((HPMA$_{120}$)-*co*-EGDMA$_{0.95}$). It is also noted here that a large fraction of these polymer samples appears to be of linear architecture, eluting at much higher retention volumes (18-20 mL).

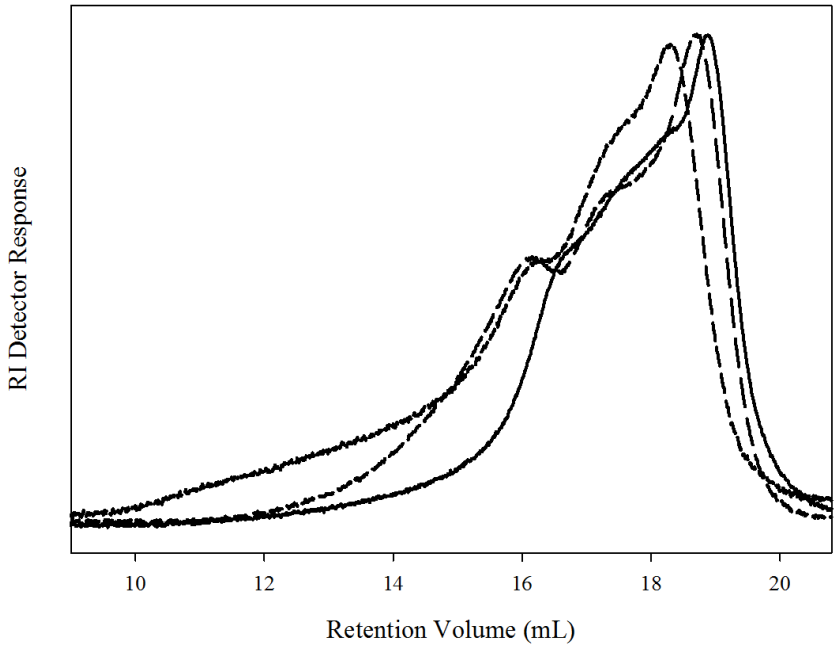


Figure 3.15: GPC (THF eluent) chromatograms for branched copolymers prepared by ambient methanolic ATRP and varying in primary chain target DP$_n$ *p*((HPMA$_{50}$)-*co*-EGDMA$_{0.95}$) (solid line), *p*((HPMA$_{80}$)-*co*-EGDMA$_{0.95}$) (medium dashed line), *p*((HPMA$_{120}$)-*co*-EGDMA$_{0.95}$) (small dashed line).

Table 3.3 shows molecular weights and molecular weight distributions of branched copolymers where the data suggests that as target $DP_n$ increases for the primary chains, branched copolymer molecular weight and dispersity increase.

| Sample | $M_n$ (g mol$^{-1}$) (theory) | $M_n$ (g mol$^{-1}$) (GPC) | $M_w$ (g mol$^{-1}$) (GPC) | $M_w/M_n$ | Conversion (%) |
|---|---|---|---|---|---|
| *p*((HPMA$_{50}$)-*co*-EGDMA$_{0.95}$) | / | 57600 | 374400 | 6.5 | > 99 |
| *p*((HPMA$_{80}$)-*co*-EGDMA$_{0.95}$) | / | 169000 | 1217000 | 7.2 | > 99 |
| *p*((HPMA$_{120}$)-*co*-EGDMA$_{0.95}$) | / | 230000 | 2392000 | 10.4 | > 99 |

Table 3.3: Data obtained *via* triple detection GPC (THF eluent) for the copolymerisation of *p*((HPMA$_x$)-*co*-EGDMA$_{0.95}$) with increasing target $DP_n$.

It is important to note that analysis by GPC utilises RALS, LALS and IV detectors. Similarly to section 3.2, the signals from all detectors are shown for *p*((HPMA$_{50}$)-*co*-EGDMA$_{0.95}$) as a comparison with previous results, Figure 3.16.

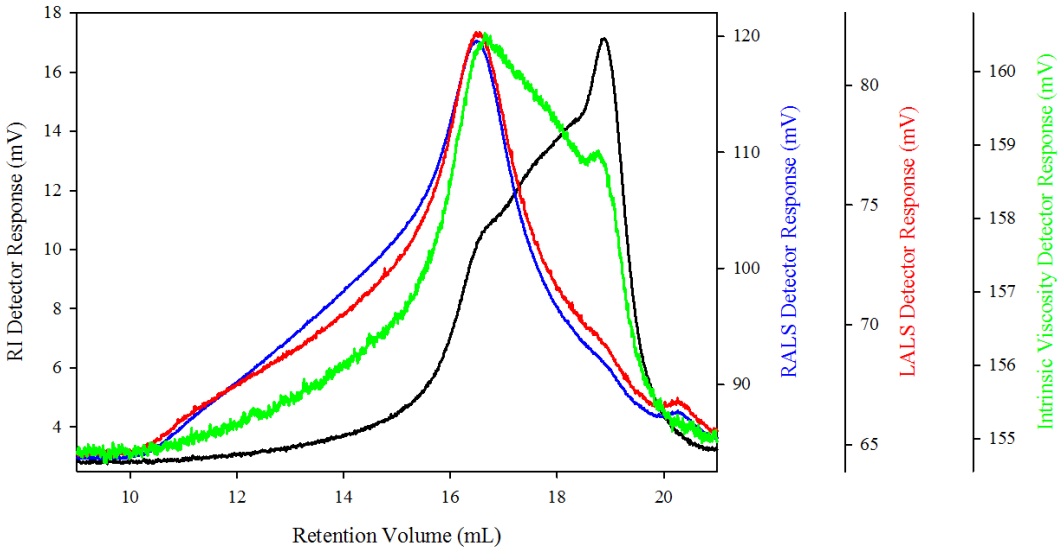


Figure 3.16: GPC (THF eluent) chromatograms of *p*((HPMA$_{50}$)-*co*-EGDMA$_{0.95}$) showing RI (black line), RALS (blue line), LALS (red line) and Intrinsic Viscosity (green line) responses.

The data in Figure 3.16 suggests the presence of very high molecular weight material. Both RALS and LALS detector responses are much more heavily weighted towards lower retention volumes, due to the higher amount of scattering for large highly branched materials. It should be noted that similar to RI detector response, the RALS and LALS detectors show lower molecular weight material present within the sample.

Figure 3.15 and Figure 3.16 both suggest high molecular weight material is formed during the copolymerisation of HPMA and EGDMA with no experimental difficulty, however, investigation into the kinetics of these copolymerisation is extremely important in order to determine when branching is occurring and at what point it becomes significant in these systems with respect to the ATRP mechanism, if at all.

### 3.3.1 Kinetic Studies for the Branched Copolymerisation of *p*((HPMA$_x$)-*co*-EGDMA$_{0.95}$), ($x$ = 50, 80, 120)

Primary chains with target DP$_n$ values of 50, 80 and 120 monomer units were chosen to study branched copolymer kinetics as these are easily comparable to the linear kinetics data described in section 3.2.2. All three reactions were performed within one week and regular sampling at hourly intervals was performed to allow analysis by $^1$H NMR spectroscopy (DMSO-$d_6$) and triple detection GPC (THF eluent). (see Chapter 2 section 2.3.2).

A linear semi-logarithmic plot is observed in the branched copolymerisation of HPMA and EGDMA with a target primary chain DP$_n$ of 50 monomer units (shown in Figure 3.17) indicating a constant concentration of radicals throughout the polymerisation, along with a high rate of conversion in the early stages of the reaction. It appears the reaction is typical for ATRP and that addition of EGDMA has not affected reaction kinetics. Kinetic experiments were conducted in the same manner for target DP$_n$ of 80 and 120 monomer units with similar behaviour (seen in Figure 3.18 and Figure 3.19.

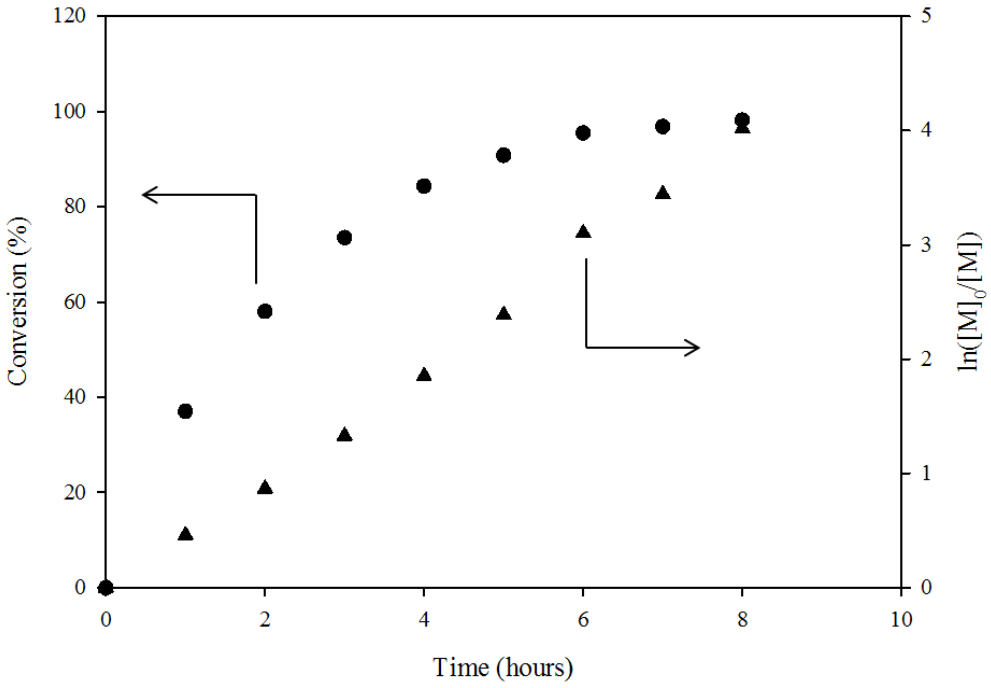


Figure 3.17 Kinetics plot for the synthesis of *p*((HPMA$_{50}$)-*co*-EGDMA$_{0.95}$) in methanol by ambient ATRP.

Similar to the linear homopolymerisation kinetic study in section 3.2.2, the reaction rate appears to reduce as target DP$_n$ increases. As the reactions have an equal molar ratio of monomer, this is clearly evident, however, a lower radical concentration is the probable cause due to the targeting of longer primary chains. The period of time necessary to reach higher conversion was found to be considerably longer for copolymerisations with higher target DP$_n$ (Figure 3.18).

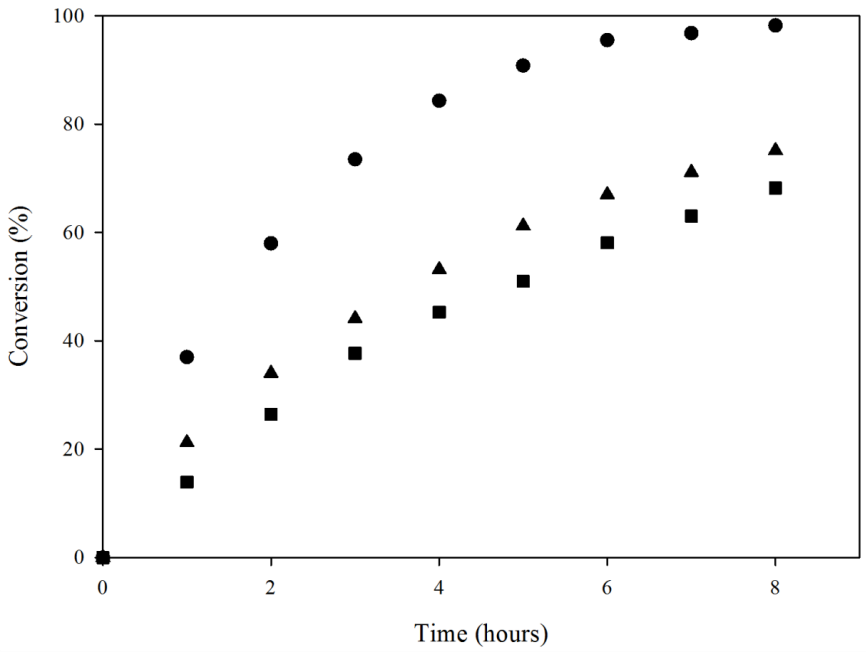


Figure 3.18: Conversion *vs*. Time for the copolymerisation of HPMA and EGDMA by methanolic ambient ATRP. *p*((HPMA$_{50}$)-*co*-EGDMA$_{0.95}$) (circle), *p*((HPMA$_{80}$)-*co*-EGDMA$_{0.95}$) (triangle), and *p*((HPMA$_{120}$)-*co*-EGDMA$_{0.95}$) (square).

Similar to linear homopolymerisations, the semi-logarithmic plots for branched copolymerisations are linear (Figure 3.19); it is therefore assumed the radical concentration is constant throughout each reactions and first order kinetics are observed during the polymerisation. The gradient of the plots decrease as target DP$_n$ increases (comparable to linear homopolymerisation) due to the diminishing concentration of propagating radicals in the copolymerisation reaction as target DP$_n$ increases. The difference in reaction rate is dramatically affected when the targeted DP$_n$ varies from 50 to 80 monomer units, compared to linear homopolymerisations, where rate retardation is most affected when target DP$_n$ varies from 80 to 120 monomer units.

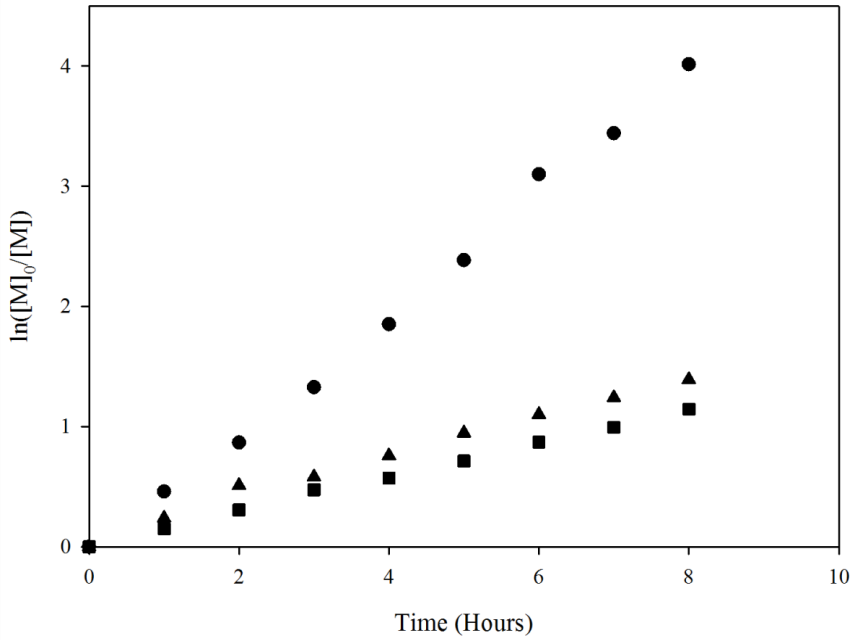


Figure 3.19: Semi-logarithmic plot for the copolymerisation of HPMA and EGDMA by methanolic ambient ATRP. *p*((HPMA$_{50}$)-*co*-EGDMA$_{0.95}$) (circle), *p*((HPMA$_{80}$)-*co*-EGDMA$_{0.95}$) (triangle), and *p*((HPMA$_{120}$)-*co*-EGDMA$_{0.95}$) (square).

Figure 3.20 shows the comparison between the reaction kinetics of a linear and branched copolymerisation with a target DP$_n$ of 50 monomer units for both the linear polymer and the primary *p*(HPMA) chains of the branched copolymer. The data suggests that despite the addition of EGDMA, reaction kinetics remain relatively similar. The copolymerisation of *p*((HPMA$_{50}$)-*co*-EGDMA$_{0.95}$) is slightly slower than its linear counterpart, possibly due to the change in concentration of the monomer in the copolymerisation reaction (due to addition of brancher). It cannot be due to changes in the concentration of initiator, as they were identical in both reactions. Similar results have been shown by Rannard and co-workers where

retardation of reaction rate was observed due to the addition of EGDMA brancher in comparison to a linear counterpart.[10]

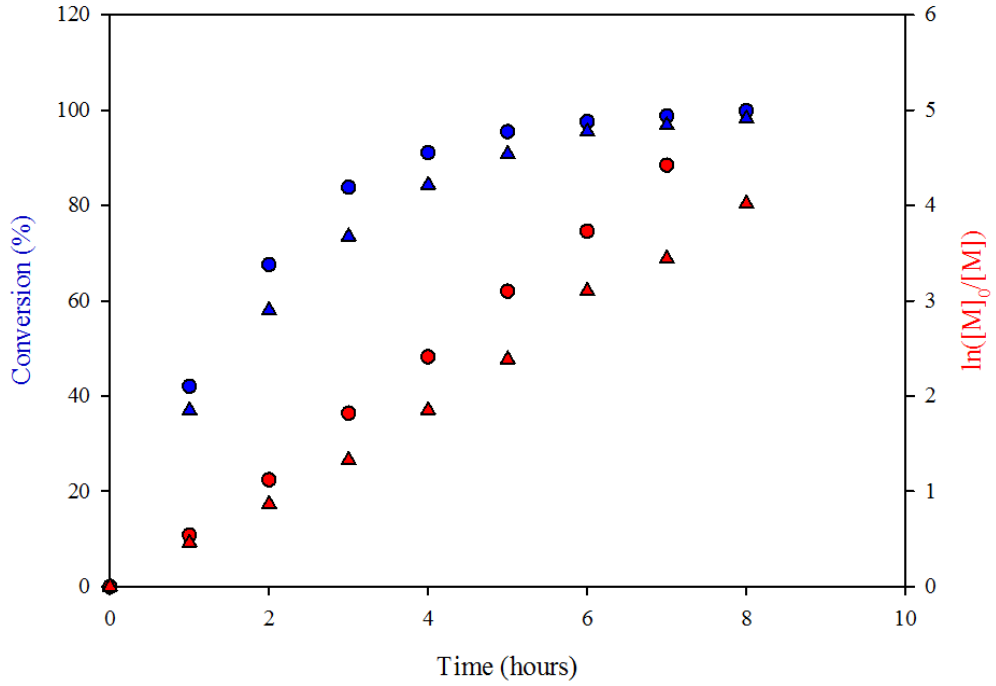


Figure 3.20: Comparison of the kinetics studies for the linear homopolymerisation and copolymerisations of HPMA and HPMA/EGDMA by methanolic ambient ATRP. *p*(HPMA$_{50}$) (circles) and *p*((HPMA$_{50}$)-*co*-EGDMA$_{0.95}$) (triangles).

Figure 3.21 displays the GPC chromatograms of copolymer samples taken from the reaction of *p*((HPMA$_{50}$)-*co*-EGDMA$_{0.95}$) over eight hours of copolymerisation. It is noted that peaks begin to broaden significantly after around 4 hours of copolymerisation (corresponding to a conversion of 84 %), however, slight peak broadening is seen prior to 4 hours reaction. Chromatograms continue to broaden throughout the copolymerisation until 8 hours reaction time (98 % conversion). GPC chromatograms performed for the kinetic studies of *p*((HPMA$_{80}$)-*co*-EGDMA$_{0.95}$) and *p*((HPMA$_{120}$)-*co*-EGDMA$_{0.95}$) are found in Appendix 3.1 and 3.2, respectively.

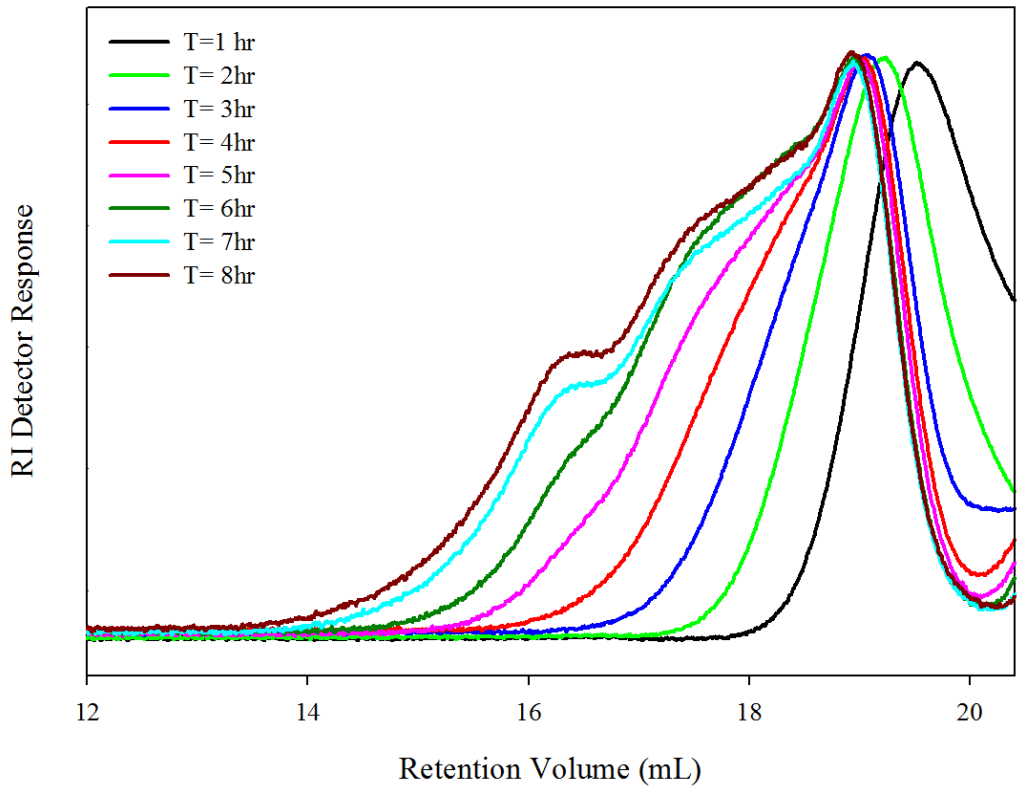


Figure 3.21: GPC (THF eluent) chromatograms for the kinetics study of the copolymerisation of HPMA and EGDMA by methanolic ambient ATRP to form *p*((HPMA$_{50}$)-*co*-EGDMA$_{0.95}$).

Figure 3.22 shows the overlay of the GPC chromatograms of *p*(HPMA$_{50}$) and *p*((HPMA$_{50}$)-*co*-EGDMA$_{0.95}$), showing significant peak overlap at high retention volumes (approximately 18-20 mL). This clearly suggests the presence of a clear linear fraction within the molecular weight distribution of the branched material. This also occurs in GPC chromatograms for DP$_n$ = 80 and 120 monomer units, shown in Appendix 3.3 and 3.4 respectively.

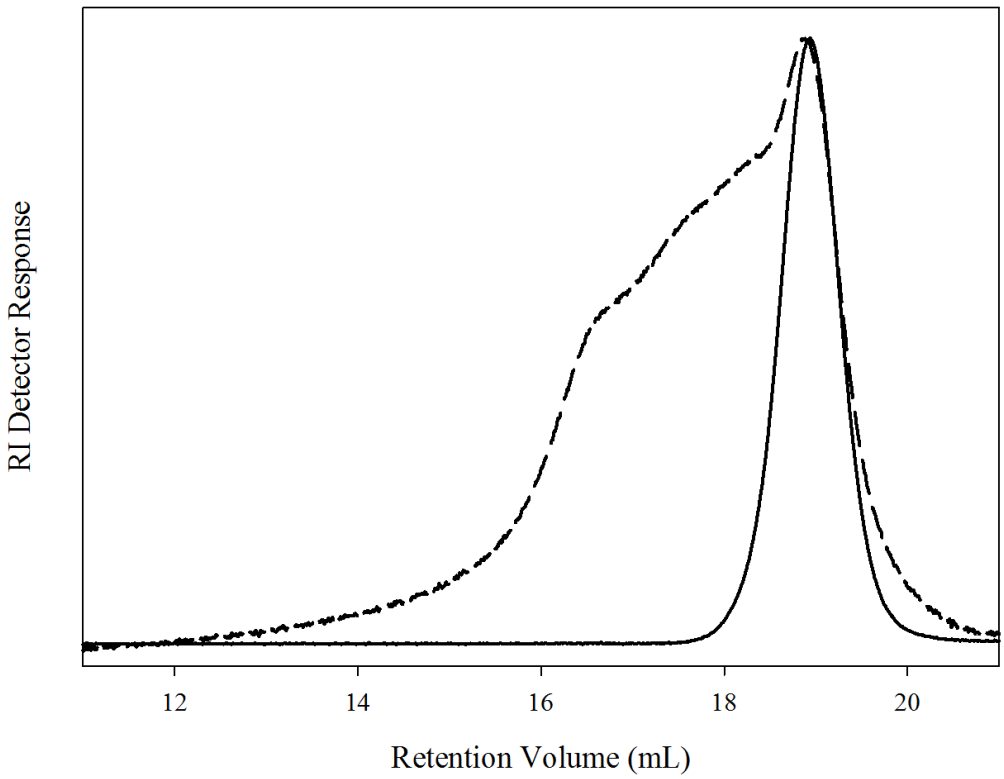


Figure 3.22 Overlaid GPC chromatograms of *p*(HPMA$_{50}$) (solid line) and *p*((HPMA$_{50}$)-*co*-EGDMA$_{0.95}$) (dashed line).

This mixture of linear and branched material existing in branched ATRP copolymerisations agrees well with the work reported by Armes and co-workers[26] whose Monte Carlo simulation models of branched systems concluded that statistically, there exist multiple copolymer architectures existing when a divinyl branched is incorporated such as linear material, highly branched material and chains containing intramolecular loops. In their previous reports investigating branched *p*(HPMA),[10] Armes and co-workers do not report significant overlap of GPC chromatograms for linear and branched material, unlike the data reported here. Other literature also report a complete shift in elution volume (suggesting a complete

architectural change from linear to branched polymer) when copolymerisations reach high conversion.[22, 23]

Some possibilities as to why branched copolymers contain linear material are:

1. Multiple branchers reacting between two primary chains intermolecularly, therefore reducing the number of pendant vinyl groups for reaction with other propagating chains.
2. Cyclisation within linear copolymer chains to yield copolymers unable to react intermolecularly with growing branched polymers. These would not be readily detectable *via* GPC analysis.

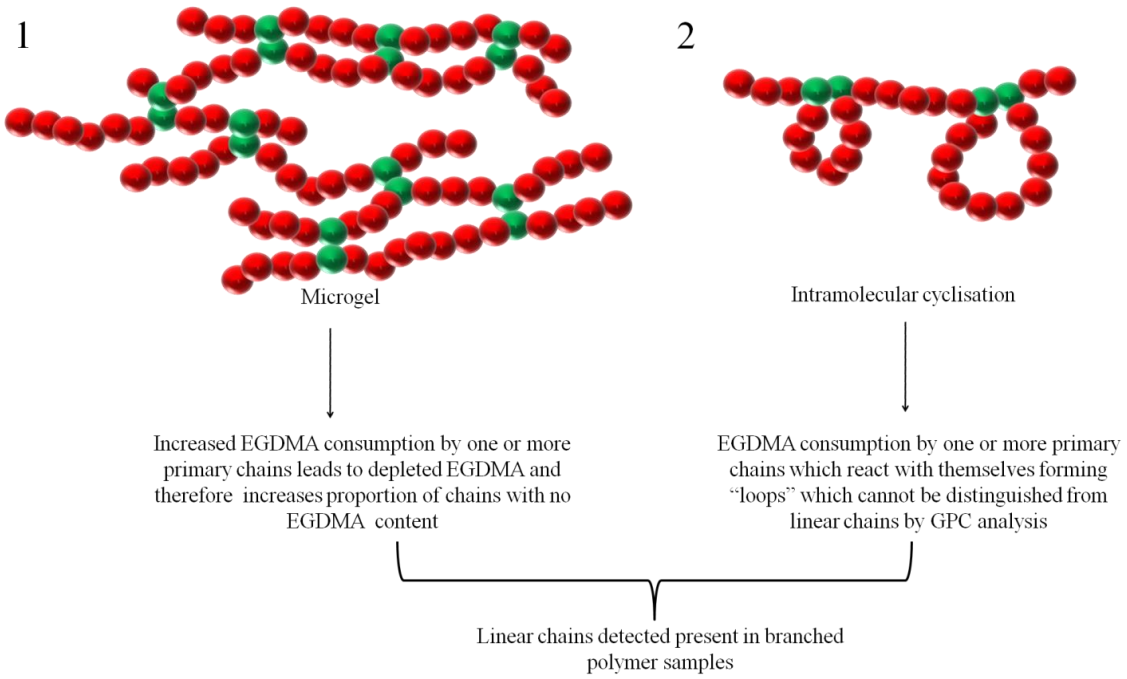


Scheme 3.4: Representation of proposed reactions leading to branched copolymer samples containing linear material.

In Scheme 3.4, two copolymerisation structures are proposed, which may ultimately contribute to the presence of linear material within branched copolymer samples. If

Scheme 3.4(1) occurs, it would be highly likely that gelation would also occur, causing network formation or microgelation. Gelation did not occur in branched the copolymerisations, either visually or observed within the GPC analysis. Micro-gelation may have occurred, with material being removed prior to injection or by the guard column in the GPC instrument, however, during sample filtration prior to injection, no adverse pressure was observed. If Scheme 3.4(2) is occurring, it is thought it would be most significant in the early stages of the polymerisation, as reaction mixtures becomes highly viscous at high conversion where monomer addition becomes diffusion controlled. It is proposed intramolecular cyclisation would be hindered where active chain ends are much more likely to react with other chains rather than with themselves.[20]

The formation of cycles is also predicted by Monte Carlo theory and very small differences in conversion, attained prior to deliberate termination of the reaction, can generate large differences of $M_n$ and $M_w$ in copolymer samples, due to the steep gradient of increasing molecular weight at very high conversion.

As expected, all three branched copolymers experienced a considerable increase in the observed number average molecular weights, weight average molecular weights and molecular weight distributions as reactions proceeded to high conversions, due to the covalent bonding of multiple linear chains. As seen in Figure 3.23, molecular weight distribution in the branched copolymerisation of *p*((HPMA$_{50}$)-*co*-EGDMA$_{0.95}$) increases dramatically with conversion, consistent with the theory of chain linking occurring with monomer depletion. Similar relationships for *p*((HPMA$_{80}$)-*co*-EGDMA$_{0.95}$) and *p*((HPMA$_{120}$)-*co*-EGDMA$_{0.95}$) can be found in Appendix 3.5 and 3.6, respectively.

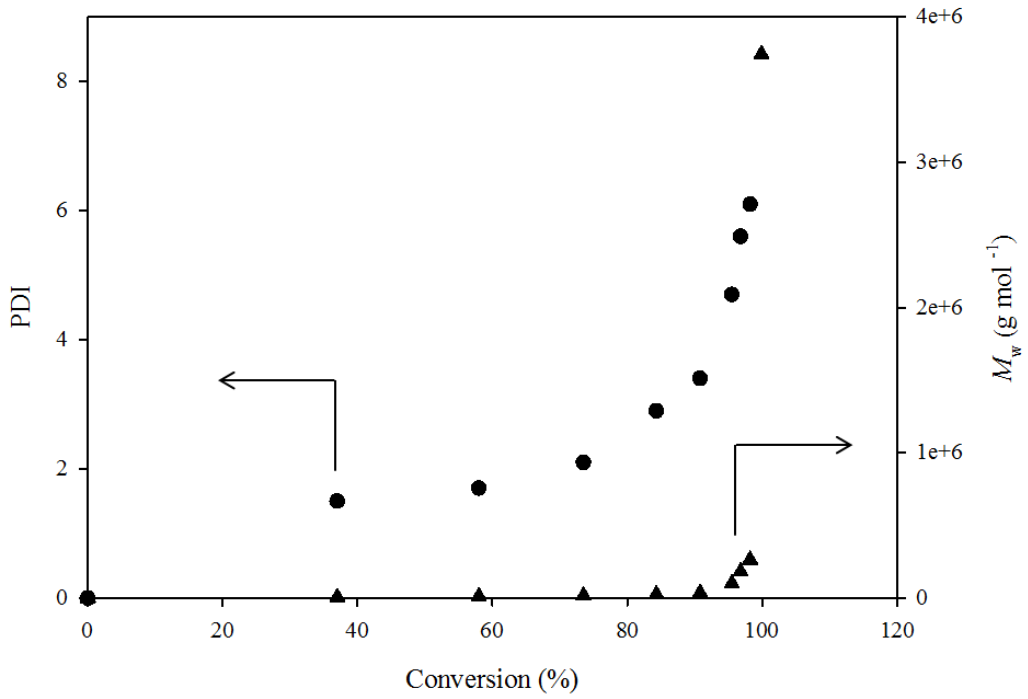


Figure 3.23: Weight average molecular weight and dispersity *vs*. conversion (%) plots determined during the kinetics study of the copolymerisation of HPMA and EGDMA by methanolic ambient ATRP to form *p*((HPMA$_{50}$)-*co*-EGDMA$_{0.95}$).

Figure 3.24 shows, the dramatic variation of number average molecular weight during the branched copolymerisation. $M_n$ begins to increase exponentially when conversion reaches > 80 % conversion where branching dominates the latter part of the reaction and HPMA monomer concentration is significantly reduced. As noted previously, when left at high conversion for extended periods, reactions become insoluble gelled networks, where it is proposed active chain ends of the branched copolymers terminate by combination.

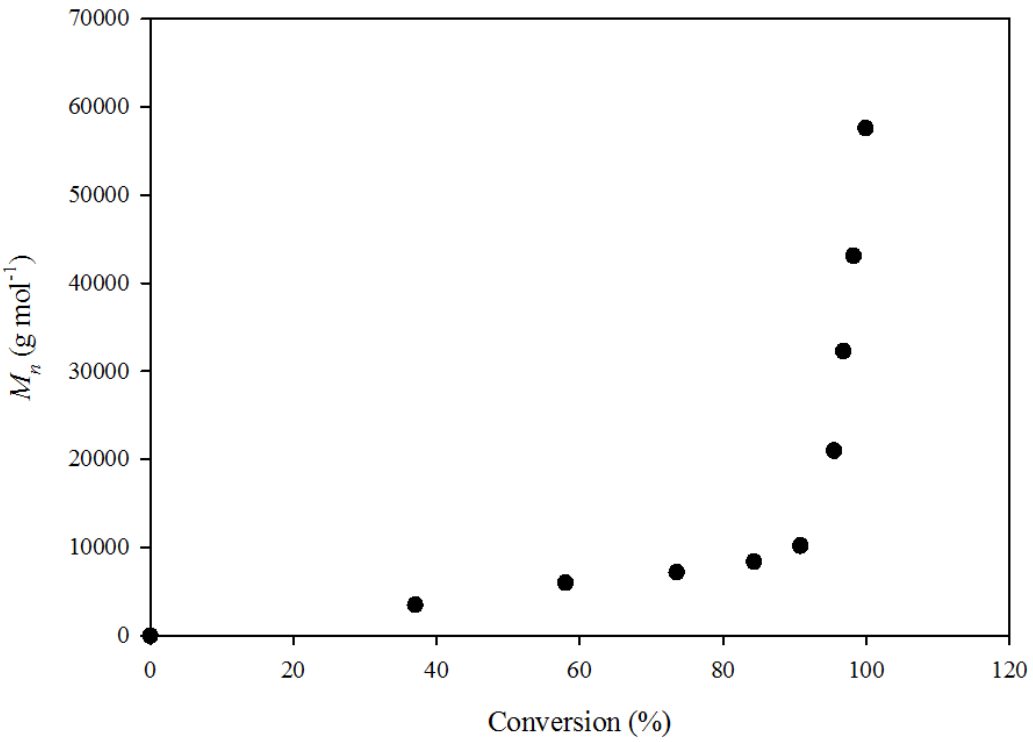


Figure 3.24: $M_n$ *vs*. conversion plot for the copolymerisation of HPMA and EGDMA by methanolic ambient ATRP polymerisation to form *p*((HPMA$_{50}$)-*co*-EGDMA$_{0.95}$).

## 3.3.2 Proposed Mechanism of Branched Vinyl Polymerisation using ATRP.

Scheme 3.5 represents the proposed mechanism of branching within the ATRP synthesis of *p*((HPMA$_x$)-*co*-EGDMA$_{0.95}$)). The reaction has been separated into three phases; Phase I represents the essentially linear growth of copolymer chains where the concentration of EGDMA is insignificant in comparison to the unreacted HPMA monomer; no branching behaviour is observed as EGDMA acts almost identically to the HPMA monomer with only one vinyl group predominantly undergoing polymerisation. When incorporated into a propagating chain, the second vinyl group in EGDMA is pendant to the growing linear chain. Phase II represents

the onset of branching as observed in the experimental deviation from linearity of $M_n$ *vs*. conversion curves and an increase in dispersity. Intramolecular coupling of linear copolymer chains begins *via* reaction of pendant vinyl groups of EGDMA with other growing linear copolymer chains. Here the concentration of the pendant vinyl groups becomes sufficient to allow intermolecular reaction between chains. Within Phase III, copolymer primary chains continue to grow linearly yet the molecular weight increase is dominated by the growing number of branch points between chains until all monomer has been depleted.

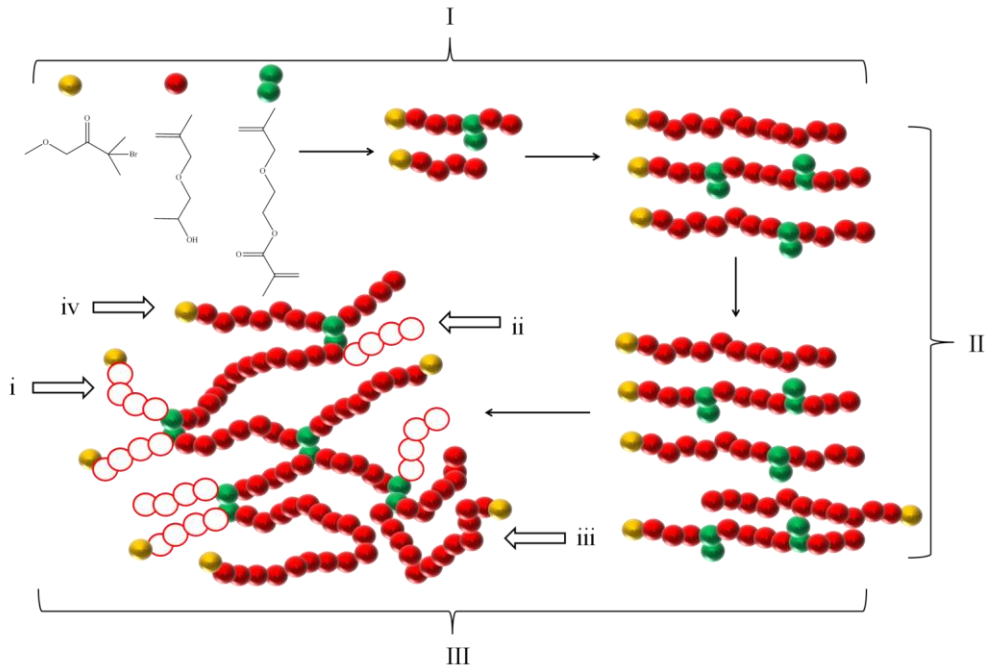


Scheme 3.5: Schematic representation of *p*(HPMA) branched copolymerisation. Phase I (oligomer formation), Phase II (initial inter-chain reaction), Phase III (intermolecular branching at high conversion) – chain-end oligomers formed at low conversion (i) and high conversion (ii) and long chain end groups (iii and iv) are highlighted.

In summary the synthesis of soluble, high molecular weight copolymers has been reported using a one-pot ATRP methodology. Reaction kinetics have been explored with varying target $DP_n$ and compared to their linear homopolymer data, followed by a proposed mechanism of branching.

### 3.3.3 Chain Extension using Branched Copolymers of HPMA and EGDMA – Exploring the Variation of Architecture by Sequential Monomer Addition.

Section 3.2.3 reported the chain extension, or self-blocking, of linear *p*($HPMA_x$) generating a block copolymer with low molecular weight distribution, with no experimental difficulty. This section aims to investigate whether chain ends in branched copolymerisations still remain active after sequential addition of additional monomer feeds. This may be done in three ways, one of which would be to copolymerise chains of branched polymers and after reaching high conversion, add another batch of monomer and brancher to give a doubly branched copolymer.

This reaction was not performed as it was highly likely that a gelled network would result, due to previous experiments where insoluble copolymer mass was formed after leaving copolymerisations which had reached > 100 % conversion.

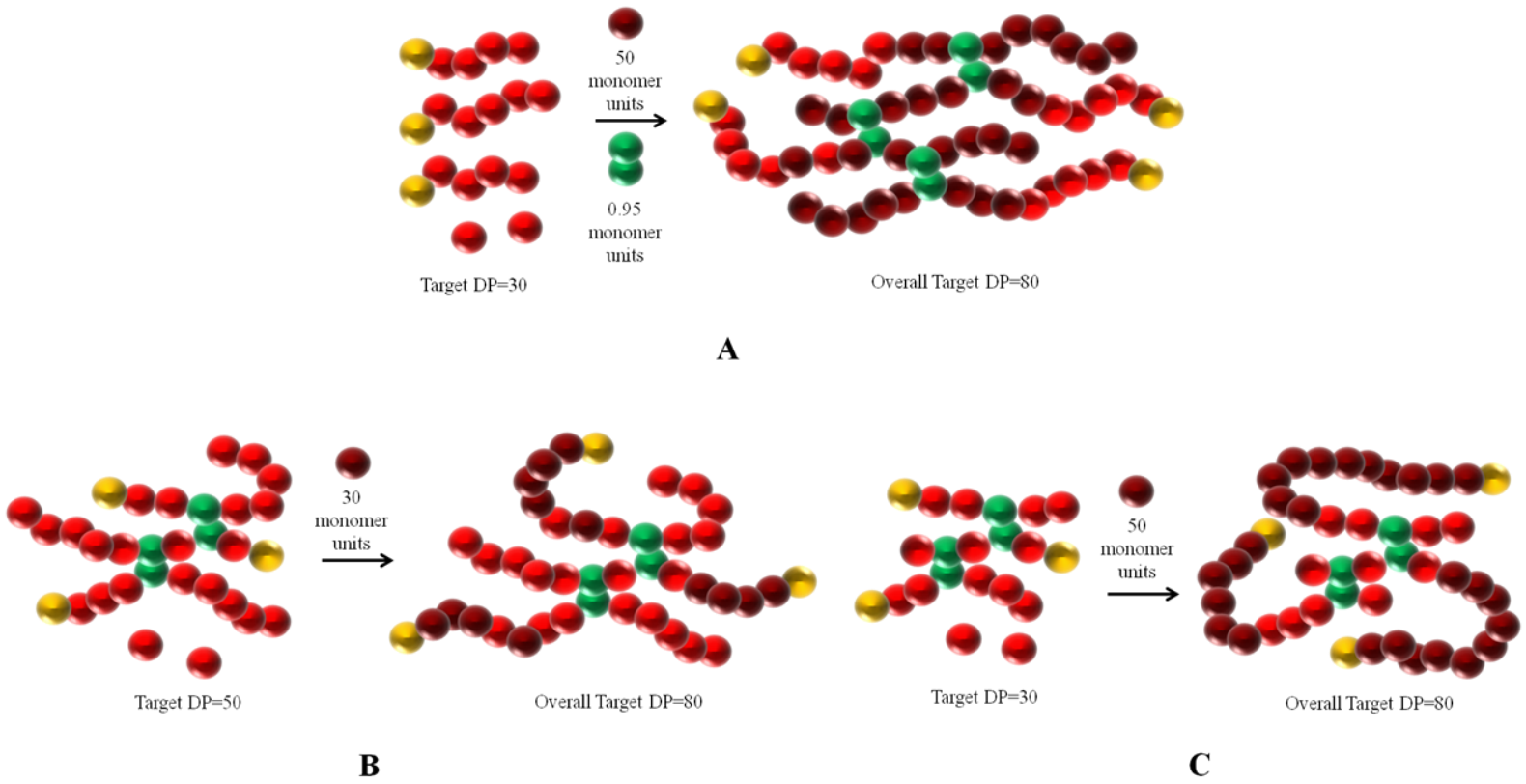


Scheme 3.6: Representation of the chain extension process to give an overall $DP_n$ of 80 monomer units. A) *p*(HPMA$_{30}$)-*b*-*p*((HPMA$_{50}$)-*co*-EGDMA$_{0.95}$). B) *p*(HPMA$_{50}$)-*b*-*p*((HPMA$_{30}$)-*co*-EGDMA$_{0.95}$). C) *p*((HPMA$_{30}$)-*co*-EGDMA$_{0.95}$)-*b*-*p*(HPMA$_{50}$).

Scheme 3.6 represents some of the different architectures which could be generated by varying the order of monomer and brancher addition. A) may be seen as an "arms-first" approach, B) and C) both could be seen as a "core-first" approach to generate branched block copolymers where maroon spheres represent the outer (or second) block of monomer. B) was attempted several times; despite successful addition of the second linear block, all reactions gelled. The exact reason for this is unclear but the presence of unreacted pendant vinyl groups which become available when the second monomer feed is added may lead to further branching and gelation. This would occur if, rather adding and an essentially linear chain to the branched polymer end groups, the longer chain ends are able to access hidden pendant reactive functionality. It may also be that the polymerisation reactions were left for too long after high conversion of the second monomer feed and gelation occurred due to termination by combination reaction. It is proposed that if reactions are terminated before gelation ensues, the architecture will be more similar to those previously synthesised rather than the block copolymer depicted in Scheme 3.6(B).

Route (A) shown in Scheme 3.6, was conducted with the initial formation of *p*($HPMA_{30}$) chains (red spheres) and, after achieving relatively high conversion, a second batch of HPMA monomer (equivalent to a $DP_n$ = 80 monomer units) containing EGDMA brancher (green spheres) at an initiator:brancher ratio of 1:0.95 was added. The second aliquot of monomer is represented in Scheme 3.6(A) by maroon spheres and a controlled copolymerisation was expected, however, the resulting copolymer was also expected to form a dramatically different architecture when compared to the formation of a branched copolymer from the direct copolymerisation of HPMA and EGDMA with a primary chain target $DP_n$ = 80

monomer units. The synthesis of a soluble branched copolymer was expected, as only a small quantity of brancher was added and hypothetically, the introduction of a short chain of *p*(HPMA) prior to the addition of brancher should have no negative impact on the polymerisation and crosslinking should not occur. $^{1}$H NMR spectroscopy and GPC analysis were used to monitor the reaction over time, with a sample taken just before addition of the second monomer batch to ensure relatively high conversion had been reached. Triple detection GPC (THF eluent) was used to analyse the samples, as shown in Figure 3.25.

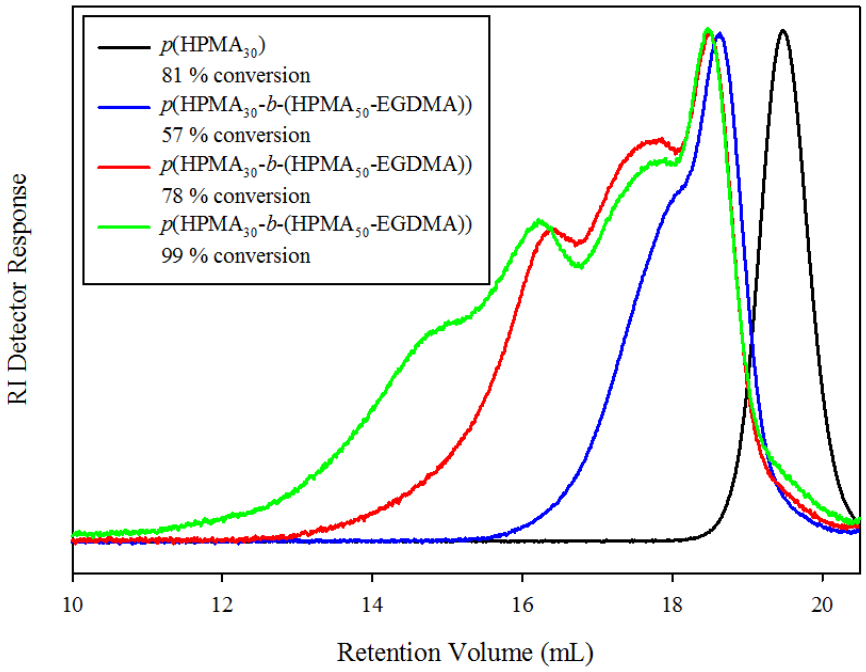


Figure 3.25: GPC chromatograms at varying points during a branched chain extension using methanolic ATRP to form *p*((HPMA$_{30}$)-*b*-((HPMA$_{50}$)-*co*-EGDMA$_{0.95}$)).

It is clear from Figure 3.25 that high molecular weight material is formed, due to brancher introduced within the second batch of monomer. Molecular weight distribution increases as conversion increases suggesting that branching dominates at extremely high conversion. Again, as previously noted, a linear peak appears at high

retention volume, suggesting a proportion of these copolymer chains are not branched, even at high conversion. Importantly, no linear polymer from the initial formation of the linear *p*($HPMA_{30}$) chains are observed in the final polymer. This suggests a very efficient propagation of the second mixed monomer:brancher feed without termination of the initial propagating chains. The presence of linear polymer in the final branched polymer sample must therefore be derived from the addition of the second HPMA monomer feed but without successful intermolecular branching of these chains.

Table 3.4 displays the data obtained during this reaction where no theoretical molecular weights could be calculated as EGDMA incorporation is statistical. Very high number average and weight average molecular weight was obtained ($M_n$ = 185000 g $mol^{-1}$, $M_w$ = 1128500 g $mol^{-1}$) alongside a molecular weight distribution of 6.1 when > 99 % conversion had been reached.

| Sample | $M_n$ (g mol$^{-1}$) (theoretical)* | $M_n$ (g mol$^{-1}$) (GPC) | $M_w$ (g mol$^{-1}$) (GPC) | $M_w/M_n$ | Conversion (%) |
|---|---|---|---|---|---|
| *p*(HPMA$_{30}$) | 3500 | 3300 | 3600 | 1.09 | 81 |
| *p*(HPMA$_{30}$)-*b*-*p*((HPMA$_{50}$)-*co*-EGDMA$_{0.95}$) | / | 25400 | 51200 | 2.10 | 57 |
| *p*(HPMA$_{30}$)-*b*-*p*(HPMA$_{50}$)-*co*-EGDMA$_{0.95}$) | / | 50000 | 245000 | 4.90 | 78 |
| *p*(HPMA$_{30}$)-*b*-*p*(HPMA$_{50}$)-*co*-EGDMA$_{0.95}$) | / | 185000 | 1128500 | 6.10 | 99 |

Table 3.4: Data for the branching chain extension of *p*(HPMA) using a statistical copolymerisation of HPMA and EGDMA utilising methanolic ATRP. *Theoretical values are based on the measured conversion values using $^1$H NMR (DMSO-d$_6$).

Similar to Section 3.2.3 where, linear block copolymers, synthesised from a self-blocking experiment with an overall target DP$_n$ = 80 monomer units, were compared to *p*(HPMA$_{80}$) synthesised in a single reaction, Figure 3.26 shows the GPC chromatograms (RI detector response) of *p*((HPMA$_{80}$)-*co*-EGDMA$_{0.95}$) overlaid with the same chromatogram from *p*(HPMA$_{30}$)-*b*-*p*((HPMA$_{50}$)-*co*-EGDMA$_{0.95}$). The branched self-blocked copolymer begins to elute at a lower retention volume in comparison to the branched copolymer prepared with EGDMA being present at all

times. Previous analysis of the RI chromatograms of branched polymers synthesised during this study have shown that a significant fraction of linear polymer is present in the final branched copolymers. The overlaid chromatograms in Figure 3.26 also suggest the presence of linear polymers, however, despite the nominal equivalent chain length of the linear polymers ($DP_n$ = 80 monomer units), when EGDMA is added in the second monomer feed, the linear fraction of the polymer distribution can be seen at a lower elution volume.

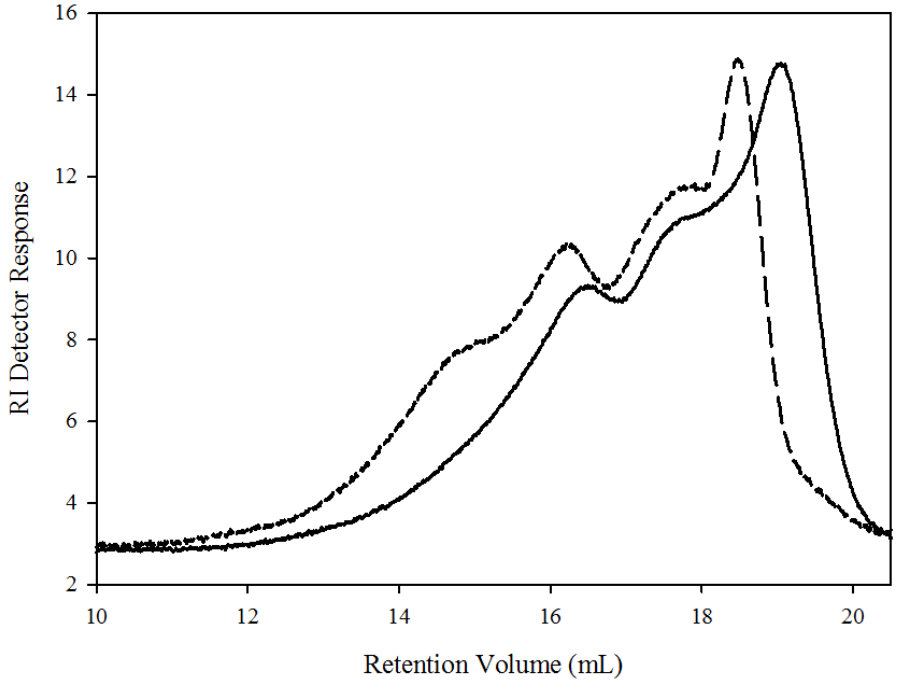


Figure 3.26: Overlaid Refractive Index chromatograms from GPC analysis (THF eluent) of *p*((HPMA$_{80}$)-*co*-EGDMA$_{0.95}$) (solid line) and *p*(HPMA$_{30}$)-*b*-*p*(HPMA$_{50}$)-*co*-EGDMA$_{0.95}$) (dashed line).

The presence of longer $DP_n$ linear chains may contribute to the observed decrease in dispersity of 6.1 for *p*((HPMA$_{30}$)-*b*-*p*(HPMA$_{50}$)-*co*-EGDMA$_{0.95}$)) compared to 7.2

for *p*((HPMA$_{80}$)-*co*-EGDMA$_{0.95}$). The reason for the higher molecular weight fraction in the chain extended copolymer is not clear; as this reaction was only performed once, it may be that temperature and/or experimental protocol were slightly different. Homogeneity of the reaction mixture will be altered as the second monomer feed is added, and as diffusion may be hindered it may lead to less than ideal EGDMA incorporation.

Figure 3.27 shows the GPC chromatograms for *p*(HPMA$_{30}$)-*b*-*p*((HPMA$_{50}$)-*co*-EGDMA$_{0.95}$) and *p*((HPMA$_{120}$)-*co*-EGDMA$_{0.95}$), where near complete overlap of peaks at approximately 18 mL is noted.

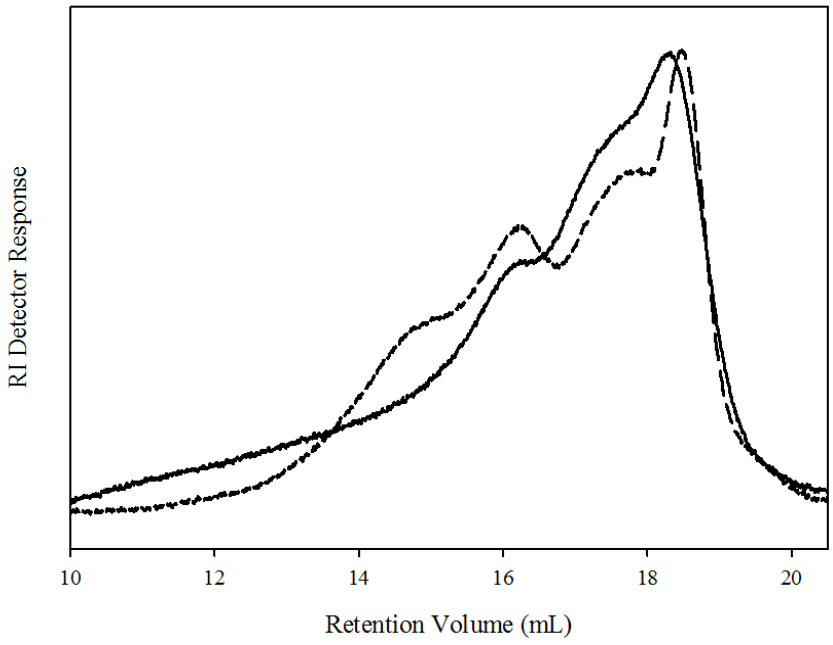


Figure 3.27: Overlaid Refractive Index chromatograms from GPC analysis (THF eluent) of *p*((HPMA$_{120}$)-*co*-EGDMA$_{0.95}$)) (solid line) and *p*(HPMA$_{30}$)-*b*-*p*((HPMA$_{50}$)-*co*-EGDMA$_{0.95}$)) (dashed line).

The data suggests that the linear material present within the chain extended copolymer is much more likely to have a $DP_n$ of approximately 120 monomer units, suggesting that despite an overall target $DP_n$ of 80 monomer units, the generation of linear material of a higher chain length is formed. It is possible that these are lightly branched chains or possibly dimers, produced by linear chains of $DP_n$ = 80 monomer units and enhanced incorporation of EGDMA is seen through this approach.

## 3.4 Summary

This chapter has reported the facile ATRP synthesis of linear *p*($HPMA_x$) homopolymers where detailed kinetic experiments were performed, confirming reactions proceeded in a controlled manner. A self-blocking experiment also confirmed that chain end functionality was maintained at relatively high conversion, generating block copolymers with a narrow molecular weight distribution and accurate molecular weight. It is believed this is the first report of branched *p*(HPMA) copolymer synthesis investigated in significant detail.

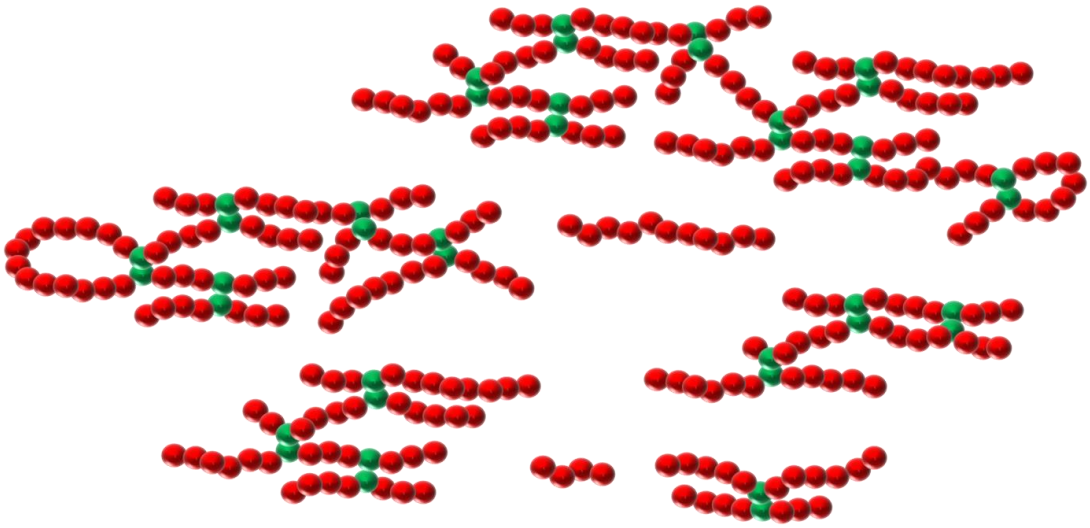

Figure 3.28: Representation of the range of materials believed to be present within *p*((HPMA$_x$)-*co*-EGDMA$_{0.95}$) samples.

From kinetic GPC analysis, a mechanistic scheme of the branching process has been proposed. High molecular weight soluble materials have been synthesised simply by controlling the monomer:brancher ratio. It has been noted that leaving these polymerisations to stand whilst still active induces gelation, yet by monitoring reaction kinetics, this can be suppressed and reactions can be manually terminated at > 99 % conversion. It is thought that the Monte Carlo modelling approach clearly correlates with the observed branching process; essentially based on statistics and predicting intramolecular cyclisation, linear chains and as branched copolymers, all of which are believed to be present in *p*((HPMA$_x$)-*co*-EGDMA$_{0.95}$) copolymer samples.

Figure 3.28 maps out a range of architectures believed to be synthesised during the branching process. This diverse range of architectures is due to the extreme retention volume ranges seen during GPC analysis. It may be possible to fractionate linear material to give purely branched copolymers, but this was not attempted.

## 3.5 References

1. Patten, T. E., Matyjaszewski, K., *Adv Mater,* **1998**, *10*, 901.

2. Matyjaszewski. K., *Chem Eur J,* **1999**, *5*, 3095.

3. Save. M., Weaver. J. V. M., Armes. S. P., *Macromolecules*, **2002**, *35*, 1152.

4. Chen. J. M., Yang. Y. L., *Spectrosc Spectral Anal*, **2001**, *21*, 47.

5. Hutchinson. R. A., Beuermann. S., Jackson. C., *Macromolecules*, **1998**, *31*, 1542.

6. Wang. Y-J., Liu. J-M, Yuan. C-D., Liu. J-F., Tan. X., Cao. T-Y., *Polym Int*, **2001**, *50*, 326.

7. Poinescu. I. C., Vlad. C., Ghiocel. I., *Polym-Plast Technol*, **1997**, *36*, (*6*), 841.

8. Long. M., Thornwaite. D. W., Rogers. S. H., Bonzi. G., Livens. F. R., Rannard. S. P., *Chem Commun*, **2009**, *42*, 6406.

9. Wu. T., Mei. Y., Cabral. J. T., Xu. C., Beers. K. L., *J Am Chem Soc*, **2004**, *126*, 9880.

10. Bannister. I., Billingham. N. C., Armes. S. P., Rannard. S. P., Findlay. P., *Macromolecules*, **2006**, *39*, (*22*), 7483.

11. Singha. N. K., de Ruiter. B., Schubert. U. S., *Macromolecules* **2005**, *38*, 3596.

12. Lee. S. B., J. Russell. A. J., Matyjaszewski. K., *Biomacromolecules*, **2003**, *4*, 1386.

13. Wang. J., Matyjaszewski. K., *Macromolecules*, **1995**, *28*, 7901.

14. Wang. X., Armes. S. P., *Macromolecules*, **2000**, *33*, 6640.

15. Bouhier. M., Cormack. P. A. G., Graham. S., Sherrington. D. C., *J Polym Sci Part A: Polym Chem*, **2007**, *45*, 2375.

16. Ma. I. Y., Lobb. E. J., Billingham. N. C., Armes. S. P., Lewis. A. L., Lloyd. A. W., Salvage. J., *Macromolecules*, **2002**, *35*, 9306.

17. Matyjaszewski. K., Xia. J. *Chem Rev*, **2001**, *101*, 2921.

18. Angot. S., Murthy. K. S., Taton. D., Gnanou. Y., *Macromolecules*, **1998**, *31*, 7218.

19. Shipp. D. A., Matyjaszewski. K., *Macromolecules*, **1999**, *32*, 2948.

20. Li. W., Yoon. J. A., Zhong. M., Matyjaszewski. K., *Macromolecules*, **2011**, *44*, 3270.

21. Li. Y., Armes. S. P., *Macromolecules*, **2005**, *38*, 8155.

22. Haidan. G., Wenyan. H., Dongliang. Z., Fanghong. G., Chunlin. L., Yang. Y., Jianhai. C., Bibiao. J., *Polymer*, **2008**, *49*, 4101.

23. Gao. H, Min. K., Matyjaszewski. K., *Macromolecules*, **2007,** *40*, 7763.

24. Rosselgong. J., Armes. S. P., *Macromolecules*, **2010**, *43*, 2145.

25. Sherrington. D. C., Saunders. G., *J Macromol Sci B*, **2005**, *44*, (*6*), 88.

26. Bannister. I., Billingham. N. C., Armes. S. P., *Soft Matter*, **2009**, *5*, 3495.

The research described in Chapter 4 has been partially published as

"Architecture-driven aqueous stability of hydrophobic, branched polymer nanoparticles prepared by rapid nanoprecipitation."

R. A. Slater, T. O. McDonald, D. J. Adams, E. R. Draper, J. V. M. Weaver and S. P. Rannard.

*Soft Matter*, **2012**, 8(38), 9816 – 9827.

# 4. Synthesis of Polymeric Nanoparticles using *p*(HPMA)

## 4.1 Introduction

The formation of nanoparticles from amphiphilic block copolymers has been reported using several methods.[1, 2] For hydrophobic homopolymers and copolymers, the use of nanoprecipitation has been shown to be particularly successful if conditions can be found to prevent macrophase separation and guarantee the formation of colloidally stable sub-micron particles. Polymers such as polystyrene[3] and poly(D,L-lactide-co-glycolide)[4] have been shown to produce near monodisperse nanoparticles in surfactant-free procedures and without obvious hydrophilic stabilising chains.

In this chapter, the formation of nanoparticles from linear and branched *p*(HPMA) was evaluated using various precipitation methods. Mechanisms of formation are postulated and a range of studies are used to investigate the aqueous nanoparticle stability and the effects of polymer architecture.

## 4.2 Nanoprecipitation of Linear *p*(HPMA$_x$) ($x$ = 50, 80, 120)

Linear polymers comprising different lengths of *p(*HPMA) (50, 80, 120 monomer units), synthesised using methanolic ATRP, were subjected to a solvent switch in order to generate nanosupensions in water. It should be noted here that no additional surfactants were added at any stage, and therefore the stability of the nanoparticles can only be attributed to the experimental protocol, polymer chemistry and concentration, giving a true insight into the process. Following nanoparticle

preparation, our aim was to avoid additional purification techniques (including dialysis, filtration, centrifugation and dilution) as although these may be common practice, these processes eliminate polymer mass and the final concentration is often unknown or unstated within literature reports.[5] Such purification techniques are also costly and time-consuming. It was believed a bottom-up approach to these experiments was required in this research, especially as materials of this nature have not been widely researched, and in this way experiments can be built upon based on the generated data results.

Schubert and co-workers often use dialysis or a slow dripping method for the preparation of nanoparticles[6] by nanoprecipitation and in order to initially investigate the full spectrum of nanoprecipitation techniques it was decided the first experiments would be based around these two methods. Representations of these processes are shown in Scheme 4.1 and Scheme 4.2 and individual experimental protocols are found in Chapter 2 section 2.5.1.2 and section 2.5.1.3.

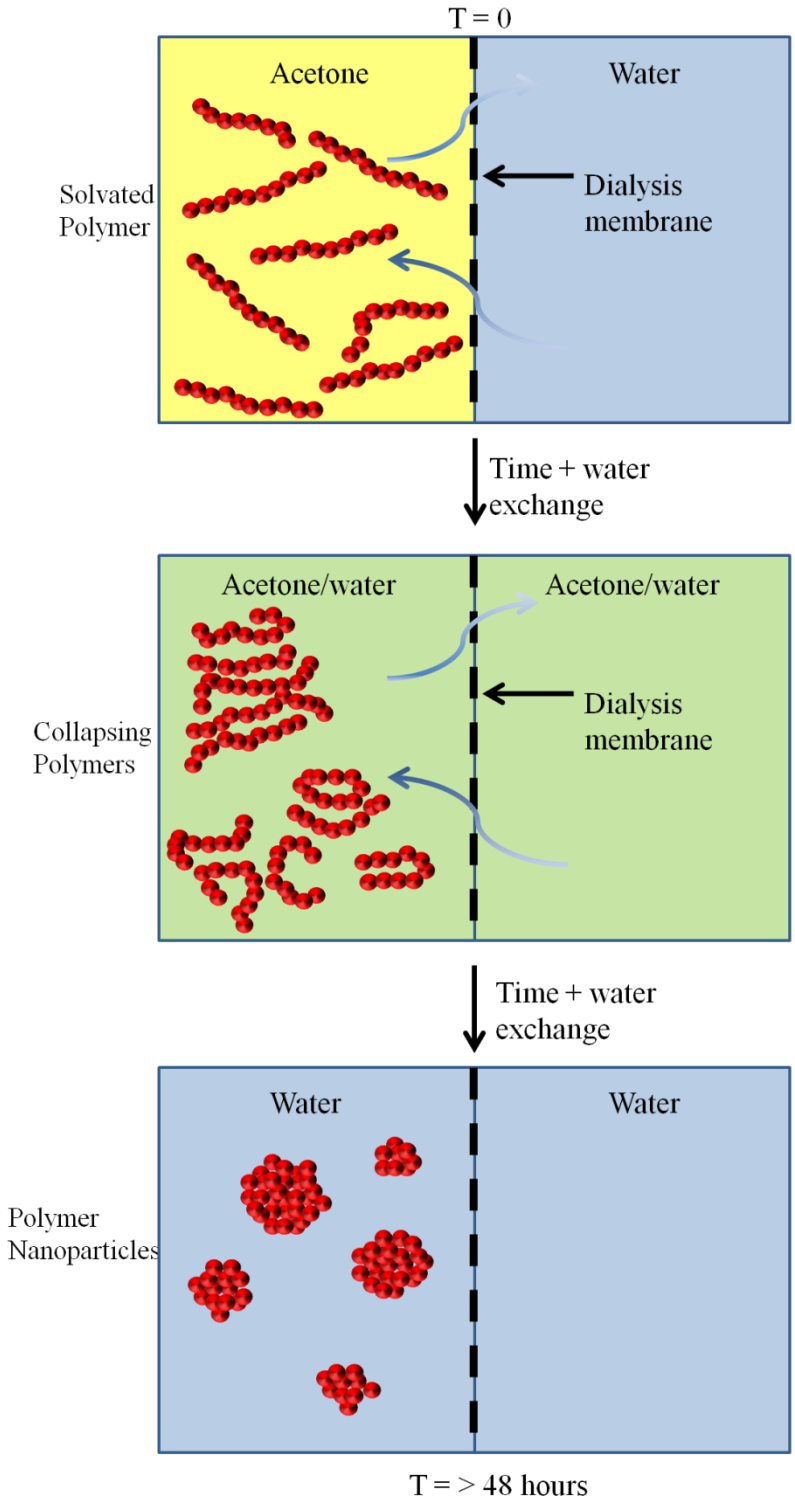


Scheme 4.1: Representation of nanoparticle production *via* dialysis using solvated linear homopolymers in acetone in a dialysis membrane and continual water exchange for > 48 hours.

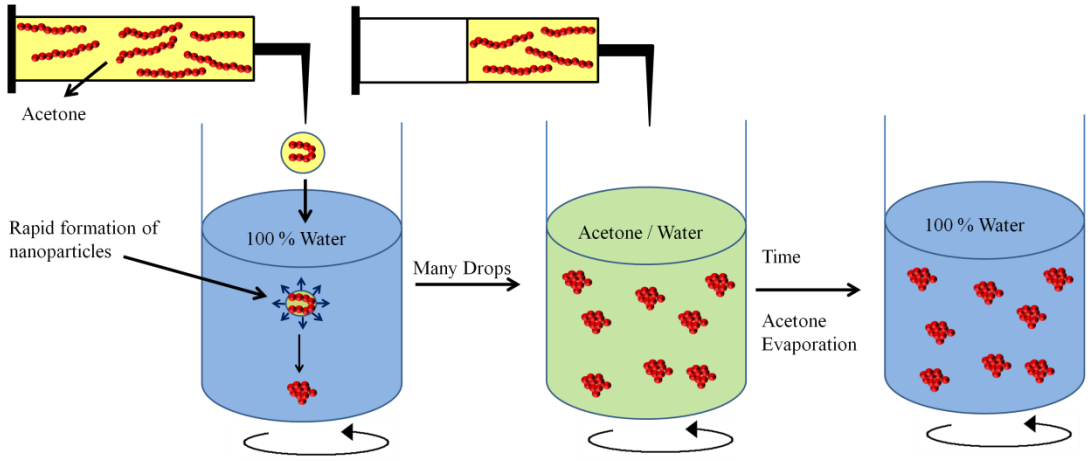


Scheme 4.2: Representation of the dripping method where linear homopolymer/acetone solution is dripped into stirring water over approximately ten minutes.

To investigate these two methods of nanoparticle preparation one polymer was selected *p*(HPMA$_{80}$) and dissolved in acetone at a concentration of 5 mg mL$^{-1}$ in a sealed vial and placed on a rolling machine overnight. The polymer/acetone solution was separated into two identical samples (2 x 1 mL) and individually slowly dripped into two vials filled with 5 mL of distilled stirring water using syringe pumps operating at 0.1 mL min$^{-1}$. One of these samples was subsequently transferred into dialysis tubing and left in a 1 L beaker filled with distilled water. After exchanging water for two days the sample was collected and analysed by DLS (see Figure 4.1). The other sample was left stirring overnight at 40°C to remove acetone and was also analysed by DLS, shown in 4.1.

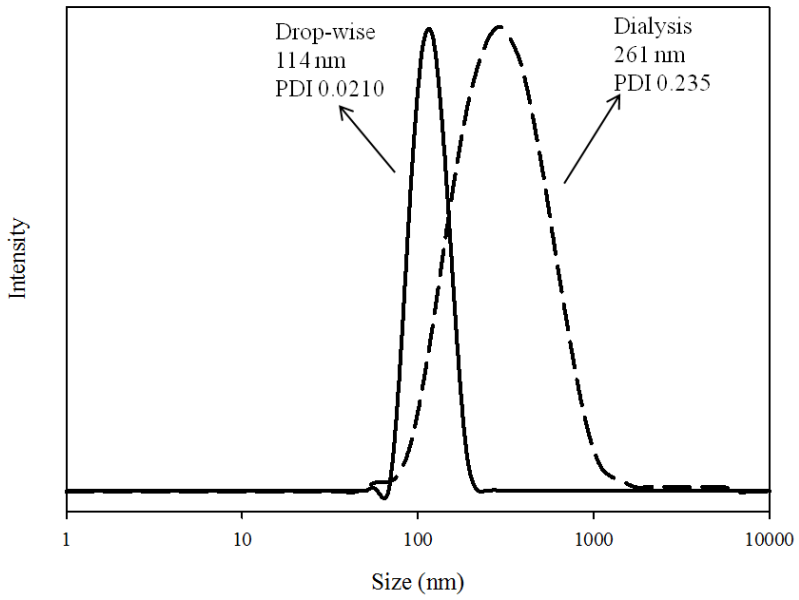


Figure 4.1: Z-average diameter analysis of nanoparticles comprising of *p*($HPMA_{80}$) at 1 mg $mL^{-1}$ using two methods; dripping method (solid line) and dialysis (dashed line).

These results seemed promising as Figure 4.1 shows monomodal distributions of nanoparticles have indeed been formed from the hydrophobic linear polymer. The dripping method with subsequent solvent evaporation formed nanoparticles with a very low polydispersity (0.021) in comparison to those from the dialysis method (0.235). The z-average diameters of these dispersions are dramatically different (114 nm and 261 nm for dripping/evaporation and dialysis, respectively), thus demonstrating a degree of control over z-average diameter by using different experimental procedures. However, upon leaving these samples standing for approximately three hours, precipitate began forming until very large amounts were present at the bottom of the sample vials after approximately five hours. This was rather unsurprising as there is no apparent stabilising force to prevent aggregation as these are solely comprised of hydrophobic starting materials. However, another

method to form stable nanoparticles using linear chains was attempted. This approach was significantly less time consuming in the hope that by drastically altering the way in which solvent exchange occurs this may affect nanoparticle z-average diameter, polydispersity and stability. This simplistic approach is essentially identical to the dripping method apart from the transfer of the polymer/acetone solution into the stirring water. Rather than a very slow dropwise addition, the entire volume was added rapidly (over less than two seconds), into pre-heated (40°C) water and left overnight to remove residual acetone. $^{1}$H NMR spectroscopy was performed on a nanoparticle suspension comprised of *p*((HPMA$_{80}$)-*co*-EGDMA$_{0.95}$) in $D_2O$ where the acetone resonance (2.22 ppm) was not evident (see Appendix 4.1).

To investigate this rapid approach to generating nanoparticles, three linear polymers, *p*(HPMA$_{50}$), *p*(HPMA$_{80}$), *p*(HPMA$_{120}$), were dissolved in acetone at 10 mg mL$^{-1}$ overnight on a rolling machine in sealed vials in order to reduce any acetone evaporation. The entire sample (1 mL) was rapidly added to stirring warmed water (5 mL, 40°C) using an adjustable pipette. Following overnight acetone evaporation, precipitation was not evident and the 2 mg mL$^{-1}$ nanosuspension were analysed *via* DLS (see experimental). Filtration/centrifugation was deemed unnecessary as DLS measurements failed to detect any large aggregates and/or dust particles, which would have led to failed measurements. DLS characterisation of the three nanoparticle suspensions comprised of *p*(HPMA$_{50}$), *p*(HPMA$_{80}$) and *p*(HPMA$_{120}$) are shown in Figure 4.2.

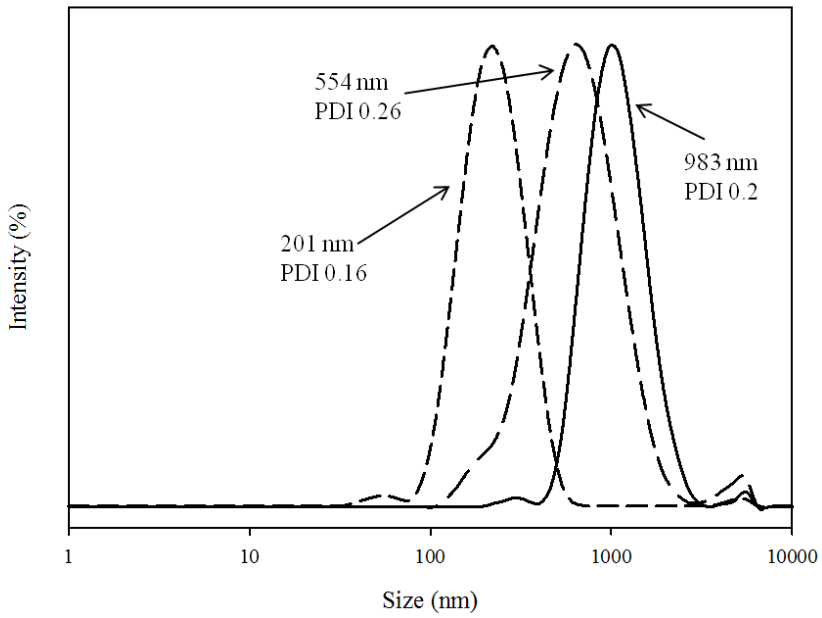


Figure 4.2: DLS characterisation of rapidly nanoprecipitated linear polymers from a starting concentration of 10 mg $mL^{-1}$ in acetone giving a final aqueous concentration of 2 mg $mL^{-1}$. *p*($HPMA_{50}$) (solid line), *p*($HPMA_{80}$) (large dashed line)and *p*($HPMA_{120}$) (small dashed line).

All of the DLS measurements shown in Figure 4.2 exhibit relatively low polydispersities (0.16 to 0.26) and interestingly the nanoparticles made from *p*($HPMA_{50}$) are approximately five times larger than those comprised of *p*($HPMA_{120}$) despite the same mass of polymer present in the final solution. The rationale behind this trend will be discussed later in Section 4.4.4. Initially this experiment seemed to provide an effective route to prepare nanoparticles consisting solely of hydrophobic polymer, yet several hours after these measurements were conducted and sample vials were allowed to rest unstirred at room temperature, large amounts of precipitate began to form. This is expected due to the hydrophobic nature of the polymers. To try to overcome the precipitation, or at least reduce the rate of precipitation, a further experiment with the same three linear polymers was

conducted. It has been suggested that lower concentrations might be preferred in order to produce more stable nanoparticles, as they would be better dispersed in the initial solvent.[6] The same precipitation protocol was followed but the initial polymer concentration in acetone was reduced to 5 mg $mL^{-1}$ and was subsequently diluted five-fold (5 mL water) to give a final concentration in water of 1 mg $mL^{-1}$ after acetone removal. It was thought that the nanoparticles would remain more stable by lowering the actual mass present in the sample, and that aggregation would be reduced. Again these samples were able to be analysed using DLS and these measurements are shown in Figure 4.3.

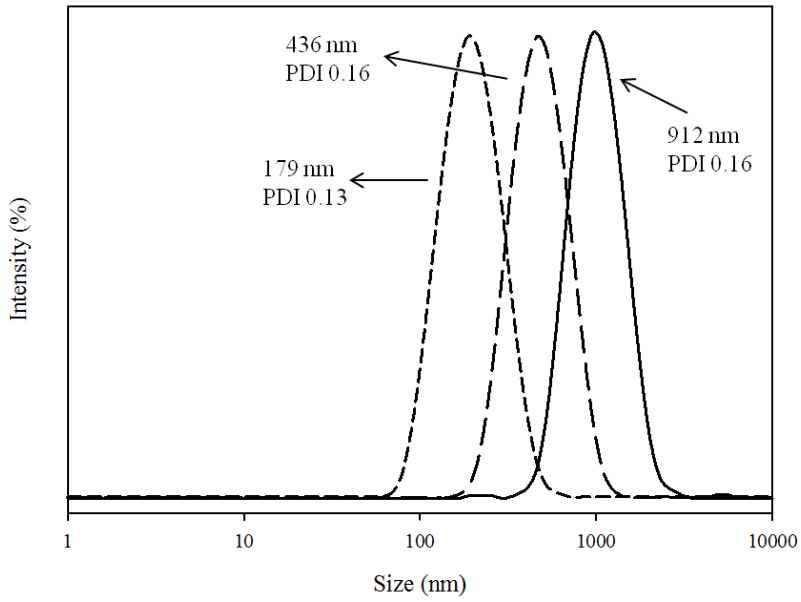


Figure 4.3: DLS characterisation of nanoprecipitated linear polymers from a starting concentration of 5 mg $mL^{-1}$ in acetone giving a final aqueous concentration of 1 mg $mL^{-1}$. *p*($HPMA_{50}$) (solid line), *p*($HPMA_{80}$) (large dashed line)and *p*($HPMA_{120}$) (small dashed line).

The DLS analyses shown in Figure 4.3 are all monomodal with very low polydispersities (approximately 0.15); lower polydispersities compared to their

counterparts in the previous experiment which used double the mass of polymer within the nanoprecipitation experiments. Having less material present in the original acetone solution (5 mg $mL^{-1}$) and obtaining similar nanoparticle z-average diameters compared to a more saturated solution (10 mg $mL^{-1}$) may suggest fewer actual particles are being formed. As this process is a nucleation and growth mechanism these results suggest there are fewer nucleation events and potentially a more controlled precipitation rate, which may also account for the increased uniformity of particle z-average diameters formed when using a more dilute polymer/acetone solution. This process is not explored in much detail here, but will feature heavily in later discussion. As observed previously, and also unsurprisingly, all nanoparticle samples began to precipitate out of solution after several hours standing, exhibiting metastability. From these experiments it has been shown that simply using a rapid solvent switch method of forming nanoparticles comprised of linear hydrophobic polymers was successful, however, the particles were unstable to even limited storage times and no further adjustments to the experimental protocol were attempted.

## 4.3 Nanoprecipitation of *p*((HPMA$_x$)-*co*-EGDMA$_{0.95}$) ($x$ = 50, 80, 120) using Dialysis and Dripping methods

The formation of stable nanoparticles *via* rapid nanoprecipitation was highly unsuccessful for linear polymers of various chain lengths of *p*(HPMA$_x$), but herein the extremely high stability of those formed from their branched counterparts is reported. Previous reports on polymer nanoparticle formation mainly focuses on using either dialysis or a dropping method in which polymer is firstly dissolved in a suitable solvent and then slowly dripped into a non-solvent (namely water) after

which the polymers self-assemble into nanostructures. In section 4.2, all attempted methods of nanoprecipitation were unsuccessful in forming stable materials, but it was not assumed this would be the case for branched copolymers as, although chemically identical, their architectures are dramatically different and may affect their behaviour during precipitation. A schematic representation of nanoparticle formation using branched copolymers is shown in Scheme 4.3 (dialysis) and Figure 4.4 (dripping method).

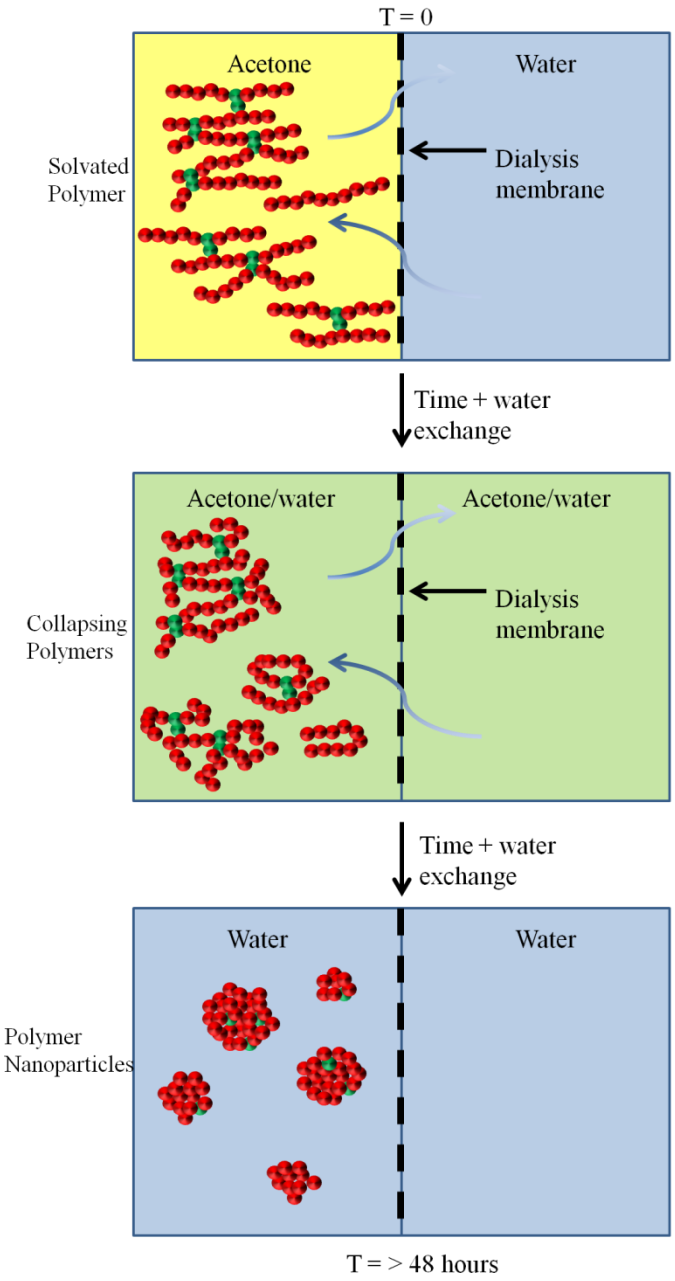


Scheme 4.3: Representation of nanoparticle production *via* dialysis using solvated branched copolymers in acetone in a dialysis membrane and continual water exchange for > 48 hours.

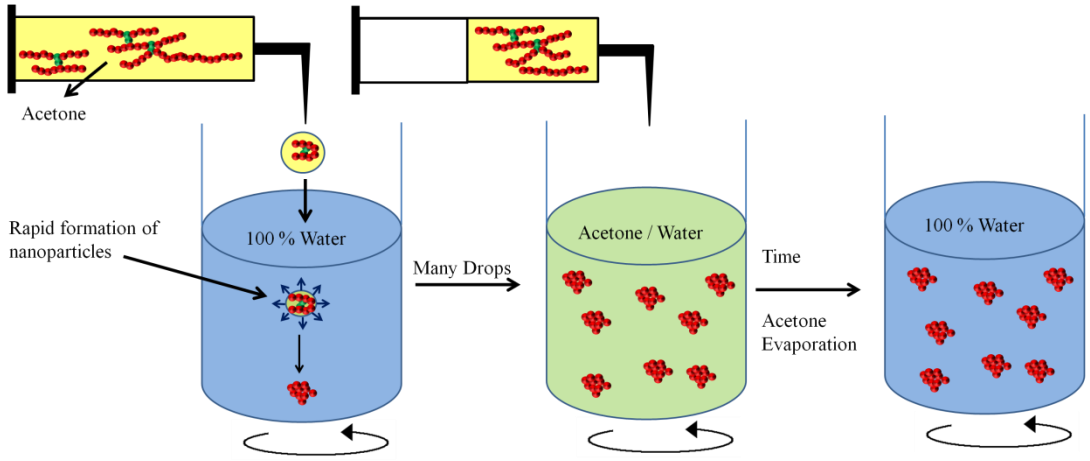


Scheme 4.4: Representation of the dripping method where branched copolymer/acetone solution is dripped into stirring water over approximately ten minutes.

To determine which method was most suitable for these copolymers, all of the aforementioned methods were compared by using *p*((HPMA$_{80}$)-*co*-EGDMA$_{0.95}$) dissolved in acetone at a concentration of 5 mg mL$^{-1}$ and precipitating into distilled water (5 mL) finally giving a copolymer concentration of 1 mg mL$^{-1}$.

The three nanoparticle suspensions remained very stable without obvious precipitation and therefore analysis was performed after the acetone had been completely removed, their DLS measurements are shown in Figure 4.4.

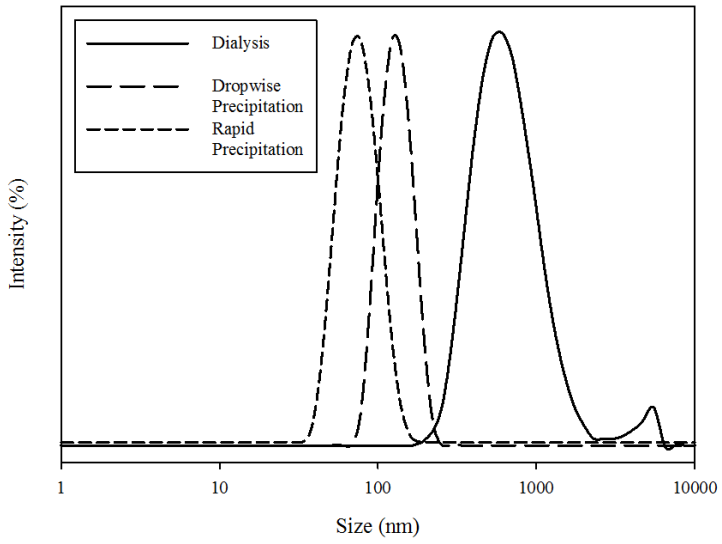


Figure 4.4: DLS measurements of nanoparticles (1 mg $mL^{-1}$) formed from *p*((HPMA$_{80}$)-*co*-EGDMA$_{0.95}$) *via* three different preparation routes. Dialysis (sold line), Dropwise (medium dashed line), Rapid (small dashed line).

The particles formed using dialysis were considerably larger when compared to the other two methods and displayed a higher polydispersity (610 nm and 0.22, respectively). Similar observations have been previously reported.[7] Particles formed by the slow addition/evaporation are markedly larger than those of the rapid addition/evaporation (72 nm and 127 nm, respectively). Both polydispersities are extremely low 0.05 and 0.02 for the dripping and rapid addition, respectively. The range of particle z-average diameters that have been formed from this single polymer is dramatic and, due to the larger z-average diameters produced as well as being more experimentally demanding, further dialysis experiments were not performed (indeed generating 1 nanoparticle sample takes > 48 hours and approximately 3 litres of distilled water and dialysis tubing). The wide range of z-average diameters recorded from a single copolymer solution concentration strongly suggests a self-

assembly of smaller entities, driven by a reduction in interfacial tension. The mechanism of the postulated self-assembly will be discussed in Section 4.4.4.

A further experiment was conducted using the more conventional dripping method to investigate concentration dependence on final nanoparticle dispersions. *p*((HPMA$_{50}$)-*co*-EGDMA$_{0.95}$) was dissolved in acetone at two different concentrations (10 mg mL$^{-1}$ and 5 mg mL$^{-1}$). Using two separate syringe pumps, solutions (1 mL) were dripped into stirring water (5 mL) achieving identical five-fold dilutions but with different final copolymer concentrations in water. Figure 4.5 shows the DLS analysis data.

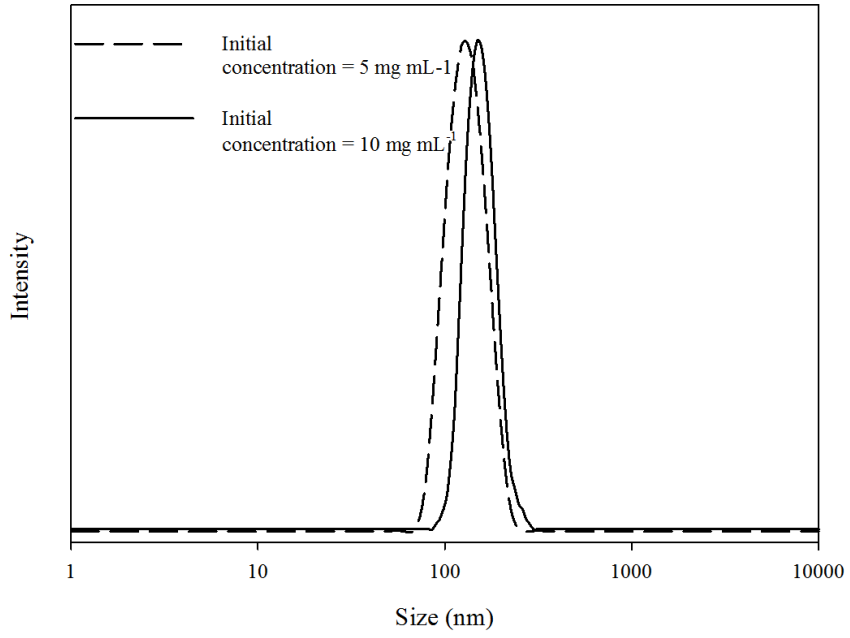


Figure 4.5: Comparison of nanoparticles formed from *p*((HPMA$_{50}$)-*co*-EGDMA$_{0.95}$) using two different starting copolymer/acetone concentrations each achieving a five-fold dilution. 5 mg mL$^{-1}$ (dashed line), 10 mg mL$^{-1}$ (solid line).

Here it is shown that varying the initial copolymer/acetone solution produces nanoparticles of differing z-average diameters *via* the dripping method for the same

dilution level. The sample with an initial concentration of 10 mg $mL^{-1}$ led to particles with a z-average diameter of 203 nm whereas starting with a 5 mg $mL^{-1}$ gave particles with a z-average diameter of 146 nm. This led us to believe that a degree of control of particle z-average diameter is apparent simply by varying the starting copolymer concentration, where higher concentrations lead to larger particles due to increasing the number of molecules per unit volume in the initial solvent.[8] This control is explored in detail in further studies later in this chapter, although using rapid precipitation rather than the dripping method. It would appear that the dripping technique is favourable due the extremely low polydispersities generated (in comparison to the rapid precipitation), yet this method (which is widely utilised),[6, 9, 10, 11] was not chosen for a more detailed nanoparticle production investigation during this study. The reasoning for this is two-fold;

1. The slow dripping/evaporation process is time consuming, taking approximately 10 minutes to produce a 5 mL sample, excluding preparation time and evaporation.

2. Syringe pumps were utilised to controllably and slowly drip the copolymer/acetone solution into water and availability limited the number of samples that could be generated and evaluated.

Due to these reasons, it was felt that rapid precipitation was the most appropriate method for a detailed study as this generates large numbers of variable volumes of low polydispersity samples that are not considerably different to the slower technique. Although all of the branched copolymer nanoparticles generated by these three different methods were stable relative to their linear counterparts, it was felt rapid precipitation outweighed the more conventional dripping method, and this was chosen to produce all of the remaining nanoparticle samples.

## 4.4 Nanoprecipitation of *p*((HPMA$_x$)-*co*-EGDMA$_{0.95}$) (*x*= 50, 80, 120) using a Rapid Solvent Switch

Although the linear *p(*HPMA) polymer nanoparticles precipitated when left standing unstirred for several hours, their DLS data suggested a trend whereby increasing the target DP$_n$ of the polymer chain produced smaller nanoparticles. To further investigate this possible trend, their branched copolymer counterparts, *p*((HPMA$_{50}$)-*co*-EGDMA$_{0.95}$), *p*((HPMA$_{80}$)-*co*-EGDMA$_{0.95}$), *p*((HPMA$_{120}$)-*co*-EGDMA$_{0.95}$), were subjected to rapid nanoprecipitation using an initial copolymer concentration in acetone of 5 mg mL$^{-1}$ and adding 1 mL of this solution to water (5 mL at 40°C) to give a final copolymer concentration in water of 1 mg mL$^{-1}$. Overnight the acetone was evaporated using a hotplate stirrer set to 40℃ as this was warm enough to provide sufficient acetone evaporation yet would not allow excessive water evaporation; indeed no significant water loss occurred after samples were collected. After the samples were left to stand and adjust to room temperature, 1 mL was analysed using DLS. Precipitation was not observed after approximately 1 hour of standing as observed with the linear nanoparticle samples (where the onset of precipitation occurred after several hours of standing) and no further purification was necessary to obtain good quality measurements. Their analysis is shown in Figure 4.6 where the three samples are displayed.

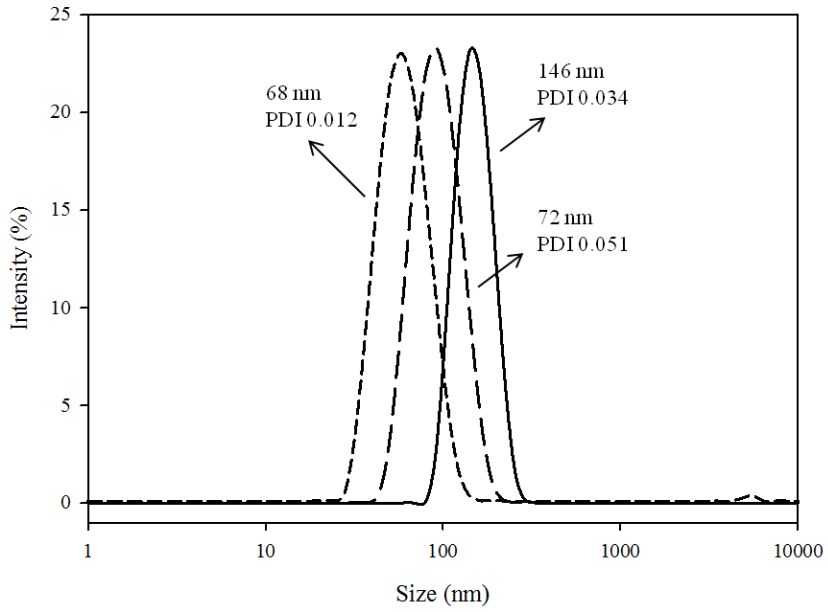


Figure 4.6: DLS measurements for the nanoparticles of *p*((HPMA$_{50}$)-*co*-EGDMA$_{0.95}$) (solid line), *p*((HPMA$_{80}$)-*co*-EGDMA$_{0.95}$) (large dashed line) and *p*((HPMA$_{120}$)-*co*-EGDMA$_{0.95}$) (small dashed line) prepared using rapid nanoprecipitation (starting copolymer concentration = 5 mg mL$^{-1}$, final copolymer concentration = 1 mg mL$^{-1}$).

The same trend also appeared in this experiment, with the largest particles being formed from the copolymer with a primary chain length of 50 monomer units (146 nm, 0.034 polydispersity) reducing to 72 nm for 80 monomer units and the smallest nanoparticles (68 nm) obtained using copolymers with 120 monomer units in the primary chain showing that the smallest particles are forming from the sample which has the longest primary chain (120 monomer units). All traces are monomodal with extremely low polydispersities and did not precipitate after several hours of standing unlike their linear counterparts (this observation will be discussed later).

### 4.4.1 Adjustment of Branched Copolymer Concentration

The use of a wt/vol % ratio to describe copolymer solution concentration during comparative nanoprecipitations of varying copolymer molecular weights or $DP_n$, may not be strictly appropriate. Many literature reports of nanoprecipitation discuss nanoparticles formed from different polymers whilst keeping the wt/vol % constant and this appears to be the standard approach.[12] Considering a sample of linear polymer chains with a $DP_n$ of 50 monomer units; there would be many more chains in the solution for any given polymer mass compared to samples where polymer chains have a $DP_n$ of 120 monomer units. If a *p*(HPMA) polymer chain with 50 monomer units has an $M_n$ of approximately 7200 g $mol^{-1}$ then there would be approximately 1.388 $e^{-4}$ moles of chains in a 1 g sample whereas a chain with 120 monomer units with an approximate $M_n$ of 17300 g $mol^{-1}$ would contain approximately 1.5780 $e^{-5}$ moles in a 1 g sample. To ensure an equal molar concentration of polymer chains, and allow a comparative molar nanoprecipitation, the initial masses would therefore need to be adjusted. To account for this, the masses of the branched polymers in acetone were normalised to the ratio of $DP_n$ of the corresponding primary chains. Two experiments were conducted, attempting to reflect the number of species in the solution, assuming the number of primary chains which form the branched copolymers was similar across the molecular weight distributions of different copolymers, and target primary chain length was achieved. This would lead to a normalised molar concentration of branched copolymer in each nanoprecipitation. A *p*(HPMA) primary chain with a $DP_n$ of 80 monomer units ($DP_{80}$) is 1.6 times longer than that of a $DP_{50}$ chain and 0.666 times as long as a $DP_{120}$ chain, therefore the concentrations of *p*(($HPMA_{50}$)-*co*-$EGDMA_{0.95}$) and *p*(($HPMA_{120}$)-*co*-$EGDMA_{0.95}$) in acetone were changed to 3.125 mg $mL^{-1}$ and 7.5

mg $mL^{-1}$, respectively and these were subsequently diluted (five-fold) into water to give final aqueous dispersions of 0.625 mg $mL^{-1}$and 1.5 mg $mL^{-1}$, respectively. This adjustment led to a dramatic change in their nanoparticle z-average diameters and these are shown in Figure 4.7.

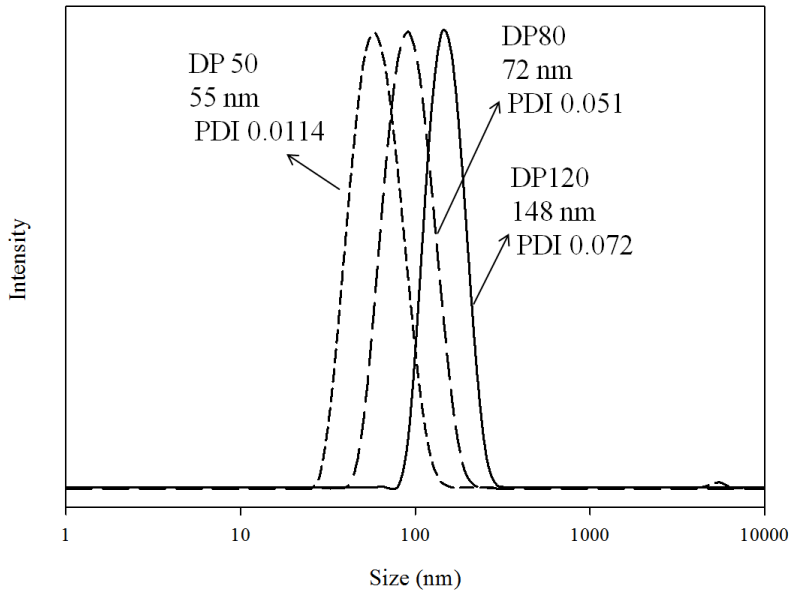


Figure 4.7: DLS nanoparticle distributions with adjusted initial concentrations for primary chain lengths. *p*((HPMA$_{50}$)-*co*-EGDMA$_{0.95}$) (3.125 mg $mL^{-1}$ starting concentration, 0.625 mg $mL^{-1}$ final concentration) (short dashed line), *p*((HPMA$_{80}$)-*co*-EGDMA$_{0.95}$) (5 mg $mL^{-1}$ starting concentration, 1 mg $mL^{-1}$ final concentration) (medium dashed line) and *p*((HPMA$_{120}$)-*co*-EGDMA$_{0.95}$) (7.5 mg $mL^{-1}$ starting concentration, 1.5 mg $mL^{-1}$ final concentration) (solid line).

As with the previous experiments at consistent mg/mL ratios, all samples have extremely low polydispersities and this experiment provides a more intuitive order of increasing nanoparticle z-average diameters. As expected, from a molar basis, copolymers with lower primary chain length produce smaller nanoparticles, completely opposite to the previous experiment which provided the smallest particles

from the longest primary chains (120 monomer units). Yet this data fails to provide sufficient evidence that this assumption is valid and true. Research into nanoprecipitation of copolymers usually reports wt/vol ratios of dissolved copolymer in solvent,[13,14,15] and although no research into nanoparticle production using hydrophobic branched copolymers has been conducted to date, it was thought using this format would provide at least some comparison to the work already published in this area. Therefore no further experiments using molar ratios of primary chain length of copolymers were conducted.

### 4.4.2 Reproducibility and scale up of Nanoprecipitation using *p*((HPMA$_{80}$)-*co*-EGDMA$_{0.95}$)

To demonstrate the reproducibility of the rapid nanoprecipitation of branched copolymers three separate experiments were conducted over a period of three months using *p*((HPMA$_{80}$)-*co*-EGDMA$_{0.95}$) to generate nanosuspensions using a 5 mg mL$^{-1}$ starting concentration of copolymer in acetone and leading to a final aqueous concentration of 1 mg mL$^{-1}$. The samples were all left overnight for acetone evaporation and were subsequently analysed using DLS where z-average diameter and polydispersity were recorded as an average of six measurements. Their measurements are reported in Figure 4.8.

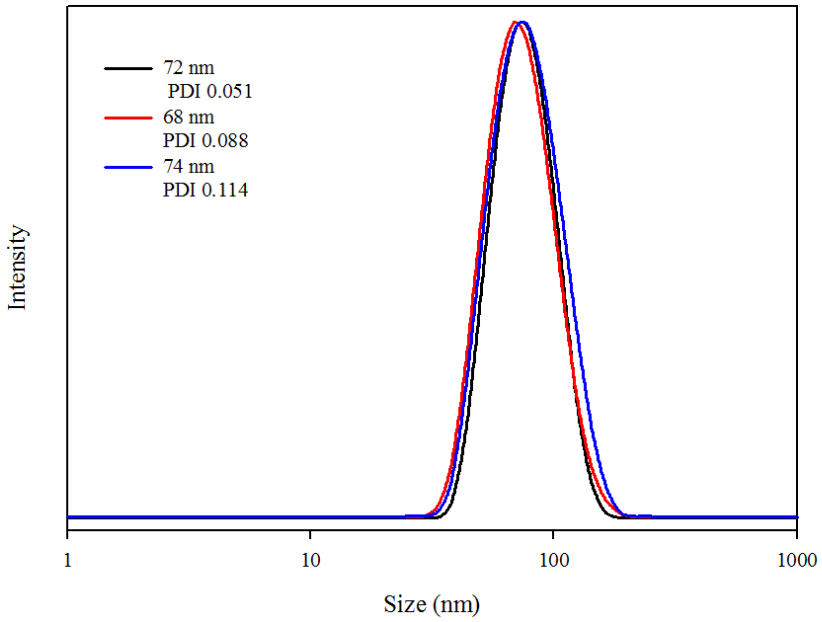


Figure 4.8: DLS measurements of rapidly precipitated nanoparticles comprising of *p*((HPMA$_{80}$)-*co*-EGDMA$_{0.95}$) (5 mg mL$^{-1}$ starting concentration; 1 mg mL$^{-1}$ final concentration) prepared on three separate occasions.

Figure 4.8 demonstrates high reproducibility of generating nanoparticle suspensions using rapid precipitation of *p*((HPMA$_{80}$)-*co*-EGDMA$_{0.95}$). A difference of only 6 nm is shown between the z-average diameters of the three samples with polydispersities ranging from 0.051 to 0.114.

All of the experiments thus far conducted have involved taking a 1 mL copolymer/acetone solution and diluting into 5 mL of distilled water. This was deemed an adequate volume as DLS measurement requires 1 mL of the suspension. To investigate whether these nanoprecipitations could be scaled up and yield reproducible nanoparticles with consistent z-average diameters, a further experiment in which a 10 mL sample of *p*((HPMA$_{80}$)-*co*-EGDMA$_{0.95}$) (5 mg mL$^{-1}$) was rapidly precipitated into warmed stirring water (50 mL) and left at 40 °C until the acetone

had evaporated. The two suspensions were compared (z-average diameter and polydispersity) using DLS (Figure 4.9).

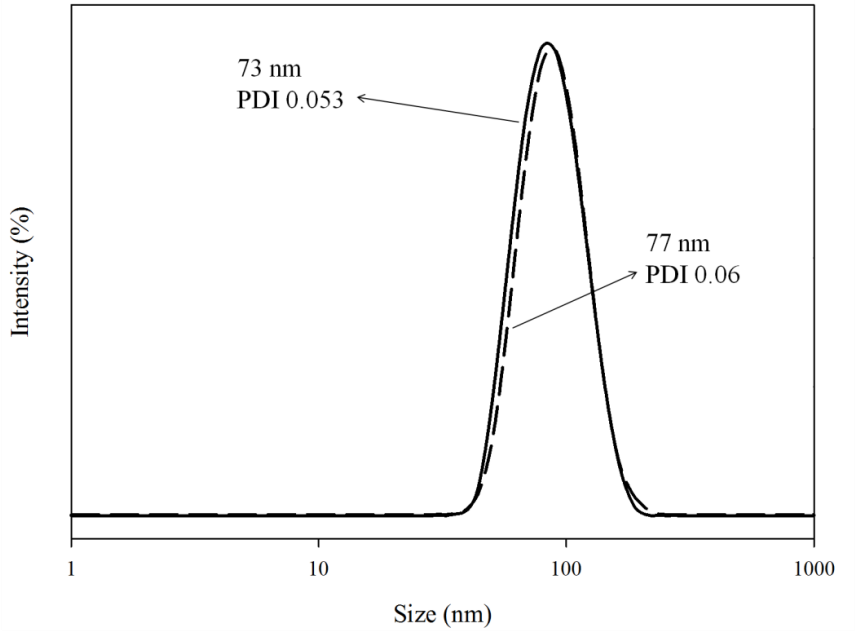


Figure 4.9: DLS characterisation of nanoprecipitated *p*((HPMA$_{80}$)-*co*-EGDMA$_{0.95}$) using 5 mg mL$^{-1}$ starting concentration; 1 mg mL$^{-1}$ final concentration. 1 mL starting volume; 5 mL final volume (solid line), 10 mL starting volume; 50 mL final volume (dashed line).

The two traces show almost identical traces confirming that indeed these precipitations can be performed on much larger scales, which may be useful for future nanoparticle applications.

This section has shown that synthesis of nanoparticles comprised of branched material is reproducible, where three separate nanoprecipitations gave extremely similar z-average diameter data. The scale up experiment where 50 mL of a 1 mg mL$^{-1}$ nanoparticle suspension was generated is believed to be an unusually high volume of nanosuspension to be reported.

### 4.4.3 Control of Nanoparticle z-Average Diameter using Rapid Nanoprecipitation

The trend towards the possible control of nanoparticle z-average diameter was observed in previous experiments where both the starting concentration of copolymer/acetone solution, and the dilution of the solution were varied independently; yielding differing nanoparticle z-average diameters. To expand on these observations, branched copolymers were subjected to rapid precipitation; achieving a variety of target dispersion concentrations. *p*((HPMA$_{50}$)-*co*-EGDMA$_{0.95}$), *p*((HPMA$_{80}$)-*co*-EGDMA$_{0.95}$), and *p*((HPMA$_{120}$)-*co*-EGDMA$_{0.95}$) were dissolved in acetone at three different concentrations (wt/vol) (10, 5 and 1 mg mL$^{-1}$) and subsequently individually precipitated into water at six different dilution ratios (1, 0.8, 0.4, 0.2, 0.05, 0.01). Dilution ratios were calculated as Final Concentration/ Initial concentration, e.g. Final Concentration (4 mg mL$^{-1}$)/ Initial concentration (5 mg mL$^{-1}$) gives a dilution ratio of 0.8. These were selected as they represent a wide range of dilutions from zero to one hundred-fold, thus allowing a much more detailed insight into copolymer self-assembly during nanoprecipitation than previously reported, and would perhaps allow the limits of this process to be explored. Table 4.1 shows the data obtained from these experiments and a number of trends are readily observed from this large data set.

1. For each branched copolymer, using a starting concentration of 10 mg mL$^{-1}$ generated the largest nanoparticles despite varying the dilution ratio and conversely the smallest particles are formed when initial copolymer concentration was at its lowest value (1 mg mL$^{-1}$).

2. Increasing the dilution factor within each set of dilution ratios produced smaller nanoparticles.
3. The lowest $DP_n$ values for primary copolymer chains generated the largest nanoparticles (already been noted in previous experiments).
4. Polydispersity of copolymer nanoparticles decreased as dilution increased i.e. the particles with the lowest polydispersities were generally obtained when the largest dilution was applied.

| Initial concentration (mg mL$^{-1}$) | Final concentration (mg mL$^{-1}$) | Dilution ratio | Primary chain length of branched copolymer *p*((HPMA$_x$)-*co*-EGDMA$_{0.95}$ | | | | | |
|---|---|---|---|---|---|---|---|---|
| | | | HPMA DP$_n$ = 50 | | HPMA DP$_n$ = 80 | | HPMA DP$_n$ = 120 | |
| | | | Diameter (nm) | Polydispersity | Diameter (nm) | Polydispersity | Diameter (nm) | Polydispersity |
| 10 | 10 | 1 | 786 | 0.435 | 564 | 0.326 | 273 | 0.116 |
| | 8 | 0.8 | 432 | 0.070 | 322 | 0.152 | 157 | 0.074 |
| | 4 | 0.4 | 200 | 0.030 | 161 | 0.051 | 88 | 0.080 |
| | 2 | 0.2 | 203 | 0.024 | 85 | 0.061 | 92 | 0.096 |
| | 0.5 | 0.05 | 175 | 0.006 | 80 | 0.057 | 58 | 0.079 |
| | 0.1 | 0.01 | 177 | 0.008 | 82 | 0.096 | 92 | 0.051 |
| 5 | 5 | 1 | 427 | 0.205 | 247 | 0.240 | 154 | 0.118 |
| | 4 | 0.8 | 226 | 0.168 | 223 | 0.153 | 107 | 0.038 |
| | 2 | 0.4 | 178 | 0.011 | 108 | 0.112 | 91 | 0.049 |
| | 1 | 0.2 | 146 | 0.034 | 72 | 0.051 | 68 | 0.012 |
| | 0.25 | 0.05 | 144 | 0.015 | 65 | 0.062 | 69 | 0.057 |
| | 0.05 | 0.01 | 144 | 0.023 | 71 | 0.095 | 66 | 0.009 |
| 1 | 1 | 1 | 273 | 0.115 | 181 | 0.055 | 150 | 0.037 |
| | 0.8 | 0.8 | 178 | 0.012 | 146 | 0.034 | 129 | 0.250 |
| | 0.4 | 0.4 | 180 | 0.009 | 88 | 0.084 | 108 | 0.053 |
| | 0.2 | 0.2 | 145 | 0.020 | 62 | 0.110 | 65 | 0.069 |
| | 0.05 | 0.05 | 144 | 0.014 | 59 | 0.139 | 69 | 0.111 |
| | 0.01 | 0.01 | 146 | 0.008 | 121 | 0.253 | 73 | 0.049 |

Table 4.1: Formation of branched copolymer nanoparticles generated using rapid nanoprecipitation from acetone.

This large data set provides an indication that branched copolymer nanoparticles comprising hydrophobic *p*(HPMA) can indeed be generated and moreover, the particle diameter can be tuned simply be altering the copolymer concentration in solution prior to nanoprecipitation and the range of dilutions involved in the nanoprecipitation process. Here we have produced particles with remarkably different z-average diameters from approximately 60 nm to 800 nm using the same simple rapid nanoprecipitation method and only three copolymers.

Figure 4.10 (A) shows z-average diameters of *p*((HPMA$_{50}$)-*co*-EGDMA$_{0.95}$) nanoparticles using various starting concentrations in acetone (10 mg mL$^{-1}$, 5 mg mL$^{-1}$ and 1 mg mL$^{-1}$) where dilution ratio is varied; indicating the largest particles are formed using starting concentrations of 10 mg mL$^{-1}$ and 5 mg mL$^{-1}$ and dilution ratios of 1 and 0.8. This same trend is found for *p*((HPMA$_{80}$)-*co*-EGDMA$_{0.95}$) and *p*((HPMA$_{120}$)-*co*-EGDMA$_{0.95}$) (see Appendix 4.2 and 4.3 respectfully). Individual DLS chromatograms are found in Appendix 4.4.

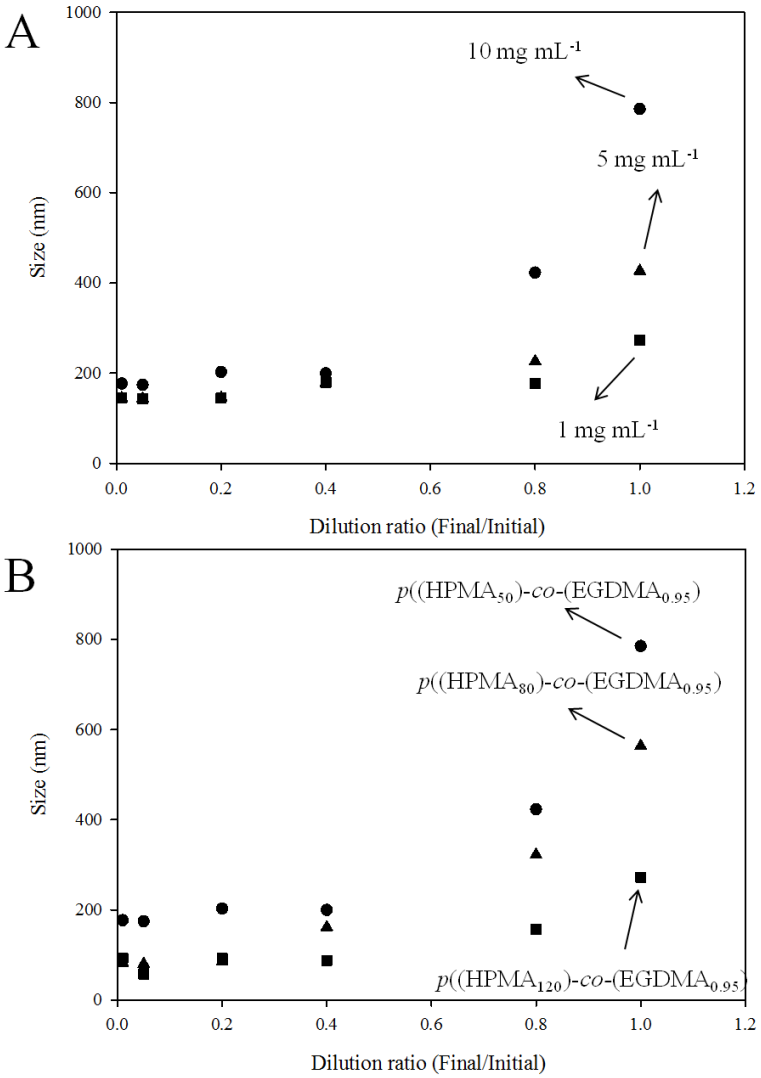


Figure 4.10: Z-average diameters of nanoparticles prepared using rapid nanoprecipitation from acetone. (A) Control of particle z-average diameter by varying initial copolymer concentration in acetone for *p*((HPMA$_{50}$)-*co*-EGDMA$_{0.95}$). (B) DLS characterisation of nanoprecipitated *p*((HPMA$_x$)-*co*-EGDMA$_{0.95}$). Demonstrating control of nanoparticle z-average diameter by varying primary chain length. DP$_n$ =50 (circles), 80 (triangles), 120 (squares).

By utilising Scanning Electron Microscopy (SEM), it is possible to obtain images of these particles and Figure 4.11 shows the dispersions of particles formed using

*p*((HPMA$_{80}$)-*co*-EGDMA$_{0.95}$) with an initial concentration of 5 mg mL$^{-1}$, leading to final concentrations of 5 mg mL$^{-1}$, 2 mg mL$^{-1}$ and 1 mg mL$^{-1}$ (see Chapter 2 section 2.2.4). In the DLS measurements, polydispersity decreased dramatically upon increasing the dilution and this correlates well with SEM images.

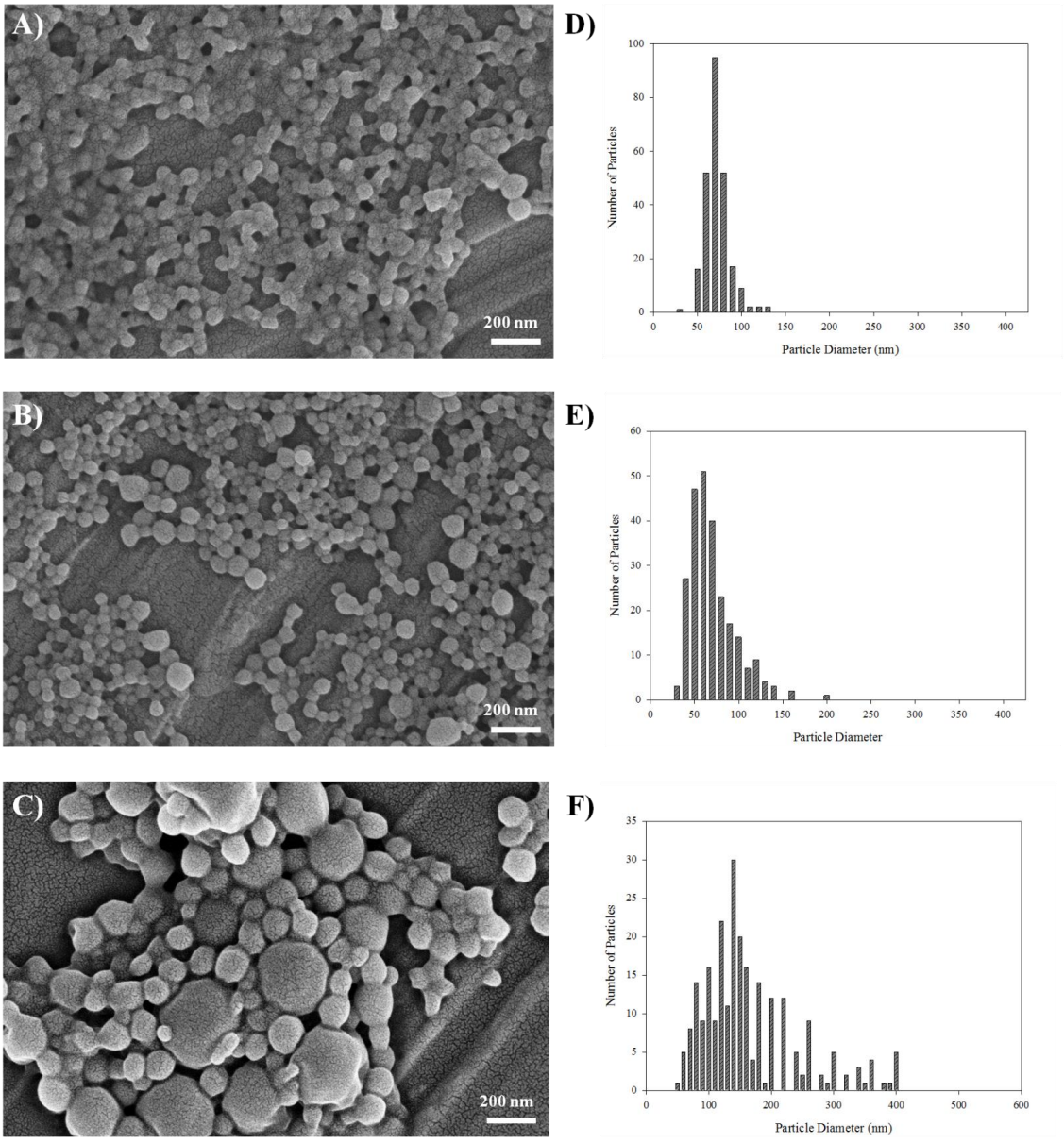


Figure 4.11: Scanning electron microscopy images of nanoprecipitated *p*((HPMA$_{80}$)-*co*-EGDMA$_{0.95}$) and histogram distributions derived from the analysis of 250 individual nanoparticles. Variation of dilution from an initial concentration of 5 mg mL$^{-1}$ in acetone to give final concentrations of; 1 mg mL$^{-1}$ (A and D) (mean 77 nm, sd 13.8 nm), 2 mg mL$^{-1}$ (B and E) (mean 75 nm, sd 26.2 nm) and 5 mg mL$^{-1}$ (C and F) ( mean 173 nm, sd 83.8 nm).

As the dilution increases, it is clearly visible from the SEM images that polydispersity decreases. This is supported by direct measurement of nanoparticles from the SEM images (n = 250 in each analysis) generating histograms where it is clear that monodispersity increases with decreasing dilution factor (i.e. higher dilution). Along with polydispersity, the images show how nanoparticle z-average diameter differs upon changing dilution factor, with the smallest being formed when the highest dilution is employed; conversely at the lowest dilution (Figure 4.11 (C)) the largest particles are clearly visible. Although the individual particle structure is not visible, all particles appear to be homogenous in composition, which is similar to a previous report of the nanoprecipitation of linear polymers.[16] Figure 4.12 shows further SEM images of copolymer nanoparticles, these images were expanded to show a larger surface area conveying the homogenous nature of nanoparticles.

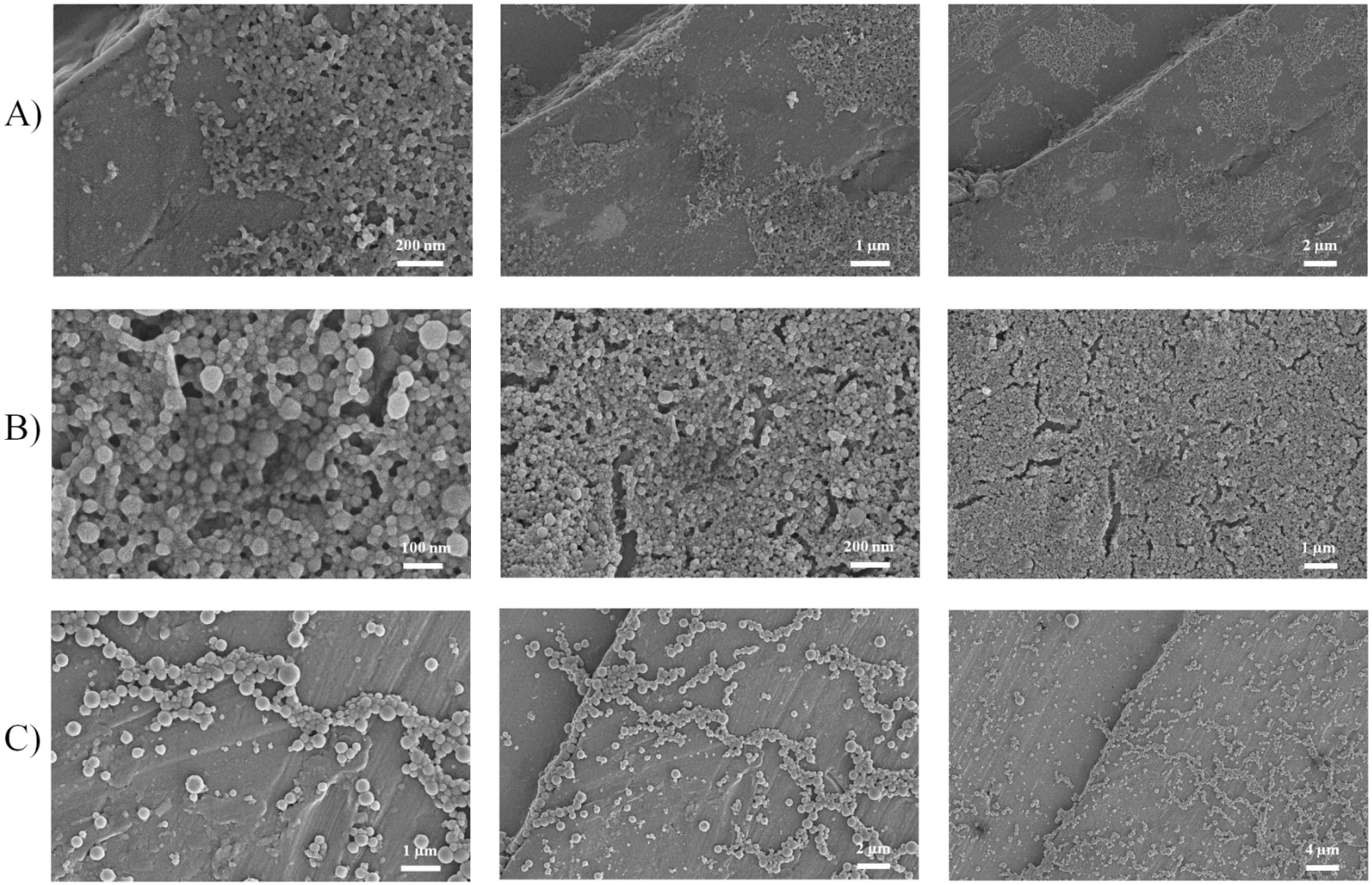


Figure 4.12: Further scanning electron microscopy images of nanosuspensions comprising of *p*($HPMA_{80}$)-*co*-$EGDMA_{0.95}$) with variation of dilution from an initial concentration of 5 mg $mL^{-1}$ in acetone to give final concentrations of; 1 mg $mL^{-1}$ (A), 2 mg $mL^{-1}$ (B) and 5 mg $mL^{-1}$ (C).

### 4.4.4 Proposed Mechanism of Nanoparticle Formation

Due to the large range of nanoparticle z-average diameters generated by simply changing the initial copolymer/acetone concentration it is proposed that a nucleation and growth mechanism occurs during precipitation. Simple collapsing of single branched copolymer chains to form single-chain nanoparticles is discounted, as it has been shown that although a large proportion of the branched copolymer samples have extremely high molecular weights composed of multiple chains, the polydispersity of branched copolymers is so large that a significant amount of lower molecular weight and also linear material present. If these were to individually collapse as precipitation occurs the resulting particles would be expected to have a wide range of z-average diameters. Indeed, it has already been shown that linear polymer samples are not stable and precipitate out of solution and as this does not occur in the branched copolymer samples (which contain linear material).

If the collapsing of a mixture of individual multiply-branched and linear chains occurred it would be expected that some precipitation would ensue, which is not the case here. Supporting the nucleation and growth concept is the DLS characterisation of branched copolymers dissolved in acetone. Three branched copolymers, *p*((HPMA$_{50}$)-*co*-EGDMA$_{0.95}$), *p*((HPMA$_{80}$)-*co*-EGDMA$_{0.95}$) and *p*((HPMA$_{120}$)-*co*-EGDMA$_{0.95}$) were dissolved in acetone at 10 mg mL$^{-1}$ overnight and subsequently analysed by DLS (Shown in Figure 4.13).

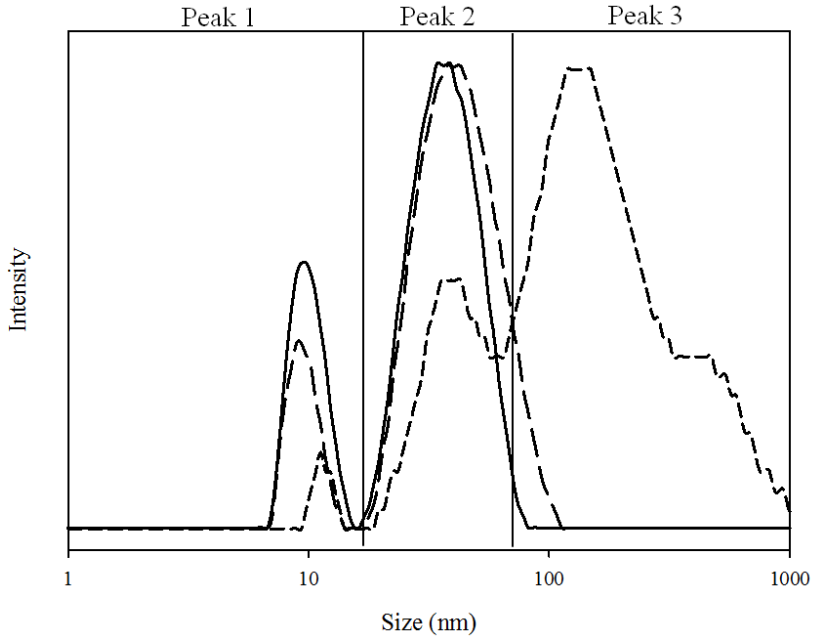


Figure 4.13: DLS characterisation of branched copolymers in acetone at 10 mg $mL^{-1}$. *p*((HPMA$_{50}$)-*co*-EGDMA$_{0.95}$) (solid line), *p*((HPMA$_{80}$)-*co*-EGDMA$_{0.95}$) (medium dashed line), *p*((HPMA$_{120}$)-*co*-EGDMA$_{0.95}$) (small dashed line).

| Copolymer | Peak 1 Diameter (nm) | Peak 2 Diameter (nm) | Peak 3 Diameter (nm) | Polydispersity | Attenuator | Derived Count Rate (kcps) |
|---|---|---|---|---|---|---|
| *p*((HPMA$_{50}$)-*co*-EGDMA$_{0.95}$) | 10 | 38 | - | 0.245 | 9 | 19664.5 |
| *p*((HPMA$_{80}$)-*co*-EGDMA$_{0.95}$) | 9 | 45 | - | 0.263 | 8 | 16636.1 |
| *p*((HPMA$_{120}$)-*co*-EGDMA$_{0.95}$) | 11 | 40 | 226 | 0.46 | 7 | 16123.4 |

Table 4.2: Data from the measurement of branched *p*(HPMA) copolymers in acetone at 10 mg $mL^{-1}$.

All three traces are multi modal showing that at least two distinct species are present, with a definitive peak at around 10 nm (peak 1) which is assigned to single solvated linear polymer chains. Alongside this are peaks with sizes ranging from 38 nm to 45 nm and, in the case of *p*($HPMA_{120}$)-*co*-$EGDMA_{0.95}$), a third peak with a size of 226 nm. This data may suggest single linear polymer chains (peak 1) and branched copolymer chains (peak 2 and peak 3) and/or possible aggregation in the solution or multiple scattering. It should also be noted from Table 4.2 that the attenuator is very high in all of these experiments (7 to 9) and indicates very low scattering, consistent with solubilised copolymer with very little refractive index difference. The data here shows that it is very unlikely that subsequent nanoparticles consist of single polymer chains.

Scheme 4.5 demonstrates the proposed processes involved during the nanoprecipitation of branched copolymers. Initially, it is thought each copolymer within the large volume of copolymer/acetone begins to collapse as the acetone/ water gradient rapidly changes. This continues as copolymers enter into a water rich environment until a critical point where aggregation of these collapsed chains occurs. At this point the collapsed copolymers associate until a size that is commensurate with colloidal stability is reached and are, thereafter, able to remain dispersed without further aggregation and subsequent precipitation. The rationale of this behaviour is consistent with other reports of nanoprecipitation.[17, 18, 19] The data suggest that the smaller nanoparticles form when the initial copolymer/acetone concentration is low and contains fewer collapsed branched copolymers.

Conversely, higher initial concentration results in larger particles containing more copolymers per particle. Their higher polydispersities are attributed to the loss of control when collapsed branched copolymers aggregate as the copolymers are in a much closer proximity as the acetone/water gradient shifts resulting in some particles containing many more copolymer chains, yet in our studies they do not reach sizes which are large enough to result in their sedimentation.

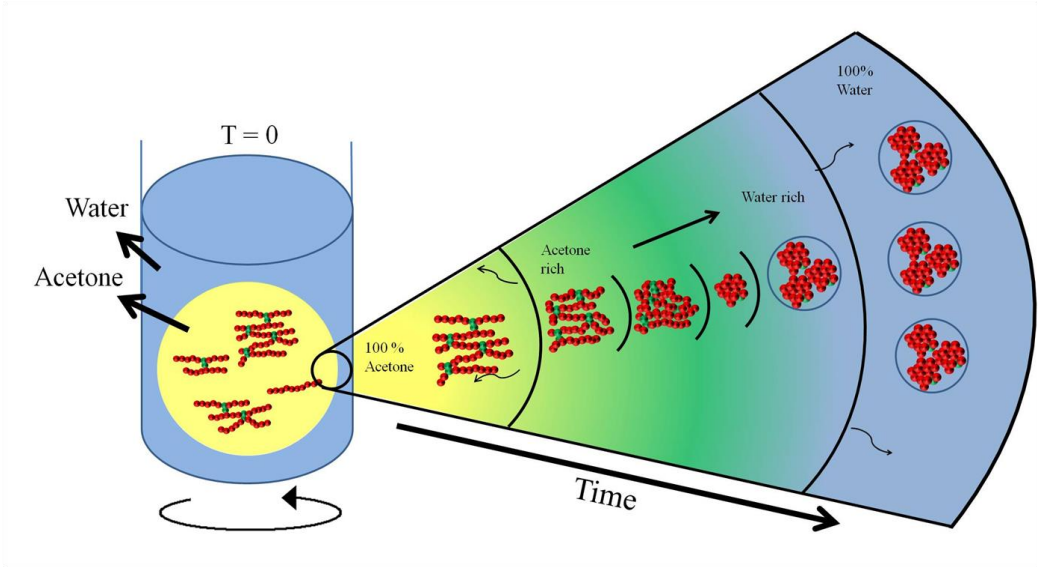


Scheme 4.5: Proposed mechanism of the nanoprecipitation process using the rapid precipitation method from acetone.

## 4.4.5 Aqueous Stability of *p*((HPMA$_{80}$)-*co*-EGDMA$_{0.95}$)

As discussed previously, it is strongly believed that particles are formed by aggregation of smaller components as z-average diameters have been shown to vary substantially. As such, it was investigated whether dilution would lead to disassembly as would be expected if the particles have a critical aggregation concentration. To identify how stable these nanoparticles are, it was decided to serially dilute a suspension and monitor any change in z-average diameter and polydispersity to determine at what point these systems cease to behave as

nanoparticles. This experiment aims to identify an aggregation concentration to discover if these particles are reversibly aggregated like colloidal particles.

For the aqueous dilution experiment, *p*((HPMA$_{80}$)-*co*-EGDMA$_{0.95}$) was rapidly nanoprecipitated into water from a starting concentration of 5 mg mL$^{-1}$ to give a final concentration of 1 mg mL$^{-1}$. 1 mL of this sample was analysed by DLS giving a z-average diameter and polydispersity which were extremely similar to previous data (74.5 nm, 0.05 polydispersity). This was then diluted to give a concentration of 0.5 mg mL$^{-1}$ and then again diluted serially to give a final concentration of 0.0078 mg mL$^{-1}$.

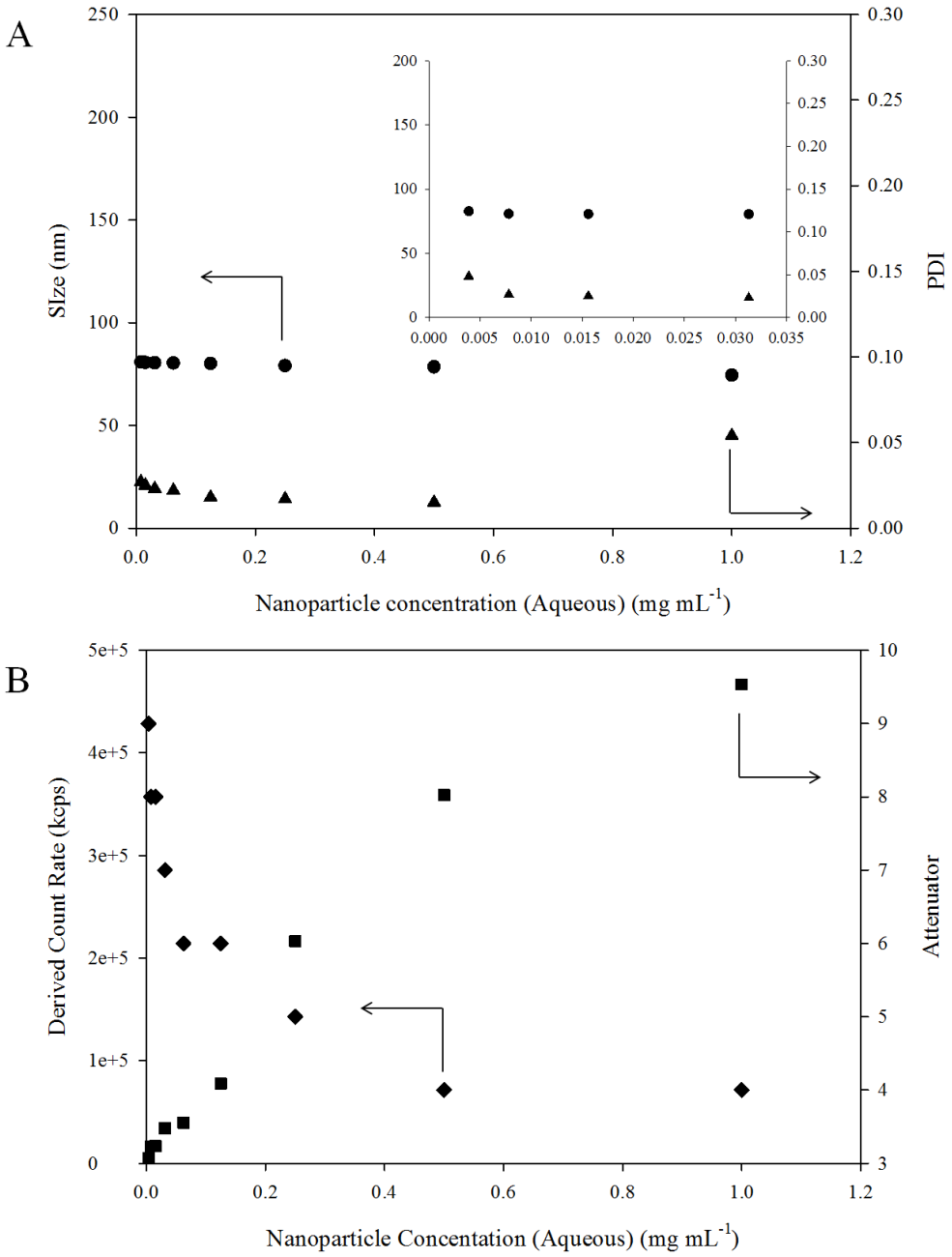


Figure 4.13: Serial dilution data for the nanoparticles comprised of *p*((HPMA$_{80}$)-*co*-EGDMA$_{0.95}$) with a starting and finishing concentration of 5 and 1 mg mL$^{-1}$, respectively. A) Nanoparticle diameter and polydispersity *vs*. Concentration of suspension. B) Derived count rate and Attenuator *vs*. Concentration of suspension.

Figure 4.13 (A) shows that these particles are stable to dilution in respect to particle diameter and also polydispersity as subjecting these to a two hundred and fifty-fold dilution led to almost no difference in either of these measurements, suggesting these are highly stable materials. Throughout the experiment the DLS detector also recorded attenuator levels and the derived count rate (shown in Figure 4.13 (B)). The former is indicative of the concentration of the overall solution whereby the attenuator must increase as solutions become more dilute in order to achieve reliable analysis measurements. This data shows that indeed the solution is becoming more dilute. Apart from z-average diameter and polydispersity measurements, the DLS detector also records a derived count rate during each measurement. This figure is indicative of the number of particles present in the suspension and is directly related when the attenuator is set at a single value, unsurprisingly this figure drops dramatically and almost linearly as the sample is serially diluted; this suggests that besides becoming diluted, these particles are not dissociating. If dissociation was occurring, the derived count rate would be expected to increase as the number of species present would have increased on break up of any aggregated nanoparticles. From this experiment it is clear highly stable materials (with respect to aqueous dilution) have been synthesised and further dilutions were abandoned due to the attenuator reaching > 9 where measurements become unreliable as the machine is unable to analyse the highly dilute sample.

### 4.4.6 Solvent Stability of *p*((HPMA$_{80}$)-*co*-EGDMA$_{0.95}$)

As well as aqueous stability, investigation into particle stability with increasing volumes of organic solvent was also explored. Adding solvent to the particles should ultimately lead to particle dissolution to give similar DLS measurements as

when they are dissolved in acetone alone. Due to the fact that these copolymers are soluble in a range of solvents, it was expected that the particles would become more solubilised as the ratio of solvent in the aqueous sample increased. It was thought that perhaps the reverse of the actual precipitation process could occur, where the gradual switching of solvent would initially swell the particles and lead to dissociation of the branched copolymers in the particles into individual branched copolymer chains. Acetone was used in preparation of the particles but due to its high volatility, experimentally adding small aliquots over an extended period of time would undoubtedly lead to inaccurate results as significant evaporation would occur despite using a lid on the sizing cuvette. Therefore methanol was chosen as this is also a good solvent for *p*(HPMA), indeed it was used in the synthesis of these copolymers and minimal evaporation would be expected to occur during DLS analysis. In this experiment a 1 mL sample of a 1mg $mL^{-1}$ nanoparticle suspension comprised of *p*((HPMA$_{80}$)-*co*-EGDMA$_{0.95}$) prepared by rapid precipitation was diluted with methanol over time until 910 µL had been added. When an aliquot of methanol was added, the glass sizing cuvette was manually swirled gently prior to sizing to attempt to evenly distribute the methanol (see Chapter 2 section 2.5.2.3). It should also be noted that the sample remains in the DLS machine for approximately 4-5 minutes while sizing measurements are taking place and giving sufficient time for the sample to equilibrate.

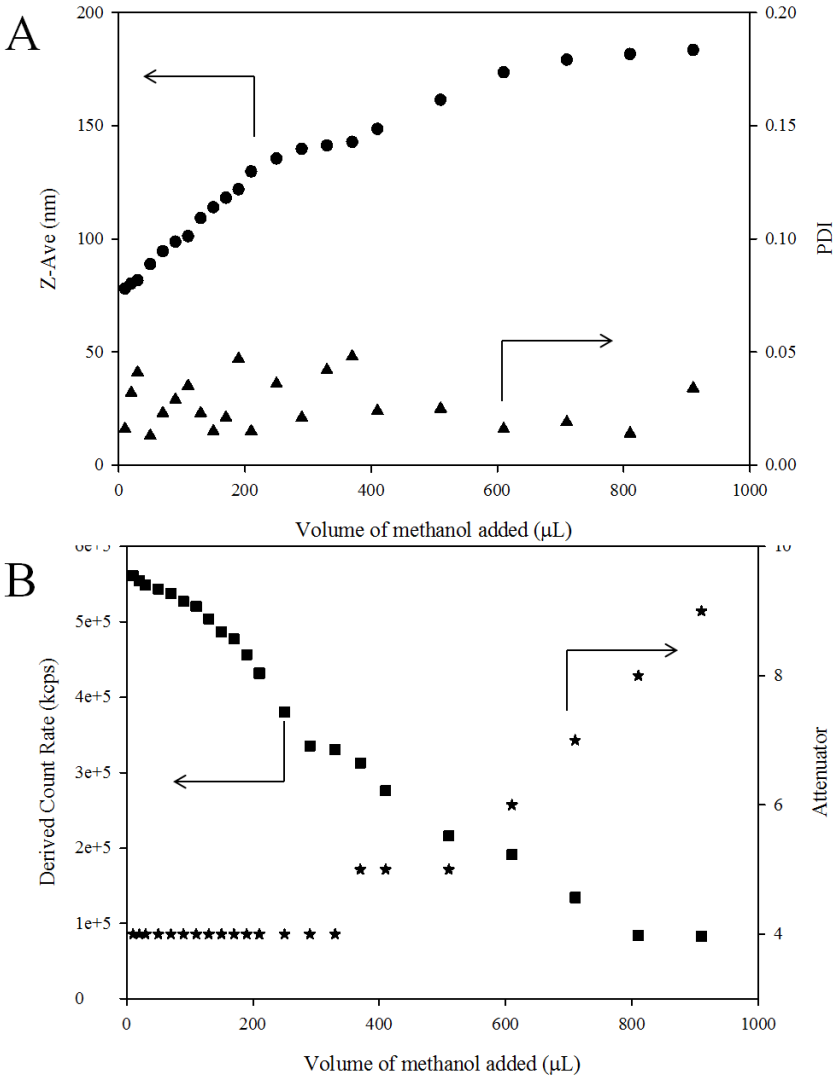


Figure 4.14: Studies into the response of methanol addition to nanoprecipitated *p*((HPMA$_{80}$)-*co*-EGDMA$_{0.95}$) (5 mg mL$^{-1}$ initial concentration; 1 mg mL$^{-1}$ final aqueous concentration. (A) Z-average diameters and polydispersity. (B) Derived count rate and Attenuator both measured using DLS.

As can be seen in Figure 4.14 (A), the branched copolymer nanoparticles continually increase in z-average diameter with addition of methanol from approximately 80 nm to 185 nm where 910 µL has been added to the 1 mL sample. The particles increased almost linearly for the first 250 µL of methanol after which the gradient decreased whilst a further 120 µL was added followed by an increase until the last measurement was recorded. Accompanying this data, polydispersity, although remaining low throughout the experiment did fluctuate until around 370 µL had been added after this it remained almost constant until the end of the experiment. This data may suggest these particles are uniformly swelling (increase in z-average diameter, low polydispersity) followed by reorganisation of the particles due to methanol uptake (plateau in z-average diameter) and finally uniform swelling until 910 µL has been added. Supporting this theory is the plot of derived count rate and attenuator seen in Figure 4.41 (B). Similar to the aqueous dilution of *p*((HPMA$_{80}$)-*co*-EGDMA$_{0.95}$) nanoparticles, the derived count rate decreased throughout the experiment suggesting that the amount of scattering is reducing as dilution occurs, and this is directly proportional to the concentration as long as the attenuator is constant and although it is not the case here, where the appropriate attenuator is automatically determined by the Zetasizer instrument, it supports the theory that particles are not dissociating with increasing dilution. It is shown that the attenuator increases during this experiment as the intensity of the scattered light from particles must be within a range for the detector to measure. The intensity would also be expected to decrease as the particles swell and affect the density with a change in refractive index, however, a larger particle would be expected to provide higher scattering. When samples do not scatter much light, as may be the case with low concentrations and/or when very small particles are present, the attenuator will

automatically allow more laser light into the sample and therefore the attenuator figure will increase, which is found on the recorded data. Taking into account all of the data shown in Figure 4.14, it is strongly suggestive that particles are swelling due to the uptake of methanol, without dissociating. Both organic and aqueous dilution of nanoparticles demonstrates their robustness and further dilution analysis was only limited due to experimental techniques.

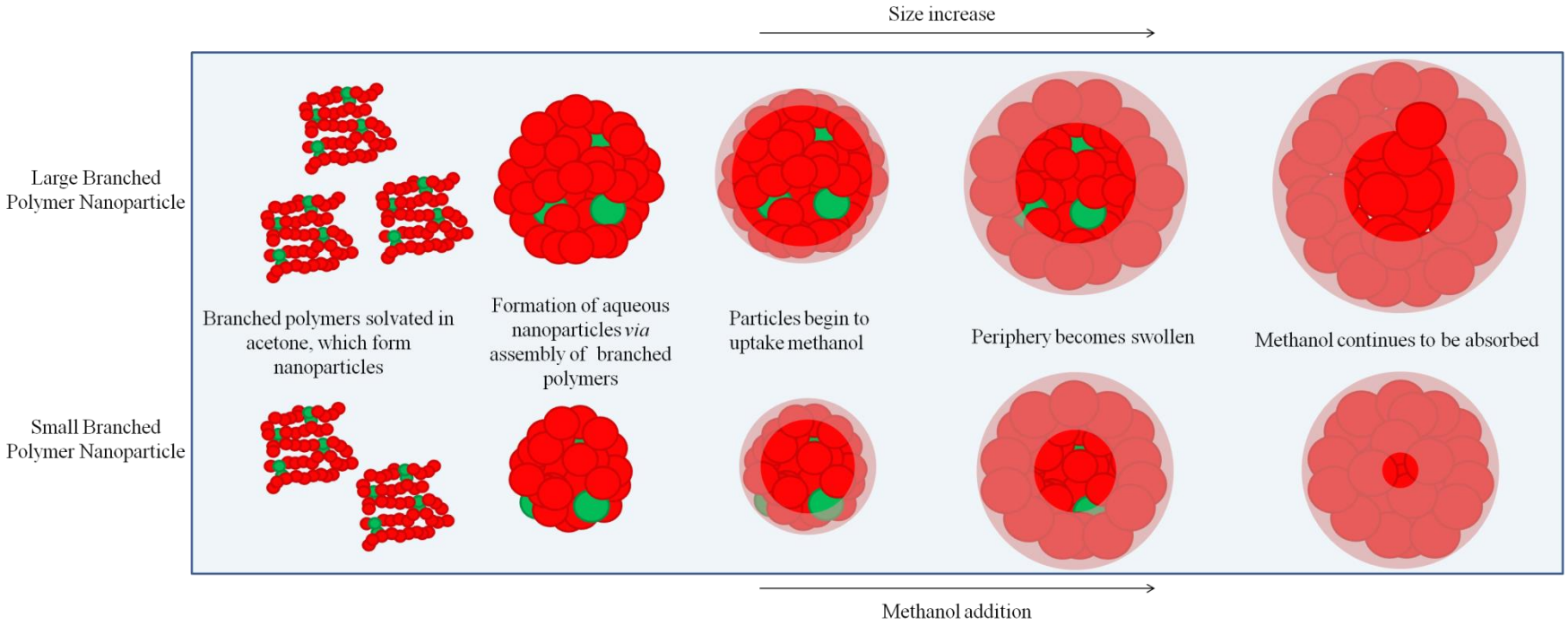


Scheme 4.6: Representation of nanoparticle swelling during methanol addition where both small and large particles are taken into account.

### 4.4.7 Long-term Stability of Nanoparticles (*p*((HPMA$_{80}$)-*co*-EGDMA$_{0.95}$)

Branched copolymer nanoparticles remained stable on standing at room temperature for several days assessed by no noticeable precipitate forming in sample vials. In order scale up to investigate long term stability, *p*((HPMA$_{80}$)-*co*-EGDMA$_{0.95}$) nanoprecipitates prepared by rapid precipitation from a starting concentration of 5 mg mL$^{-1}$ to final concentrations of 5 mg mL$^{-1}$, 4 mg mL$^{-1}$, 2 mg mL$^{-1}$, 1 mg mL$^{-1}$ and 0.25 mg mL$^{-1}$ were analysed after one day and seven months.

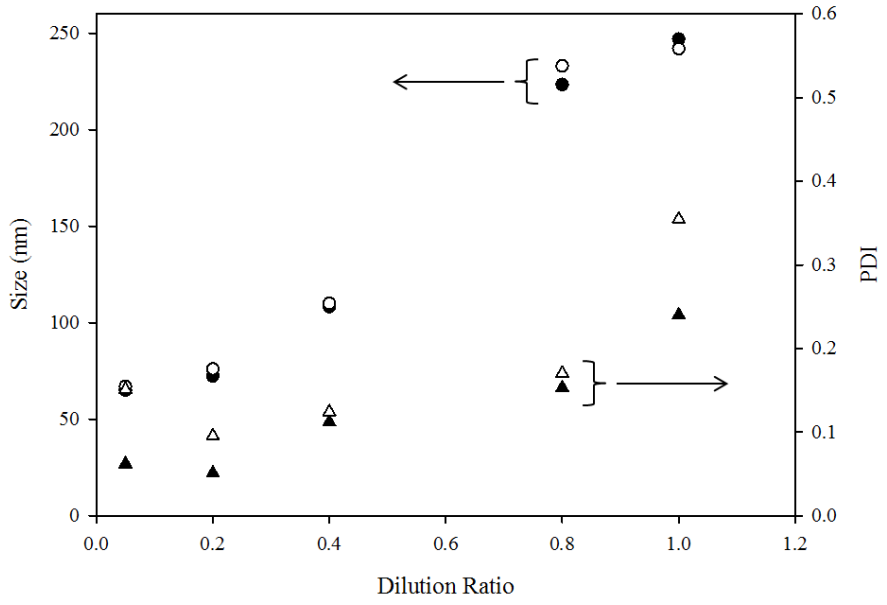


Figure 4.15: Z-average diameter and polydispersity measurements of nanoparticles comprised of *p*((HPMA$_{80}$)-*co*-EGDMA$_{0.95}$) using a starting concentration of 5 mg mL$^{-1}$ and varying the dilution ratio from 1 to 0.05 Solid symbols indicate measurements after one day, open symbols indicate measurements after seven months.

The z-average diameters of nanoparticle suspensions comprising *p*((HPMA$_{80}$)-*co*-EGDMA$_{0.95}$) after seven months were in good agreement with their counterparts

which were analysed after one day, as shown in Figure 4.15. Polydispersity had increased slightly within each dilution ratio, however, the z-average diameters of these materials were almost unchanged with the majority only increasing slightly. These data show the nanoparticles are extremely stable over extended periods of time with varying nanoparticle concentration. Linear counterparts to these samples showed onset of precipitation after several hours with significant precipitation after 2 weeks and were therefore unable to be assessed in this way. The dramatic difference in the appearance of stored samples of linear and branched nanoparticles, with decreasing dilution ratio (starting at 5 mg $mL^{-1}$), is shown in Figure 4.16.

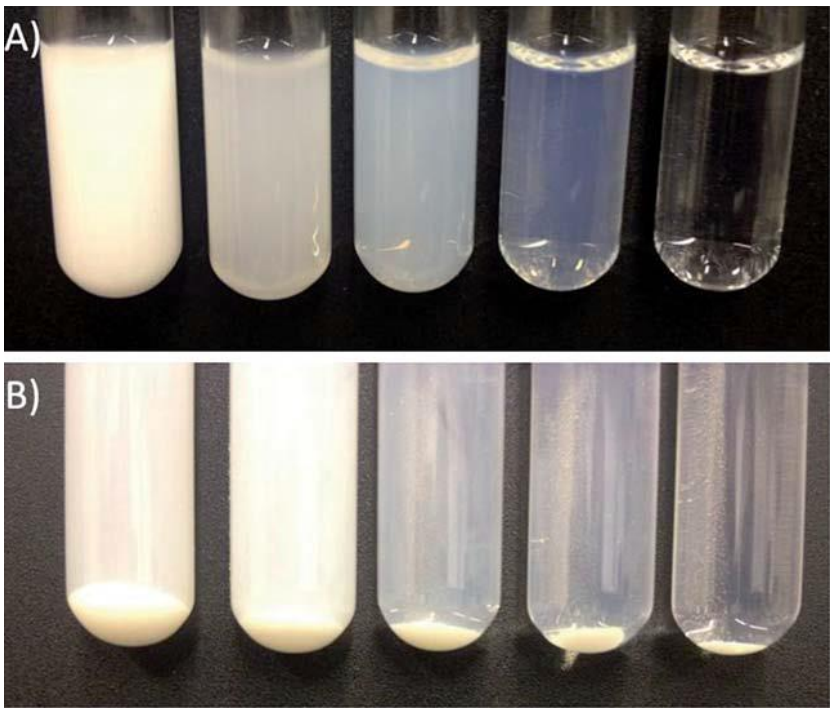


Figure 4.16: Comparison of nanoprecipitated *p*(HPMA) from an initial concentration of 5 mg $mL^{-1}$ in acetone to give varying final aqueous dispersions from 5 mg $mL^{-1}$ (far left), 4 mg $mL^{-1}$, 2 mg $mL^{-1}$, 1 mg $mL^{-1}$, 0.25 mg $mL^{-1}$ (far right). (A) *p*(HPMA-$_{80}$-*co*-EGDMA$_{0.95}$) branched copolymer seven months after nanoprecipitation; (B) *p*(HPMA$_{80}$) linear polymer two weeks after nanoprecipitation.

The change in transparency from high to low dilution ratio within Figure 4.16 is also evident where samples of 5 mg $mL^{-1}$ are completely opaque and upon decreasing the dilution ratio, they become more transparent. This is expected due to the mass of copolymer present in the far left samples scattering much more light, and as the sample becomes more dilute, scattering reduces.

### 4.4.8 Thermal Stability of Nanoparticles prepared from *p*((HPMA$_{80}$)-*co*-EGDMA$_{0.95}$)

To investigate their stability further, suspensions of nanoparticles comprised of *p*((HPMA$_{80}$)-*co*-EGDMA$_{0.95}$) were subjected to a gradual temperature increase to investigate whether changes in this parameter has any effect on their properties in solution.

In this experiment the aqueous dispersion was heated from 25 °C to 78 °C using settings within the DLS instrument; as with previous sizing measurements the recorded data is an average taken from six measurements. As can be seen in Figure 4.17, increasing the temperature has no effect on the z-average diameter or the polydispersity of the particles as they remained constant throughout the temperature range. This small and simple experiment demonstrates the particles stability and their ability to withstand temperature changes.

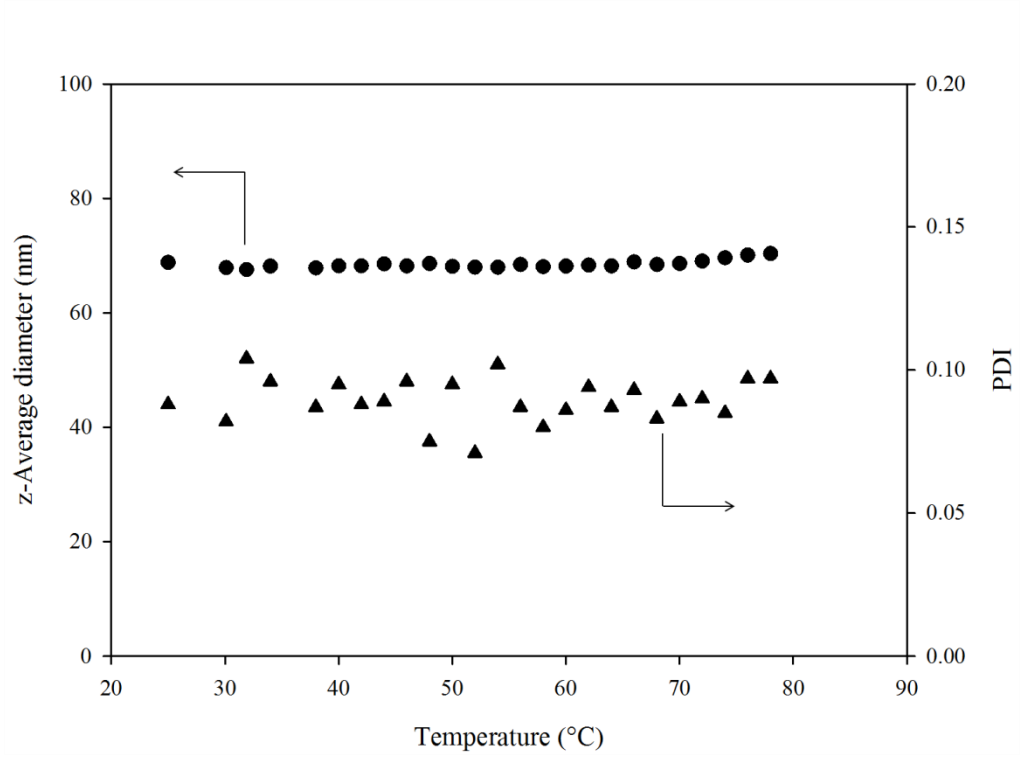


Figure 4.17: Temperature studies on nanoprecipitated *p*((HPMA$_{80}$)-*co*-EGDMA$_{0.95}$) prepared by rapid precipitation (5 mg mL starting concentration; 1 mg mL final concentration). z-average diameter (circles) and polydispersity (triangles).

### 4.4.9 Sonication Stability of nanoprecipitates prepared from *p*((HPMA$_{80}$)-*co*-EGDMA$_{0.95}$)

Prior investigations into the stability of our branched copolymer nanoparticles showed they are extremely robust. In an attempt to fully dissociate the particles, introducing extreme external force was necessary in order to give better insight into how these particles are remaining stable for such extended periods of time. Using ultrasound waves in this manner has not been widely researched; to our knowledge only three reports in the literature has investigated how sound waves impart force and fragment polymeric nanomaterials. One report refers to shell crosslinked

micelles where no z-average diameter change is apparent after 20 minutes of sonication (40 W) unlike their un-crosslinked counterparts which begin to fragment after just 1 minute.[20] Another report shows that the weight average length of sonicated micelles decreases as a function of sonication time[21] and the final publication reports the splitting of polymeric aggregates into monodisperse micelles.[22] The literature therefore suggests that materials reduce in z-average diameter as a consequence of sonication and due to the high stresses causing fragmentation.

Prior to carrying out this experiment, four possible outcomes were considered:

1. Significant cleavage of the nanoparticles resulting in significantly sized nanoparticles (e.g. half or a quarter of the original nanoparticle) present in solution. Fragments of the nanoparticles would be suspended in water, possibly in the size range of 10-50 nm, and would be detectable in DLS characterisation. This would also cause the attenuator to decrease as the overall concentration of particles would increase along with the derived count rate increasing due to increased scattering.
2. Peripheral fragmentation of the nanoparticles, with very small particles becoming more significant as sonication time increases. This would cause an increase in the derived count rate as scattering increases yet may not affect the attenuator as only very small polymer fractions would fragment with time and therefore the scattering may not increase significantly. The measured z-average diameter may remain very similar, but a decrease would be expected as sonication time increases, leading to a larger overall copolymer fragment population. Significant scattering from very small fragments may not be detectable by DLS depending on the size of the fragments formed.

3. Nanoparticle fragmentation (significant cleavage or small fragments) forming unstable materials with subsequent aggregation of material leading to precipitation. Material that has become dissociated from the nanoparticles may aggregate due to their hydrophobic nature, causing them to precipitate out of solution. This would be visually observable in the sample vial and associated with subsequent increasing attenuator values to counteract the lessening scattering intensity due to less dispersed material. DLS measurements assume particles are spherical and the average size of particles may be unaffected until a significant proportion of material has been fragmented, after which the z-average diameter of nanoparticles would reduce.
4. Single collapsed branched copolymers, which dissociate from particles into the surrounding solution. This is proposed as the literature suggests aggregated materials which are not covalently bound to each other, can dissociate into their single components.[22] It has been suggested nanoparticles are composed of multiple branched copolymers, and if sonication causes these to become single entities, a dramatic reduction in the z-average diameter of particles would occur as sonication increases, assuming these single branched copolymers are stable in aqueous solution. As the concentration of material present would increase, as stated previously, this causes more scattering, causing the derived count rate to increase and the attenuator to lower.

A preliminary sonication experiment was conducted due to the lack of literature reports describing the sonication of copolymer aggregates without a probe. It was believed that the high intensity could immediately fragment the particles without

being able to monitor the process effectively; therefore a duty cycle of 100 and 50 % intensity was selected as the treatment parameters on the sonicator software. A nanosuspension comprising of *p*((HPMA$_{80}$)-*co*-EGDMA$_{0.95}$) (5 mg mL$^{-1}$ starting concentration; 1 mg mL$^{-1}$ final concentration) was subjected to sonication using focused ultrasound waves in a water-bath with a controlled temperature of 10 °C for 5 seconds, where the sample was promptly resized. As no significant changes to the DLS size distribution occurred, the same sample was transferred back into the water-bath and sonicated for a further 60 seconds and, again, no significant change in z-average diameter was apparent, however, a slight trend to larger z-average and increased polydispersity was seen. This process was repeated once more where the sample remained in the sonicator for further 300 seconds, giving a total sonication time of 365 seconds, after which the appearance of the sample was visually unchanged. For full experimental protocol, see Chapter 2 section 2.5.2.1.

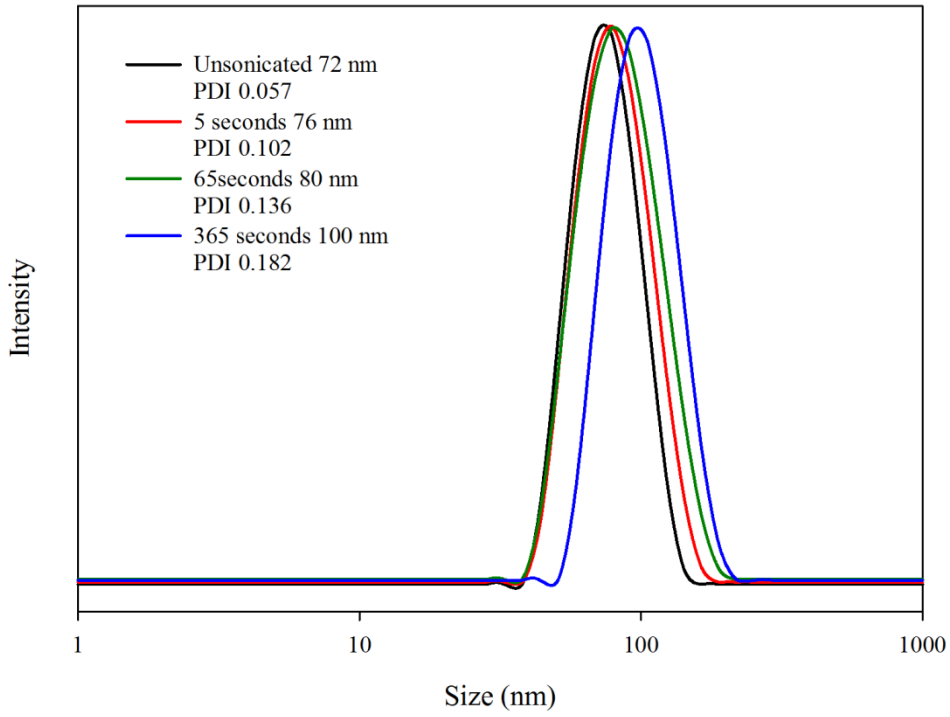


Figure 4.18: DLS characterisation of sonicated *p*((HPMA$_{80}$)-*co*-EGDMA$_{0.95}$) nanosuspension prepared by rapid precipitation (5 mg mL$^{-1}$ starting concentration; 1 mg mL$^{-1}$ final concentration) using 50 % intensity over 365 seconds.

Figure 4.18 shows clearly that fragmentation leading to smaller nanoparticles has not occurred as major decreases in the z-average diameter (with increasing polydispersity) would have been seen compared to the unsonicated trace. After 365 seconds the z-average diameter of particles increased by only 28 nm and polydispersity increased from 0.057 to 0.182. Surprisingly this preliminary experiment suggests these materials are highly stable when subjected to sonication. It was thought this sample may not fragment sufficiently using only 50 % intensity or it may have taken an extended period of exposure. Therefore a new sample of *p*((HPMA$_{80}$)-*co*-EGDMA$_{0.95}$) was prepared (identical nanoprecipitation protocol) and sonicated using 100 % intensity as it was thought monitoring of the sonication

process would allow a better insight to the stability of the suspension over a series of shorter exposure times.

The 1 mg $mL^{-1}$ sample was first analysed and then subsequently transferred into the Covaris S2x and sonicated for 5 seconds using 100 % intensity and a duty cycle of 100 and then promptly re-analysed. This process was repeated until the sample had been sonicated for approximately 4 minutes. The DLS measurements during this process are reported in Figure 4.19 over the course of the experiment.

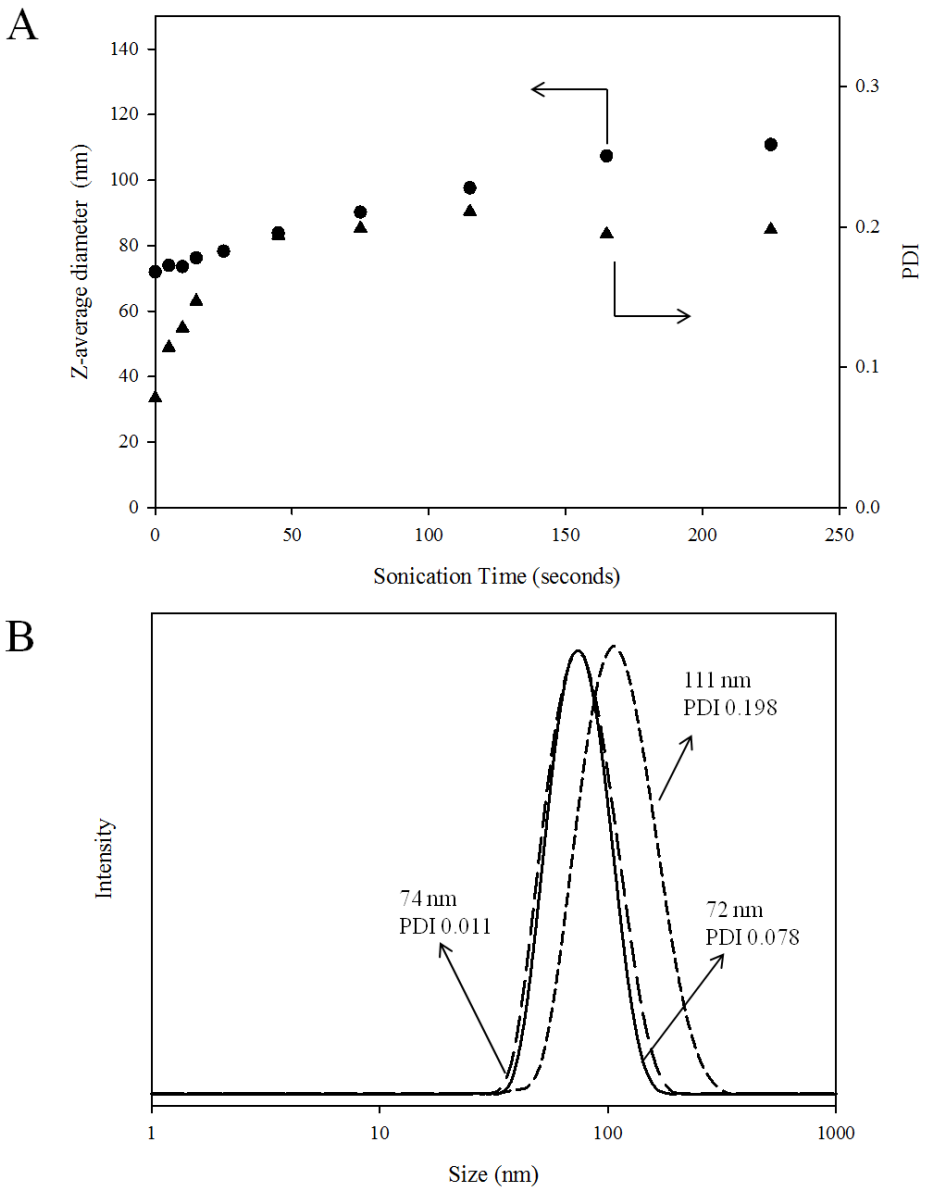


Figure 4.19: Sonication studies of nanoprecipitated *p*((HPMA$_{80}$)-*co*-EGDMA$_{0.95}$) aqueous suspension. (5 mg mL$^{-1}$ initial concentration; 1 mg mL$^{-1}$ final concentration). (A) Z-average diameter and polydispersity *vs*. sonication time. (B) DLS characterisation of particles at various sonication times. Time = 0 seconds (solid line) 5 seconds (medium dashed line), 225 seconds (small dashed line).

According to data shown in Figure 4.19 (A) the nanoparticles do not completely dissociate when exposed to sonication. Indeed they increase in diameter from 72 nm to 111nm. The first three sonication exposures (15 seconds total sonication) showed little effect on the nanosuspension but after a total sonication time of 115 seconds the particles had reached 98 nm which is approximately a 50 % increase in particle diameter. Further sonication (total time from 115 seconds to 225 seconds) led to only a moderate increase in z-average diameter of particles (98 nm) to give a final diameter of 111 nm. Polydispersity of the nanoparticles increased from 0.078 to 0.198. DLS measurements for three sonication times were selected (time = 0 seconds, 5 seconds and 225 seconds) and are shown in Figure 4.19 (B) which also displays both z-average diameter and polydispersity increase with sonication.

As well as z-average diameter and polydispersity, the derived count rate was also recorded during the experiment and is shown in Figure 4.20. As explained previously, this is directly related to the amount of scattering of the nanosuspension and can be a measure of nanoparticle concentration at constant attenuator values. The attenuator remained (automatically) at a value of 5 throughout the experiment, indicating that the instrument did not require adjustment.

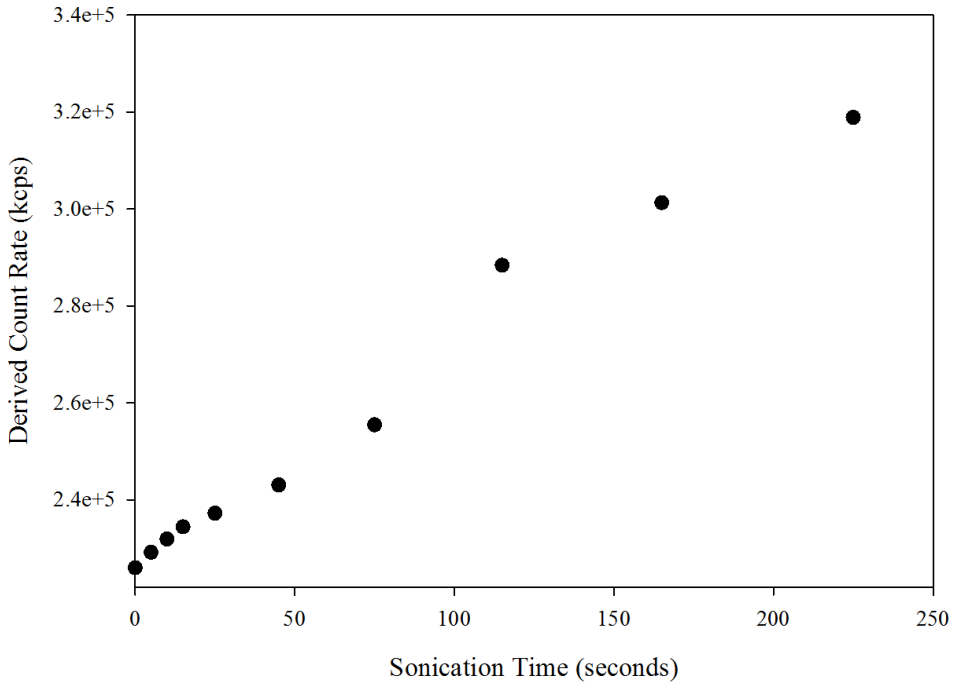


Figure 4.20: Sonication studies of nanoprecipitated *p*((HPMA$_{80}$)-*co*-EGDMA$_{0.95}$) aqueous suspension. (5 mg mL$^{-1}$ initial concentration; 1 mg mL$^{-1}$ final concentration). Derived count rate against total sonication time.

4.4.9.1 Rationale of stability during sonication

Analysis of the experimental data has shown that none of the expected behaviour occurred. Significant cleavage of copolymer from nanoparticles was discounted as the z-average diameter of particles increased throughout the experiment. If major cleavage had occurred, the attenuator would automatically be lowered in order to reduce the amount of scattered light reaching the detector. The attenuator remained constant (automatically) throughout the experiment, showing that the scattering has not increased considerably and indicating concentration of material present did not change significantly and the derived count rate increased but not over a large range. Large scale cleavage was therefore thought to be minimal.

If the particles within the sample remained substantially intact as imagined, the derived count rate would be extremely similar throughout the experiment. Yet it is seen to gradually increase from 225996 kcps to 318857 kcps (Figure 4.20), suggesting only a slight increase in scattering is occurring as sonication time increases; the range over which this change is occurring is relatively small and the same order of magnitude of scattering is seen throughout the sonication treatment. The data presented suggests two possible scenarios:

1) Fragmentation of peripheral copolymer units, which associate/aggregate onto nearby nanoparticles. This may occur as the small fragments would not be large enough to sediment but are also not stable enough to exist within the solution. Initially no significant z-average diameter change is apparent when these small fragments are transferring to other particles as the DLS measurements assume particles are perfect spheres and a small addition to a larger nanoparticle would be within the error of the measurement. Yet over time as more fragmentation occurs, a larger z-average diameter and polydispersity will ensue, due to some particles (perhaps the smallest) fragmenting more, and therefore the larger particles gain more copolymer fragments causing an increase in their z-average diameter. The derived count rate is thought to increase due to the larger particles now present in the solution scattering slightly more light.

2) Reordering of the internal nanoparticle structure. Sound waves penetrating the nanoparticles may cause motion within the individual components of the nanoparticles resulting in less dense nanoparticles after a rearrangement of the packing but without fragmentation of the nanoparticle. This was proposed due to the steady increase in the diameter of particles as sonication time increases, yet with

relatively small change in polydispersity. The increased derived count rate may, again, be due to the larger size of the particles and hence more scattering.

It is not clear which process is occurring within the nanoparticles during sonication, however, the materials appear to be highly robust with the ability to withstand extremely high and lengthy sonication.

## 4.4.10 Determination of Charge Stabilisation of Nanoparticles

Nanoparticles comprised of branched copolymers have been shown to be highly stable i.e. little change in z-average diameter or polydispersity over time. The reasons for this could be either steric repulsion, electrostatic repulsion or a combination of both. To investigate whether these particles have surface charge, nanoparticle suspensions were prepared by rapid nanoprecipitation (*p*((HPMA$_x$)-*co*-EGDMA$_{0.95}$)) ($x$ = 50, 80, 120) (5 mg mL$^{-1}$ starting concentration; 1 mg mL$^{-1}$; final concentration) and zeta potential measurements were performed. Experimental procedure is found in Chapter 2 section 2.2.3.1.

| Copolymer | Zeta Potential (mV) |
|---|---|
| *p*((HPMA$_{50}$)-*co*-EGDMA$_{0.95}$) | -41.1 |
| *p*((HPMA$_{80}$)-*co*-EGDMA$_{0.95}$) | -34.0 |
| *p*((HPMA$_{120}$)-*co*-EGDMA$_{0.95}$) | -44.5 |

Table 4.3: Zeta Potential results for nanoparticles comprised of *p*((HPMA$_x$)-*co*-EGDMA$_{0.95}$) ($x$ = 50, 80, 120) prepared by rapid nanoprecipitation (5 mg mL$^{-1}$ starting concentration; 1 mg mL$^{-1}$; final concentration).

Table 4.3 shows that nanoparticles are negatively charged (irrespective of *p*(HPMA) primary chain length) with no clear trend between samples, suggesting that stability

of suspensions arises from electrostatic repulsion. The exact reasons for negative surface charges is unknown but may be due to slightly negatively charged hydroxyl groups present in *p*(HPMA) chains. Hydrolysis of *p*(HPMA) chains (producing methacrylic acid) may also be a possible reason, however, this has not been investigated.

### 4.4.11 Branched Copolymer Nanoparticle Stability to Salt Addition

The effect of electrolyte addition to nanoparticles was studied due to the observed negative zeta-potential in previous experiments suggesting charge stabilisation as the likely mechanism for colloidal stability. Salt addition should lead to de-stabilisation through the screening of negative electrostatic repulsion between the nanoparticles. A sample of *p*((HPMA$_{80}$)-*co*-EGDMA$_{0.95}$) was nanoprecipitated, as previously described, and subjected to successive additions of small aliquots (2 µL) of aqueous NaCl (0.5M); achieving a total addition of 16 µL. After each addition the sample cuvette was gently shaken to distribute the electrolyte throughout the solution (see Chapter 2 section 2.5.2.4. Prompt analysis was performed afterwards and the recorded data are displayed in Figure 4.21.

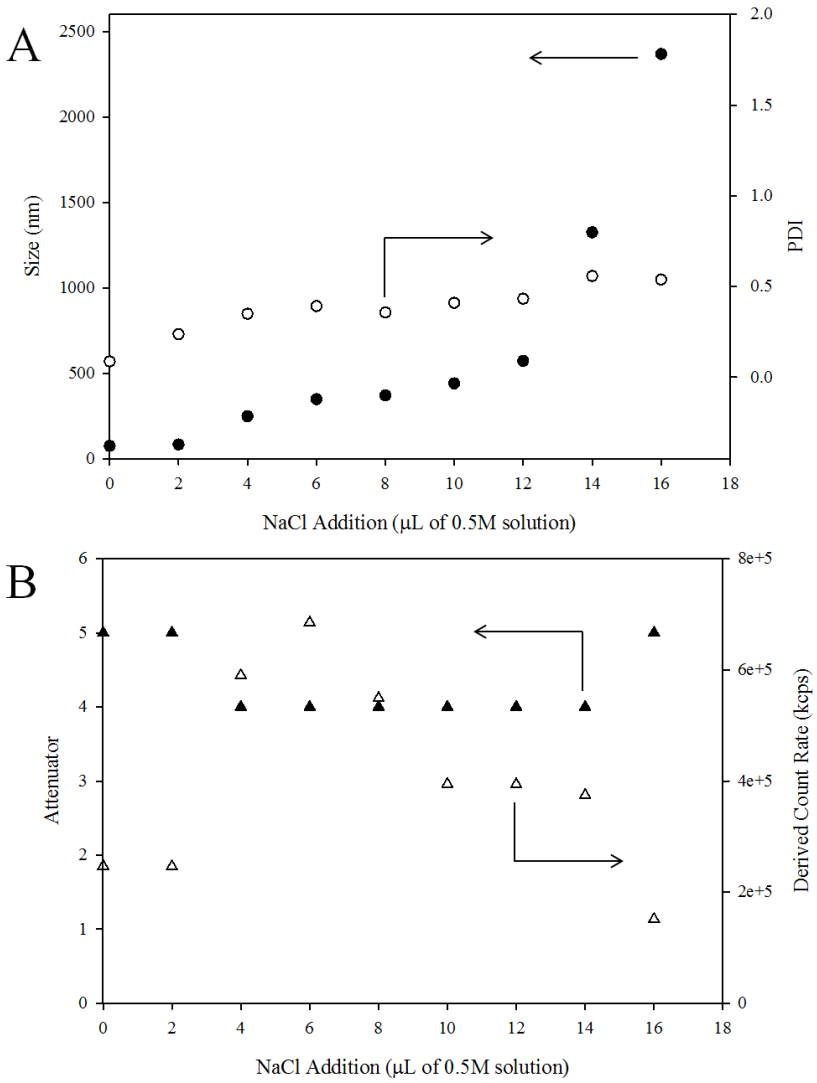


Figure 4.21: DLS characterisation of nanoprecipitated *p*((HPMA$_{80}$)-*co*-EGDMA$_{0.95}$) 5 mg mL$^{-1}$starting concentration; 1 mg mL$^{-1}$ final concentration. Response to electrolyte (0.5M NaCl) addition. (A) Z-average diameter (solid circles), Polydispersity (open circles) (B) Attenuator (solid triangles), Derived count rate (open triangles).

It is clear that small amounts of NaCl impart a great effect on z-average diameter, polydispersity and derived count rate. The z-average diameter increased slowly (from 75 nm) until 12 µL had been added (572 nm), after which the z-average diameter increased dramatically with observable precipitation. Measurements by

DLS of nanoparticles > 1000 nm are unreliable, however, the very high polydispersity (approximately 0.5) and nanoparticle diameter, is highly indicative of the response to the electrolyte. The initial additions of salt led to increasing polydispersity, with large amounts of precipitate forming in the sample vial. As the attenuator value remained constant throughout the majority of the experiment we can infer that the derived count rate is responding to the decrease in the concentration of nanoparticles (through association and precipitation) even though a subsequent increase in scattering would be expected from the larger materials.

### 4.4.12 Rationale of Nanoparticle Stability

Clearly the dramatic architectural difference between linear and branched *p*((HPMA)-*co*-EGDMA$_{0.95}$) copolymers is the reason behind the aqueous stability of branched copolymer nanoparticles. Despite their predominantly identical chemistry, copolymers formed from multiple linear chains (branched) have produced stable nanosuspensions for more than seven months where as their linear counterparts aggregated and precipitated after only several hours. It is possible that these copolymers exert some affinity for their aqueous environment, despite *p*(HPMA) being highly insoluble in water. The development of branching in the copolymerisation of *p(*HPMA) was studied in more detail in an attempt to rationalise the different behaviour observed in nanoparticle stability.

Initially, the synthesis of branched vinyl polymers was considered to establish whether common features of the mechanism would lead to architectural similarities between polymers with different target primary chain lengths. The branched copolymerisation will undergo three clear phases during the propagation of *p*(HPMA) and the growth of branched copolymers.

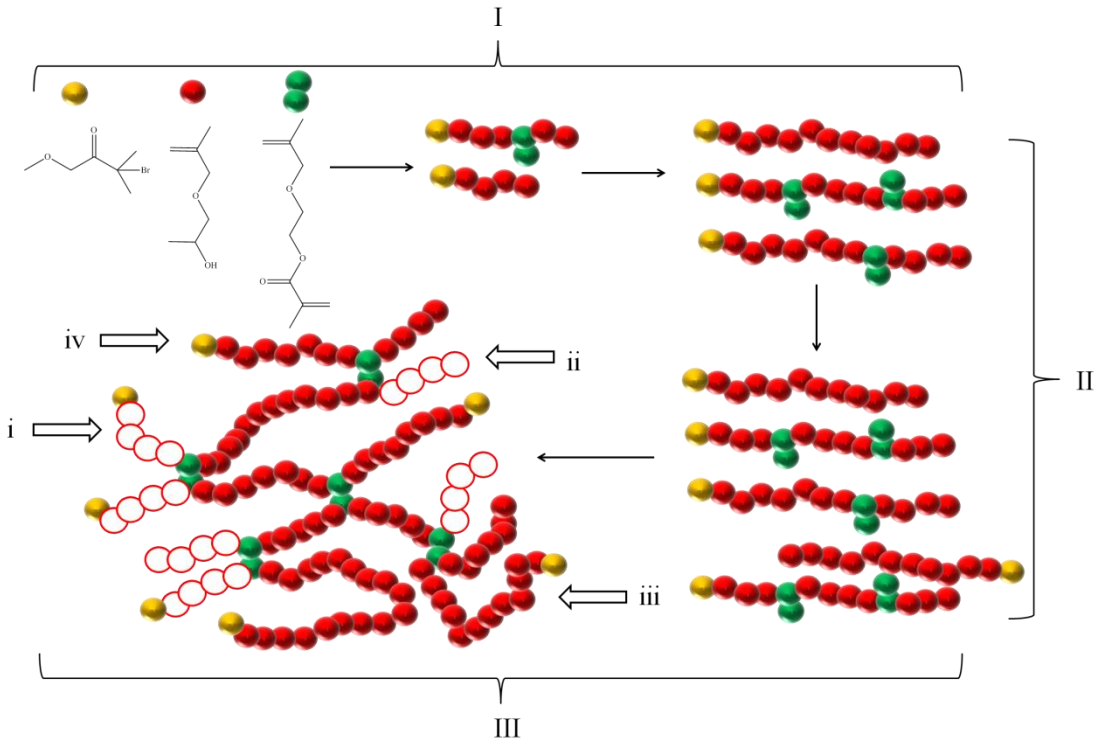


Scheme 4.7: Schematic representation of the development of branching during ATRP copolymerisation. Phase I oligomer formation), Phase II (initial inter-chain reaction), Phase III(intermolecular branching at high conversion) – chain-end oligomers formed at low conversion (i), high conversion (ii) and long chain end groups (iii and iv).

Scheme 4.7 shows the proposed stages during the branching copolymerisation Phase 1 involves statistical incorporation of EGDMA (with an un-reacted pendant vinyl group) into a primary chain before branching becomes significant. Therefore a proportion of the EGDMA will become incorporated at an early stage (low conversion) when small oligomers predominate within the reaction. This generates a small oligomeric chain preceding the branching point shown as (i) in Scheme 4.7. Conversely those chains where EGDMA is initially incorporated at a later stage (higher conversion) will produce longer pendant chains after significant branching

has occurred, indicated as (iii) in Scheme 4.7. In Chapter 3 section 3.3.1 it was shown that at high conversion, inter-chain branching predominates rather than linear chain growth, indicated by the dramatic increase in molecular weight at high conversion. Scheme 4.7 (ii) represents chain ends formed when an active chain end reacts with a pendant double bond within an environment of low monomer content and produces short oligomeric chains after the introduction of the branch point. As conversion approaches 100 %, small chain ends are guaranteed to form. Small chain ends containing approximately 10 monomer units (or less) should form after branch points which have been generated above 80 % conversion where the target $DP_n$ of the primary chain is 50 monomer units (i.e. only 10 monomer units are left to add to the propagating chains). Similarly for this example, inter-chain branching at 90 % conversion would generate small chain ends comprising of five monomer units or less. Therefore during Phase III extremely high molecular weight material is generated as linear copolymer chains become covalently bonded, but as a consequence of this, short oligomeric chain ends are also formed. However, as previously mentioned, not all chain ends will be oligomeric.

## 4.5 Synthesis of Oligomeric *p*(HPMA)

In simulation studies of linear, star and branched copolymers, specifically to understand solubility,[23] chain ends have been shown to be highly mobile and able to interact with solvent environments to a far greater extent than other areas of the polymer chains. In lightly branched structures, considerable immobility of chains is noticed over considerable timescales; therefore the chain ends described above may have a considerable impact on the behaviour of the branched copolymers. HPMA is a water soluble monomer, however, as molecular weight increases during its polymerisation it rapidly becomes insoluble. To our knowledge there are no reports

in the literature which have systematically investigated onset of insolubility (or molecular weight) of HPMA during polymerisation. As a result, a series of oligomers with target $DP_n$ = 5, 7, 10, 13, 15 and 17 monomer units were synthesised using the same experimental protocol as described for previously synthesised linear *p*(HPMA) materials in order to investigate the aqueous solubility of *p*(HPMA) oligomers (see Chapter 2 section 2.3.1).

| Target $DP_n$ | $M_n$ (g $mol^{-1}$) (GPC, acetone) | $M_w/M_n$ (GPC, acetone) | Calc $DP_n$ (GPC, acetone) | $M_n$ (g $mol^{-1}$) (GPC, THF) | $M_w/M_n$ (GPC, THF) | Calc $DP_n$ (GPC, THF) | Calc $DP_n$ ($^1$H NMR, $d_6$-DMSO) |
|---|---|---|---|---|---|---|---|
| 5 | 1800 | 1.17 | 12 | 1900 | 1.5 | 13 | 7 |
| 7 | 2300 | 1.15 | 15 | 3000 | 1.6 | 20 | 8 |
| 10 | 2600 | 1.12 | 18 | 3300 | 1.3 | 22 | 10 |
| 13 | 3200 | 1.06 | 22 | 1900 | 1.18 | 13 | 14 |
| 15 | 3200 | 1.06 | 22 | 2200 | 1.18 | 15 | 16 |
| 17 | 3300 | 1.09 | 23 | 2400 | 1.12 | 17 | 18 |

Table 4.4: GPC and $^1$H NMR spectroscopic analysis of *p*(HPMA) oligomers using ambient methanolic ATRP.

Table 4.4 shows the molecular weight analysis of the targeted oligomers after purification *via* precipitation into cold *n*-hexane. Triple detection GPC (acetone eluent) analysis gave relatively high molecular weights (and therefore calculated $DP_n$) for these polymers, despite polydispersity remaining low across all samples (see Figure 4.22 (B)). A second analysis using THF as an eluent was performed and, again, the calculated $DP_n$ for the oligomers was higher than predicted, where the

highest was $DP_n$ = 22 monomer units for a target $DP_n$ of 10 monomer units, individual GPC chromatograms are shown in (see Figure 4.22 (A)). The measured molecular weight distributions were generally higher when using THF than those recorded when using acetone as the eluent; nevertheless, all GPC traces were monomodal and the molecular weight increased steadily with increasing target $DP_n$.

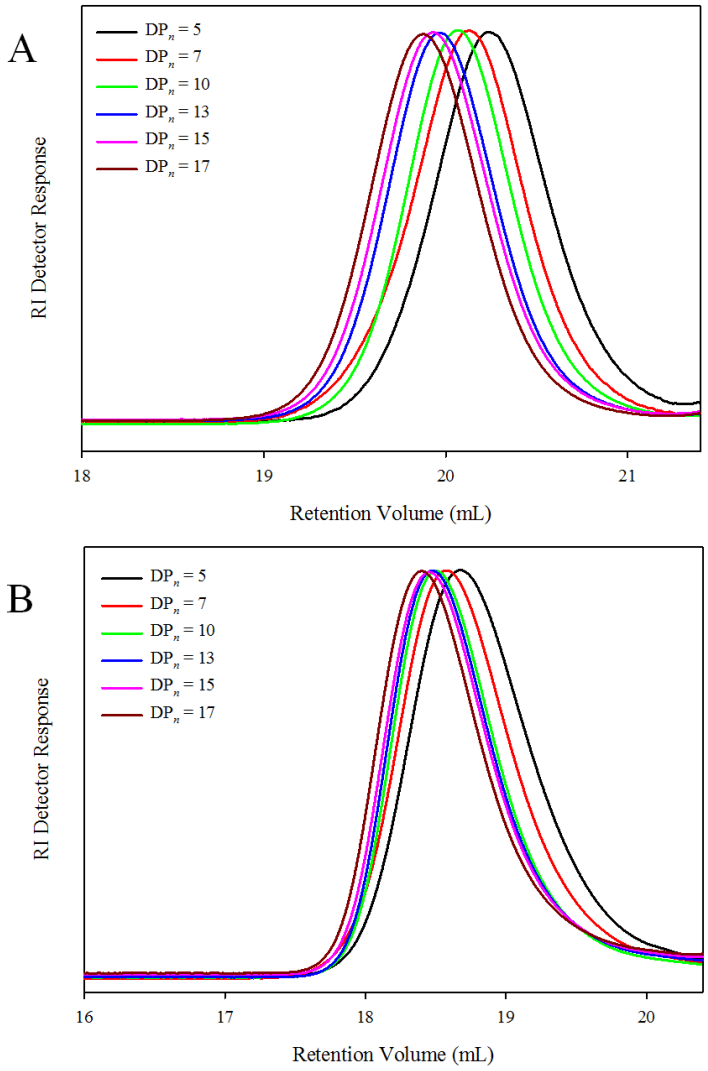


Figure 4.22: Triple Detection GPC analysis of *p*(HPMA) oligomers. THF eluent (A). Acetone eluent (B).

Unsurprisingly, the $DP_n$ values calculated by $^1H$ NMR spectroscopy are extremely similar to the target $DP_n$, as this only confirms the reaction of vinyl groups in the monomer, and assuming this is close to 100 % (as has been shown to be the case in previous polymerisations of *p*(HPMA)), then it is likely to be very close to the target $DP_n$. Also, the presence of unreacted initiator will lead to an underestimation of $DP_n$ using NMR techniques. The higher than expected molecular weights generated during these experiments are likely to be due to initiator efficiency, where fewer chains were initially generated and therefore longer chains were formed. Although the EBiB initiator has been used extensively in the previous chapter, with little inefficiency in the resulting polymer analysis, the target $DP_n$ values were significantly higher than those targeted here (50, 80, 120 monomer units). It becomes extremely difficult to obtain narrow molecular weight distributions at low target $DP_n$ using ATRP as the initiator efficiency needs be extremely high and the dormant/active nature of the equilibrium does mean that any differences in chain propagation (i.e. not all chains initiate and propagate at the same time) during the early stages of polymerisation do not balance/average across all chains, as would be expected for longer chain lengths and polymerisation times. Also, at low target $DP_n$, differences of one-five monomer units represent a large percentage of the overall targeted chain length, hence affecting the molecular weight distribution dramatically. The oligomers synthesised here do, however, represent a series of systematically varying chain lengths to facilitate the solubility of *p*(HPMA) oligomers.

### 4.5.1 Aqueous Solubility of Oligomeric *p*(HPMA)

The aqueous solubility of the oligomeric *p*(HPMA) chains and linear *p*($HPMA_{50}$), *p*($HPMA_{80}$) and *p*($HPMA_{120}$) were investigated. Saturated aqueous solutions of the

aforementioned polymers were prepared by attempting to dissolve approximately 500 mg of each sample into distilled water (14 mL). Removal of the supernatant (10 mL) after three days, and transfer of the solution into three pre-weighed aluminium dishes, allowed the dissolved polymer to be quantified after water evaporation (covered) at room temperature for one week. The dishes were re-weighed and the saturated concentration was recorded as an average of the three samples (see Chapter 2.3.6).

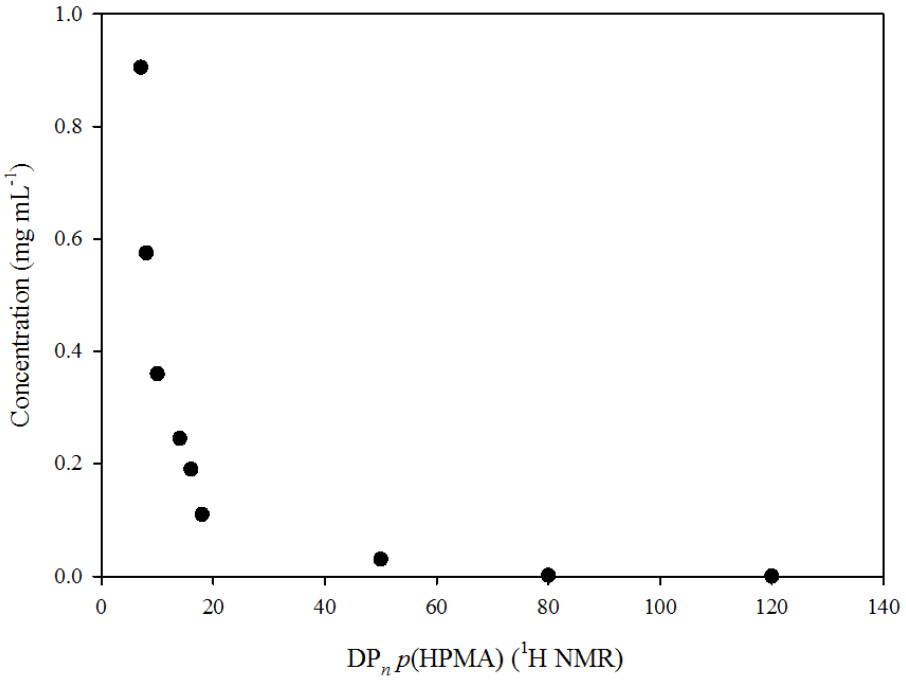


Figure 4.23: Aqueous solubility study of *p*(HPMA) with varying chain length ($DP_n$).

$DP_n$ values calculated by $^1H$ NMR spectroscopy were used to plot the solubility curve in Figure 4.23; however, using values obtained by GPC (acetone or THF eluent) also generate the same curve with the difference being that the *X* axis is shifted slightly. Data shown in Figure 4.2, demonstrate how *p*(HPMA) does indeed exhibit some aqueous solubility which increases as chain length decreases. A

concentration of 0.905 mg $mL^{-1}$ was found for the lowest recorded *p*(HPMA) chain ($DP_n$ = 7 by $^1H$ NMR spectroscopy). Aqueous solubility drastically decreased as chain length increased until the chain lengths reach approximately 18 monomer units, after which solubility is negligible. This data is intuitive with monomeric HPMA being soluble in water and suggests a potential role for the oligomeric chain ends within the branched polymer architectures (unlike their linear counterparts) possessing some affinity for an aqueous environment.

### 4.5.2 LCST Behaviour of Oligomeric *p*(HPMA)

To study the hypothesis that small oligomeric *p*(HPMA) chains are present within branched *p*(HPMA) copolymers imparting aqueous solubility and allowing nanoparticles to remain stable, a crude Lower Critical Solution Temperature (LCST) experiment was performed to determine a cloud point value. An aqueous solution (1 mL, 0.57 mg $mL^{-1}$) of *p*(HPMA) ($DP_n$ = 8 monomer units according to $^1H$ NMR spectroscopy) was placed into the DLS instrument where the temperature was set at 25 °C and the sample was analysed during increasing temperature at increments of 3 °C until the temperature reached 55 °C. It should be noted that, as with previous size analyses, the data recorded are averages of six measurements and are shown in Figure 4.24.

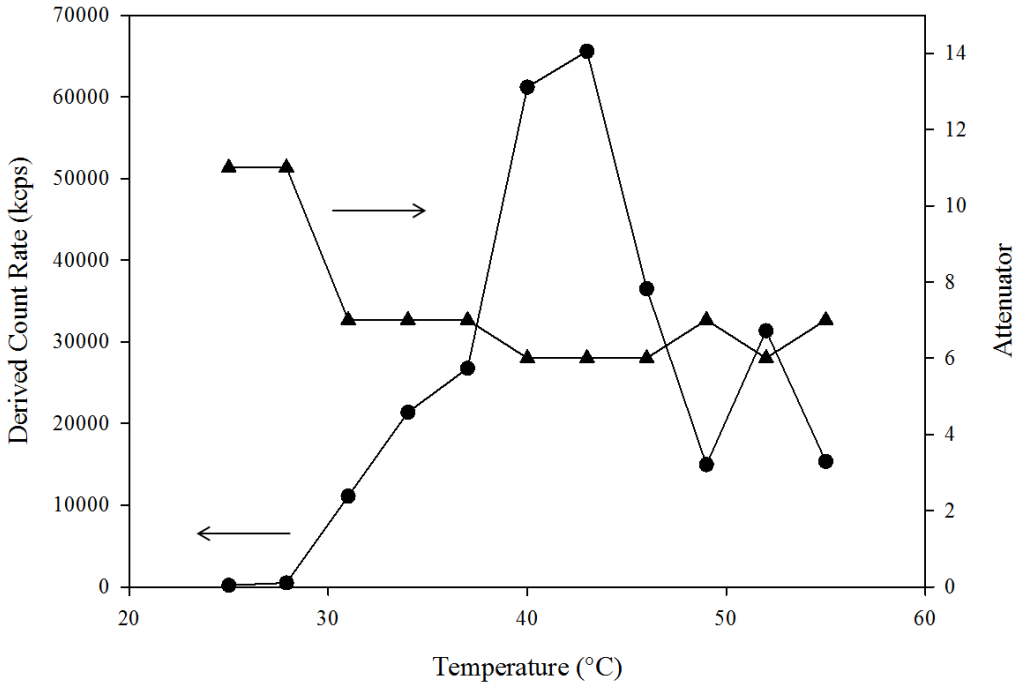


Figure 4.24: Study of the effect of temperature on an oligomer of *p*(HPMA) ($DP_n$ = 8 by $^1H$ NMR spectroscopy). Derived count rate and attenuator measure during heating within the DLS instrument.

As the oligomer is extremely small and the concentration is low, the observed scattering is extremely low and z-average diameters could not be recorded, however, we believe the derived count rate and the attenuator give some indication of the onset of LCST behaviour. From 25 °C to 31 °C virtually no scattering was observed, judged by the extremely high automatic attenuator setting (11) which substantially decreases upon temperature increase and remains between 6 and 7 for the remainder of the experiment indicating a much higher amount of scattering occurring and also correlating with values in previous experiments. The derived count rate shows a sharp increase from 197 kcps to 11095 kcps from 25 °C to 31 °C reaching 65574 kcps at 43 °C. Above this temperature the derived count rate falls dramatically until the final temperature is reached (55 °C). Although only two parameters were

examined, both indicate that oligomers of *p*(HPMA) potentially possess LCST behaviour, and subsequent interaction with water, and therefore may have the potential to provide aqueous stability to branched polymer nanoparticles independent of the main branched polymer core *via* a small amount of steric repulsion. The LCST behaviour of oligomeric *p*(HPMA) does not correlate with the thermal stability data shown in section 4.4.8, where no significant change in z-average diameter or polydispersity was observed, however, the observed highly negative zeta potential is clearly also playing an important role.

## 4.6 Removing the Impact of Oligomeric Chain Ends

To investigate the role of the short oligomeric chains in greater detail, the removal of a large number of the chains formed during the early stages of the branching process was conducted. As described previously in Chapter 3 section 3.3.3, a linear-branched chain extension reaction was conducted to study the kinetics and control during branhced polymerisation. This leads to a more architecturally complex branched copolymer being synthesised. It is very difficult to completely prevent oligomeric *p*(HPMA) chains being formed during the branched copolymerisation, however, the synthesis of *p*((HPMA$_{30}$)-*b*-*p*((HPMA$_{50}$)-*co*-EGDMA$_{0.95}$)) does eliminate the oligomers that are formed during Phase I of Scheme 4.7. The architectural differences between linear, branched and the modified branched block copolymer are shown in Scheme 4.8.

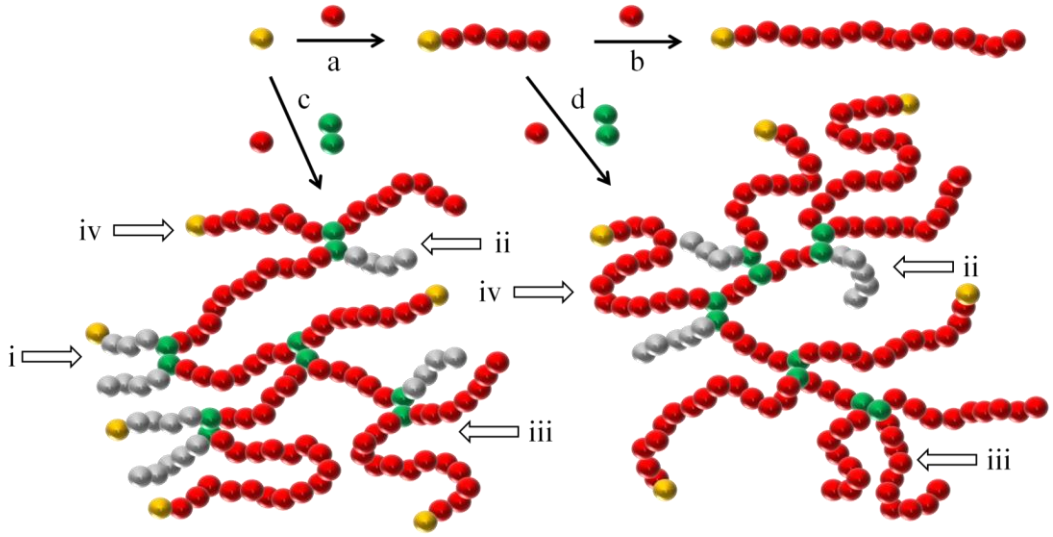


Scheme 4.8: Representation of three synthesis strategies of *p*(HPMA). (a + b) generates linear polymers. (a +c) generates branched polymers. (a + d) generates linear-*b*-branched copolymers. Chain-end oligomers formed at low conversion (i), high conversion (ii) and long chain end groups (iii and iv).

Two chain extension (or self-blocking) experiments were carried out in parallel; the first generated a linear *p*(HPMA$_{30}$-*b*-HPMA$_{50}$) (equivalent to *p*(HPMA$_{80}$)) and the second generated *p*((HPMA$_{30}$)-*b*-*p*((HPMA$_{50}$)-*co*-EGDMA$_{0.95}$)) (see Chapter 2 section 2.3.3 and 2.3.4. In the former experiment, after approximately 88 % conversion (as judged by $^{1}$H NMR spectroscopy) of the first block with a target DP$_n$ of 30 monomer units, a second batch of monomer (with a target DP$_n$ of 50 monomer units) was added to the reaction mixture and left to polymerise until > 99 % conversion had been reached. An identical protocol was used in the second experiment with the addition of EGDMA in the second batch addition to induce branching (1: 0.95 monomer:brancher) where conversion had reached 81 %.

| Sample | Description | $M_n$ (g mol$^{-1}$) (GPC) | $M_w$ (g mol$^{-1}$) (GPC) | $M_w/M_n$ | Conversion (%) |
|---|---|---|---|---|---|
| *p*(HPMA$_{30}$) | Linear | 3800 | 4200 | 1.11 | 88 |
| *p*(HPMA$_{30}$-*b*-HPMA$_{50}$) | 2$^{nd}$ monomer addition | 15300 | 18400 | 1.20 | 88 |
| *p*(HPMA$_{30}$)-*b*-(HPMA$_{50}$) | Purified linear polymer | 16000 | 17500 | 1.09 | > 99 |
| *p*(HPMA$_{30}$) | Linear | 3300 | 3600 | 1.09 | 81 |
| *p*(HPMA$_{30}$-*b*-(HPMA$_{50}$-*co*-EGDMA$_{0.95}$)) | 2$^{nd}$ monomer and brancher addition | 50000 | 319300 | 6.40 | 77 |
| *p*(HPMA$_{30}$-*b*-(HPMA$_{50}$-*co*-EGDMA$_{0.95}$)) | Purified branched polymer | 98300 | 1550000 | 15.77 | > 99 |

Table 4.5: Triple detection GPC analysis of self-blocked linear *p*(HPMA) and self blocked linear-*b*-branched *p*(HPMA).

Table 4.5 shows the dramatic difference in molecular weights between the two blocking experiments; where EGDMA is not incorporated in the second block, an $M_n$ of 16000 g mol$^{-1}$ is achieved (which is comparable to the synthesis of *p*(HPMA$_{80}$)), where an $M_n$ of 11700 g mol$^{-1}$ was found in Chapter 3 section 3.3; an $M_n$ of 98300 g mol$^{-1}$ was found for the sample which has EGDMA incorporated. Their molecular weight distributions also show a marked difference; 1.11 was found for the linear polymer sample, which is well within the range for a general linear ATRP reaction where as the branched counterpart gave a molecular weight distribution of 15.77 clearly demonstrating that branching has occurred which has generated a wide range of molecular weights.

Figure 4.25 demonstrates the dramatic molecular weight differences between the two blocking experiments, where the initial linear block (target DP$_n$ = 30) in both cases has low polydispersity and have extremely close retention volumes, correlating well with their similar conversions. It should also be noted here that linear material exists in the *p*(HPMA$_{30}$-*b*-(HPMA$_{50}$-*co*-EGDMA$_{0.95}$)) polymer sample indicated by an almost identical peak at approximately 18.5 mL elution volume, which has been found with previous branching experiments (Chapter 3 section 3.3). This experiment demonstrates the ability to self-block *p*(HPMA), with linear blocked polymer (*p*(HPMA$_{30}$-*b*-HPMA$_{50}$)) achieving a similar molecular weight to its unblocked counterpart (*p*(HPMA$_{80}$)) and also maintaining a low molecular weight distribution throughout polymerisation.

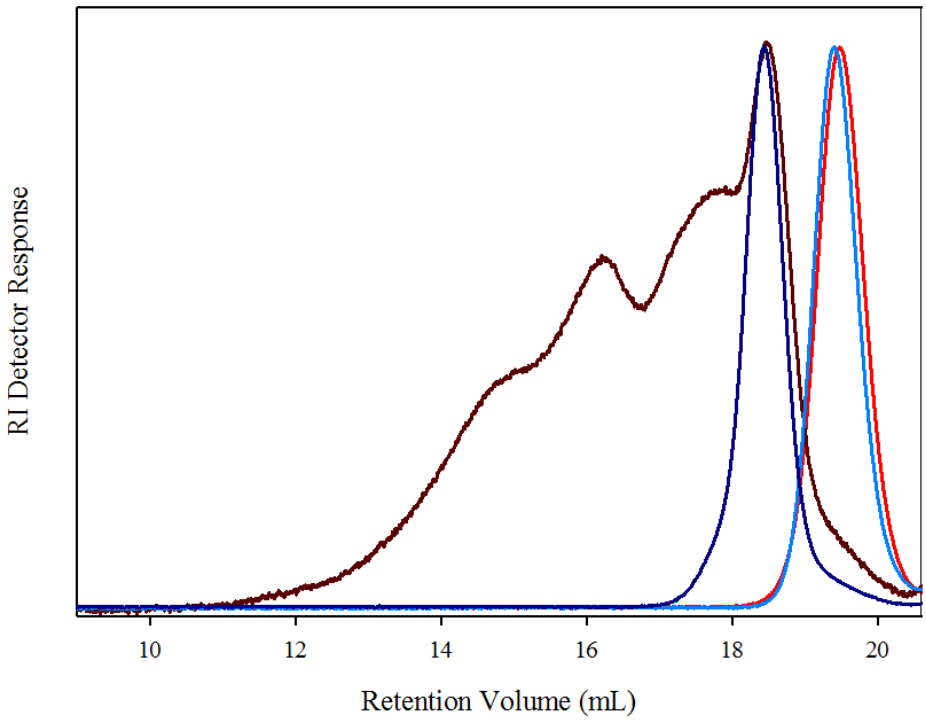


Figure 4.25: GPC chromatograms (THF eluent) of *p*(HPMA) blocking experiments. Linear-*b*-linear; block 1 (88 % conversion) (blue line), final block copolymer (> 99 % conversion) (dark blue line). Linear-*b*-branched; block 1 (81 % conversion) (red line), final branched block copolymer (> 99 % conversion) (dark red line).

Although both *p*((HPMA$_{80}$)-*co*-EGDMA$_{0.95}$) and *p*((HPMA$_{30}$)-*b*-(HPMA$_{50}$-*co*-EGDMA$_{0.95}$)) have target primary chain lengths of 80 monomer units, structurally, the latter polymer is guaranteed to contain chain ends of approximately 30 monomer units due to the first linear block which has no appreciable water solubility (according to section 4.5.1). Therefore it is assumed that branching in *p*((HPMA$_{30}$)-*b*-(HPMA$_{50}$-*co*-EGDMA$_{0.95}$)) is now restricted to the last 62.5 % of the primary chains (if each chain has a combined DP$_n$ of 80 monomer units) and may result in more densely branched materials. Statistically there will be some short oligomeric chain ends present within this modified branched polymer sample (indicated by (ii) in Scheme 4.8, but here it is assumed the number of these is now limited.

Both *p*((HPMA$_{80}$)-*co*-EGDMA$_{0.95}$) and *p*((HPMA$_{30}$)-*b*-(HPMA$_{50}$-*co*-EGDMA$_{0.95}$)) were subjected to rapid precipitation from acetone (5 mg mL$^{-1}$ initial concentration; 1 mg mL$^{-1}$ final concentration) to investigate whether the resulting nanoparticles behave differently in terms of stability.

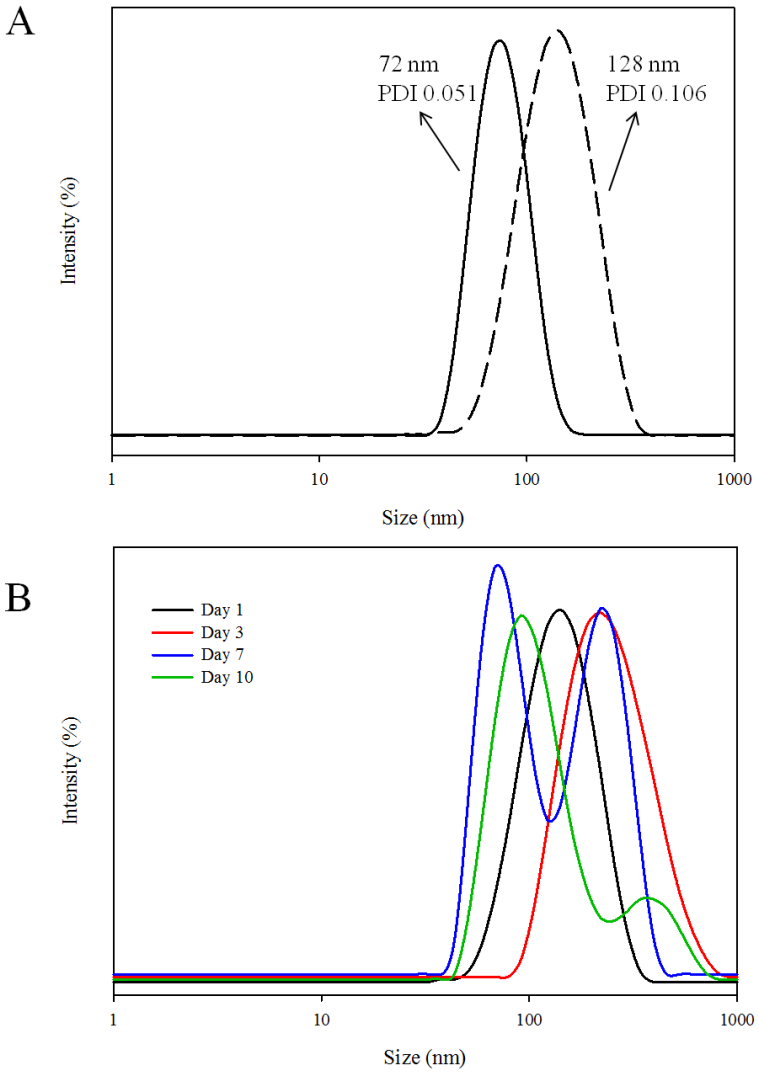


Figure 4.26: DLS characterisation of *p*((HPMA$_{30}$)-*b*-(HPMA$_{50}$-*co*-EGDMA$_{0.95}$)). A) *p*((HPMA$_{80}$)-*co*-EGDMA$_{0.95}$) (solid line) and *p*((HPMA$_{30}$)-*b*-(HPMA$_{50}$-*co*-EGDMA$_{0.95}$)) (dashed line). B) *p*((HPMA$_{30}$)-*b*-(HPMA$_{50}$-*co*-EGDMA$_{0.95}$)) nanoparticle analysis over time. (5 mg mL$^{-1}$ starting concentration; 1 mg mL$^{-1}$ final concentration).

The modified block branched copolymer *p*((HPMA$_{30}$)-*b*-(HPMA$_{50}$-*co*-EGDMA$_{0.95}$)) successfully formed nanoparticles which had a z-average diameter of 128 nm and a molecular weight distribution of 0.106 which are both markedly higher than the un-blocked branched counterpart (*p*((HPMA$_{80}$)-*co*-EGDMA$_{0.95}$)). The reason for this difference is unknown, but can only be attributed to the architectural difference in copolymer structure. The nanoparticle suspension (1 mg mL$^{-1}$) was characterised using DLS over ten days, with measurements performed after one, three, seven and ten days (see Figure 4.26 (B). After three days, both z-average diameter and polydispersity increases; which may be attributed to the onset of particle aggregation. Following this measurement small copolymer precipitate began to appear in the bottom of the sample vial; nevertheless DLS measurements were performed using the supernatant of the sample. At seven and ten days, DLS measurements are bimodal; with distinct peaks < 100 nm. The reason for this is unknown, but it is speculated that that these small nanoparticles are not involved during the onset of precipitation.

Nevertheless, the nanoparticle suspension comprised of *p*((HPMA$_{30}$)-*b*-(HPMA$_{50}$-*co*-EGDMA$_{0.95}$)) showed significantly different stability behaviour when compared to *p*((HPMA$_{80}$)-*co*-EGDMA$_{0.95}$). This supports the theory that small oligomeric *p*(HPMA) chains within branched copolymer samples exert some aqueous solubility and stability to the nanoprecipitates. Increasing the chain length of the oligomeric *p*(HPMA) chains (through blocking) may have reduced the overall aqueous interactions of nanoparticles leading to aggregation and subsequent precipitation.

## 4.7 Summary

Different methods of precipitation have been investigated, utilising both linear and branched *p*(HPMA) with linear polymer nanoparticles showing little aqueous stability. Branched copolymer nanoparticles have been shown to be highly stable with respect to dilution (aqueous and methanolic), time, temperature and sonication. Z-average diameters and polydispersity can also be systematically controlled through variation of concentration parameters, using a rapid solvent switch approach. Nanoparticle formation has been shown to be highly reproducible with a nucleation-growth mechanism proposed as the method of nanoparticle formation. Data has suggested that nanoparticle stability arises from electrostatic repulsion whereby nanoparticles de-stabilise during the addition of a salt solution. It has been proposed that small oligomeric units of *p*(HPMA) present within branched copolymer samples exert some aqueous stability and branched-block copolymers were synthesised to remove these chains and test the hypothesis. Subsequent nanoparticles showed limited stability, characterised by precipitation after approximately seven days supporting this theory.

## 4.8 References

1 Peracchia. M. T., Vauthier. C., Demaele. D., Gulik. A., Dediu. J-C., Demoy. M., d'Angelo. J., Couvreur. P., *Pharm Res*, **1998**, *15*¸(*4*), 550.

2 Johnson. B. K., Prud'homme. R. K., *Aust J Chem*, **2003**, *56*, 1021.

3 Zhang. C., Pansare. V. J., Prud'homme. R. K., Priestley. R. D., *Soft Matter*, **2012**, *8*, 86.

4 Cheng. F. Y., Wang. S. P. H., Su. C. H., Tsai. T. L., Wu. P. C., Shieh. D. B., Yeh. C. S. *Biomaterials*, **2008**, *29*, (*13*), 2104.

5 Bilati. U., Allémann. E., Doelker. E., *Eur J Pharm Sci*, **2005**, *24*, 67.

6 Hornig. S., Heinze. T., Remzi Becer. C., Schubert. U. S., *J Mater Chem*, **2009**, *19*, 3838.

7 Perevyazko. I., Vollrath. A., Hornig. S., Pavlov. G. M., Schubert. U. S., *J Polym Sci, Part A: Polym Chem*, **2010**, *48*, 3924.

8 Perevyazko. I. Y., Vollrath. A., Pietsch. C., Schubert. S., Pavlov. G. M., Schubert. U. S., *J Polym Sci Part A: Polym Chem*, **2012**, *50*, 2906.

9 Zhang. C., Chung. J. W., Priestley. R. D., *Macromol Rapid Commun*, **2012**, *33*, 1798.

10 Hornig. S. Heinze. T., *Biomacromolecules*, **2008**, *9*, 1487.

11 Hui. G., Ma. Y., Lu. X., Liang. Y., Chen. B., Ma. J., *Eur Polym J*, **2011**, *47*, 1232.

12 Remzi Becer. C., Babiuch. K., Pilz. D., Hornig. S., Heinze. T., Gottschaldt. M., Schubert. U. S., *Macromolecules*, **2009**, *42*, 2387.

13 Chan. J. M., Zhang. L., Yuet. K. P., Liao. G., Rhee. J. W., Langer. R., Farokhzad. O. C., *Biomaterials*, **2009**, *30*, 1627.

14 Calvo. P., Remuñán-López. C., Vila-Jato. J. L., Alonso. M. J., *J Appl Polym Sci*, **1997**, *1*, (*63*), 125.

15 Karnik. R., Gu. F., Basto. P., Cannizzaro. C., Dean. L., Kyei-Manu. W., Langer. R., Farokhzad. O. C., *Nano Lett*, **2008** *8*, (*9*), 2906.

16 Schubert. S., Delaney. J. T., Schubert. U. S., *Soft Matter*, **2011**, *7*, 1581.

17 Lamer. V. K., Dinegar. R. H., *J Am Chem Soc*., **1950**, *72*, 4847.

18 CNRS, (1998). *Process for the preparation of dispersible colloidal systems of a substance in the form of nanoparticles*, US Patent, US5118528.

19 Fessi. H., Puisieux. F., Devissaguet. J. P., Ammoury. N., Benita. S., *Int J Pharm*., **1989**, *55*, R1.

20 Wang. X., Liu. K., Arsenault. A. C., Rider. D. A., Ozin. G. A., Winnik. M. A., Manners. I., *J Am Chem Soc*, **2007**, *129*, 5630.

21 Guérin. G., Wang. H., Manners. I., Winnik. M. A., *J Am Chem Soc*, **2008**, *130*, 14763.

22 Zhao. J., Pispas. S., Zhang. G., *Macromol Chem Phys*, **2009**, *210*, 1026.

23 Milner. S. T., McLeish. T. C. B., Likhtman. A. E., *J Rehol*, **2001**, *45*, 539.

# 5. Linear and Branched ATRP of 2-Hydroxypropyl Methacrylate using PEG Macroinitiators

## 5.1 Introduction

The aim of this work was to synthesise a series of copolymers with well-defined compositions and structures in order to investigate the effect of architectural variation, and also introduce variability within hydrophobic/hydrophilic content, on the resultant nanoparticle properties. Copolymerisation was carried out using one-pot methanolic ATRP and a range of hydrophilic initiators were utilised in the synthesis of hydrophobic polymer chains of *p*(HPMA). The reaction kinetics of model systems were investigated using three types of hydrophilic initiator and one target primary chain length, to ensure adequate control of the polymerisations was achieved for linear and branched systems. A series of copolymers containing poly(ethylene oxide) and 2-hydroxypropyl methacrylate have been successfully prepared, with nine compositions and two different architectures; a total of eighteen linear and branched copolymers.

A macroinitiator approach to generate hydrophilic/hydrophobic block copolymers was chosen rather than the polymerisation of a hydrophilic block and the sequential addition of a second hydrophobic monomer to the reaction;[1] in all cases, experimental simplicity (all copolymer components present at the time of initiation) would considerably aid reproducibility.[2, 3] In this way, the reaction can be left to polymerise undisturbed until sufficient conversion has been reached, at which point manual termination *via* exposure to air plus suitable solvent addition is performed.

As methanol dissolves both PEG and HPMA and is a suitable ATRP solvent for vinyl monomers,[1, 4, 5] it was chosen as the solvent for all ATRP reactions conducted during this part of the current study, in addition to the synthesis of linear and branched *p*HPMA, found in Chapter 3 (sections 3.2 and 3.3).

Armes and co-workers investigated ATRP with HPMA in various solvents (aqueous, methanolic and water/methanol solution).[2] They reported molecular weight distributions as low as 1.09 within a few hours using methanol, with reaction time significantly reduced when a 50/50 water/methanol mixture was introduced, although slightly higher molecular weight distributions were obtained ($M_w/M_n$ = 1.17). Another rationale for using solely methanol is the high aqueous solubility of PEG. It can be extremely difficult to sufficiently remove water during the work up of the copolymer requires one or more of the following: freeze drying, precipitation, extraction with other solvents, and/or prolonged heating during rotary evaporation.

The Armes group was the first to investigate aqueous ATRP at ambient temperature, demonstrating the well-controlled polymerisation of monomethoxy-capped oligo(ethylene glycol) methacrylate (OEGMA) in water at 20 °C[6,7] where 95 % monomer conversion was reached after 30 minutes, with molecular weight distributions as low as 1.12. DMAEMA and 2-(diethyl amino)ethyl methacrylate (DEAEMA) have also been shown to polymerise well in water.[8] This work does not focus on investigating optimum conditions for ATRP of PEG containing *p*(HPMA) polymers, a simple reaction procedure and work up is favoured, however, studies of the success of each reaction are made. In Chapter 3 (section 3.2.2), plots of $\ln([M_0]/[M])$ *vs*. time for the homopolymerisation of HPMA (linear and branched) in methanol suggested a controlled polymerisation with fast initiation and insignificant

termination. It was proposed that similar results would be observed for copolymers synthesised using PEG macrointiators.

## 5.2 Synthesis and characterisation of monomethoxy poly(ethylene oxide) (PEG-OH) macroinitiators.

A range of PEG-Br macrointiators have been prepared by reacting the corresponding hydroxyl group of commercially available monomethoxy poly(ethylene oxide) with 2-bromoisobutyryl bromide in the presence of triethylamine (TEA) and 4-dimethylaminopyridine (DMAP). This esterification reaction is based on a method reported by Jankova *et al.*[9] Three commercially available PEG-OH materials were used to generate initiators, with reported number average molecular weights of 750, 2000 and 5000 g $mol^{-1}$. Full experimental protocol is found in Chapter 2 section 2.4.1.

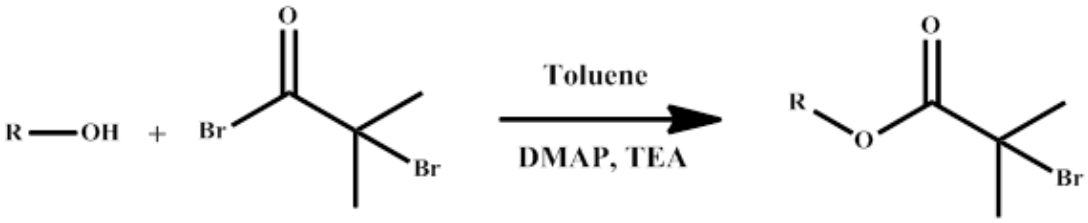


Scheme 5.1: General esterification of hydroxyl containing species, R-OH, generating an ATRP initiator R-OCO$(CH_3)_2$Br.

Scheme 5.1 shows the general esterification reaction to convert the mono-methyl PEG-OH into an ATRP initiator. Before carrying out any reactions, $^1$H NMR spectroscopy was used to confirm the precursor PEG-OH number average degree of polymerisation ($DP_n$). The ratio of the integration of the methoxy end-group and the

methylene signal should generate a number average degree of polymerisation for each polymer. $DP_n$ was therefore calculated by the integration of the terminal methyl signal at 3.38 ppm to the O-$CH_2$-$CH_2$ repeat unit at 3.64 ppm, where $DP_n = \frac{3}{a} \times \frac{b}{4}$ (see Figure 5.1). It was found that the $DP_n$ of $PEG_{17}$-OH was 17.5 ethylene oxide repeat units corresponding to a number average molecular weight of 770 g $mol^{-1}$ (by multiplying $DP_n$ by the molecular weight of the ethylene oxide repeat unit (44 g $mol^{-1}$)); in close agreement with the manufacturer's description. Applying the same method, a $DP_n$ value of 47.9 ethylene oxide repeat units was determined for $PEG_{45}$-OH (number average molecular weight = 2100 g $mol^{-1}$) and a $DP_n$ value of 126.3 ethylene oxide repeat units was found for $PEG_{113}$-OH (number average molecular weight = 5600 g $mol^{-1}$). All values are slightly higher than the averaged values reported by the manufacturer.

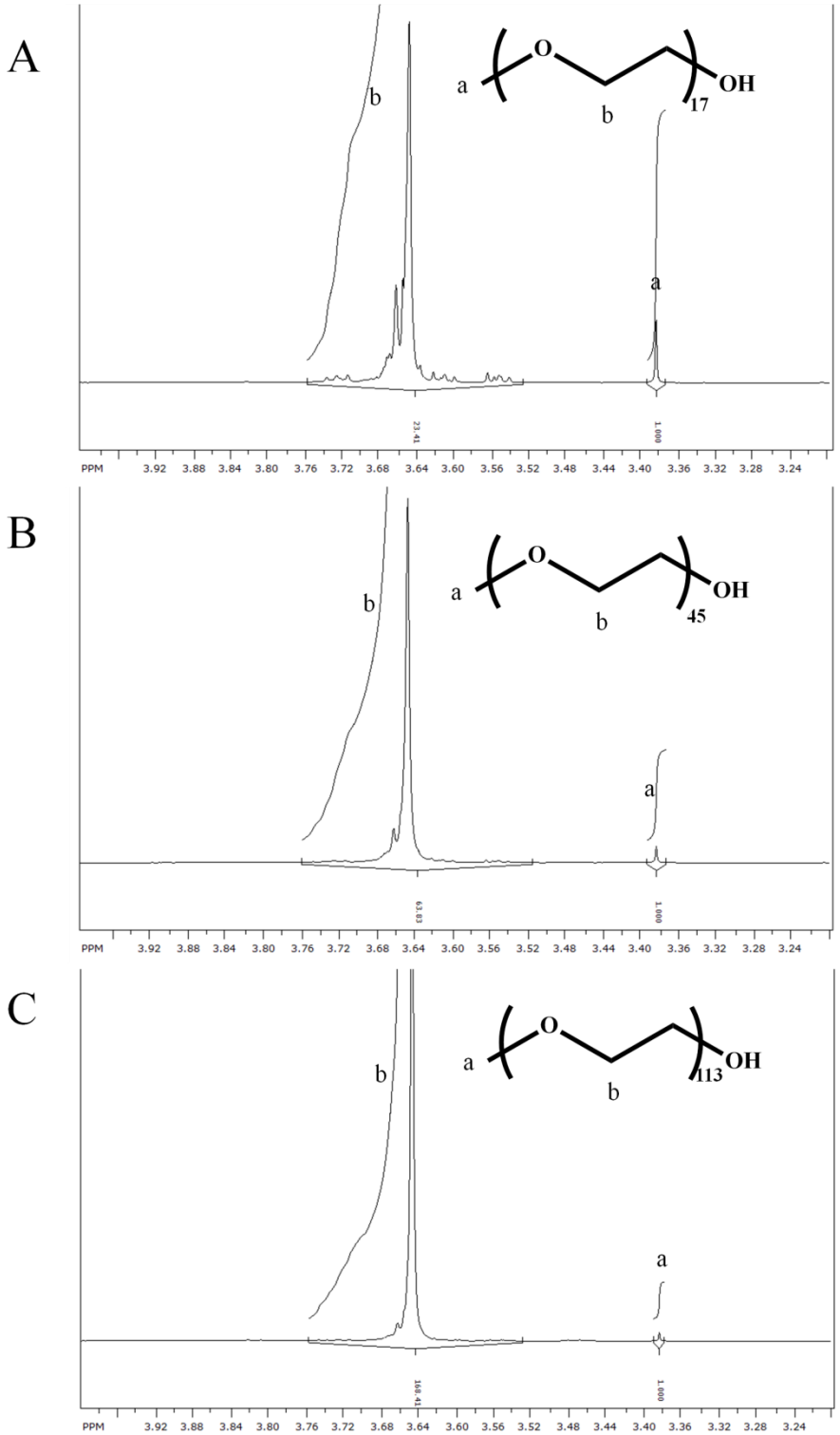


Figure 5.1: $^{1}$H NMR spectra in $CDCl_3$ of $PEG_x$-OH. (A) $PEG_{17}$-OH. (B) $PEG_{45}$-OH. (C) $PEG_{113}$-OH.

Figure 5.2(A) shows a $^{1}H$ NMR spectrum of a monomethoxy PEG-OH where proton environments are assigned. After esterification a new signal at 1.95 ppm appears as shown in Figure 5.2(B) from the new equivalent methyl resonances of the tertiary bromide group. The resonance at 4.33 ppm is attributed to the $CH_2$ group adjacent to the ester.

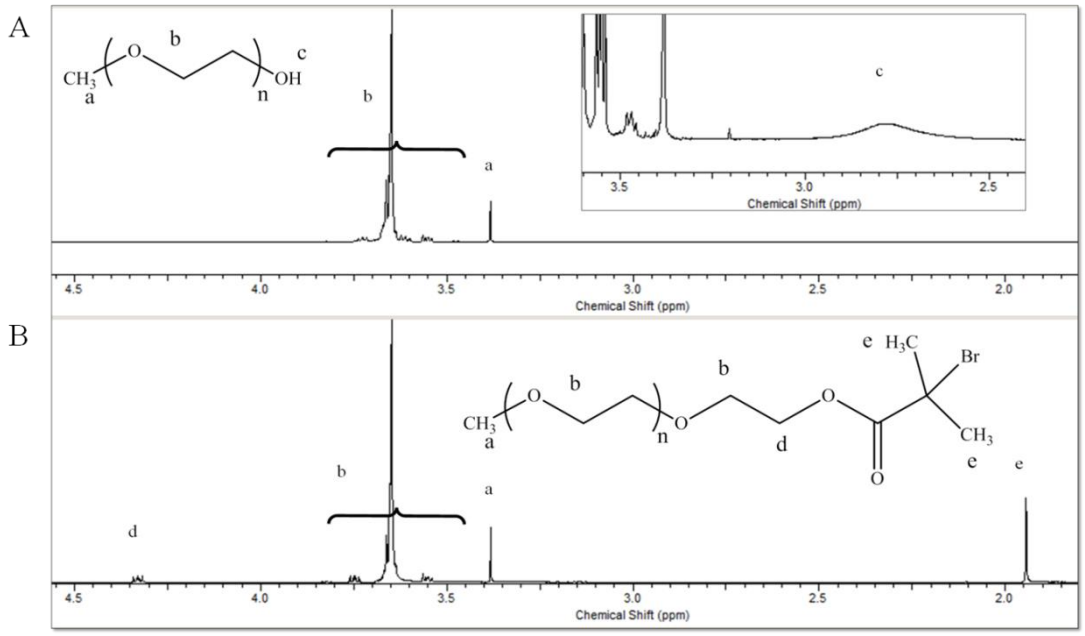


Figure 5.2: $^{1}H$ NMR spectra of (A) monomethoxy PEG-OH and (B) Esterified monomethoxy PEG-Br recorded in $CDCl_3$.

The extent of esterification was calculated using the ratio of the monomethoxy $CH_3$ and ester $CH_2$ signals, which should give a ratio of 3:2. Theoretically, the percentage esterification should be < 100 %, yet the ratio of monomethoxy $CH_3$ and ester $CH_2$ signals in Figure 5.3 is slightly higher, suggesting that extremely high conversions have been reached in conjunction with integral error.

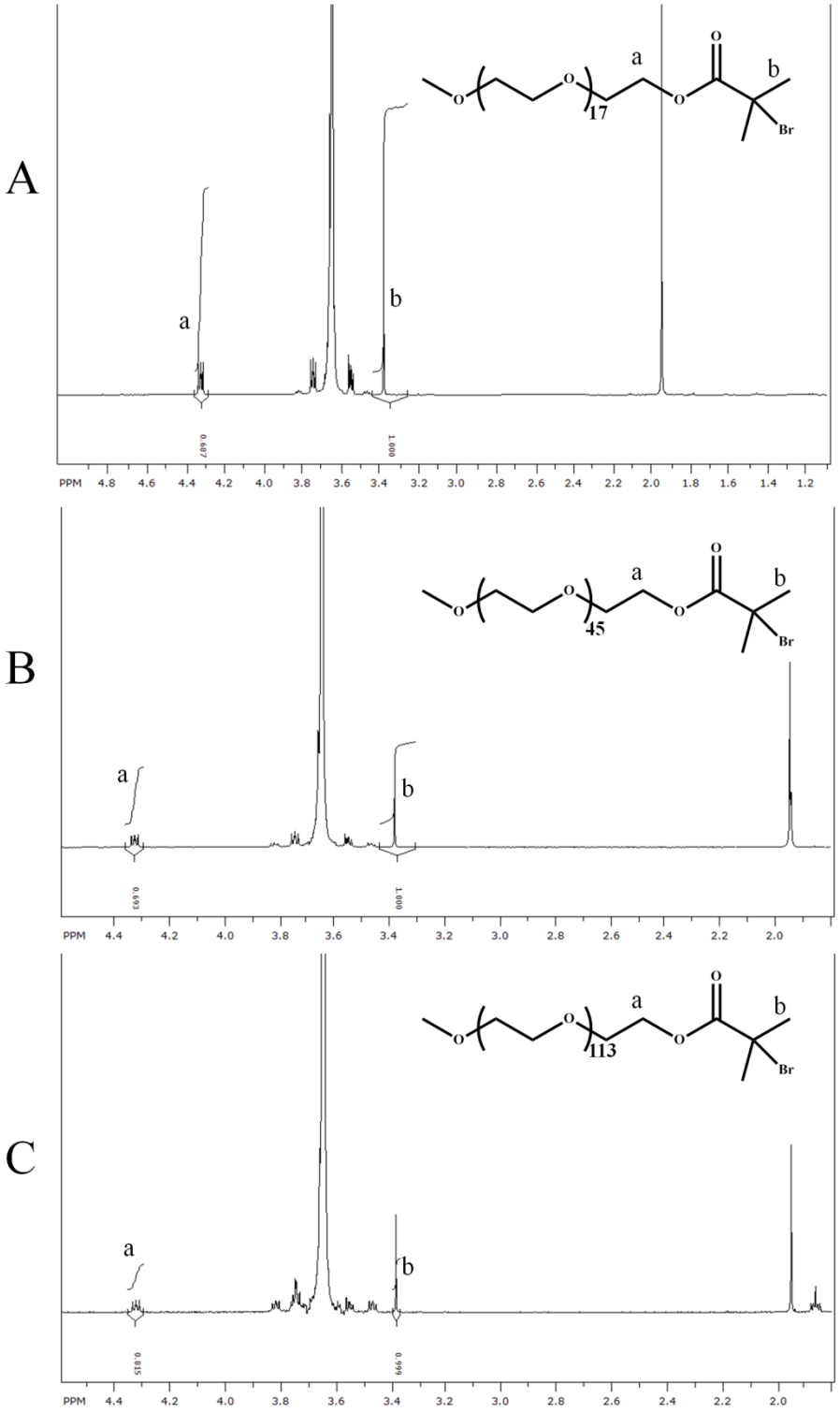


Figure 5.3: $^{1}$H NMR spectra in $CDCl_3$ of $PEG_x$-Br. A) $PEG_{17}$-Br. B) $PEG_{45}$-Br. C) $PEG_{113}$-Br.

Figure 5.3 (A) suggests 100 % esterification has been reached for $PEG_{17}$-Br, however, integration gives values > 2 protons for the ester methylene for $PEG_{45}$-Br

and $PEG_{113}$-Br, (2.1 and 2.4 respectively) (Figure 5.3(B)&(C)). The extent of esterification was not calculated using a ratio of the monomethoxy and the two methyl groups of the bromo end group as this does not confirm the reaction. This peak may also contain proton signals from other materials such as hydrolysed bromoisobutyric acid.

$M_n$, $M_w$ and molecular weight distributions were measured by triple detection GPC (THF eluent) after esterification for $PEG_{45}$-Br and $PEG_{113}$-Br which showed relatively narrow molecular weight distributions and accurate molecular weights with respect to those calculated.

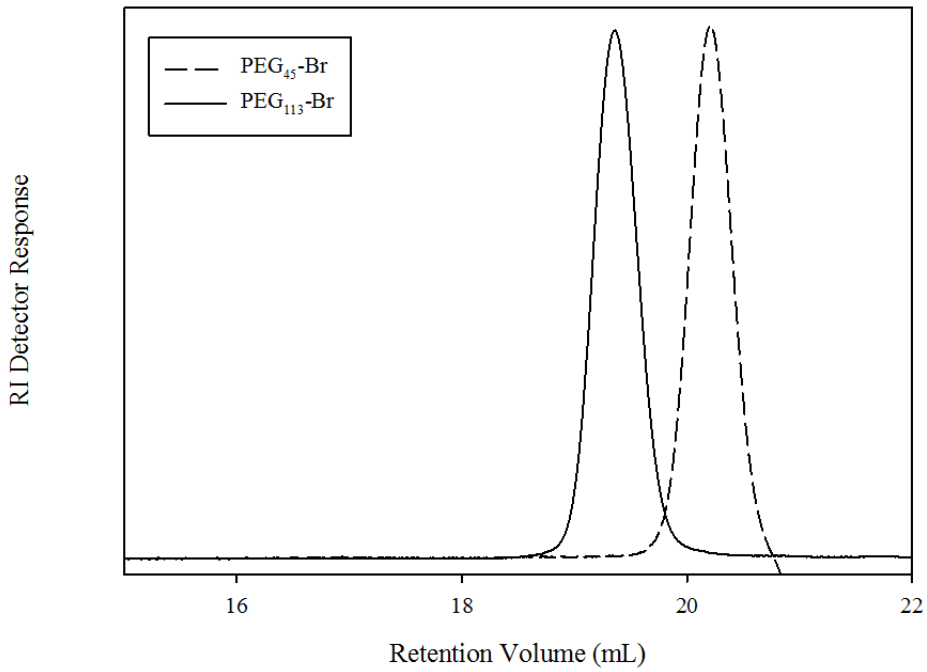


Figure 5.4: GPC chromatograms of two PEG macroinitiators. $PEG_{45}$-OH ($M_n$ = 2100; $M_{n\ theory}$ = 2000; dashed line) and $PEG_{113}$-OH ($M_n$ = 5600, $M_{n\ theory}$ = 5000; solid line).

The GPC chromatograms are shown in Figure 5.4. Unfortunately the $PEG_{17}$-Br initiator could not be analysed using this method due to its low molecular weight being beyond the elution limit of the columns; however it is possible to analyse polymers of this molecular weight using different columns designed for low molecular weight analysis but these were not available here. $PEG_{45}$-OH eluted extremely close to the solvent front and therefore the accuracy of molecular weight determination was not high. A summary table of the GPC data of these polymers is shown in Table 5.1.

| Sample | Nominal | | $^1$H NMR | | GPC | | |
|---|---|---|---|---|---|---|---|
| | $M_n$ (theory g mol$^{-1}$) | DP$_n$ | $M_n$ (g mol$^{-1}$) | DP$_n$ | $M_n$ (g mol$^{-1}$) | $M_w$ (g mol$^{-1}$) | $M_w/M_n$ |
| PEG-OH | 750 | 17 | 770 | 17.5 | / | / | / |
| PEG-Br | 840 | 17 | 748 | 17 | / | / | / |
| PEG-OH | 2000 | 45 | 2 100 | 48 | / | / | / |
| PEG-Br | 2080 | 45 | 1940 | 44 | 2200 | 3100 | 1.36 |
| PEG-OH | 5000 | 113 | 5600 | 126.3 | / | / | / |
| PEG-Br | 5080 | 113 | 4900 | 111 | 5100 | 7200 | 1.3 |

Table 5.1:Summarising data obtained *via* $^1$H NMR and GPC for the commercial PEG-OH ($M_n$ 750, 2000 and 5000 g mol$^{-1}$) and their respective macroinitiators.

## 5.3 Synthesis of $PEG_x$-*b*-*p*($HPMA_y$) block copolymers ($x$ = 17, 45, 113, $y$ = 50, 80, 120)

Using macrointiators rather than sequential A-B block copolymerisation can be seen as more experimentally facile, as a second monomer is not added and reactions can

be left until all monomer is consumed, as determined by $^{1}$H NMR spectroscopy, avoiding gradient copolymer formation and assuring distinct block segments. HPMA monomer was chosen as the hydrophobic segment due to its biocompatibility, commercial availability, and previous successful synthesis by ATRP in other research groups.

For each macroinitiator synthesised, three subsequent polymerisations were carried out, utilising HPMA monomer at varying target chain lengths (target $DP_n$ = 50, 80, 120 monomer units). In short, the initiator was first dissolved in methanol (50 w/v %) (monomer/solvent) after which the monomer feed was added (50 w/v %) (monomer/solvent), reactions were stirred and carefully degassed using a nitrogen purge for approximately 10 minutes at room temperature. Reactions were initiated after the addition of Cu(I)Cl/BPY in a ratio of 1/2.5 and left until > 98% conversion had been reached as assessed by $^{1}$H NMR spectroscopy. The reactions were purified as stated in the Chapter 2 section 2.4.2. A total of nine polymers were synthesised and a schematic representation of the effect of varying both components of the polymer chains is shown in Figure 5.5.

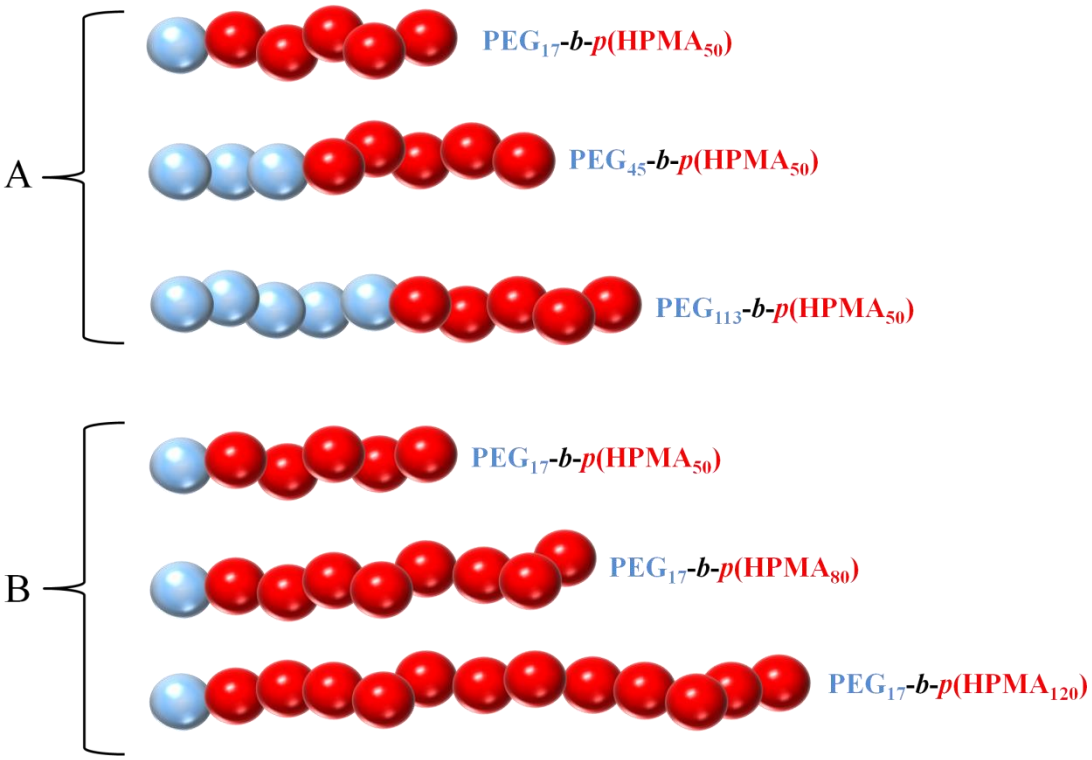


Figure 5.5: Representation of amphiphilic copolymers with varying both hydrophilic (PEG) (A) and hydrophobic (HPMA) (B) content

Figure 5.5 is not directly to scale in terms of actual PEG/HPMA content in the polymer chains; there are three ways to depict the content of each polymer block (shown below) where the polymer $PEG_{113}$-*b*-*p*($HPMA_{50}$) was chosen as an example.

1) Mole ratio of monomers = ethylene oxide repeat unit/HPMA repeat unit = 113/50 = 2.26
2) Mole ratio of each polymer = $HPMA_{50}/PEG_{113}$ = 1/1 = 1
3) Weight ratio of each polymer = $HPMA_{50}/PEG_{113}$ = (50 x 144.2)/(113 x 44) = 7200/5000 = 1.44

The three different calculations above give useful information which shows the

relative ratios of each polymer component in these amphiphilic copolymers. 1) shows that, for this particular polymer, the PEG segment is approximately 2.26 times as long as the *p*(HPMA) chain, although this does not take into account the molecular weight of each repeat unit. 2) is simply the calculation which is used to calculate the target $DP_n$ of the primary chain length, where there is one initiator per chain and *x* number of HPMA monomer units. 3) takes into account the relative molecular weights of each polymer segment, where PEG is approximately 5000 g $mol^{-1}$ and HPMA is 7200 g $mol^{-1}$ for this polymer example, therefore in the overall copolymer the HPMA chain has approximately 1.44 times the mass of the PEG containing initiator. Out of all nine copolymers synthesised, $PEG_{113}$-*b*-*p*($HPMA_{50}$) has components whose weight ratios are closest to 1. Conversely in $PEG_{17}$-*b*-*p*($HPMA_{120}$) the weight ratio of *p*(HPMA) is approximately 23 times higher than that of the PEG initiator, providing the most "un-balanced" copolymer in terms of their respective molecular weights. By synthesising this diverse range of polymers it is believed that useful insight can be gained into their individual reactions, subsequent copolymer characteristics and optimisation of reaction conditions using PEG containing copolymers by ATRP.

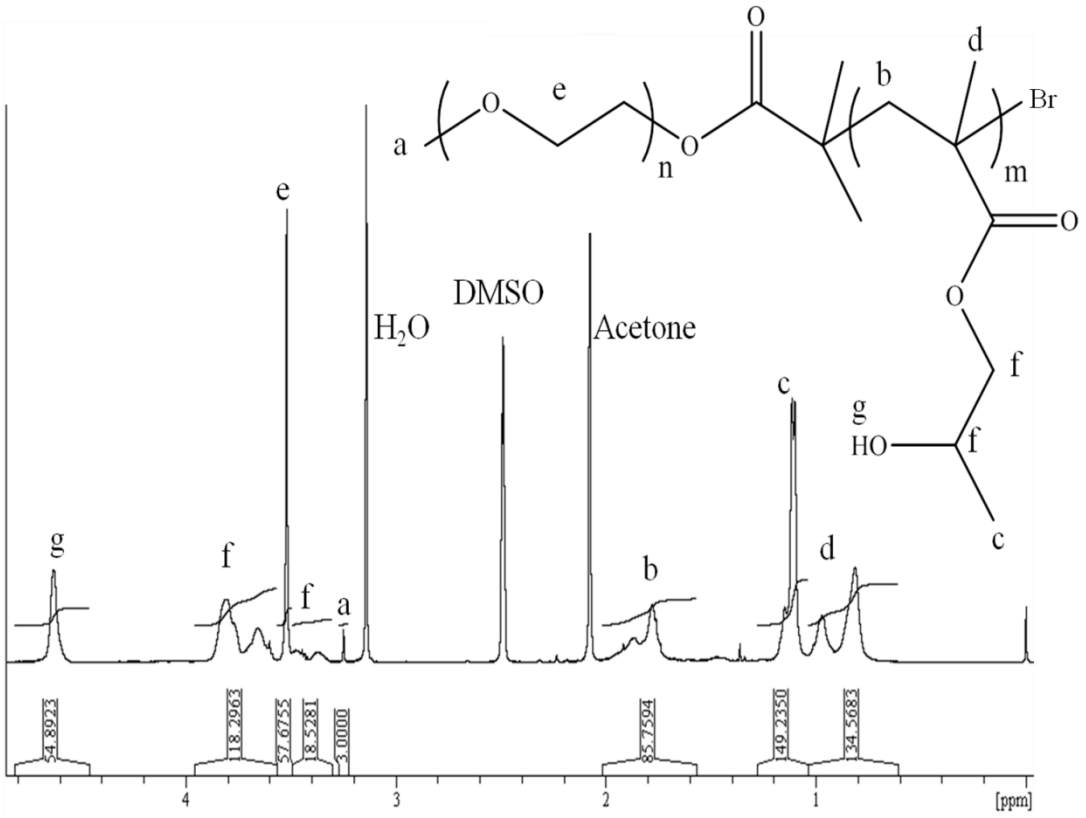


Figure 5.6: $^{1}$H NMR spectrum of $PEG_{17}$-*b*-*p*($HPMA_{50}$) in DMSO-$d_6$.

The $^{1}$H NMR spectrum of $PEG_{17}$-*b*-*p*($HPMA_{50}$) (Figure 5.6) shows the integration and assignment of the protons present in the copolymer. It should be noted that residual solvents still remain; acetone is present due to insufficient drying after the cleaning of the NMR tube, it is believed $H_2O$ is present due to the hygroscopic nature of the PEG and DMSO was the solvent in which the analysis was performed. The $DP_n$ of the *p*(HPMA) polymer can be calculated by several methods to double check values achieved, using the ratio of either the terminal methyl group (a) or the ethylene oxide repeat unit (e) of the initiator against any of the HPMA proton environments (b, c, d, f, g). For example,

$$A)\ DP_n = \frac{c}{3}$$

$$B)\ DP_n = \frac{d}{3}$$

using A) gives a $DP_n$ of 50 monomer units whereas B) gives a $DP_n$ of 45 for this polymer. These figures should be identical as both (c) and (d) come from HPMA protons, and highlights the inaccuracy of $^1$H NMR spectroscopic analysis. It should be noted that these equations are correct when the integral of the methoxy $CH_3$ is set to 3. $DP_n$ was not calculated using the ethylene oxide repeat units in the initiator due to the significant overlap of the $CH_2$ and CH groups in HPMA, and in turn these signals (f) could not be used themselves to give any accurate values. The integral of protons (g) was also not used in analysis as it is believed there was significant exchange with water and as such the values calculated using this signal are markedly lower than those using (c) or (d). Copolymer analysis by $^1$H NMR spectroscopy is best used to determine conversion of monomer to polymer through the depletion of vinyl signals from the monomer. When analysing the final recovered polymer, a ratio of initiator to polymerised monomer may be hampered by unreacted initiator residues which cannot be easily determined. In addition, no information of the molecular weight distribution is available.

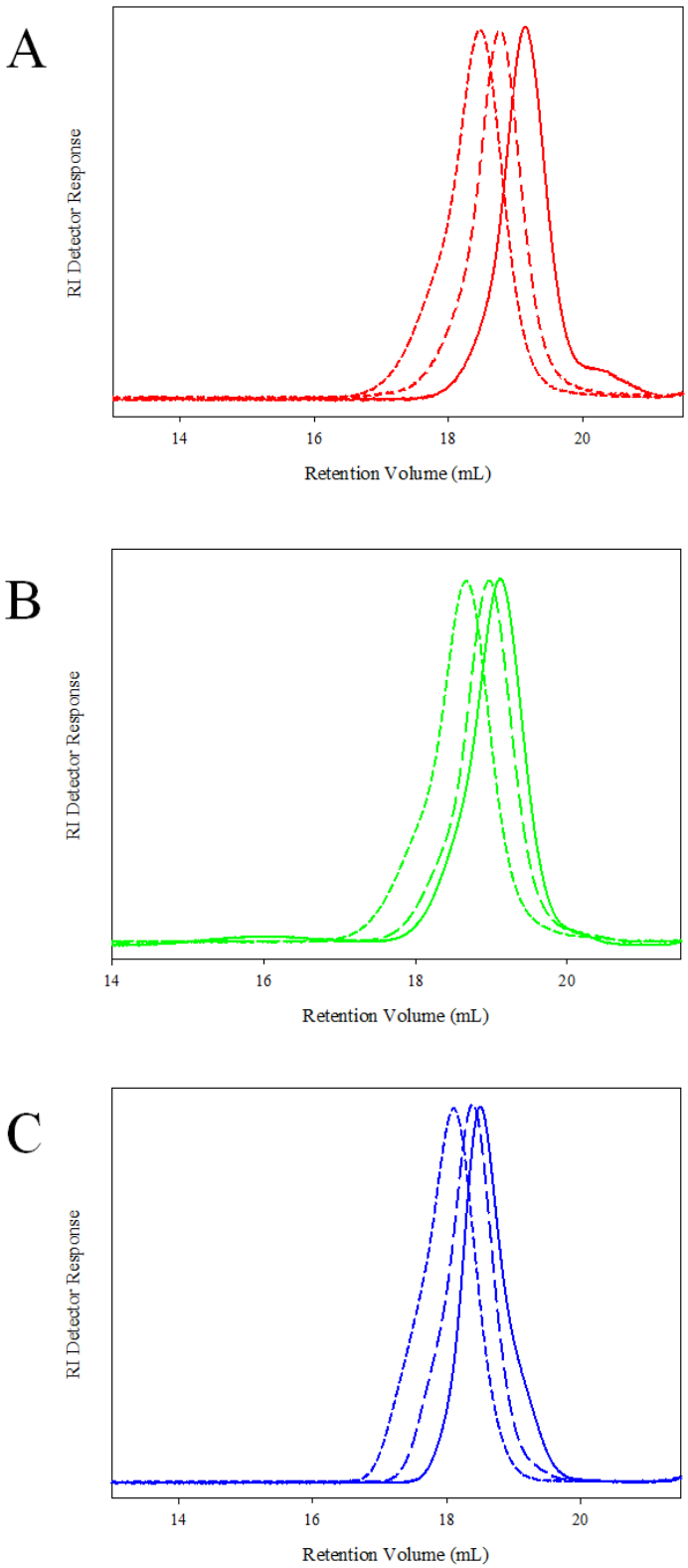


Figure 5.7: GPC chromatograms of $PEG_x$-Br initiated linear *p*HPMA copolymers. (A) $PEG_{17}$-*p*($HPMA_x$) (B) $PEG_{45}$-*p*($HPMA_x$) (C) $PEG_{113}$-*p*($HPMA_x$). $DP_n$ = 50 (solid lines), $DP_n$ = 80 (medium dashed lines) $DP_n$ = 80 (small dashed lines)

Triple detection GPC (THF eluent) was performed (5 mg $mL^{-1}$) on the nine polymers synthesised as described above, utilising three $PEG_x$ based initiators varying target $DP_n$ (50, 80, and 120 monomer units). From Figure 5.7, it is clear that linear copolymers elute at lower retention volumes as target $DP_n$ increases, as expected. Conversely, copolymers with the longest target *p*(HPMA) chains (target $DP_n$ = 120 monomer units) have the highest molecular weight distributions. All linear copolymer molecular weight distributions exhibit a lack of symmetry, with shoulders extending to higher retention volumes. This may be due to a small amount of chain termination during the reaction.

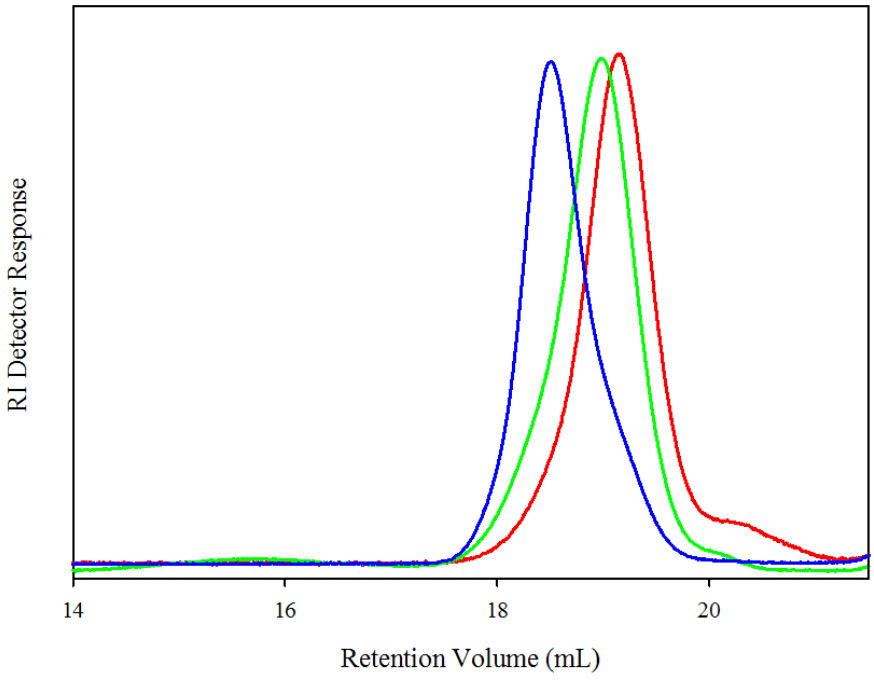


Figure 5.8: GPC chromatograms of $PEG_{17}$-*b*-*p*($HPMA_{50}$) (red line), $PEG_{45}$-*b*-*p*($HPMA_{50}$) (green line), $PEG_{113}$-*b*-*p*($HPMA_{50}$) (blue line).

The three linear copolymers with a target $DP_n$ = 50 monomer units (shown in Figure

5.8) also show distinct shoulders at lower retention volumes, potentially due to unreacted initiator or due to termination during the early stages of polymerisation. By overlaying these chromatograms, shoulders at lower retention volumes in each polymer sample can be clearly seen. Across the linear copolymer series, the most symmetrical chromatograms are found when targeting a $DP_n$ of 80 monomer units irrespective of the macroinitiator used (see Figure 5.8). The exact reason for this is unknown but this trend also appeared during the polymerisation of *p(*HPMA) homopolymers in Chapter 3 (section 3.2), which showed the lowest molecular weight distribution when the target $DP_n$ = 80 monomer units. A summary of the nine linear copolymer characterisation data is shown in Table 5.2.

| Sample | $M_n$ (g mol$^{-1}$) (Theory) | $M_n$ (g mol$^{-1}$) (GPC)* | $M_w$ (g mol$^{-1}$) (GPC)* | $M_w/M_n$ (GPC)* | Conversion (%) |
|---|---|---|---|---|---|
| $PEG_{17}$-*b*-*p*($HPMA_{50}$) | 8000 | 8100 | 9800 | 1.21 | > 99 |
| $PEG_{17}$-*b*-*p*($HPMA_{80}$) | 12300 | 13100 | 15100 | 1.15 | > 99 |
| $PEG_{17}$-*b*-*p*($HPMA_{120}$) | 18100 | 19300 | 23500 | 1.22 | > 99 |
| $PEG_{45}$-*b*-*p*($HPMA_{50}$) | 9200 | 10100 | 12100 | 1.20 | > 99 |
| $PEG_{45}$-*b*-*p*($HPMA_{80}$) | 13500 | 13900 | 16600 | 1.19 | > 99 |
| $PEG_{45}$-*b*-*p*($HPMA_{120}$) | 19300 | 20100 | 24900 | 1.24 | > 99 |
| $PEG_{113}$-*b*-*p*($HPMA_{50}$) | 12200 | 13300 | 16800 | 1.26 | > 99 |
| $PEG_{113}$-*b*-*p*($HPMA_{80}$) | 16500 | 17600 | 21500 | 1.22 | > 99 |
| $PEG_{113}$-*b*-*p*($HPMA_{120}$) | 22300 | 23400 | 30700 | 1.31 | > 99 |

Table 5.2: Summarising data obtained for linear polymers $PEG_x$-*b*-*p*($HPMA_y$) where $x$ = 17, 45, 113 and $y$ = 50, 80, 120. * THF eluent.

The molecular weight data obtained and shown in Table 5.2 are consistently higher than those predicted, yet this was also observed for the homopolymerisations of *p*(HPMA$_x$) in Chapter 3 (section 3.2). The most accurate molecular weights are obtained using the PEG$_{17}$-Br macroinitiator; whereas increased inaccuracy is seen as the molecular weight of the macroinitiator is increased. For example, PEG$_{17}$-*b*-*p*(HPMA$_{50}$) has an $M_n$ of 8100 g mol$^{-1}$, which is extremely close to that predicted (8000 g mol$^{-1}$), whereas PEG$_{113}$-*b*-*p*(HPMA$_{50}$) has an $M_n$ of 23400 g mol$^{-1}$; significantly higher than predicted (22300 g mol$^{-1}$). This discrepancy is most likely due to initiator efficiency decreasing as the molecular weight of the initiator increases, causing monomer to react with fewer than predicted initiating sites. There could also be complications during GPC analysis as the solubility of the copolymers in THF may vary as the relative ratio of PEG to *p*(HPMA) increases.

In this section it has been shown that a range of PEG based macroinitiators were able to successfully polymerise HPMA to three target primary chain lengths (50, 80 and 120 monomer units). All reactions proceeded to > 99% conversion and the subsequent polymers gave molecular weights (and therefore DP$_n$) comparable to those targeted. The molecular weight distributions of polymers (1.15 to 1.31) suggest controlled polymerisations took place.

### 5.3.1 Copolymerisation Kinetic Studies of PEG$_{17}$-*b*-*p*(HPMA$_{80}$), PEG$_{45}$-*b*-*p*(HPMA$_{80}$) and PEG$_{113}$-*b*-*p*(HPMA$_{80}$)

In order to determine if the reactions of the previously synthesised amphiphilic copolymers proceeded in a controlled manner to high conversion, kinetic studies were performed on a subset of polymers utilising all three previously synthesised

initiators whilst maintaining the target $DP_n$. It should be noted here that due to the higher molecular weight of these PEG-Br based macroinitiators in comparison to EBiB (used throughout Chapter 3), it was necessary to increase the volume of solvent in order for all components to be suitably solubilised, and also to ensure the viscosity of the polymerisation mixture at high conversions did not significantly affect the diffusion of polymer chains. The volume of methanol was adjusted, and took into account the mass of the initiator as well as HPMA monomer, therefore overall reactions were 50 w/v % (monomer,initiator/solvent) (see Chapter 2 section 2.4.2.2) Reactions were monitored with regular sampling of the polymerisation mixtures which were subsequently analysed by $^1$H NMR spectroscopy in DMSO-$d_6$ and triple detection GPC (THF eluent).

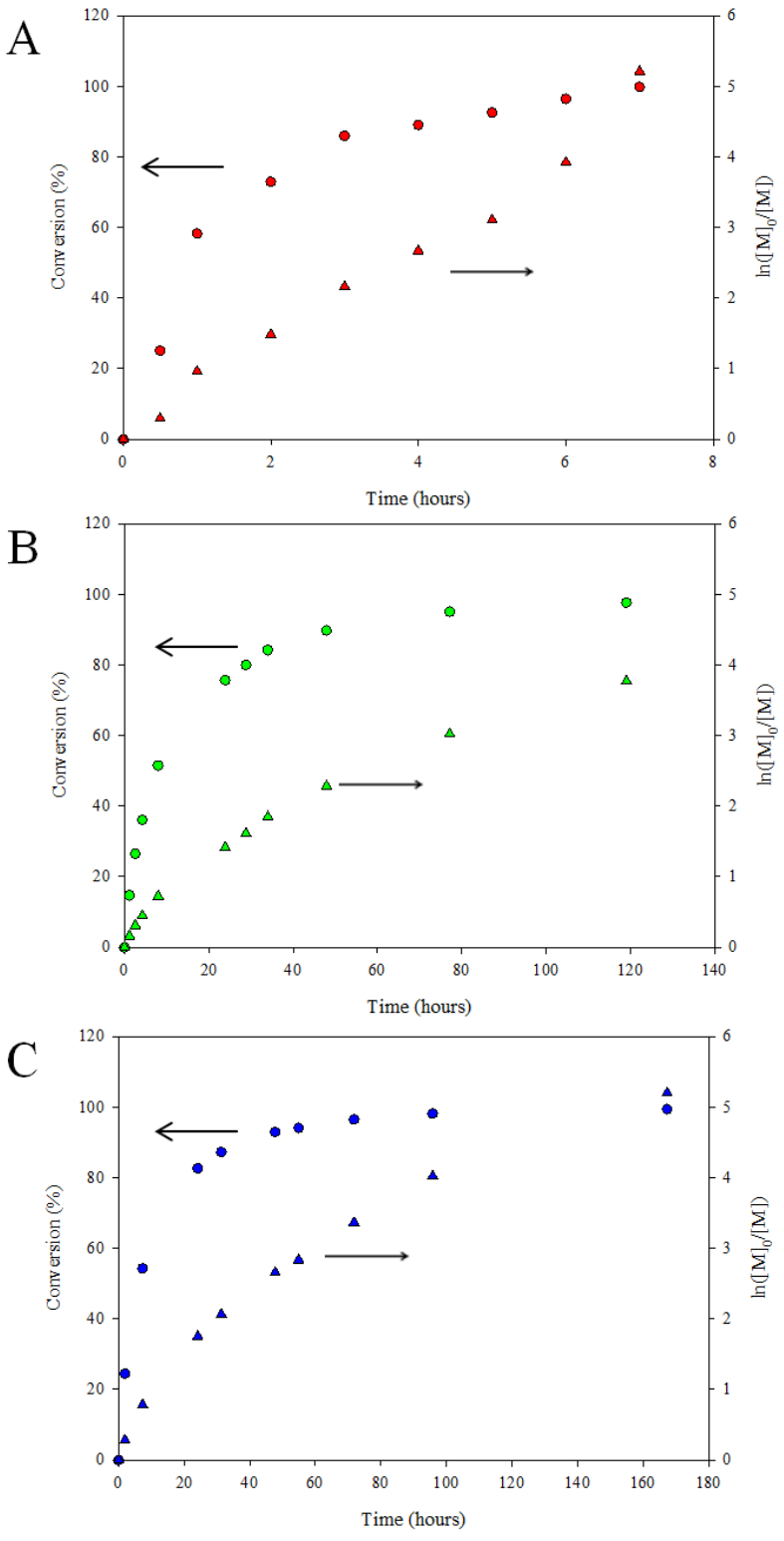


Figure 5.9: Kinetic studies of *p*(HPMA$_{80}$) using PEG-Br based macroinitiators. A) PEG$_{17}$-*b*-*p*(HPMA$_{80}$). B) PEG$_{45}$-*b*-*p*(HPMA$_{80}$). C) PEG$_{113}$-*b*-*p*(HPMA$_{80}$).

Figure 5.9 shows the kinetic data for the copolymerisation of *p*(HPMA$_x$) using various PEG-Br based macroinitiators, maintaining a target DP$_n$ of 80 monomer units. Despite varying the molecular weight of the initiator, data suggests reactions proceeded *via* conventional ATRP, as the percentage consumption of monomer is high at low conversion and at high conversion, where little un-reacted monomer is available, rates of reaction are dramatically reduced. All of the semi logarithmic plots appear to be relatively linear, indicative of the maintenance of radical concentration throughout the copolymerisation and as such, these kinetic experiments were thought to be successful. In order to draw solid conclusions of how varying the molecular weight of initiator affects reaction kinetics, it was necessary to overlay the data, which can be seen in Figure 5.10.

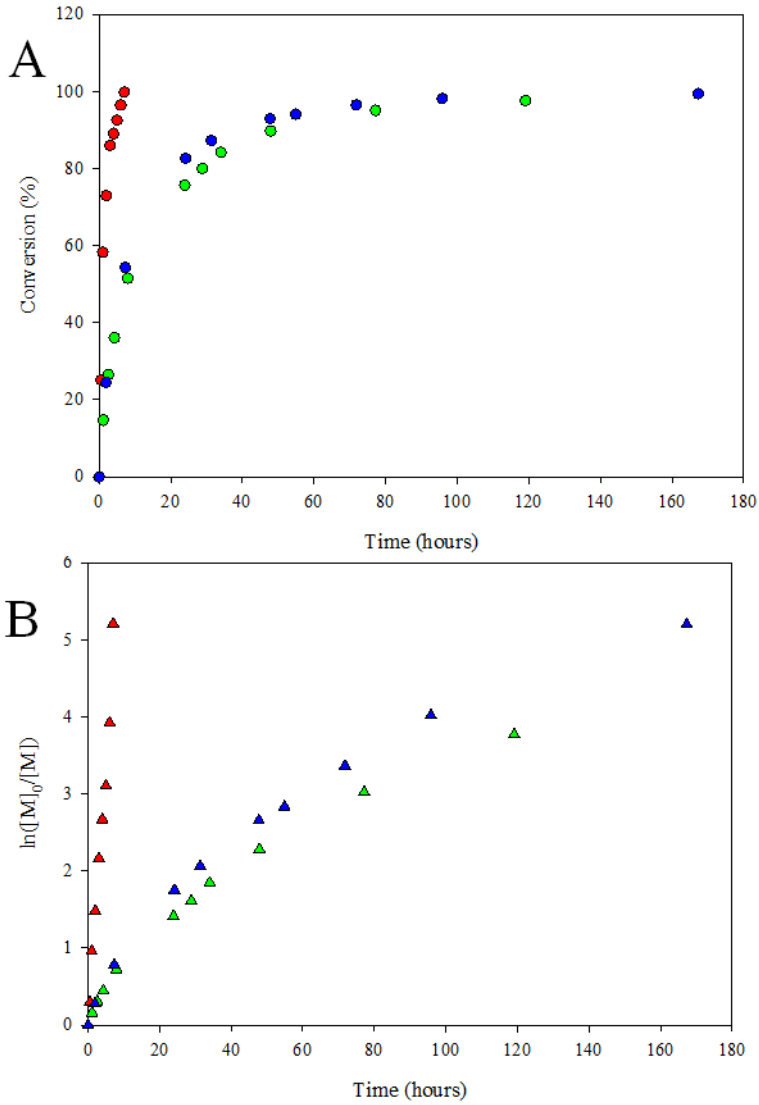


Figure 5.10: Kinetic studies of *p*(HPMA$_{80}$) polymerisation using PEG-Br based macroinitiators. A) Conversion *vs*. time. PEG$_{17}$-Br (red), PEG$_{45}$-Br (green), PEG$_{113}$-Br (blue). B) Semi-logarithmic plot. PEG$_{17}$-Br (red), PEG$_{45}$-Br (green), PEG$_{113}$-Br (blue).

By grouping the sets of data in this way, it becomes clearer to see the effect of varying initiator molecular weight with respect to kinetic data. From Figure 5.10(A), it can be seen that by using PEG$_{17}$-Br (the lowest molecular weight initiator) high conversion is reached in a significantly shorter time (> 99 % in 7 hours), compared to

the other initiators where approximately 100 hours reaction time was necessary in order to achieve the same conversion. It is believed the reason for this in mostly due to the extremely high viscosity of the solution, even at relatively low conversions in comparison to $PEG_{17}$-Br. Viscosity undoubtedly affects the diffusion and mobility of the active polymer chains and it is unsurprising that these highly viscous solutions require much longer reaction times to reach > 99 % conversion. However, the observed conversion *vs*. time curves using $PEG_{45}$-Br and $PEG_{113}$-Br are typical for reported ATRP reactions. It is apparent from Figure 5.10(A) that higher conversions are reached in slightly shorter reaction times using $PEG_{113}$-Br when compared to $PEG_{45}$-Br; this result was not anticipated as it was thought that the molecular weight of the initiator had a direct effect on reaction rates and should therefore be the "slowest" reaction. The differences are not large and it should be noted that these reactions were only conducted once, on different days and at varying ambient temperatures which may have affected the reaction rate slightly. Figure 5.10(B) shows the semi logarithmic plots for these three reactions; rather unsurprisingly the fastest rate is found by using the $PEG_{17}$-Br initiator with the lowest molecular weight. As noted previously, it was expected that utilising $PEG_{113}$-Br would have the slowest rate, but this was not the case here. The plots are also not perfectly linear, as would be expected for first order kinetics, but show a sight curvature for the longest two macroinitiators. Again, it is believed this may be due to slight temperature changes and also possible termination reactions over the extended reaction times at ambient temperature. Despite these possible discrepancies, no conclusive trends can be interpreted from this data, as the concentration of these reactions was 50 w/v % (initiator, monomer/solvent), causing the concentration of catalyst/ligand and also HPMA monomer to be unavoidably changed in all three polymerisations. It is likely

this would result in different semi logarithmic plots and therefore, no direct trends can be found in this study. Unfortunately there is no possible way to overcome this concentration difference. If the opposite approach was taken, where the volume of methanol was maintained throughout the reactions, the concentration of all other components in the polymerisation would vary from reaction to reaction. This is due to the same number of moles of initiator being utilised, undoubtedly affecting the actual mass added to the reaction mixture as initiator varies, and therefore the catalyst/ligand and HPMA monomer concentration will vary as a result. As reaction kinetics are affected by concentration, and it has been shown that this cannot be maintained successfully, it is impossible to quantitatively report how the kinetics of the polymerisation of *p*(HPMA$_x$) are affected by using various PEG$_x$-Br based initiators from the reactions carried out.

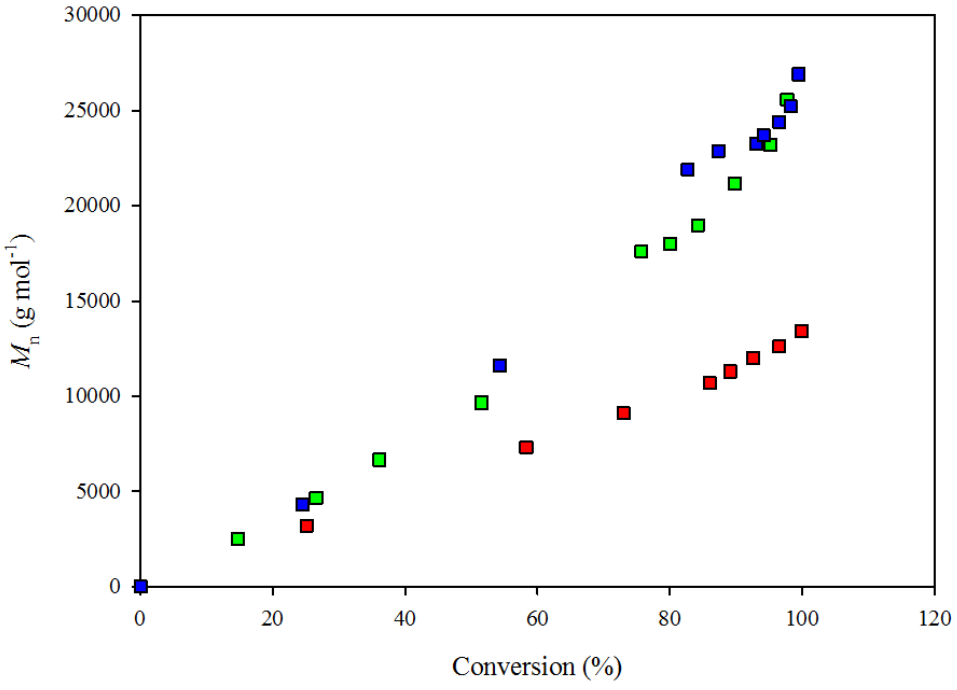


Figure 5.11: Evolution of molecular weight with conversion. PEG$_{17}$-Br (red), PEG$_{45}$-Br (green), PEG$_{113}$-Br (blue).

It is suggested that these polymerisations proceed *via* conventional ATRP, where molecular weight is expected to increase linearly with conversion, suggesting good control during the entire polymerisation. From Figure 5.11 it is shown that when employing $PEG_{17}$-Br (the lowest molecular weight initiator), good linearity between $M_n$ and conversion is seen. For copolymerisations utilising $PEG_{45}$-Br and $PEG_{113}$-Br, their respective results deviate away from linearity after approximately 70 % conversion. This suggests that after this point, these two polymerisations do not show good control and as such, are not proceeding *via* conventional ATRP. The plots of $M_n$ *vs*. conversion actually curve upwards at high conversion suggestive of termination, and therefore there are more monomer units available to polymerise with fewer active chains. This result coincides with their respective semi logarithmic plots, which curve downwards suggesting there are fewer radicals present within the respective reactions.

In summary, it has been shown that utilising the $PEG_{17}$-Br initiator to copolymerise *p*($HPMA_x$) to a target $DP_n$ of 80 monomer units was well controlled, and proceeded *via* conventional ATRP mechanisms. As the molecular weight of the initiator increased ($PEG_{45}$-Br and $PEG_{113}$-Br) control begins to break down after approximately 60 % conversion, although copolymers with relatively low polydispersities (<1.3) have been successfully polymerised with these initiators. Optimisation of these experiments (concentration, temperature etc) could result in kinetic results indicative of conventional ATRP.

### 5.3.2 Copolymerisation Kinetic Studies of $PEG_{17}$-*b*-*p*($HPMA_{30}$), $PEG_{17}$-*b*-*p*($HPMA_{50}$) and $PEG_{17}$-*b*-*p*($HPMA_{100}$)

In the previous section it was shown that varying the number of ethylene oxide repeat units in a $PEG_x$-Br based macroinitiator does have an effect on reaction kinetics when the target $DP_n$ of the HPMA polymer chains is maintained. In this section, one initiator was selected ($PEG_{17}$-Br) and used to polymerise HPMA to three different target chain lengths ($DP_n$ = 30, 50 and 100 monomer units). These experiments aim to highlight the capability of the $PEG_{17}$-Br initiator to successfully initiate and yield copolymers with accurate molecular weights (with respect to the target $DP_n$) whilst maintaining low molecular weight distributions under conventional ambient ATRP conditions. Similar experiments were carried out in Chapter 3 utilising EBiB as the initiator and comparisons between these two studies will be reported here. In the last section, solid conclusions were not found regarding the comparison of reaction kinetics utilising different initiators, due to unavoidably inconsistent reaction concentrations. In this study, the same initiator is employed ($PEG_{17}$-Br), therefore the volume of solvent is only altered due the increasing target $DP_n$ of the polymer chain to give an overall concentration of 50 w/v % (initiator, monomer/ solvent). Linear *p*($HPMA_x$) chains with a target $DP_n$ of 30, 50 and 100 monomer units were chosen, the molar ratio of the initiator was maintained aiming to ensure the same number of potential initiating chains was kept constant throughout the reaction. Reactions were conducted in parallel using methanol (50 w/v%; initiator+monomer/solvent) at ambient temperature. Kinetic sampling was employed whereby two samples, one for $^1$H NMR spectroscopy and one for GPC analysis were taken at regular intervals throughout the reactions. These experiments were conducted to ensure that any further polymers synthesised using PEG based macroinitiators proceeded *via* conventional ATRP.

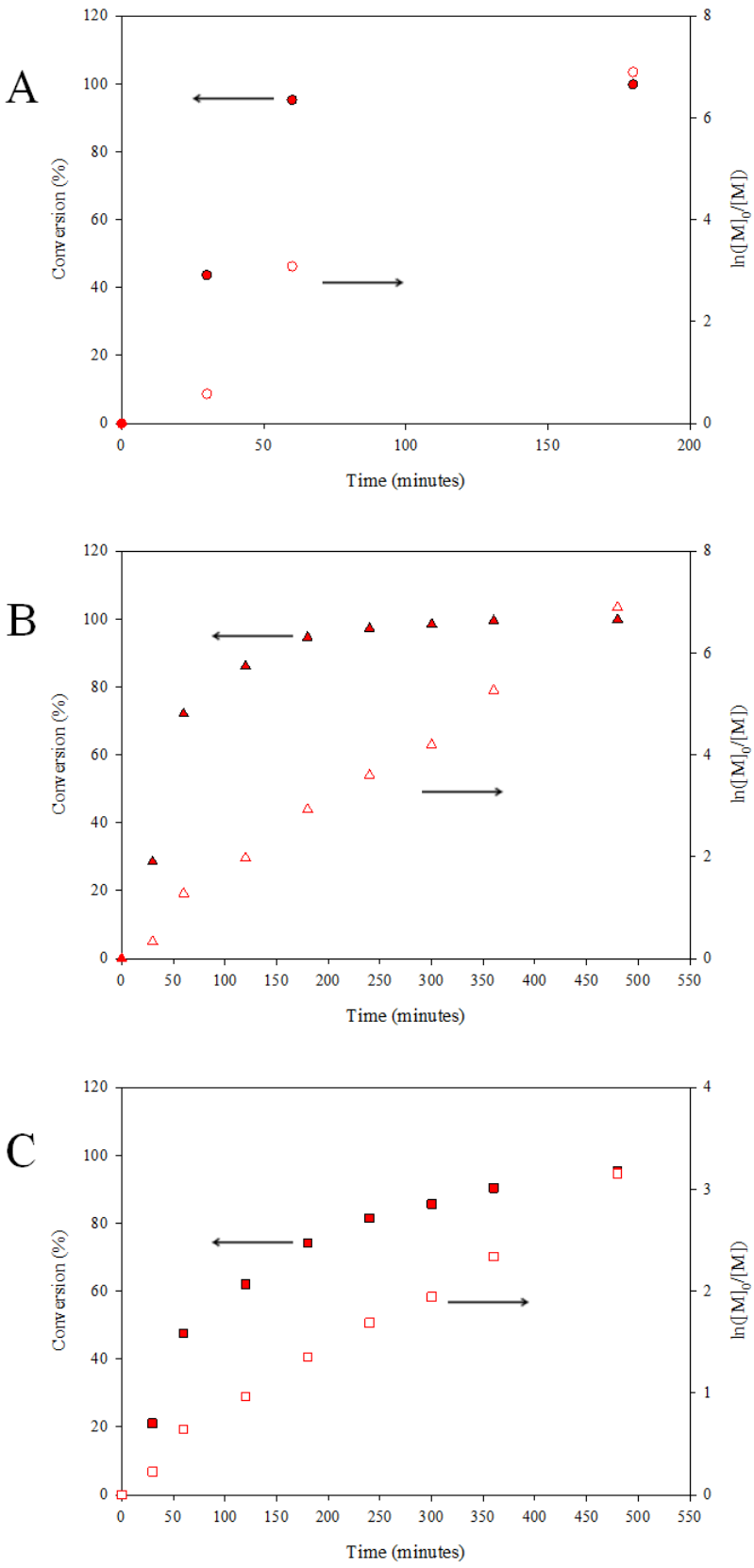


Figure 5.12: Kinetic studies of *p*(HPMA$_x$) using PEG$_{17}$-Br initiator. A) PEG$_{17}$-*b*-*p*(HPMA$_{30}$). B) PEG$_{17}$-*b*-*p*(HPMA$_{50}$). C) PEG$_{17}$-*b*-*p*(HPMA$_{100}$).

The data in Figure 5.12 suggests that all three polymerisations proceeded *via* typical ATRP mechanisms, identified by the high rate of reaction at low conversion where the concentration of monomer high. Whereas when monomer concentration begins to deplete at much higher conversions, a much slower rate of reaction is found. In conjunction to this, all of the semi logarithmic plots in Figure 5.12 are linear with respect to reaction time, indicative of a constant concentration of radicals present throughout the reactions. It is therefore assumed monomers are polymerising at a steady rate.

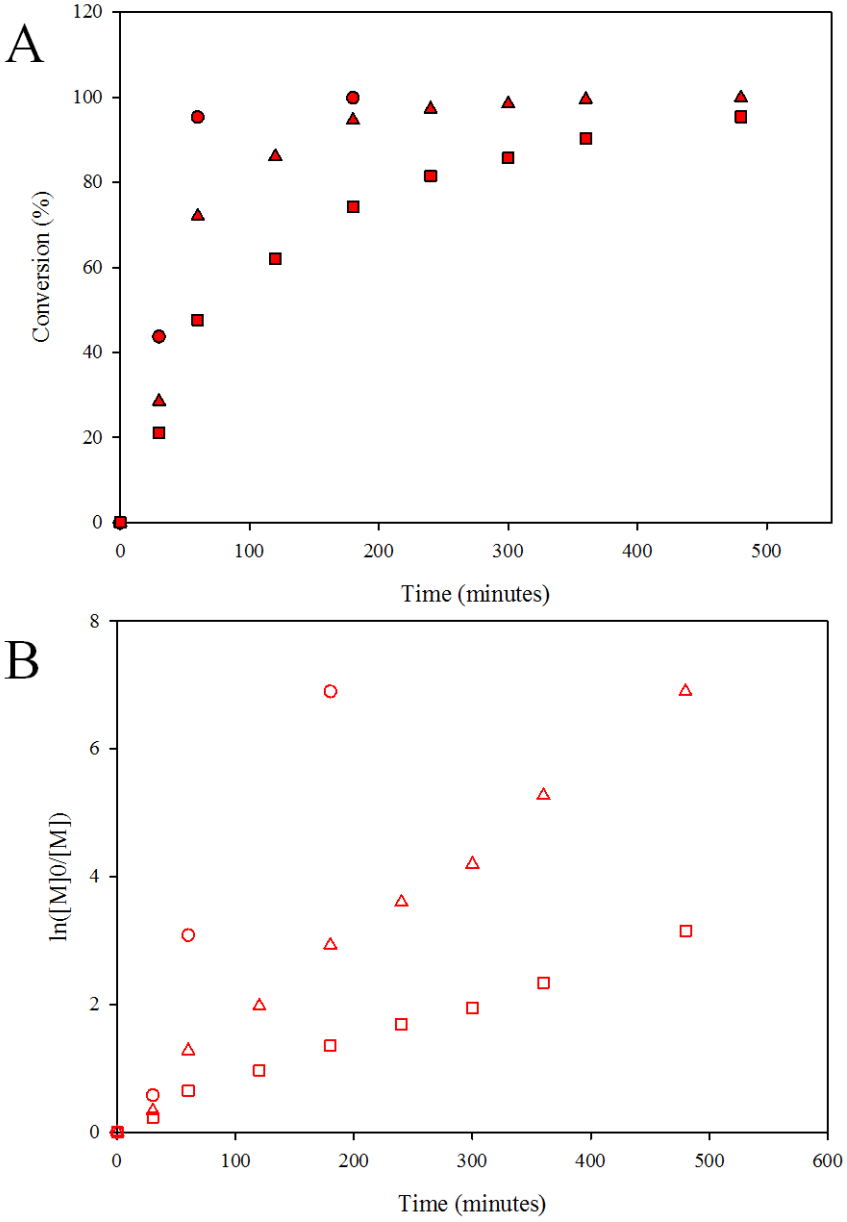


Figure 5.13: Kinetic studies of *p*(HPMA$_x$) using PEG$_{17}$-Br macroinitiator. A) Conversion *vs*. time. $x$ = 30 (filled circles), $x$ = 50 (filled triangles), $x$ = 100 (filled squares). B) Semi-logarithmic plot. $x$ = 30 (open circles), $x$ = 50 (open triangles), $x$ = 100 (open squares).

By grouping the data, the effect of increasing target DP$_n$ of *p*(HPMA) with respect to kinetic data can be seen. Figure 5.13(A) suggests the reaction with the lowest target DP$_n$ (30 monomer units) is the fastest polymerisation, followed by DP$_n$ = 50

monomer units and then 100 monomer units. This is essentially the same trend encountered in Chapter 3 (section 3.2.2) where EBiB was utilised as the initiator. The data suggests that regardless of the size and chemical composition, the fastest reactions for the polymerisation of *p*(HPMA) is found when targeting shorter primary chain lengths. The semi logarithmic plots are all linear with respect to monomer conversion as seen in Figure 5.13(B); these trends are comparable to those found in Chapter 3 (section 3.2.2). Despite varying the primary chain length, no detectable termination occurred at any stage of polymerisation and again, the rate of reaction lessens with increasing target $DP_n$, (also observed in Chapter 3 (section 3.2.2). The difference in rate directly relates to the change in concentration of the catalyst/ligand within the reaction; this change is unavoidable due to the reactions being carried out at 50 w/v % (initiator+monomer/solvent). Therefore, in the copolymerisation of $PEG_{17}$-*b*-*p*($HPMA_{50}$), the concentration of catalyst/ligand will be less than in the polymerisation of $PEG_{17}$-*b*-*p*($HPMA_{120}$), as more monomer (and therefore solvent) will have to be used in order to maintain 50 w/v %. Also, the variation in monomer concentration is expected to have an effect on the rate of reaction.

In summary, data suggests that despite varying the primary chain length of *p*($HPMA_x$) reactions proceed *via* conventional ATRP mechanisms. The trends appearing in this study are identical to those found during the kinetic analysis of *p*($HPMA_x$) in Chapter 3 (section 3.2.2).

## 5.4 Synthesis of $PEG_{17}$-*b*-*p*($HPMA_x$) Block Copolymers ($x$ = 20, 30, 50, 60, 70, 80, 100, 120)

A wide range of *p*($HPMA_x$) primary chain lengths were targeted using a selected initiator ($PEG_{17}$-Br). The previous studies have focused heavily on targeting only $DP_n$ = 50, 80 and 120 monomer units; here, much shorter polymer chains were targeted in order to investigate the limits of using $PEG_x$-Br macroinitiators to polymerise HPMA using methanolic ATRP. A wide range of polymers with accurate molecular weights and low polydispersities were obtained, where target $DP_n$ = 20, 30, 50, 60, 70, 80, 100, and 120 monomer units.

Copolymers were synthesised as described in Chapter 2 section 2.4.2 with the number of moles of initiator remaining constant, therefore the molar ratio of HPMA monomer was adjusted in order to achieve the correct target $DP_n$. Aiming to ensure the same number of initiating species is present at the beginning of all reactions, and minimising the possibility of experimental error. For example: $PEG_{17}$-Br (0.5 g, 0.547 mmol) was added to HPMA monomer (target $DP_n$ = 20 monomer units; 1.58 g, 11 mmol) or HPMA monomer (target DP = 30 monomer units; 2.37 g, 16 mmol). All reactions were left to polymerise until conversion of > 98% was reached (as assessed by $^1$H NMR spectroscopy) and terminated *via* exposure to the atmosphere and addition of approximately 200 mL of methanol whilst maintaining sufficient stirring. The copolymer solution was reduced under vacuum and precipitated into cold *n*-hexane. Molecular weight and molecular weight distributions were determined by GPC (THF eluent).

| Initiator | Target $DP_n$ | Target $M_n$ (g mol$^{-1}$) | GPC (THF eluent) | | | |
|---|---|---|---|---|---|---|
| | | | $DP_n$ | $M_n$ (g mol$^{-1}$) | $M_w$ (g mol$^{-1}$) | $M_w/M_n$ |
| $PEG_{17}$-Br | 20 | 3800 | 25 | 4600 | 6300 | 1.37 |
| $PEG_{17}$-Br | 30 | 5200 | 30 | 5200 | 6800 | 1.28 |
| $PEG_{17}$-Br | 50 | 8000 | 43 | 7100 | 8300 | 1.17 |
| $PEG_{17}$-Br | 60 | 9400 | 50 | 8100 | 9100 | 1.13 |
| $PEG_{17}$-Br | 70 | 10900 | 57 | 9100 | 10600 | 1.16 |
| $PEG_{17}$-Br | 80 | 12400 | 60 | 9500 | 11000 | 1.16 |
| $PEG_{17}$-Br | 100 | 15300 | 74 | 11500 | 13400 | 1.18 |
| $PEG_{17}$-Br | 120 | 18000 | 97 | 14800 | 17300 | 1.17 |

Table 5.3: Summary of data obtained for the copolymerisations of $PEG_{17}$-*b*-*p*-($HPMA_x$).

The data obtained through analysis of the eight copolymers synthesised using the $PEG_{17}$-Br initiator shown in Table 5.3. $DP_n$ was not analysed *via* $^1$H NMR spectroscopic analysis using the methoxy signal at 3.24 ppm due to extreme inaccuracy resulting from peak overlap, due to the water signal in the spectra. However, GPC analysis generally (apart from the polymer with a target *p*(HPMA) of $DP_n$ = 20 monomer units) gives molecular weights which are lower than those predicted; this will be explained later in the section. Overall, the data suggests considerable control has been achieved during each polymerisation, as molecular weights increase as target $DP_n$ increases whilst maintaining relatively narrow molecular weight distributions.

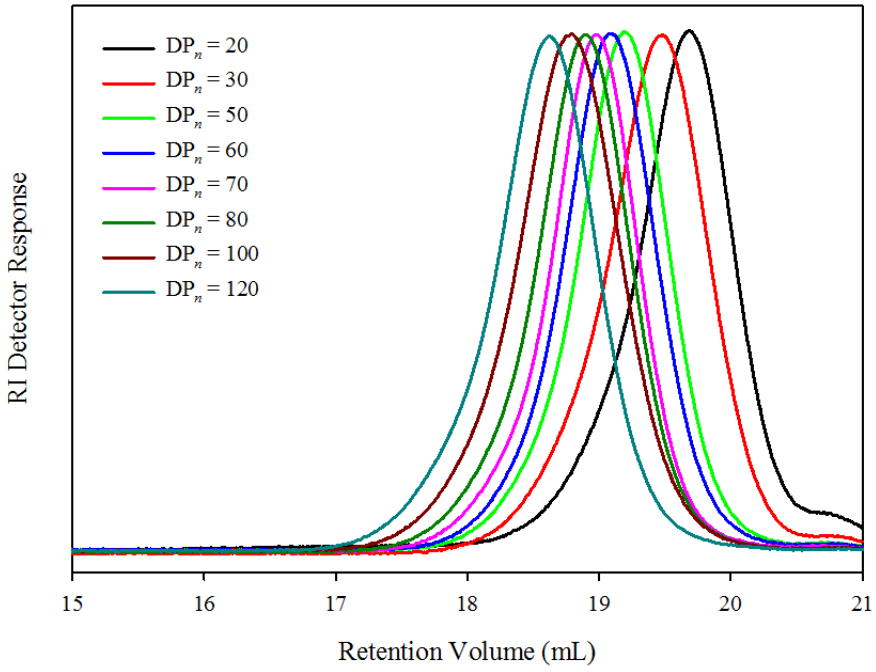


Figure 5.14: GPC chromatograms (THF eluent) for $PEG_{17}$-Br initiated *p*(HPMA) copolymers with target $DP_n$ ranging from 20 to 120 monomer units.

Figure 5.14 shows GPC traces for copolymers with target $DP_n$ ranging from 20 to 120 monomer units which are highly symmetrical. It should be noted that a small shoulder appears for copolymers with very low molecular weight (namely $DP_n$ = 20 monomer units), which is likely to be due to termination within the reaction at low conversion, directly impacting on the molecular weight distribution ($M_w/M_n$ = 1.37). By targeting low molecular weight copolymer chains it is unavoidable that their molecular weight distributions will be higher with respect to those with longer chains; adding just 3 more monomer units onto a chain (for a target $DP_n$ of 20 monomer units) results in a 15 % molecular weight increase, whereas molecular weight increases by < 3 % when applied to a target $DP_n$ of 120 monomer units.

To demonstrate this further, Figure 5.15 shows the measured dispersities *vs*. target $DP_n$ across the range of synthesised polymers; a sharp decrease in molecular weight distribution is seen as $DP_n$ increases. By targeting higher $DP_n$ values (> 60 monomer units), other factors may contribute to the increased molecular weight distribution, such as chain termination and or chain coupling due to longer reaction times needed to reach > 99 % conversion.

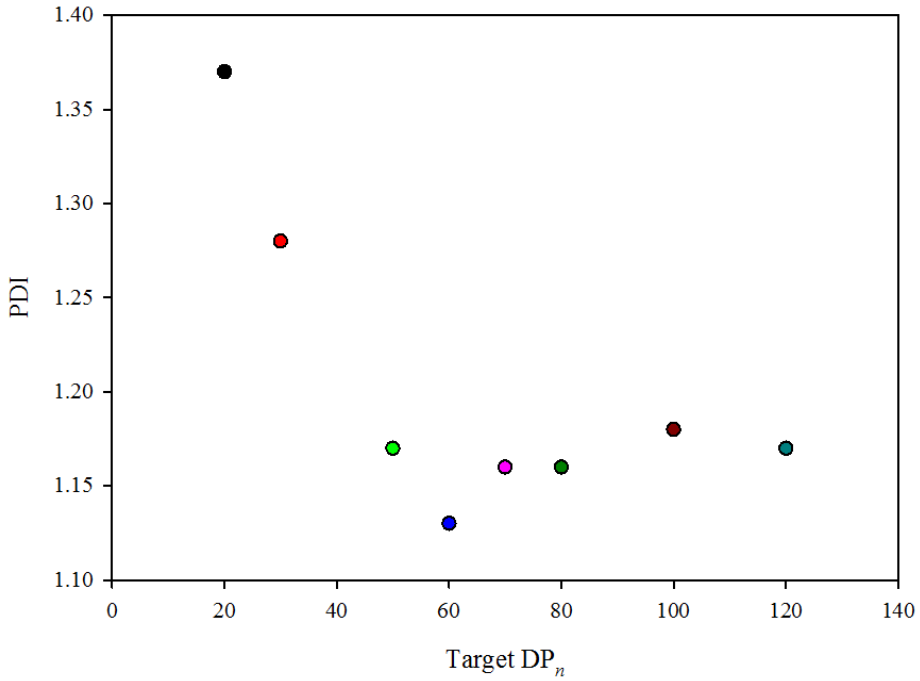


Figure 5.15 Dispersity *vs*. target $DP_n$ for $PEG_{17}$-Br initiated polymers. (Symbol colours are indicative of those used for individual GPC chromatograms in Figure 5.14).

Figure 5.16 demonstrates the accuracy of the number average molecular weights obtained for the polymers with respect to their targeted molecular weight. Plots of theoretical $M_n$ *vs*. actual $M_n$ acquired from $^1$H NMR spectroscopy and GPC analysis are both linear, suggesting good control is achieved consistently across all

synthesised polymers. Apart from $DP_n$ = 20 monomer units, all of the molecular weights obtained *via* GPC are lower than those from $^1$H NMR spectroscopic analysis; this is believed to be due to $^1$H NMR spectroscopic analysis accounting for all of the initiator added to the reaction, including residual initiator which may not have initiated efficiently and have not been removed during purification; the actual $DP_n$ is unsurprisingly close to the theoretical $DP_n$ if this is the case. However, these results are reassuring as it indicates consistently high levels of accuracy being achieved in terms of experimental protocols. GPC analysis does not account for low molecular weight unreacted initiators as they are generally undetectable due their high elution volume.

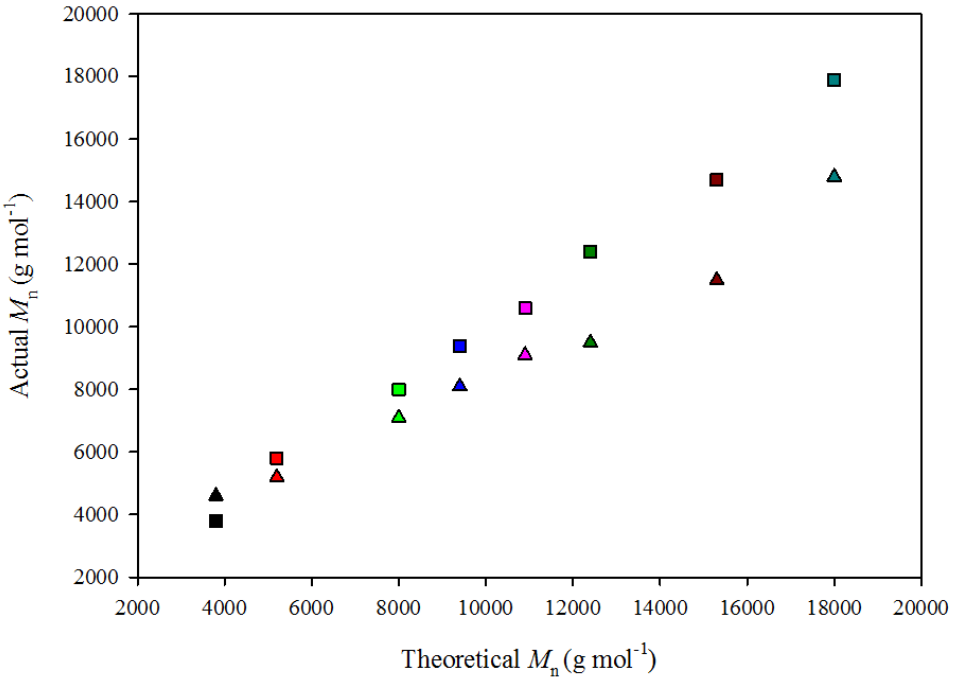


Figure 5.16: Target *vs*. Actual $M_n$ for $PEG_{17}$-Br initiated copolymers with target $DP_n$ ranging from 20 to 120 monomer units. $^1$H NMR (squares) GPC (triangles). (Symbol colours are indicative of those used for individual GPC chromatograms in Figure 5.14 and Figure 5.15).

As the resultant molecular weights of the synthesised polymers correlate well with those predicted, it is suggested that accurate control can be achieved upon varying the primary chain length of *p*(HPMA$_x$). All polymer GPC chromatograms are monomodal and highly symmetrical with molecular weight distributions ranging from 1.13 to 1.37 which is typical for linear ATRP polymerisations. Further experiments to investigate the upper and lower limits in terms of target DP$_n$ where ATRP mechanisms begin to fail and control begins to break down have not been explored here.

## 5.5 Chain Extension of PEG$_{17}$-*b*-*p*(HPMA$_x$) Block Copolymer ($x$ = 30, 50, 100)

The previous section showed that utilising the PEG$_{17}$-Br initiator to polymerise *p*(HPMA) to various chain lengths was highly successful, due consistently accurate molecular weights with respect to their target DP$_n$, alongside kinetic investigations confirming reactions were highly controlled and indicative of a controlled ATRP mechanism. This section focuses on the attempted chain extension of PEG$_{17}$-Br initiated *p*(HPMA); analogous to the chain extension experiment reported in Chapter 3 (section 3.2.3) which utilised EBiB as the initiator and was deemed highly successful. By conducting these current experiments, it is aimed to show that chain ends remain active at relatively high conversion and are able to polymerise a second batch of HPMA monomer. These experiments are "self-blocking" polymerisations as both monomer batches are identical. HPMA was polymerised using PEG$_{17}$-Br to three different target DP$_n$ values (30, 50 and 100 monomer units) after which a second batch of HPMA monomer (equivalent to a DP$_n$ of 30 monomer units) was added when the polymerisations had reached high conversions (88 % to 98%). The

molar ratio of initiator was kept constant through the experiments and the molar ratio of HPMA monomer was changed in order to achieve the correct target $DP_n$. The reactions were left until > 98% conversion (as judged by $^1H$ NMR), terminated, and purified *via* precipitation into cold *n*-hexane. A representation of chain extension is shown in Scheme 5.2.

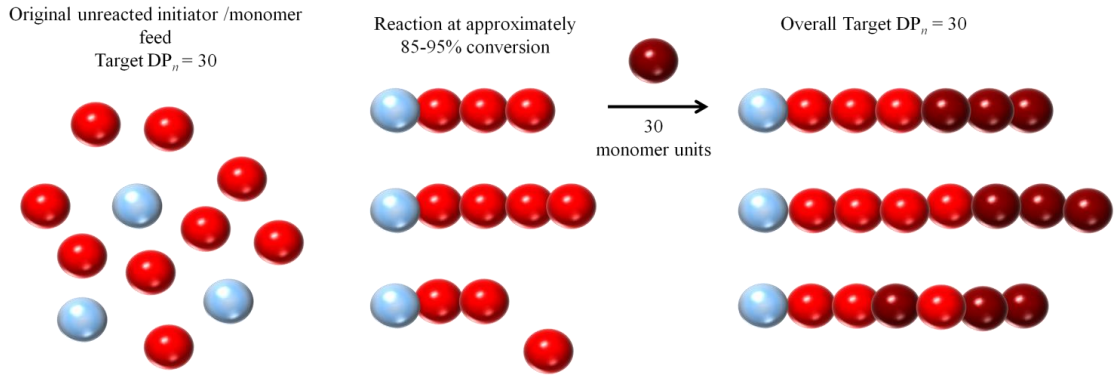


Scheme 5.2: Representation of the chain extension process in methanol for linear $PEG_{17}$-*b*-*p*($HPMA_{30}$)-*b*-*p*($HPMA_{30}$) employing $PEG_{17}$-Br as the initiator. (Initiator: monomer feed is not to scale).

Performing reaction kinetics was necessary in order to determine approximately at what time the second batch of monomer should be added. If high conversion was not reached, there would remain much more un-reacted monomer in the vessel (remaining monomer from the first block, plus monomer from second block) leading to a much higher molecular weight second block, although the overall calculated molecular weight and therefore $DP_n$, would be unaffected. Conversely, if reactions were left to reach full conversion before addition of the second batch, i.e. solely consisting of radical containing chain ends, the likelihood of two of these coupling (and terminating) is much higher, with the remaining chains still able to propagate and consume the available monomer. This lack of uniformity would ultimately lead to a much broader molecular weight distribution. According to previous reports,[10]

approximately 95% conversion is optimal for chain extension to achieve a high blocking efficiency. Prior kinetic experiments allowed for the determination of time taken for reactions to achieve approximately 95 % conversion. Experimentally, two samples were removed from the polymerisation pot after high conversion had been reached followed by the addition of a second HPMA monomer feed in quick succession. As kinetic analysis for $PEG_{17}$-*b*-*p*($HPMA_{30}$), $PEG_{17}$-*b*-*p*($HPMA_{80}$) and $PEG_{17}$-*b*-*p*($HPMA_{120}$) has been discussed in Section 5.1.2.2, the timing of the second monomer feed addition could be approximated as the molar ratios of initiator:monomer were kept constant for chain extension experiments.

Having analysed the pre-experiment kinetic results, three chain extension reactions were performed. As previously stated, samples for GPC measurement were taken as the second monomer feed was added and quickly terminated in THF before removal of catalyst by addition of resin beads and followed by passing over a small basic alumina column. This process was repeated on a larger scale once the polymerisation had reached > 99 % conversion where a sample was taken for GPC (THF eluent) analysis.

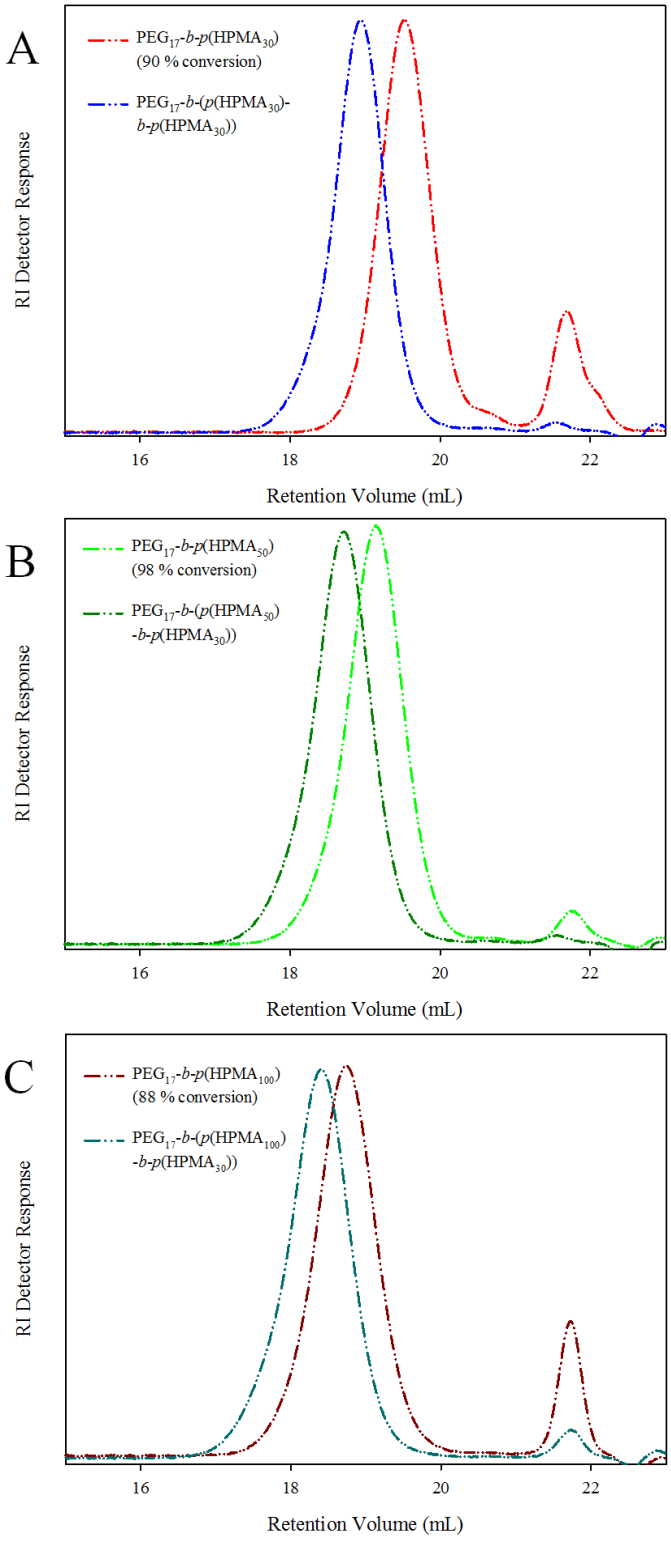


Figure 5.17: Triple detection GPC chromatograms for the chain extension of *p*(HPMA$_x$) utilising PEG$_{17}$-Br initiator. (A) PEG$_{17}$-*b*-(*p*(HPMA$_{30}$)-*b*-*p*(HPMA$_{30}$)). (B) PEG$_{17}$-*b*-(*p*(HPMA$_{50}$)-*b*-*p*(HPMA$_{30}$)). PEG$_{17}$-*b*-(*p*(HPMA$_{100}$)-*b*-*p*(HPMA$_{30}$)).

Figure 5.17 shows the GPC chromatograms for the three chain extension experiments. It should be noted here that the colours utilised in Figure 5.17 (apart from $PEG_{17}$-*b*-(*p*($HPMA_{100}$)-*b*-*p*($HPMA_{30}$)) correlate to those used in Figure 5.14. The first copolymer blocks (ranging from 88 % to 98 % conversion) all elute at a lower retention volumes than the final chain extended copolymers. The remaining monomer is also visible at an elution volume of approximately 21-22 mL; after the second monomer feed this peak in Figure 5.17(A)&(B) is almost indistinguishable from the baseline. This un-reacted monomer peak is still visible in Figure 5.17(C) which may be due to the reaction reaching a slightly lower conversion (98 %), but could also be due to less blocking efficiency, as the target $DP_n$ of the first block was relatively high (100 monomer units).

| Initiator | Target $DP_n$ | Target $M_n$ (g $mol^{-1}$) | $^1H$ NMR | | | GPC | | |
|---|---|---|---|---|---|---|---|---|
| | | | Conv (%) | $M_n$ (g $mol^{-1}$) | $DP_n$ | $M_n$ (g $mol^{-1}$) | $M_w$ (g $mol^{-1}$) | $M_w$/ $M_n$ |
| $PEG_{17}$-Br | 30 | 5100 | 90 | 4600 | 27 | 4600 | 4900 | 1.06 |
| $PEG_{17}$-Br | 30+30 (60) | 9400 | 99 | 9400 | 57 | 9000 | 9900 | 1.10 |
| $PEG_{17}$-Br | 50 | 8000 | 98 | 7800 | 40 | 6500 | 7700 | 1.19 |
| $PEG_{17}$-Br | 50+30 (80) | 12300 | 99 | 12300 | 77 | 11900 | 13300 | 1.12 |
| $PEG_{17}$-Br | 100 | 15200 | 88 | 13400 | 86 | 13200 | 14900 | 1.13 |
| $PEG_{17}$-Br | 100+30 (130) | 19500 | 98 | 19500 | 117 | 17600 | 20200 | 1.15 |

Table 5.4: Summarising data obtained from $PEG_{17}$-Br initiated chain extension experiments.

The data shown in Table 5.4 suggests most of the polymer chains are still capped with halogen atoms at high conversion and therefore sufficient chain extension occurs. An $M_n$ = 4600 g $mol^{-1}$ and a dispersity of 1.06 was achieved for a target $DP_n$ of 30 monomer units for the first batch of HPMA monomer and a final $M_n$ = 9000

g mol$^{-1}$. This figure is approximately twice the initial number average molecular weight and the dispersity was virtually unchanged at 1.10. The GPC chromatograms for this experiment (Figure 5.17) indicate high self-blocking efficiencies suggesting relatively good controlled radical character under these conditions. Blocking efficiency appears to be reduced as the target DP$_n$ increases. This is shown for a final target DP$_n$ of 130 monomer units, where a final $M_n$ = 17600 g mol$^{-1}$ is found. This is much lower than the expected $M_n$ (19500 g mol$^{-1}$) although the dispersity remains low at 1.15; this roughly equates to a chain that is 13 monomer units shorter than expected on average.

The final copolymers show predictable molecular weights with dispersities as low as 1.06 at 90 % conversion for PEG$_{17}$-*b*-*p*(HPMA$_{30}$), where shoulders at lower retention volumes are not observed within the GPC analysis, indicating negligible termination of the *p*(HPMA) chains, even at high conversion.

Figure 5.18 demonstrates the reproducibility of PEG$_{17}$-Br initiated copolymerisations and also allows for a direct comparison between linear copolymers and linear chain extended copolymers. By overlaying a copolymer counterpart GPC chromatogram; that is a copolymer that was synthesised using a single monomer addition and whose target DP$_n$ is equal (or similar) to that of the combined target DP$_n$ of chain extended copolymers, it is clear to see the impact of adding a second batch of monomer to an already polymerising reaction.

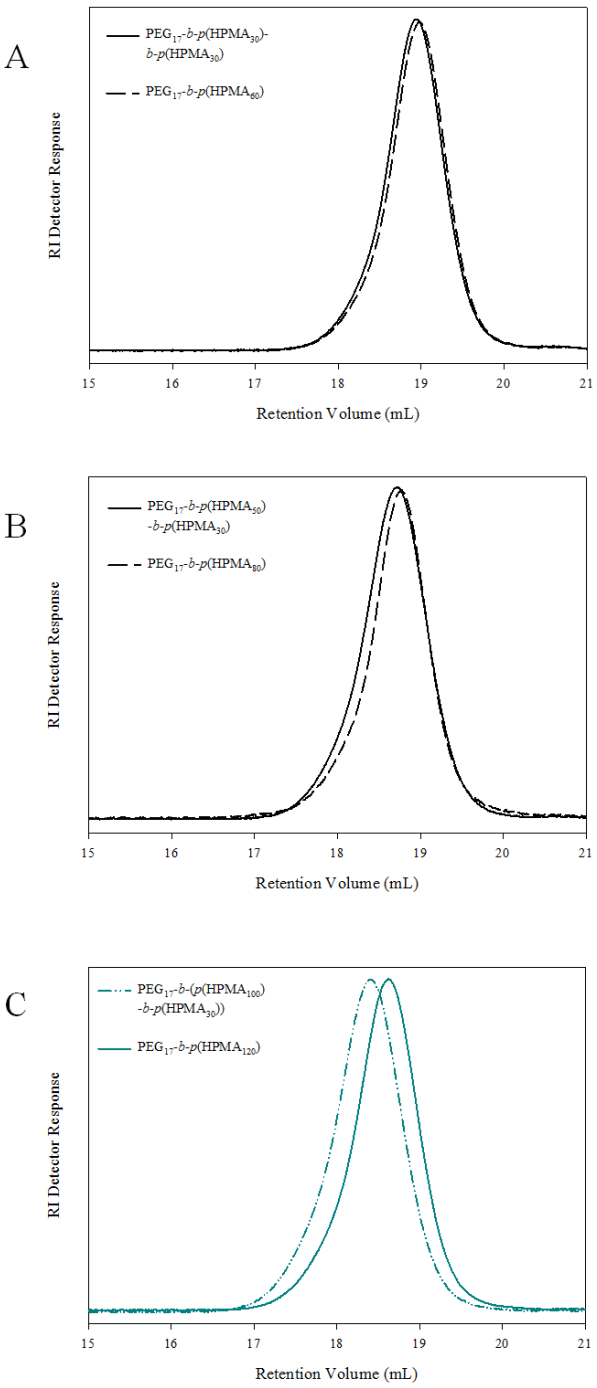


Figure 5.18: GPC chromatograms of $PEG_{17}$-Br initiated chain extended HPMA polymers (dot-dot-dashed lines) and their linear non-extended counterparts (solid lines). (A) Overall $DP_n$ = 60 monomer units. (B) Overall $DP_n$ = 80 monomer units. (C) Chain extended polymer - overall $DP_n$ = 130 monomer units and non-extended polymer - overall $DP_n$ = 120 monomer units.

A near-perfect overlay of GPC chromatograms is seen in Figure 5.18(A) as expected due to both copolymers containing virtually the same number of monomer units (60). The same near-perfect overlay is found in Figure 5.18(B), where both polymers contain approximately 80 monomer units. Figure 5.18(C) does not show complete overlay of the chromatograms as these copolymers have different targeted chain lengths.

In short summary the synthesis and characterisation of a wide range of *p*($HPMA_x$) copolymers utilising a variety of PEG based macroinitiators has been reported with individual kinetics explored. Linear copolymers are capable of chain extension where little to no termination occurred during multiple reactions. In conjunction to the high blocking efficiencies, reproducibility of copolymer synthesis was demonstrated.

## 5.6 Synthesis of Branched $PEG_x$-*b*-(*p*($HPMA_y$)-*co*-$EGDMA_{0.95}$)) Block Copolymers ( $x$ = 17, 45, 113, $y$= 50, 80, 120)

In the previous sections it has been shown that methanolic ATRP can be used to synthesise linear polymers consisting of *p*($HPMA_x$) at various chain lengths utilising $PEG_x$-Br based macroinitiators (of different molecular weight). The facile one pot methanolic polymerisation of branched *p*($HPMA_x$) using these PEG based macroinitiators is described here; reactions are based on the previously reported branched polymerisations utilising EBiB as the initiator in Chapter 3 section 3.3 with 0.95 equivalents of EGDMA brancher employed to yield high molecular weight materials with complex branched A-B amphiphilic block copolymer architectures. These reactions were carried out at ambient temperatures and 50 w/v % (initiator+monomer/solvent) and left to polymerise until > 99% conversion (judged

by $^{1}$H NMR spectroscopy) followed by manual termination *via* exposure to the atmosphere and addition of methanol.

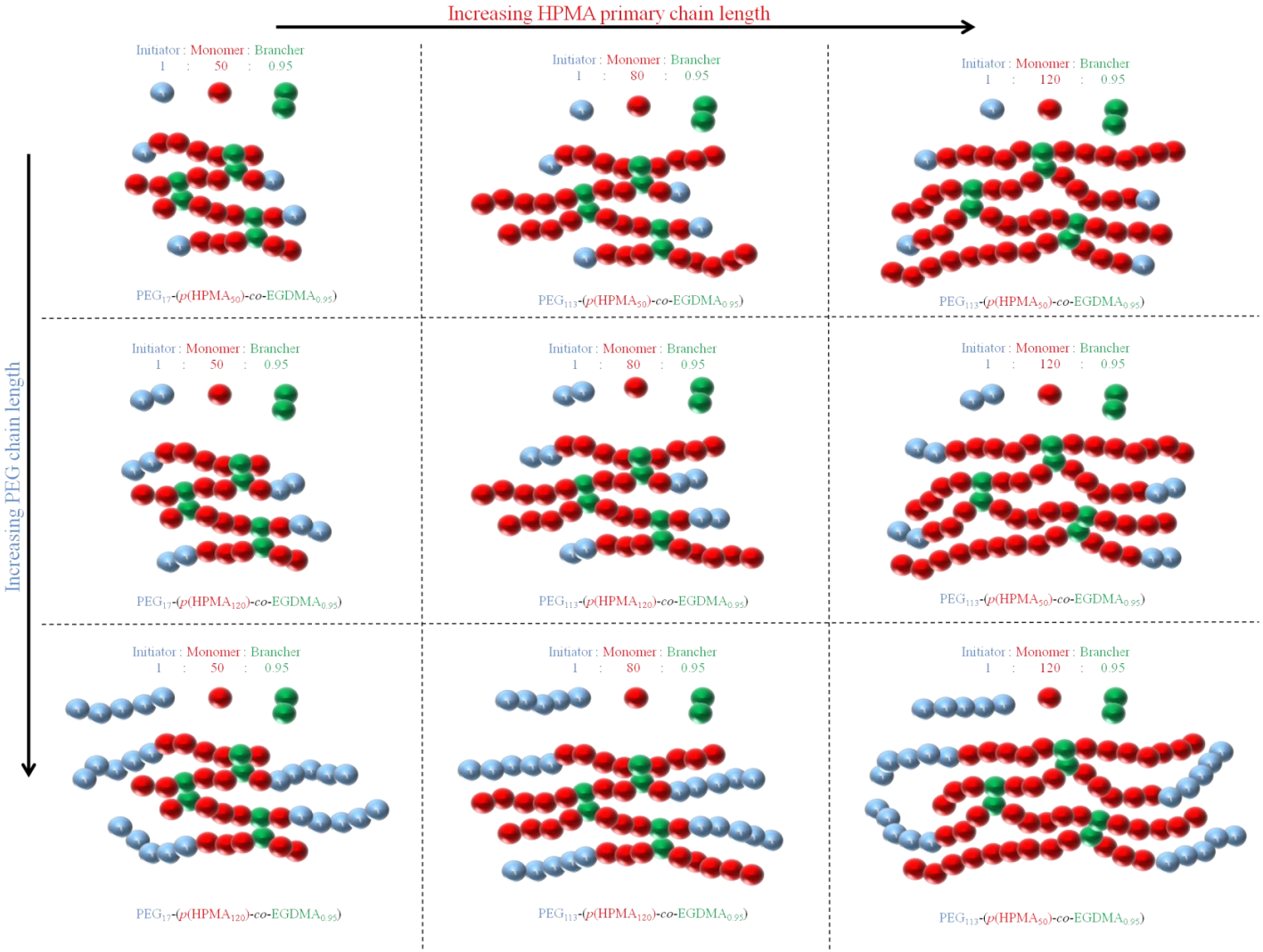


Figure 5.19: Representation of the targeted branched $p(HPMA_x)$ copolymers utilising $PEG_x$-Br based macroinitiators.

Figure 5.19 displays representations of branched copolymer structures utilising $PEG_x$-Br macroinitiators and demonstrating the architectural effect of varying both components of the copolymer. For example, the overall target molecular weight of the linear copolymer in $PEG_{113}$-*b*-(*p*($HPMA_{120}$)-*co*-$EGDMA_{0.95}$)) (bottom right of Figure 5.19) is approximately three times higher than that in $PEG_{17}$-*b*-(*p*($HPMA_{50}$)-*co*-$EGDMA_{0.95}$)) (top left of Figure 5.19). Providing that the branching process is unaffected by these various initiators, this indicates that the former branched copolymer should generate much higher molecular weight material. This representation aims to highlight the various branched structures synthesised by altering two parameters (ethylene oxide repeat units in the initiator, and HPMA monomer feed). Unlike their linear counterparts, a target $M_n$ of the overall polymer sample cannot be determined due to the inclusion of a brancher molecule (EGDMA) which covalently links otherwise linear chains. The number of chains involved in these branched structures cannot be predicted as EGDMA is incorporated statistically, however, the primary chains of the branched architectures will be monodisperse and have the target $M_n$ values of the linear materials produced in the absence of EGDMA. In Chapter 3 section 3.3, analysis showed that the distribution of molecular weight for branched materials is extremely high, suggesting copolymers do not consist of solely *x* number of primary chains. It should be noted that the copolymer representations in Figure 5.19 contain four primary *p*($HPMA_x$) chains which was simply for demonstrative purposes. A total of nine branched copolymers were synthesised containing $PEG_x$ ($x$ = 17, 45, 113) and *p*(HPMA) where target $DP_n$ = 50, 80, 120 monomer units. No visual gelation occurred and as such triple detection GPC (THF eluent) was performed. These chromatograms are

shown in Figure 5.20.

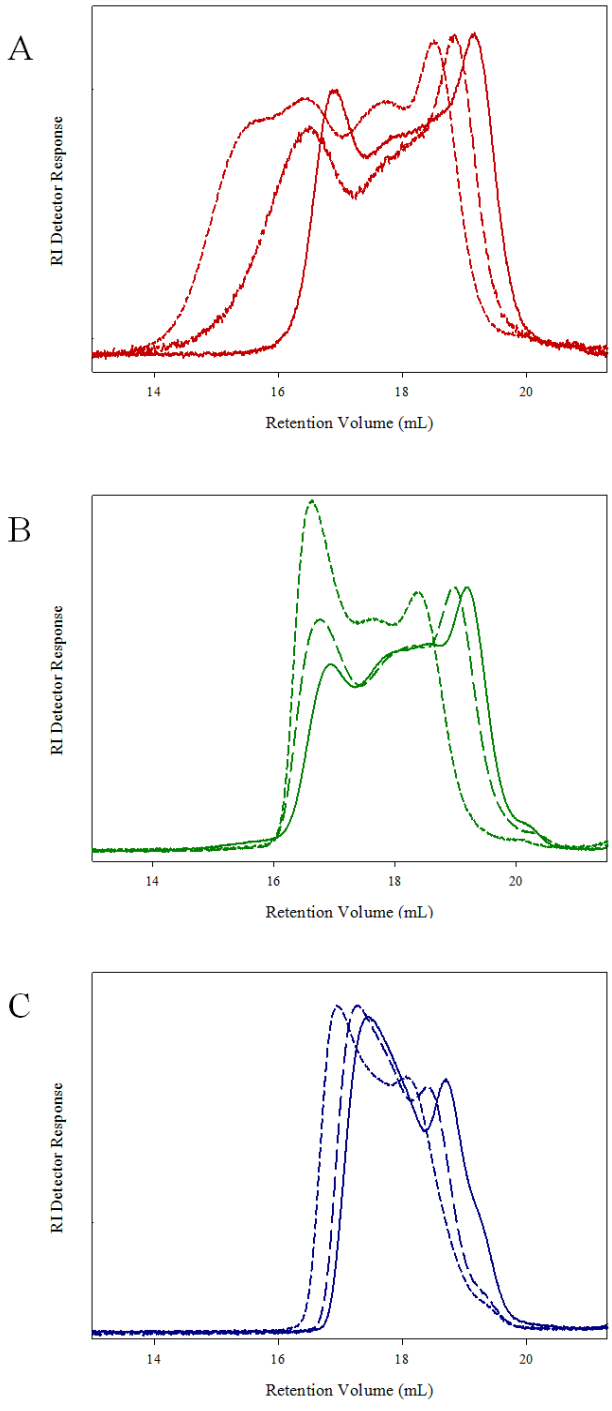


Figure 5.20: GPC chromatograms of $PEG_x$-Br initiated branched *p*(HPMA$_)$ copolymers. (A) $PEG_{17}$-*b*-(*p*($HPMA_x$)-*co*-$EGDMA_{0.95}$)) (B) $PEG_{45}$-*b*-(*p*($HPMA_x$)-*co*-$EGDMA_{0.95}$)) (C) $PEG_{113}$-*b*-(*p*($HPMA_x$)-*co*-$EGDMA_{0.95}$)). *X* = 50 (solid lines), *X* = 80 (medium dashed lines) *X* = 120 (small dashed lines).

Figure 5.20 suggests high molecular weight materials have been synthesised, due to the detection of large concentrations of material eluting at low retention volumes. It should be noted that Figures 5.20 (A), (B) and (C) are shown with the same retention volume scales, as such, it is apparent that increasing the molecular weight of the PEG initiator hinders the production of extremely high molecular weight material. For example, $PEG_{17}$-*b*-(*p*($HPMA_{120}$)-*co*-$EGDMA_{0.95}$)) begins to elute at approximately 14 mL whereas $PEG_{113}$-*b*-(*p*($HPMA_{120}$)-*co*-$EGDMA_{0.95}$)) begins to elute at 16.2 mL, indicative of lower molecular weight materials; this will be discussed later in the section.

| Sample | $M_n$ (g mol$^{-1}$) (GPC) | $M_w$ (g mol$^{-1}$) (GPC) | $M_w/M_n$ (GPC) | Conversion (%) |
|---|---|---|---|---|
| $PEG_{17}$-*b*-(*p*($HPMA_{50}$)-*co*-$EGDMA_{0.95}$)) | 57200 | 150400 | 2.63 | > 99 |
| $PEG_{17}$-*b*-(*p*($HPMA_{80}$)-*co*-$EGDMA_{0.95}$)) | 76500 | 274600 | 3.59 | > 99 |
| $PEG_{17}$-*b*-(*p*($HPMA_{120}$)-*co*-$EGDMA_{0.95}$)) | 95900 | 448800 | 4.68 | > 99 |
| $PEG_{45}$-*b*-(*p*($HPMA_{50}$)-*co*-$EGDMA_{0.95}$)) | 43300 | 110400 | 2.55 | > 99 |
| $PEG_{45}$-*b*-(*p*($HPMA_{80}$)-*co*-$EGDMA_{0.95}$)) | 45900 | 137200 | 2.99 | > 99 |
| $PEG_{45}$-*b*-(*p*($HPMA_{120}$)-*co*-$EGDMA_{0.95}$)) | 52400 | 163500 | 3.12 | > 99 |
| $PEG_{113}$-*b*-(*p*($HPMA_{50}$)-*co*-$EGDMA_{0.95}$)) | 45400 | 118500 | 2.61 | > 99 |
| $PEG_{113}$-*b*-(*p*($HPMA_{80}$)-*co*-$EGDMA_{0.95}$)) | 47800 | 119900 | 2.51 | > 99 |
| $PEG_{113}$-*b*-(*p*($HPMA_{120}$)-*co*-$EGDMA_{0.95}$)) | 49600 | 135900 | 2.74 | > 99 |

Table 5.5: Summary of the data obtained for the copolymerisations of $PEG_x$-*b*-(*p*($HPMA_y$)-*co*-$EGDMA_{0.95}$)) where $x$ = 17, 45, 113 and $y$ = 50, 80, 120.

The data presented in Table 5.5 for all nine branched copolymers demonstrates that despite each copolymer containing EGDMA, weight average molecular weights vary dramatically from 110400 to 163500 g mol$^{-1}$, as well as molecular weight distribution (2.5 to 4.7). On average, the highest molecular weights are obtained when utilising the lowest molecular weight initiator ($PEG_{17}$-Br), which also has the broadest molecular weight distributions. The data suggests that the PEG based macroinitiators are in some way directing the branching process. Intuitively, the working hypothesis assumed that, if the branching is independent of initiator

structure and/or molecular weight, the highest molecular weight copolymers should be $PEG_{113}$-*b*-(*p*($HPMA_{120}$)-*co*-$EGDMA_{0.95}$)). As this is not the case here, it is assumed that branching is hindered as the molecular weight of the initiator increases. This observation will be discussed in more detail later in the section.

## 5.7 Reproducibility of Branched Copolymer Synthesis

It was questioned whether the systematic variation in the shape of the GPC chromatograms seen in the previous section were in fact due to the effect of the initiator molecular chain length and whether the statistical branching process was reproducible. What can is evident from Figures 5.21, 5.22 and 5.23 are three distinct sections within each of the chromatograms, the first section (at high retention volumes) is attributed to linear material, following with lightly branched material and finally high molecular weight material (at low retention volumes). As the molecular weight of the initiator increases, GPC traces fail to reach extremely low retention volumes, indicative of very highly branched polymers. In order to determine whether this is a true trend, each polymerisation was conducted again. It should be noted that these polymerisations were conducted at ambient temperature and reproducibility experiments were performed after a considerable time period, using different batches of HPMA, EGDMA and catalyst/ligand. The experimental protocol was, however, identical.

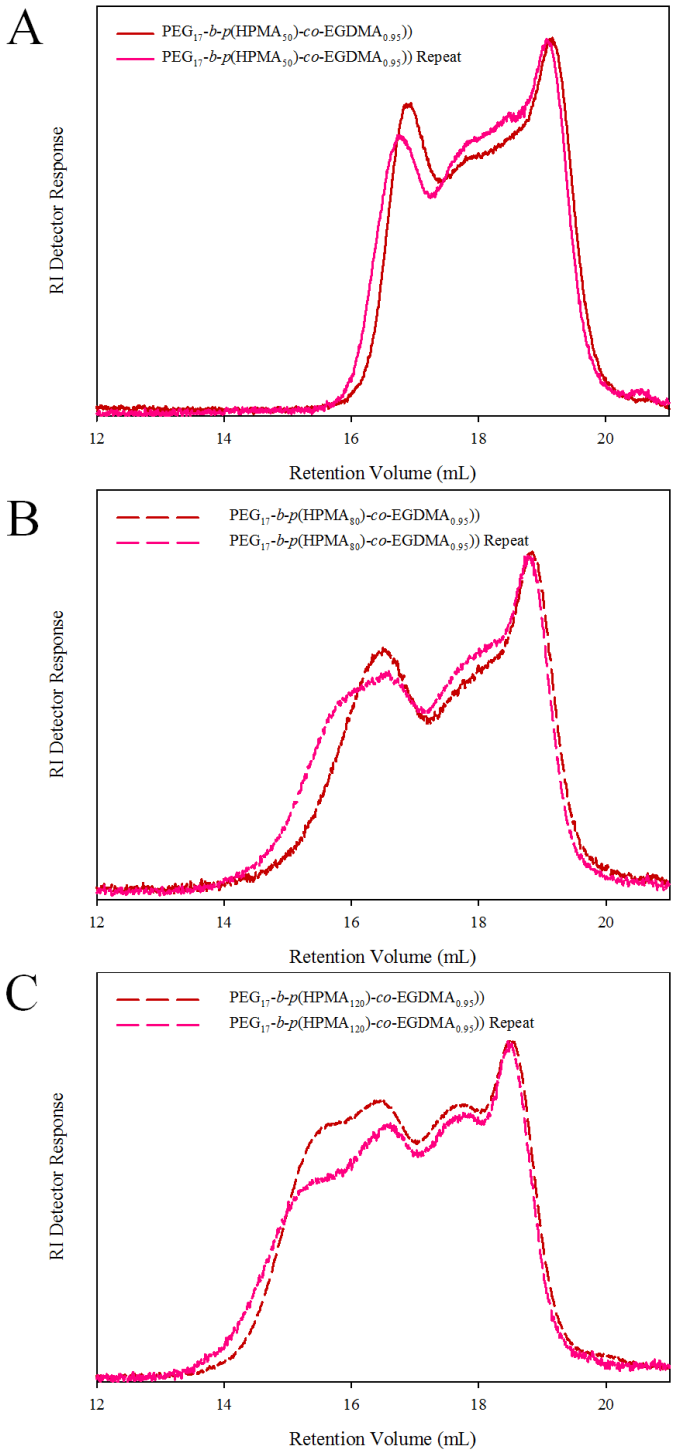


Figure 5.21: Repeat GPC Chromatograms (THF eluent) of $PEG_{17}$-*b*-(*p*($HPMA_x$-*co*-$EGDMA_{0.95}$). A) $PEG_{17}$-*b*-(*p*($HPMA_{50}$-*co*-$EGDMA_{0.95}$). B) $PEG_{17}$-*b*-(*p*($HPMA_{80}$-*co*-$EGDMA_{0.95}$). C) $PEG_{17}$-*b*-(*p*($HPMA_{120}$-*co*-$EGDMA_{0.95}$).

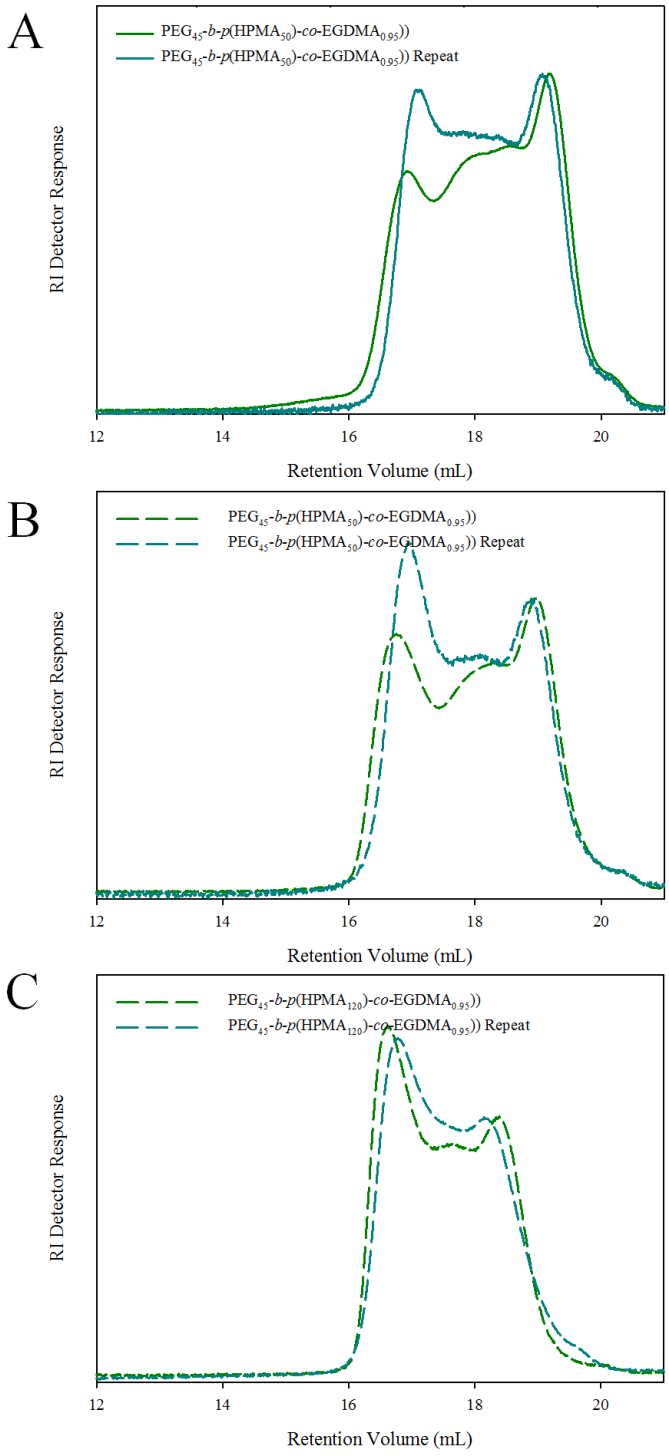


Figure 5.22: Repeat GPC Chromatograms (THF eluent) of $PEG_{45}$-*b*-(*p*($HPMA_x$-*co*-$EGDMA_{0.95}$). A) $PEG_{45}$-*b*-(*p*($HPMA_{50}$-*co*-$EGDMA_{0.95}$). B) $PEG_{45}$-*b*-(*p*($HPMA_{80}$-*co*-$EGDMA_{0.95}$). C) $PEG_{45}$-*b*-(*p*($HPMA_{120}$-*co*-$EGDMA_{0.95}$).

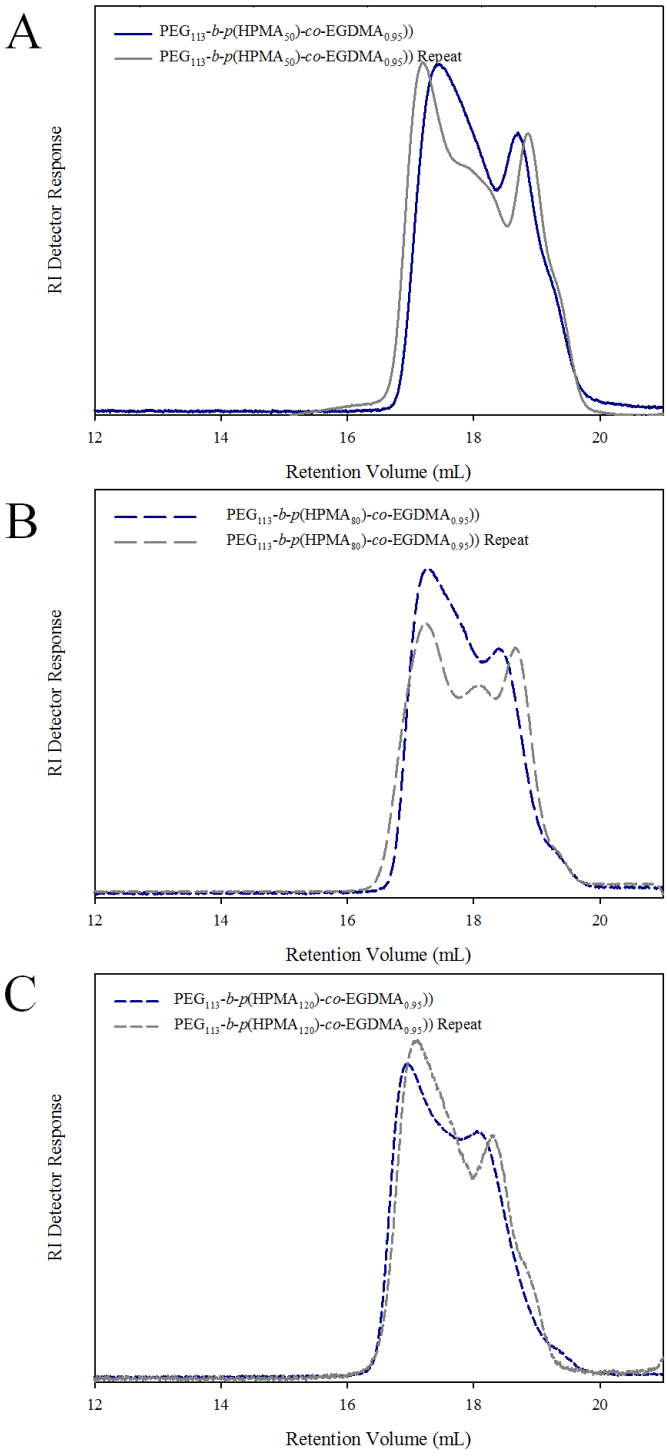


Figure 5.23: Repeat GPC Chromatograms (THF eluent) of $PEG_{113}$-*b*-(*p*($HPMA_x$-*co*-$EGDMA_{0.95}$). A) $PEG_{113}$-*b*-(*p*($HPMA_{50}$-*co*-$EGDMA_{0.95}$). B) $PEG_{113}$-*b*-(*p*($HPMA_{80}$-*co*-$EGDMA_{0.95}$). C) $PEG_{113}$-*b*-(*p*($HPMA_{120}$-*co*-$EGDMA_{0.95}$).

Clearly from all of the above chromatograms the repeat polymerisations give extremely similar RI traces in their GPC analysis. This data suggests that despite time/temperature and reagent differences, the branching process is near identical when utilising the same $PEG_x$-Br initiator. The results show that these polymerisations are robust and reproducible and no report of similar analysis can be found in the literature.

## 5.8 Further Analysis of Branched Copolymer Architecture

As previously noted, distinct peaks exist at high retention volumes which we can attributed to linear material being present within these branched copolymer samples. This occurs within all nine branched copolymers, however, a linear *p*(HPMA) and a branched copolymer with the same target $DP_n$ = 80 monomer units was chosen to highlight this in Figure 5.24. Again, this is analysis correlates well to the branched copolymers previously synthesised in Chapter 3 (section 3.3), which utilised EBiB as the initiator. This data is in good agreement with the Monte Carlo modelling of monovinyl and divinyl monomers reported by Armes and co-workers[11] which predicts that a multitude of different structures are obtained during the branching process; including linear material. What is also apparent from Figure 5.24 is the occurrence of low molecular weight shoulders within the branched copolymer chromatograms which appear to increase in size as the molecular weight of the initiator increases, believed to be due to termination during early stages of polymerisation (unlike in their linear counterparts). The exact source of the observed peaks is unknown.

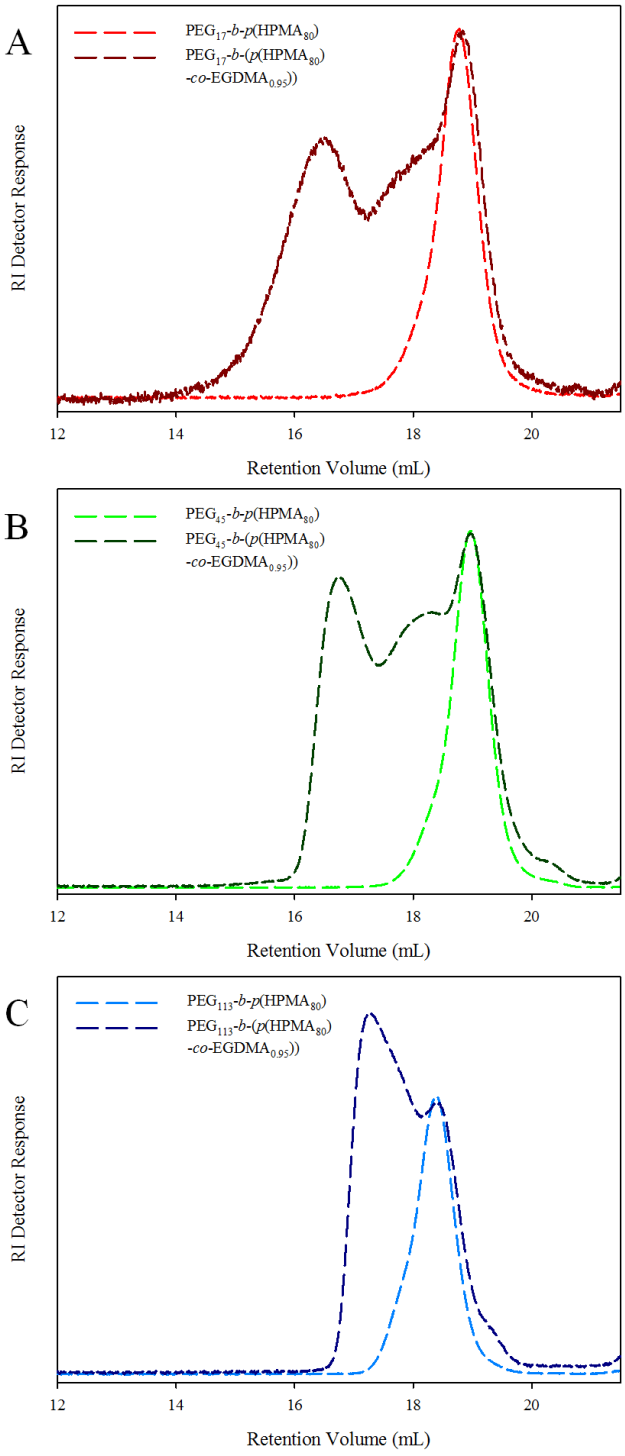


Figure 5.24: GPC (THF eluent) chromatograms of linear and branched *p*($HPMA_{80}$) utilising $PEG_x$ based initiators. A) $PEG_{17}$-Br B) $PEG_{45}$-Br C) $PEG_{113}$-Br.

Figure 5.25 shows multiple detector analyses of three branched copolymers with *p*(HPMA) primary chain lengths of 80 monomer units with varied $PEG_x$-Br macroinitiators. Refractive Index response (RI) is essentially concentration based, and as such, the fraction of linear material decreases with respect to higher molecular weight material as the molecular weight of the initiator increases based on peak heights. By analysing the Right Angle and Low Angle Light Scattering detectors (RALS and LALS) (where materials with larger hydrodynamic volumes scatter much more light (with a scattering dependence proportional to the particle radius$^6$) the majority of the copolymer samples have a branched architecture where scattering at lower retention volumes within all three copolymer samples is observed. The Intrinsic Viscosity (IV) detectors show the majority of scattering exists at lower retention volumes throughout these samples. This is due to branched materials having increased viscosity, in comparison to linear architectures, due to the increased molecular weight. In short summary, by taking into account all of the detector responses during triple detection GPC analysis of these branched copolymers, the presence of linear material is confirmed yet, significant proportions of the materials have high molecular weights and are believed to have branched architectures.

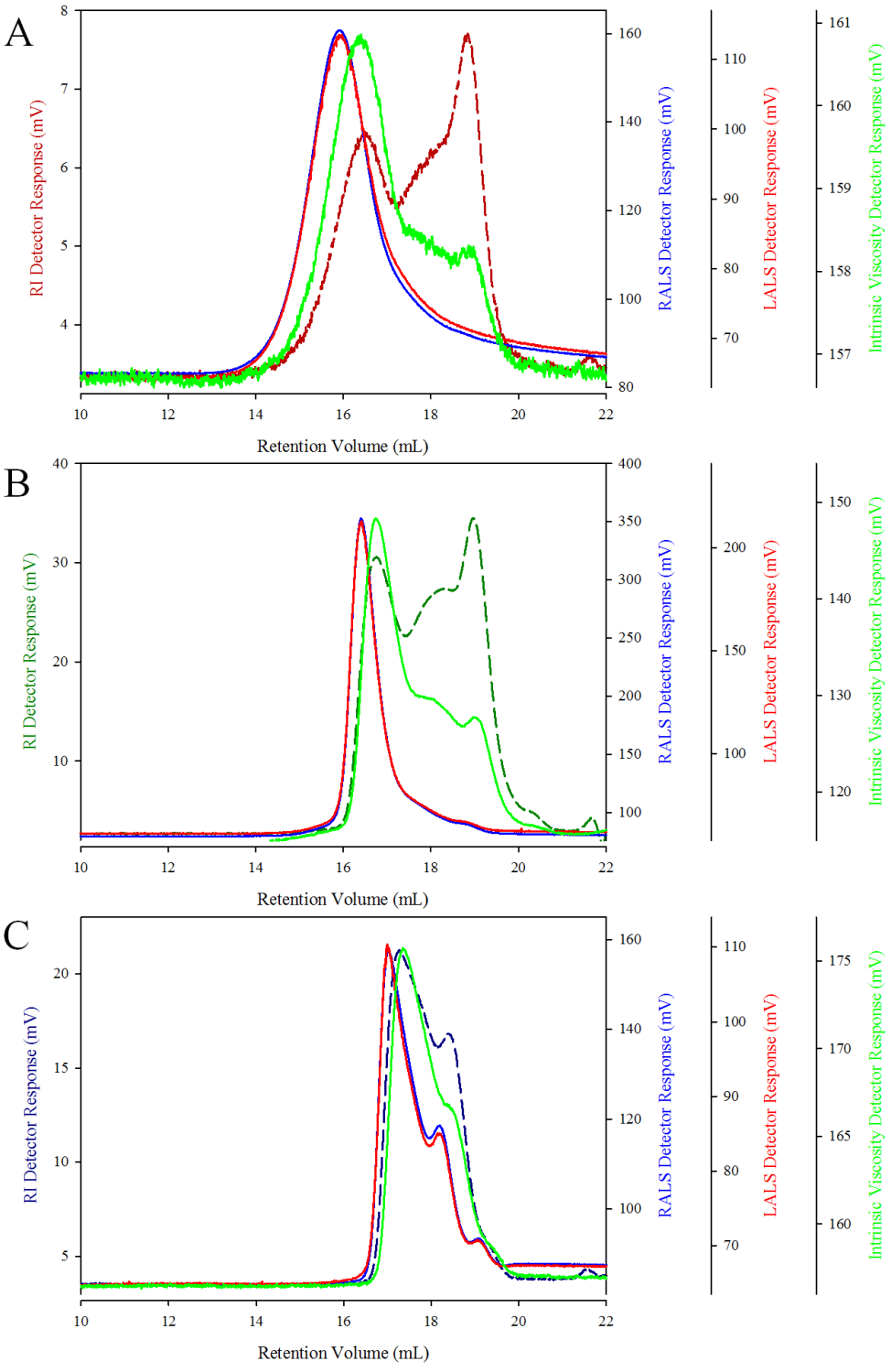


Figure 5.25: GPC chromatograms of $PEG_x$-*b*-(*p*($HPMA_{80}$)-*co*-$EGDMA_{0.95}$)). RALS (blue line), LALS (red line) and Intrinsic Viscosity (green line). A) $PEG_{17}$ RI (dark red dashed line). B) $PEG_{45}$ RI (dark green dashed line). C) $PEG_{113}$ RI (dark blue dashed line)

## 5.9 Copolymerisation Kinetic Studies for $PEG_x$-*b*-(*p*($HPMA_{80}$)-*co*-$EGDMA_{0.95}$)) ($x$ = 17, 45, 113 )

It has been shown that high molecular weight copolymers consisting of various molecular weight PEG based macroinitiators can be synthesised using methanolic ATRP by the addition of an EGDMA brancher. To determine whether these polymerisations proceed in a controlled manner, it was necessary to perform reaction kinetics. All three $PEG_x$-Br macroinitiators were used to synthesise *p*(HPMA) to one target $DP_n$ (80 monomer units) with the addition of EGDMA (0.95 equivalents). These were carried out under identical conditions to those used for their linear counterparts. Regular sampling was performed, where aliquots were analysed by $^1H$ NMR spectroscopy and triple detection GPC (THF eluent). Reactions proceeded to > 99 % conversion after which they were manually terminated.

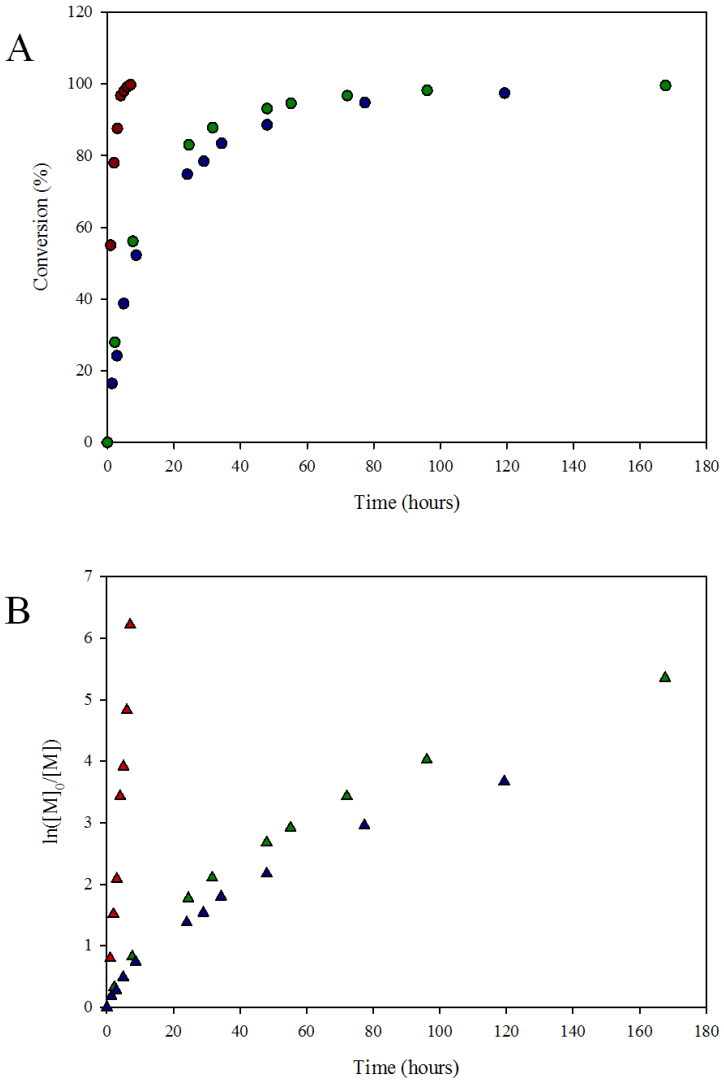


Figure 5.26: Kinetic studies of branched *p*($HPMA_{80}$) using PEG based macroinitiators. A) Conversion *vs*. Time. $PEG_{17}$-Br (dark red), $PEG_{45}$-Br (dark green), $PEG_{113}$-Br (dark blue). B) Semi-logarithmic plot. $PEG_{17}$-Br (dark red), $PEG_{45}$-Br (dark green), $PEG_{113}$-Br (dark blue).

Figure 5.26(A) shows conversion *vs*. time plots for each polymerisation conducted. All three graphs show the characteristic curvature synonymous with ATRP mechanisms, where the majority of the monomer feed is consumed within a short period of time due to the high concentration of unreacted monomer, in the early

stages of polymerisation. After approximately 80 % conversion, the rate of monomer conversion decreases, due to the depletion of HPMA monomer in conjunction with the increased viscosity of solution, until extremely high conversions are reached (where it is believed reactions are mainly diffusion controlled). It should be noted that the copolymerisation which utilises $PEG_{17}$-Br reaches > 99 % conversion in a significantly shorter space of time when compared to the other copolymerisations. This behaviour is identical to that seen for their linear counterparts, which is attributed to differences in viscosity, where the molecular weight of this initiator is significantly less than that of the other initiators. It is thought $PEG_{17}$-Br has increased chain mobility (compared to $PEG_{45}$-Br and $PEG_{113}$-Br), and therefore chains are able to polymerise at a faster rate. The semi logarithmic plot for $PEG_{17}$-*b*-(*p*($HPMA_{80}$)-*co*-$EGDMA_{0.95}$)), shown in Figure 5.26(B), is linear with respect to time although the other plots curve downwards slightly at higher reaction times, suggesting some termination is occurring during the later stages of copolymerisation. As these reactions take upwards of 80 hours to reach extremely high conversion, and coupled with the extremely high viscosity (due to the high molecular weight branched structures), the probability of active chain ends coupling with each other is higher than the probability of monomer addition.

Despite these discrepancies, data suggests that branched polymerisations follow a conventional ATRP mechanism. It is believed that this is the first report on the study of branched copolymers which utilise $PEG_x$-Br (or indeed any) macroinitiators. In Chapter 3 (section 3.3.1), linear and branched kinetics data was compared (utilising EBiB as the initiator), indicating that the branched copolymerisation proceed at slightly slower rates compared to linear counterparts. Having now reported both

linear and branched analogues for copolymerisations utilising PEG based macroinitiators, kinetics data results can be compared (shown in Figure 5.27).

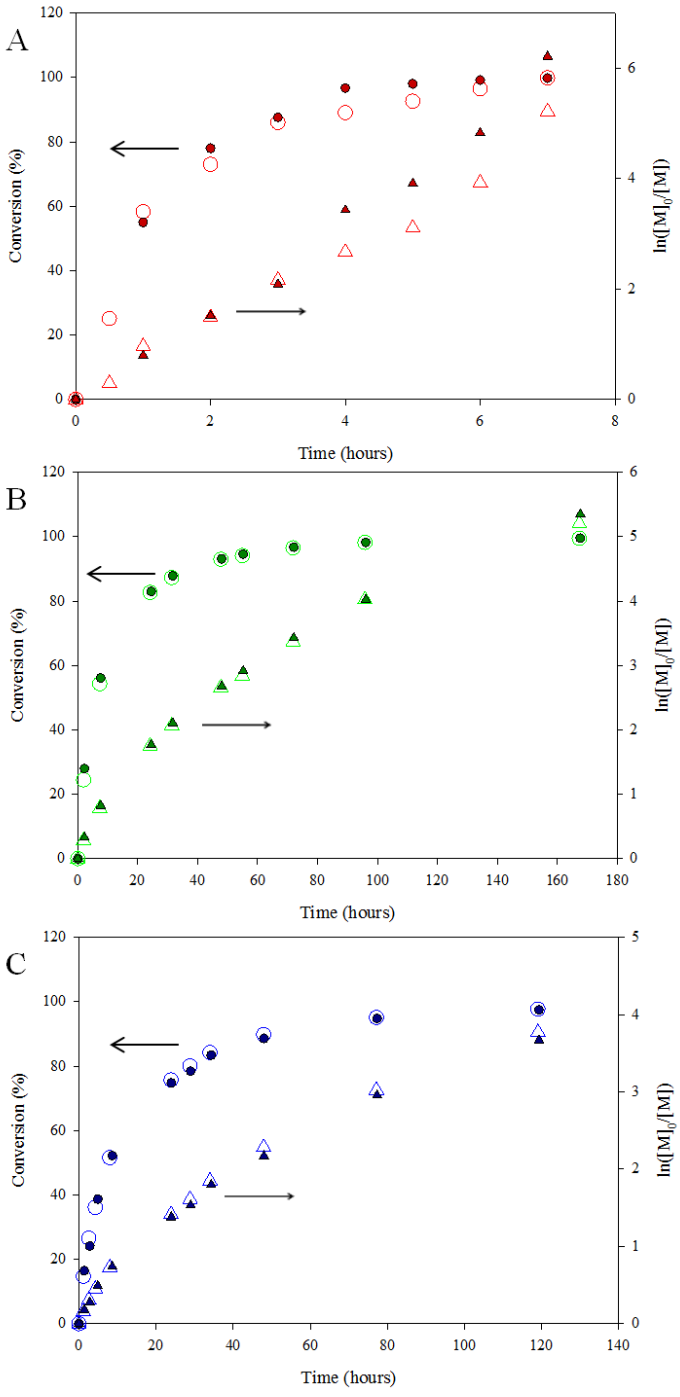


Figure 5.27: Kinetics plots for linear (open symbols) and branched (full symbols) copolymerisations of *p*(HPMA$_{80}$) using various PEG macroinitiators. A) PEG$_{17}$-Br, B) PEG$_{45}$-Br, C) PEG$_{113}$-Br.

Figure 5.27 clearly shows near identical kinetics data obtained for linear and branched copolymerisations utilising PEG macroinitiators, despite varying the molecular weight of the initiator. This consistent behaviour leads to the conclusion that, incorporation of EGDMA has absolutely little to no effect on reaction kinetics when compared to linear analogues in systems also containing PEGx-Br initiators. This is somewhat surprising, but nevertheless the data highlights the capabilities of these macroinitiators.

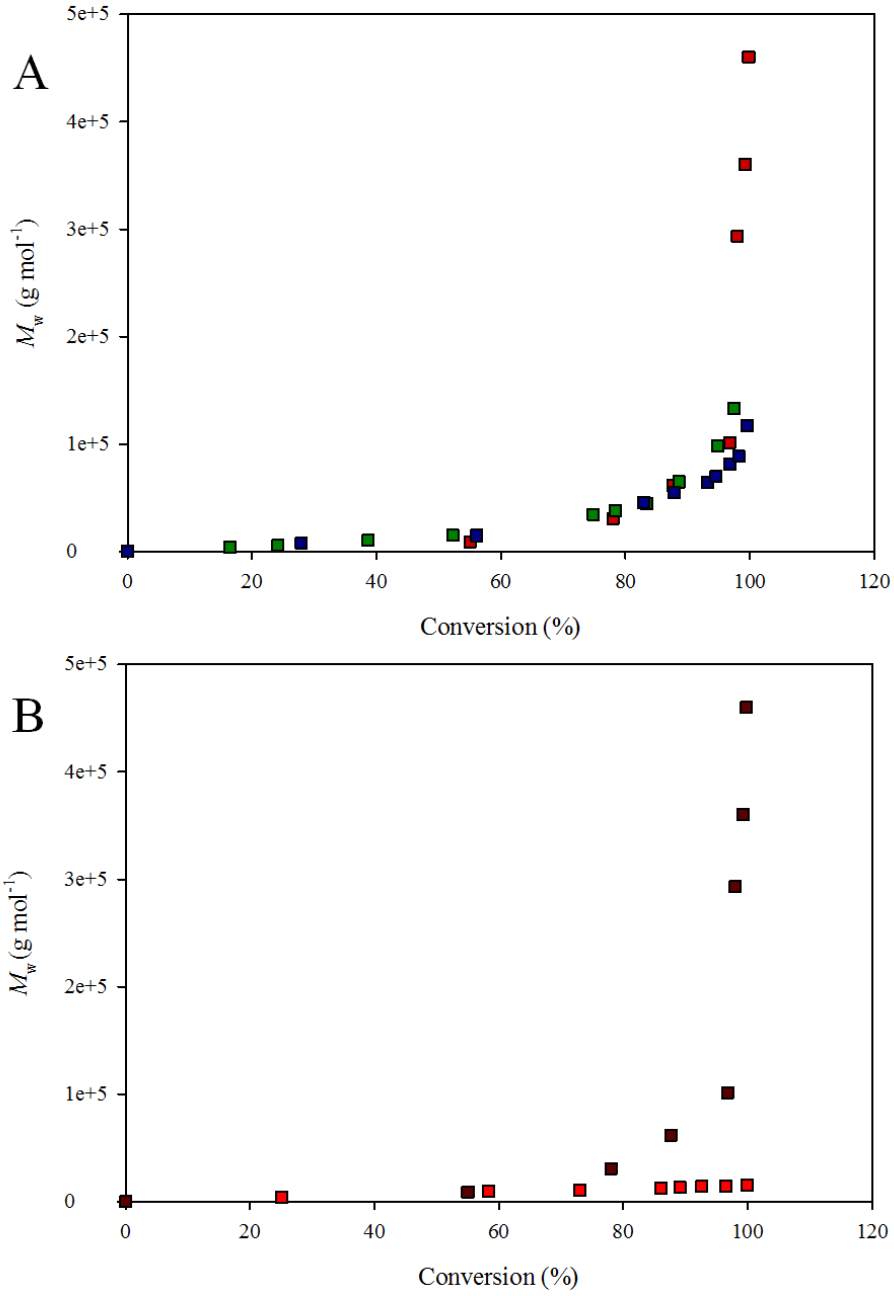


Figure 5.28: Evolution of $M_w$ with conversion. A) $PEG_x$-*b*-(*p*($HPMA_{80}$)-*co*-$EGDMA_{0.95}$)) $PEG_{17}$-Br (dark red), $PEG_{45}$-Br (dark green), $PEG_{113}$-Br (dark blue). B) $PEG_{17}$-*b*-*p*($HPMA_{80}$) (red) and $PEG_{17}$-*b*-(*p*($HPMA_{80}$-*co*-$EGDMA_{0.95}$) (dark red).

Figure 5.28 (A) shows the high molecular weights achieved during these branched copolymerisations utilising PEG macroinitiators. The molecular weights of each

copolymerisation begins to increase dramatically after approximately 85 % conversion has been reached; indicative of the covalent linking of polymer chains dominating the latter stages of copolymerisation, where monomer feed has become almost exhausted. This is in complete agreement with the results in Chapter 3 (section 3.3.1). The comparison between the evolution of molecular weight in linear and branched systems which both employ a $PEG_x$-Br macroinitiator is shown in Figure 5.28(B). This highlights the very different development of weight average molecular weight when utilising EGDMA in the initial monomer feed.

### 5.9.1 Comparison of *p*($HPMA_{80}$)-*co*-$EGDMA_{0.95}$ and $PEG_{17}$-*b*-(*p*($HPMA_{80}$)-*co*-$EGDMA_{0.95}$)) Reaction Kinetics.

The controlled branched copolymerisations of *p*($HPMA_x$) utilising PEG based macroinitiators have been discussed where trends in kinetic data are attributed to changes in the molecular weight (or number of ethylene oxide repeat units) in the PEG based macroinitiators. Here, the branched reaction kinetics of *p*($HPMA_{80}$) utilising EBiB and $PEG_{17}$-Br as initiators are compared. Unfortunately, due to their significant reaction times, it was not possible to include the reaction kinetics employing $PEG_{45}$-Br and $PEG_{113}$-Br on the same graph scales.

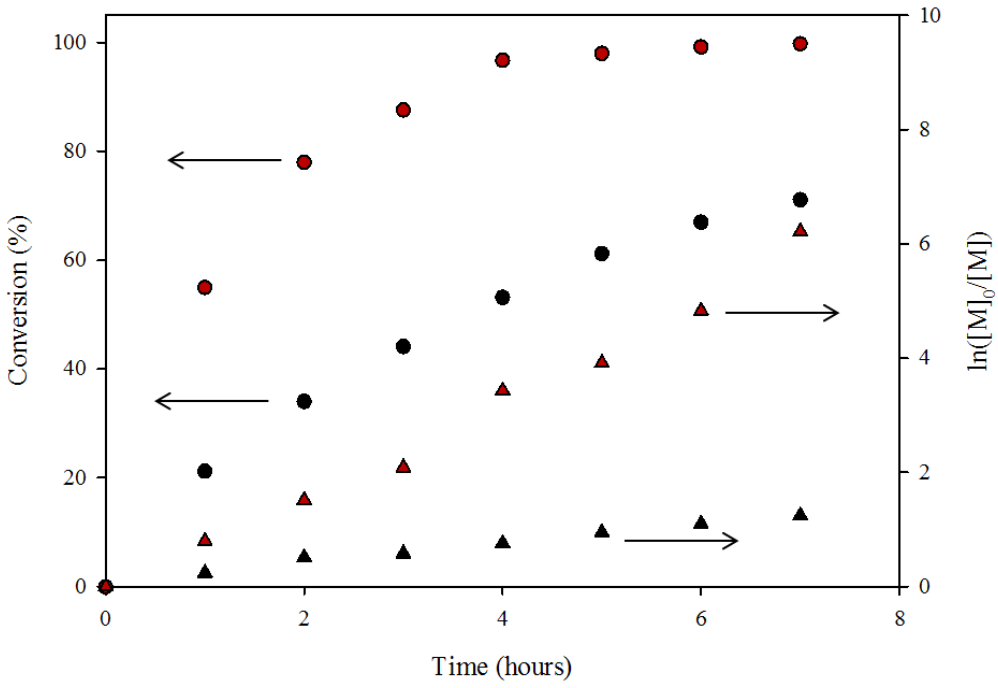


Figure 5.29: Kinetics plots for *p*(HPMA$_{80}$)-*co*-EGDMA$_{0.95}$ (black symbols) and PEG$_{17}$-*b*-(*p*(HPMA$_{80}$)-*co*-EGDMA$_{0.95}$)) (dark red symbols).

Figure 5.29 shows the marked difference in reaction kinetics between the two copolymerisations. Quite surprisingly, much more monomer is consumed during the early stages of polymerisation when the PEG based macroinitiator is employed, suggesting this initiator is more efficient than EBiB. The rate of reaction is much faster when utilising PEG$_{17}$-Br in comparison to EBiB, due to its steeper gradient. However, no solid conclusions can be drawn from this set of data due to concentration differences with respect to catalyst/ligand within the reactions. This concentration difference is unfortunately unavoidable, as the volume of solvent used is based on the mass of the initiator (and monomer) and as this has changed, the concentration of catalyst/ligand is also changed. Both reactions were conducted at ambient temperature and this also could have affected the rate of polymerisation.

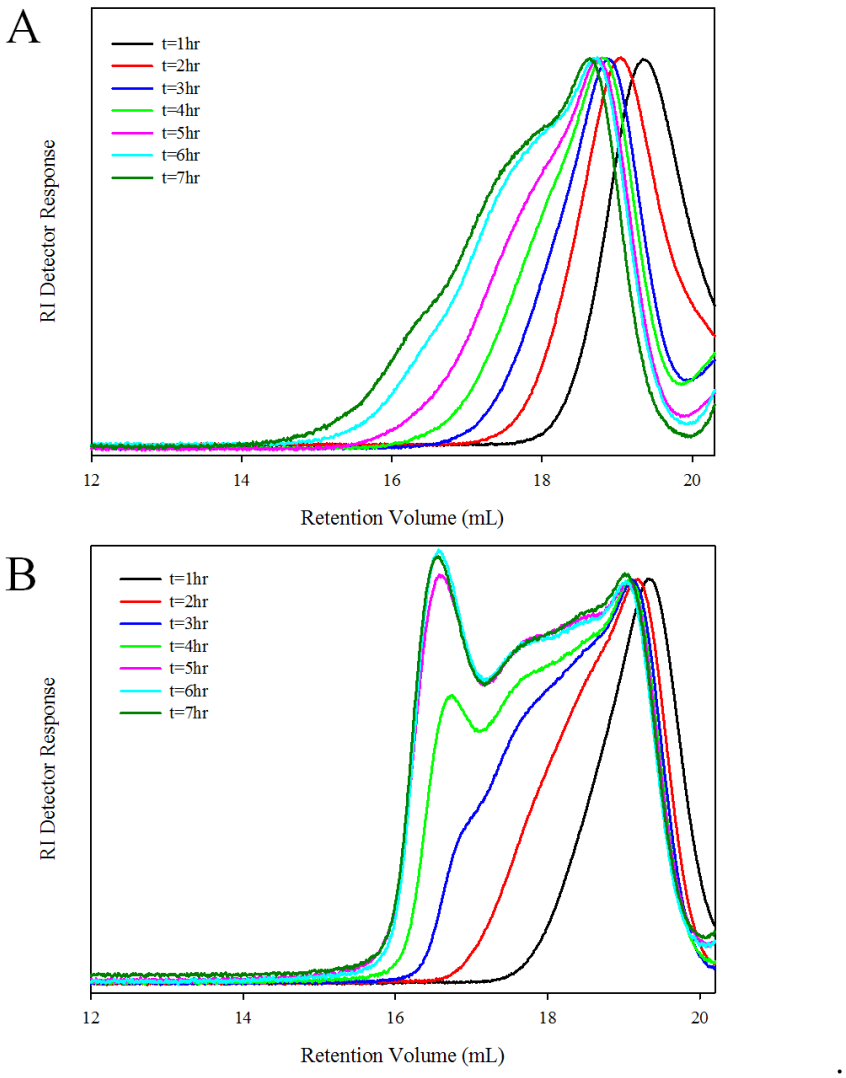


Figure 5.30: GPC chromatograms of kinetics studies for branched copolymerisations. A) *p*(HPMA$_{80}$)-*co*-EGDMA$_{0.95}$ B) PEG$_{17}$-*b*-(*p*(HPMA$_{80}$)-*co*-EGDMA$_{0.95}$)).

In the previous section it was found that as the molecular weight of the initiator increases, the ability to generate extremely high molecular weights decreases. To demonstrate this effect, Figure 5.30 shows GPC traces for kinetic experiments performed using EBiB, Figure 5.30(A), and PEG$_{17}$-Br, Figure 5.30(B), initiators where the development of branching within the systems can be seen. Figure 5.30(A) shows that the development of branching is occurring even at extremely high

conversions, indicated by the tailing of the RI trace at low retention volumes. In stark contrast to this, when utilising $PEG_{17}$-Br, Figure 5.30(B), little to no branching occurs at these high molecular weights, although the proportion of high molecular weight material in comparison to linear is much higher.

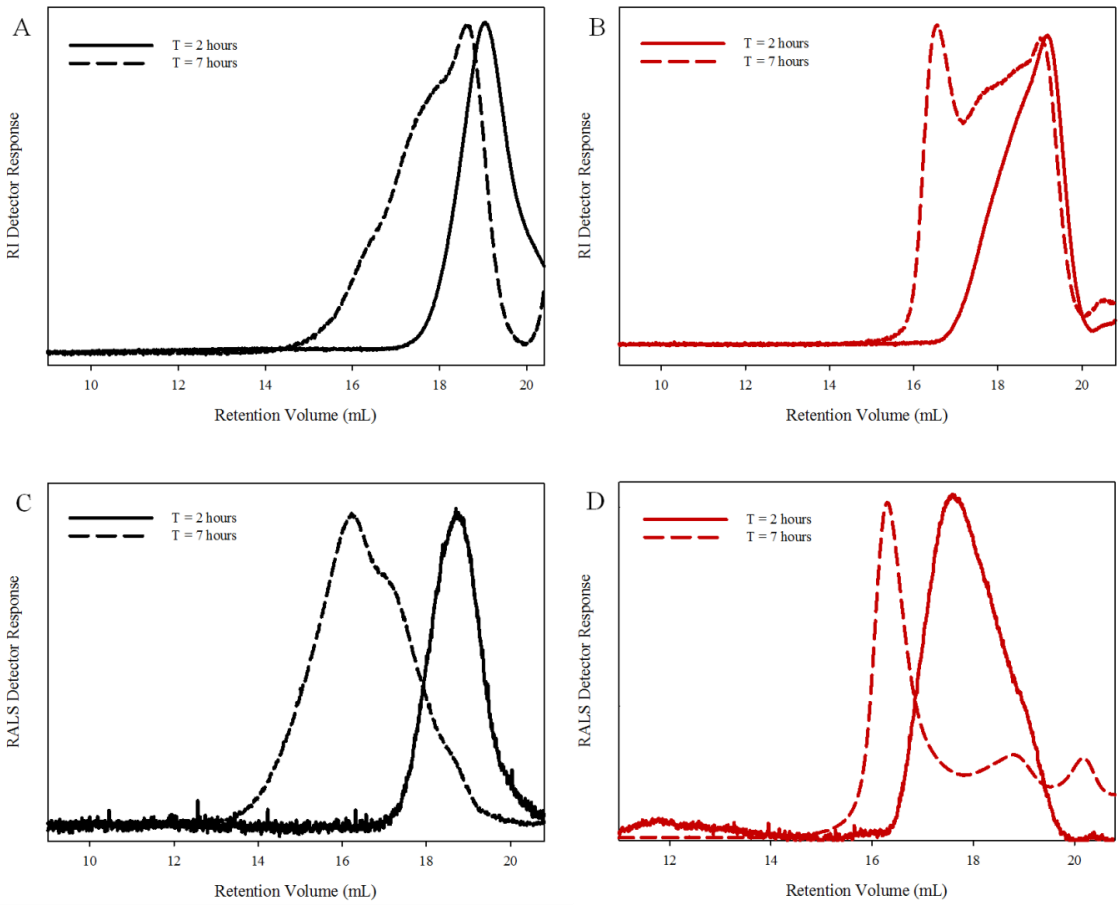


Figure 5.31: GPC chromatograms of branched copolymers at different stages of polymerisation. *p*($HPMA_{80}$)-*co*-$EGDMA_{0.95}$ (black traces), $PEG_{17}$-*b*-(*p*($HPMA_{80}$)-*co*-$EGDMA_{0.95}$)) (red traces). RI detector responses (A) and (B), RALS detector responses (C) and (D).

Along with their RI detector responses, Figure 5.31 also shows the response from the RALS detector at two selected times during branched copolymerisations, where different initiators are employed. When EBiB is employed, significant tailing at high

conversion is seen in both detectors, whereas when $PEG_{17}$-Br is utilised no tailing is observed. It should be noted here that the RALS detector evaluates the amount of light scattering and is therefore heavily weighted towards larger (higher molecular weight) materials, and as such, little scattering due to low molecular weight material is expected, as observed in Figure 5.31(D). After 7 hours, a significant proportion of linear and lightly branched material is apparent, in contrast to Figure 5.31(C). This suggests that branching is somewhat hindered when utilising PEG based macroinitiators under these conditions.

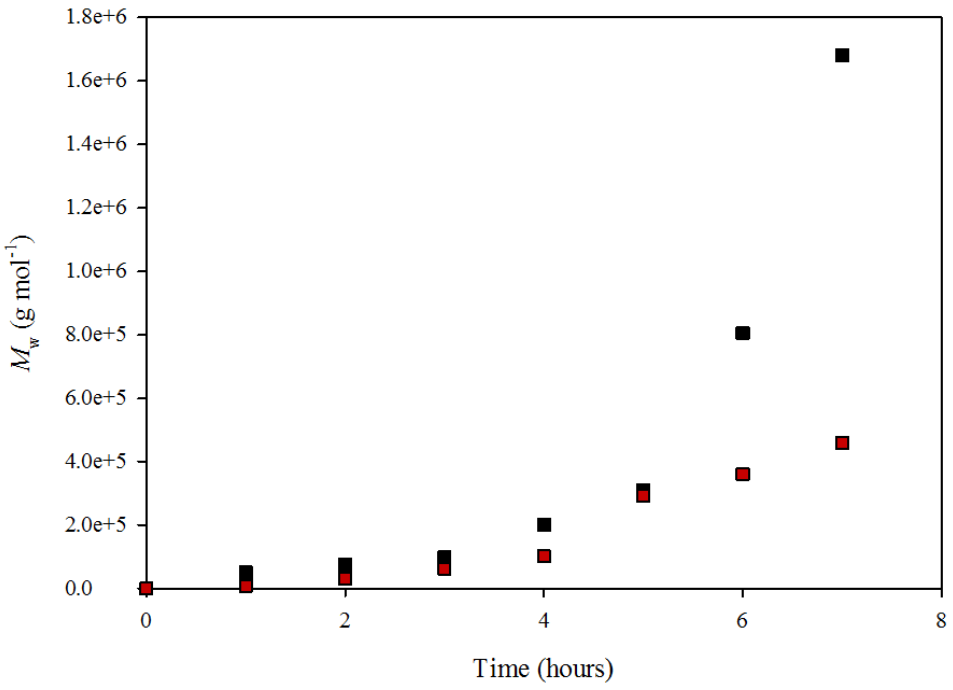


Figure 5.32: Evolution of $M_n$ during *p*(HPMA$_{80}$)-*co*-EGDMA$_{0.95}$ (black) and $PEG_{17}$-*b*-(*p*(HPMA$_{80}$)-*co*-EGDMA$_{0.95}$)) copolymerisations.

Alongside the GPC traces, the lack of tailing at low retention volumes is seen in Figure 5.32 suggests that utilising the $PEG_{17}$-Br initiator (and under near identical reaction conditions) extremely high molecular weight is not achieved, when

compared to the copolymerisation utilising EBiB. This suggests $PEG_x$-Br initiators in some way direct the branching process within these systems. In conjunction to this, as the molecular weight of the initiator increases, the system becomes increasingly unable to achieve highly branched materials. The exact reason or reasons for this are unknown, but it is likely that as the viscosity of the solution (increasing as PEG chain length increases), the active chain ends become hidden within the branched copolymer structure and are therefore unable to react with pendant vinyl groups, or even another active chain end of another branched copolymer. It may also be possible that the increasing size of the macroinitiator may prevent the physical proximity of chains required to generate intermolecular branching. If this is true, some cyclisation or abstraction of protons from the surrounding solution may be occurring and preventing copolymers reaching the extreme molecular weights seen when using EBiB as the initiator.

## 5.10 Summary

In this chapter it has been shown that a series of linear copolymers with varying $PEG_x$-Br initiators as well as varying *p*($HPMA_x$) primary chain length, can be synthesised using identical conditions to the EBiB initiated homopolymers synthesised in Chapter 3 (section 3.2), with individual kinetics data interpreted. The target primary chain length can be adjusted, yielding polymers with narrow molecular weight distributions and highly accurate targeted molecular weights. It has been shown that copolymer chains can be extended using a "self-blocking" technique, producing polymers with accurate molecular weights. The branching of these polymers has been performed (using EGDMA) with no experimental difficulty, supported by kinetic data, where high molecular weights soluble polymers can be

prepared. The difference in the branching process (characterised by GPC analysis) has been compared to that observed in Chapter 3 (section 3.3.1). Based on experimental results, there is a direct link between the chain length of the PEG based macroinitiator and the resultant molecular weight of the final branched copolymers.

## 5.11 References

1 Ma. Y. H., Tang. Y. Q., Billingham. N. C., Armes. S. P., Lewis. A. L., Lloyd. A. W., Salvage. J. P., *Macromolecules*, **2003**, *36*, 3475.

2 Save. M., Weaver. J. V. M., Armes. S. P., McKenna. P., *Macromolecules*, **2002**, *35*, 1152.

3 Darcos. V., Haddleton. D. M., *Eur Polym J*, **2003**, *39*, 855.

4 Lobb. E. J., Ma. I., Billingham. N. C., Armes. S. P., Lewis. A. L., *J Am Chem Soc*, **2001**, *123*, 7913.

5 Weaver. J. V. M., Bannister. I., Robinson. K. L., Bories-Azeau. X., Armes. S. P., Smallridge. M., McKenna. P., *Macromolecules*, **2004**, *37*, 2395.

6 Wang. X. S., Lascelles. S. F., Jackson. R. A., Armes. S. P., *Chem Commun*, **1999**, 1817.

7 Wang. X. S., Armes. S. P., *Macromolecules*, **2000**, *33*, 6640.

8 Mao B., Gan. L. H., Gan. Y. Y., Li. X., Ravi. P., Tam. K. C., *J Polym Sci, Part A: Polym Chem*, **2004**, *42*, 5161.

9 Jankova. K., Chen. X., Kops. J., Batsberg. W., *Macromolecules*, **1998**, *31*, 538.

10 Ma. I. Y., Lobb. E. J., Billingham. N. C., Armes. S. P., Lewis. A. L., Lloyd. A. W., Salvage. J., *Macromolecules*, **2002**, *35*, 9306.

11 Bannister. I., Billingham. N. C.,. Armes. S. P., *Soft Matter*, **2009**, *5*, 3495.

# 6. Synthesis of loaded and un-loaded Polymeric Nanoparticles using PEG Copolymers

## 6.1 Introduction

In Chapter 4 section 4.4.12, it was found that extremely stable nanoparticles consisting solely of branched *p*(HPMA$_x$) could be prepared using a rapid precipitation approach from acetone (see Chapter 2 section 2.5.1.1). It is believed their stability arises due to charge stabilisation and the branched architecture of the polymers. Through the variation of concentration of dissolved polymer in acetone and also the final nanoparticle concentration in water, their z-average diameters could be controlled. In this section, nanoprecipitation (from acetone) of branched PEG$_x$ containing copolymers (see synthesis and characterisation in Chapter 2 section 2.4.2) is explored in order to determine whether the same degree of control of z-average diameter is found.

It should be noted the reason for the absence of loaded nanoparticles consisting of linear copolymers is twofold; 1. All nanoprecipitation of linear copolymers produced size distributions with bimodal traces. 2. Similar to results in Chapter 4, these nanoparticles were not stable for significant periods of time with precipitation evident after 2 days. As these polymers exert partial aqueous solubility (due to the PEG$_x$ content in the polymers) it was anticipated that nanoparticles would be more stable (with respect to time) in comparison to their non-PEG$_x$ containing linear counterparts; however, this was not the case and precipitation of polymer (regardless of DP$_n$) was observed after just two days.

The rationale of branched polymer nanoparticle formation will be discussed and compared to non-$PEG_x$ containing nanoparticle formation. Following this discussion, investigation into the loading capabilities of the particles will be explored with DLS size analysis. This was achieved through co-dissolving candidate materials within the original polymer/acetone solution followed by identical nanoprecipitation protocols used for blank particle formation.

## 6.2 Rapid nanoprecipitation of $PEG_x$-*b*-*p*($HPMA_y$) where *x*= 17, 45, 113 and *y* = 50, 80, 120

Nanoparticles containing linear $PEG_x$ containing *p*($HPMA_x$) copolymers were generated using the rapid precipitation method described in the Chapter 2 section 2.5.1.1 with a starting copolymer concentration of 10 mg $mL^{-1}$ in acetone. Each of the nine previously synthesised copolymers were diluted five-fold into warmed water, giving a final aqueous concentration of 2 mg $mL^{-1}$. After acetone removal, dynamic light scattering was used to determine z-average diameters of resultant nanoparticles. It should be noted that the recorded sizes are an average of six measurements and although precipitation occurred after approximately two days these measurements were performed after one day of preparation and as such the data met the quality criteria for successful size determination (i.e. aggregation was not observed).

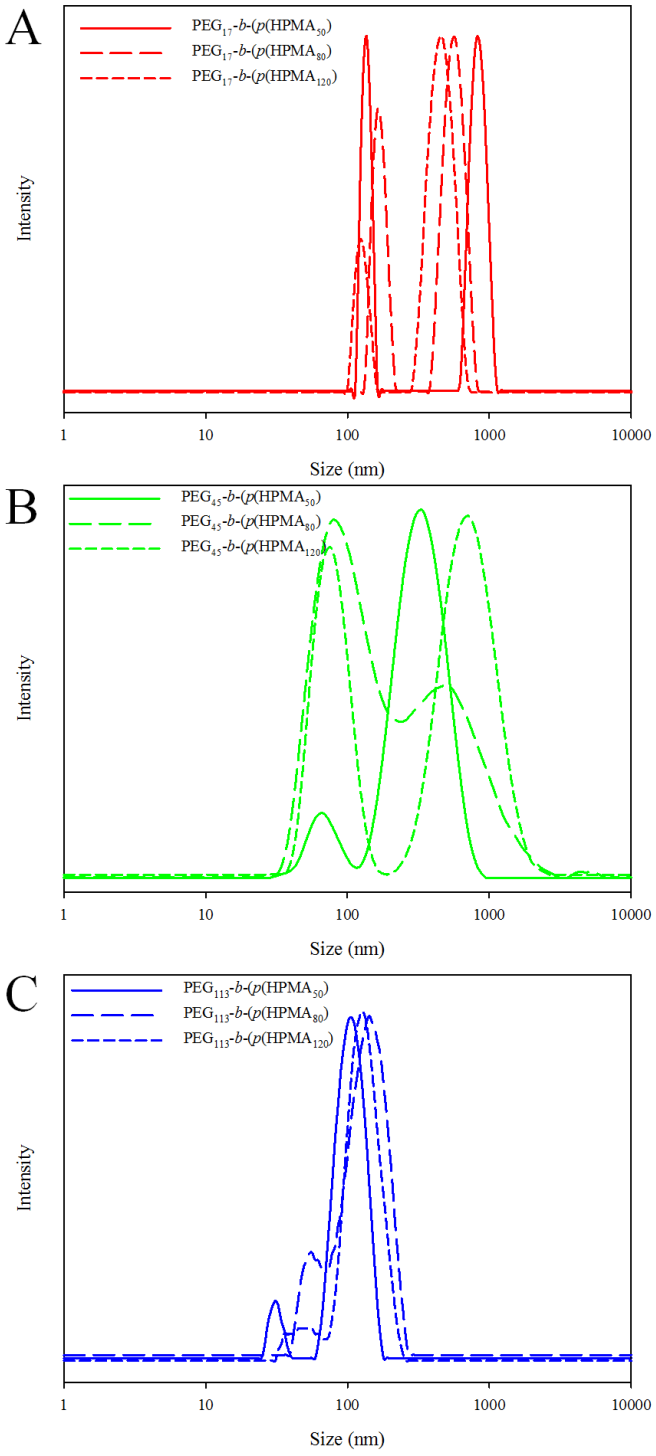


Figure 6.1: DLS measurements for linear $PEG_x$ copolymer nanoparticles using a rapid precipitation approach varying $p(HPMA_x)$ primary chain length. (10 mg $mL^{-1}$ starting concentration, 2 mg $mL^{-1}$ final concentration). A) $PEG_{17}$ B) $PEG_{45}$ C) $PEG_{113}$.

| Copolymer | Peak 1 Diameter (nm)*[a] | Peak 2 Diameter (nm)*[b] | Polydispersity Index*[c] |
|---|---|---|---|
| $PEG_{17}$-*b*-*p*($HPMA_{50}$) | 136 | 837 | 0.674 |
| $PEG_{17}$-*b*-*p*($HPMA_{80}$) | 168 | 568 | 0.269 |
| $PEG_{17}$-*b*-*p*($HPMA_{120}$) | 126 | 461 | 0.238 |
| $PEG_{45}$-*b*-*p*($HPMA_{50}$) | 70 | 348 | 0.270 |
| $PEG_{45}$-*b*-*p*($HPMA_{80}$) | 104 | 610 | 0.429 |
| $PEG_{45}$-*b*-*p*($HPMA_{120}$) | 79 | 765 | 0.643 |
| $PEG_{113}$-*b*-*p*($HPMA_{50}$) | 31 | 107 | 0.142 |
| $PEG_{113}$-*b*-*p*($HPMA_{80}$) | 56 | 141 | 0.167 |
| $PEG_{113}$-*b*-*p*($HPMA_{120}$) | 53 | 134 | 0.156 |

Table 6.1: DLS analysis of nanoparticles comprised of $PEG_x$ containing linear copolymers prepared by rapid precipitation. 10 mg $mL^{-1}$ starting concentration, 2 mg $mL^{-1}$ final concentration. *[a] peak with smallest diameter, *[b] peak with largest diameter, *[c] of both peaks.

Figure 6.1 (A-C) clearly shows the lack of monomodality and also of any apparent trends due to either variation of $PEG_x$ or *p*($HPMA_x$) chain length. This data shows that near identical behaviour to the linear *p*($HPMA_x$) containing nanoparticles (see Chapter 4 section 4.4) is observed here; although these nanoparticles contain $PEG_x$ stabilising chains this does not appear to aid in producing particles within a uniform size range. It is noted that there are particles generated which are approximately 100 nm in size which is consistent with previous nanoparticle sizes (see Chapter 4 section 4.4) yet much larger particles are also formed (> 100 nm) when utilising $PEG_{45}$ and $PEG_{113}$ macroinitiators regardless of the primary chain length of *p*($HPMA_x$) (Figure 6.1 (A) and (B)). By utilising $PEG_{17}$ two size distributions are found but both have much narrower polydispersities compared to $PEG_{45}$, where traces are not as well-defined. This can only be attributed to the influence of the

larger $PEG_x$ chains as identical experimental protocols were followed. Increasing $PEG_x$ chain length, resultant nanoparticles have much narrower polydispersities regardless of $DP_n$, (e.g. 0.142 for $PEG_{113}$-*b*-*p*($HPMA_{50}$) compared to 0.27 for $PEG_{45}$-*b*-*p*($HPMA_{50}$) and do not produce larger nanoparticles, as shown in Table 6.1. This behaviour is believed to be due to the high aqueous solubility of these polymers; however, the exact reasons are unknown.

## 6.3 Nanoprecipitation of $PEG_x$-*b*-*p*($HPMA_{80}$) using the dialysis method where *x*= 17, 45, 113

Dialysis was performed on the linear copolymers $PEG_{17}$-*b*-*p*($HPMA_{80}$), $PEG_{45}$-*b*-*p*($HPMA_{80}$) and $PEG_{113}$-*b*-*p*($HPMA_{80}$) to determine whether this method would produce well-defined and stable nanoparticles, when compared to the rapid precipitation approach. This process allows copolymers to progressively arrange themselves into the most energetically stable structure(s) through the loss of solubility and can be thought of as a thermodynamic process; in contrast, the rapid precipitation approach–subjects the copolymers to a quick solvent switch and the chains must therefore quickly arrange themselves into structures. This may be thought of as a kinetic-driven process. As described in Chapter 2 section 2.5.1.1, copolymers were first dissolved in acetone at 10 mg $mL^{-1}$ and slowly dripped into warmed stirring water to give a final copolymer concentration of 2 mg $mL^{-1}$ and the mixtures were carefully poured into sections of dialysis tubing, placed into large water filled beakers for two days and the surrounding sink water was changed approximately every eight hours. The use of slow dropping method was due to a range of literature reports that also describe this approach for amphiphilic A-B linear block copolymers.[1] Size determination was performed on the nanoparticulate

solutions without further purification and/or filtration and measurement data is displayed in Figure 6.2 and Table 6.2.

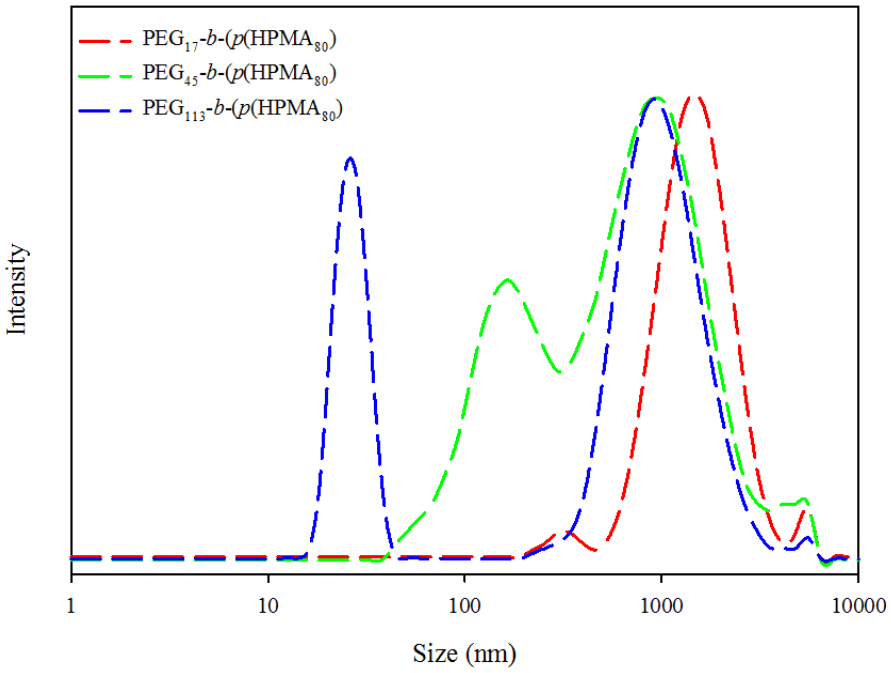


Figure 6.2: DLS size determination of nanoparticles comprising of $PEG_x$ containing linear copolymers using dialysis. 10 mg $mL^{-1}$ starting concentration, 2 mg $mL^{-1}$ final concentration.

| Copolymer | Peak 1 Diameter (nm)*[a] | Peak 2 Diameter (nm)*[b] | Polydispersity Index*[c] |
|---|---|---|---|
| $PEG_{17}$-*b*-*p*($HPMA_{50}$) | 322 | 1569 | 0.293 |
| $PEG_{45}$-*b*-*p*($HPMA_{80}$) | 168 | 1040 | 0.562 |
| $PEG_{113}$-*b*-*p*($HPMA_{80}$) | 27 | 1090 | 1 |

Table 6.2: DLS size data of nanoparticles consisting of $PEG_x$ containing linear copolymers prepared by dialysis. 10 mg $mL^{-1}$ starting concentration, 2 mg $mL^{-1}$ final concentration. *[a] peak with smallest diameter. *[b] peak with largest diameter, *[c] of both peaks.

It is clear from Figure 6.2 and Table 6.2 that this dialysis route was not able to achieve monomodal nanoparticle samples, regardless of the $PEG_x$ initiator used to prepare the A-B block copolymers. However, only a small peak at 322 nm is found using copolymers containing $PEG_{17}$, and the majority of particles are approximately 1569 nm in size. It is noted that for each polymer, Peak 1 not only decreases in size but also increases in intensity (relative to the corresponding Peak 2) as the molecular weight of $PEG_x$ increases. The exact reason for this is unknown; however, it is likely to be due to the inherent solubility of the copolymers (i.e. increasing with increasing $PEG_x$ molecular weight). In an effort to optimise the dialysis approach and produce single distributions of particles (with varying $PEG_x$ content) a lower starting concentration of polymer/acetone solution was chosen (5 mg $mL^{-1}$), however, the experimental protocol remained whereby the solution was diluted five-fold achieving a final concentration of 1 mg $mL^{-1}$. It was thought by reducing the initial polymer/acetone solution the formation of particles would be more controlled as the particles form from a more dilute solution.

By reducing the initial polymer/acetone concentration it is found that generally smaller particles form despite experimental protocols remaining the same (Figure 6.3 and Table 6.3. The largest nanoparticles are formed utilising $PEG_{45}$, generating nanoparticles which are approximately 590 nm in diameter (compared to 1569 nm, using a starting concentration of 10 mg $mL^{-1}$). Perhaps the most marked difference is found between particle diameters comprising of $PEG_{113}$-*b*-*p*($HPMA_{80}$) where not only monomodality has been achieved but nanoparticle size has been reduced by almost 1000 nm by simply altering the polymer/acetone concentration.

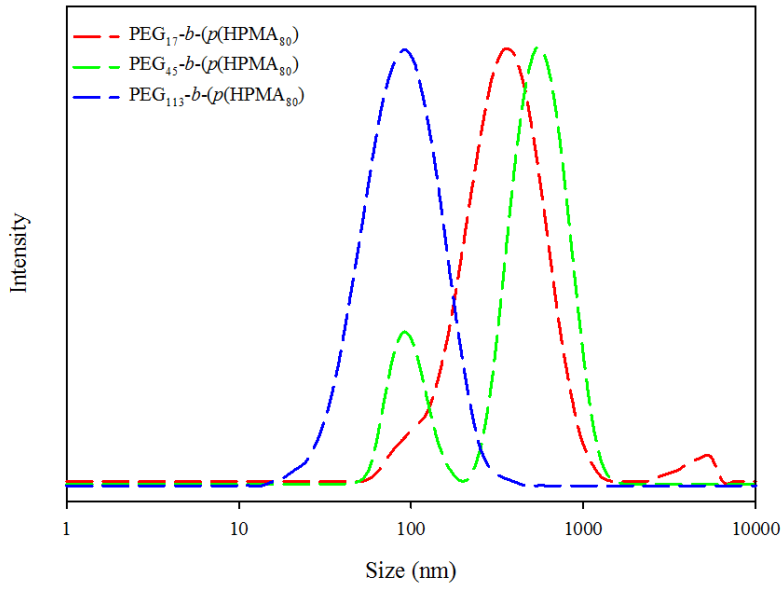


Figure 6.3: DLS size determination of nanoparticles comprising of $PEG_x$ containing linear copolymers using dialysis. 5 mg $mL^{-1}$ starting concentration, 1 mg $mL^{-1}$ final concentration.

| Copolymer | Peak 1 Diameter (nm)*[a] | Peak 2 Diameter (nm)*[b] | Polydispersity Index*[c] |
|---|---|---|---|
| $PEG_{17}$-*b*-*p*($HPMA_{80}$) | 379 | / | 0.250 |
| $PEG_{45}$-*b*-*p*($HPMA_{80}$) | 99 | 587 | 0.465 |
| $PEG_{113}$-*b*-*p*($HPMA_{80}$) | 98 | / | 0.261 |

Table 6.3: DLS size data of nanoparticles consisting of $PEG_x$ containing linear copolymers prepared by dialysis. 5 mg $mL^{-1}$ starting concentration, 1 mg $mL^{-1}$ final concentration. *[a] peak with smallest diameter. *[b] peak with largest diameter, *[c] of both peaks.

The concentration of the initial polymer/acetone solution clearly has a direct impact on resultant nanoparticle diameters (regardless of PEG chain length). As previously noted, the exact mechanism of particle formation is unknown, yet it is speculated

that the materials generated by the linear polymers are uncontrolled in their formation and can generate mixed populations. The previous dialysis techniques involved the slow addition of polymer/acetone solutions (at either 10 mg $ml^{-1}$ or 5 mg $mL^{-1}$) into warmed stirring water achieving a five-fold dilution (2 mg $mL^{-1}$ or 1 mg $mL^{-1}$); experimentally this is time consuming and syringe pumps were utilised. It was questioned whether similar size distributions of resultant nanoparticles would be found if rapid precipitation approach of polymer/acetone was employed into water, followed by dialysis. A starting concentration of 5 mg $mL^{-1}$ was chosen as this produced the smallest nanoparticles (regardless of $PEG_x$) and DLS size data is shown in Figure 6.4 and Table 6.4.

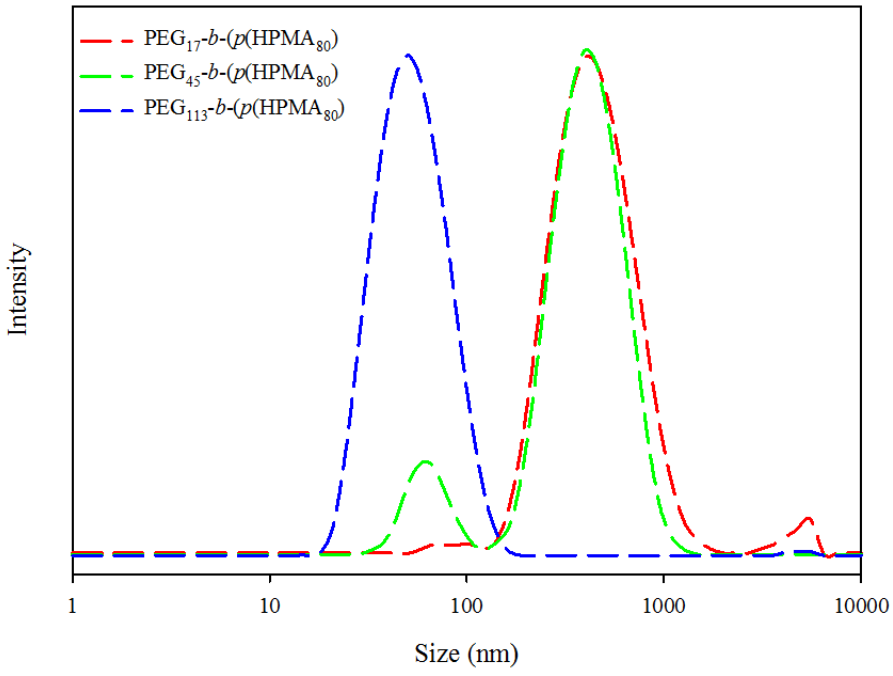


Figure 6.4: DLS size determination of nanoparticles comprising of $PEG_x$ containing linear copolymers using a modified dialysis approach . 5 mg $mL^{-1}$ starting concentration, 1 mg $mL^{-1}$ final concentration.

| Copolymer | Peak 1 Diameter (nm)*[a] | Peak 2 Diameter (nm)*[b] | Polydispersity Index*[c] |
|---|---|---|---|
| $PEG_{17}$-*b*-*p*($HPMA_{80}$) | 87 | 477 | 0.261 |
| $PEG_{45}$-*b*-*p*($HPMA_{80}$) | 65 | 441 | 0.361 |
| $PEG_{113}$-*b*-*p*($HPMA_{80}$) | 56 | / | 0.162 |

Table 6.4: DLS size data of nanoparticles consisting of $PEG_x$ containing linear copolymers prepared by a modified dialysis approach. 5 mg $mL^{-1}$ starting concentration, 1 mg $mL^{-1}$ final concentration. *[a] peak with smallest diameter. *[b] peak with largest diameter, *[c] of both peaks.

This experiment has shown that there is little difference in the shapes of size distributions by employing a rapid precipitation (followed by dialysis), rather than a slow dripping method (followed by dialysis). For example, both $PEG_{17}$ and $PEG_{45}$ contain material < 100 nm with intensity increasing with $PEG_x$ molecular weight. A difference of only 42 nm is found for $PEG_{113}$-*b*-*p*($HPMA_{80}$), and in both experiments their traces are monomodal. These findings may be important in nanoparticle formation containing polymers which cannot be formed by rapid nanoprecipitation alone i.e. using dialysis.

Despite these experiments, all of the nanoparticle suspensions began to precipitate after approximately two days, due to polymer aggregation (as seen for non-$PEG_x$ containing *p*($HPMA_x$) nanoparticles in Chapter 4 section 4.3. It is believed that the hydrophobic linear chains do not pack efficiently within the nanoparticle core and stability is not provided in spite of the stabilising ethylene glycol repeat units present; therefore these groups do not provide sufficient steric stability to the final nanoparticles.

Stable and near monodisperse amphiphilic block copolymer micelles have been reported, which were prepared by dialysis using a polymer concentration of 10 mg $mL^{-1}$ (in various organic solvents).[2] However, after nanoparticle preparation, solutions were subjected to sonication and centrifugation prior to resuspension. The authors report that these micelles are stable with respect to time, but fail to note the aqueous concentration of micelles in their studies. Therefore, it is believed further purification of $PEG_x$-*b*-*p*($HPMA_y$) nanoparticles (prepared by dialysis) may result in more monodisperse and stable suspensions. As this is extremely time consuming, no further modification was investigated.

## 6.4 Nanoprecipitation of $PEG_x$-*b*-(*p*($HPMA_{80}$)-*co*-$EGDMA_{0.95}$)) using the dialysis method where *x*= 17, 45, 113

In the previous section it was found that unstable nanoparticles with mostly bimodal size distributions resulted when utilising linear copolymers containing various $PEG_x$ molecular weights and PEG/*p*(HPMA) ratios. In this section, the primary chain length of the *p*($HPMA_{80}$) block remains constant yet the molecular weight of $PEG_x$ is varied within the branched A-B block copolymer samples. It was thought that the branched architecture of *p*($HPMA_{80}$) copolymers combined with the water soluble $PEG_x$ segments (of various molecular weight), would produce stable uniform nanoparticles through a dialysis approach.

A starting concentration of 10 mg $mL^{-1}$ was chosen; although this concentration did not aid in producing stable nanoparticles from the linear examples, the architecture of these polymers (and the overall molecular weights) is dramatically different and it would have been presumptuous to assume these materials behave in the same manner. It was thought that the branched cores would provide sufficient stability in

subsequent nanoparticles, and would perhaps be less affected by this relatively high starting polymer/acetone concentration, in comparison to linear polymer counterparts. Identical protocols were followed, whereby polymer/acetone solutions were slowly dripped into warmed stirring water followed by addition into dialysis membrane tubes followed by water exchange for two days. Nanoparticle suspensions were analysed using DLS and the data obtained is shown in Figure 6.5 and Table 6.5.

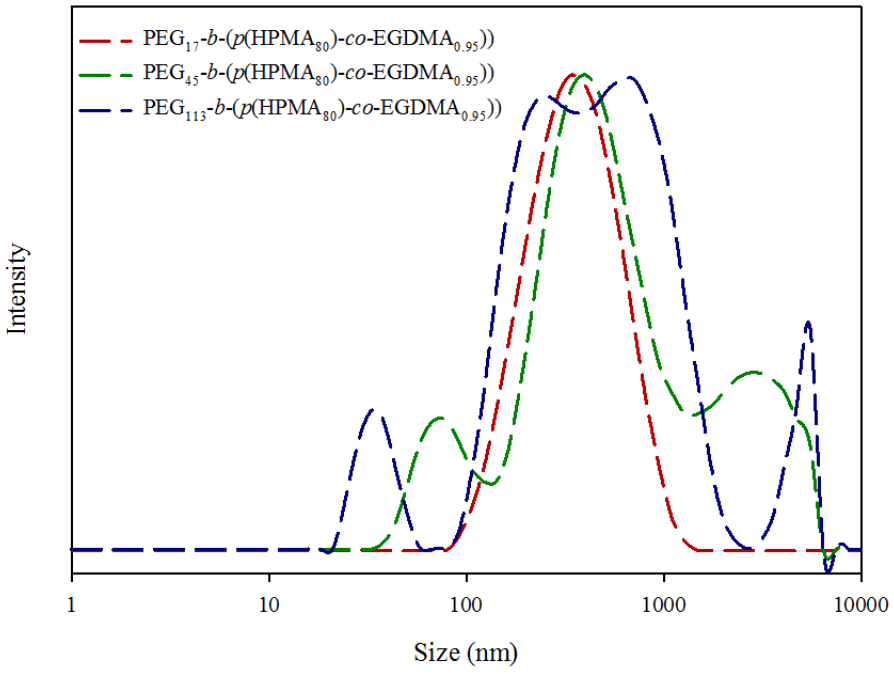


Figure 6.5: DLS size determination of nanoparticles comprising of $PEG_x$ containing branched copolymers using dialysis. 10 mg $mL^{-1}$ starting concentration, 2 mg $mL^{-1}$ final concentration.

| Copolymer | Peak 1 Diameter (nm)*[a] | Peak 2 Diameter (nm)*[b] | Peak 3 Diameter (nm)*[b] | Polydispersity Index*[c] |
|---|---|---|---|---|
| $PEG_{17}$-*b*-(*p*($HPMA_{80}$)-*co*-$EGDMA_{0.95}$)) | 392 | / | / | 0.282 |
| $PEG_{45}$-*b*-(*p*($HPMA_{80}$)-*co*-$EGDMA_{0.95}$)) | 79<br>35 | 519<br>250 | 3043<br>792 | 0.588<br>0.809 |
| $PEG_{113}$-*b*-(*p*($HPMA_{80}$)-*co*-$EGDMA_{0.95}$)) | | | | |

Table 6.5: DLS size data of nanoparticles consisting of $PEG_x$ containing branched copolymers prepared by dialysis (10 mg $mL^{-1}$ starting concentration, 2 mg $mL^{-1}$ final concentration). *[a] peak with smallest diameter. *[b] peak with largest diameter, *[c] of both peaks.

By utilising $PEG_{17}$, monomodality is found and nanoparticles are approximately 392 nm in diameter, although this diameter is markedly different than found for its linear counterpart (Peak 1, 322 nm; Peak 2, 1564 nm). The polydispersity of nanoparticles increases as the molecular weight of $PEG_x$ increases, where particle diameters of > 1000 nm are found for $PEG_{113}$-*b*-(*p*($HPMA_{80}$)-*co*-$EGDMA_{0.95}$)) (Figure 6.5), suggesting that by increasing $PEG_x$, control of producing particles within a uniform distribution is lost. Indeed, for $PEG_{113}$-*b*-(*p*($HPMA_{80}$)-*co*-$EGDMA_{0.95}$)) nanoparticles of 35 nm in diameter are found; however, it is likely that these are desolvated single branched polymer chains. For $PEG_{45}$-*b*-(*p*($HPMA_{80}$)-*co*-$EGDMA_{0.95}$)) nanoparticles of 79 nm are found, and similarly these may be either single branched polymers or aggregates of < five branched polymers (this is an approximation and is based on data not yet reported) (see section 6.9).

As for the linear counterparts, it was thought that decreasing the initial polymer/acetone concentration to 5 mg $mL^{-1}$ may increase the likelihood of

producing more well-defined nanoparticles. By diluting the initial solution, the solvated copolymers are physically more dispersed within the solution and subsequent aggregation is likely to be better controlled.

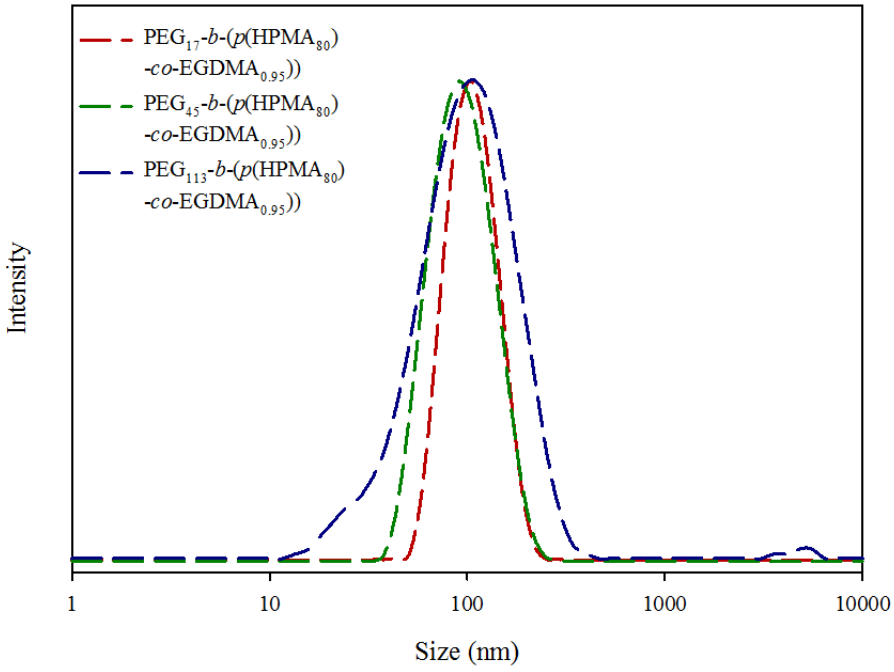


Figure 6.6: DLS size determination of nanoparticles comprising of $PEG_x$ containing branched copolymers using dialysis. 5 mg $mL^{-1}$ starting concentration, 1 mg $mL^{-1}$ final concentration.

| Copolymer | Peak 1 Diameter (nm)*[a] | Peak 2 Diameter (nm)*[b] | Polydispersity Index*[c] |
|---|---|---|---|
| $PEG_{17}$-*b*-(*p*($HPMA_{80}$)-*co*-$EGDMA_{0.95}$)) | 109 | / | 0.077 |
| $PEG_{45}$-*b*-(*p*($HPMA_{80}$)-*co*-$EGDMA_{0.95}$)) | 99 | / | 0.111 |
| $PEG_{113}$-*b*-(*p*($HPMA_{80}$)-*co*-$EGDMA_{0.95}$)) | 110 | / | 0.255 |

Table 6.6: DLS size data of nanoparticles consisting of $PEG_x$ containing branched copolymers prepared by dialysis (5 mg $mL^{-1}$ starting concentration, 1 mg $mL^{-1}$ final concentration). *[a] peak with smallest diameter. *[b] peak with largest diameter, *[c] of both peaks.

By halving the initial polymer/acetone solution (from 10 mg $mL^{-1}$ to 5 mg $mL^{-1}$) and subsequently diluting five-fold to give a final concentration of 1 mg $mL^{-1}$, it is found that extremely narrow size distributions can be achieved from the branched copolymers (Figure 6.6 and Table 6.6). It should be noted that the polydispersity of nanoparticles increases as the molecular weight of $PEG_x$ also increases; the exact reason for this is unknown, however, is likely to be due to the increased solubility of branched copolymers or the reduced content of the hydrophobic component within the polymer; each copolymer is processed from the same wt/vol concentration and the inclusion of larger block segments of $PEG_x$ leads to a reduction in the *p*(HPMA) block content at any given concentration. It is also found that the DLS trace for $PEG_{113}$-*b*-(*p*($HPMA_{80}$)-*co*-$EGDMA_{0.95}$)) is not symmetrical and contains material approximately 30 nm in diameter, consistent with single desolvated branched copolymers (see section 6.9.2 later in the chapter). The diameters of these nanoparticles do not appear to depend on the molecular weight of $PEG_x$ as they are

all approximately 100 nm. This suggests the mechanism of nanoparticle formation is near identical in all three experiments.

In the previous section it was found that altering the method (i.e. speed) of polymer/acetone solution addition had little effect on resulting nanoparticle size and distribution (regardless of PEG chain length). It was considered important to investigate whether this result would also be relevant for the branched A-B block copolymers. A 5 mg $mL^{-1}$ polymer/acetone solution was rapidly added to warmed stirring water (rather than slowly dripped), and diluted five-fold to achieve a final concentration of 1 mg $mL^{-1}$. This solution was quickly added to a dialysis membrane tube and dialysed against water for two days. The resulting nanoparticle solutions were then characterised by DLS.

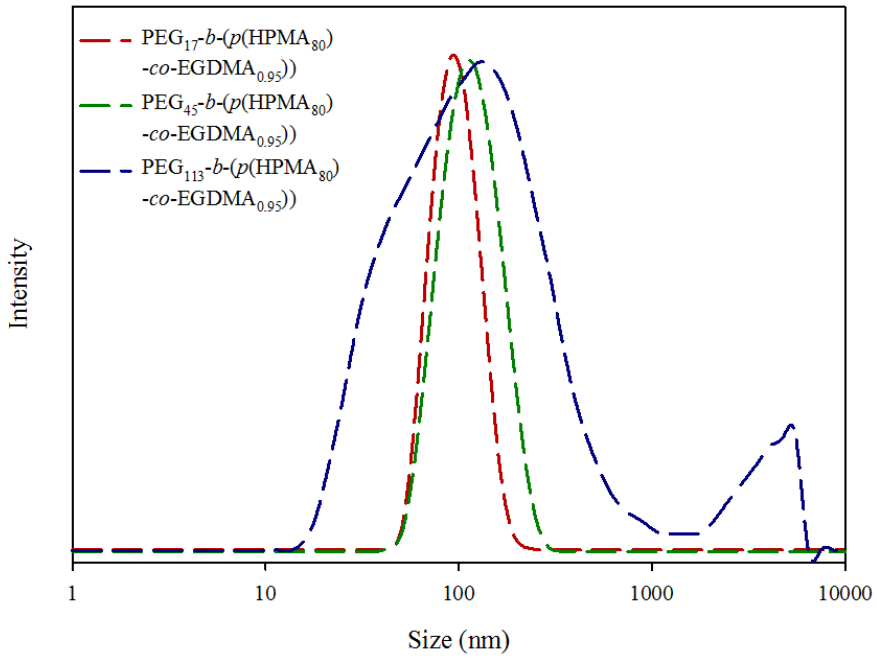


Figure 6.7: DLS size determination of nanoparticles comprising of $PEG_x$ containing branched copolymers using a modified dialysis approach . 5 mg $mL^{-1}$ starting concentration, 1 mg $mL^{-1}$ final concentration.

| Copolymer | Peak 1 Diameter (nm)*[a] | Peak 2 Diameter (nm)*[b] | Polydispersity Index*[c] |
|---|---|---|---|
| $PEG_{17}$-*b*-(*p*($HPMA_{80}$)-*co*-$EGDMA_{0.95}$)) | 99 | / | 0.051 |
| $PEG_{45}$-*b*-(*p*($HPMA_{80}$)-*co*-$EGDMA_{0.95}$)) | 120 | / | 0.100 |
| $PEG_{113}$-*b*-(*p*($HPMA_{80}$)-*co*-$EGDMA_{0.95}$)) | 155 | 3810 | 0.470 |

Table 6.7: DLS size data of nanoparticles consisting of $PEG_x$ containing branched copolymers prepared by a modified dialysis approach (5 mg $mL^{-1}$ starting concentration, 1 mg $mL^{-1}$ final concentration). *[a] peak with smallest diameter. *[b] peak with largest diameter, *[c] of both peaks.

Figure 6.7 and Table 6.7 show that near identical nanoparticle diameters and polydispersities are found for $PEG_{17}$-*b*-(*p*($HPMA_{80}$)-*co*-$EGDMA_{0.95}$)) (109 nm, polydispersity 0.077, slow dripping followed by dialysis; 99 nm, polydispersity 0.051, rapid addition followed by dialysis). Nanoparticles comprising of $PEG_{45}$-*b*-(*p*($HPMA_{80}$)-*co*-$EGDMA_{0.95}$ are also comparable in size and polydispersity (99 nm, polydispersity 0.111, slow dripping followed by dialysis; 120 nm, polydispersity 0.100, rapid addition followed by dialysis). However, nanoparticles comprising $PEG_{113}$-*b*-(*p*($HPMA_{80}$)-*co*-$EGDMA_{0.95}$)) are not unimodal and are not symmetrical; the exact reason for this is unknown but is likely to be due to the inherent solubility of this branched copolymer. It should be noted here that the nanoparticles comprising branched copolymers exerted higher stability compared to their linear counterparts however precipitation occurred after approximately three weeks. This suggests the steric or charged character of the nanoparticles is not strong enough to suppress aggregation; therefore subsequent precipitation of copolymer occurs.

Having considered these results, and taking into account the period of time which is needed to produce materials using a dialysis method, it was decided no further investigations of this nature were to be performed. It should be noted here that these materials could be filtered to remove either the high or low molecular weight material, which would isolate nanoparticles in the 100 nm region which has been previously reported.[3] Further modification of these experiments may aid the recovery of nanoparticles with low polydispersities, which may include alteration of initial polymer/acetone concentration and also choice of solvent.

## 6.5 Rapid precipitation of $PEG_x$-*b*-(*p*($HPMA_y$)-*co*-$EGDMA_{0.95}$)) where $x$ = 17, 45, 113 and $y$ = 50, 80, 120

In Chapter 4, section 4.4.3 it was found that through systematic variation of starting and final concentrations of polymer/acetone solutions nanoparticle sizes could be easily tuned for a series of hydrophobic branched p(($HPMA_x$)-co-$EGDMA_{0.95}$) copolymers when using a rapid nanoprecipitation approach. This is believed to be due to their hydrophobicity and electrostatic stability (from the negatively charged *p*(HPMA)) and here it is investigated whether this same technique can be applied to their $PEG_x$ containing branched A-B block copolymer counterparts. This process was expected to be more complex as the structure and chemistry of these polymers are different, despite both having branched hydrophobic architectures.

In this section, $PEG_{17}$-*b*-(*p*($HPMA_x$)-*co*-$EGDMA_{0.95}$)), $PEG_{17}$-*b*-(*p*($HPMA_x$)-*co*-$EGDMA_{0.95}$)) and $PEG_{17}$-*b*-(*p*($HPMA_x$)-*co*-$EGDMA_{0.95}$)) where $x$ = 50, 80 and 120 were rapidly precipitated into water using the identical protocol described in Chapter 4 section 4.4.3, to produce nanoparticles. Starting concentrations of 10 mg $mL^{-1}$, 5 mg $mL^{-1}$ and 1 mg $mL^{-1}$ were again chosen and precipitated into a range of water

volumes (dilution ratios = 1, 0.8, 0.4, 0.2, 0.05 and 0.01). It should be noted that all of the data points displayed are an average of six DLS measurements and were recorded one day after their synthesis.

| Initial concentration (mg mL$^{-1}$) | Final concentration (mg mL$^{-1}$) | Dilution ratio | Primary chain length of branched copolymer PEG$_{17}$-*b*-(*p*(HPMA$_x$)-*co*-EGDMA$_{0.95}$) | | | | | |
|---|---|---|---|---|---|---|---|---|
| | | | HPMA DP$_n$ = 50 | | HPMA DP$_n$ = 80 | | HPMA DP$_n$ = 120 | |
| | | | Diameter (nm) | Polydispersity | Diameter (nm) | Polydispersity | Diameter (nm) | Polydispersity |
| 10 | 10 | 1 | 328 | 0.249 | 175 | 0.0670 | 423 | 0.166 |
| | 8 | 0.8 | 217 | 0.195 | 156 | 0.0913 | 313 | 0.163 |
| | 4 | 0.4 | 189 | 0.155 | 111 | 0.1335 | 143 | 0.138 |
| | 2 | 0.2 | 109 | 0.114 | 84 | 0.1312 | 120 | 0.185 |
| | 0.5 | 0.05 | 115 | 0.110 | 85 | 0.1428 | 121 | 0.181 |
| | 0.1 | 0.01 | 117 | 0.168 | 83 | 0.1615 | 121 | 0.193 |
| 5 | 5 | 1 | / | / | 179 | 0.0942 | / | / |
| | 4 | 0.8 | / | / | 176 | 0.0855 | / | / |
| | 2 | 0.4 | 228 | 0.095 | 129 | 0.1205 | 156 | 0.063 |
| | 1 | 0.2 | 101 | 0.088 | 111 | 0.1233 | 127 | 0.137 |
| | 0.25 | 0.05 | 112 | 0.097 | 133 | 0.1217 | 128 | 0.159 |
| | 0.05 | 0.01 | 133 | 0.139 | 115 | 0.1367 | 123 | 0.177 |
| 1 | 1 | 1 | 120 | 0.076 | 130 | 0.071 | 168 | 0.072 |
| | 0.8 | 0.8 | 101 | 0.064 | 112 | 0.064 | 156 | 0.089 |
| | 0.4 | 0.4 | 87 | 0.070 | 96 | 0.069 | 112 | 0.148 |
| | 0.2 | 0.2 | 73 | 0.089 | 74 | 0.080 | 107 | 0.163 |
| | 0.05 | 0.05 | 87 | 0.081 | 88 | 0.054 | 110 | 0.154 |
| | 0.01 | 0.01 | 117 | 0.099 | 102 | 0.076 | 106 | 0.199 |

Table 6.8: Formation of branched PEG$_{17}$ copolymer nanoparticles generated using rapid nanoprecipitation from acetone.

| Initial concentration (mg mL$^{-1}$) | Final concentration (mg mL$^{-1}$) | Dilution ratio | Primary chain length of branched copolymer PEG$_{45}$-*b*-(*p*(HPMA$_x$)-*co*-EGDMA$_{0.95}$) | | | | | |
|---|---|---|---|---|---|---|---|---|
| | | | HPMA DP$_n$ = 50 | | HPMA DP$_n$ = 80 | | HPMA DP$_n$ = 120 | |
| | | | Diameter (nm) | Polydispersity | Diameter (nm) | Polydispersity | Diameter (nm) | Polydispersity |
| 10 | 10 | 1 | 133 | 0.107 | 190 | 0.153 | 235 | 0.199 |
| | 8 | 0.8 | 104 | 0.187 | 150 | 0.239 | 158 | 0.235 |
| | 4 | 0.4 | 81 | 0.209 | 115 | 0.205 | 143 | 0.128 |
| | 2 | 0.2 | 92 | 0.229 | 77 | 0.169 | 105 | 0.116 |
| | 0.5 | 0.05 | 145 | 0.186 | 93 | 0.129 | 110 | 0.074 |
| | 0.1 | 0.01 | 109 | 0.156 | 106 | 0.198 | 101 | 0.152 |
| 5 | 5 | 1 | 133 | 0.158 | 163 | 0.095 | 153 | 0.154 |
| | 4 | 0.8 | 119 | 0.133 | 148 | 0.152 | 149 | 0.084 |
| | 2 | 0.4 | 105 | 0.136 | 129 | 0.158 | 141 | 0.086 |
| | 1 | 0.2 | 85 | 0.144 | 79 | 0.154 | 126 | 0.119 |
| | 0.25 | 0.05 | 126 | 0.138 | 138 | 0.141 | 93 | 0.121 |
| | 0.05 | 0.01 | 117 | 0.116 | 107 | 0.124 | 108 | 0.143 |
| 1 | 1 | 1 | 239 | 0.193 | 108 | 0.156 | 121 | 0.082 |
| | 0.8 | 0.8 | 126 | 0.039 | 106 | 0.067 | 127 | 0.086 |
| | 0.4 | 0.4 | 92 | 0.064 | 80 | 0.087 | 110 | 0.097 |
| | 0.2 | 0.2 | 66 | 0.098 | 84 | 0.075 | 99 | 0.097 |
| | 0.05 | 0.05 | 86 | 0.127 | 95 | 0.062 | 122 | 0.087 |
| | 0.01 | 0.01 | 105 | 0.131 | 103 | 0.075 | 104 | 0.111 |

Table 6.9: Formation of branched PEG$_{45}$ copolymer nanoparticles generated using rapid nanoprecipitation from acetone.

| Initial concentration (mg mL$^{-1}$) | Final concentration (mg mL$^{-1}$) | Dilution ratio | Primary chain length of branched copolymer PEG$_{113}$-*b*-(*p*(HPMA$_x$)-*co*-EGDMA$_{0.95}$) | | | |
|---|---|---|---|---|---|---|
| | | | HPMA DP$_n$ = 80 | | HPMA DP$_n$ = 120 | |
| | | | Diameter (nm) | Polydispersity | Diameter (nm) | Polydispersity |
| 10 | 10 | 1 | 173 | 0.212 | 145 | 0.111 |
| | 8 | 0.8 | 154 | 0.222 | 102 | 0.168 |
| | 4 | 0.4 | 116 | 0.202 | 73 | 0.186 |
| | 2 | 0.2 | 99 | 0.211 | 77 | 0.190 |
| | 0.5 | 0.05 | 131 | 0.161 | 81 | 0.187 |
| | 0.1 | 0.01 | 129 | 0.164 | 94 | 0.150 |
| 5 | 5 | 1 | 165 | 0.184 | 144 | 0.075 |
| | 4 | 0.8 | 145 | 0.166 | 126 | 0.058 |
| | 2 | 0.4 | 109 | 0.162 | 92 | 0.150 |
| | 1 | 0.2 | 97 | 0.169 | 79 | 0.151 |
| | 0.25 | 0.05 | 117 | 0.138 | 107 | 0.133 |
| | 0.05 | 0.01 | 137 | 0.212 | 104 | 0.125 |
| 1 | 1 | 1 | 131 | 0.147 | 133 | 0.158 |
| | 0.8 | 0.8 | 113 | 0.126 | 136 | 0.045 |
| | 0.4 | 0.4 | 100 | 0.126 | 103 | 0.059 |
| | 0.2 | 0.2 | 104 | 0.101 | 104 | 0.094 |
| | 0.05 | 0.05 | 97 | 0.118 | 112 | 0.110 |
| | 0.01 | 0.01 | 99 | 0.114 | / | / |

Table 6.10: Formation of branched PEG$_{113}$ copolymer nanoparticles generated using rapid nanoprecipitation from acetone

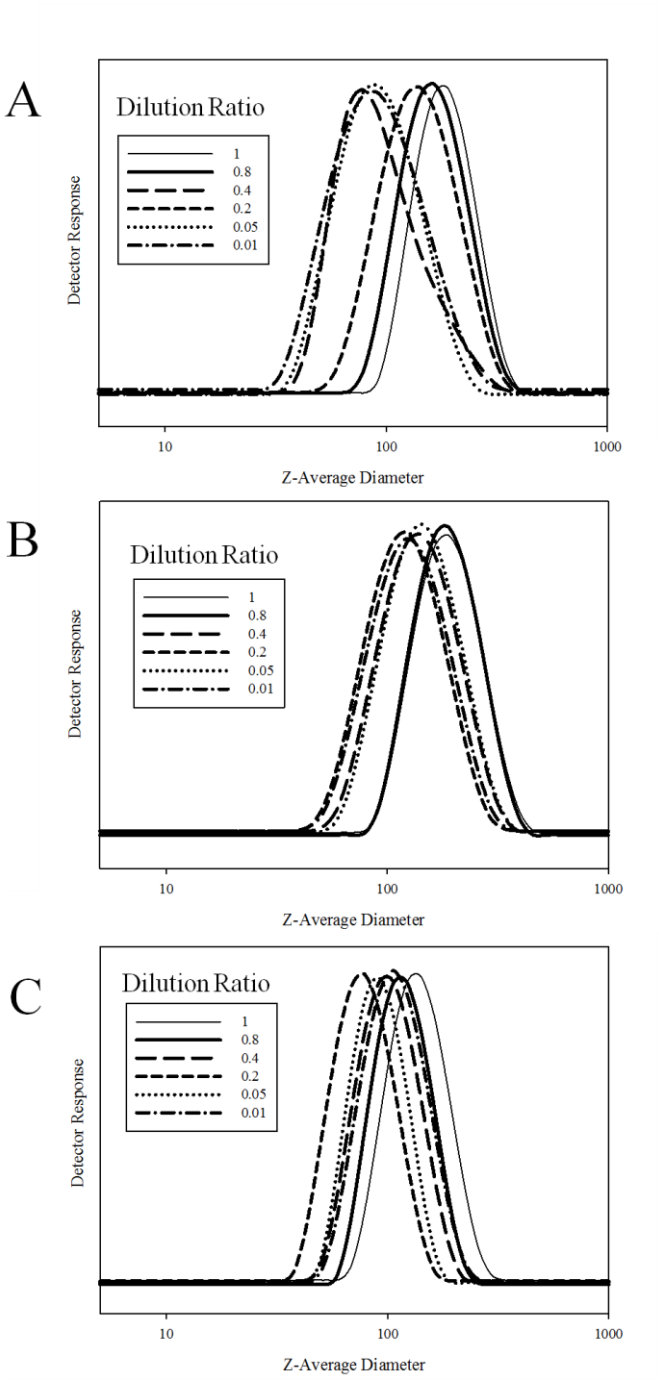


Figure 6.8: DLS analysis of nanoparticles comprised of $PEG_{17}$-*b*-*p*(($HPMA_{50}$)-*co*-$EGDMA_{0.95}$) prepared by rapid precipitation at various starting/final concentrations. (A) 10 mg $mL^{-1}$ starting concentration. (B) 5 mg $mL^{-1}$ starting concentration. (C) 1 mg $mL^{-1}$ starting concentration.

Figure 6.8 shows the DLS analysis of nanoparticles comprised of $PEG_{17}$-*b*-*p*(($HPMA_{50}$)-*co*-$EGDMA_{0.95}$). All data is presented in Tables 6.8, 6.9 and 6.10 with further size analysis found in Appendix 6.1.

Figure 6.9 shows that the nanoparticles can be formed using this technique with polymers containing the $PEG_{17}$ initiator. The systematic variation of dilution ratio and primary *p*(HPMA) chain length within the branched amphiphilic A-B block copolymers is shown. In Chapter 4 section 4.4.3, the largest nanoparticles were produced across all dilution ratios when using a starting concentration of 10 mg $mL^{-1}$, however, by introducing PEG units to the polymers; this trend is not generally seen. The smallest nanoparticles are consistently generated when using a starting concentration of 1 mg $mL^{-1}$, comparable to previous nanoparticle synthesis. The change in particle diameter across the range of dilution ratios (starting at 1 mg $mL^{-1}$) is extremely low for $PEG_{17}$-*b*-(*p*($HPMA_{50}$)-*co*-$EGDMA_{0.95}$) ( 46 nm), $PEG_{17}$-*b*-(*p*($HPMA_{80}$)-*co*-$EGDMA_{0.95}$)) (47 nm) and $PEG_{17}$-*b*-(*p*($HPMA_{120}$)-*co*-$EGDMA_{0.95}$)) (51 nm). This suggests that at this low starting concentration (1 mg $mL^{-1}$), resultant nanoparticle size is relatively unaffected by changes in dilution ratio. A number of data points in Table 6.8 and Table 6.10 have been removed as these were > 1000 nm. (($PEG_{17}$-*b*-(*p*($HPMA_x$)-*co*-$EGDMA_{0.95}$) ($x$ = 50 and 120 monomer units) dilution ratio = 1 and 0.8) the reason for these unexpectedly high results is unknown but is likely due to human error during nanoparticle preparation.

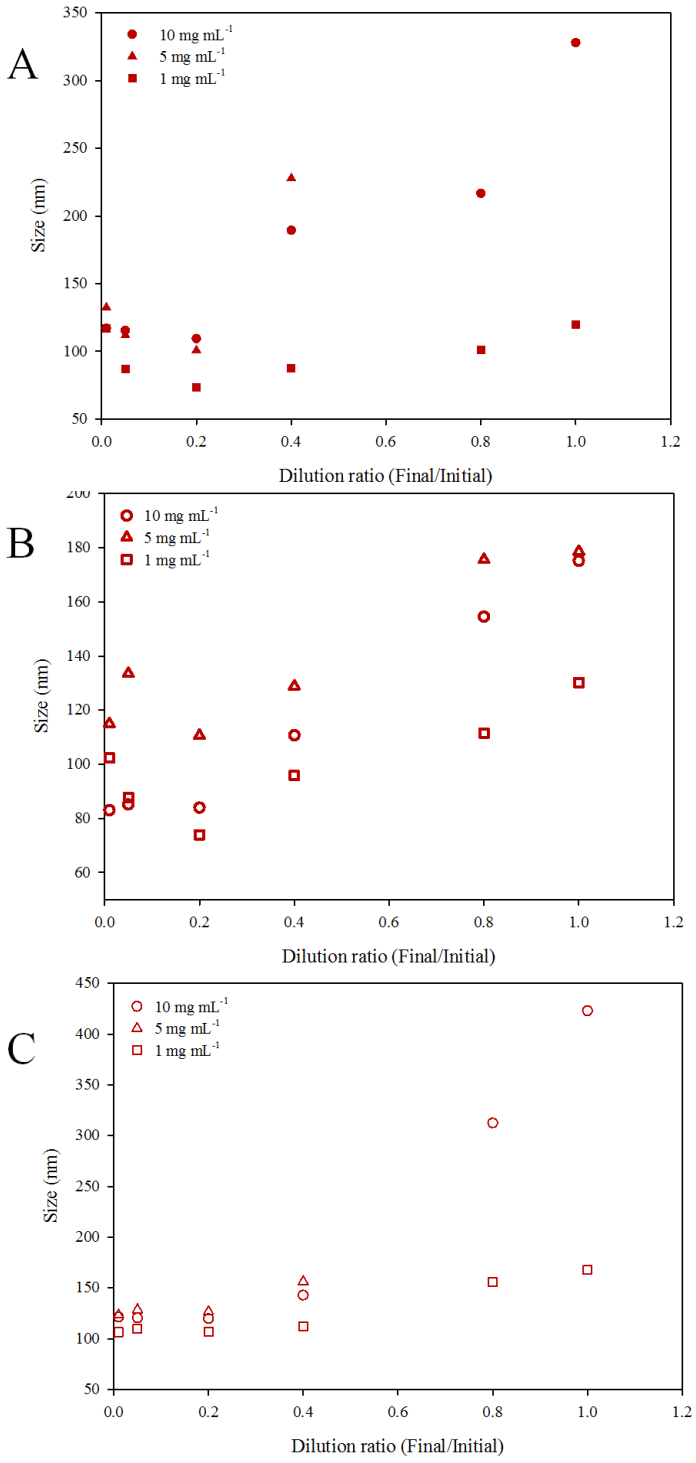


Figure 6.9: Z-average diameters of nanoparticles comprised of $PEG_{17}$-*b*-(*p*($HPMA_x$)-*co*-$EGDMA_{0.95}$)) produced *via* rapid precipitation with varied dilution ratios. Starting concentrations; 10 mg $mL^{-1}$ (circles), 5 mg $mL^{-1}$ (triangles) and 1 mg $mL^{-1}$ (squares). A) $x$ = 50 B) $x$ = 80 C) $x$ = 120.

Despite varying the primary chain length of *p*(HPMA$_x$), there appears to be a general trend, whereby the sizes of nanoparticles (regardless of starting concentration) decrease until a dilution ratio of 0.2 is reached, after which the sizes of nanoparticles increase slightly. In Chapter 4 section 4.4.3, there was insignificant change in z-average diameters beyond a dilution ratio of 0.05, yet no increase was observed as is the case here. The exact reason for this is unknown, but suggests polymers aggregate consistently differently when in extremely dilute preparation regimes. Further dilutions were not attempted here as the scattering of nanoparticles is extremely low, and DLS detectors struggle to obtain data beyond these low dilutions, often leading to inaccurate measurements.

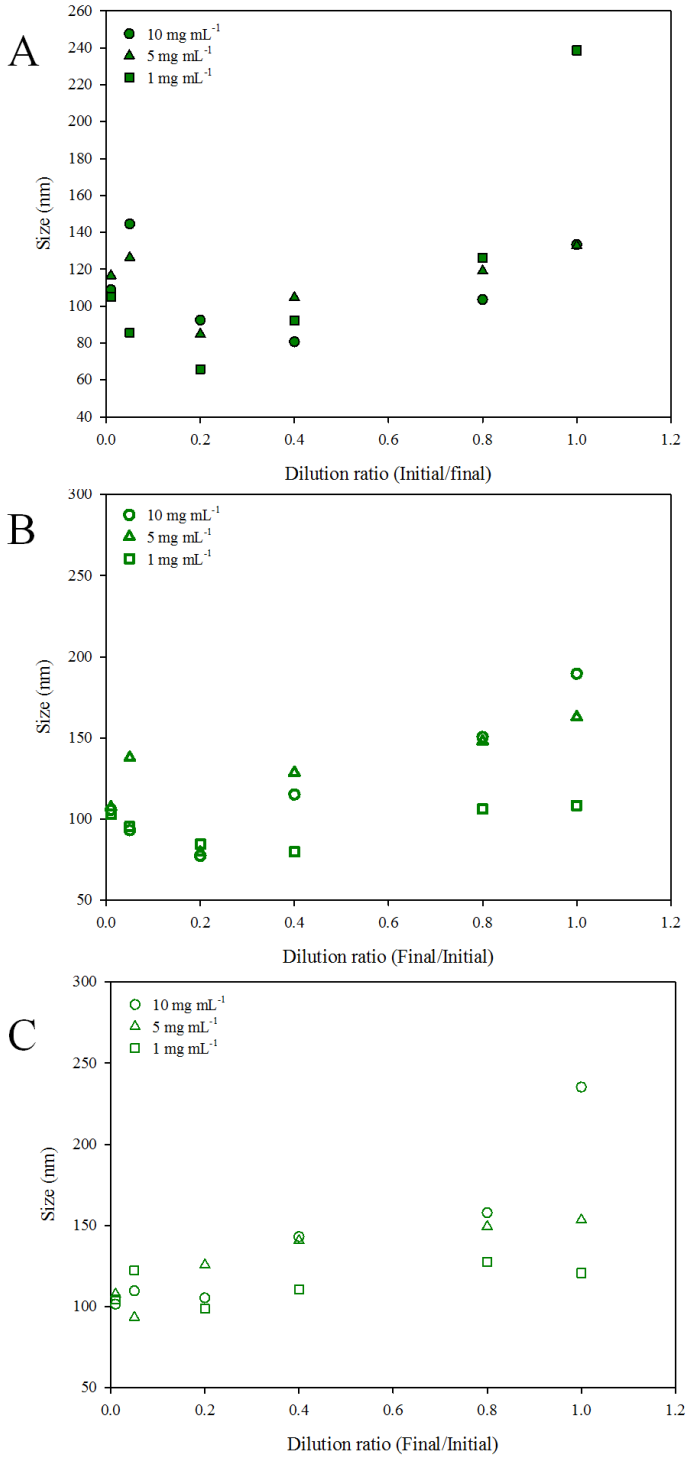


Figure 6.10: Z-average diameters of nanoparticles comprised of $PEG_{45}$-*b*-(*p*($HPMA_x$)-*co*-$EGDMA_{0.95}$)) produced *via* rapid precipitation with varied dilution ratios. Starting concentrations; 10 mg $mL^{-1}$ (circles), 5 mg $mL^{-1}$ (triangles) and 1 mg $mL^{-1}$ (squares). A) $x$ = 50 B) $x$ = 80 C) $x$ = 120.

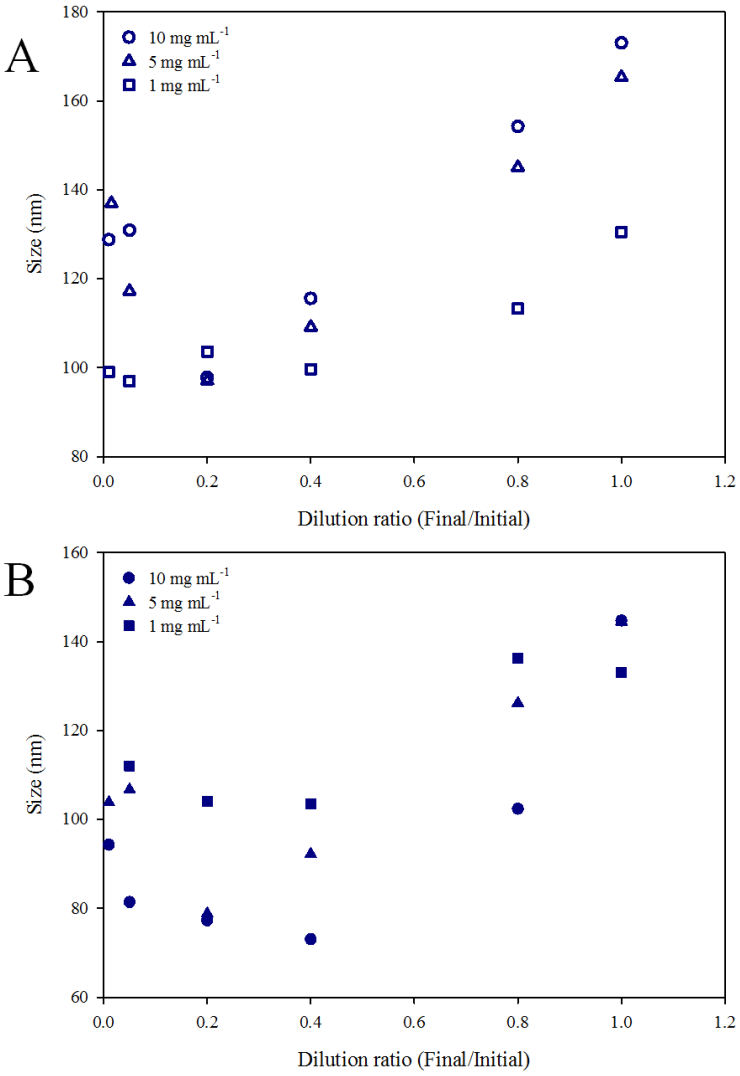


Figure 6.11: Z-average diameters of nanoparticles comprised of $PEG_{113}$-*b*-(*p*($HPMA_x$)-*co*-$EGDMA_{0.95}$)) produced *via* rapid precipitation with varied dilution ratios. Starting concentrations; 10 mg $mL^{-1}$ (circles), 5 mg $mL^{-1}$ (triangles) and 1 mg $mL^{-1}$ (squares). A) $x = 80$ B) $x = 120$.

Nanoprecipitation data using $PEG_{113}$-*b*-(*p*($HPMA_{50}$)-*co*-$EGDMA_{0.95}$)) was not obtained due to experimental errors during preparation, other attempts could not be performed due to time restraints. The same trends that were observed when utilising $PEG_{17}$ are also seen when $PEG_{45}$ and $PEG_{113}$ are employed for nanoparticle synthesis (Figure 6.10 and Figure 6.11). Z-average diameters generally decrease with

decreasing dilution ratio, with consistently higher z-average diameters beyond 0.2, despite varying $PEG_x$ chain length. There does not appear to be any consistent effect on nanoparticle size with respect to primary *p*($HPMA_x$) chain length across the dilution ranges (as noted previously), however, the at high dilution factors the order of nanoparticle sizes does seem to loosely correlate to starting polymer solution concentration. The lack of clear trends does imply that the $PEG_x$ units are directing the nanoparticle formation to a higher degree than *p*(HPMA), and nanoparticle formation is more complex and perhaps less controlled than observed in Chapter 4 section 4.4.3. The experiments in this chapter aimed to demonstrate the comparisons of z-average diameters of particles containing the same $PEG_x$ chain length; the aim was to show more clearly how nanoparticle size is affected by not only the length of the $PEG_x$ units (whilst maintaining a primary chain length (*p*($HPMA_x$) of 80 monomer units), but the starting concentration of polymer/acetone solutions.

## 6.6 $PEG_x$-*b*-(*p*($HPMA_{80}$)-*co*-$EGDMA_{0.95}$)) Nanoparticles- comparison of *p*(HPMA) primary chain length. (*x* = 50, 80, 120)

A lack of clear trends are seen when presenting an overview of the nanoprecipitation of all branched amphiphilic polymer samples, therefore an analysis of the effect of $PEG_x$ chain length on the a series of polymers with consistent *p*(HPMA) primary chain length ($DP_n$ = 80 monomer units) was generated, across the dilution factors and starting polymer concentrations.

Using a starting concentration of 10 mg $mL^{-1}$ (Figure 6.12 (A)) appears to generate nanoparticles with very similar z-average diameters irrespective of $PEG_x$ chain

length, until a dilution ratio of 0.2 is reached. However, by reducing the starting concentrations of polymer/acetone (Figure 6.12 (B) and C)), this trend begins to deviate. As previously stated, increased z-average diameters are found at higher dilution ratios than 0.2, however, for a 1 mg $mL^{-1}$ starting concentration, the range of achievable z-average diameters (regardless of $PEG_x$ chain length) over the range of dilution ratios is much lower than at 10 mg $mL^{-1}$ and 5 mg $mL^{-1}$ with these polymers.

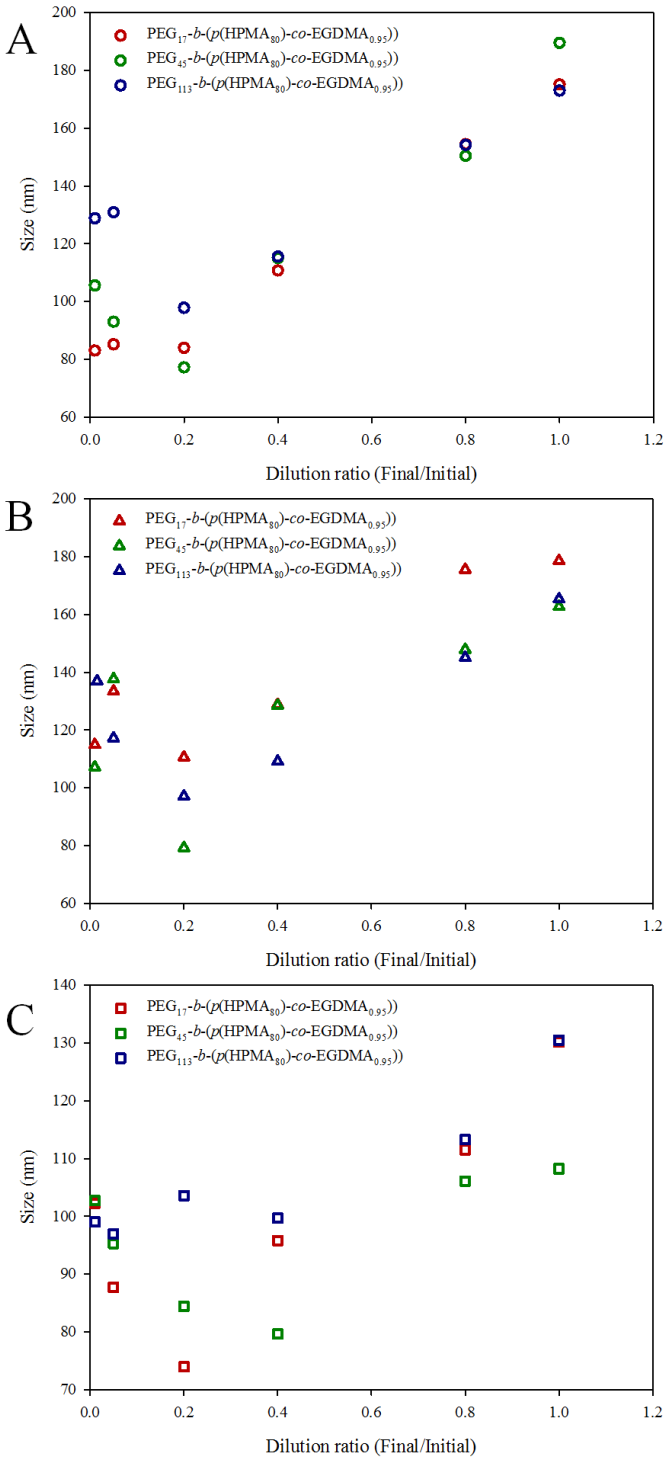


Figure 6.12: Z-average diameters of nanoparticles comprised of $PEG_x$-*b*-($p$(HPMA$_{80}$)-*co*-EGDMA$_{0.95}$)) produced *via* rapid precipitation with varied dilution ratios. A) Starting concentration = 10 mg mL$^{-1}$ B) Starting concentration = 5 mg mL$^{-1}$ C) Starting concentration = 1 mg mL$^{-1}$.

It should be noted that all of the nanoparticles generated in this section were monomodal, however, their polydispersities vary and this data is displayed in Figure 6.13. These are generally lowest when nanoparticles are formed from a starting concentration of 1 mg $mL^{-1}$, where polydispersity varies from 0.054 to 0.156 (regardless of $PEG_x$ chain length). Whereas the range of polydispersities is much larger when using a starting concentration of 10 mg $mL^{-1}$ (0.067 to 0.239), producing nanoparticles with generally larger polydispersities. From these results, it is speculated that increasing the initial polymer/acetone concentration, nanoparticle generation is less controlled, as these branched polymers are in closer proximity, and therefore produce less monodisperse particles.

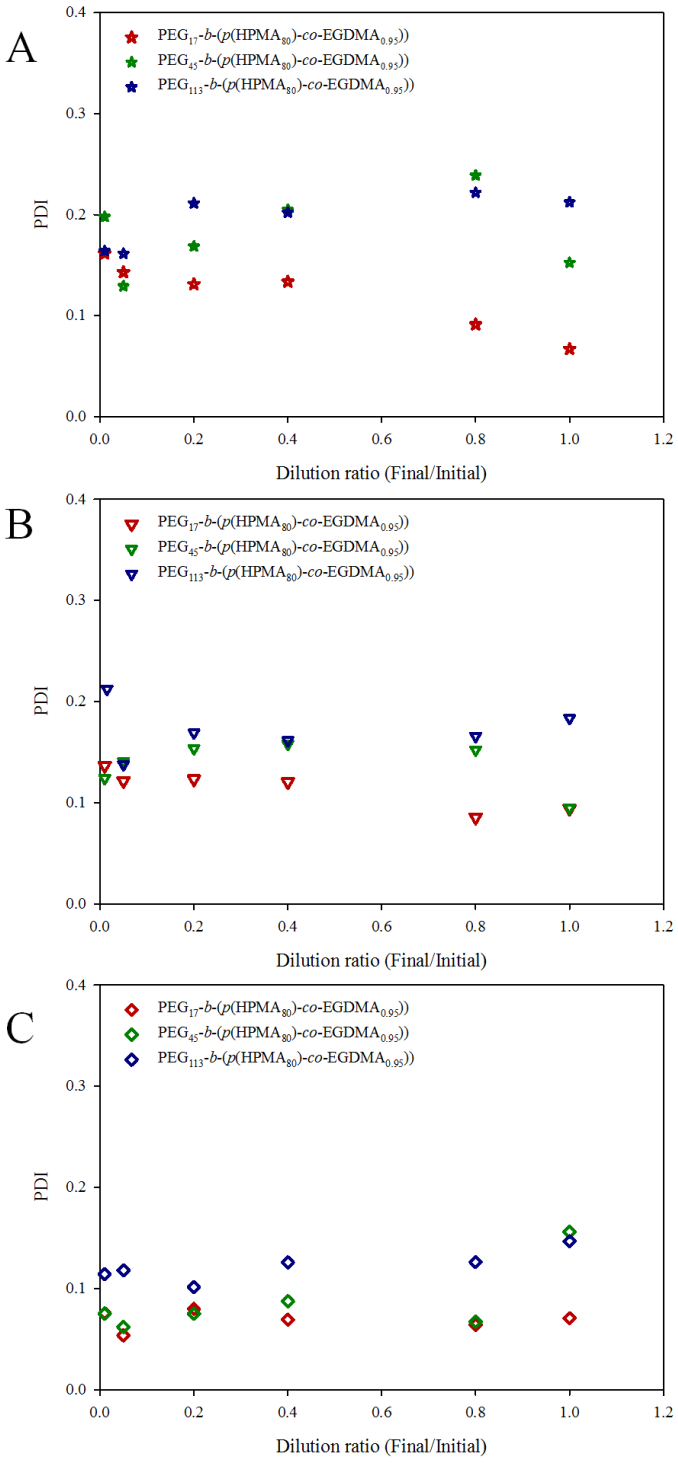


Figure 6.13: Polydispersity of nanoparticles comprised of $PEG_x$-*b*-(*p*($HPMA_{80}$)-*co*-$EGDMA_{0.95}$)) produced *via* rapid precipitation with varied dilution ratios. A) Starting concentration = 10 mg $mL^{-1}$ B) Starting concentration = 5 mg $mL^{-1}$ C) Starting concentration = 1 mg $mL^{-1}$.

Unfortunately this section has failed to produce a series of nanoparticles whose properties can be tuned by adjustment of initial/final polymer/acetone concentrations. These polymers are identical to those in utilised in Chapter 4, with the exception of their $PEG_x$ units, suggesting the ethylene glycol repeat units have a huge impact on nanoparticle formation, possibly due to the considerable solubility of $PEG_x$. A series of very monodisperse nanoparticle samples have, however, been reproducibly generated from a simple polymerisation procedure, coupled to a rapid nanoprecipitation, that have the potential for steric stabilisation and the amphiphilic character of many postulated literature drug delivery systems.

## 6.7 Aqueous serial dilution of nanoparticles comprised of $PEG_{17}$-*b*-(*p*($HPMA_{80}$)-*co*-$EGDMA_{0.95}$))

In Chapter 4 section 4.4.5, it was found that nanoparticles comprising of solely *p*($HPMA_{80}$)-*co*-$EGDMA_{0.95}$) (5 mg $mL^{-1}$ starting concentration; 1 mg $mL^{-1}$ final concentration) were highly stable with respect to aqueous dilution. It is believed that this resulted from strong hydrophobic interactions within the dense cores of the nanoparticles, combined with electrostatic repulsion between nanoparticles. Here it is investigated whether nanoparticles comprised of branched A-B block copolymers containing $PEG_{17}$ segments exert similar stability with respect to aqueous dilution.

$PEG_{17}$-*b*-(*p*($HPMA_{80}$)-*co*-$EGDMA_{0.95}$)) was dissolved in acetone at 5 mg $mL^{-1}$; this solution was added rapidly to warm stirred water and subsequently formed a 1 mg $mL^{-1}$ aqueous nanoparticle solution. DLS measurements were performed and the solution was diluted (two-fold) giving an aqueous concentration of 0.5 mg $mL^{-1}$ which was analysed. This dilution process continued until a final concentration of $2.44 \times 10^{-4}$ mg $mL^{-1}$ was achieved. It should be noted here that each data point is an

average of six measurements. By monitoring z-average diameter, polydispersity, derived count rate and the attenuator level during dilution (Figure 6.14), it is possible to speculate whether these particles are reversibly aggregated in a similar way to colloidal particles. Changes in these parameters such as an increased z-average diameter could indicate particle aggregation or dissociation.

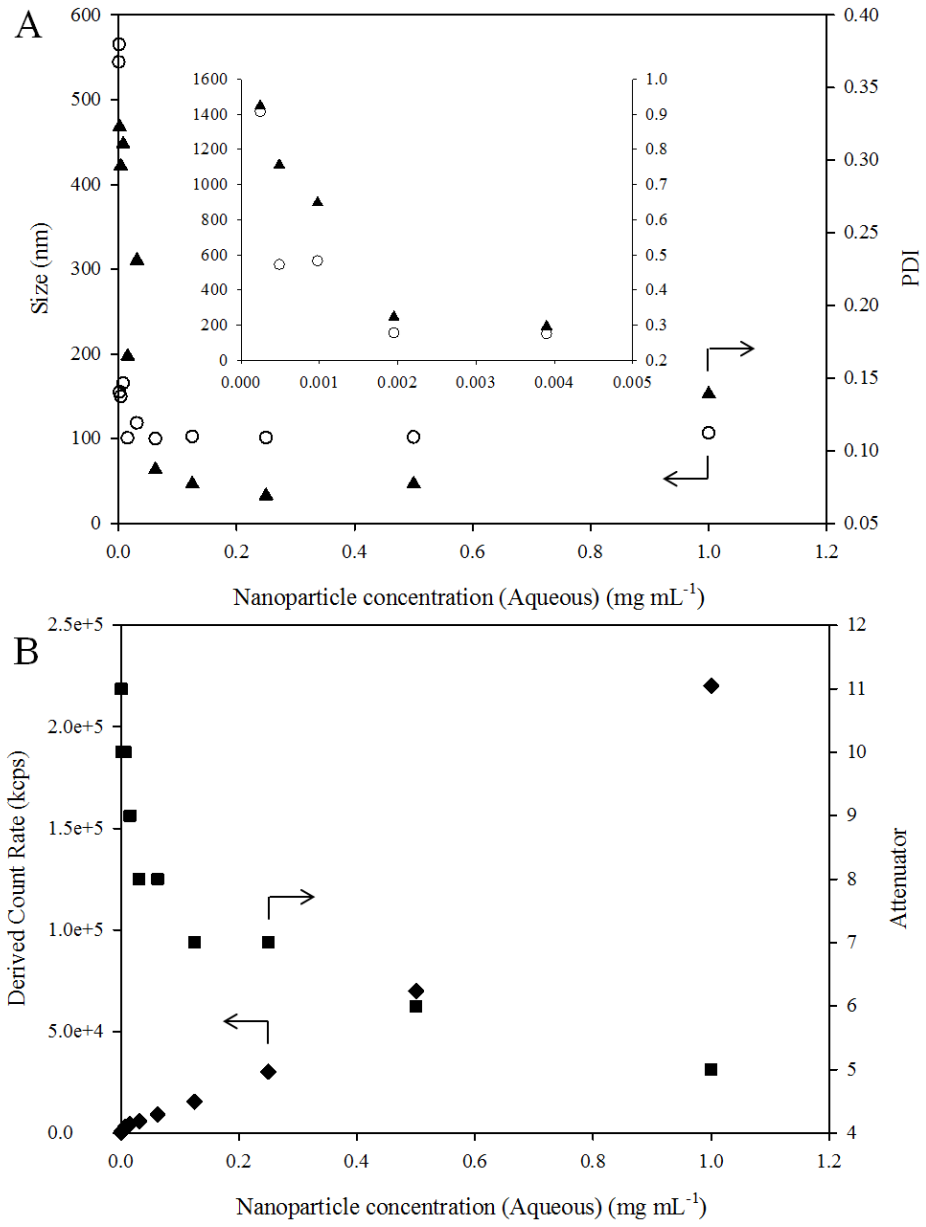


Figure 6.14: Serial dilution data of nanoparticles comprised of $PEG_{17}$-*b*-(*p*($HPMA_{80}$)-*co*-$EGDMA_{0.95}$)) with a starting and finishing concentration of 5 mg $mL^{-1}$ and 1 mg $mL^{-1}$ respectively. A) Nanoparticle diameter and polydispersity *vs*. concentration of suspension. B) Derived count rate and Attenuator *vs*. concentration of suspension.

Figure 6.14 (A) indicates these particles are extremely stable with respect to dilution as there is little change in z-average diameter and polydispersity until a concentration of 0.002 mg $mL^{-1}$ is reached which is a five hundred-fold dilution. Figure 6.14 (B) shows the derived count rate measurements during the experiment; this figure is indicative of the number of particles present in solution (this is directly related if the attenuator is set at a single value). During dilution, this figure decreases almost linearly suggesting these particles are not dissociating. An increase in derived count rate would be expected if dissociation was occurring. To support this observation, it is noted that the attenuator increases during dilution (this is automatically set by the instrument). The attenuator setting increases allowing wider areas of the sample to be analysed due to low material concentration. Once the attenuator has reached values > 9, measurements become unreliable as the instrument is unable to analyse the extremely dilute samples. Analysis of the sample beyond an attenuator setting of > 9 is shown in Figure 6.14 (B) to highlight this point; the z-average diameters and polydispersities (Figure 6.14 (B)) at these low concentration are extremely high and do not correlate well with previous measurements. These results may be due to a combination of instrument unreliability and also possibly aggregation of particles (as both z-average diameter and polydispersity increase), however, the continually decreasing derived count rate is indicative of a steadily decreasing number of particles in the sample after dilution. Further dilutions were abandoned due to the inability to record reliable measurements. This experiment shows that nanoparticles comprised of $PEG_{17}$-*b*-(*p*($HPMA_{80}$)-*co*-$EGDMA_{0.95}$)) are extremely stable to aqueous dilution, as z-average diameter and polydispersity were little affected during dilution.

## 6.8 Zeta-potential Studies

In Chapter 4 section 4.4.10, it was shown that the zeta potential of nanoparticles comprised of *p*((HPMA$_{50}$)-*co*-EGDMA$_{0.95}$), *p*((HPMA$_{80}$)-*co*-EGDMA$_{0.95}$) and *p*((HPMA$_{120}$)-*co*-EGDMA$_{0.95}$) were -34.1 mV, -41.0 mV and -44.5 mV, respectively. It is believed this arises from the pedant hydroxyl groups of *p*(HPMA), however, the exact reason for the negative charge is unknown. In this section, the zeta potential of nanoparticles comprised of PEG containing linear and branched copolymers was recorded, using the protocol found in Chapter 2 section 2.2.3.1. It is noted that nanoparticles comprised of linear copolymers were used before the onset of aggregation.

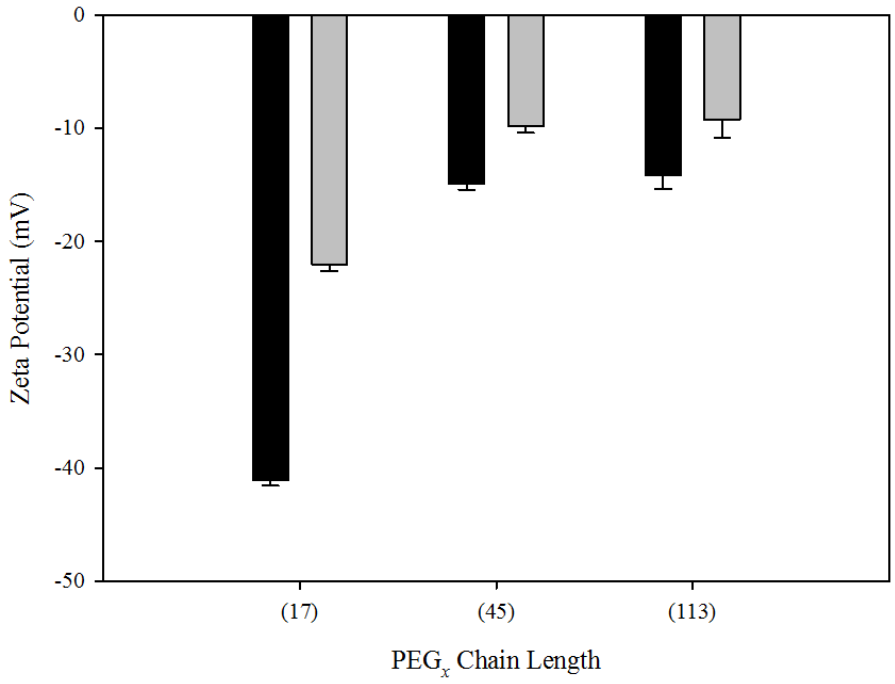


Figure 6.15: Zeta potential measurements of nanoparticles comprised of PEG$_x$-*b*-*p*(HPMA$_{80}$) and PEG$_x$-*b*-(*p*(HPMA$_{80}$)-*co*-EGDMA$_{0.95}$)), produced by rapid precipitation. 5 mg mL$^{-1}$ starting concentration; 1 mg mL$^{-1}$ final concentration. (*x* = 17, 45, 113). Linear Polymers (black), Branched Polymers (grey).

| Copolymer | Zeta Potential (mV) |
|---|---|
| $PEG_{17}$-*b*-*p*($HPMA_{80}$) | -41.1 |
| $PEG_{45}$-*b*-*p*($HPMA_{80}$) | -14.9 |
| $PEG_{113}$-*b*-*p*($HPMA_{80}$) | -14.1 |
| $PEG_{17}$-*b*-(*p*($HPMA_{80}$)-*co*-($EGDMA_{0.95}$)) | -22.00 |
| $PEG_{45}$-*b*-(*p*($HPMA_{80}$)-*co*-($EGDMA_{0.95}$)) | -9.76 |
| $PEG_{113}$-*b*-(*p*($HPMA_{80}$)-*co*-($EGDMA_{0.95}$)) | -9.23 |

Table 6.11: Summary of Zeta potential data of nanoparticles comprised of $PEG_x$-*b*-*p*($HPMA_{80}$) and $PEG_x$-*b*-(*p*($HPMA_{80}$)-*co*-$EGDMA_{0.95}$) ($x$ = 17, 45, 113).

Figure 6.15 and Table 6.11 show the comparative zeta potentials of nanoparticles comprised of linear (grey) and branched (black) copolymers with varying PEG content, maintaining *p*(HPMA) chain length ($DP_n$ = 80 monomer units). All nanoparticles are negatively charged, however, there is a clear trend seen when comparing linear and branched copolymer architectures. Nanoparticles comprised of linear copolymers are more negatively charged compared to branched counterparts, and nanoparticles generated from both architectures become less negative as PEG chain length increases.

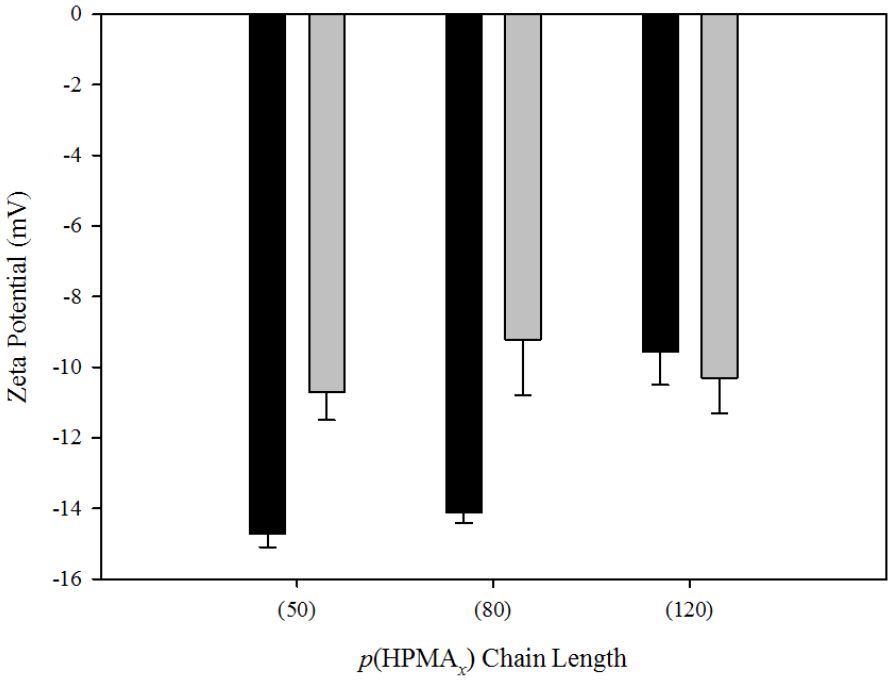


Figure 6.16: Zeta potential measurements of nanoparticles comprised of $PEG_{113}$-*b*-*p*($HPMA_x$) and $PEG_{113}$-*b*-(*p*($HPMA_x$)-*co*-$EGDMA_{0.95}$)), produced by rapid precipitation. 5 mg $mL^{-1}$ starting concentration; 1 mg $mL^{-1}$ final concentration. (*x* = 50, 80, 120). Linear Polymers (black), Branched Polymers (grey).

| Copolymer | Zeta Potential (mV) |
|---|---|
| $PEG_{113}$-*b*-*p*($HPMA_{50}$) | -14.70 |
| $PEG_{113}$-*b*-*p*($HPMA_{80}$) | -14.10 |
| $PEG_{113}$-*b*-*p*($HPMA_{120}$) | -9.55 |
| $PEG_{113}$-*b*-(*p*($HPMA_{50}$)-*co*-($EGDMA_{0.95}$)) | -10.70 |
| $PEG_{113}$-*b*-(*p*($HPMA_{80}$)-*co*-($EGDMA_{0.95}$)) | -9.23 |
| $PEG_{113}$-*b*-(*p*($HPMA_{120}$)-*co*-($EGDMA_{0.95}$)) | -10.30 |

Table 6.12: Summary of Zeta potential data of nanoparticles comprised of $PEG_{113}$-*b*-*p*($HPMA_x$) and $PEG_{113}$-*b*-(*p*($HPMA_x$)-*co*-$EGDMA_{0.95}$) (*x* = 50, 80, 120).

Nanoparticles were also prepared by rapid nanoprecipitation (5 mg $mL^{-1}$ starting concentration; 1 mg $mL^{-1}$ final concentration) from linear and branched architectures comprised of $PEG_{113}$-with varying chain lengths of *p*(HPMA) (target $DP_n$ = 50, 80, 120) and their zeta potentials were recorded. This experiment aimed to assess the impact of *p*(HPMA) primary chain length (using $PEG_{113}$) on the charge character of the final nanoprecipitates. Figure 6.16 and Table 6.12 show that as the primary chain length of *p*(HPMA) increases, subsequent nanoparticles become less negatively charged (approaching neutrality) irrespective of polymer architecture, however, for *p*(HPMA) (with target $DP_n$ values of 50 and 80 monomer units), nanoparticles comprised of linear copolymer are more negative compared to their branched counterparts. For *p*(HPMA) target $DP_n$ = 120 monomer units, nanoparticles comprised of either linear or branched material have identical zeta potentials (within experimental error). Clearly both *p*(HPMA) primary chain length and polymer architecture influence the zeta potential of nanoparticles, however, the reasons for this are unclear.

## 6.9 Solution Behaviour of Linear and Branched PEG Copolymers

### 6.9.1 Aqueous Behaviour of $PEG_{45}$-*b*-*p*($HPMA_{50}$), $PEG_{45}$-*b*-(*p*($HPMA_{50}$)-*co*-$EGDMA_{0.95}$)), $PEG_{113}$-*b*-*p*($HPMA_{50}$) and $PEG_{113}$-*b*-*p*($HPMA_x$)-*co*-$EGDMA_{0.95}$) where *x* = 50, 80, 120

A small selection of the linear and branched amphiphilic A-B block copolymers that have been synthesised appeared to have an appreciable solubility in water. This was

probably due to the balance of PEG and *p*(HPMA) content within the copolymer structures and therefore the assembly of these materials was studied in water, without the application of any of the reported precipitation methods already discussed within this thesis.

The polymers were treated as follows; linear polymers (PEG$_x$-*b*-*p*(HPMA$_y$)) and branched copolymers *p*(PEG$_x$-*b*-(*p*(HPMA$_y$)-*co*-EGDMA$_{0.95}$)) ($x$ = 17, 45, 113) ($y$ = 50, 80, 120) (50 mg) were added to distilled water (5 mL) and placed on a rolling machine overnight to dissolve. Only PEG$_{45}$-*b*-*p*(HPMA$_{50}$), PEG$_{45}$-*b*-(*p*(HPMA$_{50}$)-*co*-EGDMA$_{0.95}$)), PEG$_{113}$-*b*-*p*(HPMA$_{50}$) and PEG$_{113}$-*b*-*p*(HPMA$_x$) ($x$ = 50, 80, 120) appeared to have dissolved (where polymer was not visible to the naked eye). These 10 mg mL$^{-1}$ solutions were then analysed directly using DLS, shown in Figure 6.17.

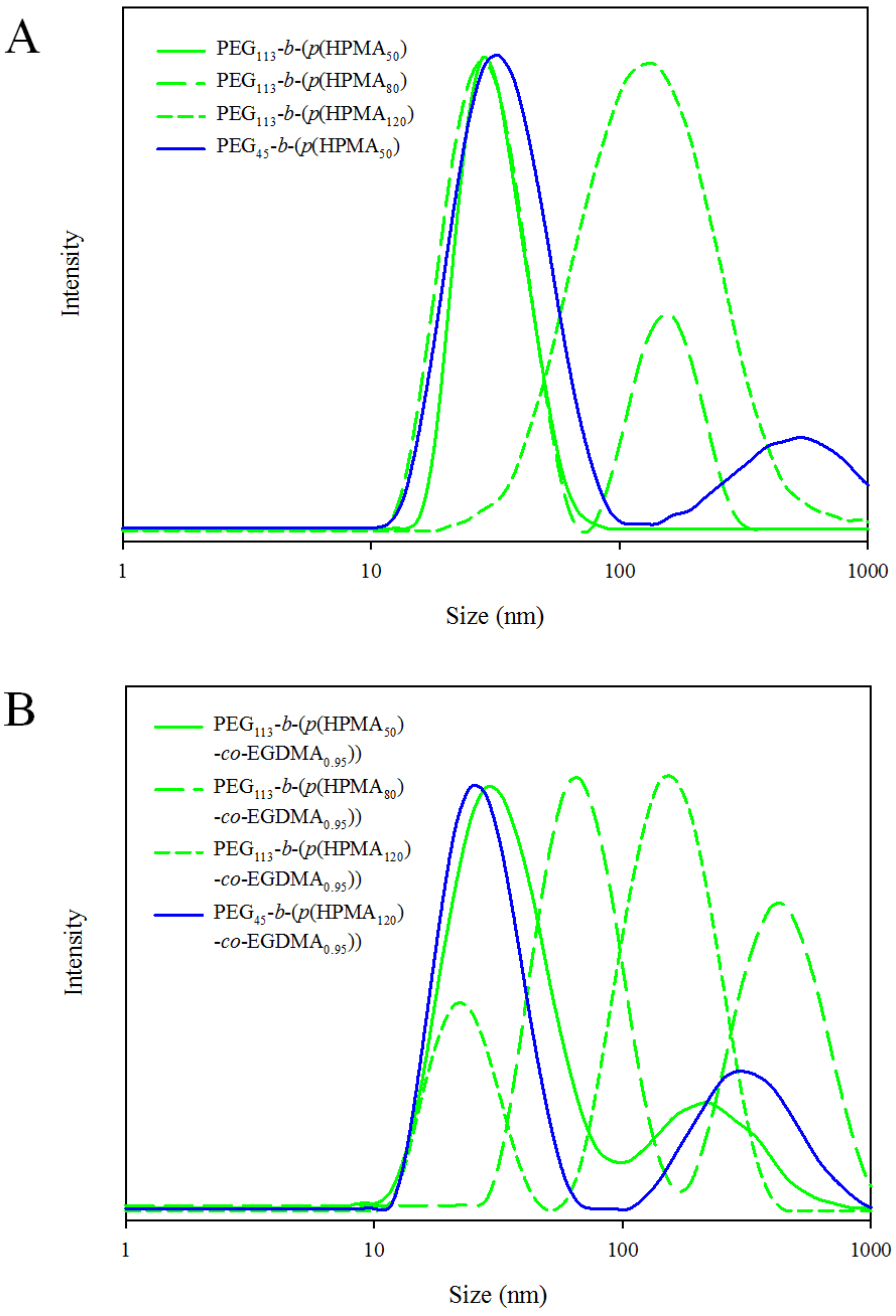


Figure 6.17: DLS size determination of (A) linear and (B) branched copolymers in water at 10 mg $mL^{-1}$. $PEG_{45}$-*b*-*p*($HPMA_{50}$) and $PEG_{45}$-*b*-(*p*($HPMA_{50}$)-*co*-$EGDMA_{0.95}$)) (blue). $PEG_{113}$-*b*-*p*($HPMA_x$) ($x$ = 50, 80, 120) and $PEG_{45}$-*b*-(*p*($HPMA_{50}$)-*co*-$EGDMA_{0.95}$)) ($x$ = 50, 80, 120) (green)

| Copolymer | Peak 1 Diameter (nm)*[a] | Peak 2 Diameter (nm)*[b] | Polydispersity Index*[c] |
|---|---|---|---|
| $PEG_{45}$-*b*-*p*($HPMA_{50}$) | 36 | 582 | 0.35 |
| $PEG_{113}$-*b*-*p*($HPMA_{50}$) | 58 | / | 0.20 |
| $PEG_{113}$-*b*-*p*($HPMA_{80}$) | 30 | 160 | 0.22 |
| $PEG_{113}$-*b*-*p*($HPMA_{120}$) | 117 | / | 0.32 |
| $PEG_{45}$-*b*-(*p*($HPMA_{50}$)-*co*-($EGDMA_{0.95}$)) | 28 | 347 | 0.40 |
| $PEG_{113}$-*b*-(*p*($HPMA_{50}$)-*co*-($EGDMA_{0.95}$)) | 35 | 235 | 0.37 |
| $PEG_{113}$-*b*-(*p*($HPMA_{80}$)-*co*-($EGDMA_{0.95}$)) | 70 | 455 | 0.69 |
| $PEG_{113}$-*b*-(*p*($HPMA_{120}$)-*co*-($EGDMA_{0.95}$)) | 23 | 166 | 0.32 |

Table 6.13: DLS size data of $PEG_x$ containing linear and branched copolymers in water (10 mg $mL^{-1}$) *[a] peak with smallest diameter. *[b] peak with largest diameter, *[c] average across full sample.

Figure 6.17(A) and Table 6.13 show DLS data for linear copolymers dissolved in water (10 mg $mL^{-1}$) where $PEG_{113}$-*b*-*p*($HPMA_{50}$) gives a monomodal distribution (58 nm, 0.20 polydispersity), $PEG_{113}$-*b*-*p*($HPMA_{80}$) is bimodal, however, there is significant overlap with the monomodal distribution of $PEG_{113}$-*b*-*p*($HPMA_{50}$. $PEG_{113}$-*b*-*p*($HPMA_{120}$) also appears to form structures within the aqueous solution with diameter of 117 nm and a higher polydispersity of 0.32. Figure 6.17 (B) shows branched copolymer structures in water where all chromatograms are bimodal with some materials > 100 nm in diameter. $PEG_{45}$-*b*-*p*($HPMA_{50}$) and $PEG_{45}$-*b*-(*p*($HPMA_{50}$)-*co*-$EGDMA_{0.95}$)) appear to form structures which are extremely similar; both distributions are bimodal and their architectural differences do not seem to have an effect on the aqueous behaviour of these materials. Clear differences are evident

between the linear and branched polymers initiated with $PEG_{113}$-Br and this may, again, be a strong indication of the modification of behaviour of linear polymers that can be achieved through the introduction of intermolecular branches as their nominal compositions (PEG/*p*(HPMA) are identical within each series.

It is unclear if any of the structures that are observed are due to the collapse of single branched A-B block copolymers; the smallest peak diameter was found to be 23 nm when subjecting $PEG_{113}$-*b*-(*p*($HPMA_{120}$)-*co*-($EGDMA_{0.95}$)) to this procedure, however, linear polymers also form structures with similar sizes.

### 6.9.2 Behaviour of $PEG_x$-*b*-*p*($HPMA_y$) and $PEG_x$-*b*-(*p*($HPMA_y$)-*co*-$EGDMA_{0.95}$)) in Acetone where $x$ = 17, 45, 113, $y$ = 50, 80, 120

It has been assumed that prior to nanoprecipitation, that copolymers are suitably solvated in acetone. The observation of particulate structures in water suggested an examination of acetone solutions of the linear and branched polymers and a suitable RI difference between solvent and polymer was expected if dense, self-assembled particles were being formed. $PEG_x$ containing copolymers (with linear and branched architectures) were therefore dissolved in acetone at 10 mg $mL^{-1}$ overnight and subsequently analysed directly by DLS.

It can be seen from Figure 6.18 (A) that a measureable DLS signal was observed for several acetone solutions; the data is shown in Table 6.13. $PEG_{17}$-*b*-*p*($HPMA_{80}$) is monomodal with a peak diameter of 7 nm; as the chain length of $PEG_x$ increases (to $PEG_{45}$), the linear copolymers exist in two distinctly separate size ranges; the

polydispersity of the individual peaks are narrow but clearly the dissolved chains do have a tendency to assemble with increasing PEG content.

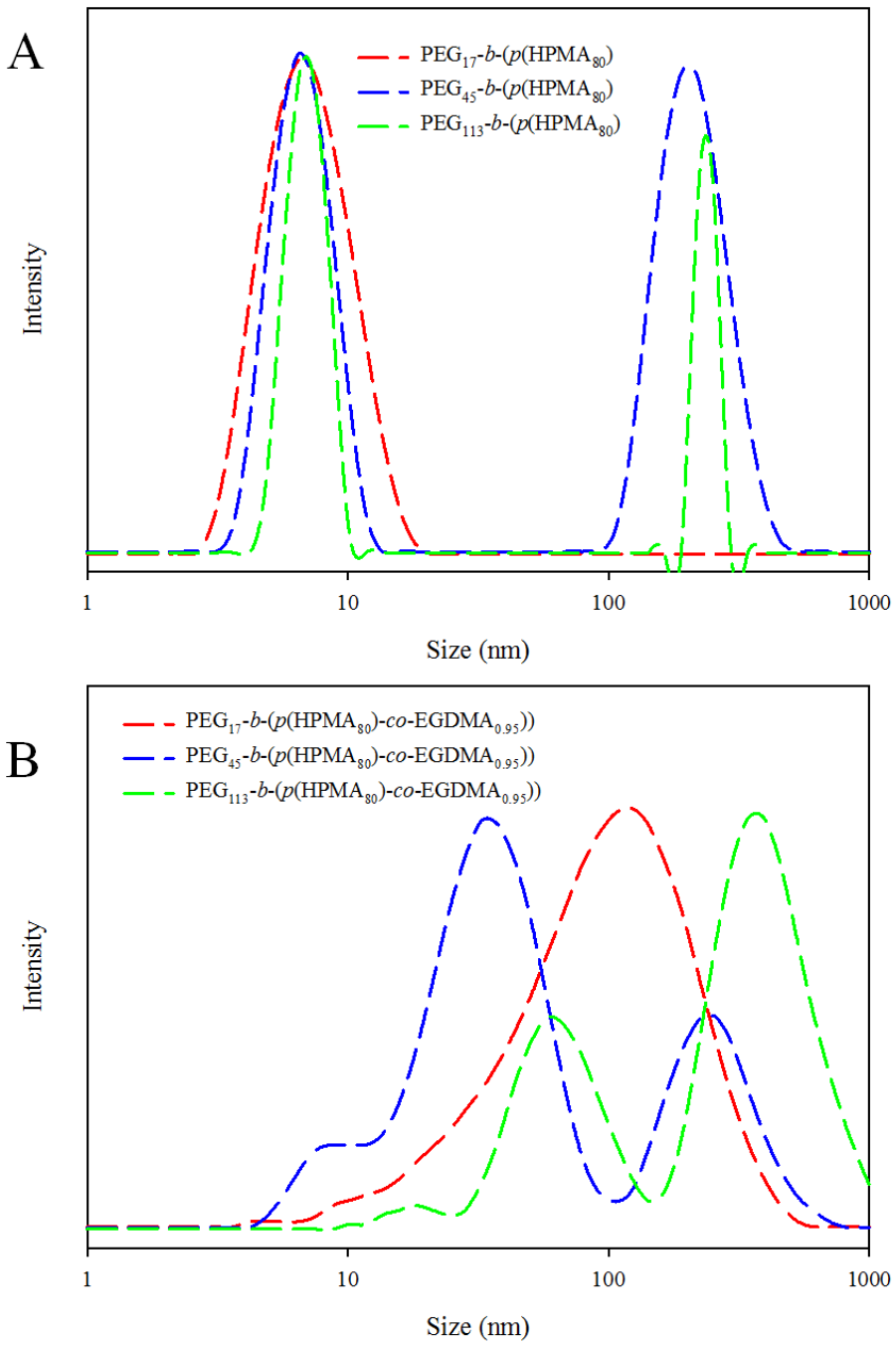


Figure 6.18: DLS size determination of linear (A) and branched (B) copolymers in acetone at 10 mg $mL^{-1}$.

| Copolymer | Peak 1 Diameter (nm)*[a] | Peak 2 Diameter (nm)*[a] | Peak 3 Diameter (nm)*[a] | Polydispersity Index*[b] |
|---|---|---|---|---|
| $PEG_{17}$-*b*-*p*($HPMA_{80}$) | 7 | / | / | 0.18 |
| $PEG_{45}$-*b*-*p*($HPMA_{80}$) | 7 | 217 | / | 0.54 |
| $PEG_{113}$-*b*-*p*($HPMA_{120}$) | 6 | 237 | / | 0.83 |
| $PEG_{17}$-*b*-(*p*($HPMA_{80}$)-*co*-($EGDMA_{0.95}$)) | 117 | / | / | 0.45 |
| $PEG_{45}$-*b*-(*p*($HPMA_{80}$)-*co*-($EGDMA_{0.95}$)) | 9 | 37 | 264 | 0.38 |
| $PEG_{113}$-*b*-(*p*($HPMA_{80}$)-*co*-($EGDMA_{0.95}$)) | 18 | 58 | 342 | 0.76 |

Table 6.13: DLS size data of $PEG_x$ containing linear and branched copolymers in acetone (10 mg $mL^{-1}$) *[a] peak mean intensity from small to large diameter. *[b] peak with largest diameter, *[b] of both peaks.

Linear $PEG_{113}$-derived copolymers also exist in two well defined regions, however, the polydispersity of the individual peaks are broader than those displayed for materials containing the shorter PEG chains. As mentioned previously, the intensity of scattering scales as the sixth power of the particle radius. Although the peaks within the intensity distribution appear to be of similar heights within Figure 6.18 (A), the relative concentrations are highly biased towards the smaller sized materials and therefore the larger aggregates are only present at very low concentrations and may signify slowly dissolving chains rather than aggregated structures. This is confirmed by measuring size distribution by the number of particles present in the sample, where no material > 10 nm is measured; DLS measurement is found in Appendix 6.2.

It is possible to potentially observe the linear fraction of the branched polymer distributions as the small shoulders that appear from 7 nm to 12 nm (Figure 6.18

(B)). It should also be noted that the automatic attenuator DLS setting during this series of studies varied from 7-10, due to the minimal difference in refractive index between copolymer and acetone.

## 6.10 Loading capacity evaluation of $PEG_x$-*b*-(*p*($HPMA_{80}$)-*co*-($EGDMA_{0.95}$)) Nanoparticles with hydrophobic guest-molecules. ($x$ = 17, 45, 113)

In order to determine whether the polymeric nanoparticles generated via rapid nanoprecipitation could efficiently encapsulate guest-molecules, co-nanoprecipitation of branched A-B block copolymers and hydrophobic guest-molecules was evaluated. It is proposed that during nanoparticle formation, hydrophobic guest-molecules co-precipitate within the hydrophobic segments of the copolymers resulting in *p*(HPMA)-material cores, with PEG coronas. Linear A-B block copolymers were not utilised here due to rapid de-stabilisation of nanoparticles. Branched A-B block copolymers with a target $DP_n$ of 80 monomer units within the *p*(HPMA) primary chain length and varying PEG block chain lengths were chosen as a model to evaluate loading. It should be noted here that preliminary experiments showed that the loading capacity of the EBiB-initiated *p*(($HPMA_x$)-*co*-$EGDMA_{0.95}$) branched polymers was extremely limited with nanoparticle aggregation apparent after only several hours.

A variety of readily available hydrophobic guest-molecules were utilised in order to evaluate stability/size data prior to investigations using the HIV/AIDS antiretroviral drug Lopinavir (LPV). This is due to the limited availability and cost of LPV, where preliminary experiments could potentially eliminate drug wastage. Oil red O, Pyrene

and Ibuprofen were chosen as hydrophobic guest-molecules for these initial scoping investigations. The various branched copolymers were co-dissolved in acetone (5 mg $mL^{-1}$) with a guest-molecule (at varied concentrations) before nanoprecipitation into water using a rapid approach and achieving a final copolymer concentration of 1 mg $mL^{-1}$ and a five-fold decrease in guest-molecule concentration. This method is outlined in Chapter 2 section 2.5.1.4 and is similar to other reported methods of drug encapsulation using nanoprecipitation.[4,5,6,7,8] The resulting nanoparticles were analysed by DLS where comparisons between loaded and un-loaded particles can be seen.

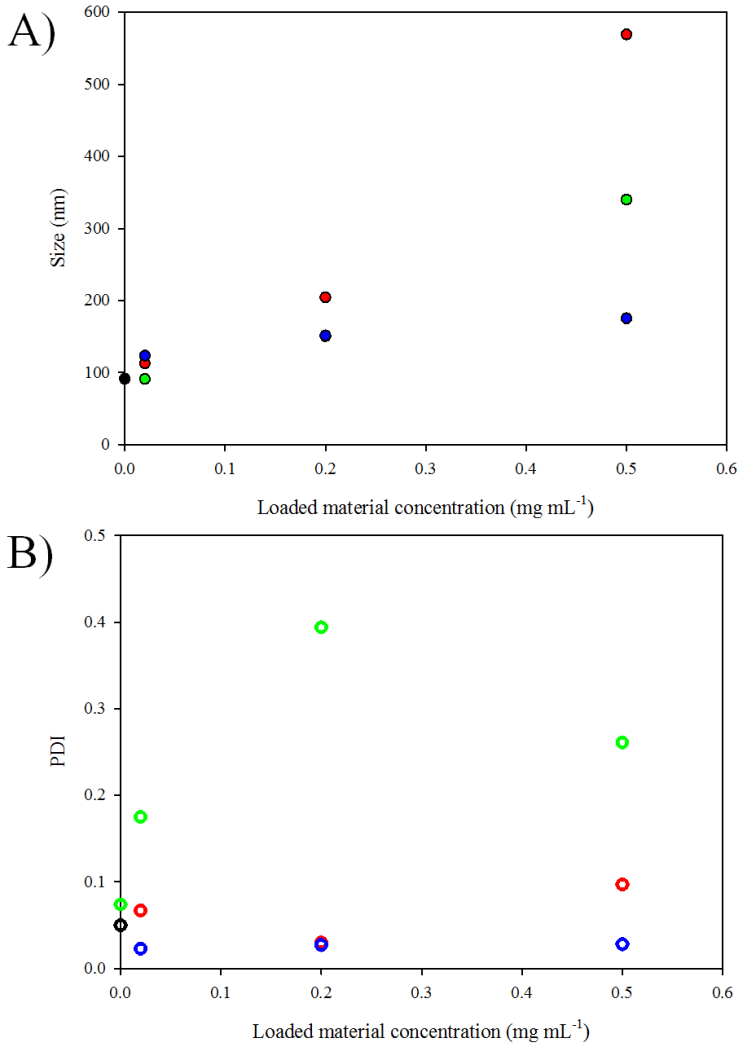


Figure 6.19: Loaded nanoparticle analysis using $PEG_{17}$-*b*-(*p*($HPMA_{80}$)-*co*-$EGDMA_{0.95}$)) using rapid nanoprecipitation (5 mg $mL^{-1}$ starting concentration; 1 mg $mL^{-1}$ final concentration), with varied loading material concentration, A) Z-average particle diameter *vs*. loading. B) Polydispersity *vs*. loading. Blank nanoparticle (black), Oil Red O (red), Pyrene (green), Ibuprofen (blue).

It is seen that $PEG_{17}$-*b*-(*p*($HPMA_{80}$)-*co*-$EGDMA_{0.95}$)) nanoparticles can successfully encapsulate guest molecules with concentrations of up to 0.5 mg $mL^{-1}$ (Figure 6.19). Higher loading concentrations were unsuccessful where nanoparticles precipitated after several hours. Figure 6.19 (B) indicates that nanoparticles which contain Pyrene have significantly higher polydispersities in comparison to Oil red O and

Ibuprofen. The exact reason for this is unknown but may be due to the rigid structure of Pyrene (planar and aromatic), where packing efficiency may be less than the other materials (see Figure 6.25). Individual DLS measurements are shown in Figure 6.20 where direct comparison between z-average diameter and guest-molecule concentration can be clearly seen.

Figure 6.20 shows the comparison between loaded and-unloaded $PEG_{17}$-*b*-(*p*($HPMA_{80}$)-*co*-$EGDMA_{0.95}$)) nanoparticles, where z-average diameter increases as loading also increases. This may suggest a similar number of nanoparticles are forming during nanoprecipitation under different conditions, whereby the incorporation of hydrophobic material ultimately leads to larger particles; however, this is only speculative. It should be noted that polydispersity of nanoparticles remains relatively low (apart from Pyrene loading), despite guest-molecule concentration increasing, suggesting nanoprecipitation mechanisms are well controlled.

An identical experimental protocol was followed using $PEG_{45}$-*b*-(*p*($HPMA_{80}$)-*co*-$EGDMA_{0.95}$)) where guest-molecule loading of up to 1 mg $mL^{-1}$ is found. It should be noted that higher loading was attempted, however, nanoparticles precipitated after less than one day and were therefore not analysed. An overview of the loading capacity of $PEG_{45}$-*b*-(*p*($HPMA_{80}$)-*co*-$EGDMA_{0.95}$)) nanoparticles is shown in Figure 6.21and Figure 6.22.

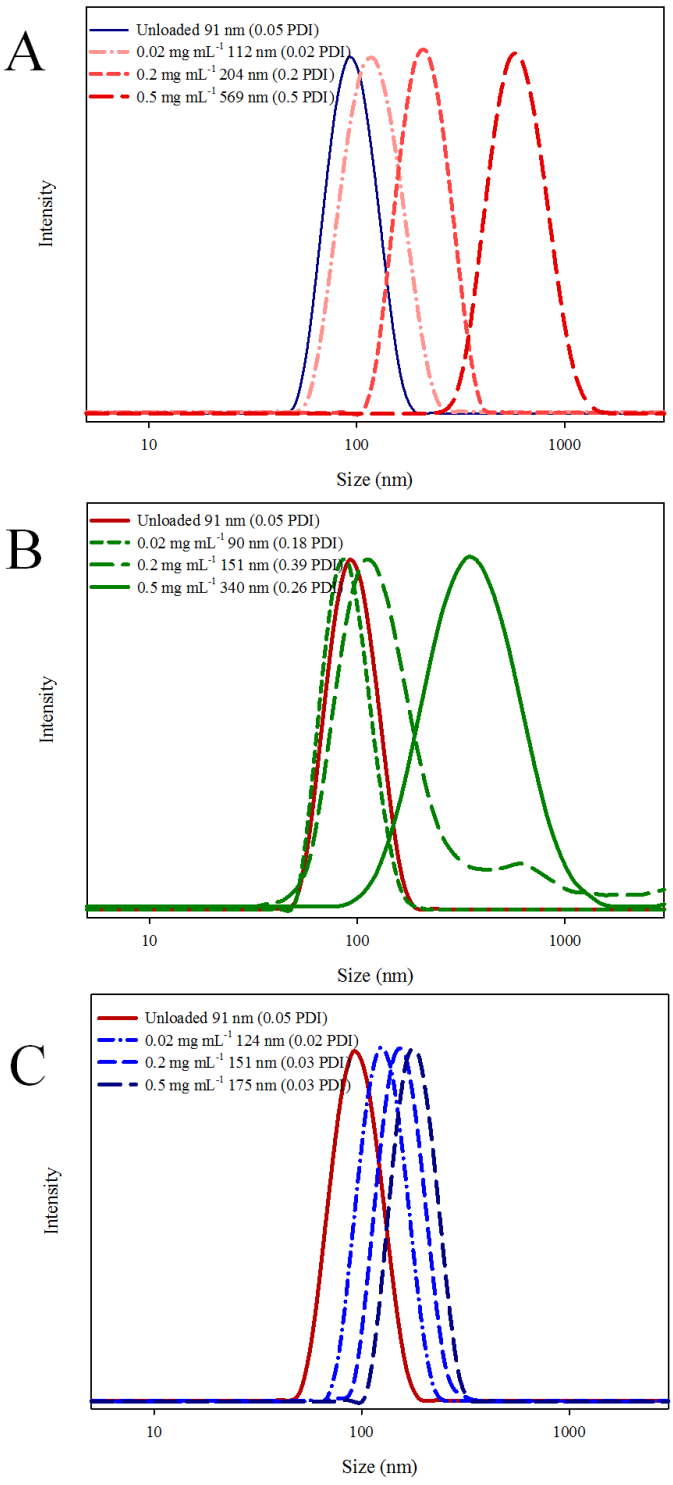


Figure 6.20: Loaded nanoparticle analysis of $PEG_{17}$-*b*-(*p*($HPMA_{80}$)-*co*-$EGDMA_{0.95}$)) using rapid nanoprecipitation (5 mg $mL^{-1}$ starting concentration; 1 mg $mL^{-1}$ final concentration), with varied loading material concentration, A) Oil Red. B) Pyrene. C) Ibuprofen.

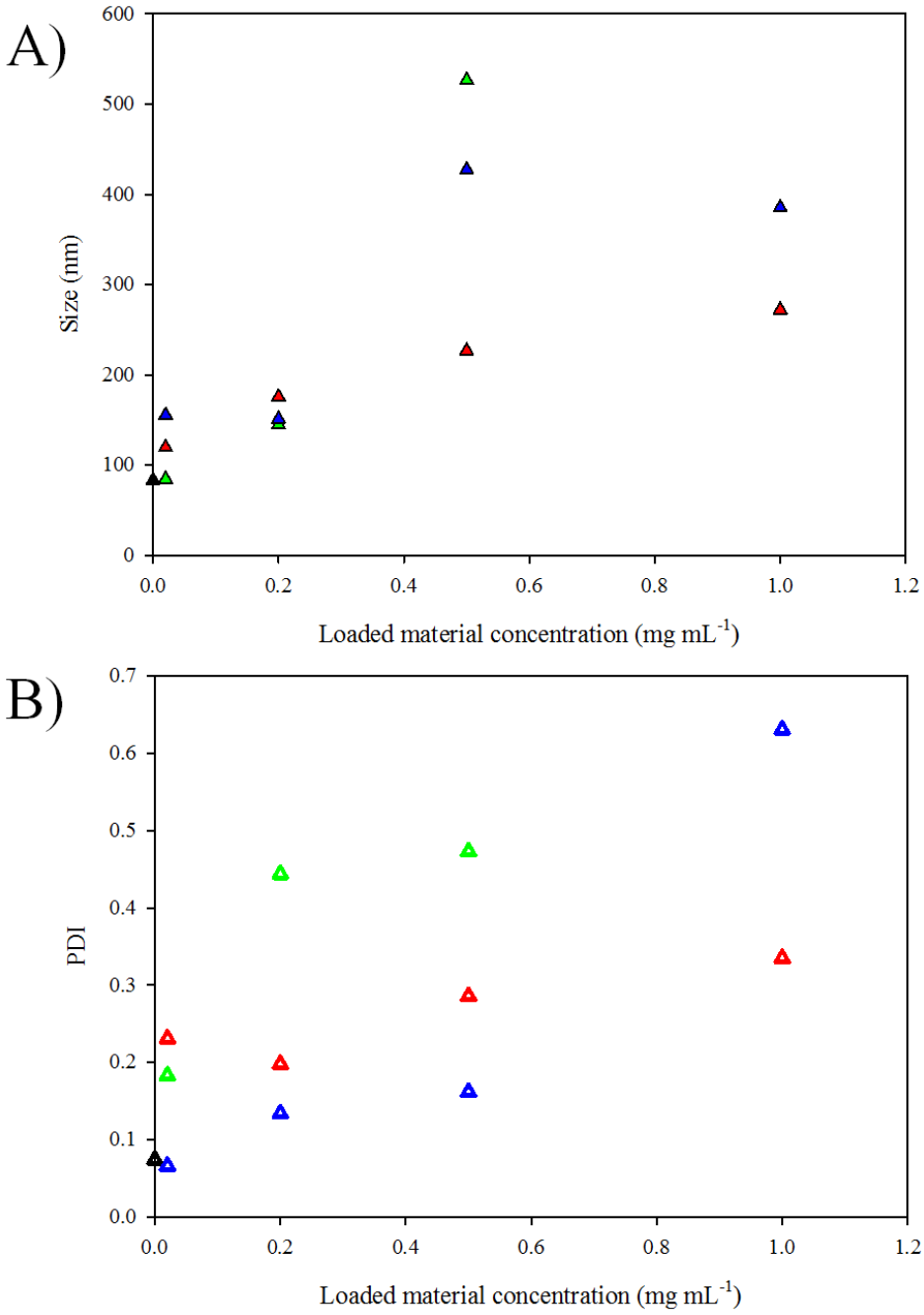


Figure 6.21: Loaded nanoparticle analysis using $PEG_{45}$-*b*-(*p*($HPMA_{80}$)-*co*-$EGDMA_{0.95}$)) using rapid nanoprecipitation (5 mg $mL^{-1}$ starting concentration; 1 mg $mL^{-1}$ final concentration), with varied loading material concentration, A) Z-average particle diameter *vs*. loading. B) Polydispersity *vs*. loading. Blank nanoparticle (black), Oil Red (red), Pyrene (green), Ibuprofen (blue).

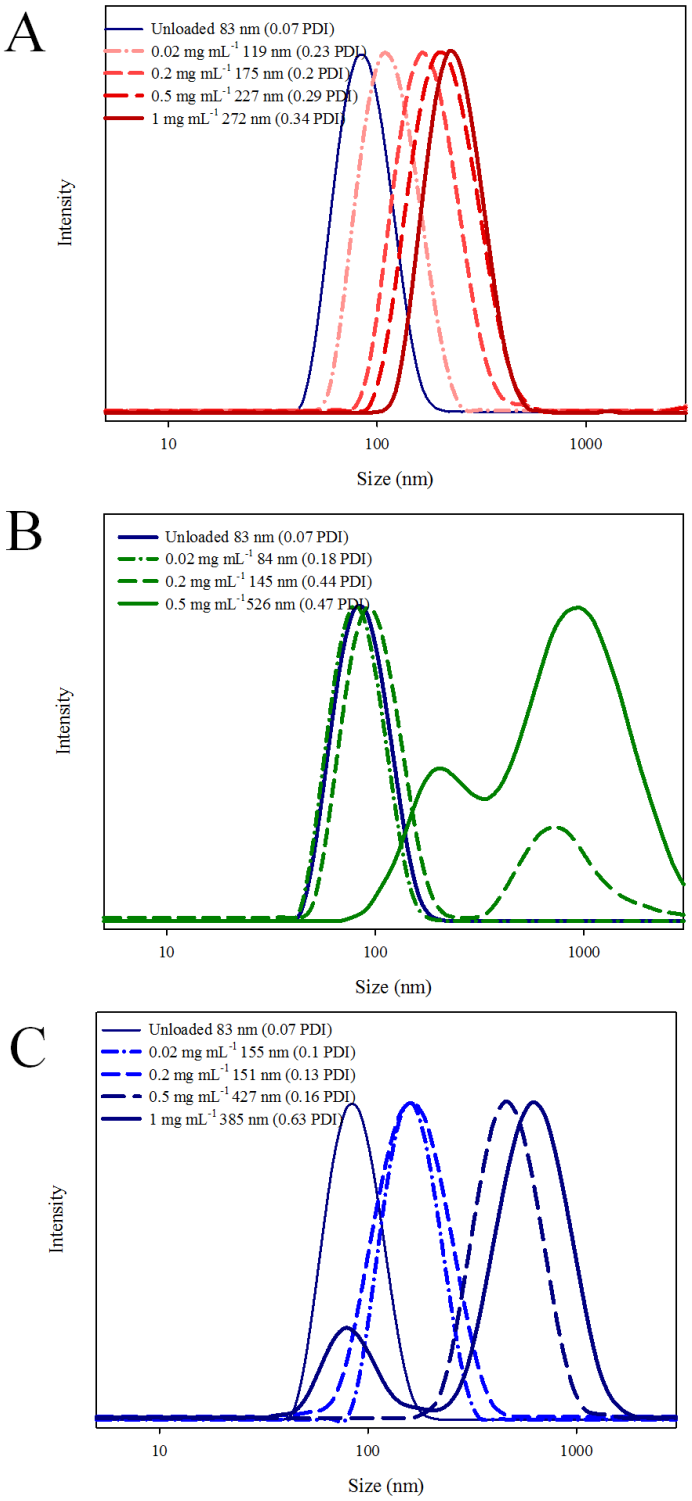


Figure 6.22: Loaded nanoparticle analysis of $PEG_{45}$-*b*-(*p*($HPMA_{80}$)-*co*-$EGDMA_{0.95}$)) using rapid nanoprecipitation (5 mg $mL^{-1}$ starting concentration; 1 mg $mL^{-1}$ final concentration), with varied loading material concentration, A) Oil Red. B) Pyrene. C) Ibuprofen.

Similarly to $PEG_{17}$-*b*-(*p*($HPMA_{80}$)-*co*-$EGDMA_{0.95}$)) nanoparticles, as Oil Red O concentration increases, z-average diameter increases whilst polydispersity remains relatively narrow (Figure 6.21). Nanoparticles with diameters of 272 nm formed with 1 mg $mL^{-1}$ of Oil Red O, compared to 83 nm for blank nanoparticles; the nanoparticle diameter has more than doubled in this case. A Pyrene loading of only 0.5 mg $mL^{-1}$ could be achieved using $PEG_{45}$-*b*-(*p*($HPMA_{80}$)-*co*-$EGDMA_{0.95}$)), where rapid precipitation occurred for higher concentrations. $PEG_{45}$-*b*-(*p*($HPMA_{80}$)-*co*-$EGDMA_{0.95}$)) nanoparticles could successfully load Ibuprofen up to 0.5 mg $mL^{-1}$ whilst maintaining monomodal size distributions; however, when 1 mg $mL^{-1}$ of Ibuprofen is co-precipitated, two discrete size distributions appear (Figure 6.22 (C)) The small peak (approximately 80 nm) shows significant overlap with un-loaded nanoparticles suggesting ibuprofen loading varies between individual nanoparticles.

In comparison to Figure 6.19, increasing $PEG_x$ chain length (from $PEG_{17}$ to $PEG_{45}$) has a direct impact on nanoparticle loading capacity. This can be observed directly, as a higher concentration of oil red, and ibuprofen (double the mass of encapsulated material with respect to total polymer concentration) could be successfully encapsulated (1 mg $mL^{-1}$, compared to 0.5 mg $mL^{-1}$) into nanoparticles, whilst maintaining copolymer concentration (1 mg $mL^{-1}$). Hypothetically, when increasing $PEG_x$ chain length, $PEG_{113}$-*b*-(*p*($HPMA_{80}$)-*co*-$EGDMA_{0.95}$)) nanoparticles should successfully load materials with higher concentrations than 1 mg $mL^{-1}$, whilst keeping copolymer concentration constant (1 mg $mL^{-1}$). Analysis of loaded $PEG_{113}$-*b*-(*p*($HPMA_{80}$)-*co*-$EGDMA_{0.95}$)) nanoparticles is shown in Figure 6.23 and Figure 6.24.

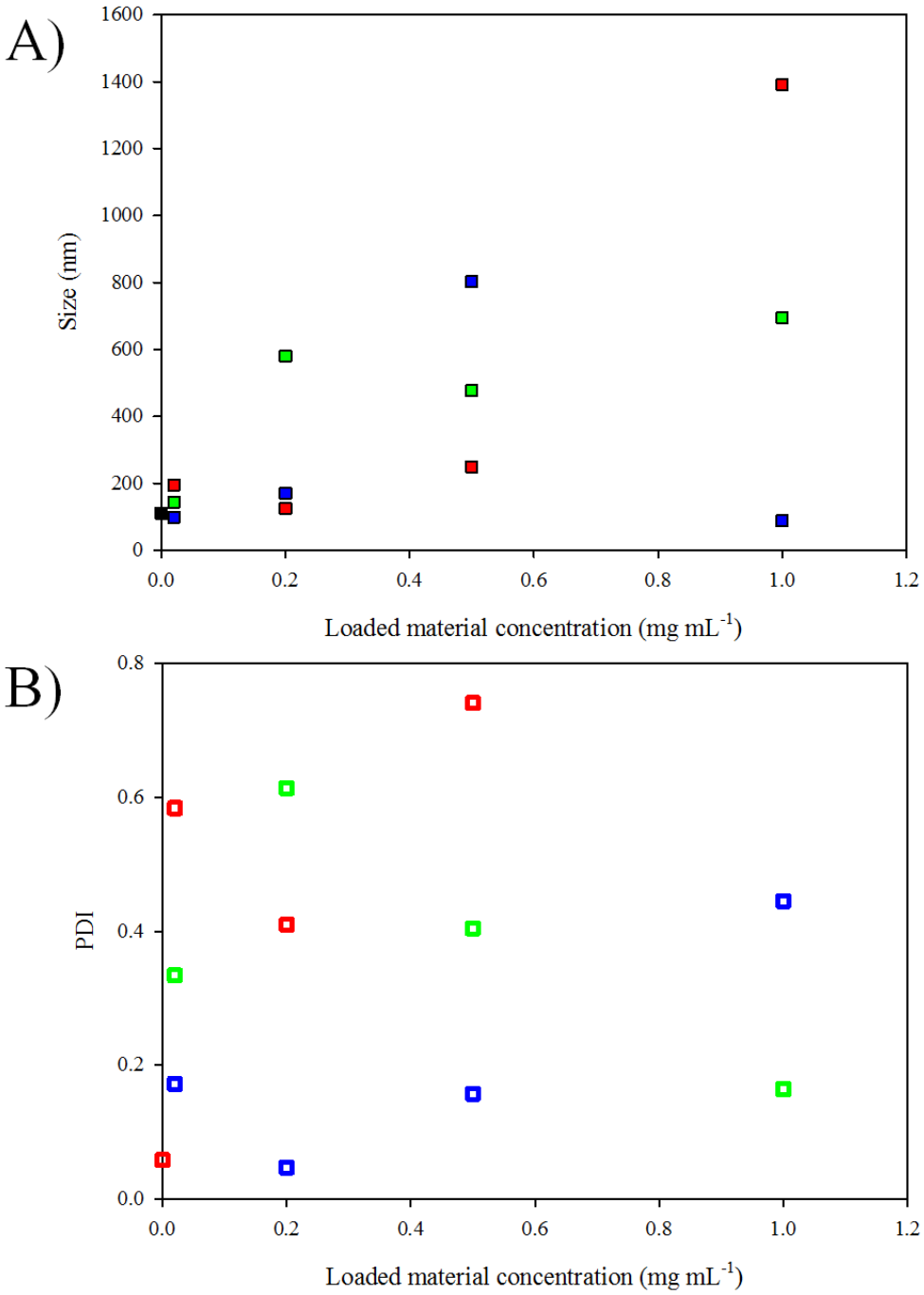


Figure 6.23: Loaded nanoparticle analysis using $PEG_{113}$-*b*-(*p*($HPMA_{80}$)-*co*-$EGDMA_{0.95}$)) using rapid nanoprecipitation (5 mg $mL^{-1}$ starting concentration; 1 mg $mL^{-1}$ final concentration), with varied loading material concentration, A) Z-average particle diameter *vs*. loading. B) Polydispersity *vs*. loading. Blank nanoparticle (black), Oil Red (red), Pyrene (green), Ibuprofen (blue).

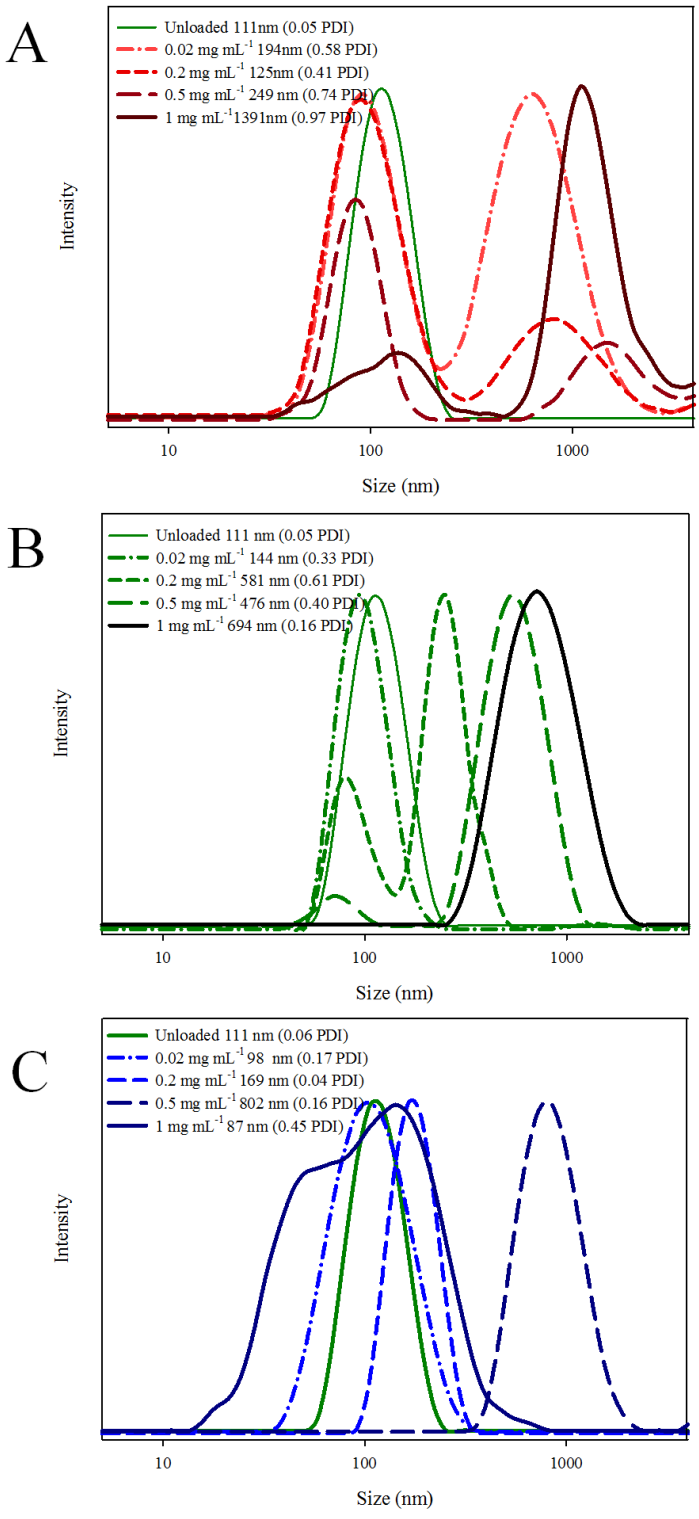


Figure 6.24: Loaded nanoparticle analysis of $PEG_{113}$-*b*-(*p*($HPMA_{80}$)-*co*-$EGDMA_{0.95}$)) using rapid nanoprecipitation (5 mg $mL^{-1}$ starting concentration; 1 mg $mL^{-1}$ final concentration), with varied loading material concentration, A) Oil Red. B) Pyrene. C) Ibuprofen.

Loading of Oil Red into $PEG_{113}$-*b*-(*p*($HPMA_{80}$)-*co*-$EGDMA_{0.95}$)) nanoparticles did not successfully encapsulate at concentrations > 1 mg $mL^{-1}$; clear monomodal traces were not found and significant overlap of unloaded material is seen in Figure 6.24 (A), however, the exact reason for this is unknown. A similar trend is found for Pyrene loading, however, a monomodal trace is reported for loading of 1 mg $mL^{-1}$ Pyrene where z-average diameter increases from 111 nm (un-loaded) to 694 nm (1 mg $mL^{-1}$ Pyrene). An attempt was made to load 2 mg $mL^{-1}$ of Pyrene into nanoparticles; however, precipitation occurred several hours after preparation. Loading $PEG_{113}$-*b*-(*p*($HPMA_{80}$)-*co*-$EGDMA_{0.95}$)) nanoparticles with a small amount of Ibuprofen (0.02 mg $mL^{-1}$) does not produce particles with a larger z-average, however, Figure 6.24 (C) demonstrates that the nanoparticles' polydispersity increases on loading with a guest molecule; possible indicating irregular distribution of Ibuprofen within nanoparticle cores. Loading of 1 mg $mL^{-1}$ Ibuprofen resulted in an unsymmetrical DLS trace, with a broad polydispersity (0.45), suggesting nanoparticle formation is irregular. It should be noted that these dispersions remained stable for > two weeks before the onset of precipitation.

It is also worth noting that the branched copolymers containing $PEG_{113}$ as the hydrophilic block segment have an appreciable solubility in water and it is possible that the high ratio of PEG within these A-B amphiphilic block copolymers hinders the formation of encapsulated material during co-nanoprecipitaion.

The data reported in these experiments suggests that loaded nanoparticle formation is highly complex; affected by factors such as guest-molecule structure and their miscibility in *p*(HPMA). The data also suggests that copolymers with longer $PEG_x$ chains can load a higher concentration of guest-molecules resulting in stable nanoparticles; however, long PEG chains that also impart some enhanced

hydrophilicity may hamper guest encapsulation. In order to consistently generate monomodal nanoparticle distributions, further optimisation experiments are necessary.

### 6.10.1 LPV Loading capacity evaluation of $PEG_x$-*b*-(*p*($HPMA_{80}$)-*co*-($EGDMA_{0.95}$)) Nanoparticles ($x$ = 17, 45, 113)

This aim of this section was to produce aqueous suspensions of stable LPV loaded nanoparticles, where variation of concentration parameters was investigated in order to optimise conditions. Ultimately, a concentrated stable nanosuspension of LPV would provide a potential oral route of drug administration for HIV/AIDS patients. Encapsulating the drug into $PEG_x$-*b*-(*p*($HPMA_y$)-*co*-$EGDMA_{0.95}$)) nanoparticles may improve bioavailability of the drug through prolonged circulation time and minimising first pass metabolism. If loaded nanoparticles are highly stable, they may successfully permeate cell membranes to reach the blood stream followed by macrophage uptake. Macrophages have been highlighted as HIV reservoir sites and it is postulated that enzymatic degradation of nanoparticles will release the drug at the site of replication. However, the aim of this chapter was to assess solely the LPV loading capacity of branched copolymer nanoparticles, which would lead to optimisation of synthetic protocol.

Section 6.10 failed to draw solid conclusions between nanoparticle loading capacity and $PEG_x$ chain length. In the experiments, 5 mg $mL^{-1}$ copolymer solutions were precipitated to give a final concentration of 1 mg $mL^{-1}$; however, this does not take into account the relative molar ratios of $PEG_x$ and HPMA monomer units. For example, a 5 mg $mL^{-1}$ sample of *p*($HPMA_{80}$)-*co*-$EGDMA_{0.95}$) contains only HPMA monomer repeat units in the copolymer primary chain (EGDMA repeat units were

not taken into account), a 5 mg $mL^{-1}$ sample of $PEG_{17}$-*b*-(*p*($HPMA_{80}$)-*co*-$EGDMA_{0.95}$)) contains PEG and less HPMA monomer units, (6.1 % PEG, 93.9 % *p*(HPMA). To maintain the same mass of HPMA in both copolymer acetone solutions, simply dividing this HPMA % by 5 achieves the corrected mass for preparing samples. (e.g. 5/0.939 = 5.32 mg $mL^{-1}$).

Before studying the encapsulation of LPV, the four molecules that have been studied as guest molecules need to be considered in detail. Figure 6.25 shows the relative chemical structures of each guest molecule studied.

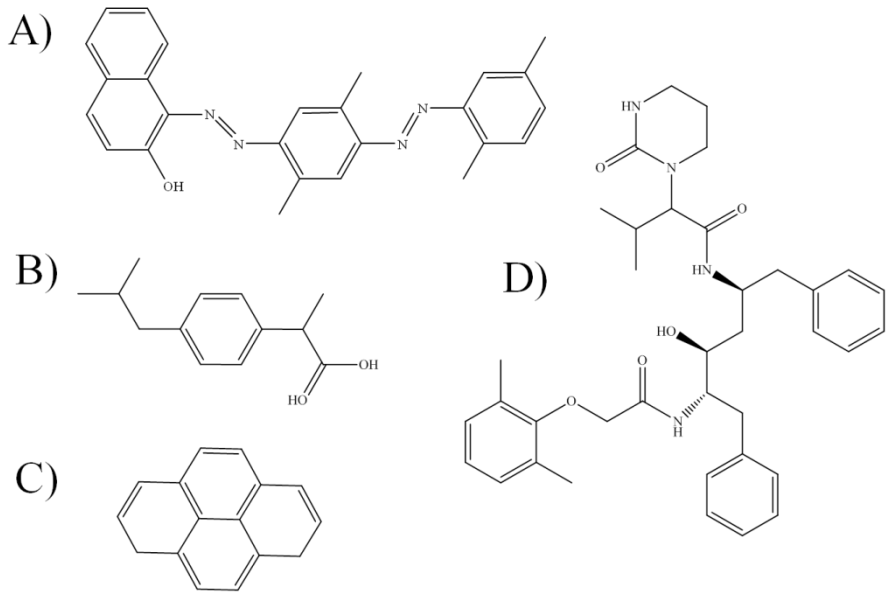


Figure 6.25: Chemical structures of hydrophobic guest-molecules. A) Oil Red O. B) Ibuprofen. C) Pyrene. D) Lopinavir.

LPV is a complex chiral compound with a high molecular mass; greater than 1.5 times the mass of Oil Red. Comparatively, Oil Red has a molecular mass of 408.5 g $mol^{-1}$; Pyrene has a molecular mass of 202.3 g $mol^{-1}$; Ibuprofen has a molecular mass of 209.3 g $mol^{-1}$; and LPV has a molecular mass of 628.8 g $mol^{-1}$. By preparing adjusted copolymer concentrations, a direct comparison between nanoparticle

loading capacities, with respect to PEG content was investigated for LPV-containing nanoparticles.

A series of copolymers were nanoprecipitated with a five-fold dilution and using adjusted concentrations to provide the same HPMA mass content in the final dispersion these were approximately 5 mg $mL^{-1}$ with respect to *p*(HPMA). Table 6.14 indicates starting and final concentrations of the polymers used alongside the DLS nanoparticle analysis.

| Copolymer | HPMA monomer content (%) | Starting Concentration (mg $mL^{-1}$) | Final Concentration (mg $mL^{-1}$) | Z-Average Diameter (nm) | Polydispersity |
|---|---|---|---|---|---|
| $PEG_{17}$-*b*-*p*((HPMA$_{50}$)-*co*-EGDMA$_{0.95}$) | 90.56 | 5.52 | 1.1 | 70 | 0.0950 |
| $PEG_{17}$-*b*-*p*(HPMA$_{80}$)-*co*-EGDMA$_{0.95}$) | 93.90 | 5.32 | 1.06 | 70 | 0.1850 |
| $PEG_{17}$-*b*-*p*(HPMA$_{120}$-*co*-EGDMA$_{0.95}$)) | 95.83 | 5.21 | 1.04 | 108 | 0.2400 |
| $PEG_{45}$-*b*-*p*(HPMA$_{50}$)-*co*-EGDMA$_{0.95}$) | 78.6 | 6.39 | 1.28 | 29 | 0.1610 |
| $PEG_{45}$-*b*-*p*(HPMA$_{80}$)-*co*-EGDMA$_{0.95}$) | 85.18 | 5.87 | 1.17 | 35 | 0.1370 |
| $PEG_{45}$-*b*-*p*(HPMA$_{120}$)-*co*-EGDMA$_{0.95}$) | 89.64 | 5.58 | 1.12 | 89 | 0.0280 |
| $PEG_{113}$-*b*-*p*(HPMA$_{50}$)-*co*-EGDMA$_{0.95}$) | 59 | 8.47 | 1.69 | 32 | 0.3120 |
| $PEG_{113}$-*b*-*p*(HPMA$_{80}$)-*co*-EGDMA$_{0.95}$) | 69.97 | 7.18 | 1.44 | 35 | 0.0580 |
| $PEG_{113}$-*b*-*p*(HPMA$_{120}$-*co*-EGDMA$_{0.95}$)) | 77.58 | 6.45 | 1.29 | 66 | 0.3830 |

Table 6.14: Nanoparticle analysis of $PEG_x$-*b*-(*p*(HPMA)-*co*-EGDMA$_{0.95}$)) using rapid nanoprecipitation (five-fold dilution). Concentrations adjusted for *p*(HPMA) content.

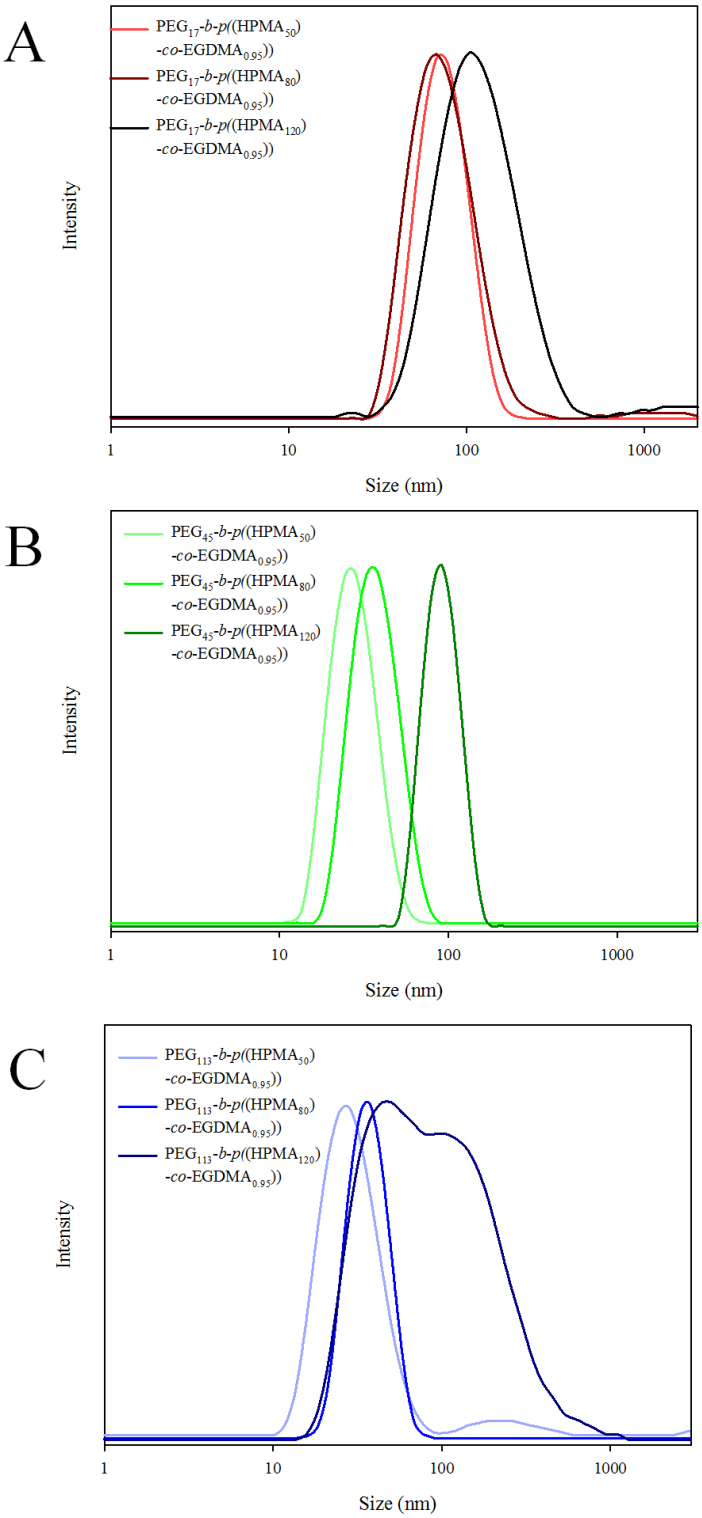


Figure 6.26: Nanoparticle analysis of $PEG_x$-*b*-(*p*(HPMA)-*co*-$EGDMA_{0.95}$)) using rapid nanoprecipitation (five-fold dilution). Concentrations adjusted for *p*(HPMA) content (see Table 6.14). (Approximately 5 mg $mL^{-1}$ starting concentration, 1 mg $mL^{-1}$ final concentration). (A) $PEG_{17}$, (B) $PEG_{45}$, (C) $PEG_{113}$.

Figure 6.26 and Table 6.14 demonstrate that the smallest nanoparticles are generally formed utilising a target $DP_n$ = 50 monomer units, where z-average diameter increases as *p*(HPMA) primary chain length increases, irrespective of $PEG_x$ chain length. Little difference is noted between nanoparticle samples in Figure 6.26 (A) however for a target $DP_n$ of 120 monomer units, z-average diameter increases to 108 nm (compared to 70 for target $DP_n$ = 50, 80 monomer units). Figure 6.26 (B) and Table 6.14 clearly shows PEG-*b*-*p*((HPMA$_x$)-*co*-EGDMA$_{0.95}$)) nanoparticle z-average diameter increasing as target $DP_n$ increases, with narrow polydispersities consistently found. Unfortunately the same clear trend could not be found for $PEG_{113}$-*b*-*p*((HPMA$_x$)-*co*-EGDMA$_{0.95}$) (Figure 6.26 (C)) where nanoparticles formed using a target $DP_n$ = 50 monomer units formed in two discrete size ranges, and particles whose copolymer had a target $DP_n$ = 50 monomer units formed a bimodal polydisperse sample. This data suggests that the size of PEG containing nanoparticles cannot be systematically varied through changes in concentration parameters, despite maintaining a constant mass of *p*(HPMA) within samples.

Nevertheless, aiming to maintain the same concentration of *p*(HPMA) within nanoparticle samples is thought to aid in the optimisation of LPV loading studies. It is presumed that LPV and *p*(HPMA) are miscible (and hydrophobic), and will therefore co-exist surrounded by a hydrophilic PEG shell. If copolymer concentrations are not adjusted to account for PEG content (i.e. maintaining a 5 mg $mL^{-1}$ starting concentration), the ratio of LPV/*p*(HPMA) decreases as PEG chain length increases.

It was not assumed that LPV would be successfully encapsulated within stable nanoparticle cores, as loading capacity will be affected by the structure/chemistry of LPV, however, using section 6.10 as a guide, and utilising the same encapsulation

protocol, a series of experiments were attempted to identify issues with LPV as a guest within these branched copolymer nanoparticle systems.

| Polymer | *p*(HPMA) $M_n$ (g mol$^{-1}$) | *p*(HPMA) Wt% | Initial polymer concentration (mg mL$^{-1}$) | Final polymer concentration (mg mL$^{-1}$) | Initial LPV concentration (mg mL$^{-1}$) | Final LPV concentration (mg mL$^{-1}$) | Stable for 1 day (mg mL$^{-1}$) | Stable for 5 days (mg mL$^{-1}$) |
|---|---|---|---|---|---|---|---|---|
| **PEG$_{17}$-*b*-*p*((HPMA$_{50}$)-*co*-EGDMA$_{0.95}$** | 7950 | 90.56 | 5.52 | 1.1 | 5 | 1 | Y | N |
| | | | 5.52 | 1.1 | 10 | 2 | N | N |
| | | | 2.76 | 0.55 | 2.5 | 0.5 | Y | N |
| **PEG$_{17}$-*b*-*p*((HPMA$_{80}$)-*co*-EGDMA$_{0.95}$** | 12300 | 93.90 | 10.65 | 2.13 | 5 | 1 | Y | N |
| | | | 5.32 | 1.06 | 5 | 1 | Y | N |
| | | | 5.32 | 1.06 | 10 | 2 | N | N |
| | | | 5.32 | 0.53 | 5 | 1 | Y | N |
| | | | 2.66 | 0.53 | 2.5 | 0.5 | Y | N |
| **PEG$_{17}$-*b*-*p*((HPMA$_{120}$)-*co*-EGDMA$_{0.95}$)** | 18000 | 95.83 | 5.21 | 1.04 | 5 | 1 | Y | N |
| | | | 5.21 | 1.04 | 10 | 2 | N | N |
| | | | 2.61 | 0.52 | 2.5 | 0.5 | Y | N |
| **PEG$_{45}$-*b*-*p*((HPMA$_{50}$)-*co*-EGDMA$_{0.95}$)** | 9200 | 78.6 | 6.389 | 1.28 | 5 | 1 | Y | Y |
| | | | 6.389 | 1.28 | 10 | 2 | Y | N |
| | | | 6.389 | 0.64 | 5 | 1 | Y | N |
| | | | 3.19 | 0.64 | 2.5 | 0.5 | Y | N |
| **PEG$_{45}$-*b*-*p*((HPMA$_{80}$)-*co*-EGDMA$_{0.95}$)** | 13500 | 85.18 | 11.74 | 2.35 | 5 | 1 | Y | N |
| | | | 5.87 | 1.17 | 5 | 1 | Y | Y |
| | | | 5.87 | 1.17 | 10 | 2 | Y | N |
| | | | 5.87 | 0.59 | 5 | 1 | Y | Y |
| | | | 2.93 | 0.59 | 2.5 | 0.5 | Y | Y |
| **PEG$_{45}$-*b*-*p*((HPMA$_{120}$)-*co*-EGDMA$_{0.95}$)** | 19300 | 89.64 | 5.58 | 1.12 | 5 | 1 | Y | N |
| | | | 5.58 | 1.12 | 10 | 2 | Y | Y |
| | | | 5.58 | 0.58 | 5 | 1 | Y | N |
| | | | 2.79 | 0.56 | 2.5 | 0.5 | Y | N |
| **PEG$_{113}$-*b*-*p*((HPMA$_{50}$)-*co*-EGDMA$_{0.95}$)** | 12200 | 59 | 8.47 | 1.69 | 5 | 1 | Y | Y |
| | | | 8.47 | 1.69 | 10 | 2 | Y | N |
| | | | 4.24 | 0.58 | 2.5 | 0.5 | Y | Y |
| **PEG$_{113}$-*b*-*p*((HPMA$_{80}$)-*co*-EGDMA$_{0.95}$)** | 16500 | 69.97 | 14.34 | 2.87 | 5 | 1 | Y | N |
| | | | 7.18 | 1.44 | 5 | 1 | Y | N |
| | | | 7.18 | 1.44 | 10 | 2 | Y | N |
| | | | 7.18 | 0.72 | 5 | 1 | Y | N |
| | | | 3.59 | 0.72 | 2.5 | 0.5 | Y | Y |
| **PEG$_{113}$-*b*-*p*((HPMA$_{120}$)-*co*-EGDMA$_{0.95}$)** | 22300 | 77.58 | 6.45 | 1.29 | 5 | 1 | Y | N |
| | | | 6.45 | 1.29 | 10 | 2 | Y | N |
| | | | 3.22 | 0.64 | 2.5 | 0.5 | Y | Y |

Table 6.15: Overview of other LPV loading studies using amphiphilic branched copolymer nanoparticles prepared *via* rapid nanoprecipitation from acetone.

Table 6.15 shows that loaded LPV nanoparticles can be generated consistently using a variety of branched copolymers. As the PEG increases in length, the ability to form loaded nanoparticles that remain stable for 1 day increases. Branched A-B block copolymers containing short PEG chains are incapable of producing loaded nanoprecipitates with LPV that remain stable for over 5 days, however, the longer chain PEG containing branched polymers do have an ability to do so under varying conditions.

Table 6.16 indicates the z-average diameters of a series of loaded nanoprecipitates, ranging from 220 nm ($PEG_{45}$-*b*-*p*($HPMA_{80}$)-*co*-$EGDMA_{0.95}$)) to 456 nm ($PEG_{113}$-*b*-*p*($HPMA_{50}$)-*co*-$EGDMA_{0.95}$)), it should be noted that these systems all remained stable for > three days before subsequent precipitation.

A higher starting LPV concentration in acetone (10 mg $mL^{-1}$), was also investigated, where copolymer concentration in acetone was kept at approximately 5 mg $mL^{-1}$ (concentration adjusted for HPMA content). Therefore, the final nanoparticle suspensions concentrations were 1 mg $mL^{-1}$ (LPV) and approximately 1 mg $ml^{-1}$ (copolymer). A target $DP_n$ of 80 monomer units for the primary chain length was chosen for this more detailed study as LPV availability was limited and other *p*(HPMA) primary chain lengths had been excluded by earlier testing. Unfortunately $PEG_{17}$-*b*-*p*($HPMA_{80}$)-*co*-$EGDMA_{0.95}$) nanoparticles rapidly precipitated after synthesis of nanoparticles and therefore could not be analysed, $PEG_{45}$-*b*-*p*($HPMA_{80}$)-*co*-$EGDMA_{0.95}$) and $PEG_{113}$-*b*-*p*($HPMA_{80}$)-*co*-$EGDMA_{0.95}$) nanoparticles, however, remained stable for > 5 days. All z-average diameters of loaded nanoparticles were higher than blank nanoparticles, indicative of LPV encapsulation. This is shown for sample copolymer-LPV systems in Figure 6.27, where target $DP_n$ = 80 monomer units.

| Copolymer | Starting Concentration (mg $mL^{-1}$) | Final Concentration (mg $mL^{-1}$) | Z-Average Diameter (nm) | Polydispersity |
|---|---|---|---|---|
| $PEG_{17}$-*b*-*p*(($HPMA_{50}$)-*co*-$EGDMA_{0.95}$) | 5.52 | 1.1 | 234 | 0.4290 |
| $PEG_{17}$-*b*-*p*($HPMA_{80}$) -*co*-$EGDMA_{0.95}$) | 5.32 | 1.06 | 284 | 0.4620 |
| $PEG_{17}$-*b*-*p*($HPMA_{120}$-*co*-$EGDMA_{0.95}$)) | 5.21 | 1.04 | 276 | 0.4850 |
| $PEG_{45}$-*b*-*p*($HPMA_{50}$) -*co*-$EGDMA_{0.95}$) | 6.39 | 1.28 | 313 | 0.2030 |
| $PEG_{45}$-*b*-*p*($HPMA_{80}$) -*co*-$EGDMA_{0.95}$) | 5.87 | 1.17 | 220 | 0.1760 |
| $PEG_{45}$-*b*-*p*($HPMA_{120}$) -*co*-$EGDMA_{0.95}$) | 5.58 | 1.12 | 255 | 0.3710 |
| $PEG_{113}$-*b*-*p*($HPMA_{50}$) -*co*-$EGDMA_{0.95}$) | 8.47 | 1.69 | 456 | 0.1370 |
| $PEG_{113}$-*b*-*p*($HPMA_{80}$) -*co*-$EGDMA_{0.95}$) | 7.18 | 1.44 | 335 | 0.2920 |
| $PEG_{113}$-*b*-*p*($HPMA_{120}$-*co*-$EGDMA_{0.95}$)) | 6.45 | 1.29 | 234 | 0.3360 |

Table 6.16: Analysis of $PEG_x$-*b*-(*p*(HPMA)-*co*-$EGDMA_{0.95}$)) /LPV loaded nanoparticles using rapid nanoprecipitation (five-fold dilution). Concentrations adjusted for *p*(HPMA) content. LPV starting concentration 5 mg $mL^{-1}$, final concentration 1 mg $mL^{-1}$.

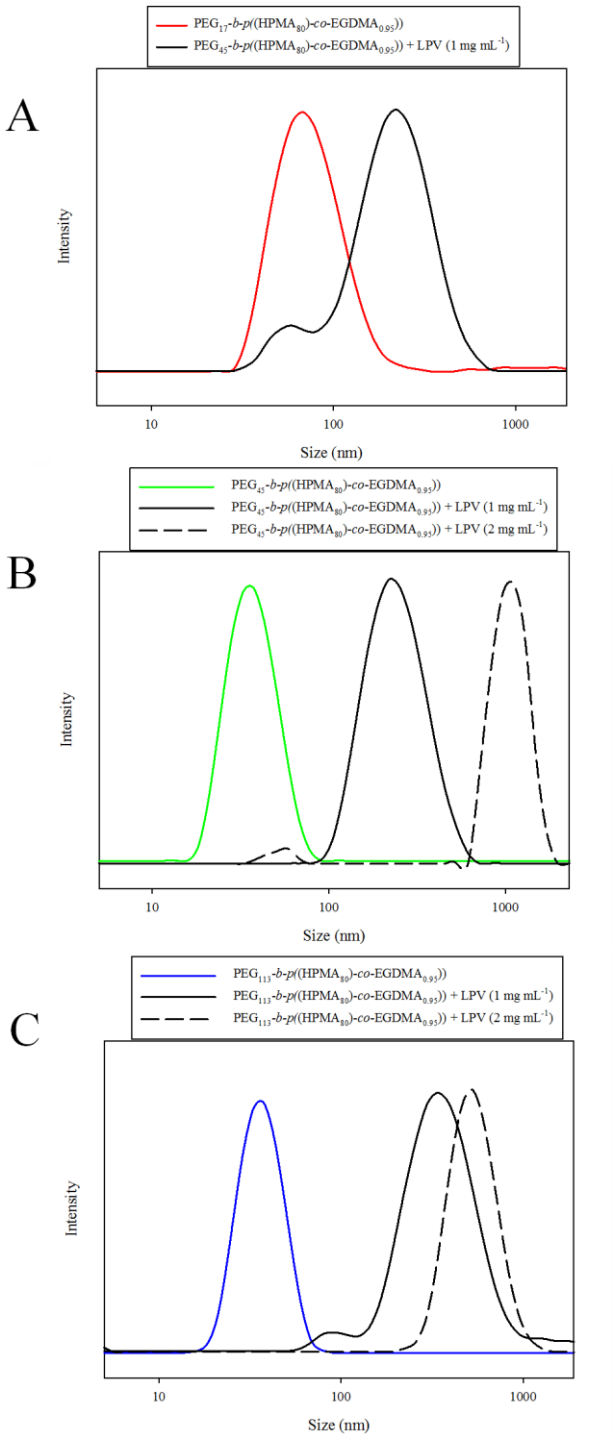


Figure 6.27: Analysis of LPV loaded $PEG_x$-*b*-(*p*(HPMA)-*co*-$EGDMA_{0.95}$)) and blank nanoparticles prepared using rapid nanoprecipitation (five-fold dilution). Copolymer concentrations adjusted for *p*(HPMA) content (see Table 6.16). (Approximately 5 mg $mL^{-1}$ starting concentration, 1 mg $mL^{-1}$ final concentration). (A) $PEG_{17}$, (B) $PEG_{45}$, (C) $PEG_{113}$.

Figure 6.27 suggests nanoparticles could successfully encapsulate LPV, characterised by an increase in z-average diameter as LPV concentration increases (for $PEG_{45}$-*b*-*p*($HPMA_{80}$)-*co*-$EGDMA_{0.95}$) and $PEG_{113}$-*b*-*p*($HPMA_{120}$-*co*-$EGDMA_{0.95}$)). Figure 6.27 (A) shows peak overlay between loaded and unloaded nanoparticles, this may suggest a proportion of nanoparticles contain no, or very little, encapsulated LPV. It is shown in Figure 6.27 (B) that z-average diameter increases as LPV concentration increases; this may indicate that similar numbers of nanoparticles are formed during nanoprecipitation which have significantly more dense hydrophobic cores. Figure 6.27 (C) shows the same trend of z-average diameter increase with increasing LPV, however in this case z-average diameter does not increase in regular intervals (seen in Figure 6.27 (B)), the reason for this is unknown.

## 6.11 Summary

This chapter has reported the facile nanoprecipitation of amphiphilic linear and branched block copolymers, where various preparation methods have been evaluated. Data consistently show that linear copolymers do not form stable nanostructures in water, whereas amphiphilic A-B block copolymers with branched *p*(HPMA) structures do form stable nanoparticles when produced by rapid nanoprecipitation. Trends in nanoparticle size/polydispersity were investigated by producing a large screen where copolymers (of varying amphiphilicity) were nanoprecipitated to various dilutions, however, clear and trends could not be found. The stability of nanoparticles has been evaluated by conducting a serial aqueous dilution experiment showing little change in z-average diameter during dilution. The

surface charge of PEG containing copolymer nanoparticles was also investigated where particles become more positive as copolymer PEG content increases. The loading capacity of a variety of copolymer nanoparticles with guest-molecules has also been evaluated with data suggesting stability/loading is proportional to PEG chain length. A series of LPV-loaded nanoparticles that exhibit stability for greater than 5 days have been produced and further research is required to evaluate these in relevant cell and in vivo models.

## 6.12 References

1 Hui. G., Yanan. M., Xueyou. L., Yongri. L., Baoquan. C., Jianbiao. M., *Eur Polym J*, **2011**, *47*, 1232.

2 Kim. S. Y.,, Shin. I. L. G., Lee. Y. M., Cho. C. S.,, Sung. Y. K., *J Control Release*, **1998**, *51*, 13.

3 Chan. J. M., Zhang. L., Yuet. K. P., Liao. G., Rhee. J., Langer. R., Farokhzad. O. C., *Biomaterials*, **2009**, *30*, (*8*), 1627.

4 Chorny. M., Fishbein. I., Danenberg. H. D., Golomb. G., *J Control Release*, **2002**, *83*, 389.

5 Govender.T., Stolnik. S., Garnett. M. C., Illum. L., Davis. S. S., *J Control Release*, **1999**, *57*, (*2*), 171.

6 Yordanov. G., Skrobanska. R., Evangelatov. A., *Colloid Surface B*, **2012**, *92*, 98.

7 Betancourt. T., Brown. B., Brannon-Peppas. L., *Nanomedicine*, **2007**, *2*, (*2*), 219.

8 Barichello. J. M., Morishita. M., Takayama. K., Nagai. T., *Drug Dev Ind Pharm*, **1999**, *25*, (*4*), 471.

# 7. Conclusions and Further Work

## 7.1 Overview of Chapter 3

Methanolic ATRP was used to synthesise linear *p*(HPMA$_x$) using a facile one-pot methodology. By varying the ratio of initiator:monomer feed, homopolymers with varying chain lengths (50, 80, 120 monomer units) could be generated. $^1$H NMR spectroscopic analysis confirmed all reactions proceeded to > 99 % conversion, judged by the disappearance of monomer vinyl proton resonances. Through GPC analysis, actual $M_n$ was found to be extremely close to predicted $M_n$ for all polymer samples, where $M_w/M_n$ remained low. Detailed kinetic analysis showed that all polymerisations proceeded in a controlled manner with excellent correlation to expected ATRP behaviour. A self-blocking experiment also confirmed that chain end functionality was maintained at relatively high conversion, generating block copolymers with a narrow molecular weight distribution and accurate molecular weight. Branched *p*(HPMA) copolymers were prepared using the same one-pot methodology where (ratio of initiator:EGDMA was kept constant at 1:0.95) producing soluble high molecular weight material analysed by triple detection GPC. It has been shown that a variety of *p*(HPMA) primary chain lengths could be targeted (DP$_n$ = 50, 80, 120 monomer units), where detailed kinetic analysis showed little differences between linear and branched reactions. The evolution of branching during copolymerisation was characterised by triple detection GPC analysis, performed at regular intervals, showing a dramatic increase in molecular weight at high conversion, consistent with reported Monte Carlo modelling predictions for branched vinyl polymerisation using controlled radical techniques. GPC analysis of

repeat polymerisations confirmed near identical molecular weights could be attained for both linear and branched materials, which has not been reported in the literature.

It is believed EGDMA has been successfully incorporated into *p*(HPMA) chains, however, GPC analysis showed that a branching density was varied in all samples; in order to determine the fraction of linear material, a UV active brancher analogue could be employed. Provided the analogue behaves similarly to EGDMA, GPC analysis using a UV detector could potentially determine the fraction of linear material present. In order to obtain solely branched copolymers, fractionation techniques could be employed.

## 7.2 Overview of Chapter 4

It has been shown that nanoparticles comprised of *p*(HPMA) polymers (with linear and branched architectures) can be prepared by a variety of methods using a solvent switch from acetone to water. The different methods were evaluated and it is proposed that using a rapid nanoprecipitation technique is an extremely reliable and reproducible method. The stability of linear polymer nanoparticles has been shown to be extremely limited; however, when polymers with a branched architecture are used, nanoparticles were shown to be highly stable with respect to time, dilution and sonication, where little changes in z-average diameter and dispersity were found. Reports in the literature of the preparation of nanoparticles comprised of branched vinyl copolymers have not been found and this research opens new avenues of investigation. Aqueous nanoparticle dispersions were analysed using DLS and variation of size from < 100 nm in diameter to over 700 nm was obtainable. The range of z-average diameters were correlated to a series of simple systematic variation of polymer and processing parameters. A large nanoparticle screen was

produced using three branched *p*(HPMA) copolymers where comparisons between primary chain length and nanoparticle z-average diameter were investigated; a link between dilution ratio and polydispersity of nanoparticles was found which has not been reported in the literature. Nanoparticle formation has been shown to be highly reproducible and a nucleation-growth mechanism has been proposed. It is speculated that nanoparticle stability arises from electrostatic repulsion whereby nanoparticles de-stabilise during the addition of a salt solution. Data has suggested that small oligomeric units of *p*(HPMA) present within branched copolymer samples exert some aqueous stability and branched-block copolymers were synthesised to remove these chains and test the hypothesis. Subsequent nanoparticles showed limited stability, characterised by precipitation after approximately seven days supporting this theory, however, repeat analysis would be necessary to support this theory. Similarly, the introduction of other monomers (hydrophilic or hydrophobic), to form branched statistical copolymers, would reveal interesting insight into the role of the chemistry of the primary polymer chains with respect to nanoparticle formation, size control and stability.

## 7.3 Overview of Chapter 5

A macroinitiator approach was used to synthesise linear and branched amphiphilic A-B block copolymers. Through simple esterification reactions, a variety of PEG-based macroinitiators were generated with varying chain length (750 g $mol^{-1}$, 2000 g $mol^{-1}$ and 5000 g $mol^{-1}$). These were used to synthesise linear and branched *p*(HPMA) to varying target $DP_n$ using an identical experimental protocol for ATRP homopolymerisations and copolymerisations with EGDMA. Kinetic analysis suggested all polymerisations proceeded by conventional ATRP mechanisms and

were shown to be reproducible. Polymer molecular weight distributions were narrow for linear architectures and extremely broad for branched polymerisations. It has been shown that amphiphilic copolymer chains can be extended using a "self-blocking" technique, producing polymers with accurate molecular weights. It is believed that this is the first report of amphiphilic branched A-B block copolymer synthesis using a macroinitiator strategy thus leading to systematic variation of branched copolymer chemistry.

## 7.4 Overview of Chapter 6

Amphiphilic linear and branched block copolymers were used to synthesise nanoparticles using various precipitation methodologies, similar to homopolymer nanoprecipitation studies. It was shown that linear copolymers do not form stable structures when processed in this way in water, similar to the linear homopolymers studied in Chapter 4. Amphiphilic branched A-B block copolymers have been shown to form stable nanoparticles using a rapid nanoprecipitation approach. Trends in nanoparticle size/polydispersity were investigated by producing a large screen where copolymers (of varying amphiphilicity) were nanoprecipitated using various dilutions. The stability of nanoparticles has been evaluated by conducting a serial aqueous dilution experiment showing little change in z-average diameter during dilution. The surface charge of PEG containing copolymer nanoparticles was also investigated where particles become less negative as copolymer PEG content increases. It has also been shown that linear and branched amphiphilic copolymers, with significant PEG content, appear to dissolve in water and acetone but close observation suggests that association does occur; the impact (positive or negative) on the nucleation and growth of nanoparticles during nanoprecipitation is unknown.

The loading capacity of a variety of copolymer nanoparticles was investigated using Oil red O, Pyrene, and Ibuprofen. Data suggested that stability/loading is proportional to PEG chain length. Fluorescence studies using Pyrene loaded nanoparticles are required to accurately determine loading capacity and confirm the presence of pyrene within the hydrophobic environment (i.e. nanoparticle cores).

The hydrophobic antiretroviral drug Lopinavir (LPV) has been used as a model for preliminary encapsulation experiments. Data has shown that the drug co-exists within a series of branched copolymer nanoparticles characterised by no visual LPV precipitation or crystallisation for up to five days in an aqueous environment. In many cases, instability and a lack of successful loading was observed. Further optimisation of experimental protocol is necessary to produce near monodisperse nanoparticle suspensions. This may be achieved through variation of concentration parameters of both polymer and LPV, perhaps using more dilute solutions to generate stable dispersions. Loading of LPV also could be analysed through $^{14}C$-radiolabelling of the drug. Rigorous toxicity screening is essential to ensure that excipients in any proposed drug formulation are safe. Therefore, performing a cytotoxicity evaluation of the following materials would be necessary.

1. Individual monomers
2. Copolymers
3. Unloaded nanoparticles
4. Loaded nanoparticles

An initial cytotoxicity screen of various candidate methacrylate monomers was performed in collaboration with the Department of Molecular and Clinical Pharmacology, University of Liverpool. In this study, the individual methacrylate

monomers (dissolved in phosphate buffered saline), were studied against Caco-2 cells, a model of the human gut epithelium and the observed luminescence is proportional to cell count, which was measured as the concentration of monomer increased from 0.01 to 5 w/v %. Figure 7.1 suggests PEGMA is not toxic to Caco-2 cell lines, as the amount of luminescence is relatively unchanged throughout the experiment.

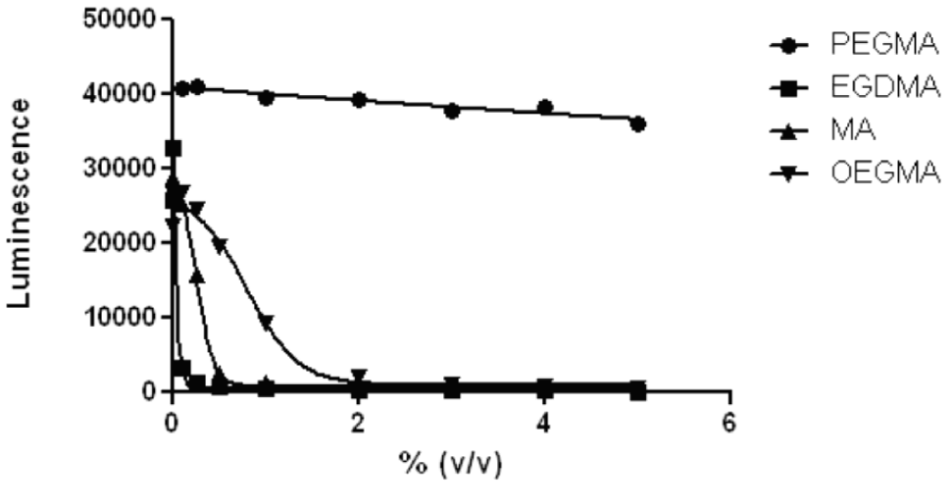


Figure 7.1: Cytotoxic assay of methacrylate monomers using a Caco-2 cell line.

All other monomers were shown to be toxic to this cell line at varying degrees, where cell death became significant at approximately 0.1 w/v % for EGDMA, for example. This experiment suggests that polymers which are used in drug delivery systems must be extensively purified in order to completely remove un-reacted monomer. Interestingly, OEGMA (a short PEG chain equivalent of PEGMA) showed significant toxicity, suggesting a correlation with PEG chain length that, to the best of our knowledge, is not reported in the literature. If polymerisations can be forced to achieve > 99 % conversion (as was the case in this thesis) the issue of

residual monomer toxicity becomes less significant and polymer toxicity must be established.

The amphiphilic branched copolymers synthesised in this thesis have the potential to form reproducible aqueous nanodispersions using an extremely facile methodology, which load LPV as a model HIV/AIDS drug. With further optimisation of synthetic conditions, it is thought z-average diameter may be controlled by the simple adjustment of concentration parameters, which may be useful for cell uptake studies.

# 8. Appendices

## Appendix 1.1

| ARV Type | FDA Approval | Brand name | Generic name | Manufacturer |
|---|---|---|---|---|
| Fusion inhibitors | 2003 | Fuzeon | Enfuvirtide (T-20) | Roche Pharmaceuticals & Trimeris |
| | 2007 | Selzentry (US) Celsentri (Europe) | Maraviroc | Viiv healthcare co |
| Nucleoside reverse transcriptase inhibitors | 1987 | Retrovir | Zidovudine (AZT) | GlaxoSmithKline |
| | 1991 | Videx | Didanosine (ddl) | Bristol-Myers Squibb |
| | 1992 | Hivid | Zalcitabine (ddC) | Roche Pharmaceuticals |
| | 1994 | Zerit | Stavudine (d4T) | Bristol-Myers Squibb |
| | 1995 | Epivir | Lamivudine (3TC) | GlaxoSmithKline |
| | 1998 | Ziagen | Abacavir (ABC) | GlaxoSmithKline |
| | 2001 | Viread | Tenofovir disoproxil (TVD) | Gilead Sciences |
| | 2003 | Emtriva | Emtricitabine (FTC) | Gilead Sciences |
| Non-nucleoside reverse transcriptase inhibitors | 1996 | Viramune | Nevirapine (NVP) | Boehringer lngelheim |
| | 1997 | Rescriptor | Delavirdine (DLV) | Pfizer |
| | 1998 | Sustiva | Efavirenz (EFV) | Bristol-Myers Squibb |
| | 2008 | Tntelence | Etravirine (ETR) | Tibotec Therapeutics |
| Protease inhibitors | 1995 | Invirase | Saquinavir (SQV) | Roche Pharmaceuticals |
| | 1996 | Norvir | Ritonavir (RTV) | Abbott Laboratories |
| | 1996 | Crixivan | Indinavir (IDV | Merck |
| | 1997 | Viracept | Nelflnavir (NFV) | Pfizer |
| | 1999 | Agenerase | Amprenavir (APV) | GlaxoSmithKline |
| | 2000 | Kaletra | Lopinavir + Ritonavir (LPV/r) | Abbott Laboratories |
| | 2003 | Reyataz | Atazanavir (ATV) | Bristol-Myers Squibb |
| | 2003 | Lexiva | Fosamprenavir (FPV) | GlaxoSmithKline |
| | 2005 | Aptivus | Tipranavir (TPV) | Boehringer lngelheim |
| | 2006 | Prezista | Darunavir (DRV) | Tibotec Therapeutics |
| Integrase inhibitors | 2007 | Isentress | Raltegravir | Merck |

FDA approved antiretroviral drugs

## Appendix 3.1

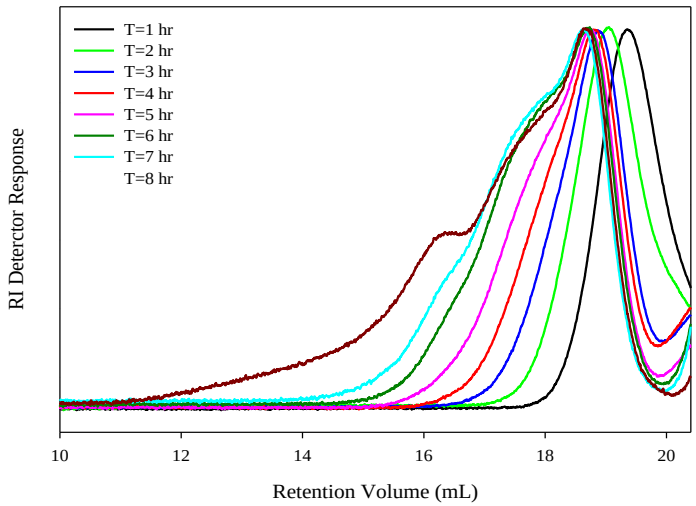


GPC (THF eluent) chromatograms for the kinetics study of the copolymerisation of HPMA and EGDMA by methanolic ambient ATRP to form *p*((HPMA$_{80}$)-*co*-EGDMA$_{0.95}$).

## Appendix 3.2

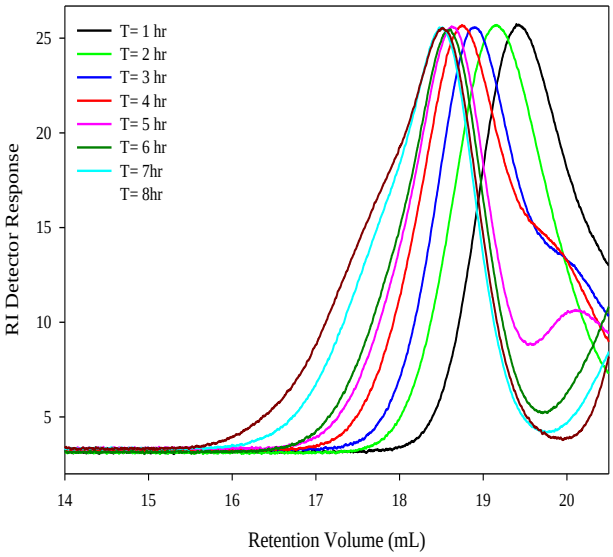


GPC (THF eluent) chromatograms for the kinetics study of the copolymerisation of HPMA and EGDMA by methanolic ambient ATRP to form *p*((HPMA$_{120}$)-*co*-EGDMA$_{0.95}$).

## Appendix 3.3

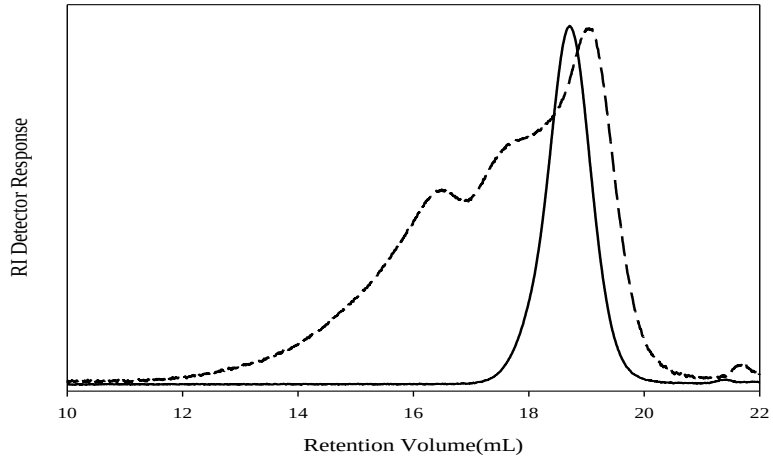


Overlaid GPC chromatograms of *p*($HPMA_{80}$) (solid line) and *p*(($HPMA_{80}$)-*co*-$EGDMA_{0.95}$) (dashed line).

## Appendix 3.4

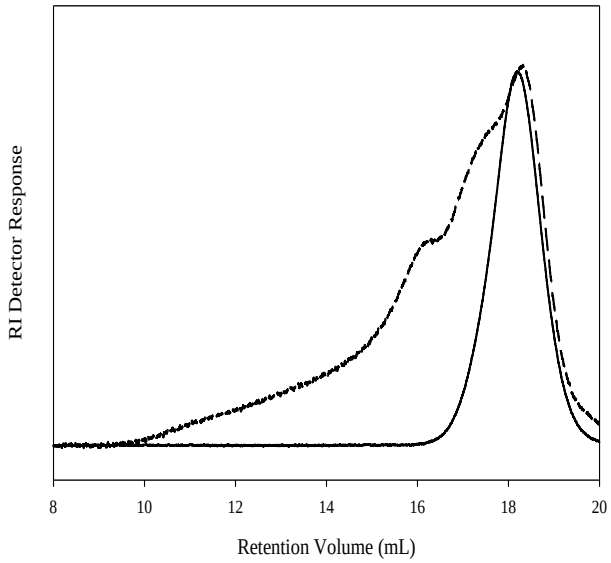


Overlaid GPC chromatograms of *p*($HPMA_{120}$) (solid line) and *p*(($HPMA_{120}$)-*co*-$EGDMA_{0.95}$) (dashed line)

## Appendix 3.5

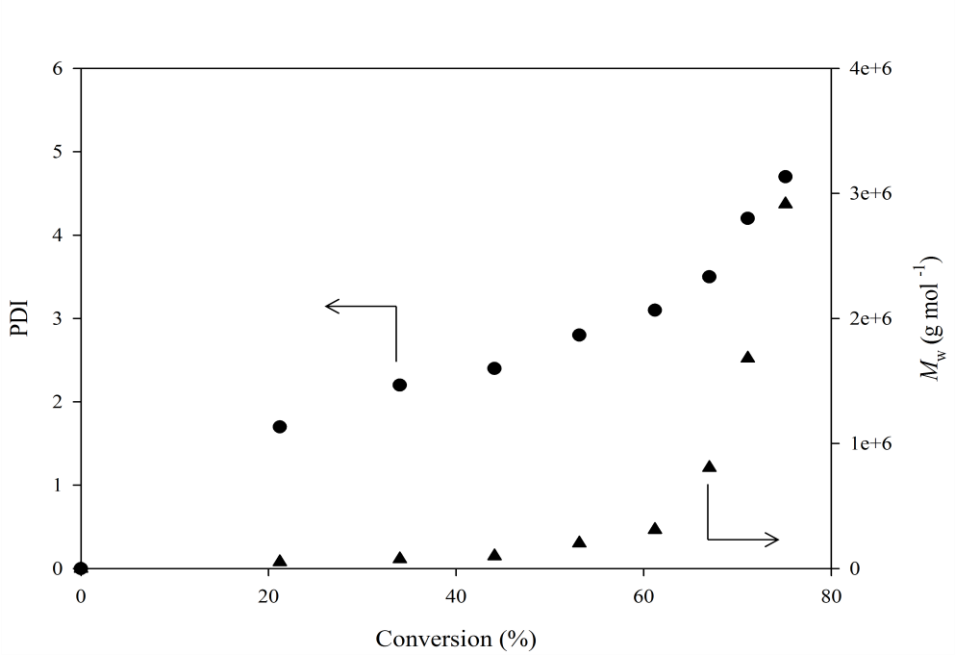


Weight average molecular weight and dispersity vs. conversion (%) plots determined during the kinetics study of the copolymerisation of HPMA and EGDMA by methanolic ambient ATRP to form *p*((HPMA$_{80}$)-*co*-EGDMA$_{0.95}$).

## Appendix 3.6

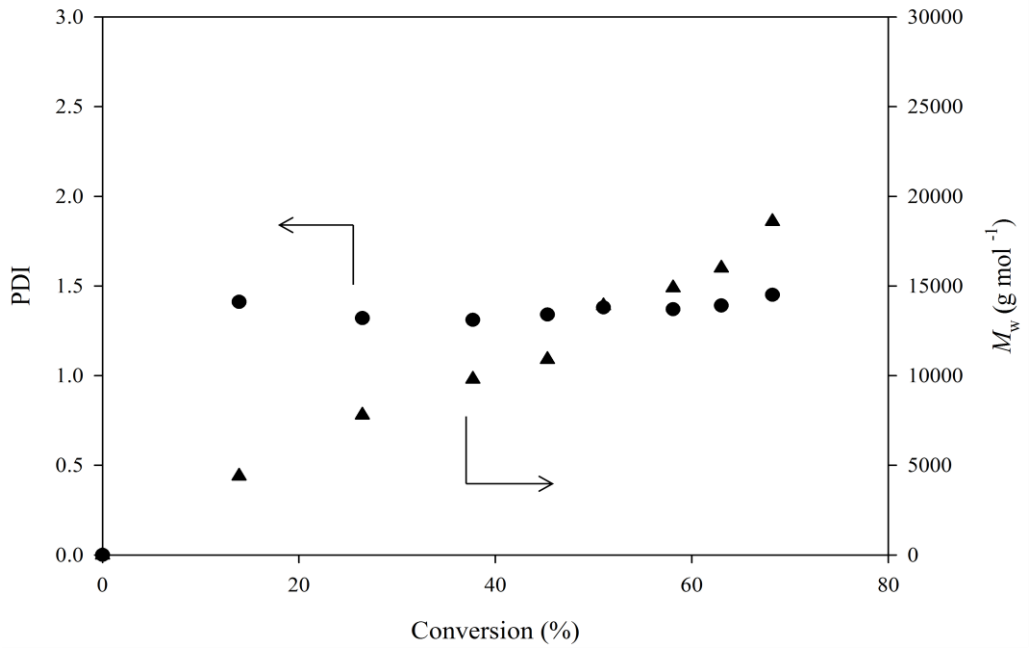


Weight average molecular weight and dispersity vs. conversion (%) plots determined during the kinetics study of the copolymerisation of HPMA and EGDMA by methanolic ambient ATRP to form *p*((HPMA$_{120}$)-*co*-EGDMA$_{0.95}$).

# Appendix 4.1

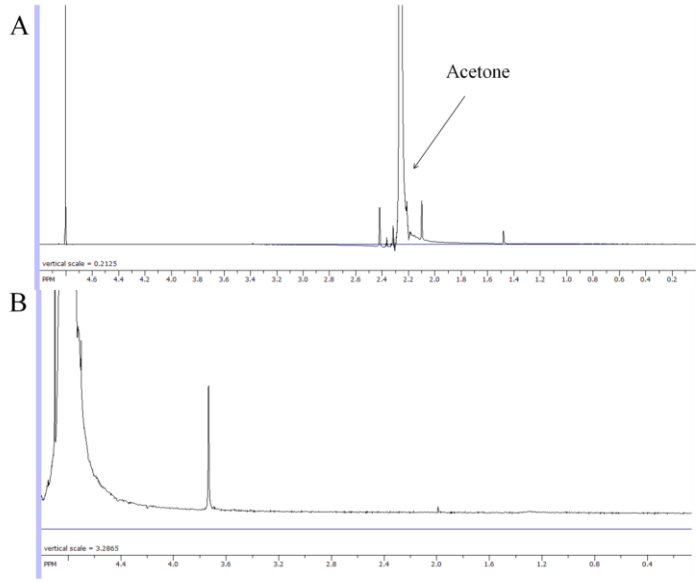


$^{1}$ H NMR of Acetone (A) and a nanosuspension comprised of *p*(HPMA$_{80}$-*co*-EGDMA$_{0.95}$) (B) showing no residual acetone. Both recorded in $D_2O$.

## Appendix 4.2

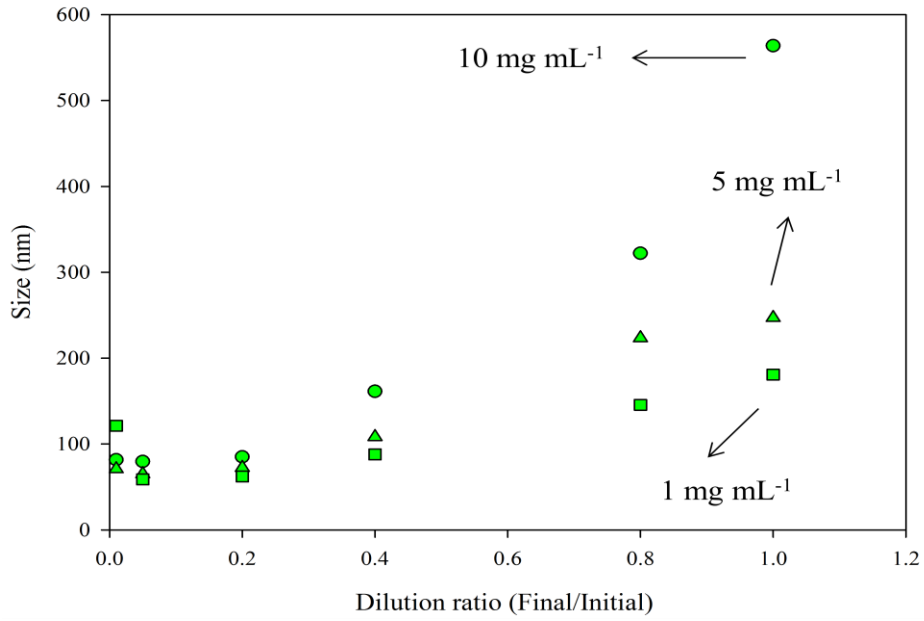


Control of particle z-average diameter by varying initial copolymer concentration in acetone for *p*((HPMA$_{80}$)-*co*-EGDMA$_{0.95}$).

## Appendix 4.3

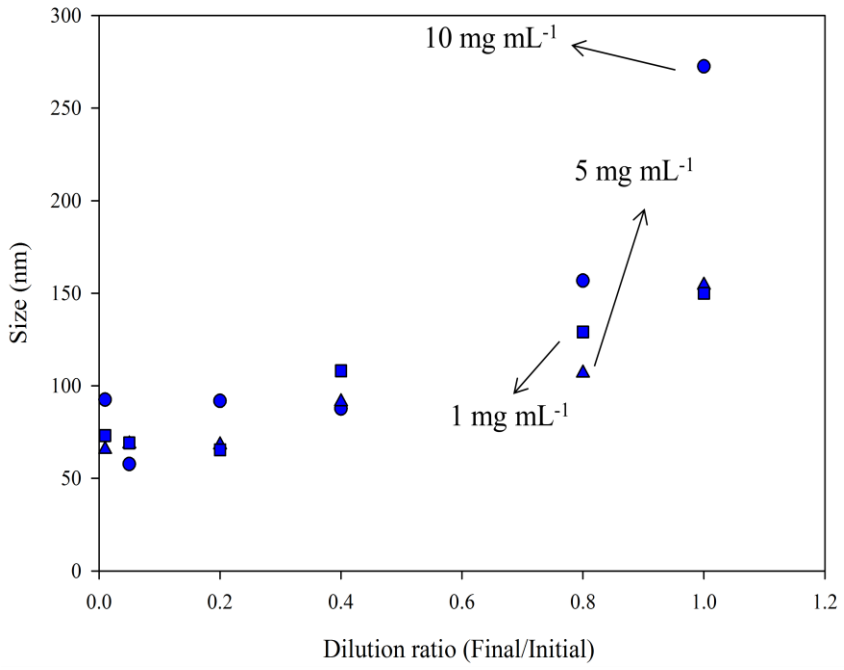


Control of particle z-average diameter by varying initial copolymer concentration in acetone for *p*((HPMA$_{120}$)-*co*-EGDMA$_{0.95}$).

# Appendix 4.4

$p((HPMA_{50})$-*co*-$EGDMA_{0.95})$
10 mg $mL^{-1}$ starting concentration

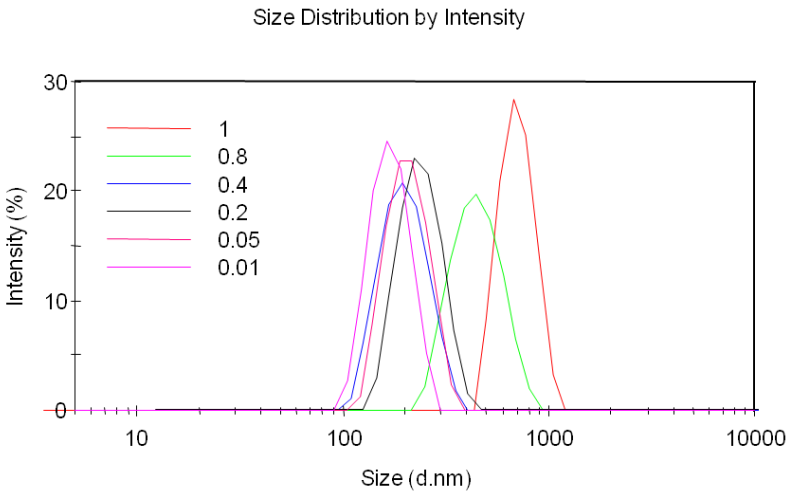


$p((HPMA_{50})$-*co*-$EGDMA_{0.95})$
5 mg $mL^{-1}$ starting concentration

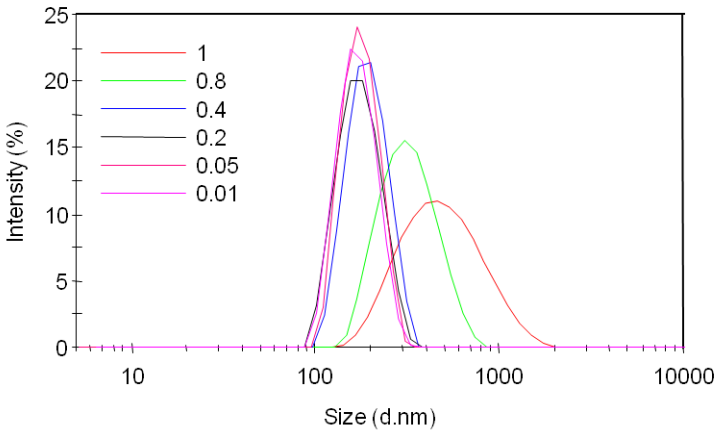

$p((HPMA_{50})$-*co*-$EGDMA_{0.95})$
1 mg $mL^{-1}$ starting concentration

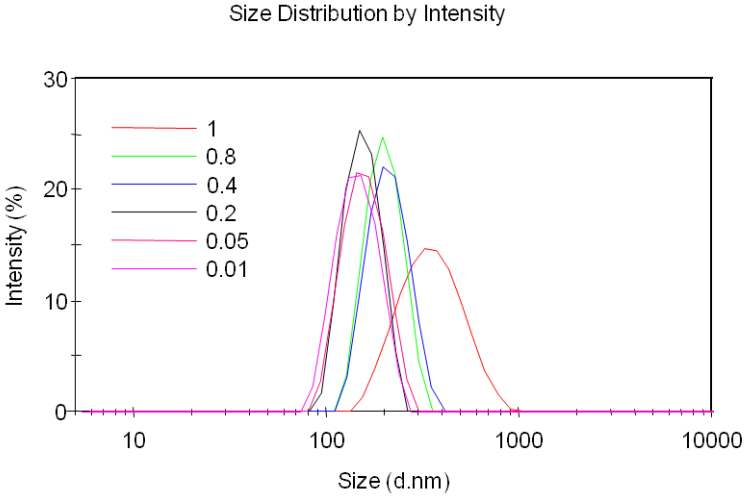


$p((HPMA_{80})$-*co*-$EGDMA_{0.95})$
10 mg $mL^{-1}$ starting concentration

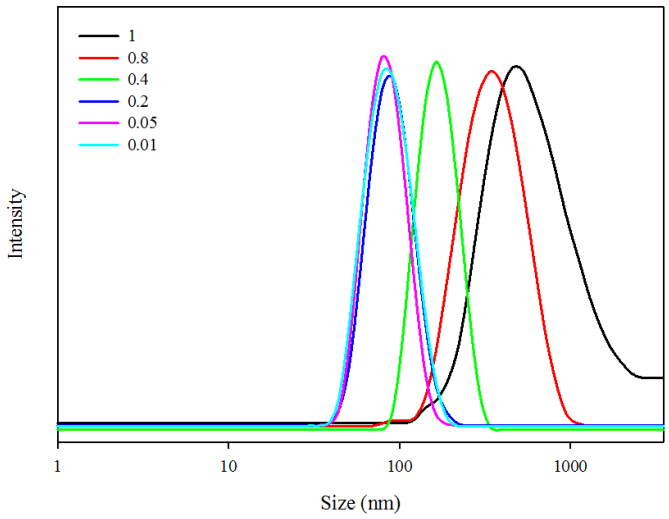

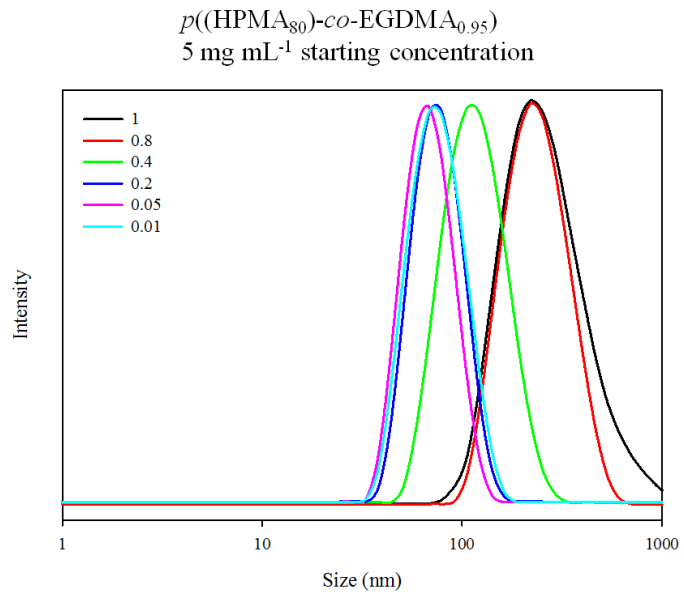
p((HPMA80)-co-EGDMA0.95)
5 mg mL-1 starting concentration
1
0.8
0.4
0.2
0.05
0.01
Intensity
1
10
100
1000
Size (nm)

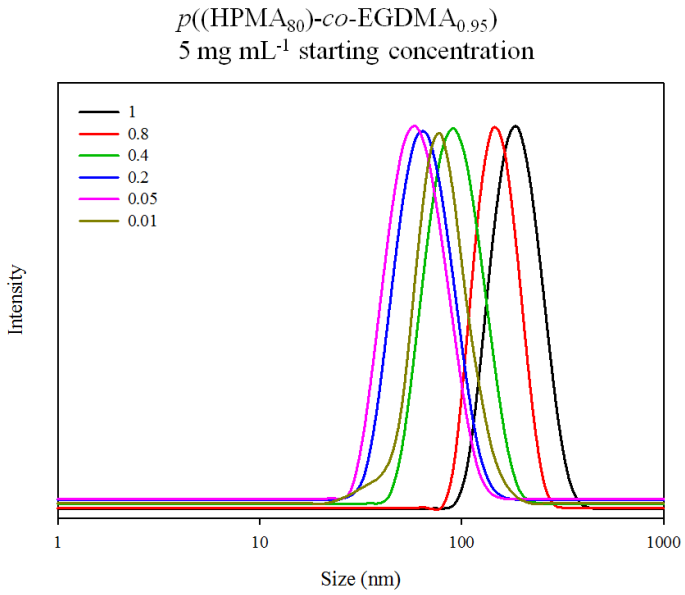
p((HPMA80)-co-EGDMA0.95)
5 mg mL-1 starting concentration
1
0.8
0.4
0.2
0.05
0.01
Intensity
1
10
100
1000
Size (nm)

# Appendix 6.1

$PEG_{17}$-*b*-*p*(($HPMA_{50}$)-*co*-$EGDMA_{0.95}$)
10 mg $mL^{-1}$ starting concentration

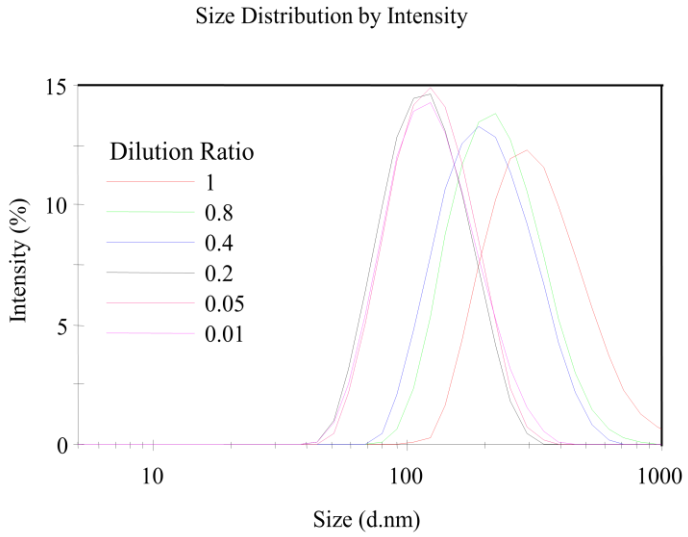


$PEG_{17}$-*b*-*p*(($HPMA_{50}$)-*co*-$EGDMA_{0.95}$)
5 mg $mL^{-1}$ starting concentration

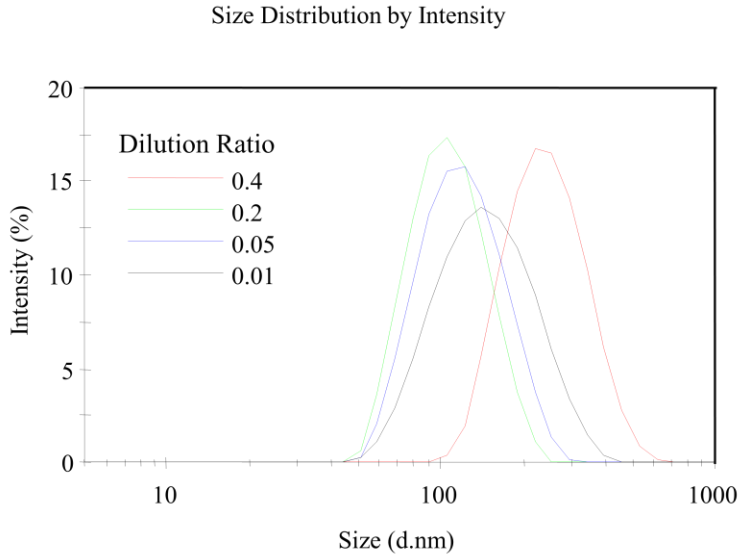

$PEG_{17}$-*b*-*p*(($HPMA_{50}$)-*co*-$EGDMA_{0.95}$)
1 mg $mL^{-1}$ starting concentration

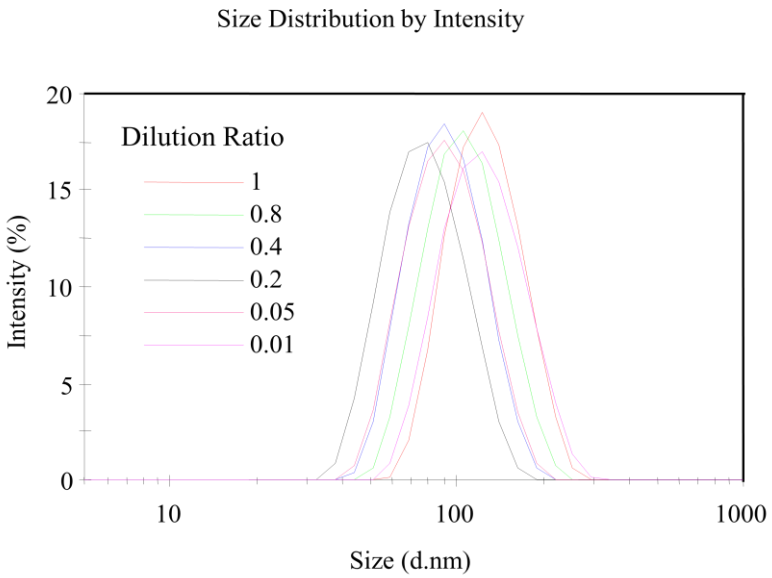


$PEG_{45}$-*b*-*p*(($HPMA_{50}$)-*co*-$EGDMA_{0.95}$)
10 mg $mL^{-1}$ starting concentration

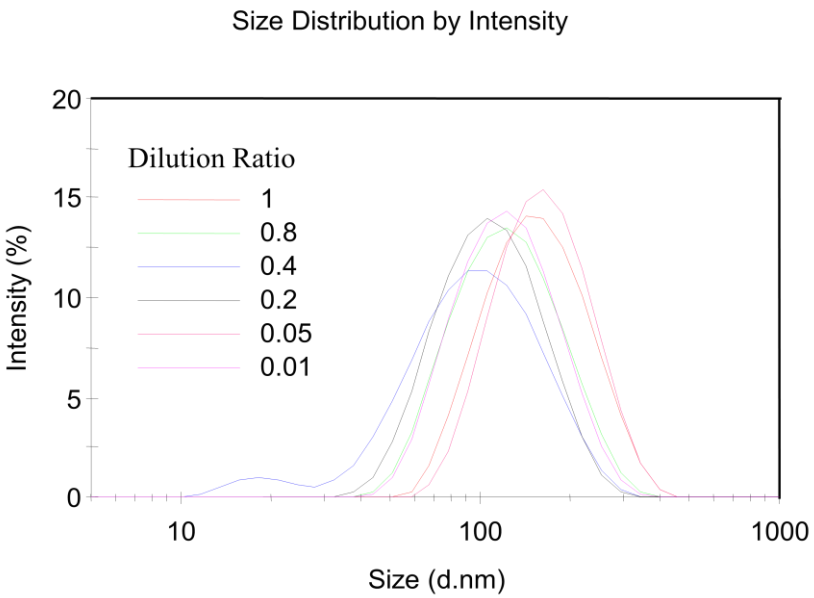

$PEG_{45}$-*b*-*p*(($HPMA_{50}$)-*co*-$EGDMA_{0.95}$)
5 mg $mL^{-1}$ starting concentration

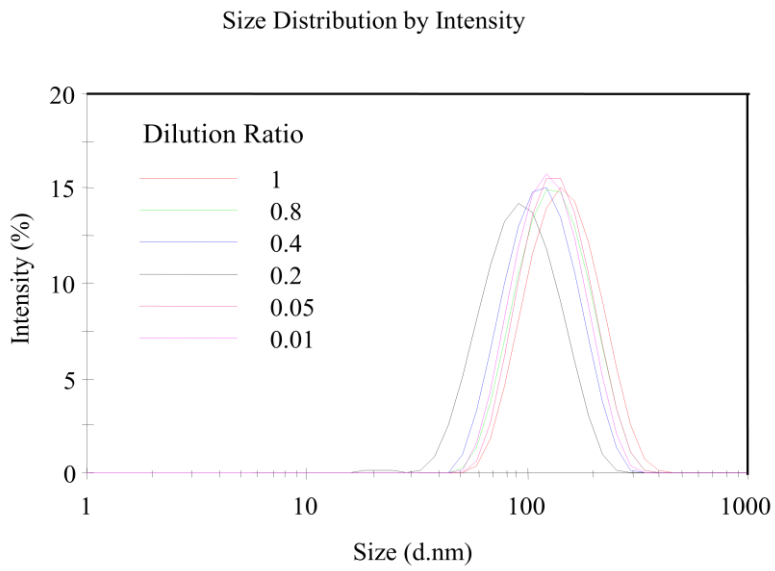


$PEG_{45}$-*b*-*p*(($HPMA_{50}$)-*co*-$EGDMA_{0.95}$)
1 mg $mL^{-1}$ starting concentration

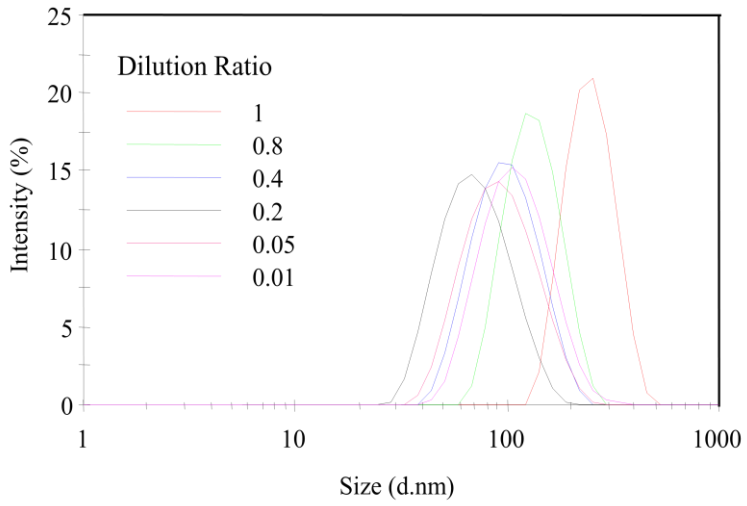

PEG$_{45}$-*b*-*p*((HPMA$_{80}$)-*co*-EGDMA$_{0.95}$)
10 mg mL$^{-1}$ starting concentration

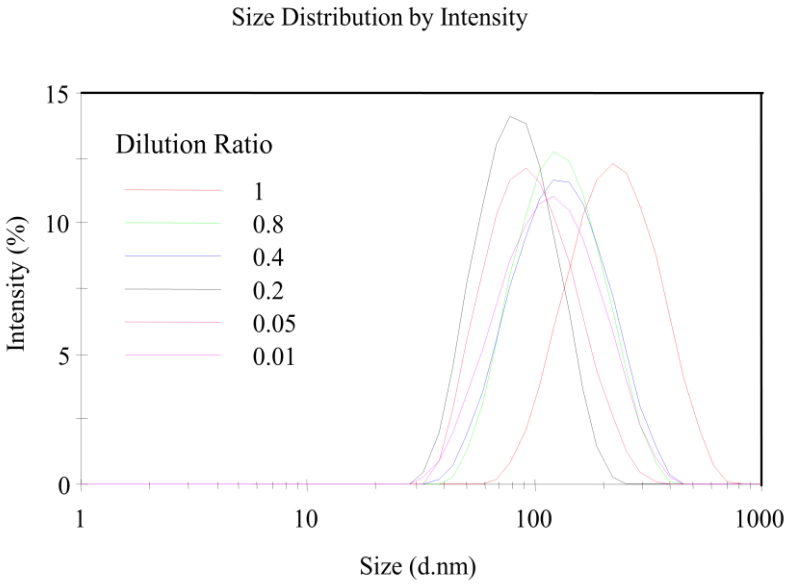


PEG$_{45}$-*b*-*p*((HPMA$_{80}$)-*co*-EGDMA$_{0.95}$)
5 mg mL$^{-1}$ starting concentration

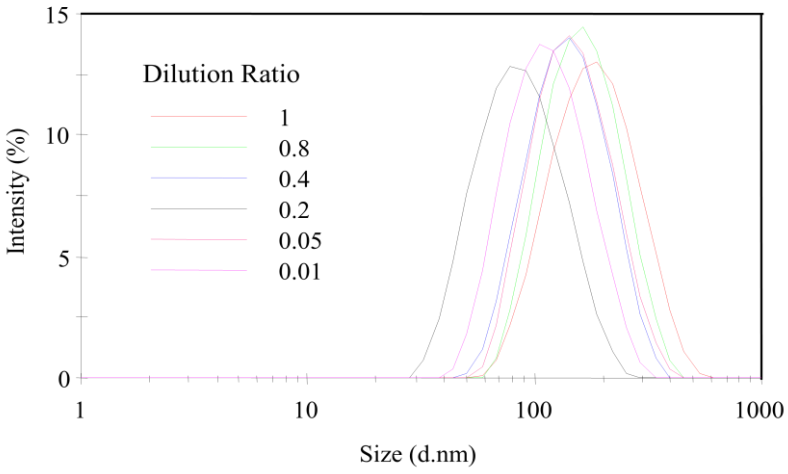

$PEG_{45}$-*b*-*p*(($HPMA_{80}$)-*co*-$EGDMA_{0.95}$)
1 mg $mL^{-1}$ starting concentration

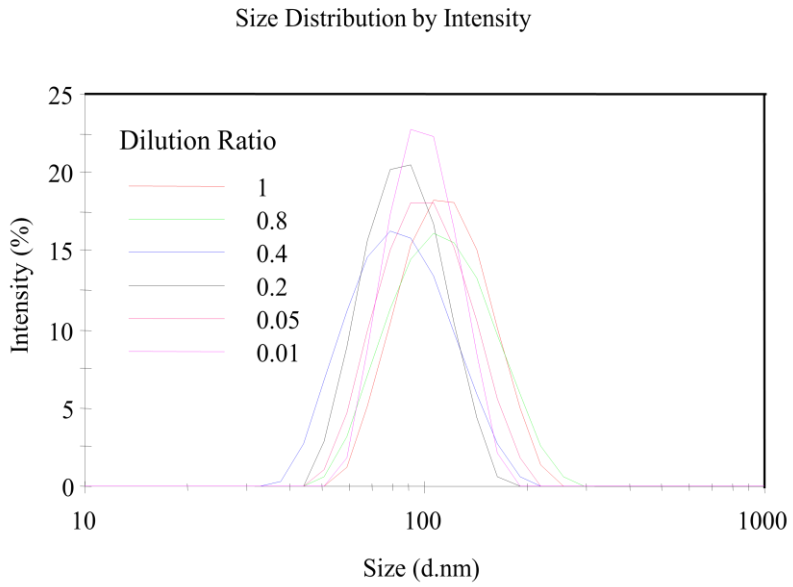


$PEG_{45}$-*b*-*p*(($HPMA_{120}$)-*co*-$EGDMA_{0.95}$)
10 mg $mL^{-1}$ starting concentration

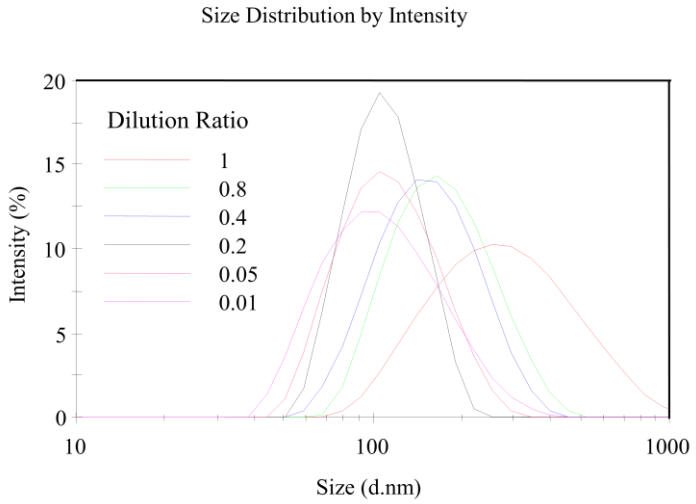

$PEG_{45}$-*b*-*p*(($HPMA_{120}$)-*co*-$EGDMA_{0.95}$)
5 mg $mL^{-1}$ starting concentration

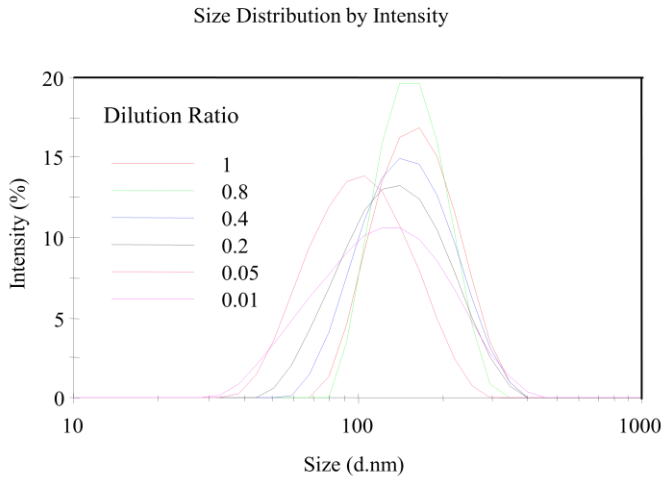


$PEG_{45}$-*b*-*p*(($HPMA_{120}$)-*co*-$EGDMA_{0.95}$)
1 mg $mL^{-1}$ starting concentration

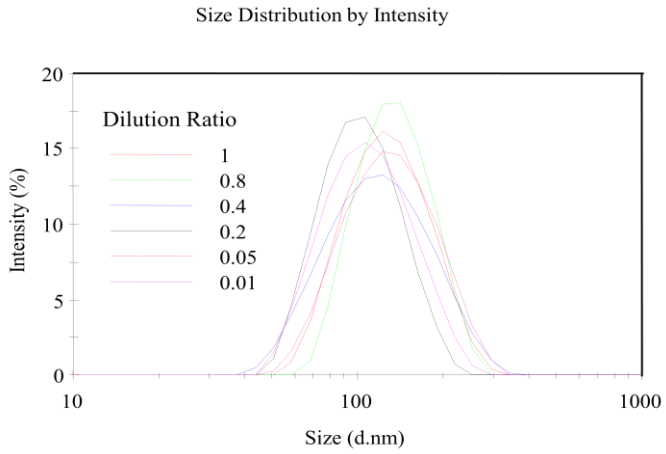


$PEG_{113}$-*b*-*p*(($HPMA_{80}$)-*co*-$EGDMA_{0.95}$)
10 mg $mL^{-1}$ starting concentration

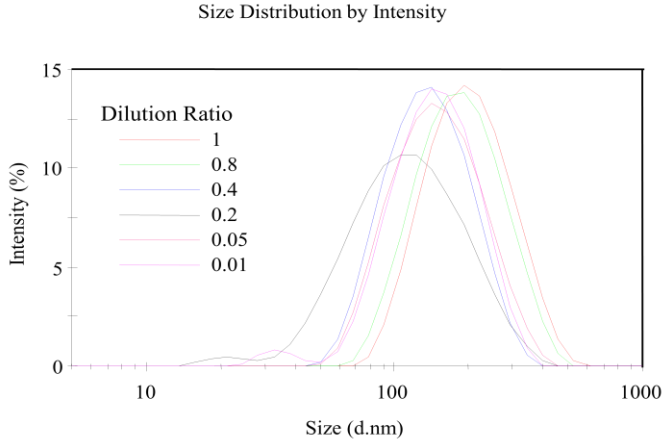

$PEG_{113}$-*b*-*p*(($HPMA_{80}$)-*co*-$EGDMA_{0.95}$)
5 mg $mL^{-1}$ starting concentration

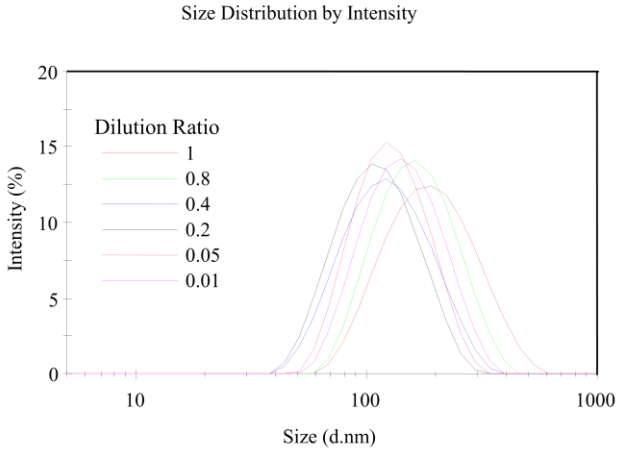


$PEG_{113}$-*b*-*p*(($HPMA_{80}$)-*co*-$EGDMA_{0.95}$)
1 mg $mL^{-1}$ starting concentration

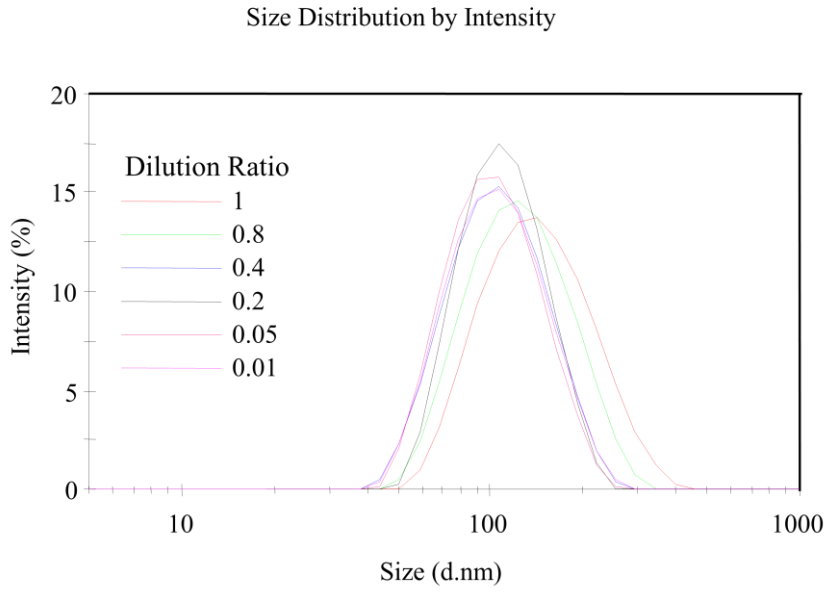

PEG$_{113}$-*b*-*p*((HPMA$_{120}$)-*co*-EGDMA$_{0.95}$)
10 mg mL$^{-1}$ starting concentration

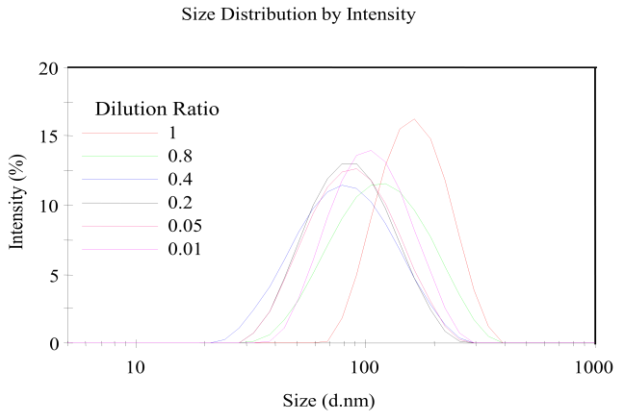


PEG$_{113}$-*b*-*p*((HPMA$_{120}$)-*co*-EGDMA$_{0.95}$)
5 mg mL$^{-1}$ starting concentration

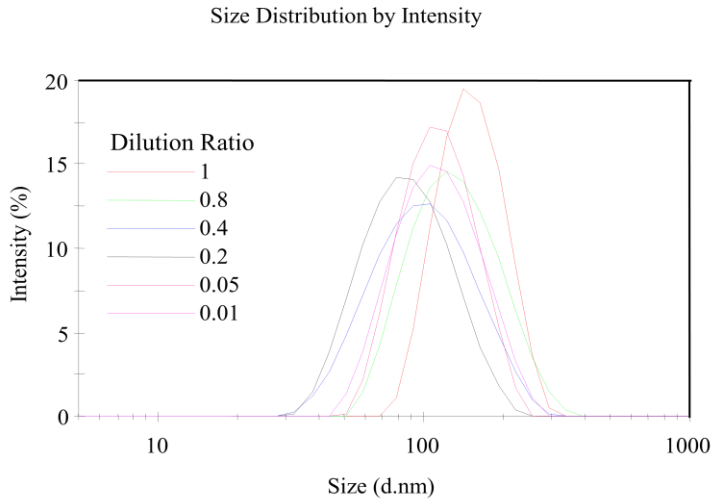

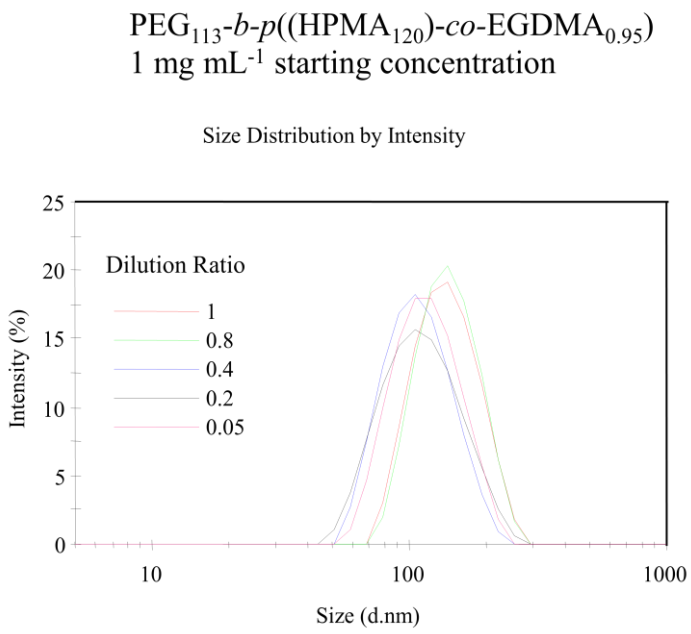


$PEG_x$-*b*-(*p*($HPMA_y$)-*co*-$EGDMA_{0.95}$) nanoparticle size analysis using rapid precipitation with varied dilution ratios.

## Appendix 6.2

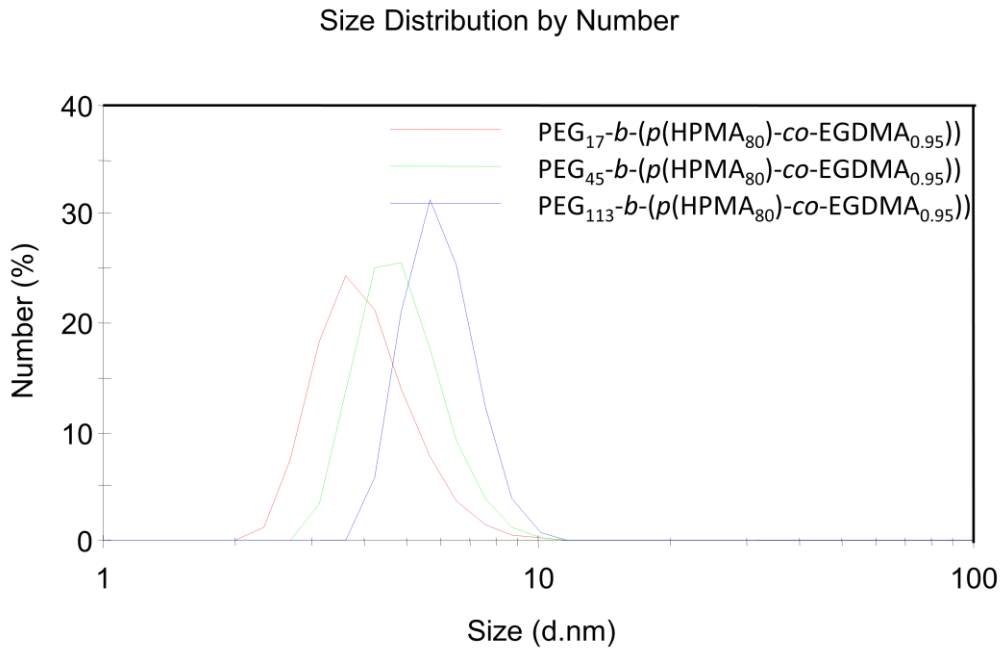


DLS characterisation of branched copolymers dissolved in acetone at 10 mg $ml^{-1}$ measuring size distribution by number.